Flexural and Shear Failure Mechanisms

of

Precast/Prestressed Concrete Members

by

Jaeman Lee

Significant advances have been accomplished in the second half of the twentieth century in the seismic protection of structures due to the development of new technologies and advanced materials. In twenty first century, the effective maintenance and management of structures built in last decades are urgent future work to realize the sustainable development society. Therefore, the design and construction of concrete structures which are friendly environment are important. Prestressed / precast concrete structures which can control the cracks due to introduction of prestressing and also enhance the workability due to production in factory and construction in field have been highlighted. The prestressed / precast concrete system can contribute to the realization of long-life structures and reduction of the construction and management cost.

Main objectives of this research are to investigate the structural behavior and failure mechanism of prestressed / precast concrete members and to develop the rational structural design procedure of prestressed / precast concrete structures.

Chapter 1 introduces the back ground, objectives, and the outline of this research.

In Chapter 2, previous research on shear and flexural behavior of reinforced / prestressed concrete members and shear design equations for reinforced / prestressed concrete members are introduced. In shear analogies, Ichinose`s truss model, Vecchio`s modified compression field theory, and current shear design equations will be introduced. In flexural behavior, inelastic deformation capacity prediction method of reinforced concrete beams failed in flexure and shear after flexural yielding will be introduced. The achievement and future work of those analogies will be also discussed.

Static loading test on shear behavior of post-tensioned precast concrete beams is described in Chapter 3. Experimental outlines and results on two series of half-scale post-tensioned precast concrete beams are reported. Structural properties of various shear failure modes (shear compression, shear tension, and diagonal tension failure etc.) will be clarified. By comparing of shear strength of post-tensioned prestressed concrete beams predicted by current shear design

analogy to the one observed from previous research, applicability of current shear analogy to post-tensioned precast concrete beams will be discussed.

An innovative shear failure analogy (Model 1) for the post-tensioned precast concrete beams will be proposed in Chapter 4. The analogy covers shear compression or bond failure as well as shear tension failure which is considered at current shear design equation procedures. The proposed analogy will be verified by comparison between the analytical results by the proposed analogy and experimental data from previous research on shear behavior of prestressed concrete in the past.

In Chapter 5, a diagonal tension failure analogy (Model 2) will be proposed. The shear analogy to be able to investigate the diagonal tension failure of reinforced / prestressed concrete members is attained by fractural energy equilibrium condition on shear crack. The proposed analogy will be verified by comparison between the analytical and experimental results (shear strength, initial shear crack width, and failure mode).

In Chapter 6, flexural shear compression failure model (Model 3) will be clarified. Based on the stress state of concrete in flexural compression zone, shear capacity at flexural shear compression failure will be evaluated. This analytical model can be very effective analytical tool to estimate the total deformation of post-tensioned precast concrete member failing in flexure as well as shear capacity of member in an integrative way.

In Chapter 7, seismic performance of prestressed concrete beam has been conducted by the FEM analysis. Two analytical parameters, bond strength of PT tendon and mild steel ratio are selected. The effect of bond strength and mild steel ratio of prestressed concrete beams on seismic performance (load-displacement relation, the maximum load capacity, energy dissipation capacity, and residual deformation) will be investigated analytically.

Chapter 8 summarizes the conclusions of this research and suggests recommendations for future work.

University. I would like to express my thanks to all of them.

Finally, I wish to express my sincere gratitude to my wife, Minhee, and my parents for their constant assistance, encouragement, understanding and support over the years.

<div align="right">

March, 2013

이재만

</div>

(Acknowledgements written in Japanese is attached at the end of this thesis)

Journal Papers (Full Referred)

1. J. Lee, M. Nishiyama, S. Kono, M. Sakashita, "Shear Resistance Mechanism of Post-tensioned Precast Concrete Members," *Journal of Structural Engineering, ASCE*. (accepted)

2. J. Lee, M. Tani, M. Skashita, S. Kono, M. Nishiyama, "Flexural and Shear Behavior of Precast Prestressed Concrete Beam with High Strength Shear Reinforcement," *Journal of Structural and Construction Engineering, AIJ*, Vol. 653, 2010, pp. 1335-1342. (in Japanese)

Conference Papers (Full Referred)

3. J. Lee, M. Tani, M. Sakashita, S. Kono, "Diagonal Tension Failure of Post-tensioned Precast Concrete Beam with High Strength Shear Reinforcement," *Proceedings of The 19th Symposium on Developments of Prestressed Concrete, JPCEA*, 21-22 Oct. 2010, pp. 77-80. (in Japanese)

4. J. Lee, M. Tani, M. Sakashita, S. Kono, "Diagonal Tension Failure of Post-tensioned Precast Concrete Beam with High Strength Shear Reinforcement," *Proceedings of Japan Concrete Institute, JCI*, Vol. 32, 7-9 July 2010, pp. 493-498. (in Japanse)

5. J. Lee, M. Nishiyama, M. Tani, "Evaluation of Shear Design Procedures for Prestressed Concrete Members," *Proceedings of The 3rd international fib Congress / PCI Annual Convention and Bridge Conference*, EAD11-455, May-June, 2010

6. J. Lee, M. Tani, M. Nishiyama, "Shear Behavior of Prestressed Concrete Beam with High Strength Shear Reinforcement," *Proceedings of The 18th Symposium on Developments of Prestressed Concrete, JPCEA*, 29-30 Oct. 2009, pp. 257-260. (in Japanse)
    [Excellent Presentation Award, *The 18th Symposium on Developments of Prestressed Concrete, JPCEA*, 2009]

Others

7. J. Lee, M. Nishiyama, "Seismic Performance of Prestressed Concrete Beams – Effect of Bond Strength and Mild Steel Ratio," *Proceedings of The 14th Taiwan-Korea-Japan Joint Seminar on Earthquake Engineering for Building Structures*, 1-2 Nov. 2012, pp. 69-78.

8. J. Lee, M. Nishiyama, "Deformation Performance of Post-tensioned Precast Concrete Columns Failing in Flexural Shear," *Proceedings of The 12th Korea-Japan-Taiwan Joint Seminar on Earthquake Engineering for Building Structures*, 26-27 Nov. 2010, pp. 11-20.

9. J. Lee, Y. Karino, M. Sakashita, M. Tani, S. Kono, M. Nishiyama, "Diagonal Tension Failure of Post-tensioned Precast Concrete Beam with High Strength Shear Reinforcement," *Summaries of Technical Papers of Annual Meeting, AIJ*, C-2, 9-11, Sep. 2010, pp. 825-828. (in Japanese)

10. J. Lee, M. Nishiyama, M. Tani, "Shear Strength of Precast Post-tensioned Concrete Beams with High Strength Shear Reinforcement," *Proceedings of The 11th Taiwan-Korea-Japan Joint Seminar on Earthquake Engineering for Building Structures*, 3-5 Dec. 2009, pp. 93-102.

11. J. Lee, Y. Karino, J. Yamamoto, Z. Hui, M. Sakashita, M. Tani, S. Kono, M. Nishiyama, "Shear Behavior of Prestressed Concrete Beams with High Strength Transverse Reinforcement," *Summaries of Technical Papers of Annual Meeting, AIJ*, C-2, 26-29, Aug. 2009, pp. 837-842. (in Japanese)

12. M. Nishiyama, M. Tani, J. Lee, "Ultimate Flexural Strength Evaluation for Prestressed Concrete Columns," *Proceedings of The 10th Japan-Taiwan-Korea Joint Seminar on Earthquake Engineering for Building Structures*, 10-11 Oct. 2008, pp. 277-285.

1. Introduction

3. Static Loading Test on Flexural and Shear Behavior of Post-tensioned Precast Concrete Beams 34

4. Analytical Model 1 for Shear Failure Mechanism of Post-tensioned Precast Concrete Members (SC and ST Model) 126

5. Analytical Model 2 for Reinforced / Prestressed Concrete Members (DT Model)152

6. Analytical Model 3 for Post-tensioned Precast Concrete Members (FSC Model) . 187

7. Effect of Bond Strength and Mild Steel Ratio on Seismic Performance of Prestressed Concrete Beams 207

8. Major Conclusions and Future Work.......... 229

1. Introduction

1.1 Background and object

The world wide consensus and expectation aim to provide a modern society with structures able to sustain a design level earthquake with limited or negligible damage have been developed for high-performance, cost-effective, and seismic resisting systems [1.1]. In addition, a broad consensus between public, politicians and engineers/scientists communities for the conservation of energy and the reduction of CO_2 emission in whole process throughout design, construction, and management of building structures seem to be achieved, recently.

As a result, in an attempt to develop adequate structural systems, prestressed / precast concrete systems are highlighted. It is because prestressed / precast concrete systems contribute for realization of sustainable developed society due to enhancement of durability and cost-effective. In the structural behavior, an introduction of prestress in concrete leads to prevention of cracking (durability). In addition, a shortening of construction period due to production of structural members in factory leads to enhancement of workability. Therefore, the damage-control design of prestressed / precast concrete systems can contribute for achievement of high-performance, cost-effective, and energy conservation structures as well as a realization of seismic resisting building structures.

Referring to the concept of damage-control design, have developed the Performance Based Design (PBD) for seismic structures. However, there are few experimental and analytical data for seismic performance of prestressed concrete members while the data for that of reinforced concrete members are extensive. For design and analysis of prestressed concrete member, many design equations or guidelines [1.1, 1.3] are currently based on the results from the research using reinforced concrete (RC) members. However, there is still

considerable disagreement among researchers in proposing and using a rational way of investigating flexure or shear failure mechanism of prestressed / precast concrete members.

In order to resolve the problems on applicability of the design or analytical analogy for RC members to prestressed concrete beams or columns, the following establishment of research object must be made.

On shear behavior of prestressed concrete members;
1. Experimental investigation on shear behavior and failure mode of post-tensioned precast concrete members.
2. Investigation on effect of experimental parameters of prestressed concrete members on failure mechanism.
3. Suggestion of analogy on shear failure mechanism of prestressed concrete members.
4. Discussion on applicability of proposed analogy to seismic design of prestressed concrete members.

On flexural behavior of prestressed concrete members;
1. Investigation of bond strength in post-tensioning (PT) tendon and amount of mild steel on structural behavior of prestressed concrete members.
2. Suggestion of flexure-shear integrative analogy on flexural and shear failure mechanism of post-tensioned precast concrete members.
3. Discussion on applicability of proposed design analogy to prestressed concrete members with unbonded PT tendons

Resolving the research object above leads to the realization of quantitative evaluation for the structural performance of prestressed/precast concrete members. Then, it is expected that the main results of this study contribute for the establishment of damage-control design based on the collapse mechanism. The quantitative evaluation for the structural performance is defined as the proposition and the estimation of the minimum required damage (crack width etc.), energy dissipation capacity, and the residual deformation to satisfy the performance levels of structure (1. serviceability, 2. reparability, 3. safety), developed as part of an attempt to provide an alternative for the PBD guide lines. The establishment of damage-control design leads to the prevention the structure

from the collapse and the maintenance of reparability of the structure.

The main results from the proposed method in this study (the evaluation of the stress in shear cracked concrete in model 1 (Chapter 4), the prediction of the primary shear crack width in model 2 (Chapter 5), and the evaluation of drift angle of precast concrete member at flexural failure in model 3 (Chapter 6)) is the criteria to investigate the structural performance of precast/prestressed concrete members. It is expected that the prediction method of failure mode of precast/prestressed concrete members in model 1 to 3 (Chapter 4 to 6) leads to the establishment of damage-control design based on the collapse mechanism of structures. Moreover, the energy dissipation capacity and residual deformation properties of prestressed concrete with unbonded PT tendon shown in Chapter 7, will be referred to achievement of structural performance level of prestressed/precast concrete structures.

1.2 Outline of research
This research is consisted of seven chapters.

In Chapter 2, previous research on shear and flexural behavior of reinforced / prestressed concrete members and shear design equations for reinforced / prestressed concrete members are introduced. In shear analogy, Ichinose`s truss model, Vecchio`s modified compression field theory, and current shear design equations will be introduced. In flexural behavior, inelastic deformation capacity prediction method of reinforced concrete beams failed in flexure and shear after flexural yielding will be introduced. The achievement and future work of those analogies will be also discussed.

Static loading test on shear behavior of post-tensioned precast concrete beams is described in Chapter 3. Experimental outlines and results on two series of half-scale post-tensioned precast concrete beams are reported. Structural properties of various shear failure modes (shear compression, shear tension, and diagonal tension failure etc.) will be clarified. By comparing of shear strength of post-tensioned prestressed concrete beams predicted by current shear design analogy to the one observed from the previous research, applicability of current shear analogy to post-tensioned precast concrete beams will be discussed.

An innovative shear failure analogy (Model 1) for the post-tensioned precast

concrete beams is proposed in Chapter 4. The analogy covers shear compression or bond failure as well as shear tension failure which is considered at current shear design equation procedures. The proposed analogy will be verified by comparison between the analytical results by the proposed analogy and experimental data from previous research on shear behavior of prestressed concrete in the past.

In Chapter 5, a diagonal tension failure analogy (Model 2) will be proposed. The diagonal tension failure is most brittle and catastrophic failure mode induced by excessive opening of primary shear crack. A different approach from Model 1 is necessary to investigate the diagonal tension failure. The shear analogy to be able to investigate the diagonal tension failure of reinforced / prestressed concrete members is attained by fractural energy equilibrium condition on shear crack. The proposed analogy will be verified by comparison between the analytical and experimental results (shear strength, initial shear crack width, and failure mode).

In Chapter 6, flexural shear compression failure model (Model 3) will be clarified. Based on the stress state of concrete in flexural compression zone, shear capacity at flexural shear compression failure will be evaluated. This analytical model can be very effective analytical tool to estimate the total deformation of post-tensioned precast concrete member failing in flexure as well as shear capacity of member in an integrative way.

In Chapter 7, seismic performance of prestressed concrete beam have been conducted by the FEM analysis. Two analytical parameters, bond strength of PT tendon and mild steel ratio are selected. The effect of bond strength and mild steel ratio of prestressed concrete beams on seismic performance (load-displacement relation, the maximum load capacity, energy dissipation capacity, and residual deformation) will be investigated analytically.

Chapter 8 summarizes the conclusions of this research and suggests recommendations for future work.

[References]

1.1 Pampanin S., "Simple and Low-Cost Technology for A Total Damage-Control: The Ultimate Challenge of Earthquake Engineering," Proceedings of Fumio Watanabe Symposium, Oct. 24-25, 2008, pp. 101-112.

1.2 Architectural Institute of Japan (AIJ), "Standard for Structural Design and Construction of Prestressed Concrete Structures," pp. 232-234, 1998.

1.3 ACI Committee 318, "Building Code Requirements for Structural Concrete (ACI-318) and Commentary", American Concrete Institute, Farmington Hills, MI, pp. 155-168, 2008.

2. Previous Research on Flexural and Shear Behavior of Reinforced / Prestressed Concrete Members

2.1 Introduction

Previous flexural and shear analogy of reinforced / prestressed concrete members are specified in Chapter 2. Further, properties and problems of the analogies will be also scrutinized.

In current earthquake design, potential plastic hinge zones are designed. In particular, for preventing brittle shear failure, the shear strength of reinforced / prestressed concrete members is designed to exceed the shear demand developed by their maximum flexural strength [2.1]. In order to design the prestressed concrete members in which shear strength is larger than their flexural strength, it is necessary to investigate and evaluate shear strength of reinforced / prestressed concrete member in a rational way. By the middle of 1980, many researches on shear analogy of reinforced / prestressed concrete members have been based on a truss analogy by Ritter and Morsch (1899). In the analogy, diagonal compressive stresses in the concrete act as the diagonal members of the truss while the stirrups act as vertical tension members [2.2]. After the truss analogy by Ritter and Morsch, extensive truss analogies such as variable angle truss analogy have been proposed by many researchers. Then, plastic theory by Nielsen and Modified Compression Field Theory (MCFT) by Vecchio [2.3] were developed.

In existing models on shear capacity of reinforced / prestressed concrete members, the shear strength and deformation capacity of the members are determined at the intersection of the shear capacity curve and the shear demand curve that represents the shear force required by the flexural action of the

member as shown in Fig. 2.1. However, the degradation curve of the shear capacity due to inelastic flexural deformation has been empirically obtained. Choi [2.1] and Nakatsuka [2.4] proposed an analytical method for predicting the degraded shear capacity and deformation capacity of reinforced concrete beams subjected to cyclic loading.
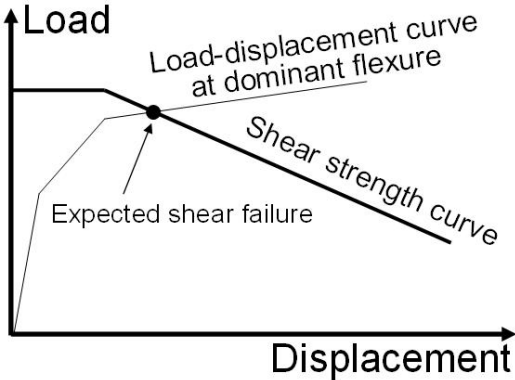
Fig. 2.1 Load-displacement relation and shear capacity

In Section 2.2 and 2.3, shear analogies on reinforced / prestressed concrete members in the previous researches [2.3, 2.5] are introduced. Current shear design equations used in the design of shear resistance members are also mentioned in Section 2.4. In Section 2.5, Choi`s [2.1] and Nakatsuka`s [2.4] model to evaluate inelastic deformation capacity of reinforced concrete beams failed in flexure and shear after flexural yielding are specified.

2.2 Ichinose`s Truss Analogy
2.2.1 Research Background
The uniform truss model as shown in Fig. 2.2 had been accepted widely in Japan for calculating shear strength of reinforced concrete members. The diagonal compressive stress in concrete strut is equilibrated with bond force of longitudinal bar and tensile force of shear reinforcement. However, the uniform truss model has two theoretical weak points: (1) compressive stress of concrete is assumed to distribute uniformly even in critical sections of member, and (2) longitudinal reinforcement is assumed to be strong enough beyond its yield strength [2.5]. To improve these weak points, Ichinose proposed the modified truss analogy with concrete struts of variable angles and shear resistance zone of cover concrete as shown in Fig. 2.3.

2.2.2 Ichinose`s Truss Model

Figure 2.3 illustrates the Ichinose`s truss model. It is assumed that uniform angle concrete struts distribute in shaded zone BEJF. In shaded zone BDF and EGJ, variable angle struts distribute. At the ends of the member, compressive stress, f_c, and shear stress, τ_c, exist at between A and C or H and K.

Uniaxial compressive stress in zone BDF push apart region BD and DF. It points out that diagonal compressive stresses in shaded zone BDF are not carried by tension in the shear reinforcement. As shown in Fig. 2.3 (b), overall section are not effective against shear because the diagonal compressive stresses in shaded zone BEJF are supported by longitudinal bars at four corners in the member section. In a view of overall section, it can be seen that member section will fail in compression at lower stress than uniaxial compressive strength, F_c.
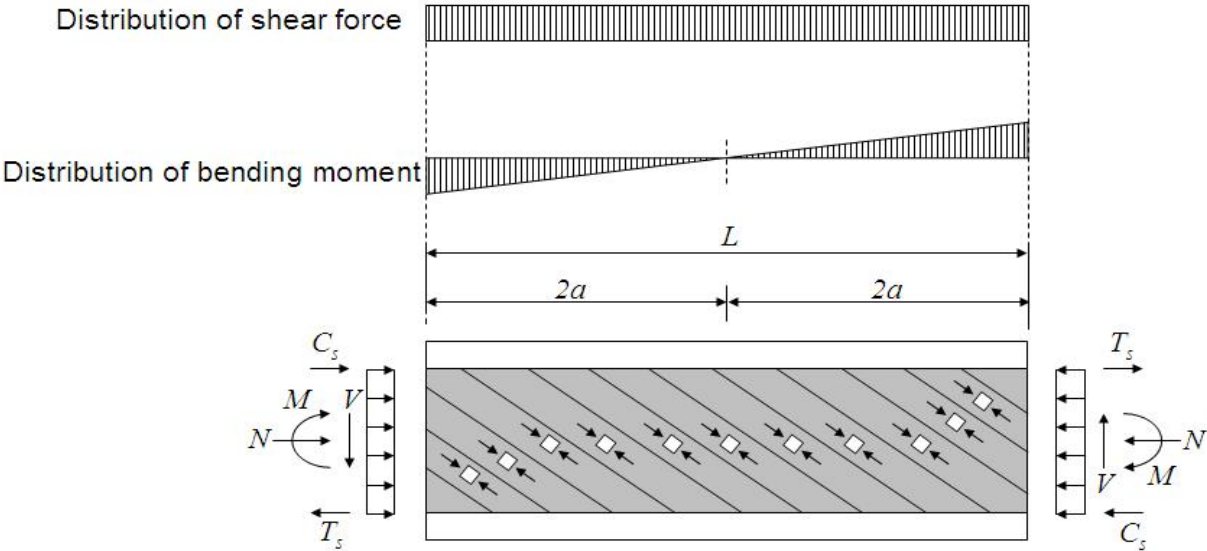
Fig. 2.2 Conventional uniform angle truss model subjected to double curvature
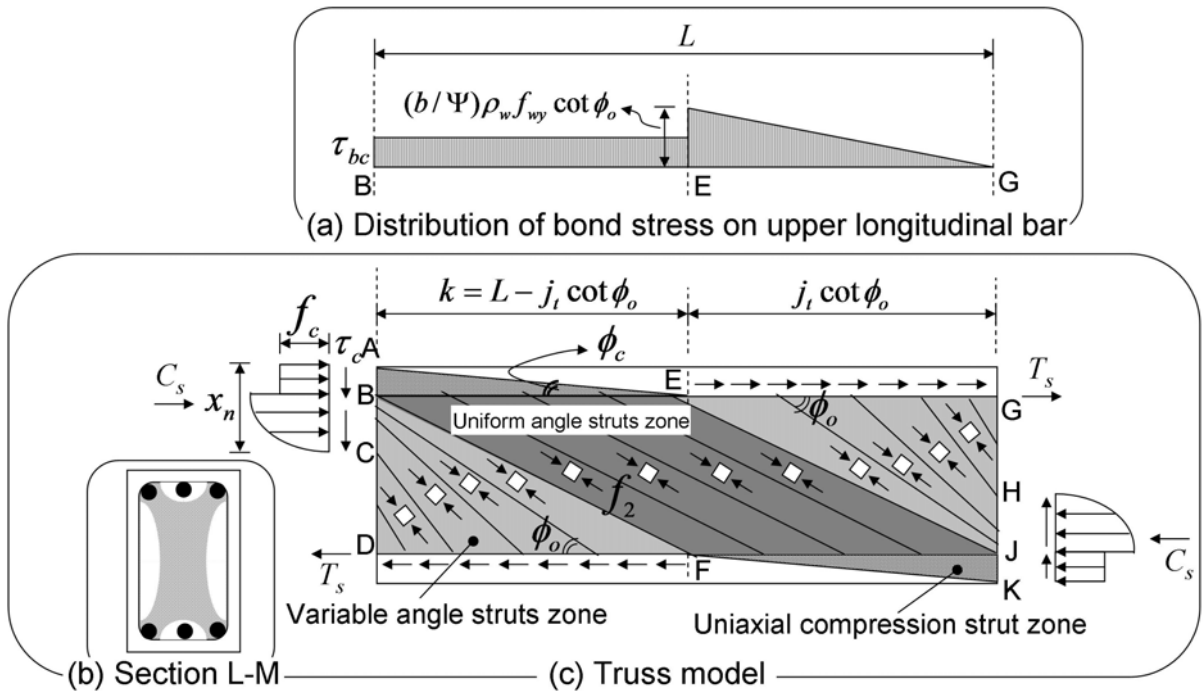
Fig. 2.3 Ichinose`s Truss model

An increase in axial compressive stress leads to an increase in axial stress of compressive mild-strength bar. However, the bond force in mild strength bars is not enough to carry the axial reaction force of diagonal compressive strut. To improve this problem, Ichinose introduced axial resistance component of compressive cover concrete as shown in Fig. 2.3 (c). Stress circles at zone ABE and BEJF are illustrated in Fig. 2.4 (a) and (b), respectively. Fig. 2.4 (c) illustrates enlarged view of region BE. Diagonal compressive stress in zone BEJF, f_2, is equilibrated with the sum of diagonal compressive stress in zone ABE, f_{co}, transverse reaction force by shear reinforcement, $\rho_w f_{wy}$, and bond stress of mild strength bar, τ_{bc}.
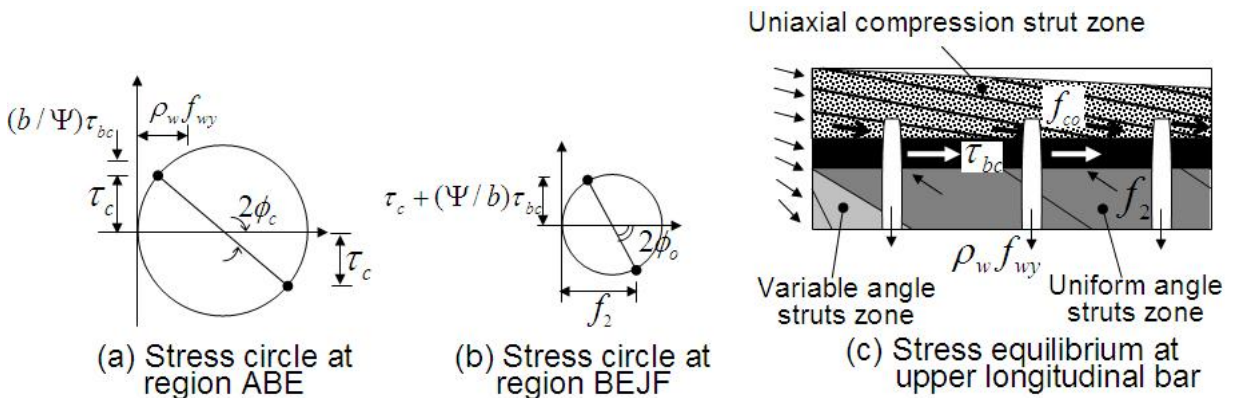
Fig. 2.4 Stress state of concrete struts in Ichinose`s truss model

Shear force in region AC, V_{AC}, is expressed as Eq. (2.1) because it is equilibrated with transverse reaction force in region EF, $\rho_w f_{wy}$.

$$V_{AC} = \int_{AC} b\tau(z)dz = \int_{EF} b\rho_w f_{wy} dx = bj_t \rho_w f_{wy} \cot \phi_o \qquad \text{Eq. (2.1)}$$

Distribution of bond stress in upper mild strength bar is shown in Fig. 2.3. (a). The bond stress in region BE, τ_{bc}, is smaller than the bond stress required in this truss model, $(b/\psi)\rho_w f_{wy}cot\phi_o$, because shear stress from AB, τ_c, is transferred to BE. In the member with high axial load, bond stress at region E, $(b/\psi)\rho_w f_{wy}cot\phi_o$, is frequently larger than τ_f. To solve this broblem, Ichinose used the required bond stress expressed as Eq. (2.2) using compressive and tensile resultant force at the flexural critical section, T` and C`.

$$\tau_f = \frac{T' + C'}{\Psi(L - d)} \qquad \text{Eq. (2.2)}$$

2.2.3 Conclusions

It can be seen that Ichinose`s truss model is effective to investigate the shear resistance mechanism of reinforced concrete member with high axial load or small bond stress of mild-strength bar. However, Ichinose has not been made the quantification on compressive stress of concrete strut, f_2, angle and compressive stress of cover concrete, ϕ_c and f_{co}, in the model. Further, Ichinose`s model can not explain that shear reinforcement does not yield at ultimate state. The verification for Ichinose`s model by comparison with experimental results is also necessary.

2.3 Modified Compression Field Theory (MCFT)
2.3.1 Research Background

Predicting the structural response involves the two interrelated tasks of determining how the load is shared among the elements of the structure (global analysis) and how each element responds to its applied loads (element analysis). [2.3]

The models for the response of reinforced concrete element analysis have not matched because of the sophistication of the structural analysis procedures while

the extensive global analysis have been developed during last 50 years. Predicting the response of the simple reinforced concrete element shown in Fig. 2.5 is not as straightforward a task as it would first appear. Under a particular set of loads, new cracks may form or pre-existing cracks may propagate. The stresses in the reinforcing bars will vary along the lengths of the bars, and will be highest at the crack locations [2.3]. Also, tensile stress will exist in the concrete lying between the cracks.
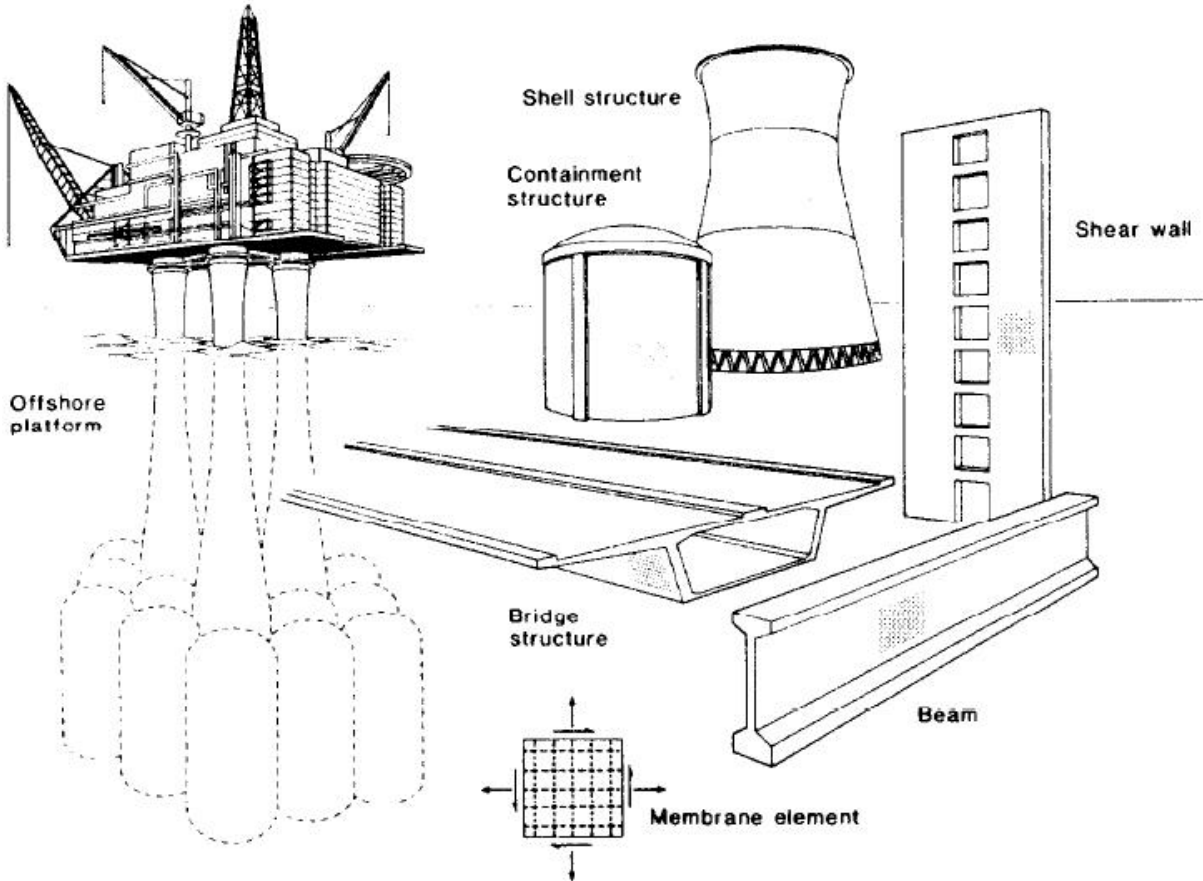
Fig. 2.5 Structures idealized as an assemblage of membrane elements [2.3]

While the Ichinose`s truss model used the only stress equilibrium condition, strain compatibility conditions as well as stress equilibriums is applied to Modified Compression Field Theory (MCFT) proposed by Vecchio. By using these conditions, Vecchio succeed in continuous simulation of the shear behavior of reinforced concrete member until failure.

In the MCFT proposed by Vecchio, the cracked concrete is treated as a new material with its own stress-strain characteristics. Equilibrium, compatibility, and stress-strain relationships are formulated in terms of average stresses and average strains [2.3]. Tensile stresses in the shear cracked concrete are taken into

account in the MCFT. Further, Vecchio verified analytical results from his theory by comparison with the experimental results for the cracked concrete.

2.3.2 Analytical Assumptions

Vecchio applied the analytical assumptions below [2.3].

1. For each strain state there exist only one corresponding stress state; situations in which the influence of loading history is significant will not be treated.
2. Stresses and strains can be considered in terms of average values when taken over areas or distances large enough to include several cracks.
3. The concrete and the reinforcing bars are perfectly bonded together at the boundaries of the element (i.e., no overall slip).
4. The longitudinal and transverse reinforcing bars are uniformly distributed over the element.

Tensile stresses and tensile strains will be treated as positive quantities while compressive stresses and strains will be taken as negative.

2.3.3 Compatibility Conditions

The initial strain in non-prestressed reinforcement is same as that in surrounding concrete. Hence

$$\varepsilon_{rx} = \varepsilon_{cx} = \varepsilon_x \qquad \text{Eq. (2.3)}$$

and

$$\varepsilon_{ry} = \varepsilon_{cy} = \varepsilon_y \qquad \text{Eq. (2.4)}$$

where ε_{rx} and ε_{ry} are axial and transverse initial strain of reinforcement, ε_{cx} and ε_{cy} are axial and transverse initial strain of concrete, ε_x and ε_y are axial and transverse initial strain in element.

If the three strain components, ε_x, ε_x, and γ_{xy} where γ_{xy} is average shear strain of element are known, the strain in any other direction can be found from geometry as shown in Fig. 2.6. Useful relationships which can be derived from its geometry include

$$\gamma_{xy} = \frac{2(\varepsilon_x - \varepsilon_2)}{\tan \theta} \qquad \text{Eq. (2.5)}$$

$$\varepsilon_x + \varepsilon_y = \varepsilon_1 + \varepsilon_2 \qquad \text{Eq. (2.6)}$$

and

$$\tan^2 \theta = \frac{\varepsilon_x - \varepsilon_2}{\varepsilon_y - \varepsilon_2} = \frac{\varepsilon_1 - \varepsilon_y}{\varepsilon_1 - \varepsilon_x} = \frac{\varepsilon_1 - \varepsilon_y}{\varepsilon_y - \varepsilon_2} = \frac{\varepsilon_x - \varepsilon_2}{\varepsilon_1 - \varepsilon_x} \qquad \text{Eq. (2.7)}$$

where ε_1 is the principle tensile strain, ε_2 is the principle compressive strain, and θ is angle of inclination of principle strains to x-axis.
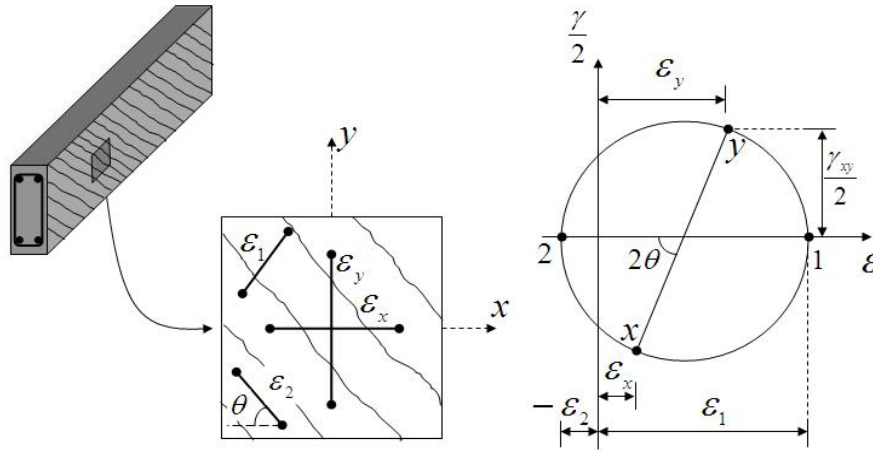
(a) Average strains in cracked element   (b) Mohr`s circle for average strains

Fig. 2.6 Compatibility conditions of shear cracked element

2.3.4 Equilibrium Conditions

The force applied to reinforced concrete element must be equilibrated with stress in concrete and reinforcements. For the free body diagram shown in Fig. 2.7, the equilibrium requirement that the forces sum to zero the x-direction can be derived as

$$\int_A f_x dA = \int_{A_c} f_{cx} dA_c + \int_{A_r} f_{rx} dA_r \qquad \text{Eq. (2.8)}$$

where f_x is average stress in x-direction, f_{cx} is stress in concrete in x-direction, f_{rx} is stress in x-reinforcement, A_c is sectional area of x-face or y-face of concrete, and A_r is sectional area of reinforcement, respectively.
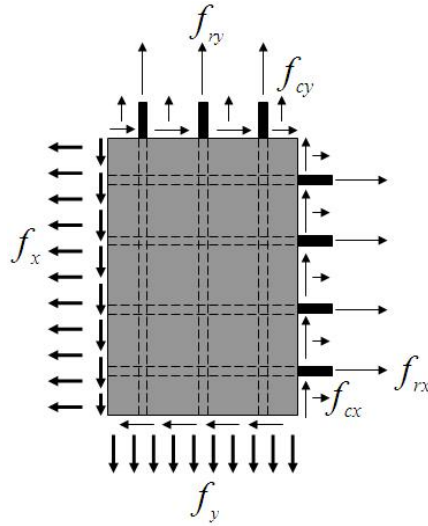
Fig. 2.7 Free-body diagram of part of element

For the overall section ignoring sectional area of reinforcement, Eq. (2.8) can be expressed as

$$f_x = f_{cx} + \rho_{rx} \cdot f_{rx}$$ Eq. (2.9)

where ρ_{rx} is reinforcement ratio for reinforcing steel in x-direction

In a similar manner, the following equilibrium conditions can be derived.

$$f_y = f_{cy} + \rho_{ry} \cdot f_{ry}$$ Eq. (2.10)

$$\tau_{xy} = \tau_{cx} + \rho_{rx} \cdot \tau_{rx}$$ Eq. (2.11)

and

$$\tau_{xy} = \tau_{cy} + \rho_{ry} \cdot \tau_{ry}$$ Eq. (2.12)

Assuming that

$$\tau_{cx} = \tau_{cy} = \tau_{cxy}$$ Eq. (2.13)

where f_y is stress applied to element in y-direction, f_{cy} is stress in concrete in y-direction, ρ_{ry} is reinforcement ratio for reinforcing steel in y-direction, f_{ry} is average stress in y-reinforcement, τ_{xy} is shear stress on element relative to x, y axes, τ_{cx} is shear stress on x-face of concrete, τ_{cy} is shear stress on y-face of concrete, τ_{rx} is shear stress on x-reinforcement, τ_{ry} is shear stress on y-reinforcement, and τ_{cxy} is shear stress on concrete relative to x, y axes, respectively.

The Mohr's circle for the concrete stresses shown in Fig. 2.8 yields the following useful relationships.

$$f_{cx} = f_{c1} - \tau_{cxy} / \tan \theta_c$$ Eq. (2.14)

$$f_{cy} = f_{c1} - \tau_{cxy} \cdot \tan \theta_c \qquad \text{Eq. (2.15)}$$

and

$$f_{c2} = f_{c1} - \tau_{cxy} \cdot (\tan \theta_c + 1/\tan \theta_c) \qquad \text{Eq. (2.16)}$$

where f_{c1} is principle tensile stress in concrete, f_{c2} is principle compressive stress in concrete, and θ_c is angle of inclination of principle stresses in concrete to *x*-axis, respectively.

(a) Average concrete stresses

(b) Principle concrete in stresses

(c) Mohr's circle for average concrete stresses
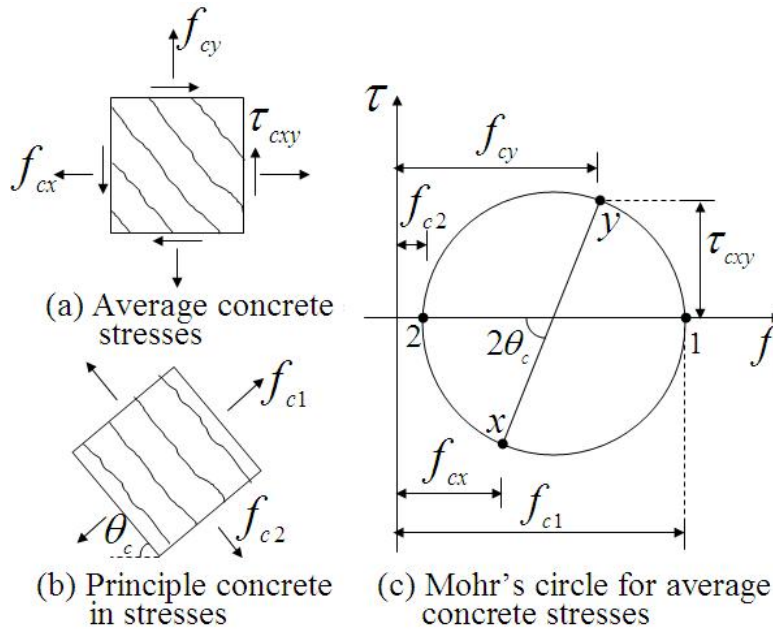
Fig. 2.8 Stresses in cracked concrete

2.3.5 Stress-strain Relationships

Constitutive laws are required to link average stresses to average strains for both the reinforcement and the concrete. These average stress-average strain relations may differ significantly from the usual local stress-local strain relations determined from the standard material tests. The axial stress in the reinforcement will be assumed to depend on only one strain parameter, the axial strain in the reinforcement [2.3]. The usual bilinear uniaxial stress-strain relationship shown in Fig. 2.9 applied in relationship between axial stress and axial strain. Thus

$$f_{rx} = E_r \varepsilon_x \le f_{yx} \qquad \text{Eq. (2.17)}$$

$$f_{ry} = E_r \varepsilon_y \le f_{yy} \qquad \text{Eq. (2.18)}$$

$$\tau_{rx} = \tau_{ry} = 0 \qquad \text{Eq. (2.19)}$$
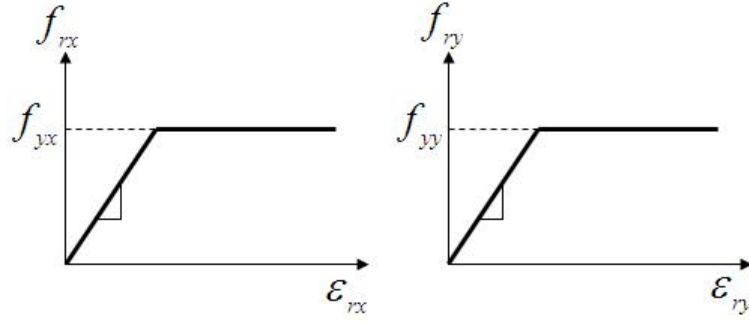
Fig. 2.9 Stress-strain relationships for reinforcement

It is assumed that principle stress axes in concrete are coincide to principle strain axes in concrete. It is expressed as follows.

$$\theta_c = \theta \qquad \text{Eq. (2.20)}$$

To investigate the structural properties of cracked concrete, Vecchio carried out 30 tests on reinforced concrete elements subjected to simple well-defined loading conditions. In the tests, known values of stress were applied to the reinforced concrete (f_x, f_y, and τ_{xy}), and the resulting specimen strains were measured (ε_x, ε_y, and γ_{xy}). For the detail of the tests, refer to reference [2.3].

The principle compressive stress in the concrete, f_{c2}, was found to be a function not only of the principle compressive strain, ε_2, but also of the co-existing principle tensile strain, ε_1. Thus, cracked concrete subjected to high tensile strains in the direction normal to the compression is softer and weaker than concrete in a standard cylinder test [2.3]. Vecchio suggested the following relationship.

$$f_{c2} = f_{c2\,\max}\left[2\left(\frac{\varepsilon_2}{\varepsilon_c'}\right) - \left(\frac{\varepsilon_2}{\varepsilon_c'}\right)^2\right] \qquad \text{Eq. (2.21)}$$

where

$$\frac{f_{c2\,\max}}{F_c} = \frac{1}{0.8 - 0.34\varepsilon_1 / \varepsilon_c'} \leq 1.0 \qquad \text{Eq. (2.22)}$$

The relationship between the average principle tensile stress in the concrete and the average principle tensile strain in nearly linear prior to cracking is as Eq. (2.23). Vecchio suggested the relationship after cracking as Eq. (2.24).

$$f_{c1} = E_c \varepsilon_1 \qquad \text{Eq. (2.23)}$$

1 6

$$f_{c1} = \frac{f_{cr}}{1 + \sqrt{200\varepsilon_1}}$$

Eq. (2.24)

To consider local variations at a shearcrack, Vecchio proposed the relationship between the shear across the crack, τ_{ci}, the crack width, w, and the required compressive stress on the crack, f_{ci}, based on the experimental studies including Walraven [2.6]. The relationship is derived as follows.

$$\tau_{ci} = 0.18\tau_{ci\,max} + 1.64f_{ci} - 0.82\frac{f_{ci}^2}{\tau_{ci\,max}}$$

Eq. (2.25)

where

$$\tau_{ci\,max} = \frac{\sqrt{-F_c}}{0.31 + 24w/(a+16)}$$

Eq. (2.26)

The crack width, w, to be used in Eq. (2.26) should be the average crack width over the crack surface. It can be taken as the product of the principle tensile strain and the crack spacing s_θ; that is

$$w = \varepsilon_1 \cdot s_\theta$$

Eq. (2.27)

where

$$s_\theta = \frac{1}{\dfrac{\sin\theta}{s_{mx}} + \dfrac{\cos\theta}{s_{my}}}$$

Eq. (2.28)

2.3.6 Conclusions

MCFT proposed by Vecciho is effective and innovative analytical tool to investigate the shear mechanism of reinforced concrete member because the simulation of shear force-deformation relationship is possible. However, further investigation for the applicability of the MCFT to post-tensioned precast concrete member needs because the MCFT does not take into account the effect of bond stress of PT tendon or cover concrete on shear resistance mechanism of members.

2.4 Current Shear Design Equations

2.4.1 ACI Shear Design Equation

The following a set of shear design equations are specified in ACI318-08. The

shear strength is based on an average shear stress on the full effective cross section, *bd*. In a member with shear reinforcement, a portion of the shear strength is assumed to be provided by the concrete and the remainder by the shear reinforcement [2.7]. The equations are consists of the concrete contribution, V_c, and the shear reinforcement contribution, V_s in S.I. units. The concrete contributions, V_c, are obtained as follows.

Concrete contribution for nonprestressed member subjected to shear and flexure only

$$V_c = \left(0.16\sqrt{F_c} + 17.24\rho w \frac{V_u d}{M_u} \right) bd \qquad \text{Eq. (2.29)}$$

Assuming that

$$V_c \le 0.29\sqrt{F_c} \quad \text{and} \quad \frac{V_u d}{M_u} \le 1.0 \qquad \text{Eq. (2.30)}$$

For reinforced concrete members subjected to axial compression, the following equation is permitted to compute V_c using Eq. (2.29) with M_m substituted for M_u and $V_u d/M_u$ not then limited to 1.0.

Concrete contribution for nonprestressed member subjected to axial compression

$$V_c = \left(0.16\sqrt{F_c} + 17.24\rho w \frac{V_m d}{M_m} \right) bd \qquad \text{Eq. (2.31)}$$

where

$$M_m = M_u - N_u \frac{(4h - d)}{8} \qquad \text{Eq. (2.32)}$$

Assuming that

$$V_c \le 0.29\sqrt{F_c}\sqrt{1 + \frac{N_u}{3.43 A_g}} \quad \text{and} \quad \frac{V_u d}{M_m} \le 1.0 \qquad \text{Eq. (2.33)}$$

For concrete contribution of prestressed concrete members subjected to shear, the concrete contribution, V_c, can be obtained by lesser of flexural shear cracking strength, V_{ci}, and web shear cracking strength, V_{cw} as.

Concrete contribution for prestressed members

$$V_c = \min(V_{ci}, V_{cw}) \qquad \text{Eq. (2.34)}$$

$$V_{ci} = 0.05\sqrt{F_c}bd_p + V_p + \frac{V_i M_{cre}}{M_{max}} \qquad \text{Eq. (2.35)}$$

$$V_{cw} = \left(0.29\sqrt{F_c} + 0.3f_{pi}\right)bd + V_p \qquad \text{Eq. (2.36)}$$

Shear strength provided by shear reinforcement is obtained as follows.
Shear reinforcement contribution for noprestressed and prestressed members

$$V_s = \frac{A_w f_{wy} d}{s} \qquad \text{Eq. (2.37)}$$

The shear design equations for the concrete contribution in ACI provision, V_c, are based on the experimental results taking into account parameters affecting shear failure of member. Therefore, the design equations can not be applied to the member in which geometric or material properties are exceed to applicable coverage. Further, an equation for the shear reinforcement contribution, V_s, underestimate the experimental results because it is based on the conventional 45 degree angle truss model.

2.4.2 AIJ Shear Design Equations for RC member

For the reinforced concrete member subjected to pure shear, the following equations are specified in Architectural Institute of Japan (AIJ) guide line for reinforced concrete memebers [2.8] which based on the strut and truss analogy. The equations consist of strut mechanism (concrete contribution) and truss mechanism (shear reinforcement contribution) as indicated in Eq. (2.38) to (2.41). The shear strength of reinforced concrete member is obtained as the lesser of V_{u1}, V_{u2}, and V_{u3}. V_{u1} in Eq. (2.39) indicates a sum of strut and truss mechanism. V_{u2} and V_{u3} in Eq. (2.40) to (2.41) represent shear strength by truss mechanism. Refer to reference [2.8] for the detail notations.

$$V_u = \min(V_{u1}, V_{u2}, V_{u3}) \qquad \text{Eq. (2.38)}$$

$$V_{u1} = \mu\rho_{we} f_{wy} bj_o + \left(\nu F_c - \frac{5\rho_{we} f_{wy}}{\lambda}\right)\frac{bD}{2}\tan\theta \qquad \text{Eq. (2.39)}$$

$$V_{u2} = \frac{\lambda\nu F_c + \rho_{we} f_{wy}}{3} bj_o \qquad \text{Eq. (2.40)}$$

$$V_{u3} = \frac{\lambda\nu F_c}{2} bj_o \qquad \text{Eq. (2.41)}$$

Figure 2.10 illustrates the relationship between amount of shear reinforcement, $\rho_{we}f_{wy}$, and shear strength, V_u, by AIJ guide line [2.8]. Variables in vertical and horizontal axis in Fig. 2.10 are dimensionless by effective compressive strength

of concrete strut, vF_c. As shown in Fig. 2.10, two shear resistance mechanisms (strut and truss mechanism) exist in reinforced concrete member with low amount of shear reinforcement. In the member with high amount of shear reinforcement, truss mechanism significantly resists against shear. It points out that the AIJ guide line [2.8] take into account the effect of amount of shear reinforcement on shear strength of reinforced concrete members.
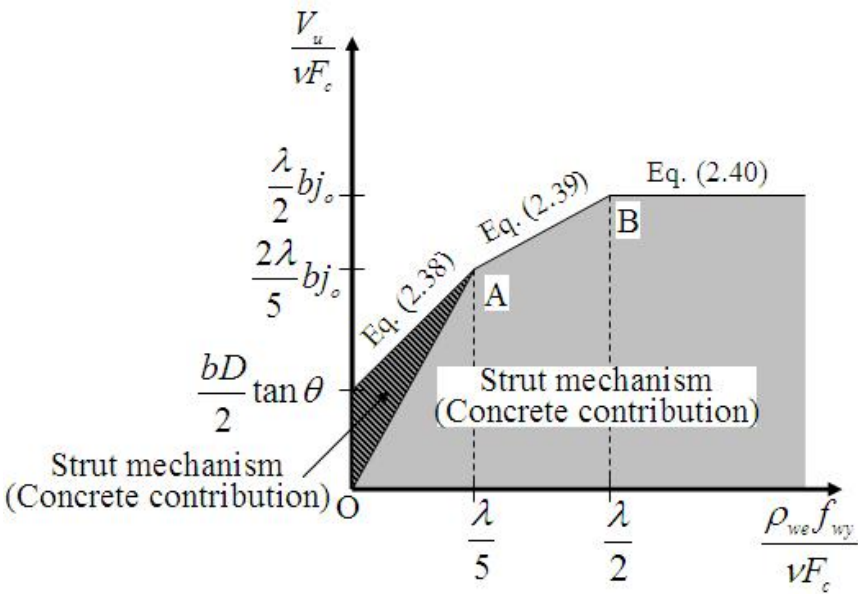
Fig. 2.10 Relationship between amount of shear reinforcement and shear strength by AIJ guide line [2.78]

The effective compressive strength represents compressive strength of concrete softened by cracks and damages. The effective compressive strength coefficient, v_1, is obtained as follows.

$$v_1 = 0.7 - \frac{F_c}{200}$$

Eq. (2.42)

The effective compressive strength is based on the lower boundary theory of plasticity theory. Then, the equations only take into stress equilibrium conditions consideration. In the equations, it is assumed that shear reinforcement yields at shear strength while it has been reported that shear reinforcement did not yield at the ultimate state [2.9-2.15]. Further investigation needs for the applicability of the shear design equations in AIJ guide line to prestressed concrete members.

2.4.3 AIJ Shear Design Equations for PC member

Equation 2.43 indicates shear design equation specified in AIJ guide line for

prestressed concrete structures [2.16]. The Eq. (2.43) is based on the strut mechanism ($0.5bD(vF_c-2\rho_w f_{wy})tan\theta$) and truss mechanism ($bj_o\rho_w f_{wy}$). In the truss mechanism, it is assumed that shear reinforcement yield at shear failure. An effective compressive strength of shear cracked concrete, v_2F_c, is considered in strut mechanism. The effective compressive strength coefficient, v_2, is obtained as Eq. (2.44). In general, increase in prestress in concrete leads to increase of shear strength of prestressed concrete members. The beneficial effect of prestress on shear strength is considered as indicated in Eq. (2.44). It points out that the shear design equation in the AIJ guide line [2.16] is useful for evaluation of shear strength of prestressed concrete members.

$$V_u = bj_o\rho_w f_{wy} + 0.5bD\left(vF_c - 2\rho_w f_{wy}\right)\tan\theta, \quad f_{wy} \leq 295MPa \quad \text{Eq. (2.43)}$$

$$v = \alpha L_r\left(1 + \frac{P_e}{bDF_c}\right) \quad \text{Eq. (2.44)}$$

where

$$\tan\theta = \sqrt{(L/D)^2 + 1} - L/D \quad \text{Eq. (2.45)}$$

$$L_r = \frac{a}{2D} \quad \text{and} \quad \alpha = \sqrt{60/F_c} \quad \text{Eq. (2.46)}$$

Assuming that

$$L_r \leq 1 \quad \text{and} \quad \alpha \leq 1 \quad \text{Eq. (2.47)}$$

However, further investigation needs for an applicability of high-strength shear reinforcement to shear strength of prestressed concrete beam, because the upper limit of yield strength of shear reinforcement is designated as 295 MPa in the AIJ guide line [2.16]. Further, the definition of distance between reinforcing bar in compression and tension, j_o, is ambiguous for post-tensioned precast concrete members. It can be taken as either the distance between the top and bottom non-prestressed longitudinal mild-strength reinforcement or the one between the top and bottom prestressig steels. Mild-strength reinforcements are usually not connected at the joint between members assembled by post-tensioning. Therefore, an effect of the bond type of prestressing steel on shear behavior should be investigated, then it is necessary to propose a new shear mechanism reflecting the results of these investigations.

2.5 Inelastic Deformation Capacity Prediction Method of RC Beam Failed in Flexure

2.5.1 Introduction

The low deformation capacity of reinforced concrete members is attributed to the fact that under cyclic loading, the shear capacity of concrete deteriorates as the flexure-shear cracks in the plastic hinge zones widen [2.1]. As shown in Fig. 2.1, the existing models determine the shear strength and deformation capacity of a reinforced concrete member using intersection of the shear capacity curve and the shear demand curve that represents the shear force required by the flexural action of the member. In the conventional analytical model, the degradation curve was empirically obtained by test results with insufficient theoretical background. To solve this problem, Choi [2.1] proposed an analytical method for predicting the degraded shear capacity and deformation capacity using the concept of the strain-based shear strength model.

2.5.2 Maximum Shear Stress Capacity of Concrete

It is assumed that the shear resistance of reinforced concrete beams is proved by the compression zone of the intact concrete and shear reinforcement, then the contributions of aggregate interlock and dowel action is neglected. Using Rankine`s failure criteria, the failure criteria by compression and tension for the concrete in compression zone are defined as follows.

$$f_1 = \frac{f_c}{2} - \sqrt{\left(\frac{f_c}{2}\right)^2 + \tau_c^2} = F_c \qquad \text{Eq. (2.48)}$$

$$f_2 = \frac{f_c}{2} + \sqrt{\left(\frac{f_c}{2}\right)^2 + \tau_c^2} = F_t \qquad \text{Eq. (2.49)}$$

where f_1 and f_2 are the principle tensile and compressive stress, and f_c and τ_c are the current normal and shear stress, respectively.

Equation (2.48) and (2.49) can be expresses using allowable maximum shear stress, τ_{ut} and τ_{uc} as follows.

$$\tau_{ut}(z) = \sqrt{-F_t(-F_t + f_c(z))} \qquad \text{Eq. (2.50)}$$

$$\tau_{uc}(z) = \sqrt{F_c(F_c - f_c(z))} \qquad \text{Eq. (2.51)}$$

2.5.3 Shear Capacity of Concrete Compression Zone

Figure 2.11 (a) and (b) illustrate the distribution of the normal strain and stress at a cracked section, which are developed by the flexural action of a beam. Fig. 2.11 (c) illustrates the shear stress capacities, τ_{ut} and τ_{uc}, respectively. In these figures, $\alpha\varepsilon_o$ is the current compressive normal strain at the extreme compression fiber of the cross section, ε_o is the compressive strain corresponding to the compressive strength of concrete. The value $\alpha\varepsilon_o$ represents the current flexural damage of the cross section [2.1].

After the compressive normal stress at the extreme compression fiber of the cross section reaches the compressive strength of concrete ($\alpha\varepsilon_o > \varepsilon_o$, Stage DE), the failure criteria in Eq. (2.49) is defined by the softened compressive strength and it is satisfied by the compressive normal stress alone. It results that the part of the compression zone experiencing compressive softening no longer provides the shear stress capacity controlled by compression [2.1].

Choi defined the governing shear stress capacity, τ_u, at a location in the compression zone as the minimum of τ_{ut} and τ_{uc} obtained from Eq. (2.50) and (2.51), respectively. When, $\alpha \le 1.0$ ($\alpha\varepsilon_o \le \varepsilon_o$), the distribution of the governing shear stress capacity, τ_u, can be simplified as the distribution of the shear capacity controlled by tension, τ_{ut}. On the other hand, when $\alpha > 1.0$ ($\alpha\varepsilon_o > \varepsilon_o$), the shear stress capacity in the region experiencing compressive softening is neglected.

After inclined tensile crack reaches the neutral axis (Stage CD in Fig. 2.11), the shear force is resisted primary by the compression zone of the intact concrete. To derive a simplified analytical model, Choi used the average normal stress, f_a, in the compression zone. The shear capacity at Stage CD is derived as follows.

$$V_{CD} = b\int_0^c \tau_{ut}(z)dz \approx b\sqrt{-F_t(-F_t + f_a)c} \qquad \text{Eq. (2.52)}$$

where b is the beam width, and c is the depth of the compression zone, which is determined based on the force-equilibrium in the cross section. Both f_a and c can be defined as the fuctions of $\alpha\varepsilon_o$.

(a) Strain distribtion

(b) Normal stress distribtion

(c) Governing allowable shear stress distribtion
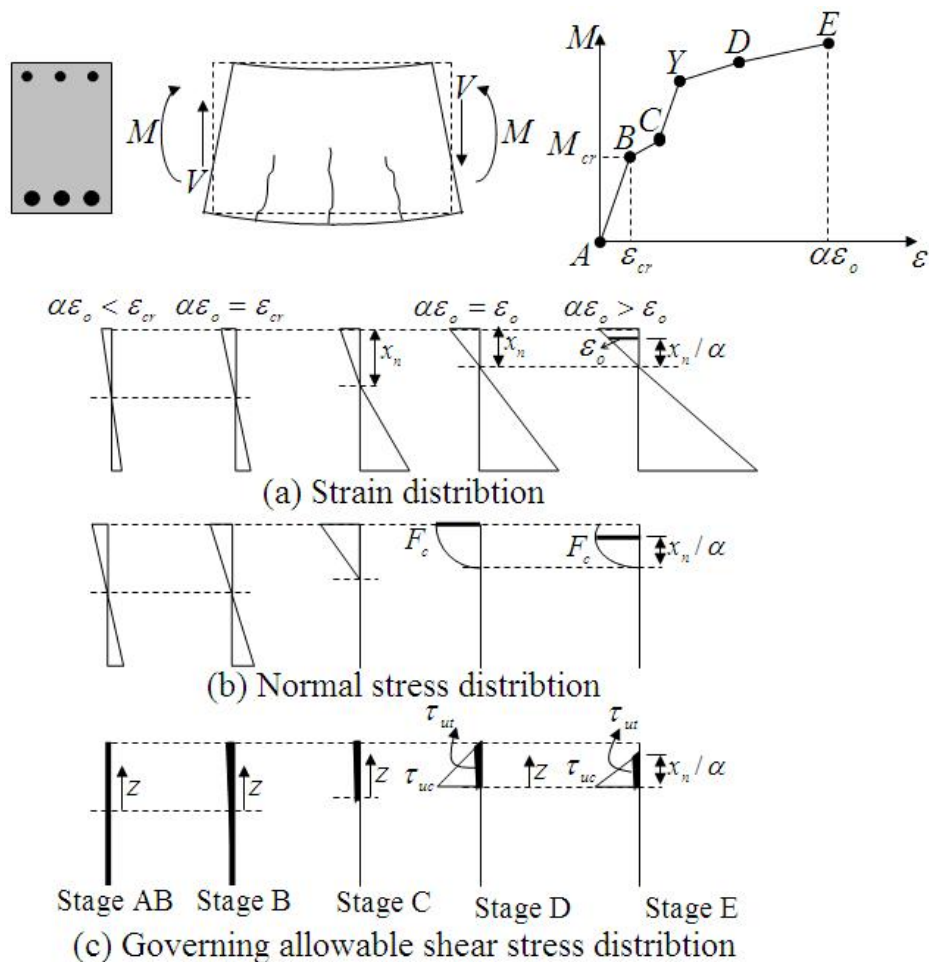
Fig. 2.11 Variations in normal stress and maximum shear stress capacity with change in flexural deformation at cracked cross section

After the compressive softening at the extreme compression fiber ($\alpha\varepsilon_o > \varepsilon_o$, Stage DE), the shear capacity of the cross section is provided only by the remaining part that did not experience the compressive softening $0 \leq z \leq c/\alpha$, because the part of the compression zone experiencing compressive softening cannot resist the shear force. The shear capacity during Stage DE is defined as follows.

$$V_{DE} \approx b\int_0^{c/\alpha} \tau_{ut}(z)dz \approx b\sqrt{-F_t\left(-F_t + f_a\right)c/\alpha} \qquad \text{Eq. (2.53)}$$

2.5.4 Evaluation of Shear Capacity and Shear Demand

Shear failure must be examined at all locations of the potential critical sections because the shear capacity and shear demand vary along the beam span. The first potential critical section becomes the actual critical section. In general, the shear failure of a slender cantilever beam with shear reinforcement occurs in the plastic hinge region at the fixed beam end [2.17-2.19]. It points out that the critical section for shear failure is located in the plastic hinge zone of the beam end, and shear demand curve can be determined by the flexural moment of the

2 4

beam. The moment at the fixed end of a cantilever beam, M_a, can be defined as a function of the normal strain, $\alpha\varepsilon_o$, at the extreme compression fiber of the cross section [2.1]. The tensile force of the reinforcing bar, $A_r f_r$ in Eq. (2.54) is defined as Eq. (2.56).

$$M_a = A_r f_r j_d \qquad\qquad \text{Eq. (2.54)}$$

where

$$j_d = \left[\int_0^c z\sigma_u(z)dz \right] / \left[\int_0^c \sigma_u(z)dz \right] + d - c \qquad\qquad \text{Eq. (2.55)}$$

$$A_r f_r = b\int_0^c \sigma_u(z)dz \le A_r f_{ry} \qquad\qquad \text{Eq. (2.56)}$$

The shear demand at the fixed end is defined as follows.

$$V_d = \frac{M_a}{a} = \frac{A_r f_r j_d}{a} \qquad\qquad \text{Eq. (2.57)}$$

In reinforced concrete beams with shear reinforcement, the overall shear capacity of the beams with shear reinforcement, V_u, is defined as the sum of the shear contributions of concrete, V_c, and shear reinforcement, V_s. The shear contribution of concrete, V_c, is obtained by Eq. (2.52) and (2.53).

$$V_u = V_c + V_s \qquad\qquad \text{Eq. (2.58)}$$

where

$$V_s = \rho_w f_{wy} \cot\theta \cdot b(d - c) \qquad\qquad \text{Eq. (2.59)}$$

where the average shear crack angle, θ, is assumed to be 45 degrees [2.20].

For the displacement, the rotation of a cantilever beam is defined as $R = \delta/a$. Choi used the following relationships to evaluate the rotation of the beam.

$$R = \phi_a(a/3) \qquad \text{for} \ \ \phi_a \le \phi_y \qquad\qquad \text{Eq. (2.60)}$$

$$R = \phi_y(a/3) + (\phi_a - \phi_y)/L_h \qquad \text{for} \ \ \phi_a \le \phi_y \qquad\qquad \text{Eq. (2.61)}$$

where ϕ_y ($=\varepsilon_y/(d-c)$) is the curvature of the beam at yielding of reinforcing bars, and L_h is the length of the plastic hinge where is estimated as $0.5d(M/V_h)$ [2.21].

An analytical model developed by Choi [2.1] is effective and rational tool to evaluate the inelastic deformation capacity of slender or intermediate beams subjected to cyclic or monotonic loading. The analytical model also covers bar buckling and bar fracture as well as flexural failure. Moreover, the proposed method is applicable to the concrete beams with a/d greater than 2.0 and shear reinforcement ratio less than 0.19%.

2.6 Inelastic Deformation Capacity Prediction Method of RC Beam Failed in Shear after Flexural Yielding

2.6.1 Introduction

In shear failure after flexural yielding of reinforced concrete member, AIJ guide line [2.8] specifies a method using relationship between rotation angle of plastic hinge and effective compressive strength of concrete strut to consider the deterioration of shear capacity of the member after flexural yielding. However, its theoretical basis is ambiguous. To investigate inelastic deformation capacity of reinforced concrete members failing in shear after flexural yielding, Nakatsuka [2.4] proposed a new analytical model using the potential shear resistance of concrete in flexural compression zone.

2.6.2 Analytical Model

To construct a relationship between the deterioration of shear capacity and the shear resistance of concrete in flexural compression zone, Nakatsuka [2.4] used the Mohr-Columb failure criteria. The following the analytical assumptions are applied.

1. Shear stress in flexural compressive zone is neglected.
2. An effect of shear stress in neutral axis on axial stress-strain curve of concrete is neglected [2.22].

Figure 2.12 illustrates resistance mechanism of reinforced concrete member subjected to shear force. As shown in Fig. 2.12, resistance mechanism of reinforced concrete member consists of four resistances: 1. shear resistance of concrete in flexural compression zone; 2. shear resistance of shear reinforcement; 3. interlocking of aggregate; and 4. dowel action of reinforcing bar. Shear resistance due to interlocking of aggregate is neglected in this study because an increase in shear crack width after flexural yielding leads to the deterioration in interlocking resistance. The effect of dowel action of reinforcing bar on shear resistance mechanism of reinforced concrete member is also neglected because shear deformation of concrete in flexural compression zone is small.
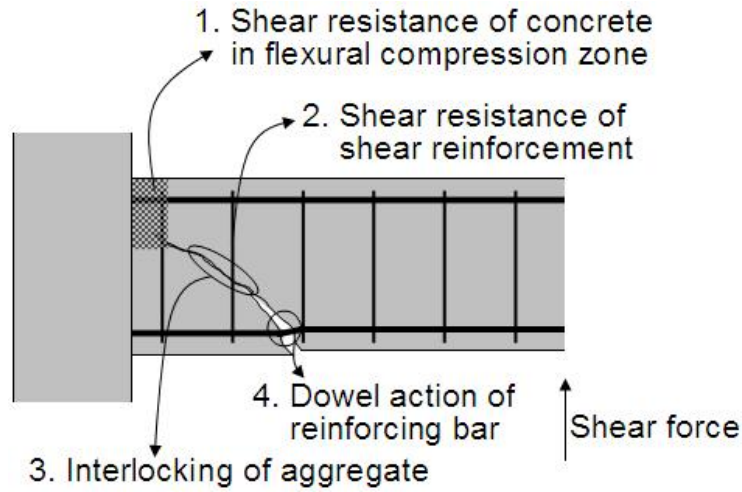
Fig. 2.12 Resistance mechanism of reinforced concrete member

Two shear resistance mechanisms (shear resistance of concrete in flexural compression zone and shear reinforcement) were considered in this study. Potential shear capacity of reinforced concrete member after flexural yielding can be expressed a sum of shear capacity of concrete in flexural compression zone, $_sV_{cu}$, and shear capacity at yield strength of shear reinforcement, $_sV_{wy}$ as shown in Eq. (2.62). Valuable β in shear capacity in yield strength of shear reinforcement, $_sV_{wy}$, can be expressed as Eq. (2.65) because it is corresponded to the range D-x_n [2.23] as shown in Fig. 2. 13.

$$_sV_u = {}_sV_{cu} + {}_sV_{wy} \qquad \text{Eq. (2.62)}$$

$$_sV_{cu} = b\int_0^{x_n} \tau_{cu}(y)dy \qquad \text{Eq. (2.63)}$$

$$_sV_{wy} = \beta Db\,v_s\,\rho_w f_{wy} \qquad \text{Eq. (2.64)}$$

$$\beta = (D - x_n)/D \qquad \text{Eq. (2.65)}$$

$$v_s = 1.0 \quad \text{for} \quad \gamma \le 0.66 \qquad \text{Eq. (2.66)}$$

$$v_s = 0.66/\gamma \quad \text{for} \quad \gamma > 0.66 \qquad \text{Eq. (2.67)}$$

$$\gamma = (\rho_w f_{wy})/\sqrt{F_c} \qquad \text{Eq. (2.68)}$$

where x_n is neutral axis depth, τ_{cu} is potential shear strength, ρ_w is shear reinforcement ratio, and f_{wy} is yield strength of shear reinforcement, respectively.

Fig. 2.13 Shear resistance of shear reinforcement

In concrete subjected to axial compression force and shear force, compressive stress, f_c, and shear stress, τ_c, at failure are satisfied with Mohr-Columb's failure criteria [2.22]. It was assumed that the shear capacity of co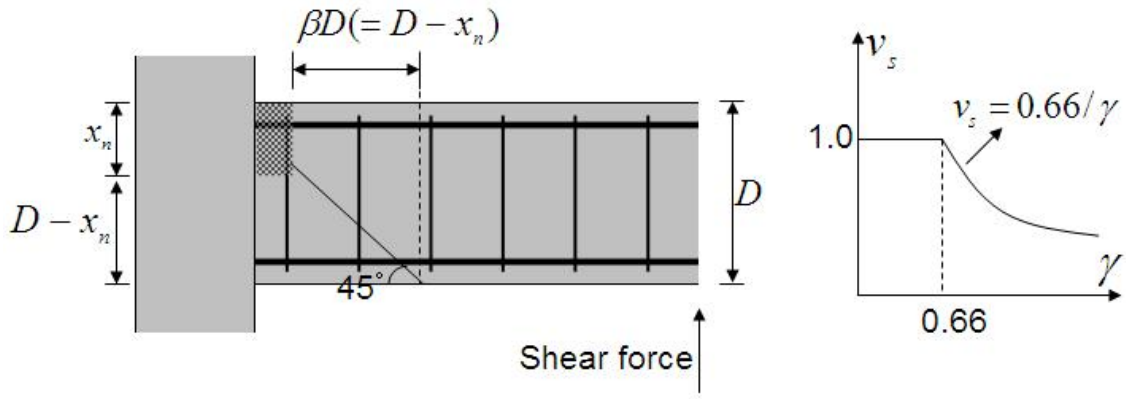ncrete in flexural compression zone is satisfied with Mohr-Columb's failure criteria in this study. Figure 2.14 illustrates calculation procedure for the potential shear capacity of the concrete in flexural compression zone. The potential shear strength, τ_{cu}, is obtained as the following procedures:

1. Estimate the strain in flexural compression fiber, ε_c.
2. Based on the plane assumption, distribution of strain at critical section can be obtained.
3. The stress distribution also can be obtained. The strain–stress relationship for the concrete subjected to compressive stress in this step is obtained as Eq. (2.69) and (2.70).
4. Calculate the potential shear strength, τ_{cu}, using Mohr-Columb's failure criteria shown in Eq. (2.71) where f_c is the stress in flexural compression zone which were obtained in step 3.
5. Calculate the potential shear capacity of the concrete in flexural compression zone, $_sV_{cu}$, as resultant force of τ_{cu}.
6. Obtain the curvature corresponded to ε_c. Then, plot the relationship between shear capacity and curvature of reinforced concrete member as shown in Fig. 2.15.

$$f_c = F_c \left[1 - \left(1 - \varepsilon / \varepsilon_o \right)^2 \right] \quad \text{for} \quad \varepsilon \le \varepsilon_o \qquad \text{Eq. (2.69)}$$

$$f_c = F_c - \left(\varepsilon - \varepsilon_o \right) \overline{E}_o \quad \text{for} \quad \varepsilon > \varepsilon_o \qquad \text{Eq. (2.70)}$$

$$\left(1 + \alpha \right)^2 \left(\frac{\tau_{cu}}{F_c} \right)^2 + \alpha \left(\frac{f_c}{F_c} - \frac{\alpha - 1}{2\alpha} \right)^2 = 1 + \frac{(\alpha - 1)^2}{4\alpha} \qquad \text{Eq. (2.71)}$$

where $\overline{E}_o$ is gradient in degradation zone of stress-strain relationship
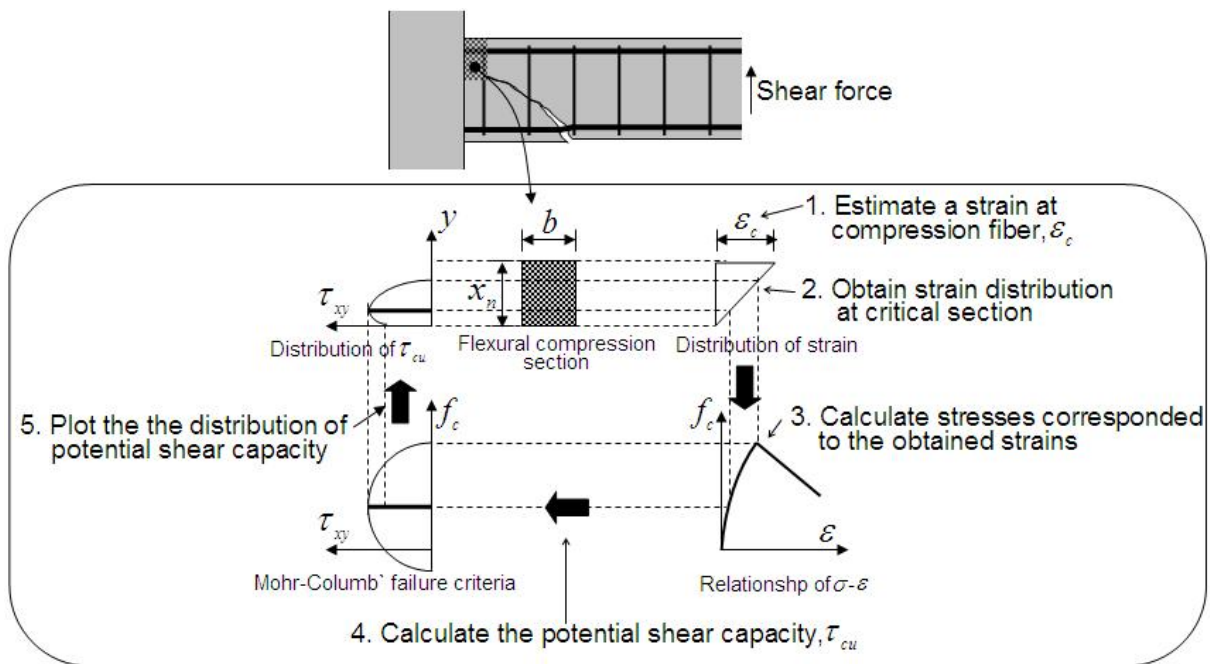
Fig. 2.14 Calculation procedure of the potential shear capacity
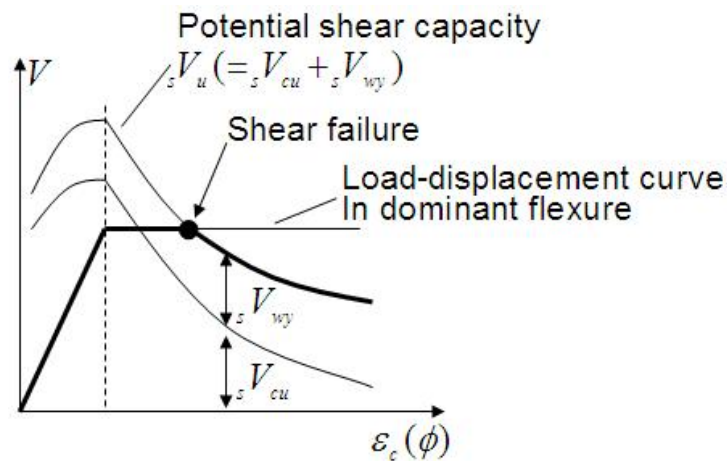
Fig. 2.15 Illustration of results obtained by proposed method for the potential shear capacity

The analytical method proposed by Nakastuka [2.24] evaluated the relationship between shear capacity and inelastic deformation capacity of reinforced concrete member failing in shear after flexural yielding in a good accuracy. It point out that Nakatsuka's model is effective method to calculate inelastic deformation capacity and to investigate the mechanism of deterioration of shear capacity after flexural yielding.

2.7 Conclusions

In Chapter 2, previous flexural and shear analogies of reinforced / prestressed concrete members were introduced. The properties and problem of previous analogies also are described.

Ichinose's truss analogy took into account the shear contribution of compressive cover concrete and required bond stress of reinforcing bar. It points out that Ichinose's truss analogy can be applied to reinforced concrete members which are subjected to axial force or with insufficient bond stress of reinforcing bars. However, the truss model did not make quantitative relationships between valuables.

MCFT proposed by Vecchio and based on the stress and strain status of concrete and reinforcement simulated shear force-deformation relation very well. As upper limit condition for calculation procedures Vecchio used yield strength of shear reinforcement, f_{wy}, and softened compressive strength of concrete strut, f_{c2max}, respectively. However, MCFT did not take into account shear contribution of compressive cover concrete. Moreover, shear resistance mechanism for reinforced / prestressed concrete members with multiple layered reinforcing bars can not be investigated by MCFT. It is necessary to develop a new shear resistance model for reinforced / prestressed concrete with shear contribution of compressive cover concrete or with multiple layered reinforcing bars.

Current shear design equations in ACI provision [2.7] and AIJ guideline [2.8, 16] were introduced. Shear design equations in the ACI provision consists of shear contribution of concrete and shear reinforcement. The shear contribution of concrete in the ACI provision was empirical equations based on the experimental parameters affecting shear behavior of reinforced concrete member. Therefore, the design equations can not be applied to the member in which geometric or material properties are exceed to applicable coverage. An equation for the shear reinforcement contribution in ACI provision underestimates the experimental results because it is based on the conventional 45 degree angle truss model. Shear design equations in AIJ guide lines were based on the strut and truss analogies as shear contribution of concrete and shear reinforcement, respectively. In order to apply the equations in AIJ guide line to prestressed concrete member with cut-off longitudinal bar at ends of the member, further investigations on the effect of bond stress of PT tendons and cover concrete on

the shear behavior need.

In order to investigate inelastic deformation capacity of reinforced concrete beams failing in flexure, analytical method proposed by Choi [2.1] was introduced. Choi used Rankine's failure criteria to investigate stress-strain relationship of concrete in flexural compression zone. Based on the shear capacity of concrete in flexural compression zone, Choi developed the analytical method to investigate the deterioration of shear capacity of slender reinforced concrete beams. However, the model can not be applied to reinforced concrete beam failing in shear or short beam. Also, to apply the model to prestressed concrete members, further investigations need.

To investigate the deterioration of shear capacity of reinforced concrete failing in shear after flexural yielding, Nakatsuka [2.4] proposed analytical model based on the Mohr-Columb's failure criteria. To simulate deterioration of shear capacity after flexural yielding, Nakatsuka [2.4] used the shear resistance capacity of concrete in the flexural compression and shear reinforcement. Nakatsuka's model is effective tool to investigate the deterioration of shear capacity of reinforced concrete beams failind shear after flexural yielding.

[References]

2.1 K. Choi, H. Park, "Evaluation of Inelastic Deformation Capacity of Beams Subjected to Cycle Loading," *ACI Structural Journal*, V. 107, No. 5, Sep.-Oct. 2010, pp. 507-515.

2.2 M. P. Collins, D. Mitchell, "Prestressed Concrete Structures," Prentice Hall, Englewood Cliffs, N. J., 1991.

2.3 F. J. Vecchio, M. P. Collins, "The Modified Compression-Field Theory for Reinforced Concrete Elements Subjected to Shear," *ACI Structural Journal*, V. 83, No. 22, 1986, pp. 219-231.

2.4 Nakatsuka T., Kojima K., "Estimation on Shear Failure of Concrete Members Based on Failure of Flexural Compression Concrete," Proceeding of Japan Concrete Institute, V. 28, No. 2, 2006, pp. 793-798 (in Japanese).

2.5 Ichinose T., "Truss Mechanism in Critical Region of RC Member," *Journal of Structural and Construction Engineering*, AIJ, No. 475, Sep.,

pp. 129-135. (in Japanese)

2.6 J. C. Walraven, "Fundamental Analysis of Aggregate Interlock," *Proceedings, ASCE*, V. 107, ST. 11, Nov., 1981, pp. 2245-2270.

2.7 ACI Committee 318, "Building Code Requirements for Structural Concrete (ACI-318) and Commentary," American Concrete Institute, Farmington Hill, MI, 2008, pp. 155-168.

2.8 Architectural Institute of Japan (AIJ), "Design Guide lines for Earthquake Resistant Reinforced Concrete Buildings Based on Inelastic Displacement Concept," 1999, pp. 142-159 (in Japanese).

2.9 Tani M., "The Evaluation of Structural Performance of Post-tensioned Precast Concrete Columns," PhD Thesis, Kyoto University, Kyoto, Japan, Mar., 2009. (in Japanese)

2.10 Mori, K., Okamura T., Ichioka, Y., Skashita, M., Tani M., Kono S., Nishiyama M., "Flexure and Shear Behavior of Post-tensioned Precast Concrete Columns Made of High Performance Materials", *Summaries of Technical Papers of Annual Meeting*, *AIJ*, Oct., 2009, pp. 843-846. (in Japanese)

2.11 Lee J., Nishiyama M., and Tani M., "Evaluation of Shear Design Procedures for Prestressed Concrete Members," *Proceedings of 3rd fib International Congress 2010*, May, 2010.

2.12 Lee J., Tani M., Kono S., and Sakashita M., "Diagonal Tension Failure of Post-tensioned Precast Concrete Beam with High Strength Shear Reinforcement," *Proceedings of the Japan Concrete Institute*, V. 32, No. 2, JCI, June, 2010, pp. 493-498

2.13 Yuasa N., Ogawa T., Kamakura M., Fukui T., Uchida R., and Hamahara M., "Experimental Study on Shear Behavior of Precast Prestressed Concrete Beams," *Summaries of Technical Papers of Annual Meeting, AIJ*, Sep., 2000, pp. 965-970. (in Japanese)

2.14 Yuasa N., Ohtaga K., Fukui T., and Hamahara M., "Experimental Study on Shear Behavior of Precast Prestressed Concrete Beams," *Summaries of Technical Papers of Annual Meeting, AIJ*, Sep., 2001, pp. 955-960. (in Japanese)

2.15 Yuasa N., Ohtaga K., and Hamahara M., "Experimental Study on Shear Behavior of Precast Prestressed Concrete Beams (Part5 Discussion of Ultimate Shear Strength of Test Beams), *Summaries of Technical Papers of Annual Meeting*, AIJ, Aug., 2002, pp. 993-994. (in Japanese)

2.16 Architectural Institute of Japan, "Standard for Structural Design and

Construction of Prestressed Concrete Structures," 1998, pp. 233-234 (in Japanese).

2.17 Xiao, Y., Esmaeily-Ghasemabadi, A. Wu H., "High-Strength Concrete Short Beams Subjected to Cyclic Shear," *ACI Structural Journal*, V. 96, No. 3, May-June, 1999, pp. 393-399

2.18 Matamoros A. B., Sozen M. A., "Drift Limits of High-Strength Concrete Columns Subjected to Load Reversals, " *Journal of Structural Engineering*, V. 129, No. 3, 2003, pp. 297-313.

2.19 Lehman D., Moehle J., Mahin S., Calderone A., Henry L, "Experimental Evaluation of the Seismic Performance of Reinforced Concrete Bridge Columns," *Journal of Structural Engineering*, V. 130, No. 6, 2004, pp. 869-879.

2.20 Sezen J., Moehle J. P., "Shear Strength Model for Lightly Reinforced Concrete Columns," *Journal of Structural Engineering*, ASCE, V. 130, No. 11, 2004, pp. 1692-1703

2.21 Lee J., Watanabe F., "Shear Deterioration of Reinforced Concrete Beams Subjected to Reversed Cyclic Loading," *ACI Structural Journal*, V. 100, No. 4, July-Aug., 2003, pp. 480-489.

2.22 Sakakura M., Araki H., Nakatsuka T., Kabayama K., "Resistance Mechanism of Confined Concrete Subjected to Shear Force," *Proceedings of the Japan Concrete Institute*, V. 25, No. 2, JCI, 2003, pp. 1033-1038.

2.23 Watanabe H., "Experimental Study on Evaluation of Ductility of Reinforced Concrete Columns," Journal of Structural and Construction Engineering, V. 590, Oct., 2002, pp. 161-168.

3. Static Loading Test on Flexural and Shear Behavior of Post-tensioned Precast Concrete Beams

3.1 Introduction

In order to investigate shear behavior of prestressed concrete beams, two series of static loading tests (Test 1 and 2) using half-scale post-tensioned precast concrete beams have been conducted. In Test 1, shear behavior of post-tensioned precast concrete beams failing in shear compression (SC) and shear tension (ST) is conducted. In Test 2, structural behavior of diagonal tension (DT) failure of prestressed concrete beams is investigated.

3.2 Test on Flexural Shear Behavior of Post - tensioned Precast Concrete Beams (Test 1)

3.2.1 Design of Specimens

To investigate flexural shear behavior of post-tensioned precast concrete beams, seven half-scale beams were designed. Figure 3.1 illustrates test specimens. Two experimental parameters were selected: shear span depth ratio, a/D, and shear reinforcement ratio, ρ_w. Table 3.1 indicates experimental parameters allocated to specimens. Table 3.2 shows the geometric and material properties applied to the specimens for the design. Fig. 3.2 illustrates the relationship of the shear capacity and a load-displacement curve of the specimens when flexure is dominant. Vertical and Horizontal axis in Fig. 3.2 represent shear force, V, and member rotation angle, R, defined as a ratio of relative displacement of beam, δ, to beam length, L. Notation (C), (S), and (Y) in Fig. 3.2 indicate expected flexural cracking, shear failure, and, yielding of prestressing steel, respectively. Flexural crack moment, M_{cr}, flexural yield moment, M_y, in Fig. 3.2 were

obtained by Eq. (3.1) to (3.3). Stiffness reduction factor, α_y, for flexural yielding was obtained by Okada [3.1] and Sugano's [3.2] model as shown in Eq. (3.4) and (3.5). Stiffness reduction factor after flexural yielding, α_3, is defined as 0.001 [3.2].

$$M_{cr} = f_{pb}Z \qquad \text{Eq. (3.1)}$$

$$M_y = 0.9M_u \qquad \text{Eq. (3.2)}$$

$$M_u = bx_n k_1 F_c\left\{\frac{D}{2} - k_2 x_n\right\} + A_{pt}f_{py}\left(d_{pt} - \frac{D}{2}\right) + A_{rt}f_{ry}\left(d_{rt} - \frac{D}{2}\right), \quad x_n = \frac{A_{pt}f_{py} + A_{rt}f_{ry} + N}{bk_1 F_c}$$

$$\text{Eq. (3.3)}$$

$$\alpha_y = \left\{0.043(1 + a/D) + 0.33\eta_N + 1.64(n_r\rho_{rt} + 3.5n_s\rho_p d_{g1})\right\}d_{rt1}^2, \quad \text{for } a/D \geq 2.0$$

$$\text{Eq. (3.4)}$$

$$\alpha_y = \left\{-0.0836 + 0.159a/D + 0.169\eta_N\right\}d_{rt1}^2, \quad \text{for } a/D < 2.0 \qquad \text{Eq. (3.5)}$$

$$R_y = \frac{M_y}{(L/2)\alpha_y K_e}, \quad K_e = \frac{12E_c I_c}{L^2} \qquad \text{Eq. (3.6)}$$

where f_{pb} is stress at the extreme tension fiber of the beam section due to prestress, Z is section modulus ($=bD^2/6$), and M_u is flexural strength obtained using stress block (k_1=0.83 and k_2=0.42) specified in the reference [3.3].
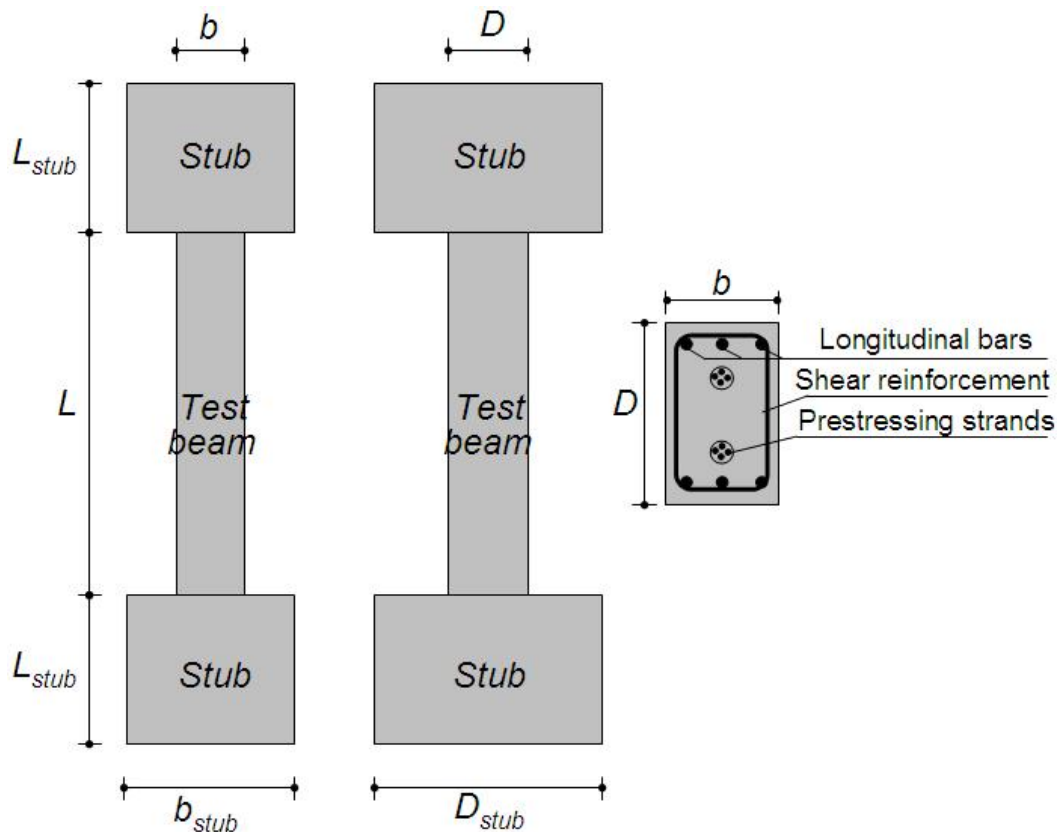

Fig. 3.1 Test specimens

Table 3.1 Experimental parameters

		ρ_w (%)		
		0.21 (2-S6@100)	0.42 (2-S6@100)	0.63 (2-S6@100)
	1.0	-	S-10-L42	S-10-L63
a/D	1.5	S-15-L21	S-15-L42	S-15-L63
	2.0	S-20-L21	S-20-L42	-

Table 3.2 Geometric and material properties applied in specimens for design

	b (mm)	D (mm)	L (mm)	a/D	F_c (MPa)	P_i (kN)	f_{wy} (MPa)	ρ_w (%)
S-10-L42			800	1.0				0.42
S-10-L63								0.63
S-15-L21								0.21
S-15-L42	300	400	1200	1.5	60	1480 (=0.8P_y)	785	0.42
S-15-L63								0.63
S-20-L21			1600	2.0				0.21
S-20-L42								0.42

Note: a = shear span; D = overall depth of section; P_i = initial prestressig force; P_y = yield force of prestressing steel; and ρ_w = shear reinforcement ratio.
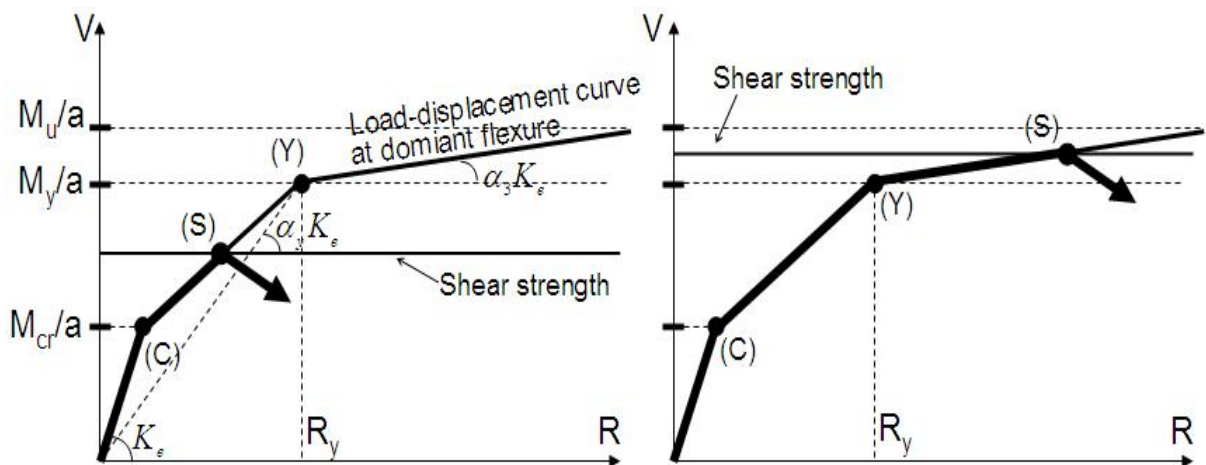

(a) Shear failure prior to flexural yielding (b) Shear failure after flexural yielding
Fig. 3.2 Load-displacement relationship and shear capacity

Figure 3.3 plots the load-displacement relationship and shear strength obtained by AIJ guide line [2.8]. The equation is specified in Eq. (2.38) to (2.41). It is

expected that five of seven specimens fail in shear prior to flexural yielding.
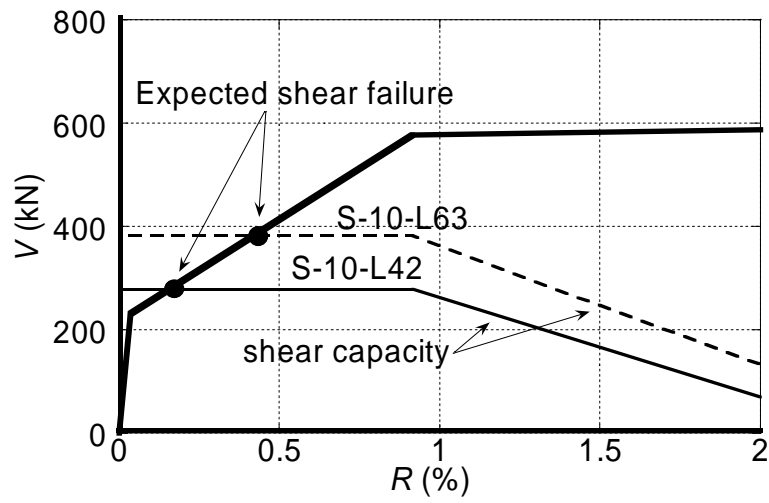
(a) Specimens with *a/D* =1.0
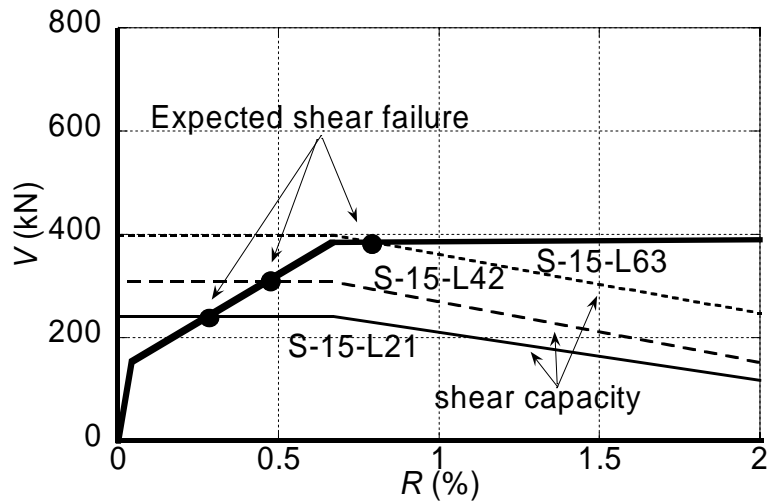
(b) Specimens with *a/D* =1.5

(c) Specimens with *a/D* =2.0

Fig. 3.3 Load displacement relationship and shear capacity obtained by AIJ guideline [2.8]

3.2.2 Materials, Construction, and Test Specimens

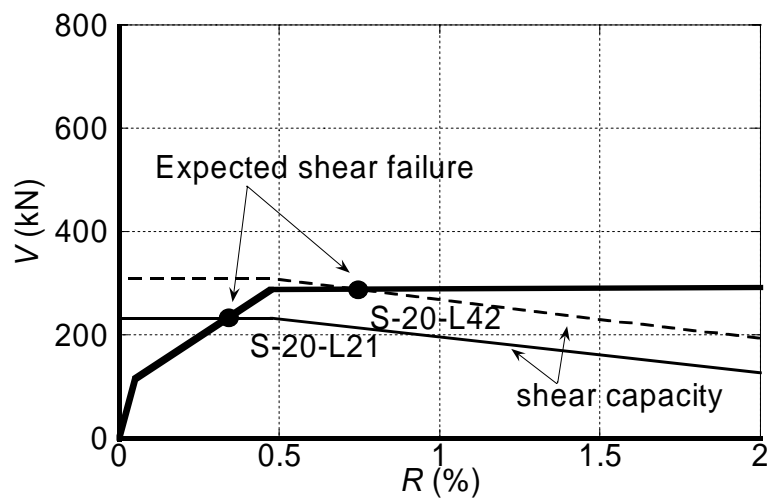Table 3.3 summarizes the geometric and material properties used in the specimens. Beam cross sections are shown in Fig. 3.4. Fig. 3.5 to 3.7 illustrate the reinforcing details of the specimens. All beams were post-tensioned by prestressing strands (2-6×φ12.7, SWPR7BL), and shear reinforced with high-strength shear reinforcement (S6, KSS785), which were supported by supplementary longitudinal reinforcing bars of mild-strength steel (D10, SD295A). The beam cross sectional dimensions is 300×400 mm. The beam length was 800, 1200, or 1600 mm. A beam and stubs were assembled by post-tensioning through a 20 mm thick high-strength non-shrinkable mortar joint. Prestressing force corresponding to approximately 80% of the yield force of the prestressing strands was introduced. Effective prestressing force, P_e, at the time of testing ranged from 1093 kN to 1419 kN as shown in Table 3.4.

Table 3.3 Geometric and material properties in test specimens

Concrete	F_c (MPa)	F_t (MPa)	E_c (GPa)
S-10-L42, S-10-L63	57.3	-	28.9
S-15-L21, S-15-L42, S-15-L63	62.3	3.26	30.0
S-20-L21, S-20-L42	55.9	3.89	28.1
Mortar at joint	F_c (MPa)	F_t (MPa)	E_c (GPa)
S-10-L42, S-10-L63	75.1	4.35	24.0
S-15-L21, S-15-L42, S-15-L63	82.1	4.14	25.8
S-20-L21, S-20-L42	83.4	3.14	30.8
Grout for prestressing steel	F_c (MPa)	F_t (MPa)	E_c (GPa)
S-10-L42, S-10-L63	55.9	3.20	15.2
S-15-L21, S-15-L42, S-15-L63	68.8	3.93	15.2
S-20-L21, S-20-L42	67.7	2.21	15.0

Reinforcements	A_s (mm)	Grade	f_y (MPa)	ε_y (%)	f_u (MPa)	E_s (GPa)
S6	31.67	KSS785	984.2*	-	1165	194.4
D10	71.33	SD295A	360.9	0.20	510	178.3
Prestressing strands		Type	P_y (kN)	P_u (kN)	ε_{uf} (%)	E_p (GPa)
6φ12.7		SWPR7BL	1069*	1188	6.0	186

*0.2% offset

Note: F_c and F_t = compressive and splitting tensile strengths; E_c = Young's

modulus; f_y and f_u = yield and tensile strengths of reinforcement; ε_y = yield strain of reinforcement; E_s and E_p = Young's modulus of reinforcement and prestressing strand; P_y and P_u = yield and tensile forces of prestressing strand; ε_{uf} = strain at failure of prestressing strand, respectively.

Table 3.4 Effective prestressing force P_e and prestressing level η

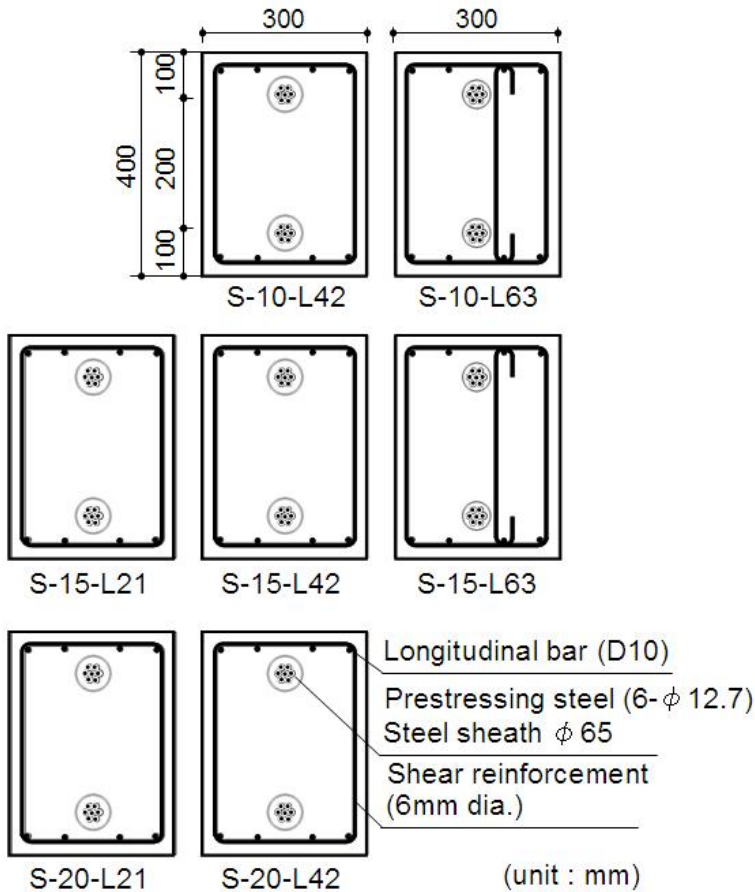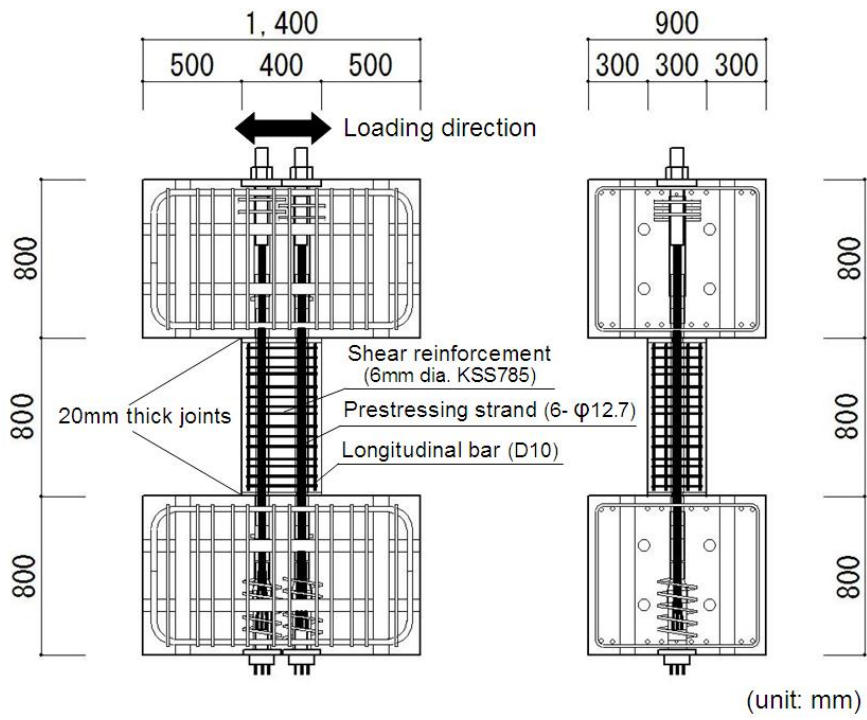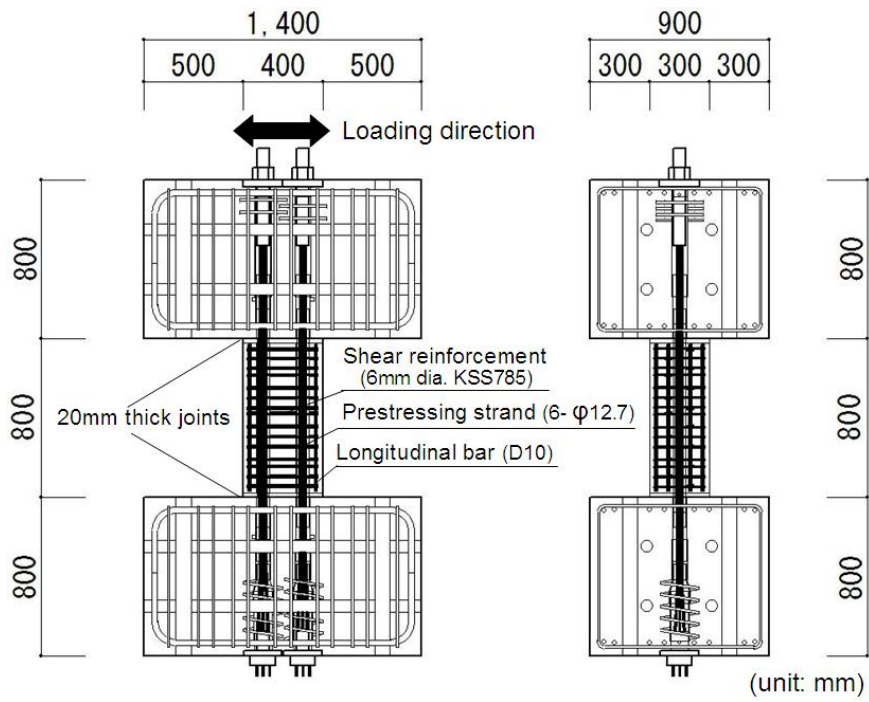| Specimen	P_e (kN)	$\eta(=P_e/bDF_c)$
S-10-L42	1204	0.175
S-10-L63	1104	0.161
S-15-L21	1115	0.150
S-15-L42	1093	0.146
S-15-L63	1178	0.158
S-20-L21	1419	0.212
S-20-L42	1396	0.208

Fig. 3.4 Beam cross section
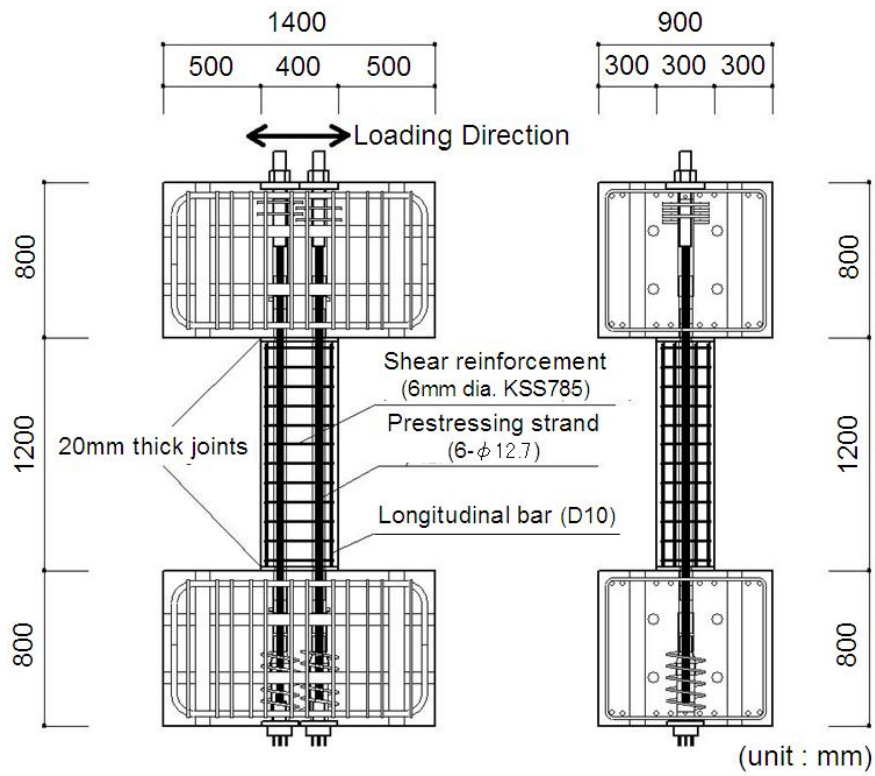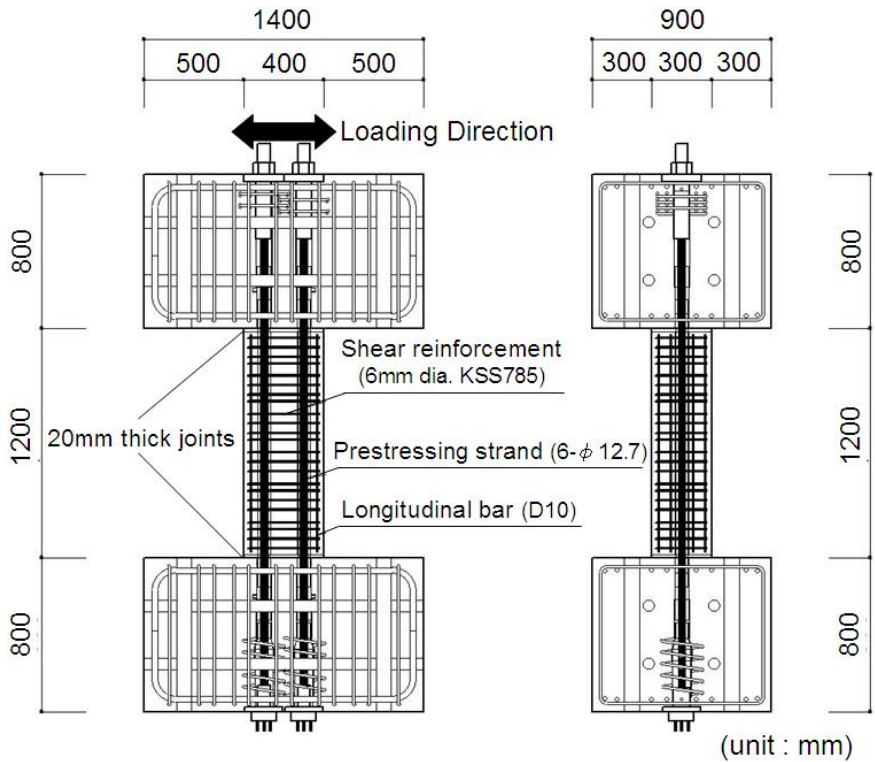
(a) S-10-L42

(b) S-10-L63

Fig. 3.5 Reinforcing details of test beam (a/D=1.0, L=800mm)

(a) S-15-L21

(b) S-15-L42

Fig. 3.6 Reinforcing details of test beam (a/D=1.5, L=1200mm)

4 1

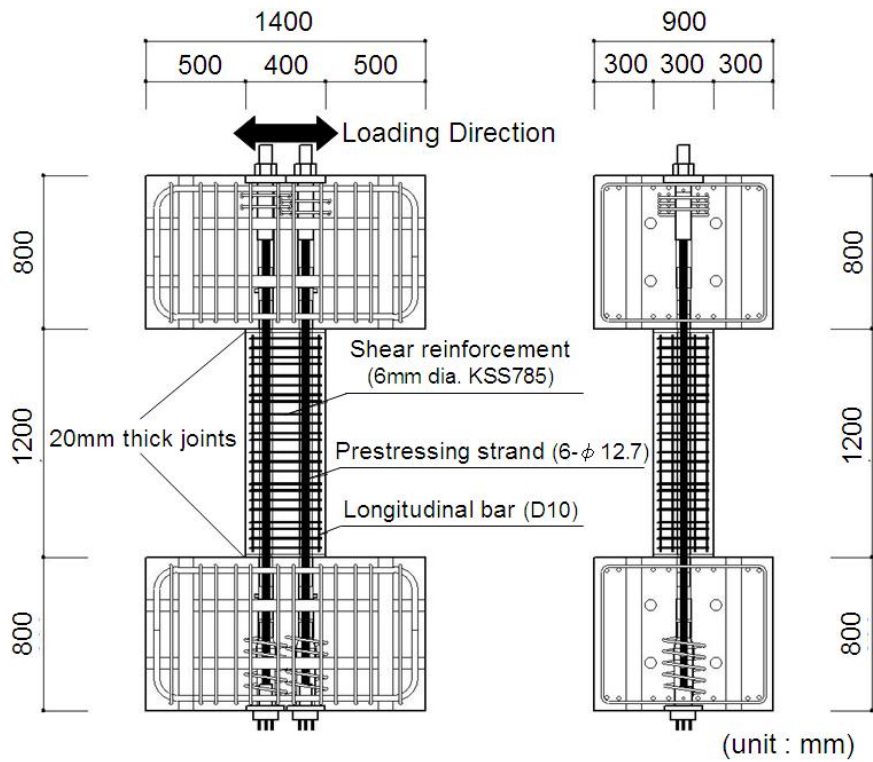(c) S-15-L63

Fig. 3.6 Reinforcing details of test beam (*a/D*=1.5, *L*=1200mm)

(a) S-20-L21

Fig. 3.7 Reinforcing details of test beam (*a/D*=2.0, *L*=1600mm)

4 2
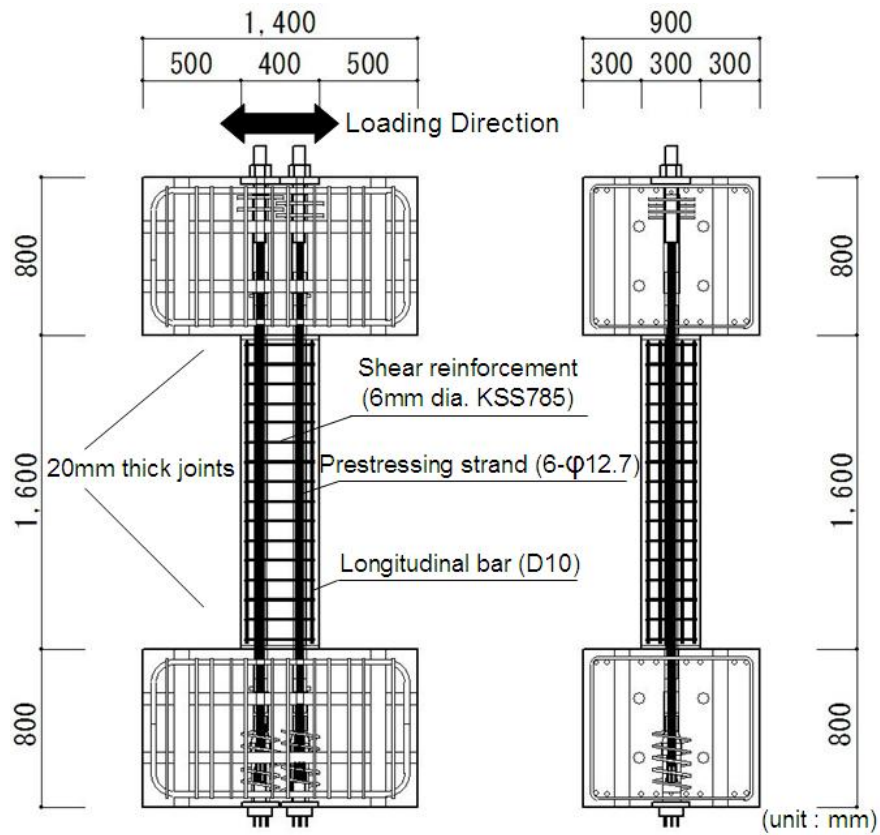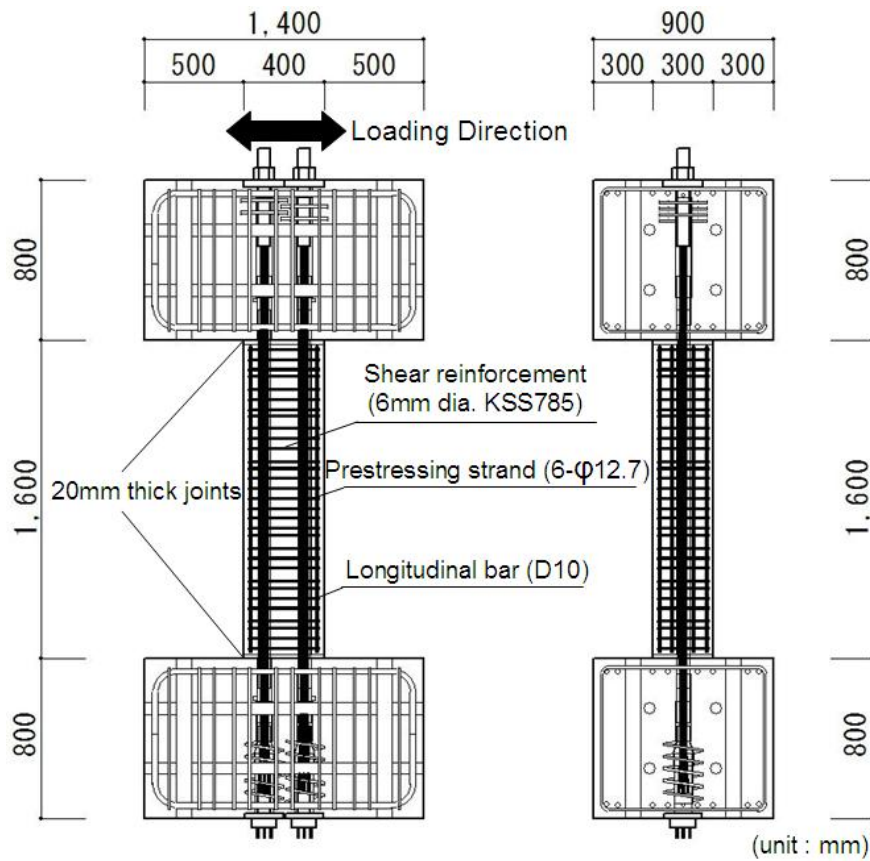
(b) S-20-L42

Fig. 3.7 Reinforcing details of test beam (*a/D*=2.0, *L*=1600mm)

3.2.3 Loading and Measurements

The specimen was rotated by 90 degrees and set in the loading rig as shown in Fig. 3.8. The loading setup consisted of a L-shape steel frame with two sets of hydraulic jacks of 2000 kN and 8000 kN capacity. To simulate a beam in the moment-resisting frame subjected to earthquake loading, the vertical jacks of 8000 kN kept the top stub horizontal during testing. The total load of these two jacks was kept zero for not applying any axial load on the beam. The horizontal loads were applied by the 2000 kN jacks. The first loading cycle was up to *R*= 1.0%, and was followed by a series of member rotation controlled cycles comprising two full cycles to each of the member rotation of 0.25%, 0.5%, 0.75%, 1.0%, 2.0%, 4.0%, and 6.0%, respectively. The loading patterns are shown in Fig. 3.9.
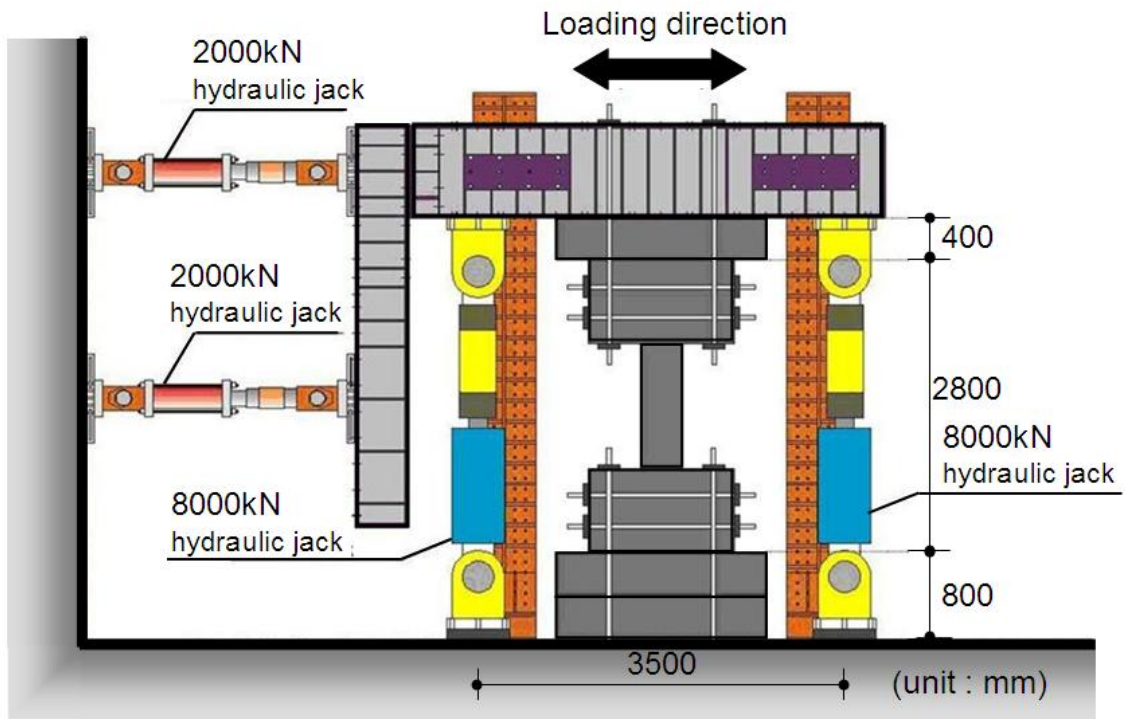
(a) Elevation
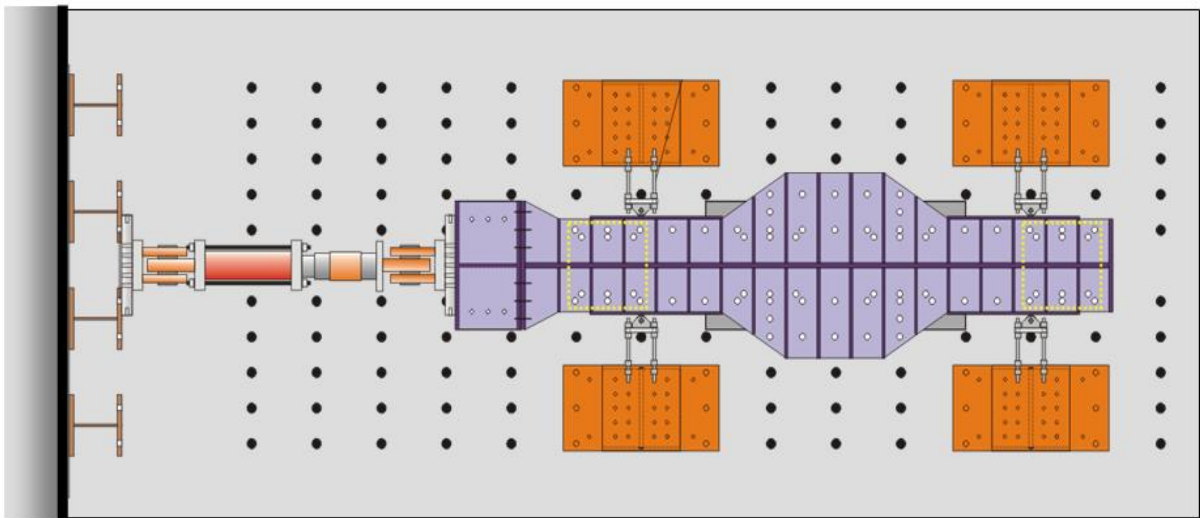
(b) Plan

Fig. 3.8 Loading setup
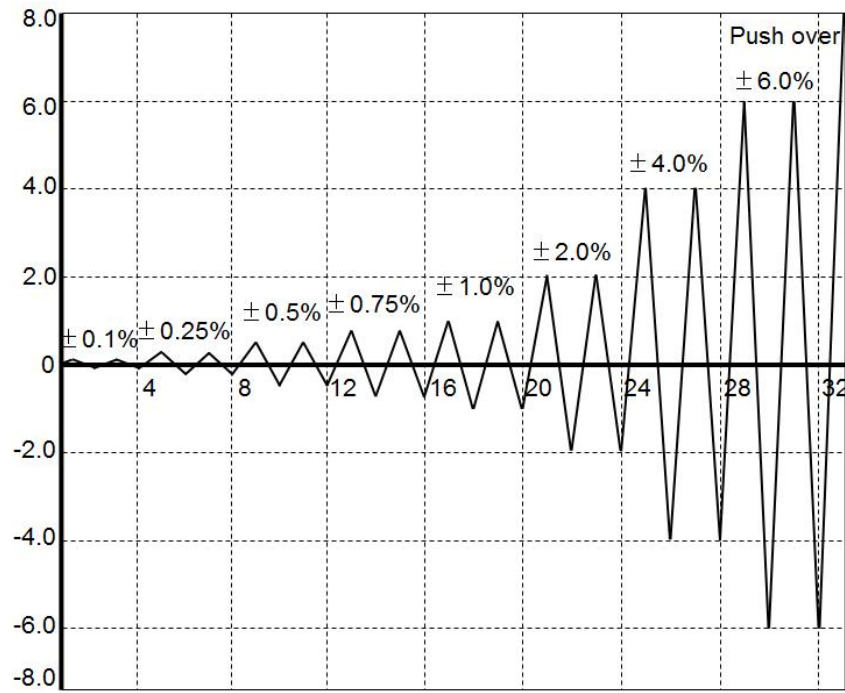
Fig. 3.9 Loading patterns

Strain gauges were attached to some of the reinforcements (e.g. PT bars, longitudinal bars, and shear reinforcements) as shown in Fig. 3.10. The strain gauges were attached at two sides of the single reinforcement. All instrumentation was monitored and recorded continuously throughout testing. Flexural and shear deformations of the beam were measured by the linear displacement transducers attached on the beam, which was divided into six to ten segments as shown in Fig. 3.11.
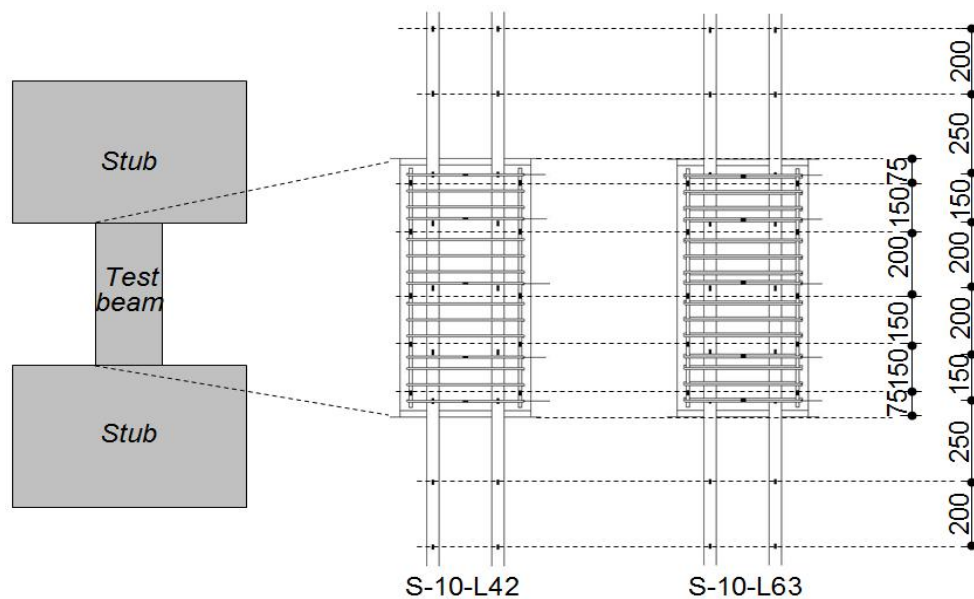
(a) Specimens with *a/D*=1.0

Fig. 3.10 Position of strain gauges attached on the reinforcements

4 5
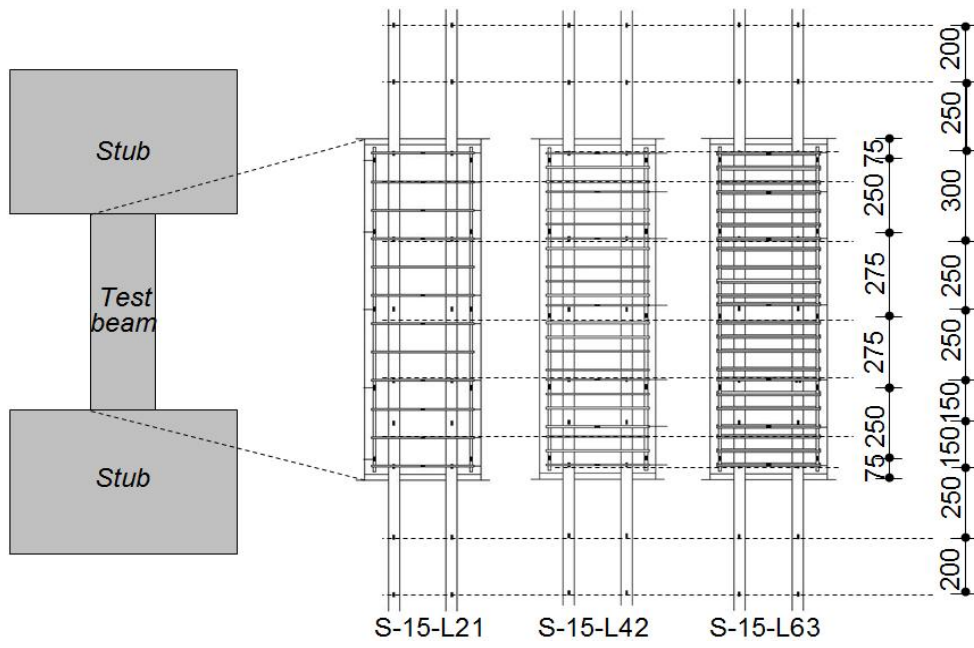
(b) Specimens with *a/d*=1.5
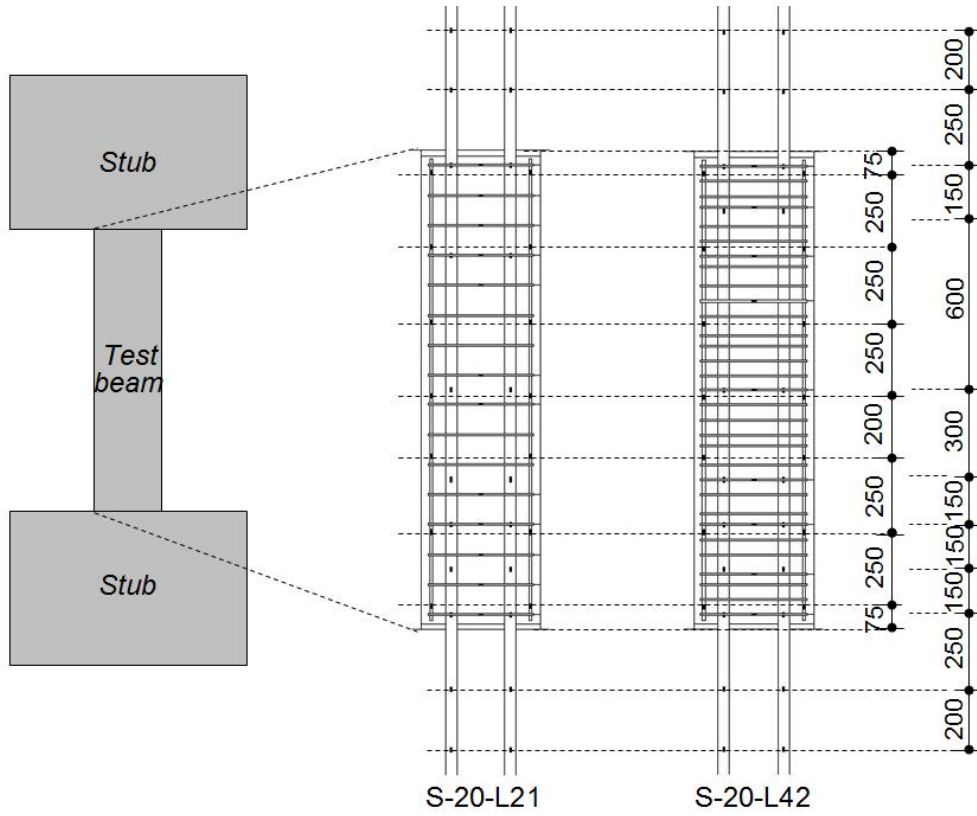
(c) Specimens with *a/D*=2.0

Fig. 3.10 Position of strain gauges attached on the reinforcements

(a) Specimens with *a/D*=1.0   (b) with *a/D*=1.5

(c) Specimens with *a/D*=2.0
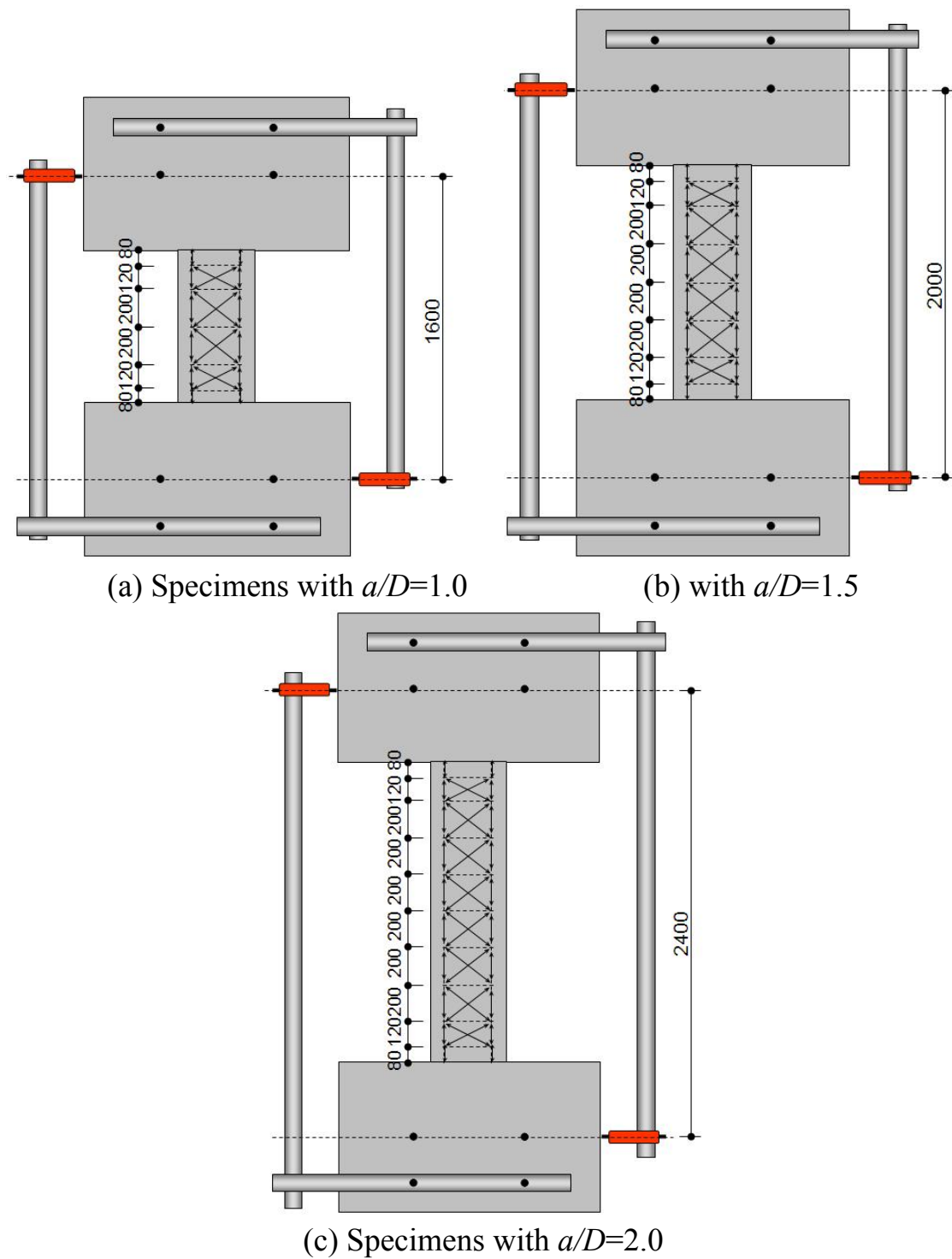
Fig. 3.11 Setup of linear displacement transducers

3.2.4 Test Results

Load-displacement relationships and crack patterns

Figure 3.12 shows beam shear force, *V,* -drift angle, *R*, relations. The shear force, *V*, is obtained as Eq. (3.37) and (3.38) considering horizontal force of leaned vertical hydraulic jacks. The drift angle, *R* is defined as a ratio of relative displacement of beam to its length ($=\delta_{exp}/L$). The horizontal dashed lines

represent shear force, V_f, at flexural strength, M_f, which is theoretically obtained using the ACI 318 concrete stress block, the ultimate concrete strain of 0.3%, and plane section assumption. Symbols ○, ●, Δ, □, and ◊ in Fig. 3.12 represent first flexural cracking, first shear cracking, peak load, yielding of prestressing strand, and yielding of shear reinforcement, respectively.

$$V = V_{top} + V_{bottom} + N_{sx} + N_{nx} \qquad \text{Eq. (3.37)}$$

$$N_{sx} = N_s \frac{\tan\theta}{\sqrt{1+\tan^2\theta}}, \quad N_{nx} = N_n \frac{\tan\theta}{\sqrt{1+\tan^2\theta}}, \quad \tan\theta = \frac{\delta_{exp}}{H} \qquad \text{Eq. (3.38)}$$

where V_{top} and V_{bottom} are shear force by two jacks, N_s and N_n are axial force by two vertical jacks, N_{sx} and N_{nx} are lateral force by two vertical jacks, $tan\theta$ is rotation angle of vertical jacks, δ_{exp} is lateral displacement of specimens, and H is height of vertical jacks (=2900 mm)
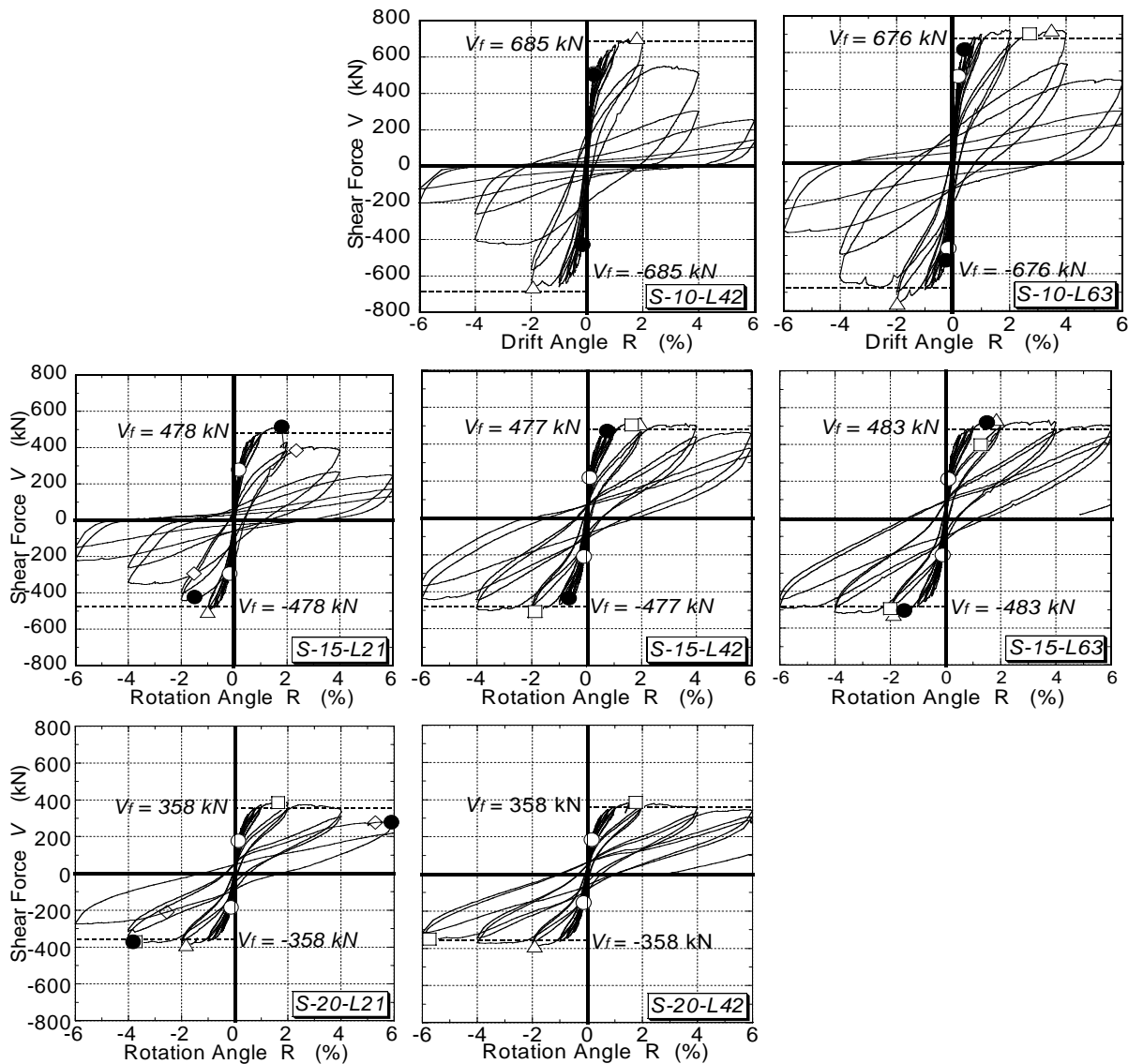
Fig. 3.12 Shear force, V – drift angle, R, relations

Table 3.5 summarizes the test results. In Table 3.5, V_{cr_f} is shear force at flexural cracking, V_{exp} is peak load, and R_{exp} is beam drift angle at peak load, respectively. Figure 3.13 shows crack patterns of beams for difference of drift angle of 0.25% to 6.0%. Seven failure modes, shear tension failure (ST), shear compression failure (SC), diagonal tension failure (DT), flexural shear compression failure (FSC), bond failure (B), flexural failure (F), and shear failure after flexural yielding (FS), are used in this study. Moreover, the shear failure can be further categorized by its definition as follows:

1. Shear tension failure (ST): Tensile stress of shear reinforcement develops due to initiation of shear crack, and it reaches its yield strength at ultimate state.

2. Shear compression failure (SC): Tensile stress of shear reinforcement develops due to initiation of shear crack. Compressive principle stress in diagonally cracked concrete reaches its compressive strength and crushes prior to yielding of shear reinforcement.

3. Diagonal tension failure (DT): Rapid decay of load carrying the shear capacity of beam due to excessive open of shear crack immediately after initiation of the crack.

4. Bond failure (B): Deterioration of shear resistance of beam due to bond failure of longitudinal bars or PT tendons.

5. Flexural shear compression failure (FSC): Decay of load carrying the capacity of a member due to deterioration of shear capacity of the concrete at flexural compression zone.

Table 3.5 Summary of test results

Specimen	Failure mode	V_{cr_f} (kN)		V_{exp} (kN)		R_{exp} (kN	
		+	-	+	-	+	-
S-10-L42	S(FSC)	510.9	-428.0	706.4	-658.6	1.79	-1.92
S-10-L63	FS	470.6	-461.0	721.6	-761.5	3.48	-1.98
S-15-L21	S(DT)	279.3	-293.1	515.7	-502.9	1.79	-1.00
S-15-L42	F	219.0	-208.2	511.8	-507.8	1.96	-1.87
S-15-L63	F	212.0	-201.7	536.0	-525.3	1.85	-1.88
S-20-L21	FS	176.8	-184.9	386.1	-387.4	1.74	-1.82
S-20-L42	F	183.9	-154.9	385.9	-386.4	1.76	-1.92

Note: S is shear failure, FS is shear failure after flexural yielding, F is flexural failure, FSC is flexural shear compression failure, and DT is diagonal tension failure, respectively.

All specimens except S-15-L63 and S-20-L42 had been designed to fail in shear prior to yielding of prestressing steel. However, only two of them (S-10-L42 and S-15-L21) failed as designed. The reason for this is that Eq. (2.43) to (2.47) which were used for design of the specimens underestimated their shear capacities. The equations have been used in practice for design of ordinary reinforced concrete members. It is useful because shear capacity deterioration with increasing inelastic deformation is included. However beneficial effect of prestress on shear resistance is not taken into consideration in the equations.

| 0.25% | 0.5% | 0.75% | 1.0% | 2.0% | 4.0% | 6.0% |

(a) S-10-L42

| 0.25% | 0.5% | 0.75% | 1.0% | 2.0% | 4.0% | 6.0% |

(b) S-10-L63

| 0.25% | 0.5% | 0.75% | 1.0% | 2.0% | 4.0% | 6.0% |

(c) S-15-L21

Fig. 3.13 Crack patterns

0.25% 0.5% 0.75% 1.0% 2.0% 4.0% 6.0%

(d) S-15-L42

0.25% 0.5% 0.75% 1.0% 2.0% 4.0% 6.0%

(e) S-15-L63

0.25% 0.5% 0.75% 1.0% 2.0% 4.0% 6.0%
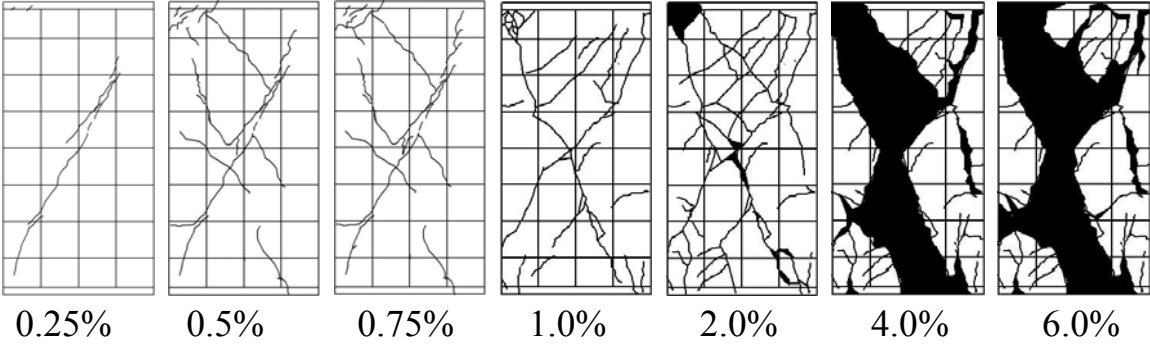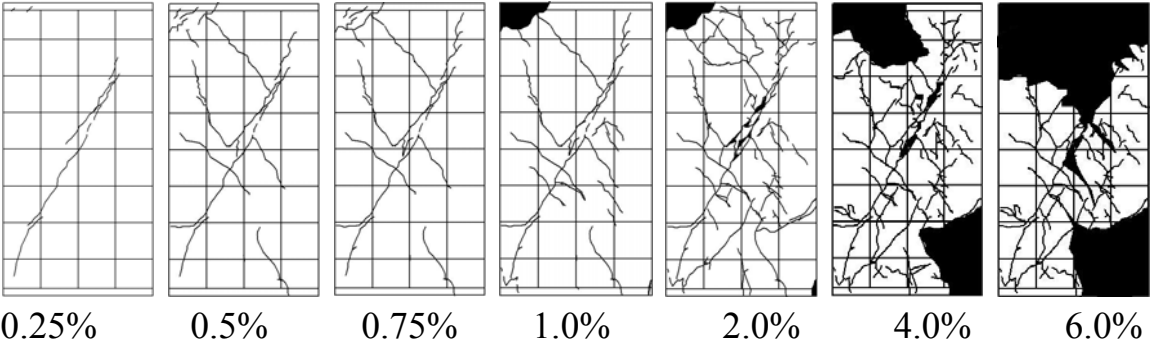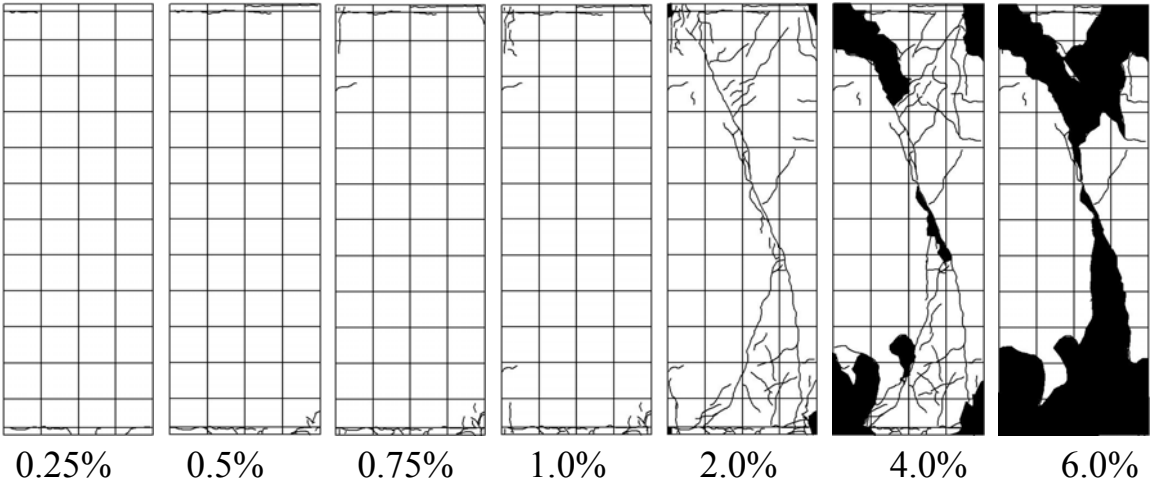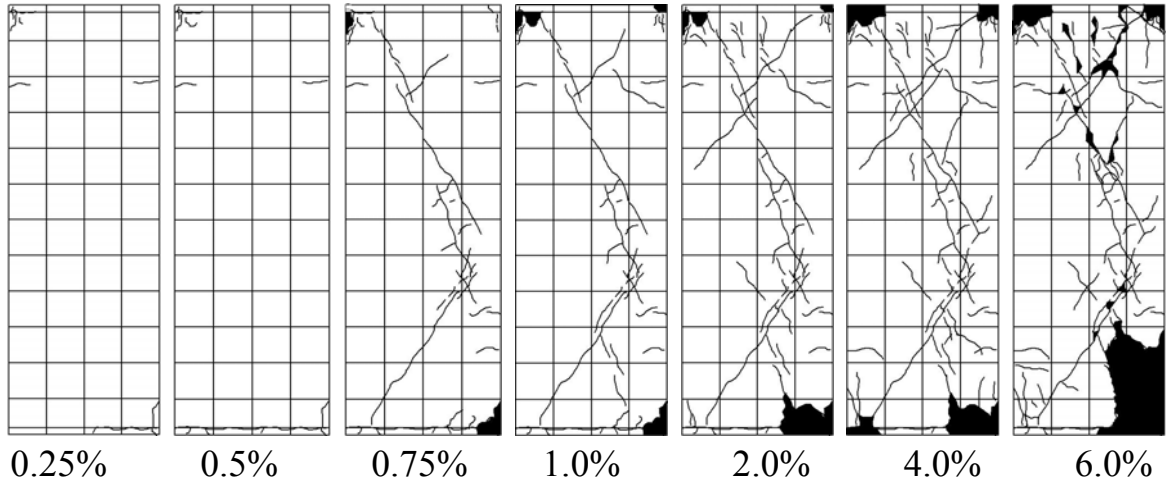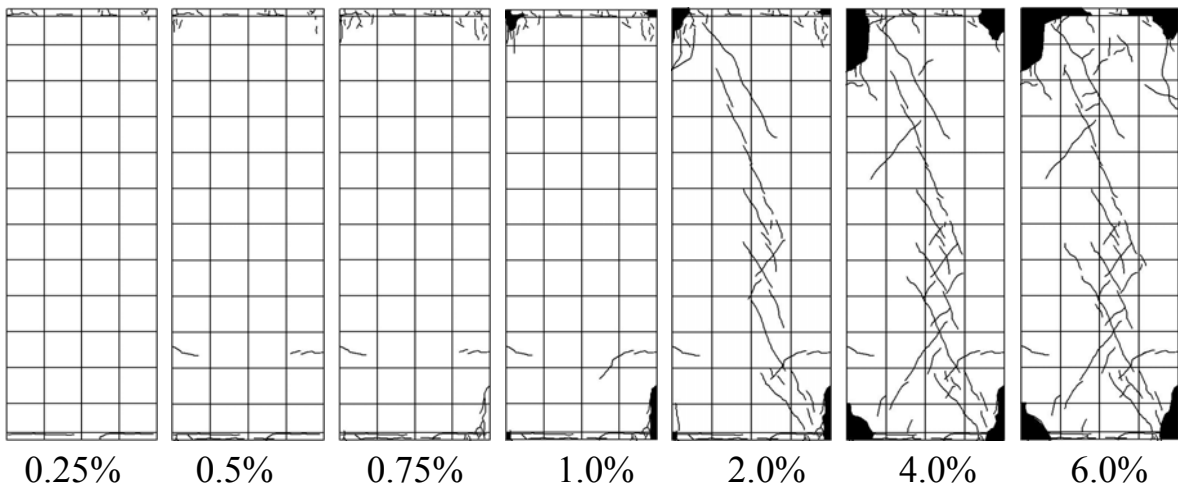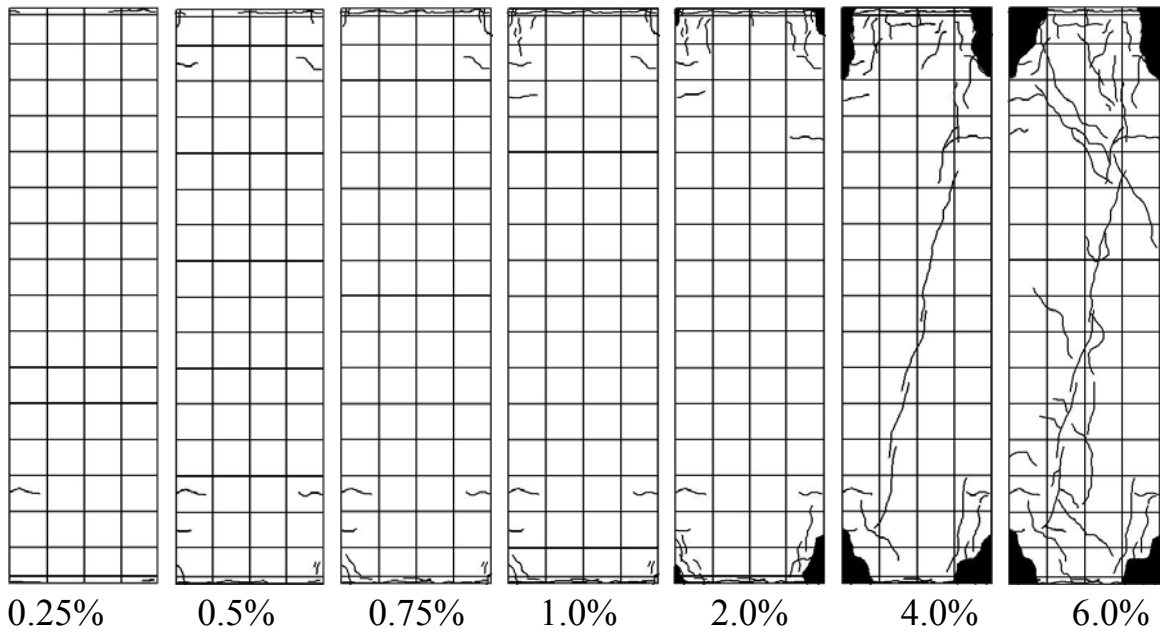
(f) S-20-L21

Fig. 3.13 Crack patterns

| 0.25% | 0.5% | 0.75% | 1.0% | 2.0% | 4.0% | 6.0% |
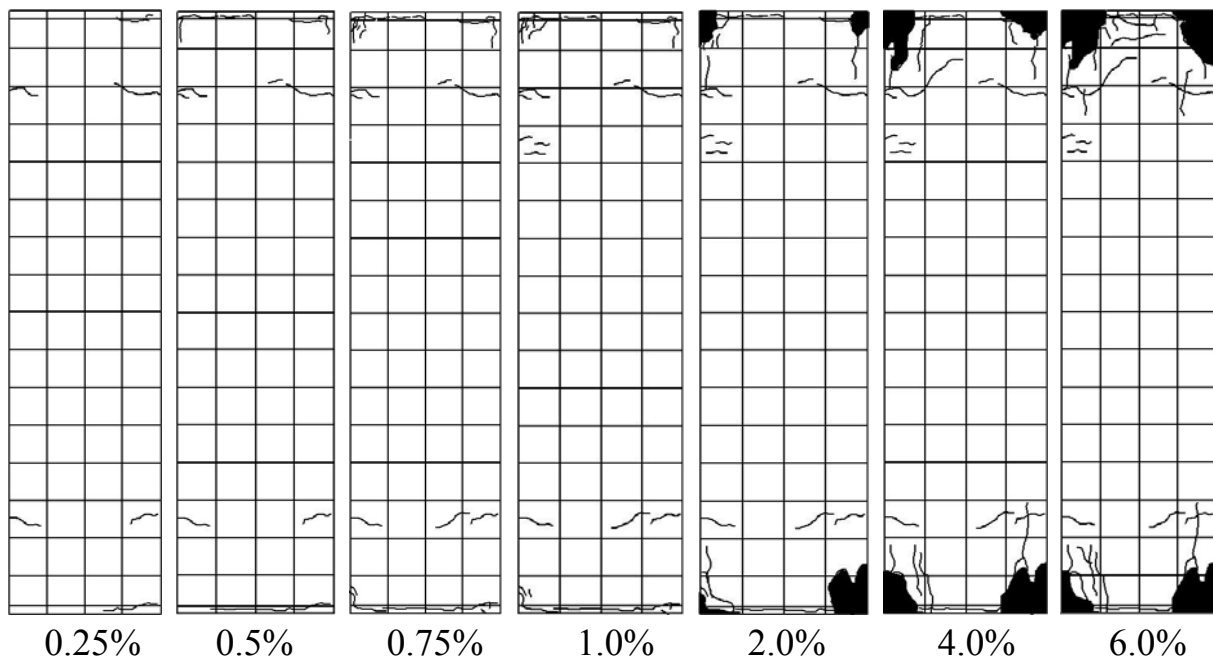
(g) S-20-L42

Fig. 3.13 Crack patterns

As shown in Fig. 3.12 to 3.13, flexural cracks in all beams were initiated in R=0.1%. In S-10-L42, shear crack was initiated at R=0.1% and propagated until peak load of R=2.0%. Shear reinforcement did not yield, and the load carrying the shear capacity of beam decayed due to crushing of concrete at flexural compression zone at R=2.0%. The failure mode of S-10-L42 is judged as FSC (flexural shear compression failure).

In S-10-L63, shear cracks were propagated after its initiation at R=0.25%. No significant deterioration of the load carrying the shear capacity is until R=2.7% in which prestressing steel yielded. The load decayed after R=4.0%. It is judged as FS (shear failure after flexural yielding).

Specimens with a/D=1.5 except S-15-L21 failed in flexure (F). Gap opening at joints occurred at R=0.25%. The load carrying the shear capacity in S-15-L21 rapidly dropped immediately after initiation of primary shear crack. It is because of deterioration of interlock resistance on shear crack due to the excessive opening of the crack. S-15-L21 is judged that it failed in diagonal tension (DT).

In S-15-L42 and S-15-L63, gap of joint at ends of beam opened at R=0.1%, and prestressing steel yielded at R=2.0 and 1.8%, respectively. No deterioration of the load carrying the shear capacity of beams is while shear crack propagated

until *R*=6.0%. They failed in flexure (F).

In S-20-L21, the prestressing steel yielded immediately after the peak load of *R*=1.8%. At *R*=3.8%, flexural shear crack was initiated, and significant decay of the load occurred. It is judged as shear failure after flexural yielding (FS).

In S-20-L42, no significant deterioration of the load in S-20-L42 was until prestressing steel yielded at the peak load of *R*=1.8%. It is judged as flexure failure (F).

Decomposition of flexural and shear deformation
To investigate the distribution of flexural and shear deformation in the beams, the flexural and shear deformation was obtained based on the displacement measured by the linear displacement transducers attached on the beam as shown in Fig. 3.11. Fig. 3.14 illustrates the relative displacement of the linear displacement transducers in decomposed flexural and shear deformation. It is noted that the relative displacements are δ_{i1}, δ_{i2}, δ_{i3}, and δ_{i4} in Fig. 3.14 are vertical and diagonal displacement measured by linear displacement transducers. Curvature, ϕ_i, and shear strain, γ_i, in segmented area i can be obtained as Eq. (3.39).

$$\phi_i = \frac{\delta_{i2} - \delta_{i1}}{L_{i1i}L_{i2}}, \quad \gamma_i = \alpha_{i1} + \alpha_{i2} = \frac{\sqrt{L_{i1}^2 + L_{i2}^2}}{L_{i1}L_{i2}} \frac{\delta_{i4} - \delta_{i3}}{2} \qquad \text{Eq. (3.39)}$$

As shown in Fig. 3.14, the relative displacement in area i and in area $i+1$ due to flexural deformation in area i can be obtained as Eq. (3.40) and (3.41). Therefore, relative displacement in a beam due to flexural deformation, δ_f, is derived as Eq. (3.42). The relative displacement due to shear deformation, δ_s, is expressed as Eq. (3.43). Total relative displacement due to flexural and shear deformation, δ_{dcp} is obtained as Eq. (3.44).

$$u_{if} = \int_0^{L_{i1}} z\phi_i dz = \frac{\phi_i}{2} L_{i1}^2 \quad \text{for area } i \qquad \text{Eq. (3.40)}$$

$$u'_{if} = (H - L_{i1})\phi_i L_{i1} \quad \text{for area } i+1 \qquad \text{Eq. (3.41)}$$

$$\delta_f = \sum_{i=1}^{n} u_{if} + u'_{if} = \sum_{i=1}^{n} \left(H - \frac{L_{i1}}{2} \right)\phi_i L_{i1} \qquad \text{Eq. (3.42)}$$

$$\delta_s = \sum_{i=1}^{n-1} \gamma_i L_{i1} = \frac{\sqrt{L_{i1}^2 + L_{i2}^2}}{L_{i2}} \frac{\delta_{i4} - \delta_{i3}}{2}, \quad \delta_s = \sum_{i=1}^{n-1} \gamma_i L_{i1} \qquad \text{Eq. (3.43)}$$

$$\delta_{dcp} = \delta_f + \delta_s \qquad \text{Eq. (3.44)}$$
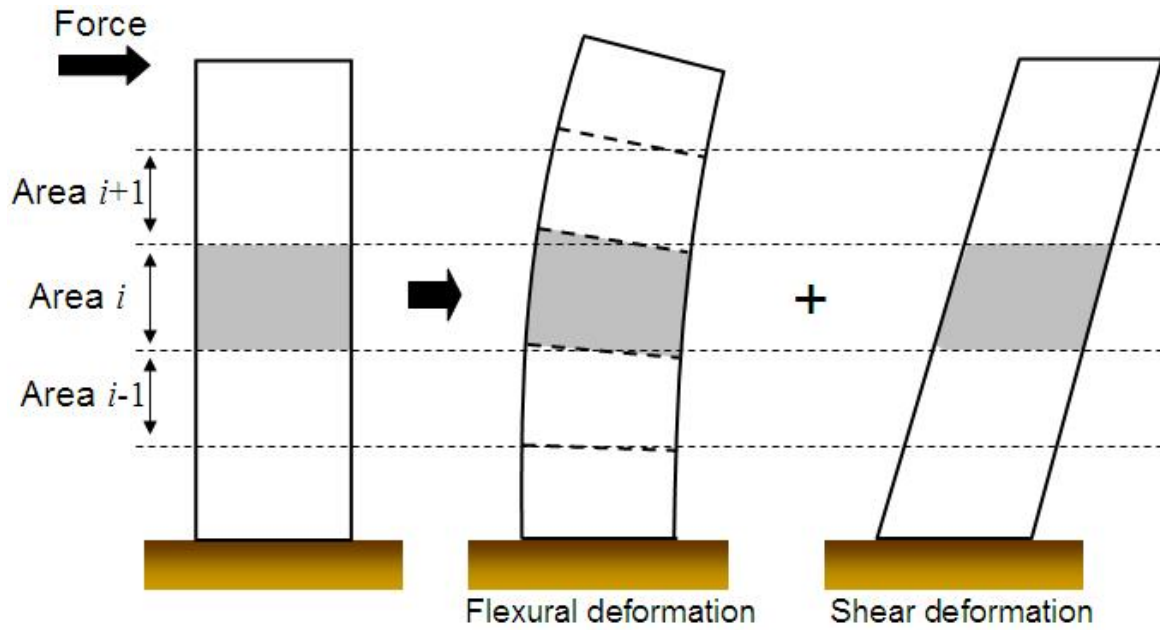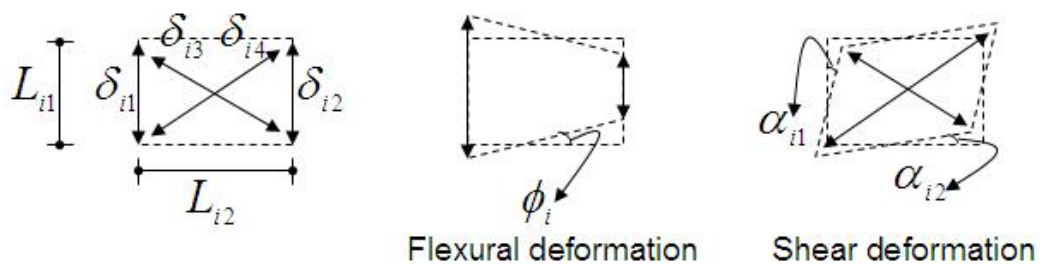
Fig. 3.14 Decomposition of flexural and shear deformation

Figure 3.15 illustrates distribution of a ratio of decomposed deformations to total deformation, δ_{dcp} /δ_{exp}. The decomposed deformation consists of flexural and shear deformation. In specimens with a/D=1.0, a ratio of shear deformation to total deformation of S-10-L42 was larger than that of S10-L63. It can be seen that amount of shear reinforcement (ρ_w) significantly affected shear deformation of beam. A ratio of flexural deformation to total deformation in specimens with a/D=2.0 (S-20-L21 and S-20-L42) gradually increased while that in specimens with a/D=1.0 (S-10-L42 and S-10-L63) did not. It points out that flexural deformation is dominant in large shear span ratio beams. It is noted that decomposed total deformation, δ_{dcp}, in large drift angle was not coincided with measured lateral displacement, δ_{exp}, well. It is necessary to develop the measurement method of flexural and shear deformation which can evaluate experimental deformation in a good accuracy.
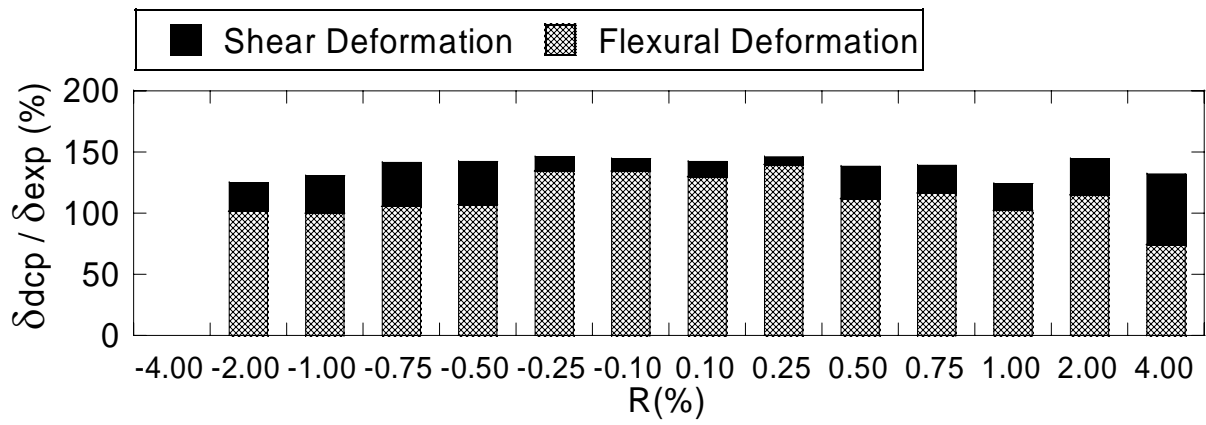
(a) S-10-L42
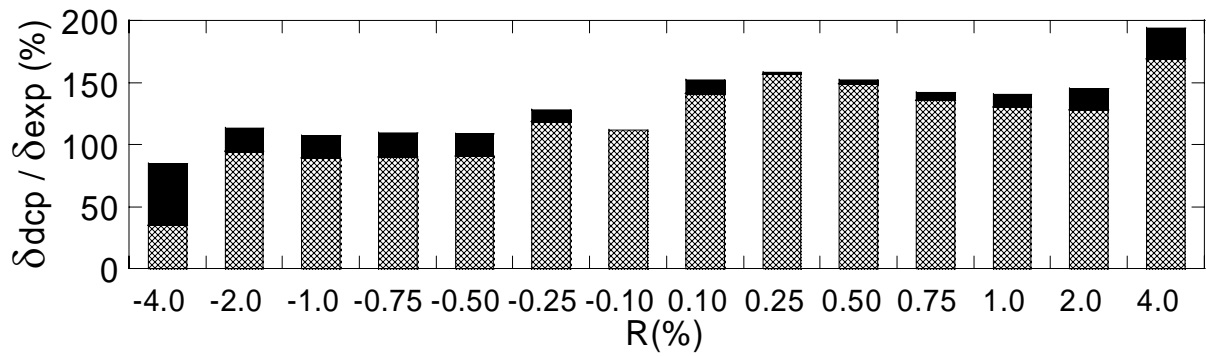
(b) S-10-L63
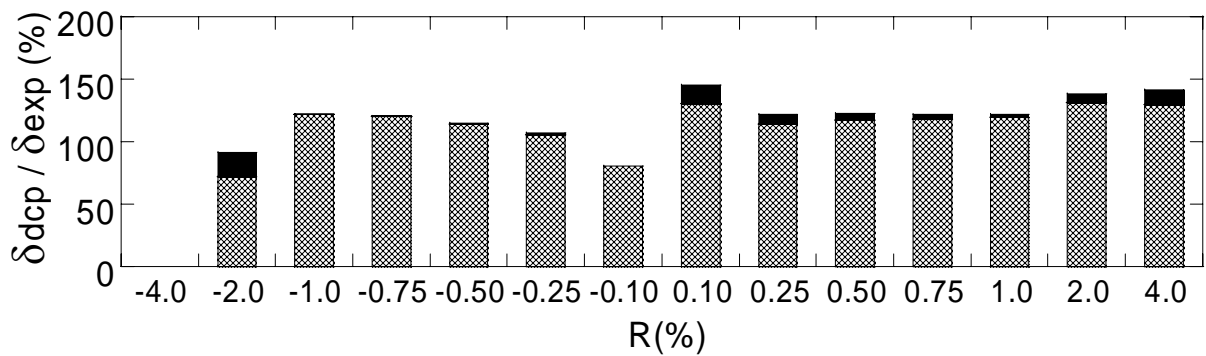
(c) S-15-L21

(d) S-15-L42

Fig. 3.15 Distribution of $\delta_{dcp}/\delta_{exp}$ for a difference of drift angle, R
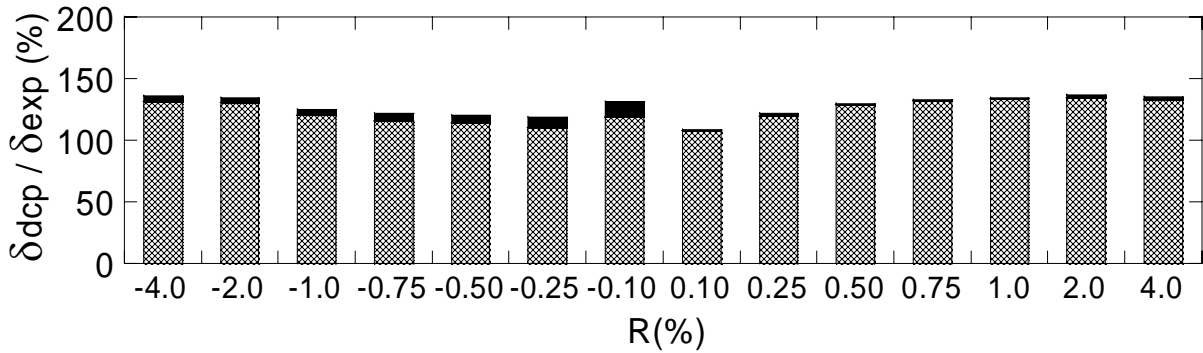
(e) S-15-L63
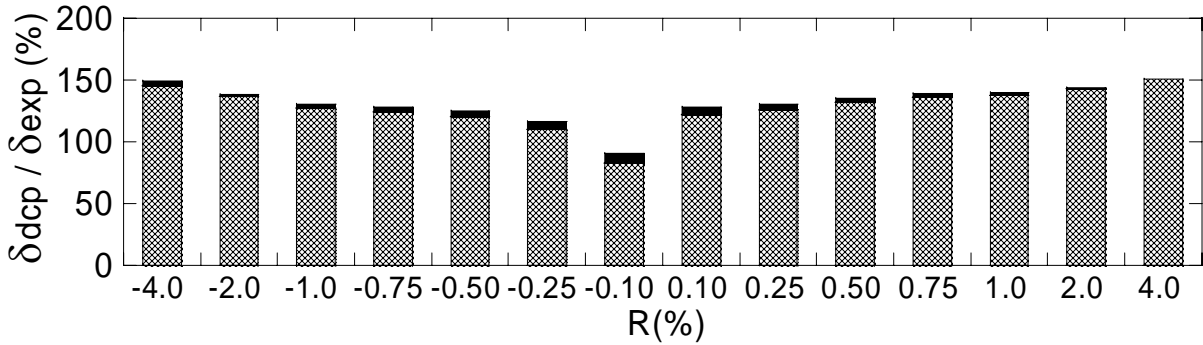
(f) S-20-L21

(g) S-20-L42

Fig. 3.15 Distribution of $\delta_{dcp}/\delta_{exp}$ for a difference of drift angle, R

Tensile stress distribution

(1) PT tendon

Figure 3.16 illustrates the stress distribution of PT tendons in test specimens for difference of drift angle, R: (a) S-10-L42; (b) S-10-L63; (c) S-15-L21; (d) S-15-L42; (e) S-15-L63; (f) S-20-L21; and (g) S-20-L42. The horizontal dashed lines represent yield strength of prestressing strands, f_{py}. Upper and lower graphs in each specimen plot the distribution of tensile stress of prestressing strands in upper and lower side, respectively. In Fig. 3.16, compression and tension fiber at critical section in positive loading direction also indicated as `Compression side` and `Tension side`, respectively.

As shown in Fig. 3.16, tensile stress of PT tendon concentrates in gap joints. It point out that flexural deformation concentrates within selected discrete regions of the member, typical referred to plastic hinge or gap joints in precast concrete members. In flexural compression zone at critical section, tensile stress of prestressing strands kept its initial prestress. It is because most compression resultant force is resisted by concrete while prestressing strands does not significantly resist against compression force.
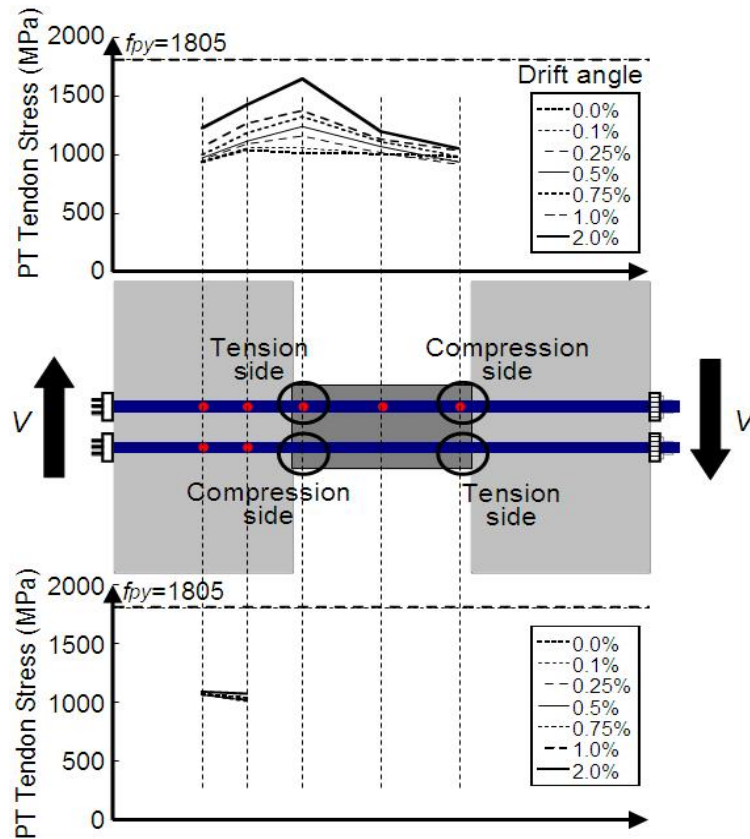
(a) S-10-L42

Fig. 3.16 Distribution of tensile stress of prestressing strands
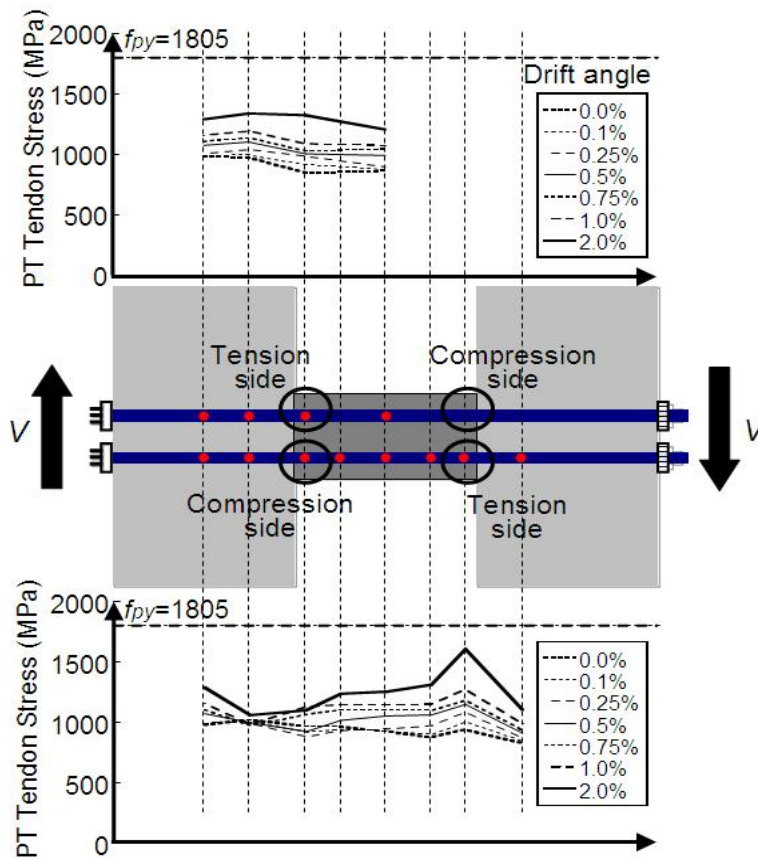
(b) S-10-L63
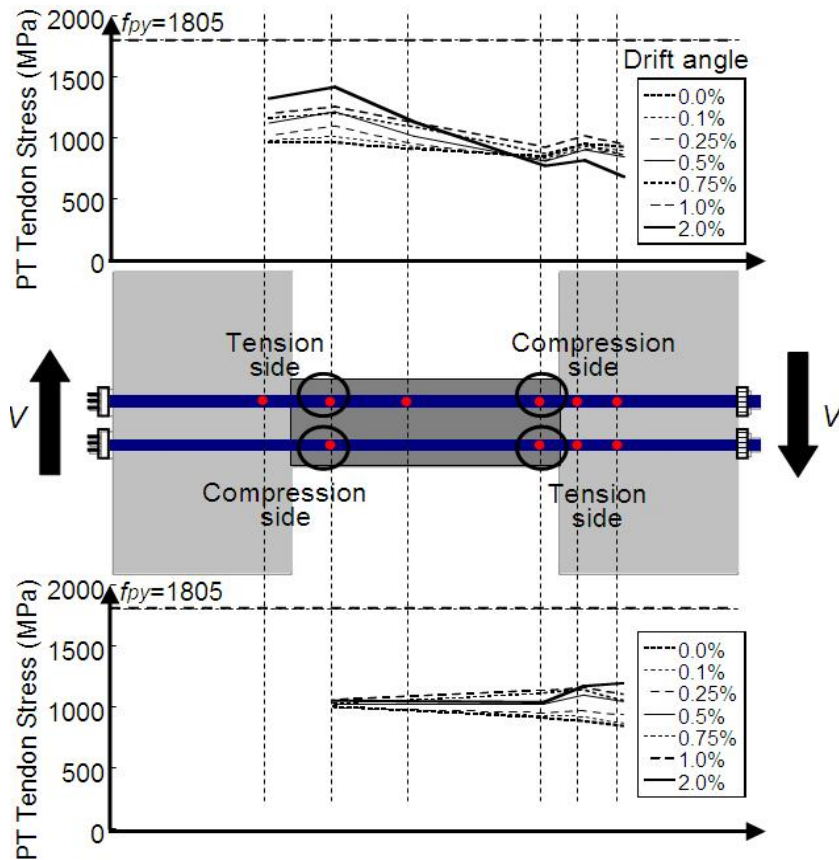
(c) S-15L21

Fig. 3.16 Distribution of tensile stress of prestressing strands
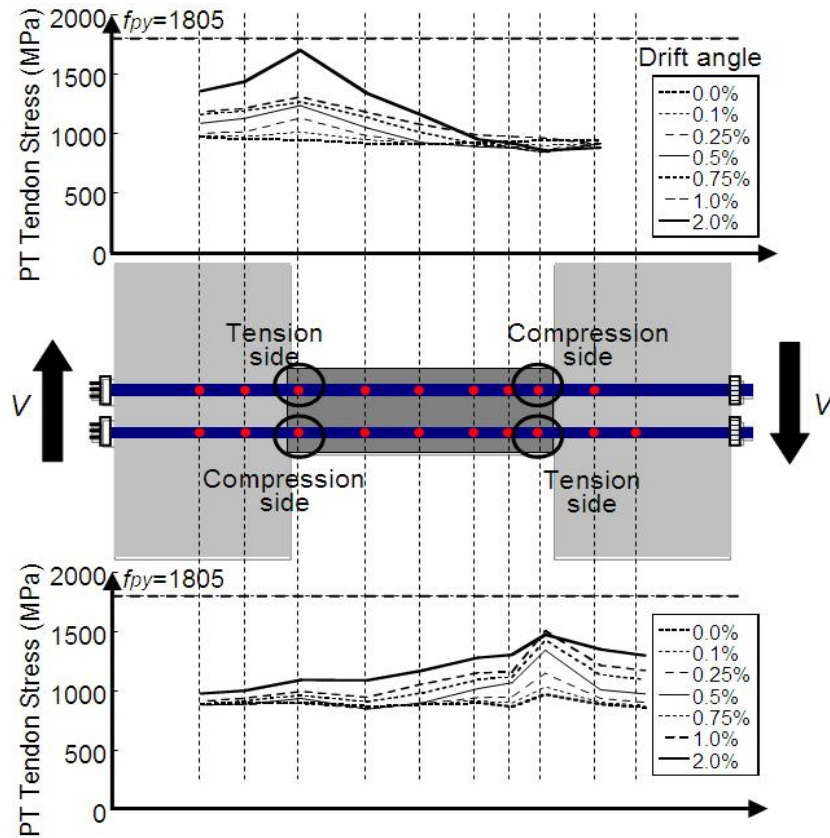
(d) S-15-L42
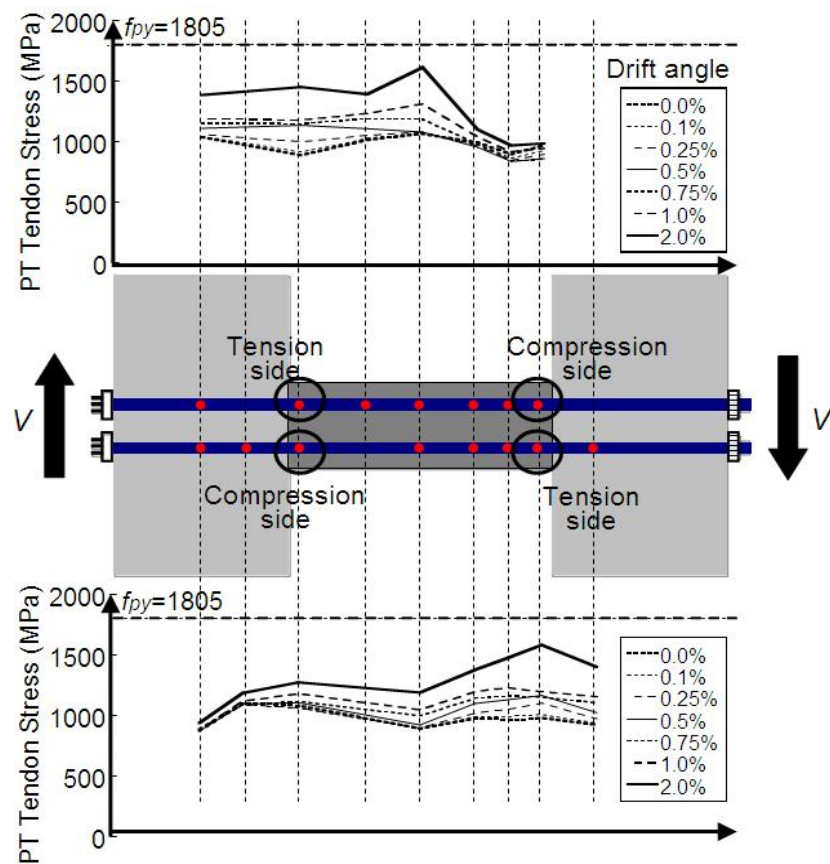
(e) S-15-L63

Fig. 3.16 Distribution of tensile stress of prestressing strands

5 9
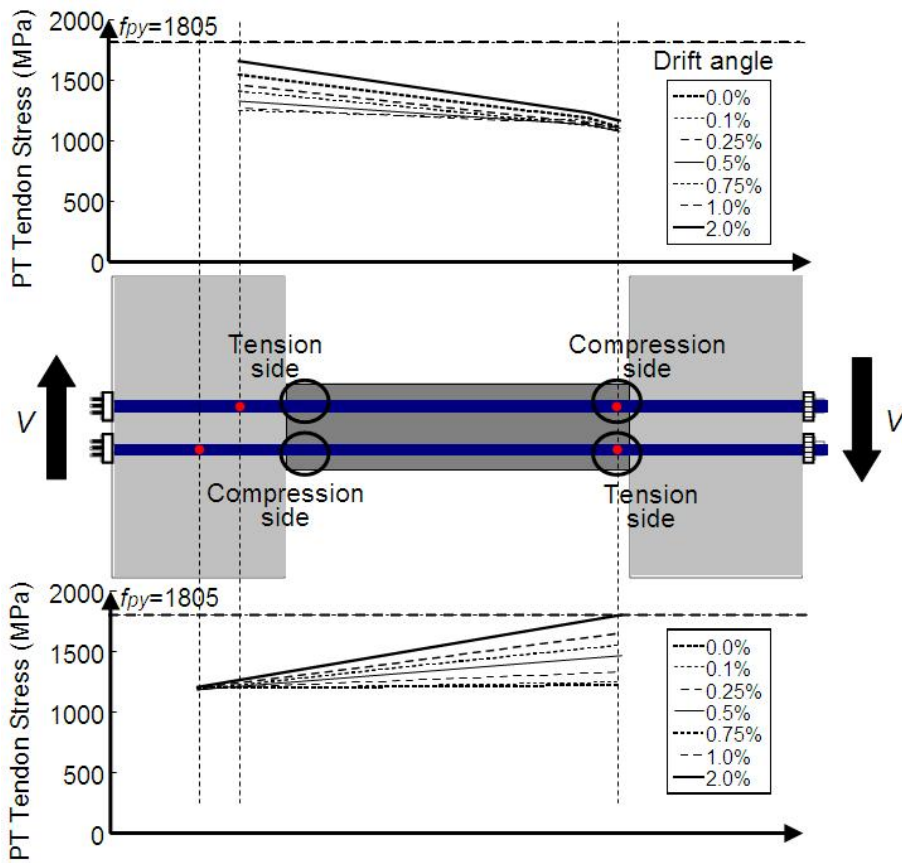
(f) S-20-L21
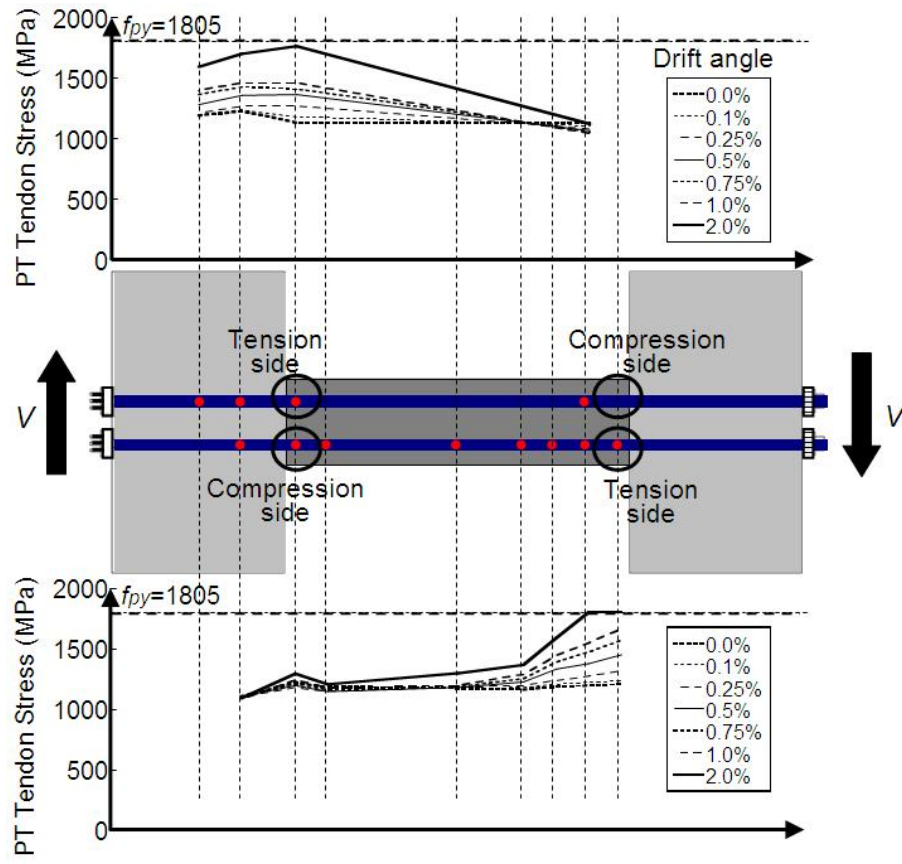
(g) S-20-L42

Fig. 3.16 Distribution of tensile stress of prestressing strands

(2) Non-prestressed longitudinal bar

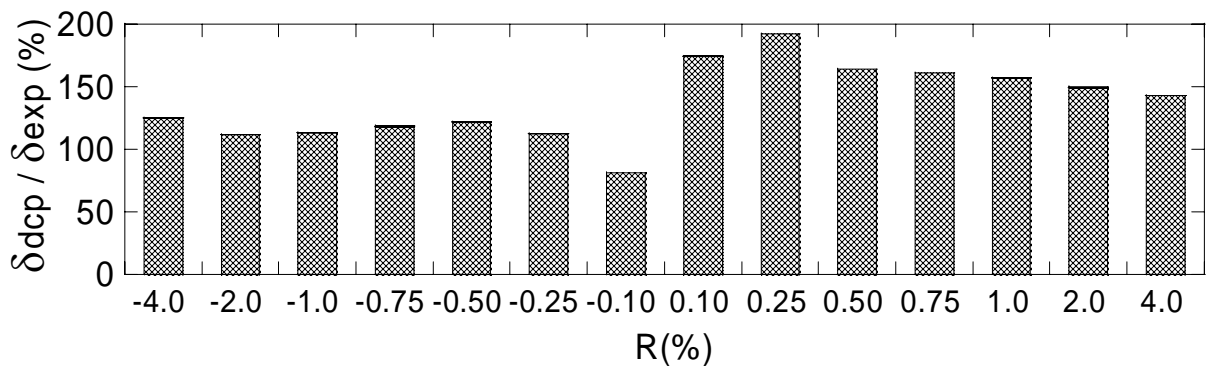Figure 3.17 illustrates the stress distribution of non-prestressed longitudinal bars in test specimens in a same manner with Fig. 3.16: (a) S-10-L42; (b) S-10-L63; (c) S-15-L21; (d) S-15-L42; (e) S-15-L63; (f) S-20-L21; and (g) S-20-L42. Compressive yield strength of longitudinal bar, f_{ry}, is also represented in Fig. 3.17. As shown in Fig. 3.17, non-prestressed longitudinal bars in flexural compression zone reached their yield strength while those in flexural tension zone did not. It is because tensile force of the longitudinal bar is hardly transferred to anchorage zones due to discontinuity of longitudinal reinforcing bars. It point out that bond stress of non-prestressed longitudinal bars due to tensile force does not significantly develop and then, shear resistance by the bond stress of longitudinal bar might small as neglected.

(a) S-10-L42
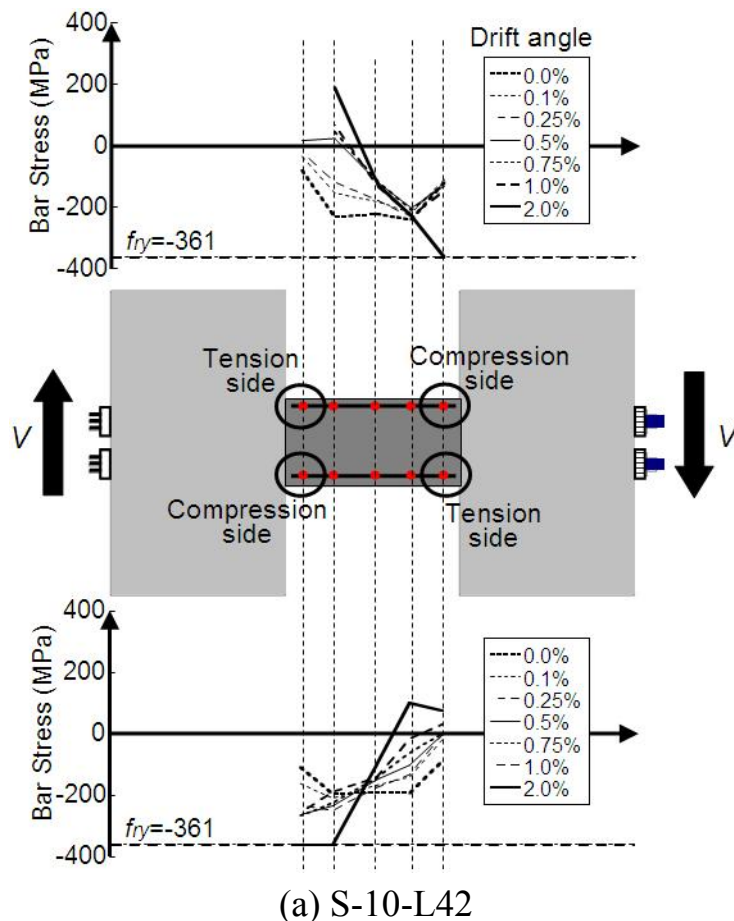
Fig. 3.17 Distribution of tensile stress of non-prestressed longitudinal bars
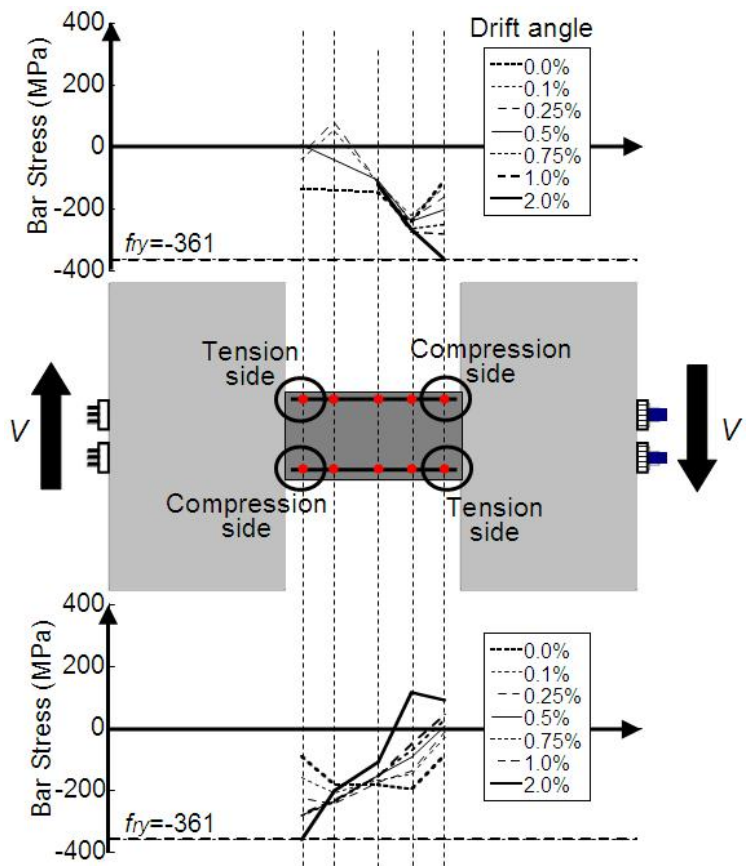
(b) S-10-L63
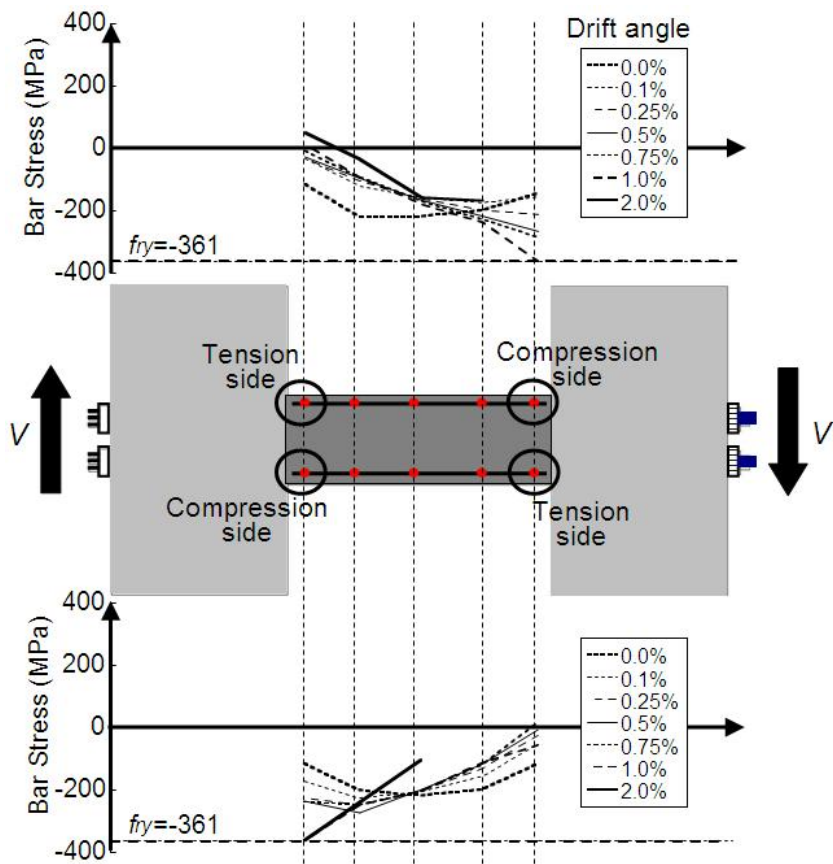
(c) S-15-L21

Fig. 3.17 Distribution of tensile stress of non-prestressed longitudinal bars

(d) S-15-L42

(e) S-15-L63

Fig. 3.17 Distribution of tensile stress of non-prestressed longitudinal bars

6 3

(f) S-20-L21

(g) S-20-L42

Fig. 3.17 Distribution of tensile stress of non-prestressed longitudinal bars

(3) Shear reinforcement

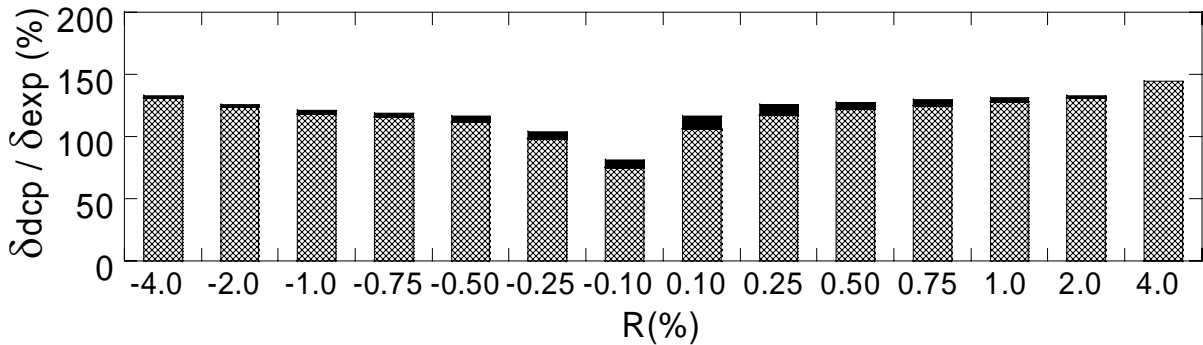Figure 3.18 illustrates the tensile stress distribution of shear reinforcements in test specimens: (a) S-10-L42; (b) S-10-L63; (c) S-15-L21; (d) S-15-L42; (e) S-15-L63; (f) S-20-L21; and (g) S-20-L42. Tensile yield strength of shear reinforcement, f_{wy}, is indicated in the figure. As shown in Fig. 3.18, no shear reinforcement yield in all specimens. In specimens failed in shear (S-10-L42 and S-15-L21) and shear after flexural yielding (S-10-L63 and S-20-L21), tensile stress of shear reinforcement at mid-span was larger than that at both ends of beam. It points out that shear strain at mid-span of the beam is the largest, then concrete strut subjected to uniaxial stress exists at both ends of the post-tensioned precast concrete beam (fan action).
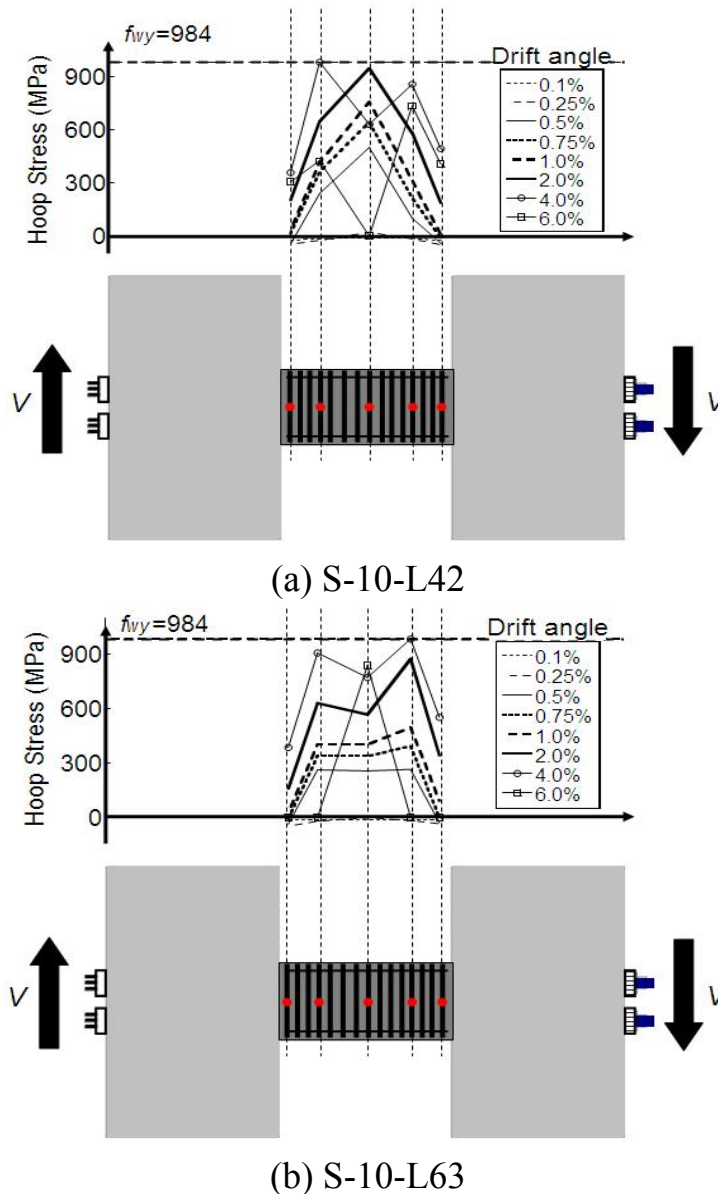
(a) S-10-L42

(b) S-10-L63

Fig. 3.18 Distribution of tensile stress of shear reinforcement

6 5
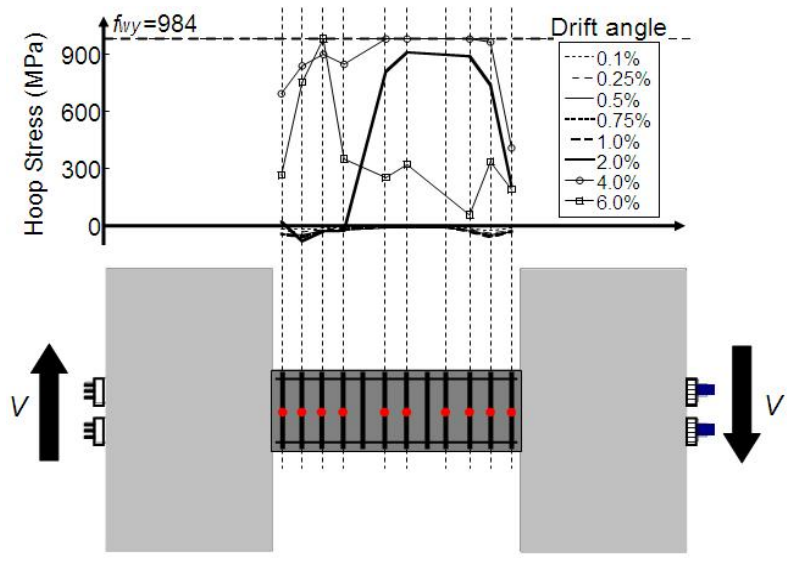
(c) S-15-L21
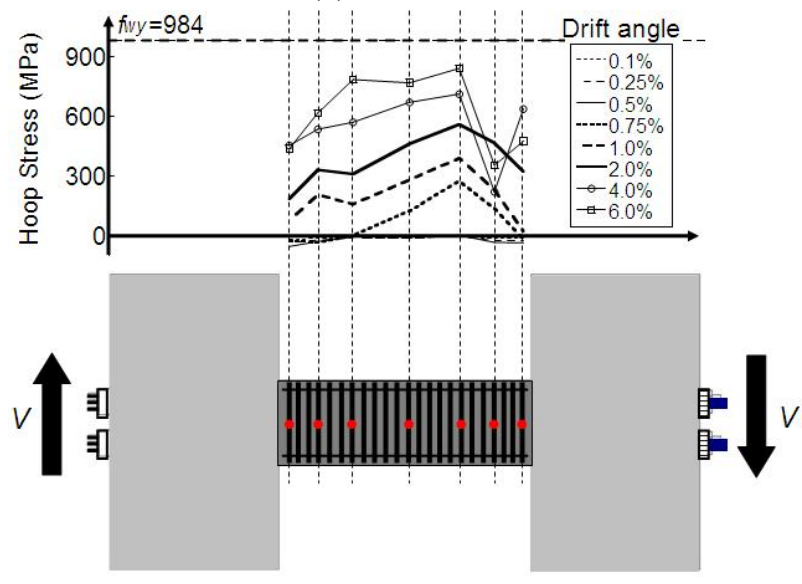
(d) S-15-L42
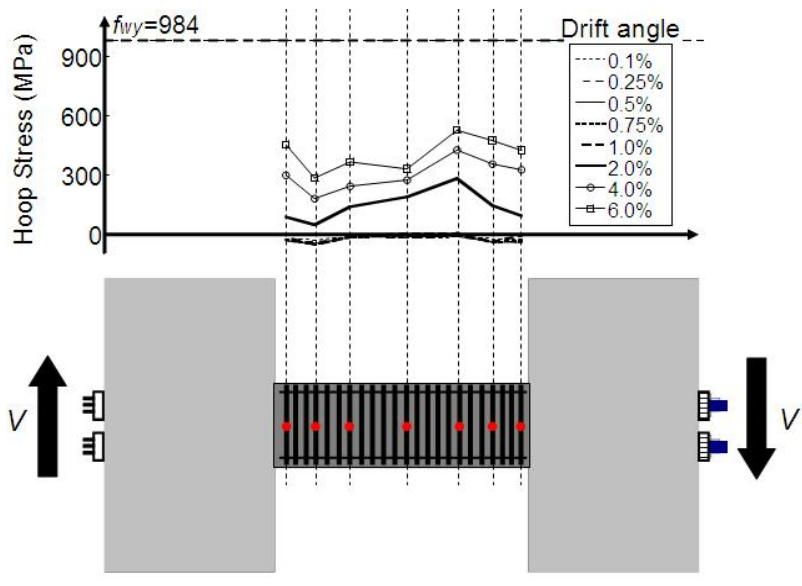
(e) S-15-L63

Fig. 3.18 Distribution of tensile stress of shear reinforcement
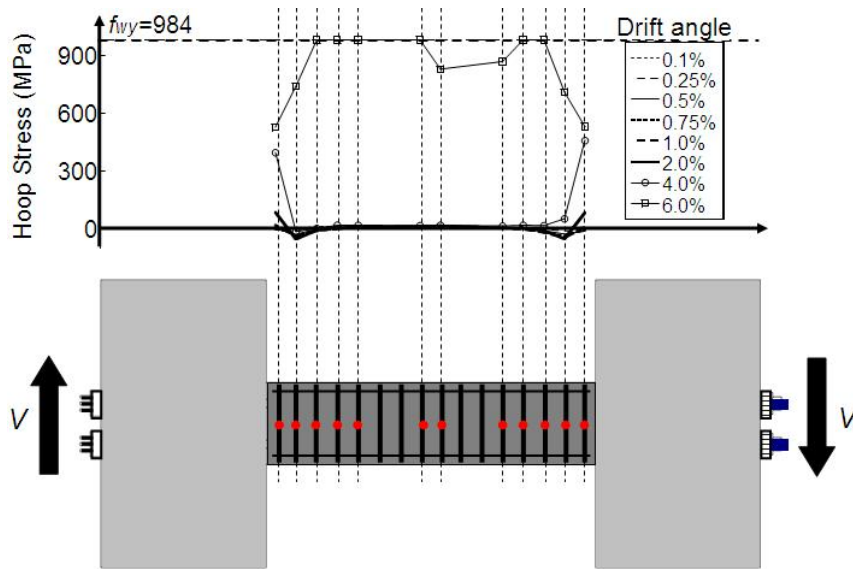
(f) S-20-L21
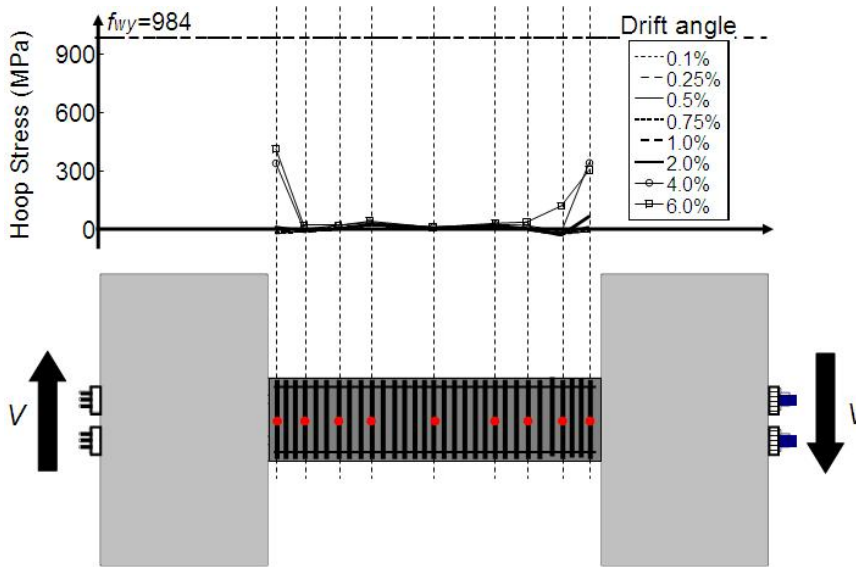
(g) S-20-L42

Fig. 3.18 Distribution of tensile stress of shear reinforcement

Residual ratio of tensile force of PT tendon

Figure 3.19 plots relationshop between the ratio of residual tensile force of PT tendon to effective prestressing force, P/P_e and drift angle, R. Vertical and horizontal axis in Fig. 3.19 represent P/P_e and R, respectively. The residual tensile forces of PT tendon, P, are obtained by measured tensile strain of PT tendon in top and bottom joints (PCL_T and PCL_B for prestressing strands in left side, and PCR_T and PCR_B for prestresiing strands in right side). P_y in Fig. 3.19 indicates yield force of prestressing strands. As shown in Fig. 3.19, P/P_e, in all specimens increase until peak load (R=2.0% cycle). It can be seen that the bond stress of prestressing strands is large enough to transfer tensile stress. In S-10-L42, S-10-L63, S-15-L21, and S-15-L42, P/P_e decreases after R=4.0%

cycle. It is because an increase in compressive axial strain due to crushing of concrete in flexural compression zone leads to the decrease in effective prestressing force of prestressing strands.
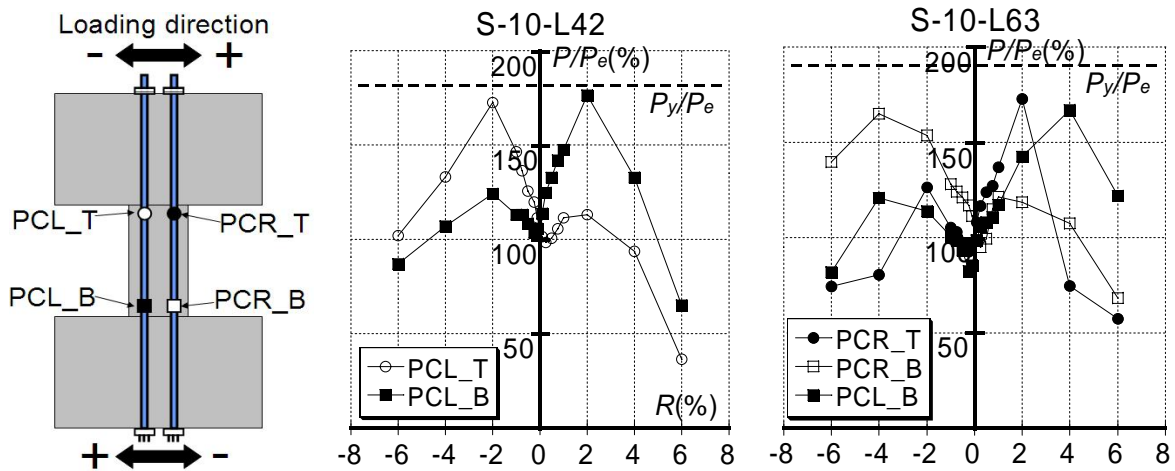
Fig. 3.19 Residual ratio of tensile force of PT tendon
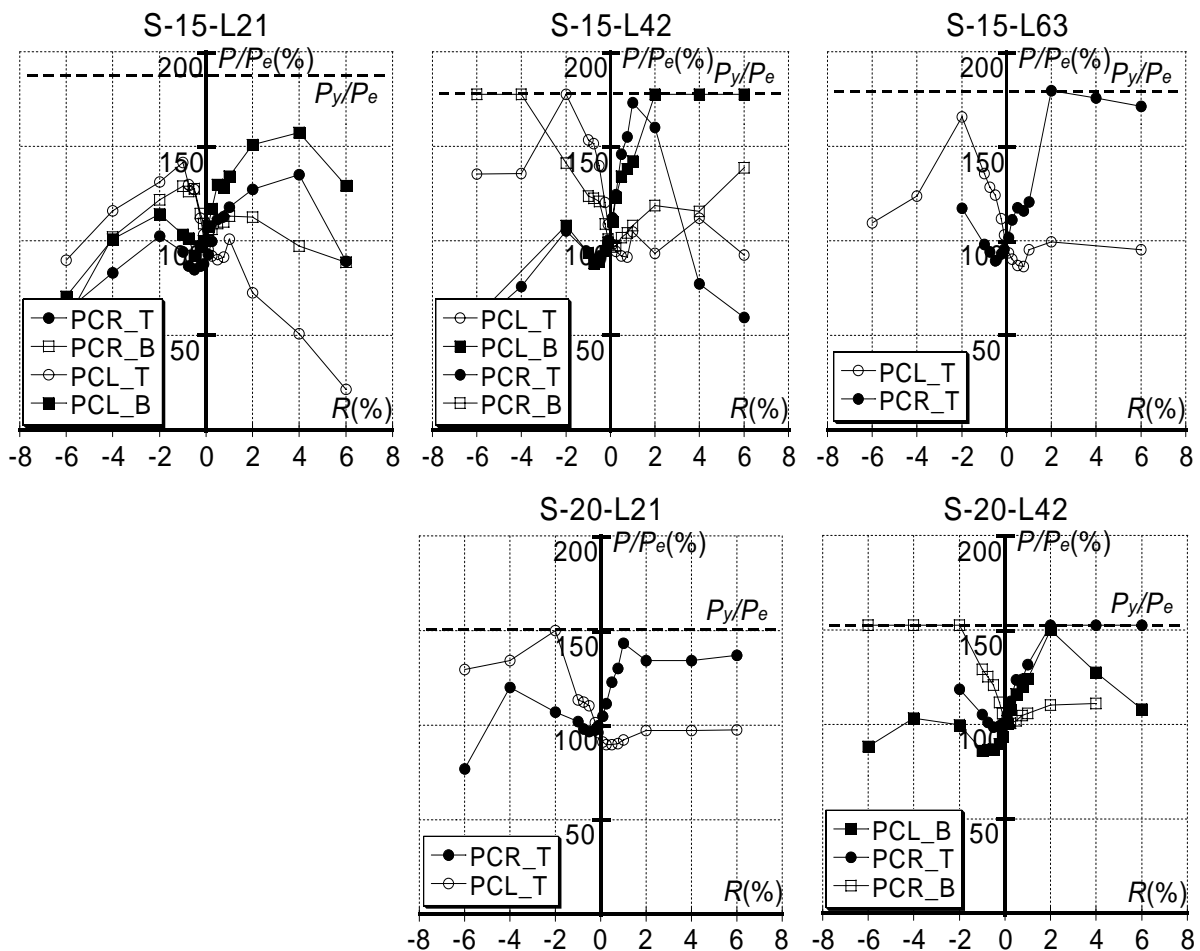
Fig. 3.19 Residual ratio of tensile force of PT tendon

Bond stress

(1) PT tendon

Figure 3.20 plots the distribution of bond stress of PT tendons. Upper and lower graphs of each specimen plot the distribution of bond stress of prestressing strands in upper and lower side, respectively. Horizontal dashed lines represent bond strength of prestressing strand, τ_{max}. For bond strength of prestressing strand, τ_{max}, it is assumed as 4 MPa referred to analytical bond strength equations [3.4-3.6] as shown in Table. 3.5. As shown in Fig. 3.20, the bond stress of prestressing strands in S-10-L63, S-15-L42, and S-15-L63 reached their bond strength. However, the bond stress of prestressing strands in the specimens did not significantly affect the shear strength. Moreover, there is negative bond stress in region A of all specimens as shown in Fig. 3.20. It is because tensile stress of prestressing strands at gap joints (region A in Fig. 3.20) is larger than the tensile stress at region B and C in Fig. 3.20. It is closely related to the deformation behavior of precast concrete member.

Table 3.5 Analytical bond strength [3.4-3.6]

Reference	Analytical bond strength	Equation
[3.4]	2.0 to 4.5	
[3.5]	4.5 to 4.9	$\tau_{max} = 0.602\sqrt{F_g}$
[3.6]	4.0 to 4.4	$\tau_{max} = 0.53\sqrt{F_g}$
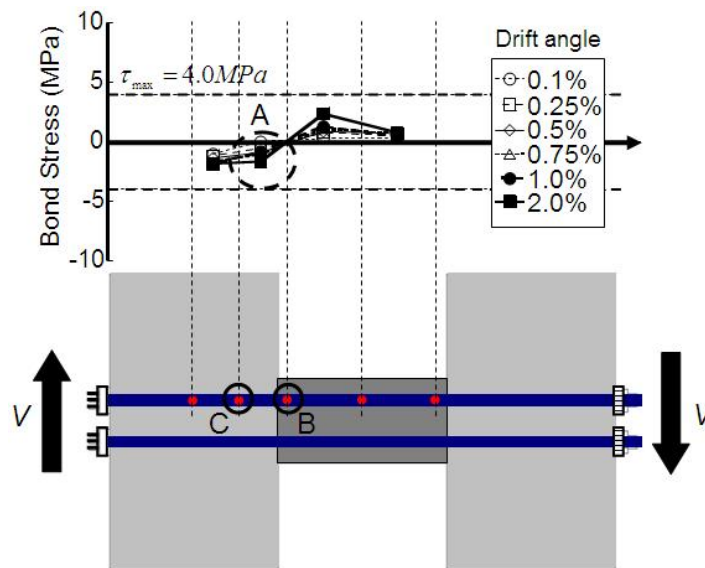
(a) S-10-L42

Fig. 3.20 Distribution of bond stress of PT tendon
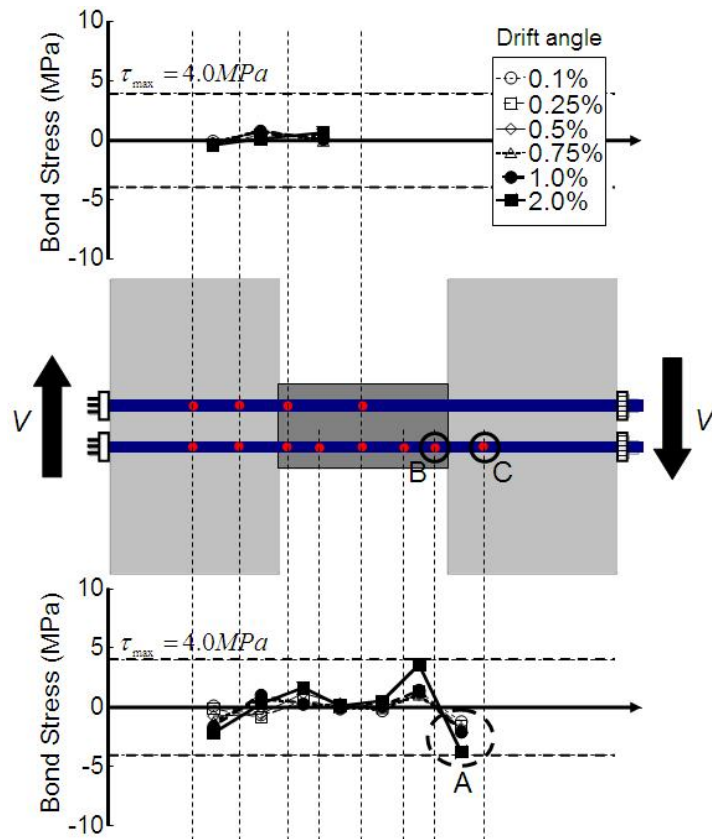
(b) S-10-L63
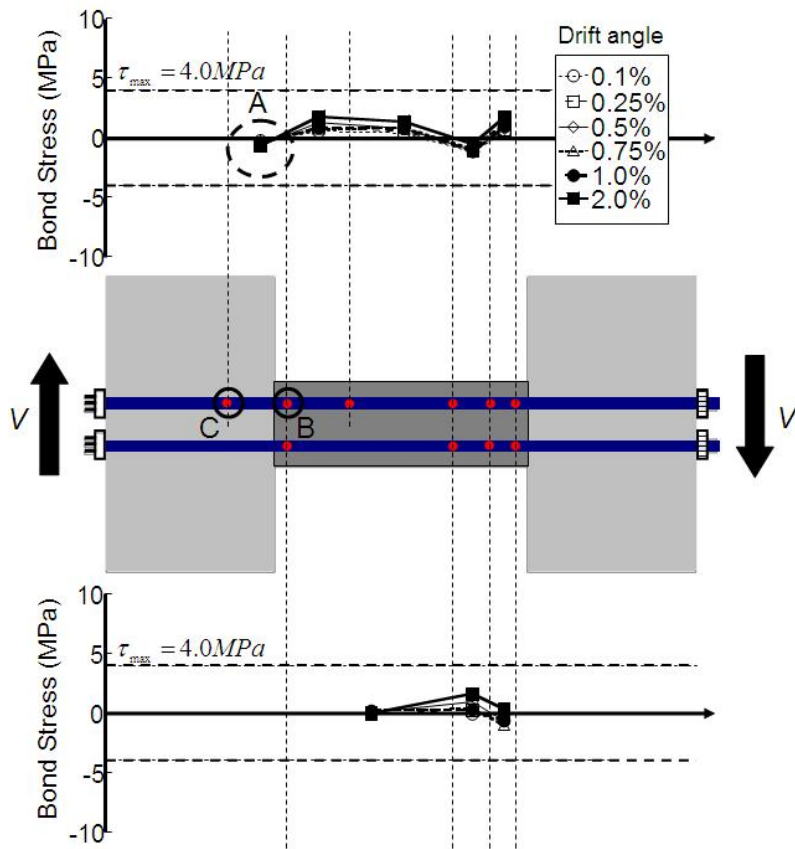

(c) S-15-L21

Fig. 3.20 Distribution of bond stress of PT tendon
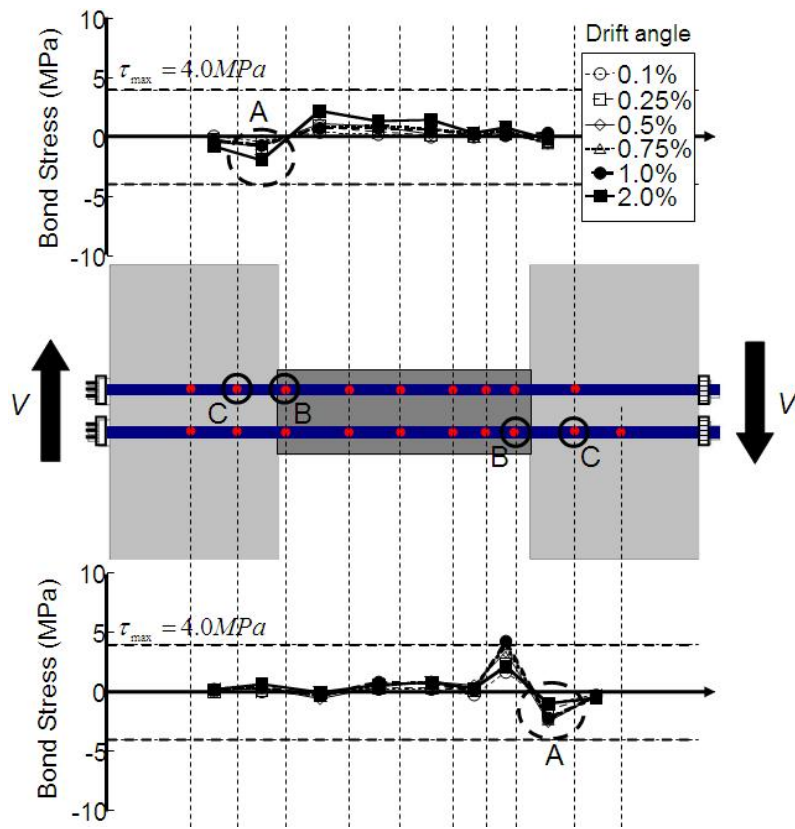
(d) S-15-L42
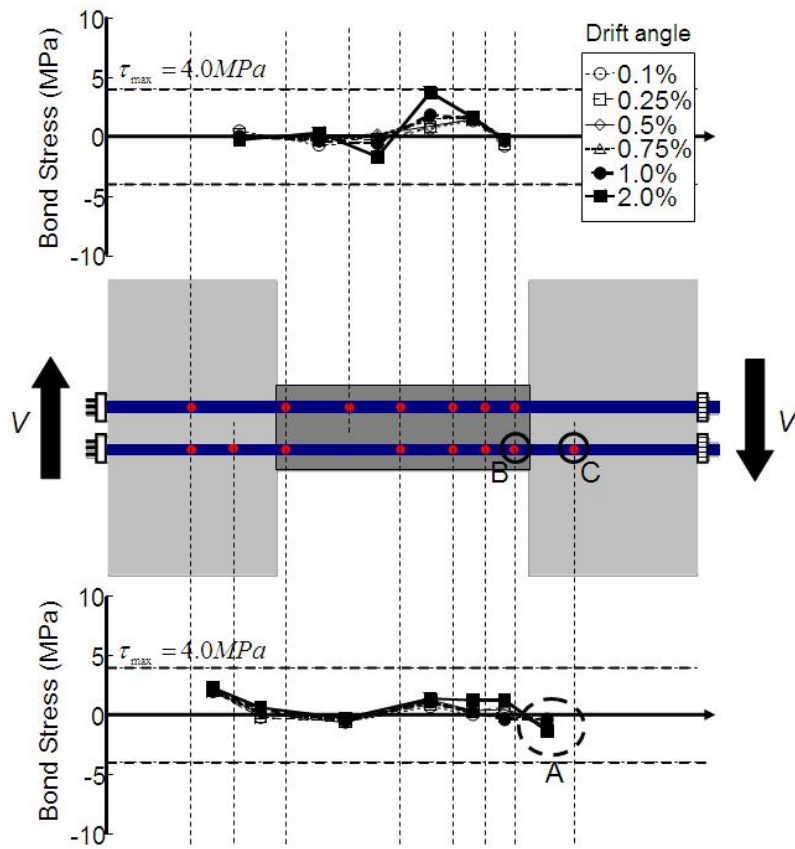
(e) S-15-L63

Fig. 3.20 Distribution of bond stress of PT tendon
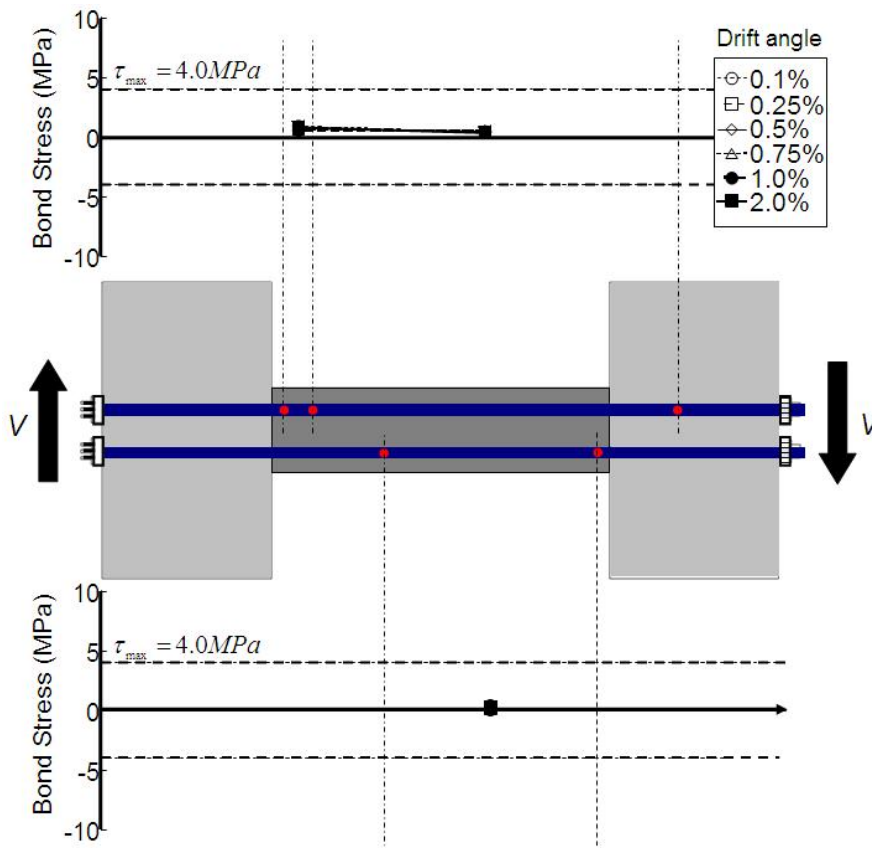
(f) S-20-L21
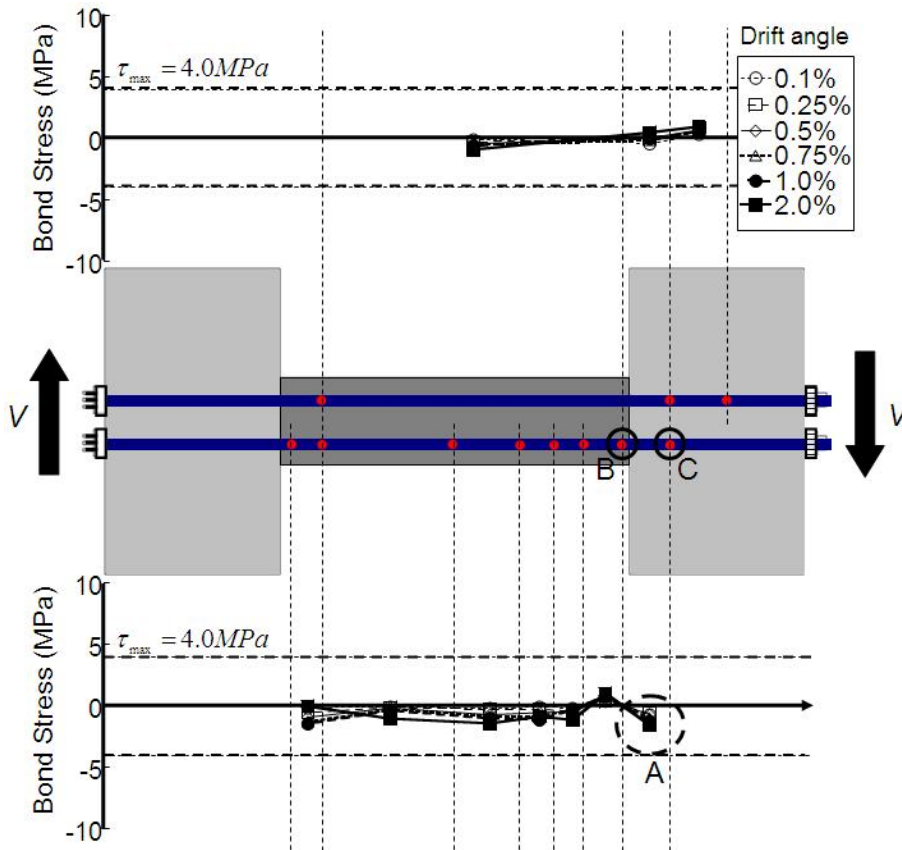
(g) S-20-L42
Fig. 3.20 Distribution of bond stress of PT tendon

(2) Non-prestressed longitudinal bar

Figure 3.21 plots the distribution of bond stress of non-prestressed longitudinal bars. The bond strength of longitudinal bar, τ_{max}, was obtained as shown in Table 3.6 referred to reference [3.7]. As shown in Fig. 3.21, no shear reinforcements in all specimens reached their bond strength. The bond stress of longitudinal bars hardly developed until peak load (R=2.0% cycle). It is coincided with Yoshida`s test results [3.8] that the bond stress of cut-off longitudinal bars in precast concrete members does not increase.

Table 3.6 Analytical bond strength [3.7]

| Specimen	Analytical bond strength
S-10-L42	6.8
S-10-L63	8.4
S-15-L21	5.9
S-15-L42	7.0
S15-L63	8.7
S-20-L21	5.6
S-20-L42	6.7
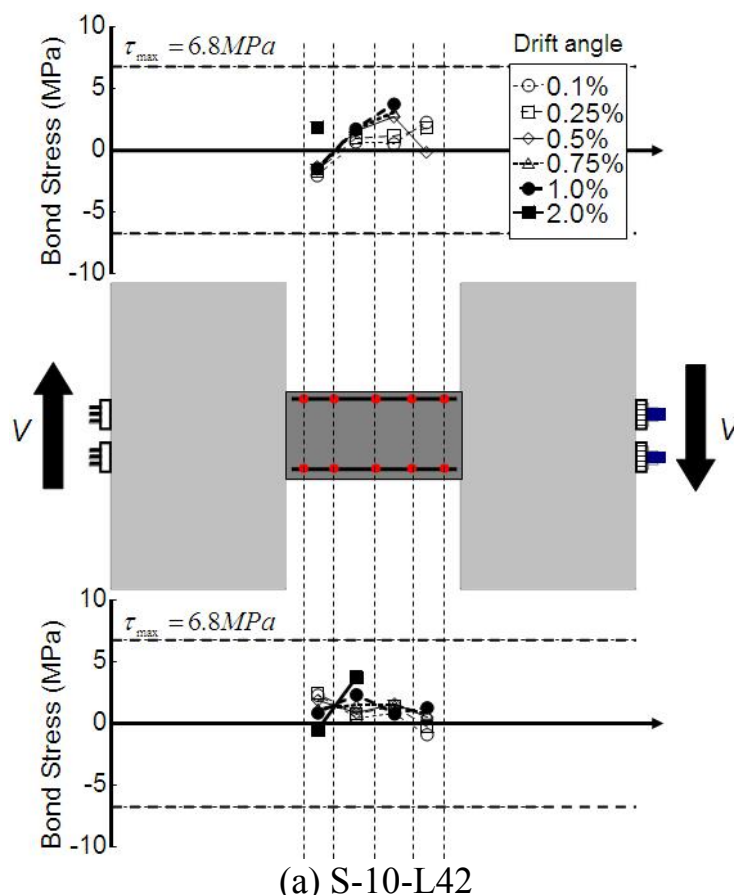
(a) S-10-L42

Fig. 3.21 Distribution of bond stress of non-prestressed longitudinal bar
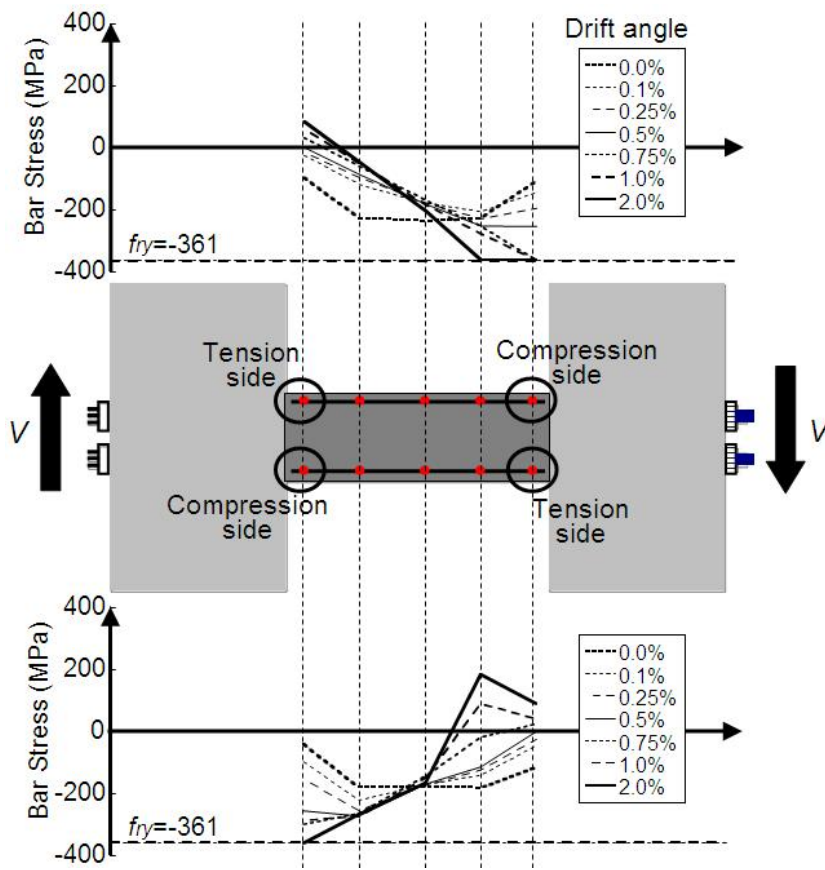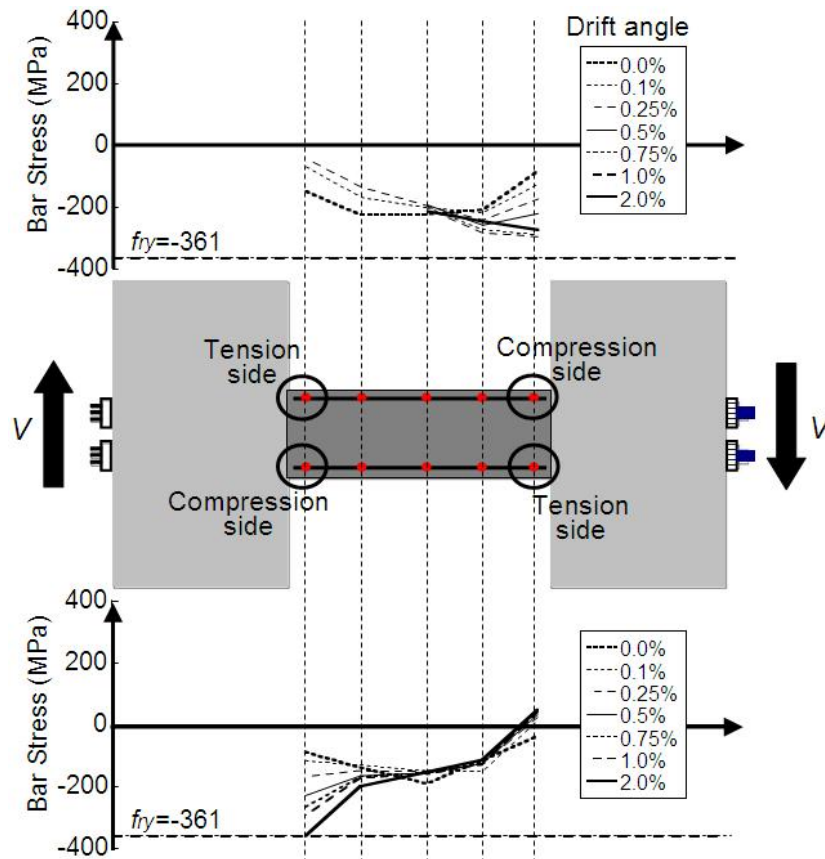
7 3
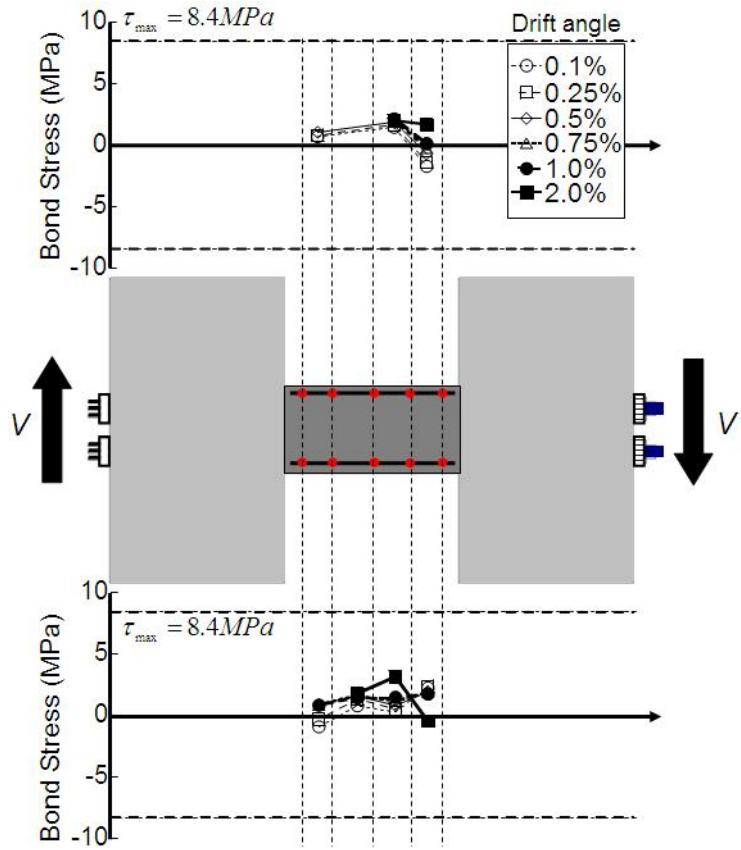
(b) S-10-L63
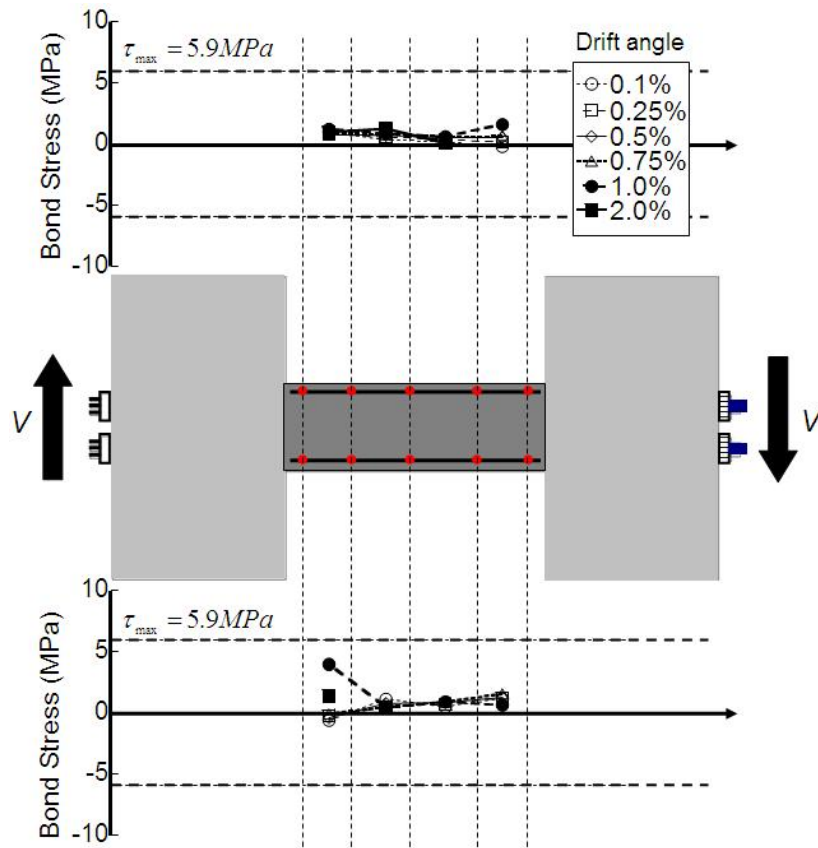
(c) S-15-L21

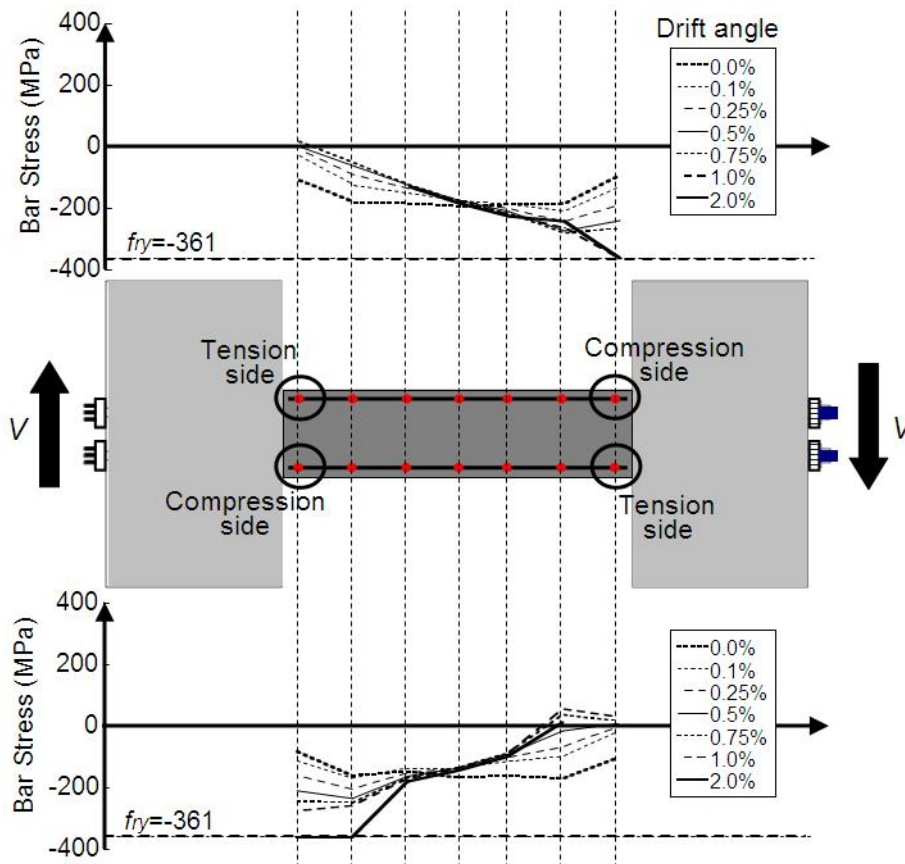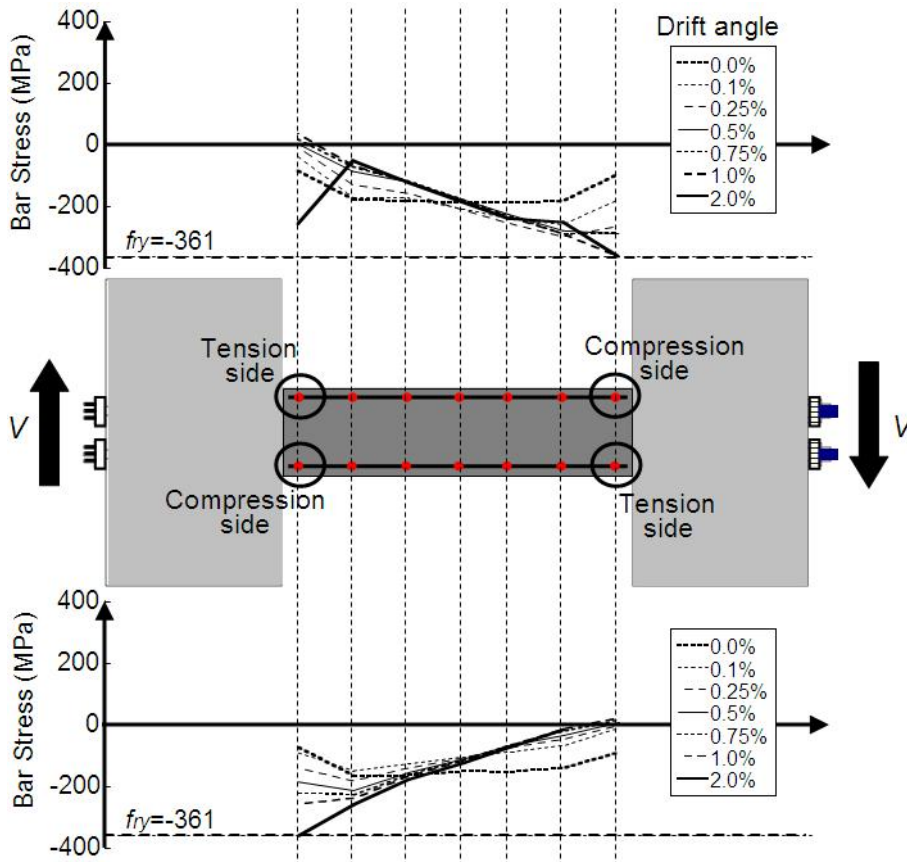Fig. 3.21 Distribution of bond stress of non-prestressed longitudinal bar

7 4
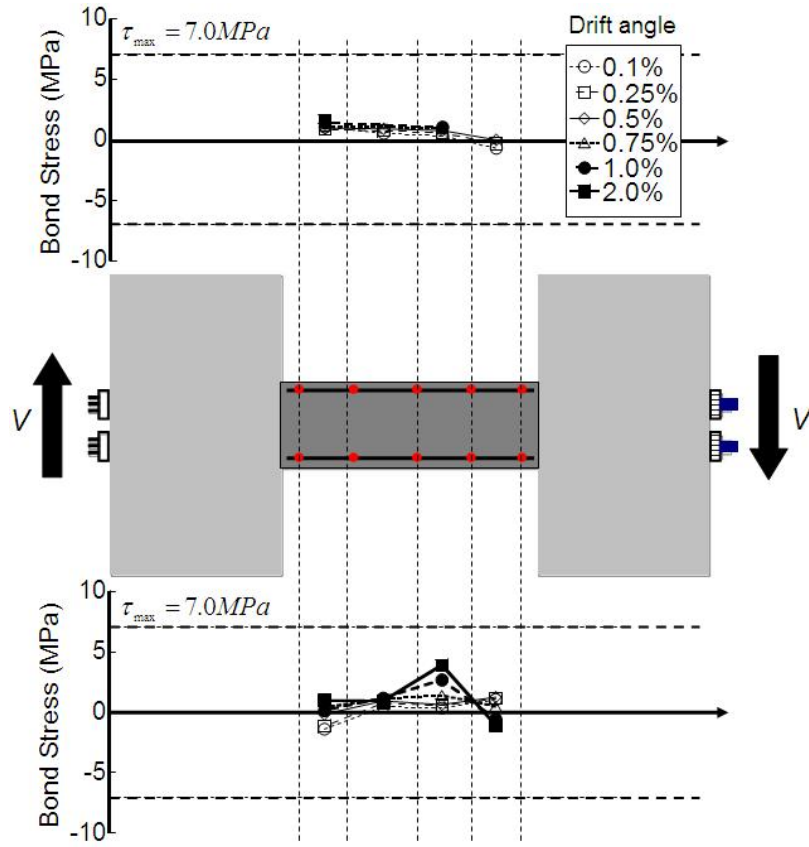
(d) S-15-L42
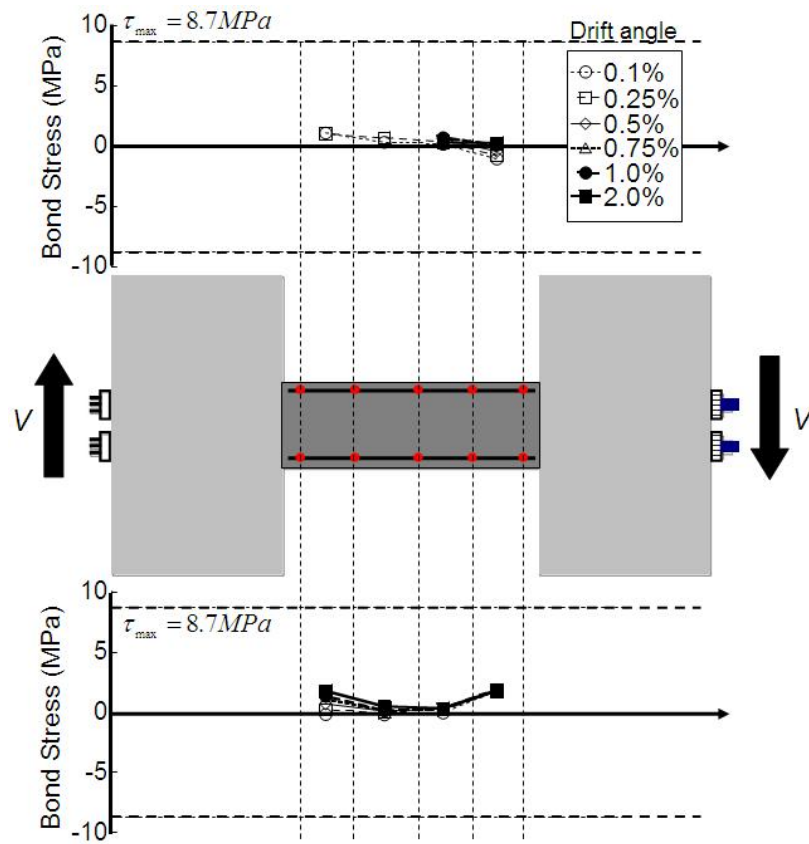
(e) S-15-L63

Fig. 3.21 Distribution of bond stress of non-prestressed longitudinal bar
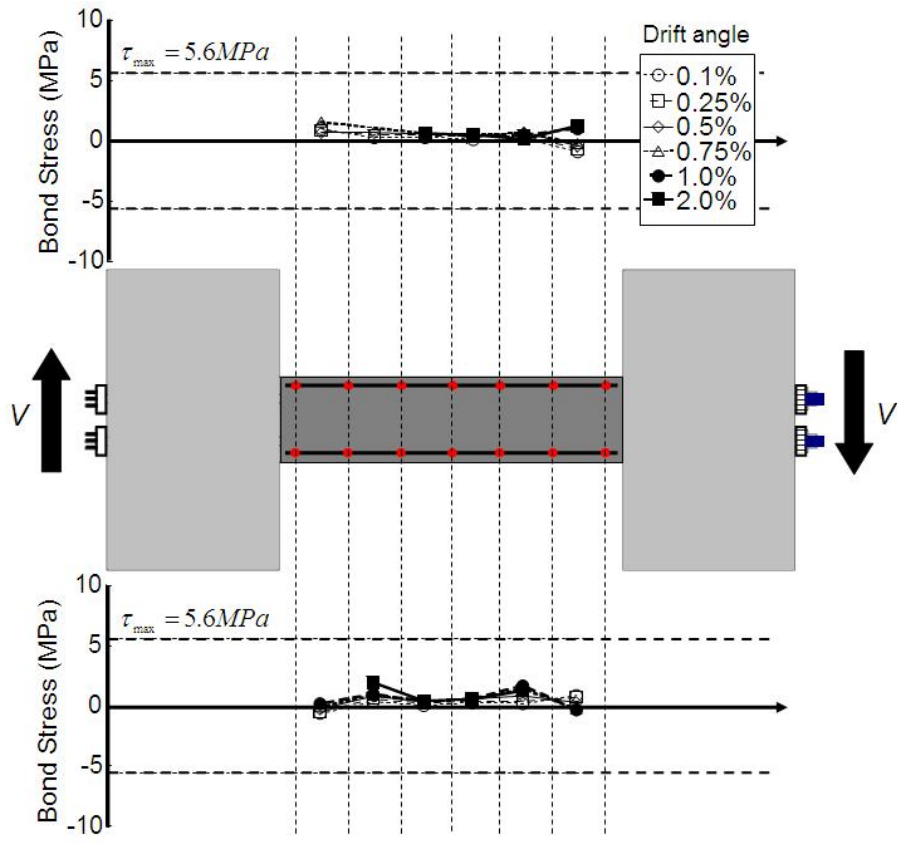
(f) S-20-L21
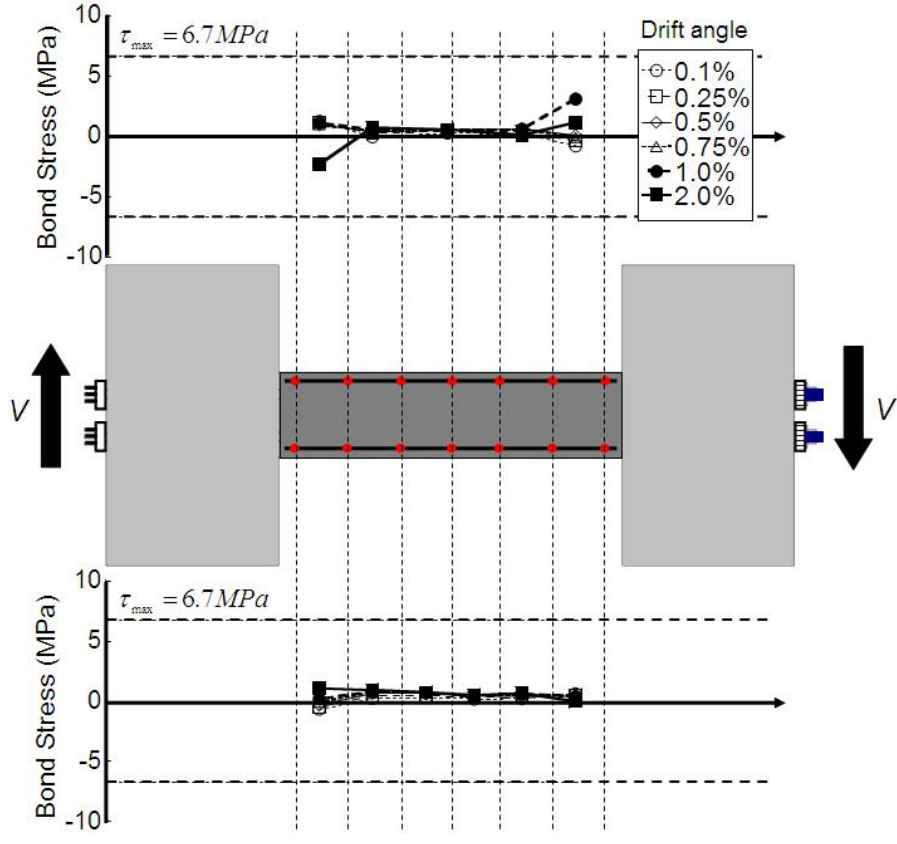
(g) S-20-L42

Fig. 3.21 Distribution of bond stress of non-prestressed longitudinal bar

7 6

Shear crack width

To investigate the behavior of shear crack, the width of shear crack had been measured by linear displacement transducer attached on the surface shown in Fig. 3.22. The width of shear crack was continuously monitored. Fig. 3.23 plots relationship shear force and observed shear crack width in S-10-L42, S-10-L63, S-15-L21, and S-15-L42. As shown in Fig. 3.23, shear crack width in specimen failed in DT (S-15-L21) rapidly increases immediately after initiation of primary shear cracking (●). In other failure mode, shear crack width gradually develops until peak load. It points out that primary opening of shear crack in member failing in diagonal tension leads to shear failure. Therefore, quantification of relationship between opening of primary shear crack and shear resistance needs for investigation of shear failure mechanism which can apply to diagonal tension (DT) failure as well as shear tension (ST), shear compression (SC), or flexural shear compression (FSC).
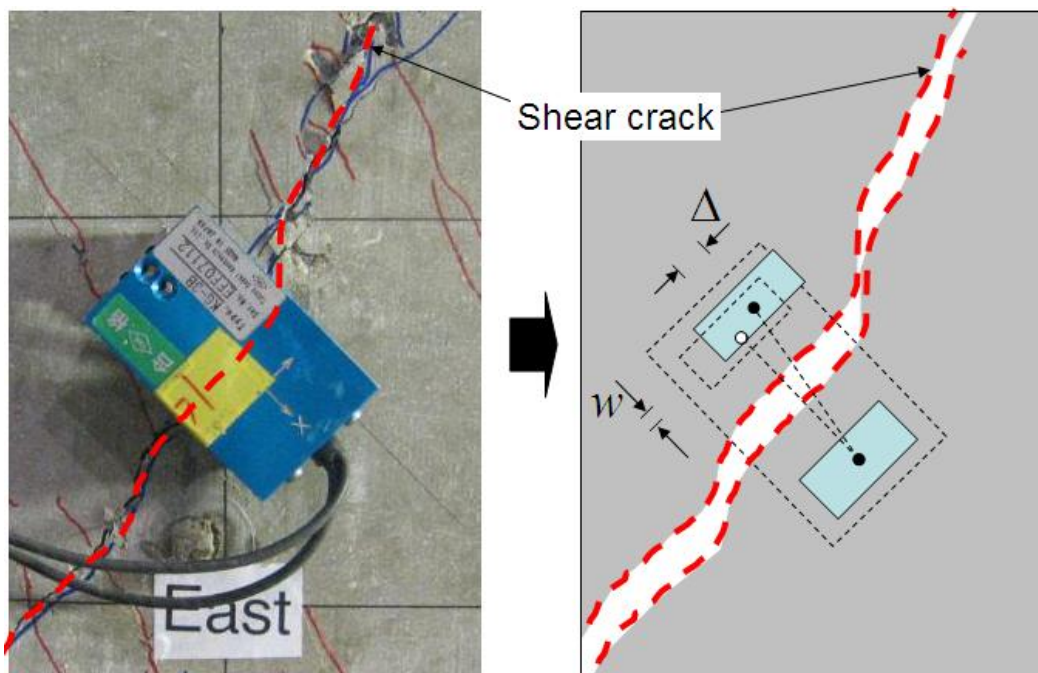
Fig. 3.22 Measurement of shear crack width by linear displacement transducer

(a) S-10-L42 (SC)　　　　　　　　(b) S-10-L63 (FS)

(c) S-15-L21 (DT)　　　　　　　　(d) S-15-L42 (F)
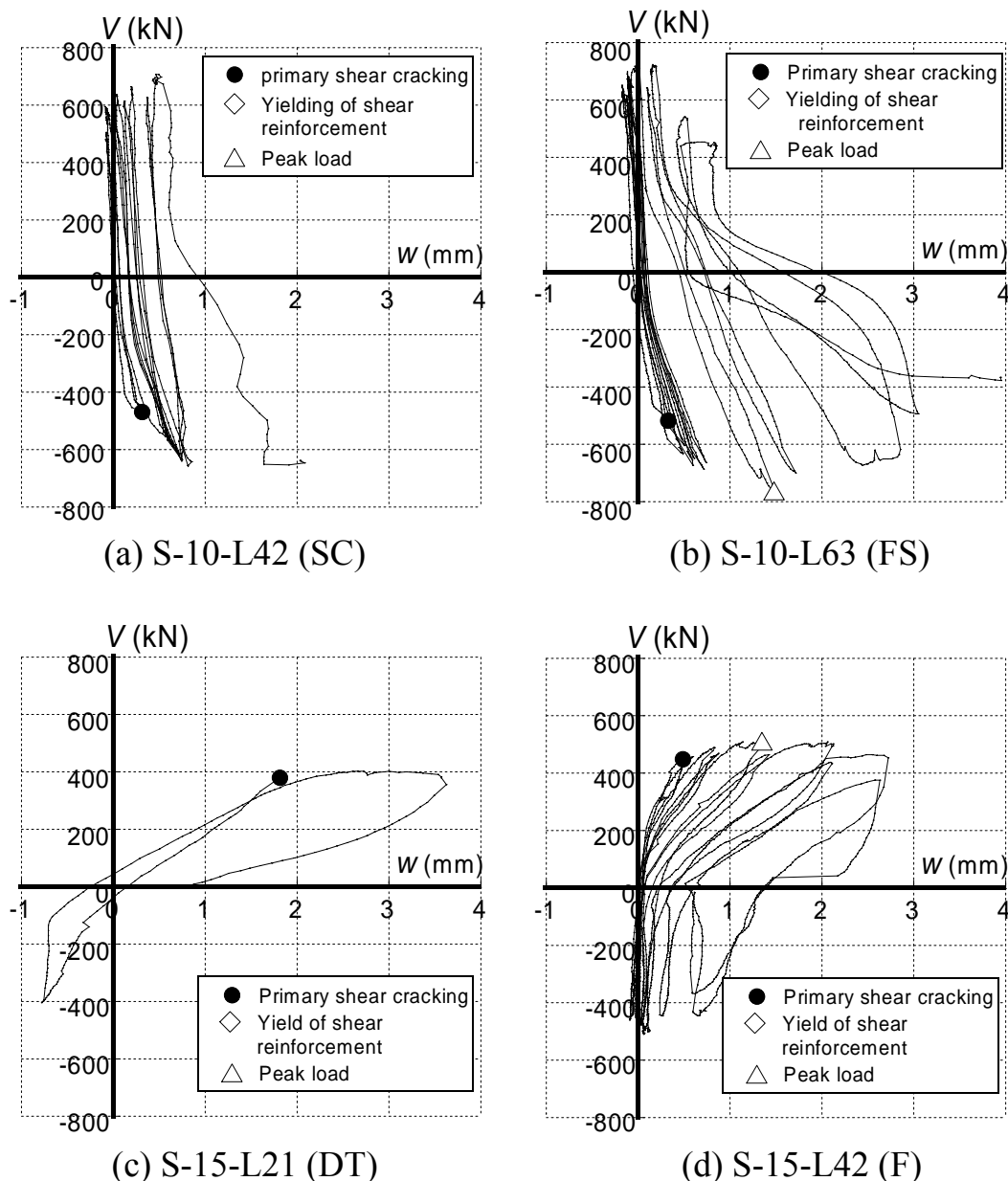
Fig. 3.23 Relationship between shear force and observed shear crack width

3.3 Test on Diagonal Tension Failure of Post-tensioned Precast Concrete Beams (Test 2)

3.3.1 Design of Specimens

To investigate structural behavior of prestressed concrete beams failing in diagonal tension, four half-scale beams were designed. Design of the specimens had been conducted with similar manner with test 1 in section 3.2. Two experimental parameters were selected: shear span depth ratio, a/D, and shear reinforcement ratio, ρ_w. Table 3.7 indicates experimental parameters allocated to specimens. Table 3.8 shows the geometric and material properties applied to the

specimens for design. Load-displacement relationship when flexure is dominant for design of specimens was obtained in a same manner with test 1 in section 3.2. Equation (3.1) to (3.6) were used for flexural crack moment, M_{cr}, flexural yield moment, M_y, Stiffness reduction factor, α_y, and member rotation angle at yielding of prestressing steel, R_y, respectively. Stiffness reduction factor after flexural yielding, α_3, is defined as 0.001 [3.2].

Table 3.7 Experimental parameters

		ρ_w (%)		
		0.00 (-)	0.10 (2-S6@200)	0.21 (2-S6@100)
a/D	1.0	-	S-10-L10	S-10-L21
	1.5	S-15-L00	S-15-L10	-

Table 3.8 Geometric and material properties applied in specimens for design

	b (mm)	D (mm)	L (mm)	a/D	F_c (MPa)	P_i (kN)	f_{wy} (MPa)	ρ_w (%)
S-10-L10	300	600	1200	1.0	60	2980 (=0.7P_y)	785	0.10
S-10-L21								0.21
S-15-L00			1800	1.5				0.00
S-15-L10								0.10

Note: a = shear span; D = overall depth of section; P_i = initial prestressig force; P_y = yield force of prestressing steel; and ρ_w = shear reinforcement ratio.

Table 3.9 Ratio of shear strength and flexural yielding strength, V_u/V_y

	M_y (kN·m)	V_y (kN)	V_u (kN)	V_u/V_y
S-10-L10	739.8	1233	893	0.72
S-10-L21			957	0.78
S-15-L00	692.1	768.6	817	1.06
S-15-L10			892	1.16

Note: M_y is bending moment at yielding of prestressing steel, V_y is shear force at yielding of prestressing steel (=M_y/a), a is shear span, and V_u is shear strength by AIJ standard [2.16].

Table 3.9 indicates ratio of shear strength and flexural yielding strength, V_u/V_y. The shear strength, V_u, was obtained by AIJ standard for PC members [2.16]. The equations are specified in (2.43) to (2.47). To evaluate expected shear

strength of post-tensioned precast concrete beams, distance between prestressing steel in compression and tension side, j_p, was applied to j_o in Eq. (2.43). Moreover, upper limit for yield strength of shear reinforcement ($f_{wy} \leq 295$ MPa) is neglected for the design of the specimens. It is expected that two specimens (S-10-L10 and S-10-L21) fail in shear prior to flexural yielding.

3.3.2 Materials, Construction, and Test Specimens

Table 3.10 summarizes the geometric and material properties used in the specimens. Beam cross sections are shown in Fig. 3.24. Fig. 3.25 to 3.26 illustrate the reinforcing details of the specimens. All beams were post-tensioned by prestressing strands (2-12×ϕ12.7, SWPR7BL), and shear reinforced with high-strength shear reinforcement (S6, KSS785), which were supported by supplementary longitudinal reinforcing bars of mild-strength steel (D10, SD295A). The beam cross sectional dimensions is 300×600 mm. The beam length was 1200 or 1800 mm. A beam and stubs were assembled by post-tensioning through a 20 mm thick high-strength non-shrinkable mortar joint. Prestressing force corresponding to approximately 70% of the yield force of the prestressing strands was introduced. Effective prestressing force, P_e, at the time of testing ranged from 2580 kN to 2650 kN as shown in Table 3.11.

Table 3.10 Geometric and material properties in test specimens

Concrete	F_c (MPa)	F_t (MPa)	E_c (GPa)		
S-10-L10, S-10-L21, S15-L00, S-15-L10	65.2	3.21	36.8		
Mortar at joint	F_c (MPa)	F_t (MPa)	E_c (GPa)		
S-10-L10, S-10-L21, S15-L00, S-15-L10	63.9	4.47	23.8		
Grout for prestressing steel	F_c (MPa)	F_t (MPa)	E_c (GPa)		
S-10-L10, S-10-L21, S15-L00, S-15-L10	53.9	1.38	14.8		
Reinforcements	A_s (mm)	Grade	f_y (MPa)	ε_y (%)	f_u (MPa)	E_s (GPa)
S6	31.67	KSS785	1006*	0.698	1183	202
D10	71.33	SD295A	381	0.202	533	183
Prestressing strands		Type	P_y (kN)	P_u (kN)	δ_u(%)	E_p (GPa)
12ϕ12.7		SWPR7BL	2088*	2316	2.3	195

Note: *0.2% offset, F_c and F_t = compressive and splitting tensile strengths; E_c = Young's modulus; f_y and f_u = yield and tensile strengths of reinforcement; ε_y = yield strain of reinforcement; E_s and E_p = Young's modulus of reinforcement and prestressing strand; P_y and P_u = yield and tensile forces of prestressing strand, respectively.

Table 3.11 Effective prestressing force P_e and prestressing level η

Specimen	P_e (kN)	$\eta(=P_e/bDF_c)$
S-10-L10	2650	0.226
S-10-L21	2580	0.219
S-15-L00	2640	0.225
S-15-L10	2640	0.225
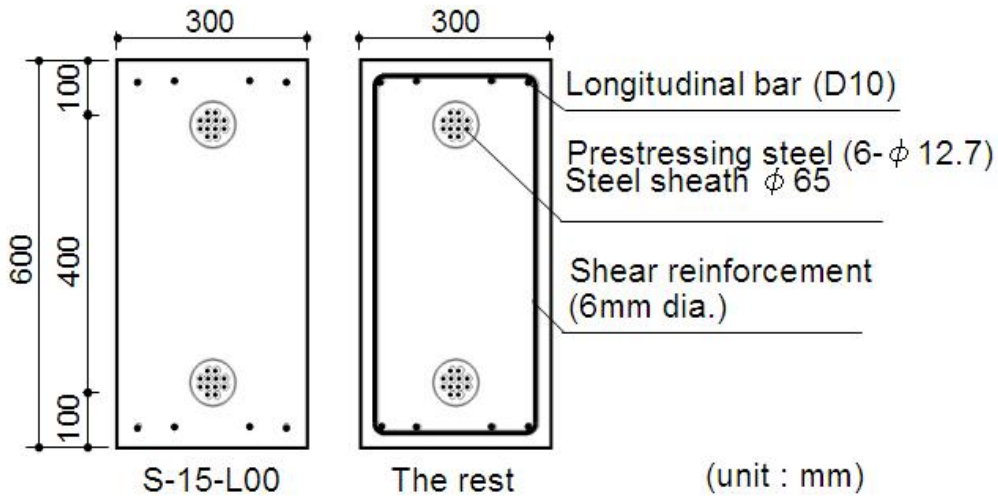
Fig. 3.24 Beam cross section
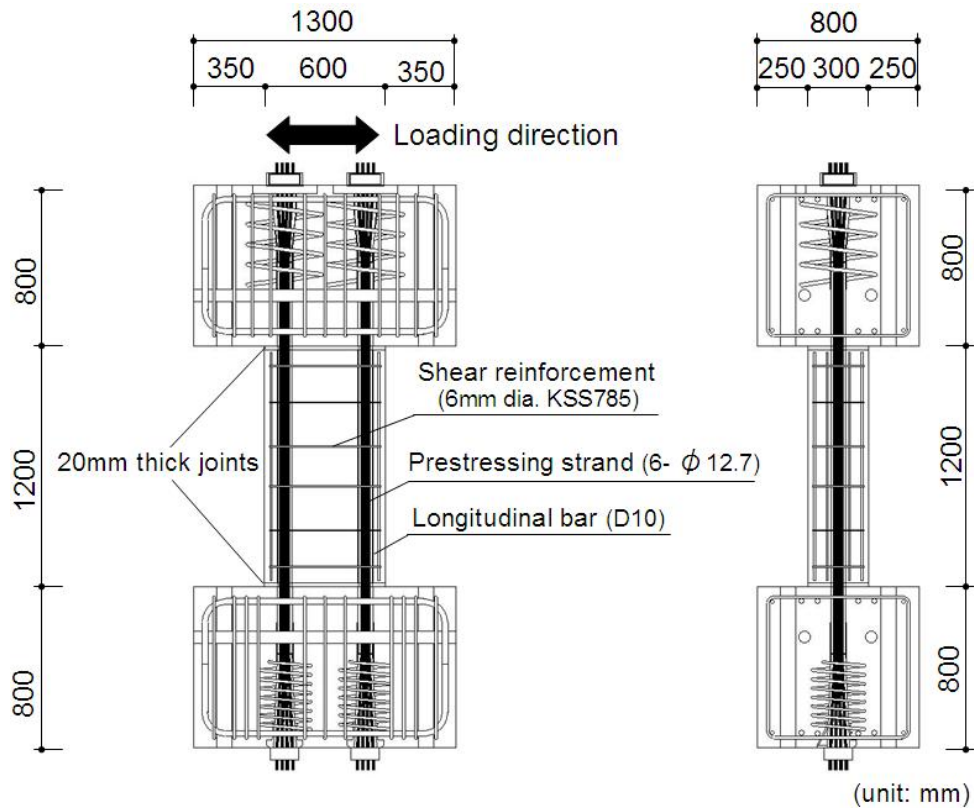
(a) S-10-L10

Fig. 3.25 Reinforcing details of test beam (*a/D*=1.0, *L*=1200mm)
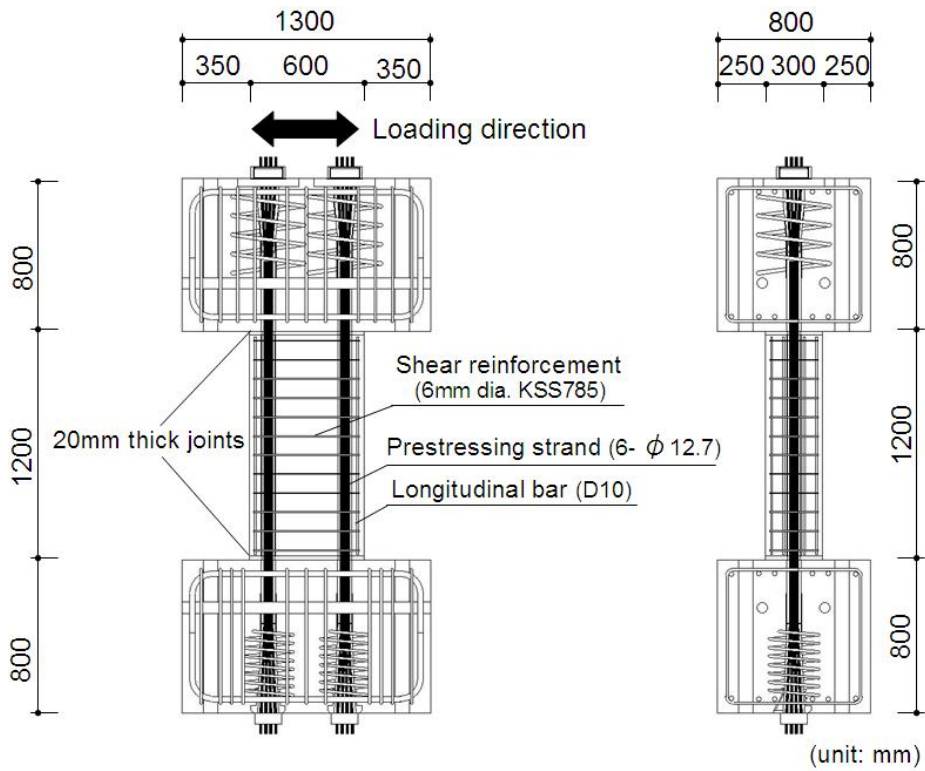
(b) S-10-L21

Fig. 3.25 Reinforcing details of test beam (*a/D*=1.0, *L*=1200mm)
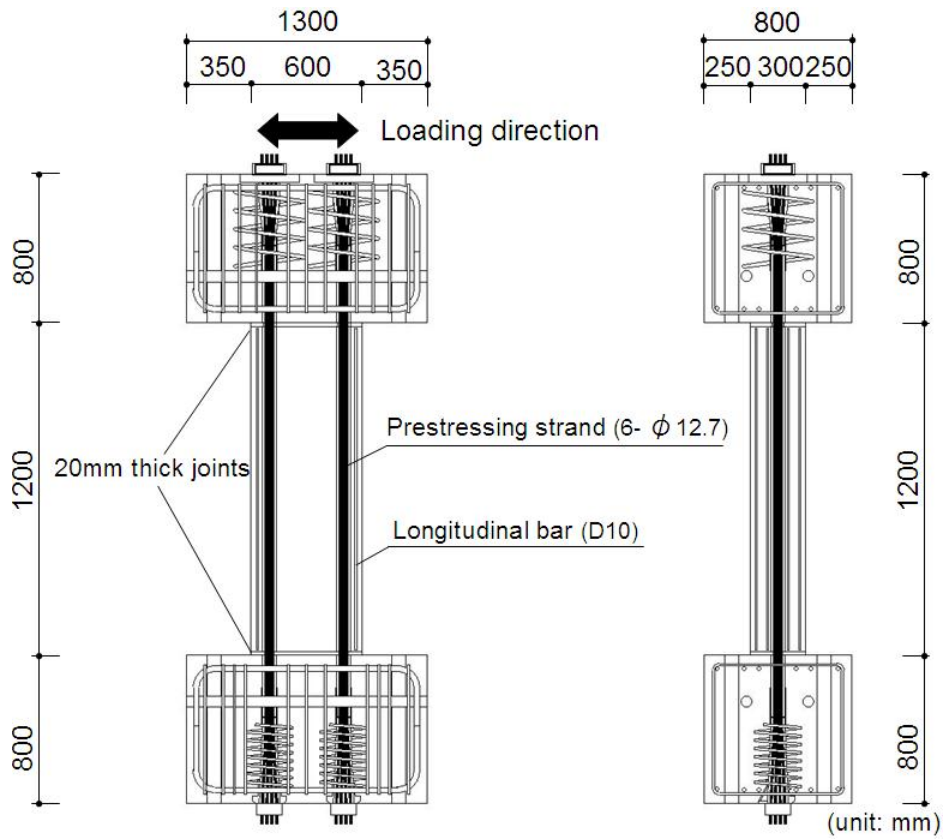
(a) S-15-L00

Fig. 3.26 Reinforcing details of test beam (*a/D*=1.5, *L*=1800mm)

8 2
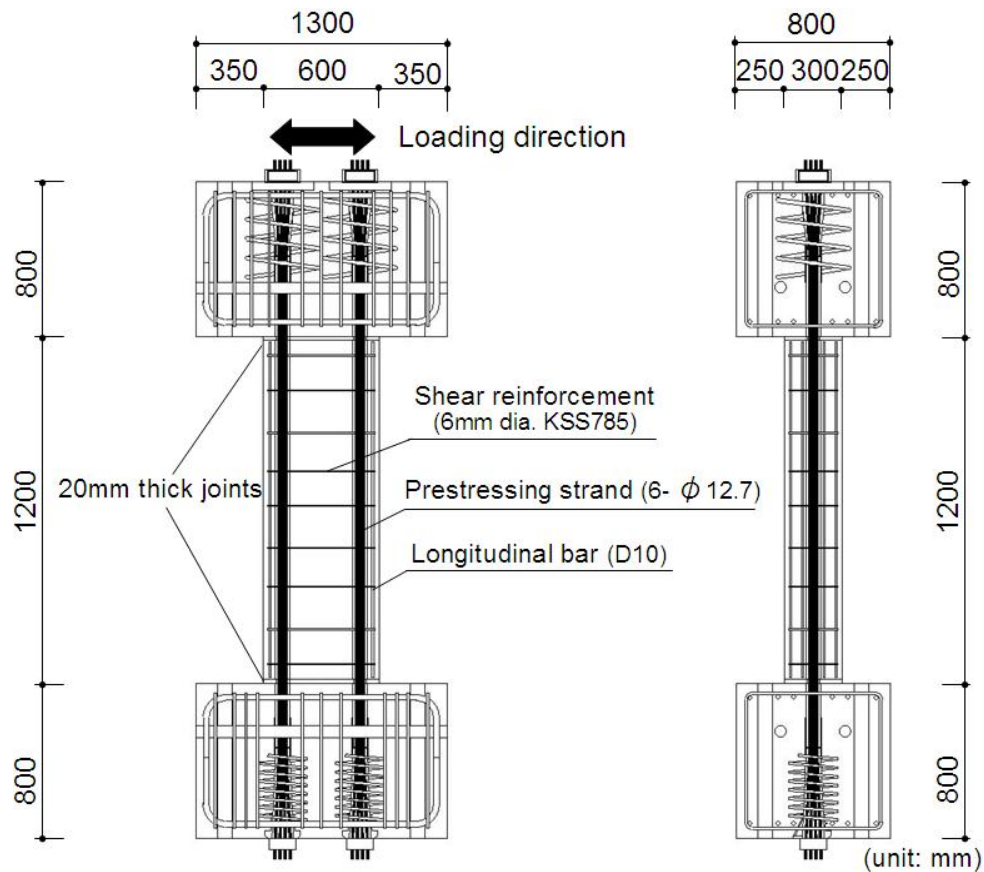
(b) S-15-L10

Fig. 3.26 Reinforcing details of test beam (*a/D*=1.5, *L*=1800mm)

3.3.3 Loading and Measurements

The loading and measurements also had been conducted in similar manner with the test 1 in section 3.2.3. The loading setup and loading patterns which are same with those of test 1 in section 3.2.3 were used as shown in Fig. 3.8 to 3.9.

Strain gauges were attached to some of the reinforcements (e.g. PT bars, longitudinal bars, and shear reinforcements). These strain gauges were placed as shown in Fig. 3.27. Fig. 3.28 illustrates the setup of linear displacement transducers attached on the beam to measure the flexure and shear deformation.

8 3
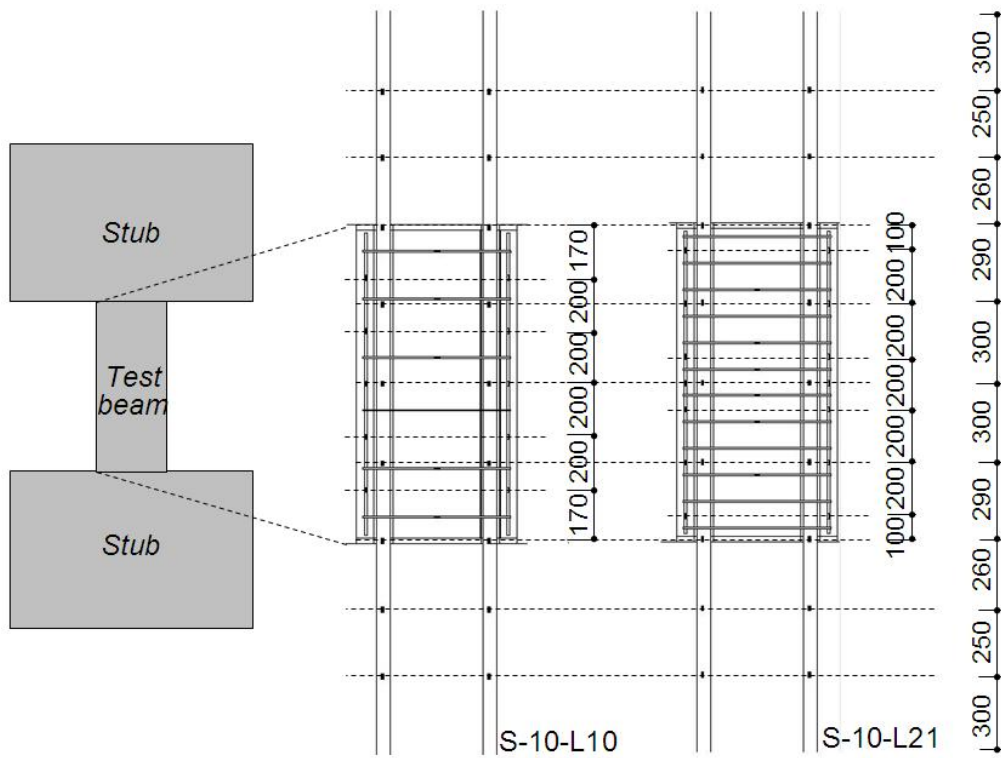
(a) Specimens with *a/D*=1.0
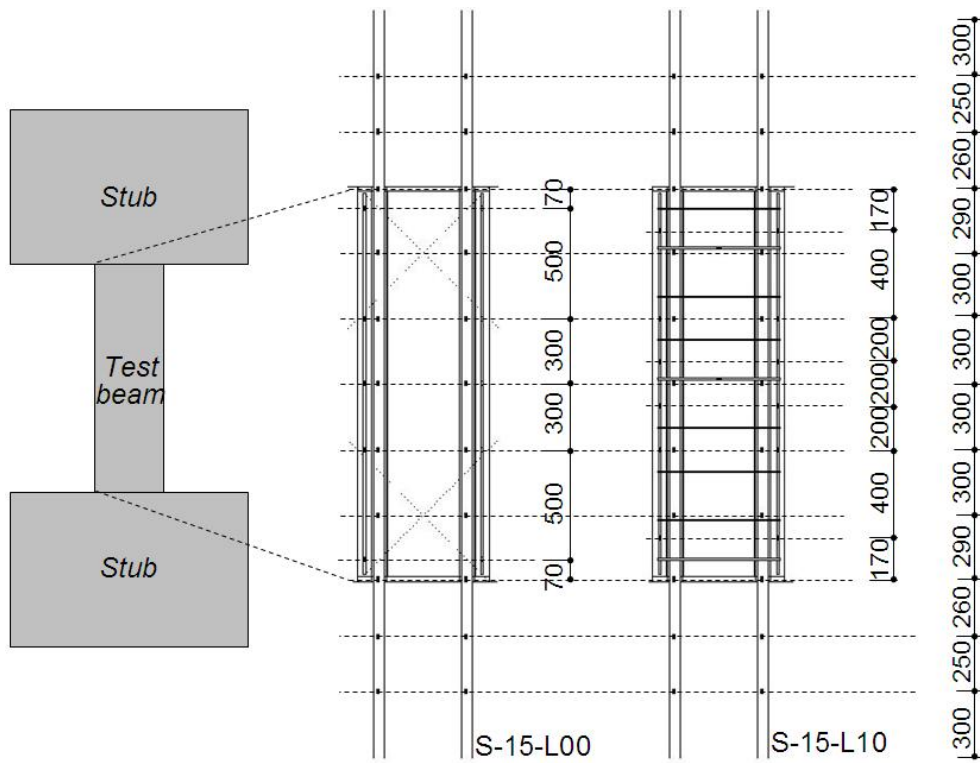
(b) Specimens with *a/d*=1.5

Fig. 3.27 Position of strain gauges attached on the reinforcements

(a) Specimens with *a/D*=1.0   (b) with *a/D*=1.5
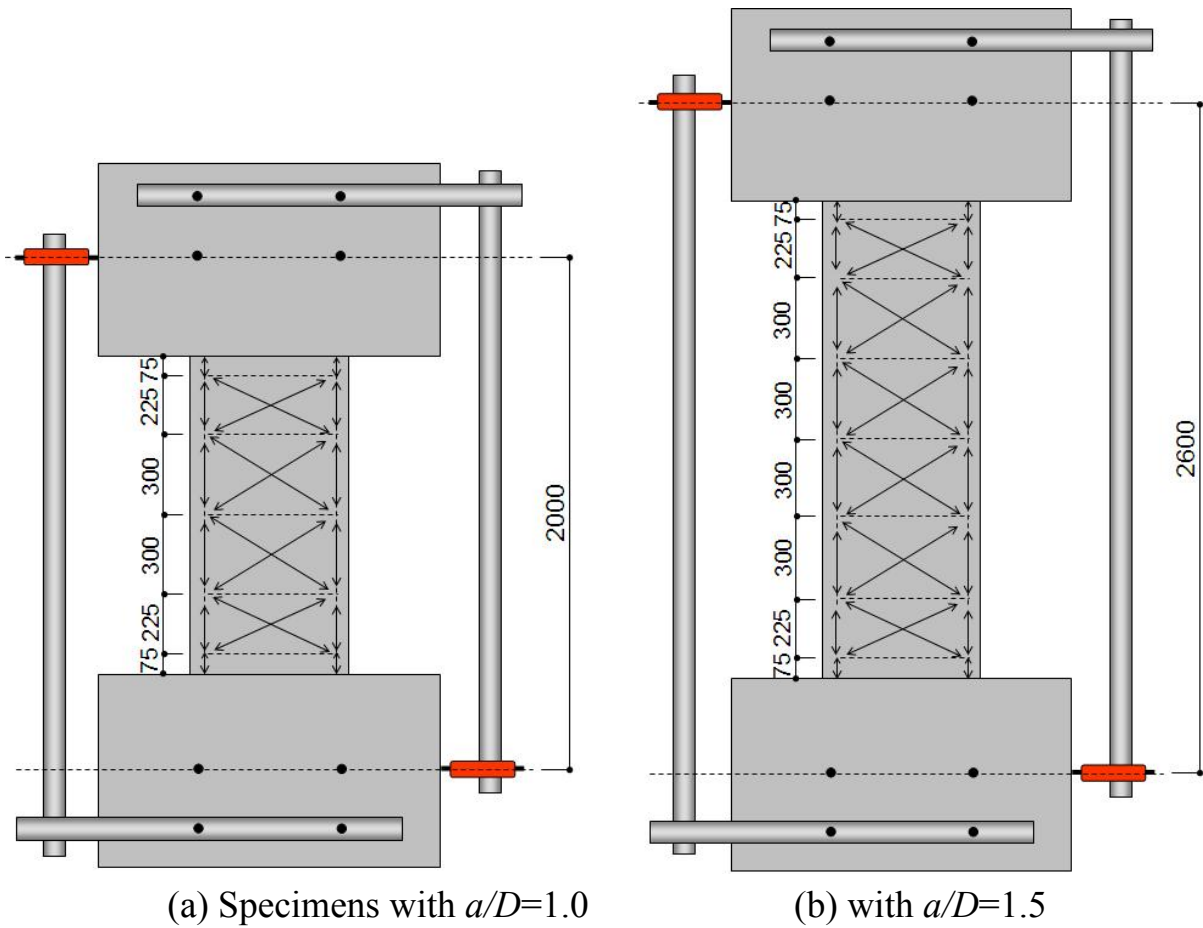
Fig. 3.28 Setup of linear displacement transducers

3.3.4 Test Results

Load-displacement relationships and crack patterns

Figure 3.29 shows beam shear force, *V,* -drift angle, *R*, relations. The shear force, *V,* is obtained as Eq. (3.37) and (3.38) considering horizontal force of leaned vertical hydraulic jacks. In a same manner with the test in section 3.2, the drift angle, *R* is defined as a ratio of relative displacement of beam to its length ($=\delta_{exp}/L$). The horizontal dashed lines represent shear force, V_f, obtained by Eq. (2.43) to (2.47) which were used for the design of the specimens [2.16]. Symbols ○, ●, Δ, and ◊ in Fig. 3.29 represent first flexural cracking, first shear cracking, peak load, and yielding of shear reinforcement, respectively.
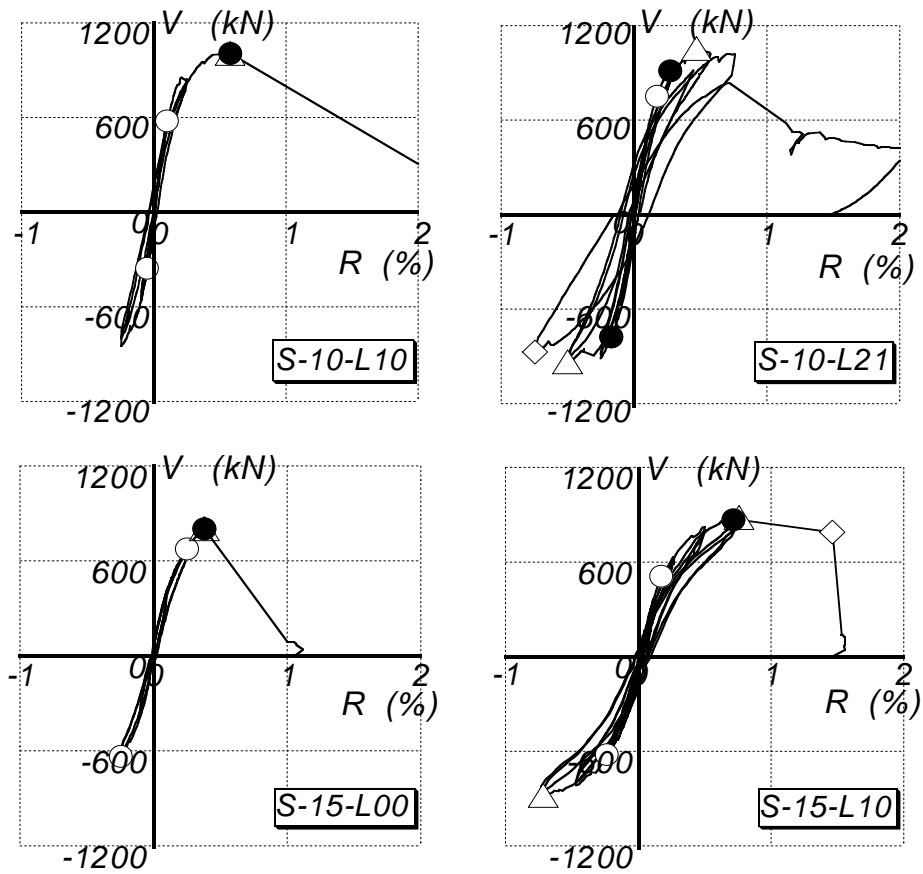
Fig. 3.29 Shear force, V – drift angle, R, relations

Table 3.12 summarizes the test results. In Table 3.12, V_{cr} is shear force at shear cracking, V_{exp} is peak load, and R_{exp} is beam drift angle at peak load, respectively. Fig. 3.30 shows crack patterns of beams from beam drift angle of 0.25% to shear failure. Fig. 3.31 plots relationships among observed drift angle, R, shear force, V, and tensile stress of shear reinforcement in shear reinforced specimens, S-10-L10, S-10-L21, and S-15-L10. Straight lines, solid circles, and open squares in Fig. 3. 31 indicate envelop curve for shear force, V, tensile stress in shear reinforcement, f_{ws}, and peak load. Tensile stress, f_{ws}, in Fig. 3.31 is obtained by measured strain of shear reinforcement which across the crack.

Table 3.12 Summary of test results

Specimen	Failure mode	V_{cr} (kN)		V_{exp} (kN)		R_{exp} (kN	
		+	-	+	-	+	-
S-10-L10	S (DT)	1006	-	1006	-848	0.576	-0.249
S-10-L21	S (ST)	913	-774	1054	-934	0.472	-0.502
S-15-L00	S (DT)	803	-	803	-640	0.378	-0.252
S-15-L10	S (DT)	871	-	884	-877	0.753	-0.736

Note: S is shear failure, and DT is diagonal tension failure, respectively.
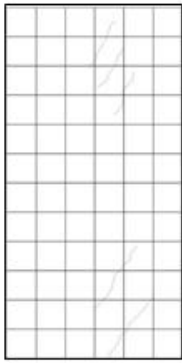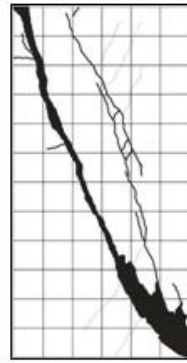
(a) S-10-L10
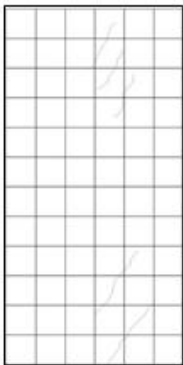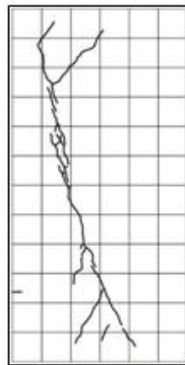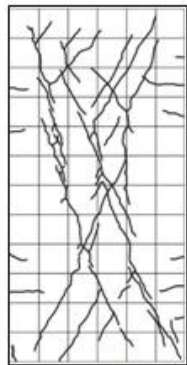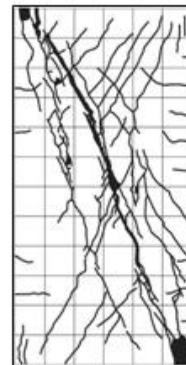
(b) S-10-L21
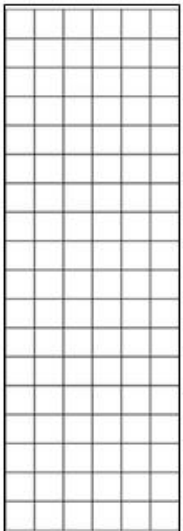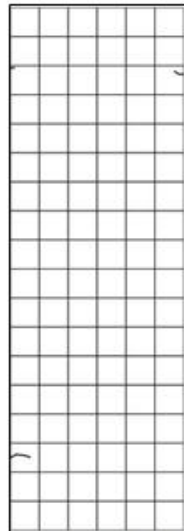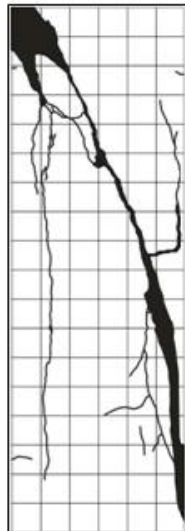
(c) S-15-L00

Fig. 3.30 Crack patterns

R=0.10% R=0.25% R=0.50% R=0.75% Shear failure (R=0.76%)
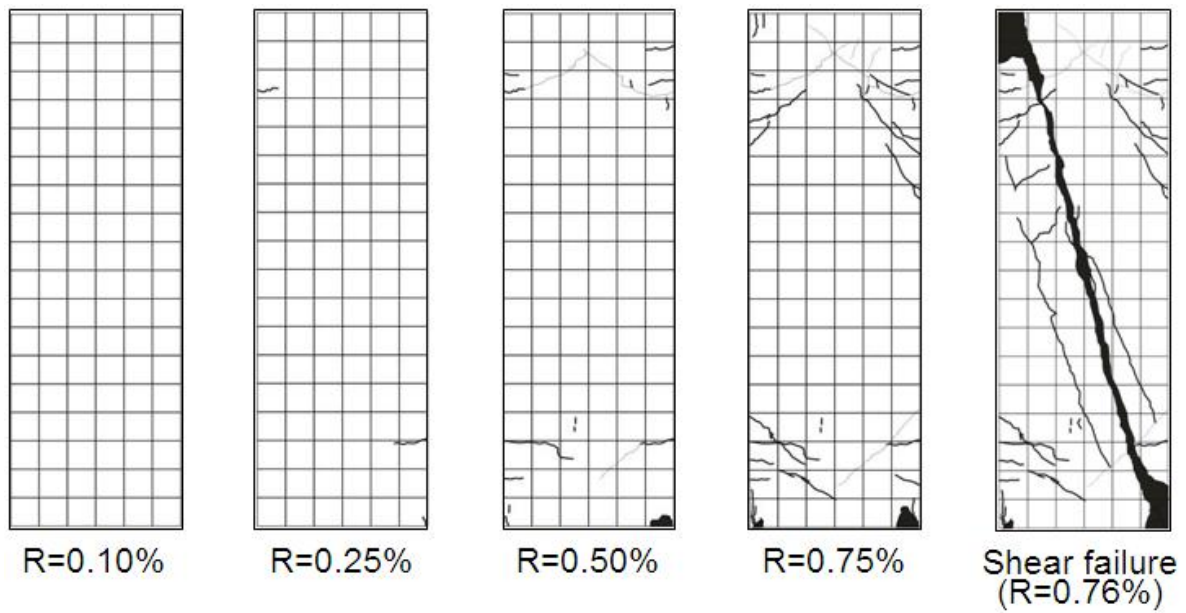
(d) S-15-L10

Fig. 3.30 Crack patterns

S-10-L10 (DT)

V (kN)

Peak load

Initiation of primary shear crack

f_{ws} (MPa)

Yielding strength, f_{wy} =1006 MPa

S-10-L21 (ST)

V (kN)

Peak load

Initiation of primary shear crack

f_{ws} (MPa)

Yielding strength, f_{wy} =1006 MPa

S-15-L10 (DT)

V (kN)

Peak load

Initiation of primary shear crack

f_{ws} (MPa)

Yielding strength, f_{wy} =1006 MPa
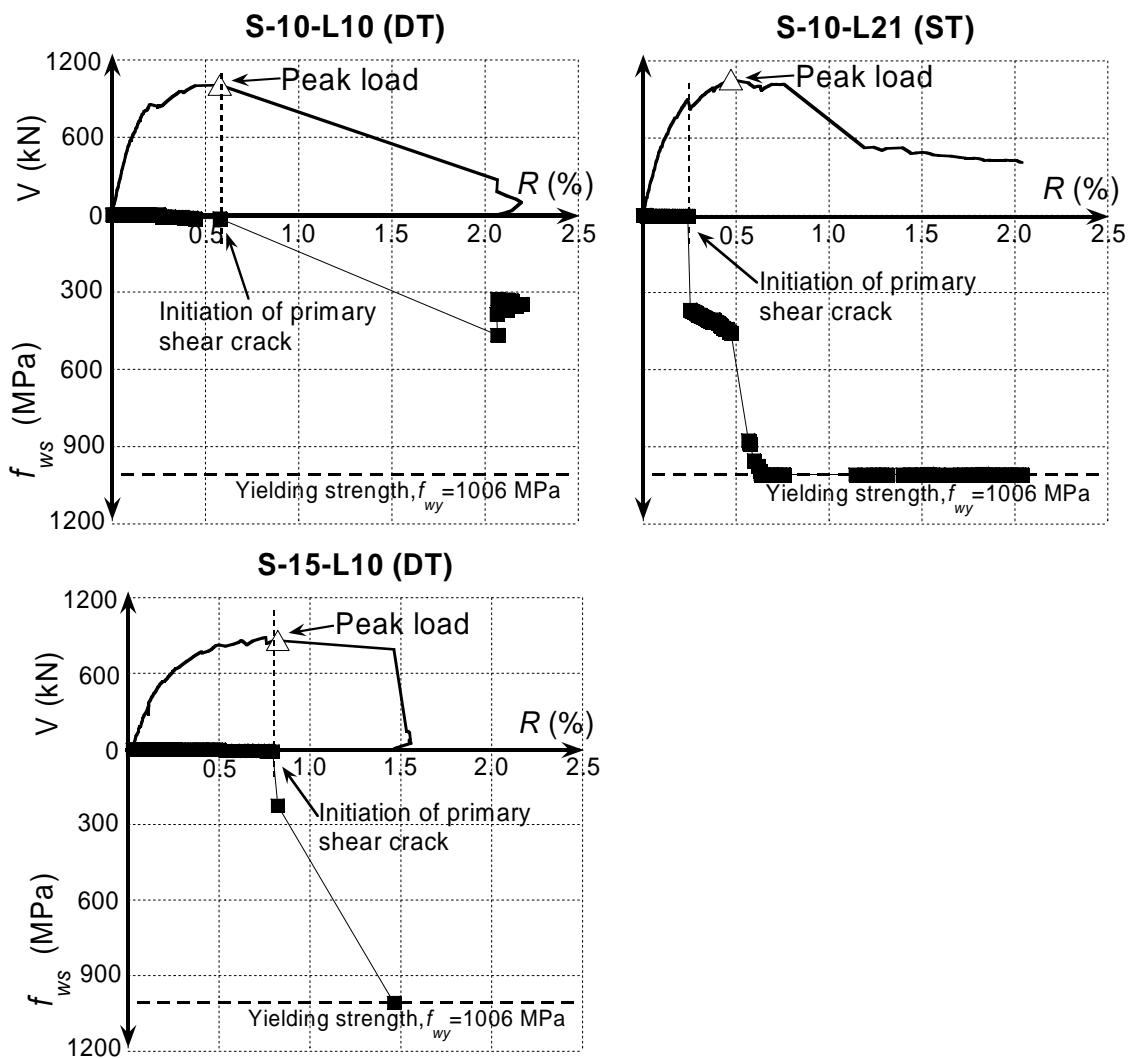
Fig. 3.31 Relationship among shear force, *V*, drift angle, *R*, and tensile stress of shear reinforcement, f_{ws}

As shown in Fig. 3.29 to 3.31, all specimens failed in shear. In particular, three of four specimens failed in diagonal tension (DT). For definition of failure mode, refer to section 3.2.4. In S-10-L10, flexural cracks was initiated in $R=0.10\%$. At $R=0.58\%$, beam failed in shear immediately after initiation of primary shear crack. The failure mode is judged as diagonal tension failure (DT) because initiation of primary web shear crack leads to rapid decay of load carrying the shear capacity of the beam. Until shear failure, tensile stress of longitudinal bars, prestressing steel, and shear reinforcement did not reached their yield strength.

In S-10-L21, tensile stress of shear reinforcement were gradually propagated after initiation of primary shear crack at $R=0.25\%$. Non-prestressed longitudinal bar in compression zone yielded at same time. Initiation of primary shear crack did not affect the deterioration of the load carrying the shear capacity. Yielding of shear reinforcement at $R=0.72\%$ leads to decay of load carrying the shear capacity. The failure mode of S-10-L21 is judged as shear tension failure (ST).

In S-15-L00, the load carrying the shear capacity in S-15-L00 rapidly dropped immediately after initiation of primary shear crack. It is because of excessive opening of shear crack without shear reinforcement. S-15-L00 is judged that it failed in diagonal tension (DT).

In S-15-L10, gap joint opened at $R=0.10\%$. Inclined flexural crack (flexural shear crack) was initiated at $R=0.75\%$. The load carrying the shear capacity of beam rapidly dropped immediately after initiation of web shear crack at $R=0.83\%$. Shear reinforcement did not yield until shear failure. It is judged that S-15-L10 failed in diagonal tension (DT).

As shown in Fig. 3.31, tensile stress of shear reinforcement, f_{ws}, in the specimens which failed in DT rapidly increased with initiation of primary shear crack. Excessive opening of shear crack leads to shear failure of beam due to deterioration of interlock resistance. On the other hand, f_{ws} in S-10-L21 which failed in shear tension (ST) continuously increased without decay of load carrying capacity until shear reinforcement yielded. In general, shear reinforcement controls crack opening and width. An increase in energy release rate at the initiation of primary shear crack leads to significant opening of shear crack. Shear capacity rapidly drops by sliding along shear crack if aggregate

interlocking resistance deteriorates. This tendency was prominent in S-10-L10, S-15-L00, and S-15-L10, with small amount of shear reinforcement because low amount of shear reinforcement ($\rho_w = 0.0$ or 0.1%) could not significantly control opening of cracks.

Based on the experimental results above, it can be seen that the first web-shear cracking load in the specimens which failed in DT represented the ultimate shear strength.

Tensile stress distribution
(1) PT tendon

Figure 3.32 plots the stress distribution of PT tendons in test specimens for difference of drift angle: (a) S-10-L10; (b) S-10-L21; (c) S-15-L00; and (d) S-15-L10. Tensile yield strength of prestressing strand, f_{py}, is also indicated in Fig. 3.32. In a same manner with Fig. 3.16, upper and lower graphs in Fig. 3.32 plot the distribution of tensile stress of prestressing strands in upper and lower side, respectively. As shown in Fig. 3.32, no prestressing strands yield in all specimens. Increasing of tensile stress of prestressing strands at flexural tension zone of critical section is prominent. Tensile stress in flexural compression zone of critical zone does not significantly decrease during increasing of drift angle. It is because prestressing strand can not effectively resist against compression resultant force. However, small tensile stress of prestressing strand decreases in S-10-L21 and S-15-L10. It is because of loss of prestressing force of the tendon. An initiation of compressive crack or crushing of concrete leads to increasing of compressive strain of concrete and loss of prestressing force of the PT tendon.
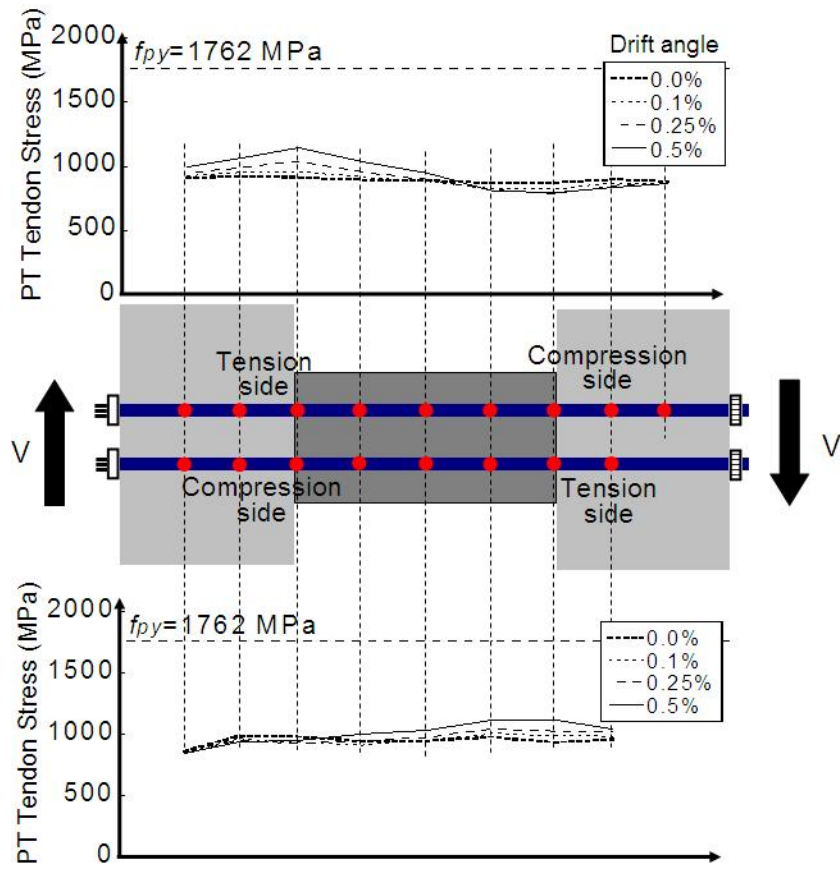
(a) S-10-L10
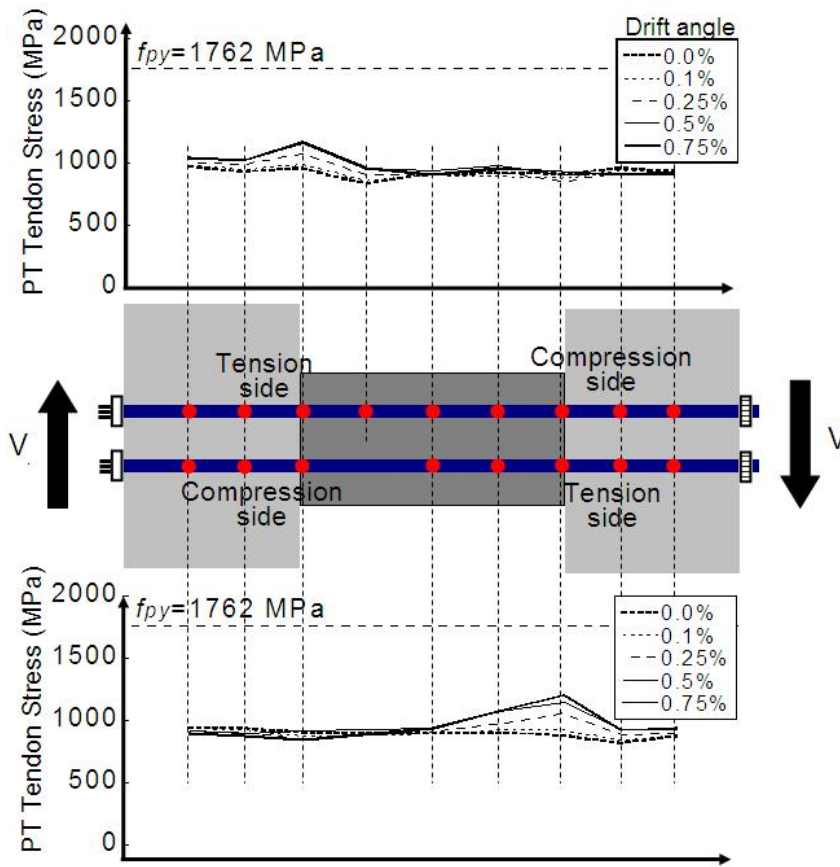
(b) S-10-L21

Fig. 3.32 Tensile stress distribution of PT tendon
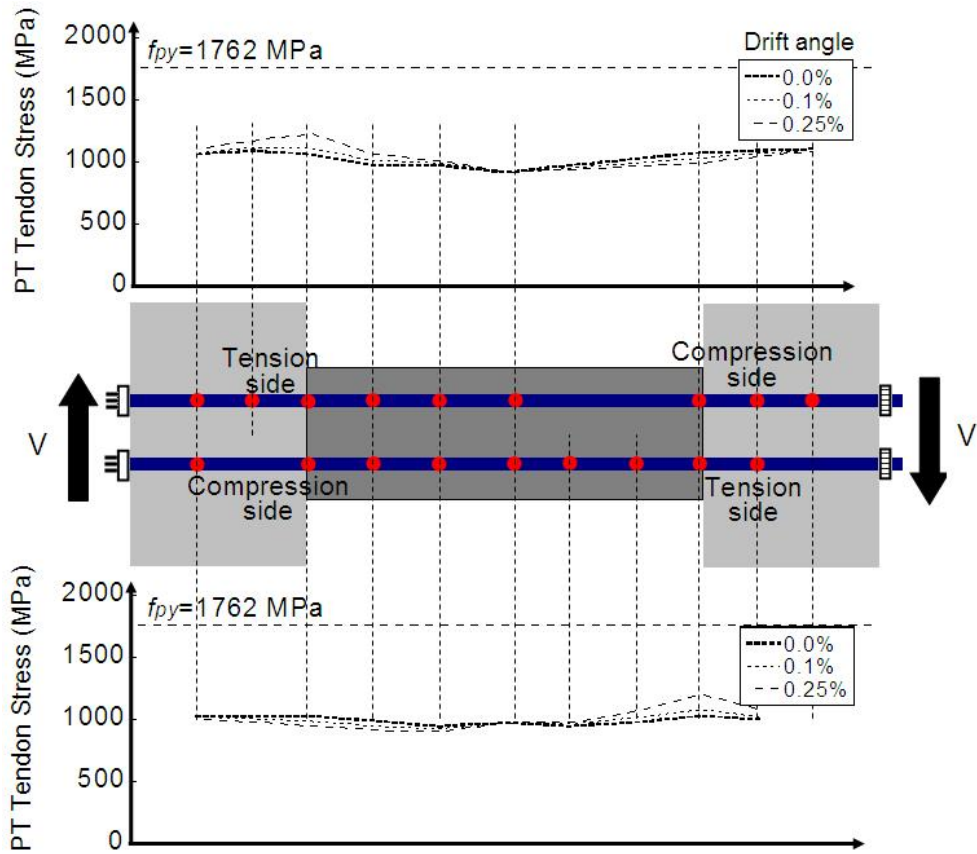
(c) S-15-L00
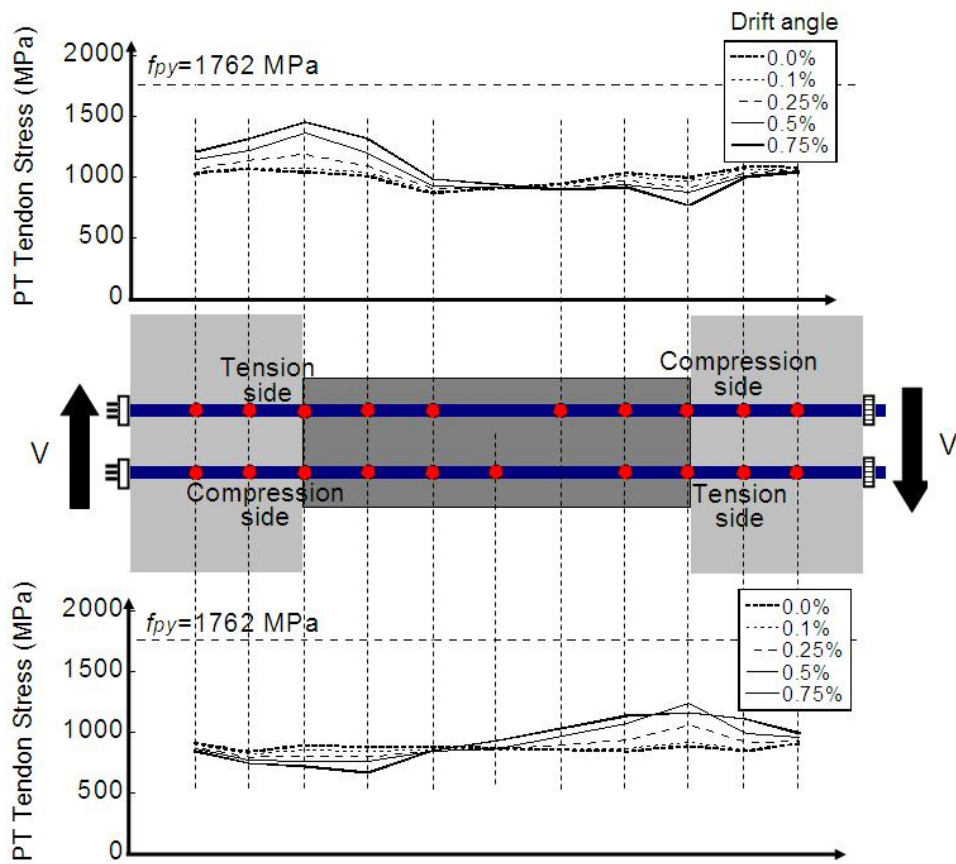
(d) S-15-L10

Fig. 3.32 Tensile stress distribution of PT tendon

92

(2) Non-prestressed longitudinal bars

Figure 3.33 illustrates the stress distribution of non-prestressed longitudinal bars in test specimens in a same manner with Fig. 3.17: (a) S-10-L10; (b) S-10-L21; (c) S-15-L00; and (d) S-15-L10. Compressive yield strength of longitudinal bar, f_{ry}, is also represented in Fig. 3.33. As shown in Fig. 3.33, non-prestressed longitudinal bars in flexural compression zone of all specimens except S-10-L10 reach their yield strength while those in flexural tension zone did not. It is because tensile force of the longitudinal bar is hardly transferred to anchorage zones due to discontinuity of longitudinal reinforcing bars.

(a) S-10-L10
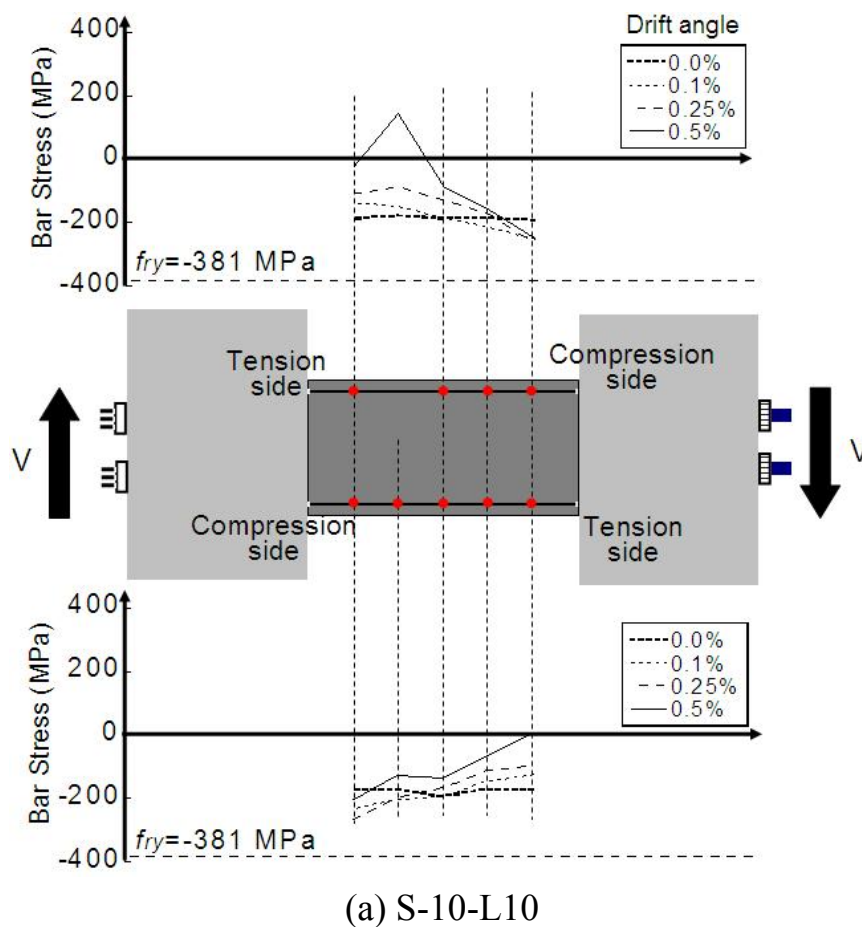
Fig. 3.33 Stress distribution of non-prestressed longitudinal bar
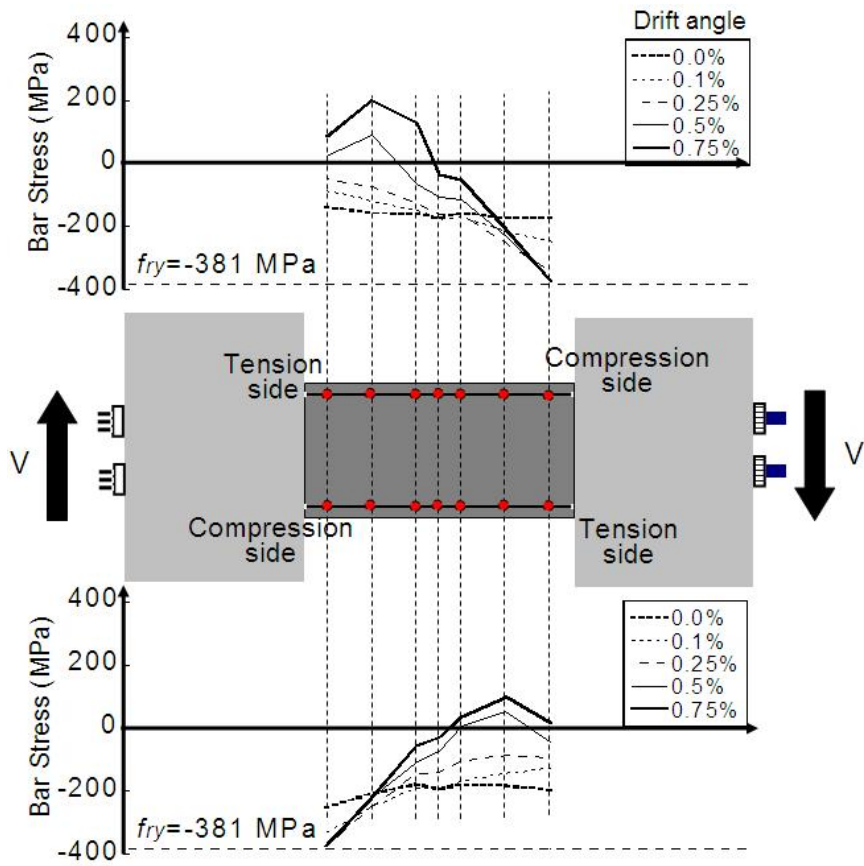
(b) S-10-L21
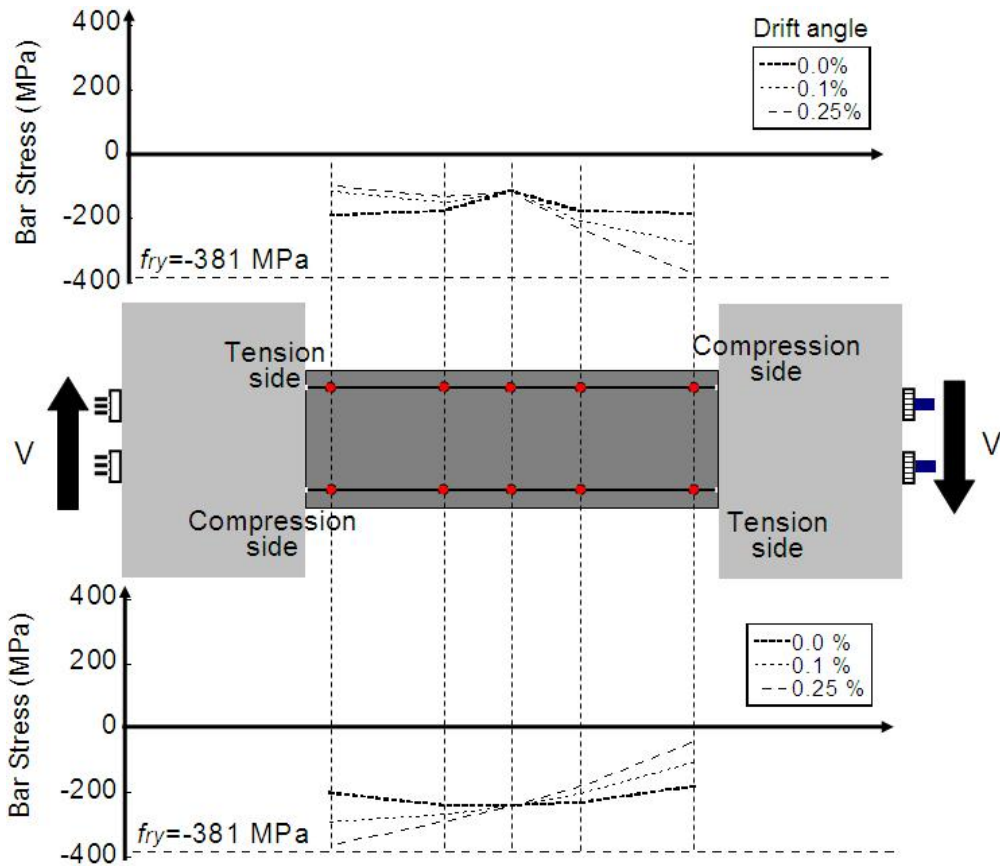
(c) S-15-L00

Fig. 3.33 Stress distribution of non-prestressed longitudinal bar
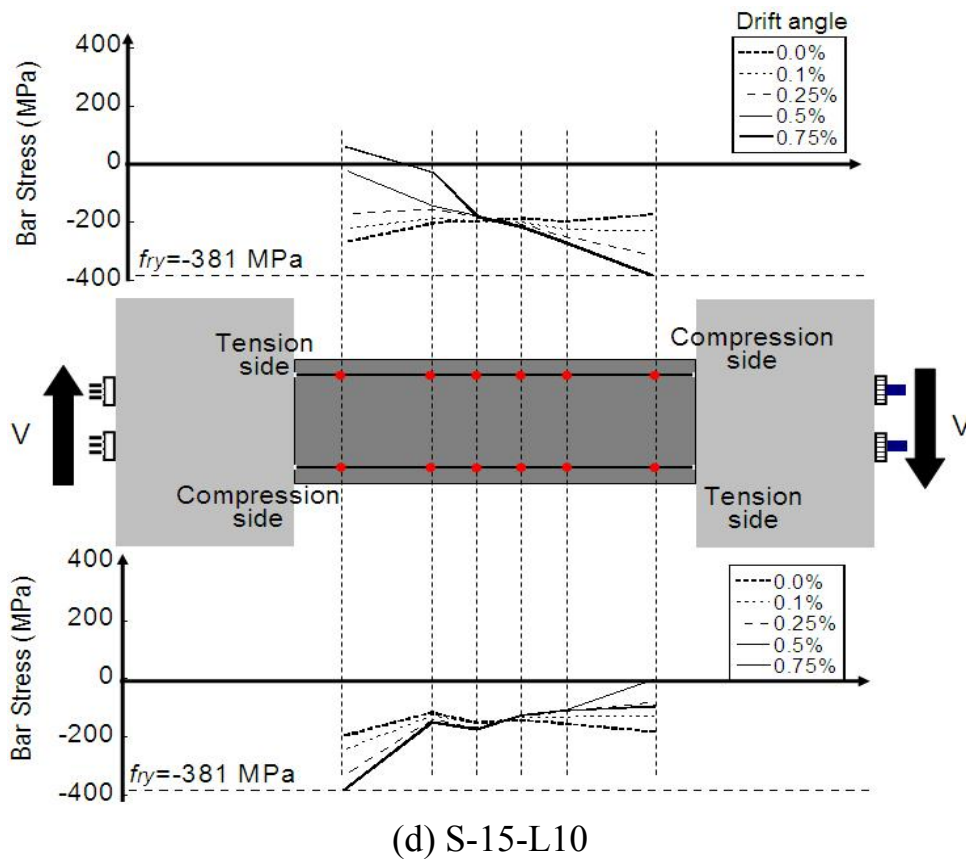
(d) S-15-L10

Fig. 3.33 Stress distribution of non-prestressed longitudinal bar

(3) Shear reinforcement

Figure 3.34 plots the tensile stress distribution of shear reinforcements in shear reinforced specimens: (a) S-10-L10; (b) S-10-L21; and (c) S-15-L10. Tensile yield strength of shear reinforcement, f_{wy}, is indicated in the figure. As shown in Fig. 3.34, tensile stress of shear reinforcement at mid-span in specimens failed in diagonal tension (S-10-L10 and S-15-L10) did not develop until shear failure (R=0.5% cycle for S-10-L10, R=0.75% cycle for S-15-L10). It is corresponded to previous research on diagonal tension failure of reinforced concrete beams [3.9-3.11]. It points out that shear reinforcement does not significantly contribute for shear resistance of beam failing in diagonal tension. In S-10-L21, the tensile stress of shear reinforcement gradually increase after initiation of primary shear crack at R=0.5% cycle. Therefore, the conventional shear design models [2.7-2.8, 2.16] in which yield strength of shear reinforcement is specified need to be modified. Further, it is necessary to develop the analytical model for diagonal tension failure of reinforced / prestressed concrete beam in which failure mechanism of diagonal tension failure is considered. It will be clarified in section 5.

9 5
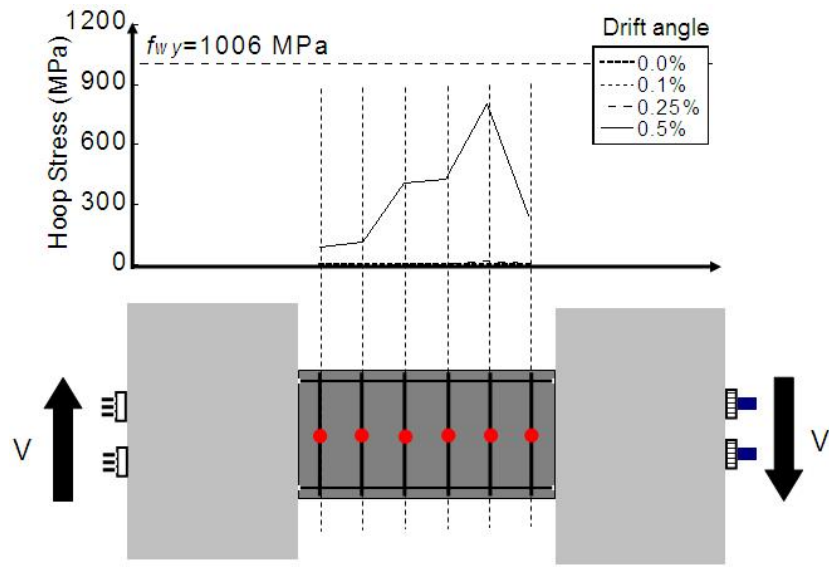
(a) S-10-L10
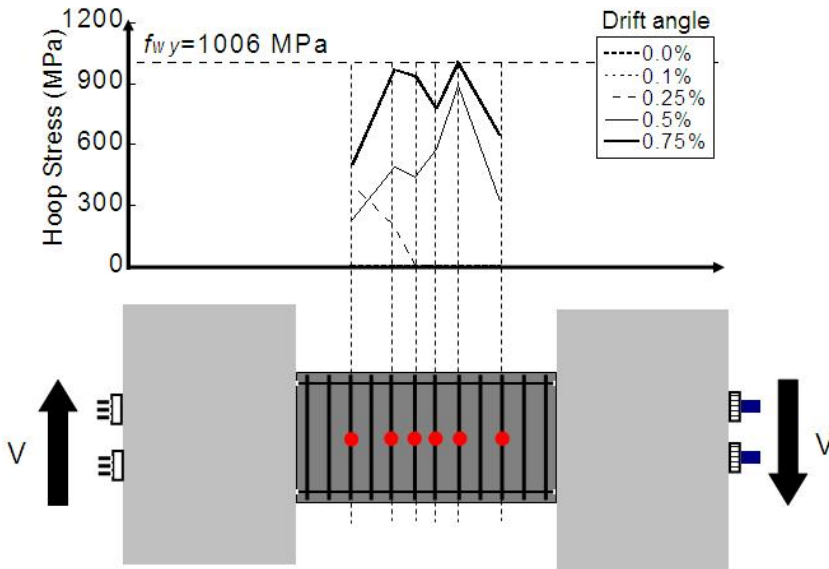
(b) S-10-L21
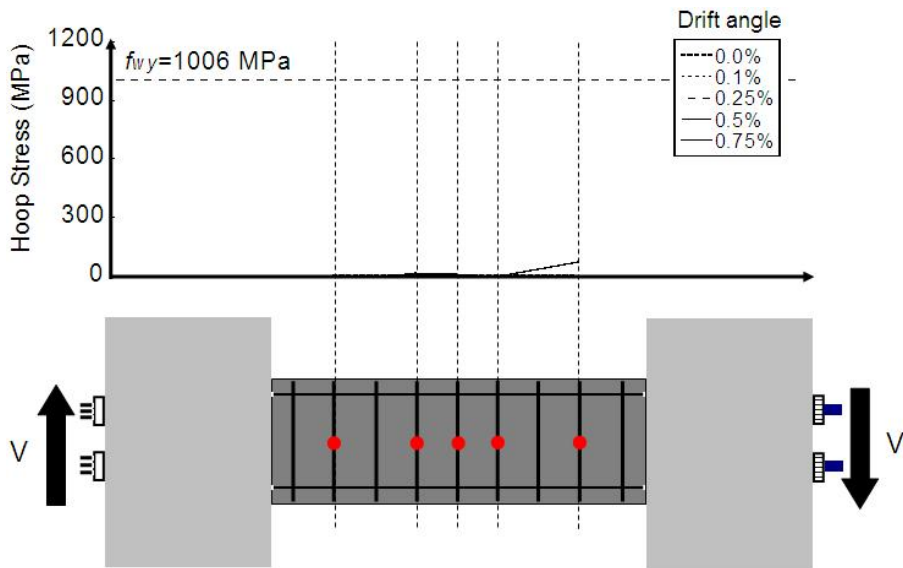
(c) S-15-L10

Fig. 3.34 Distribution of tensile stress of shear reinforcement

9 6

Bond stress

(1) PT tendon

Figure 3.35 plots the distribution of bond stress of PT tendons. Upper and lower graphs of each specimen plot the distribution of bond stress of prestressing strands in upper and lower side, respectively. Horizontal dashed lines represent bond strength of prestressing strand, τ_{max}. For bond strength of prestressing strand, τ_{max}, it is assumed as 4 MPa referred to analytical bond strength equations [3.4-3.6] as shown in Table. 3.5. As shown in Fig. 3.35, no bond stresses of prestressing strands significantly develop and reach their bond strength. It points out that bond stress of PT tendon does not significantly affect to shear resistance of beam failing in diagonal tension.
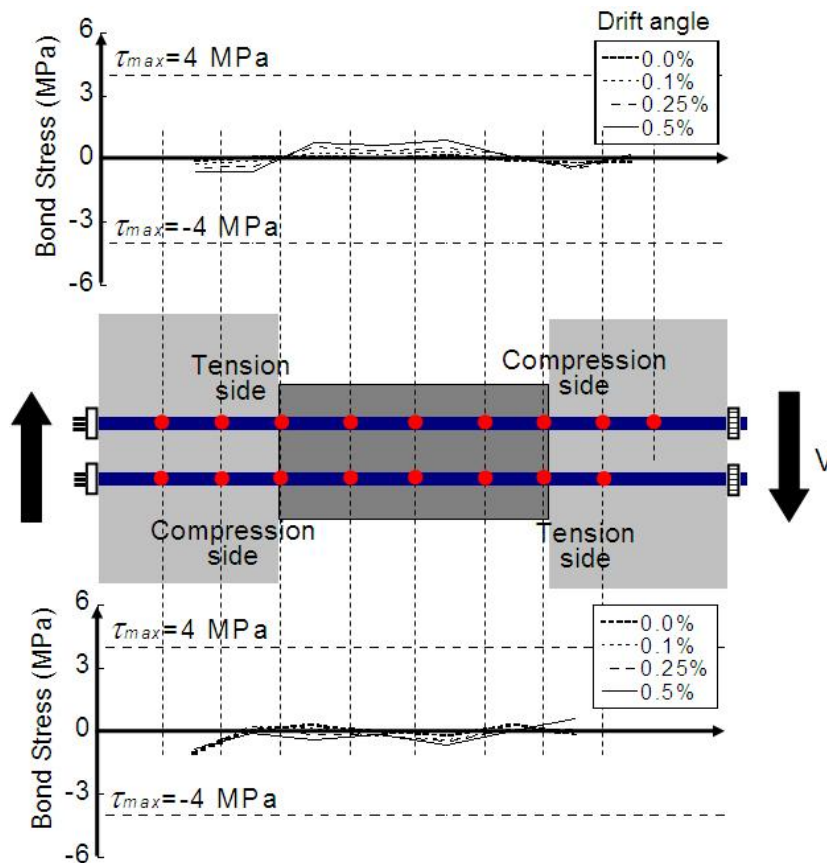
(a) S-10-L10

Fig. 3.35 Distribution of bond stress of PT tendon

(b) S-10-L21

(c) S-15-L00
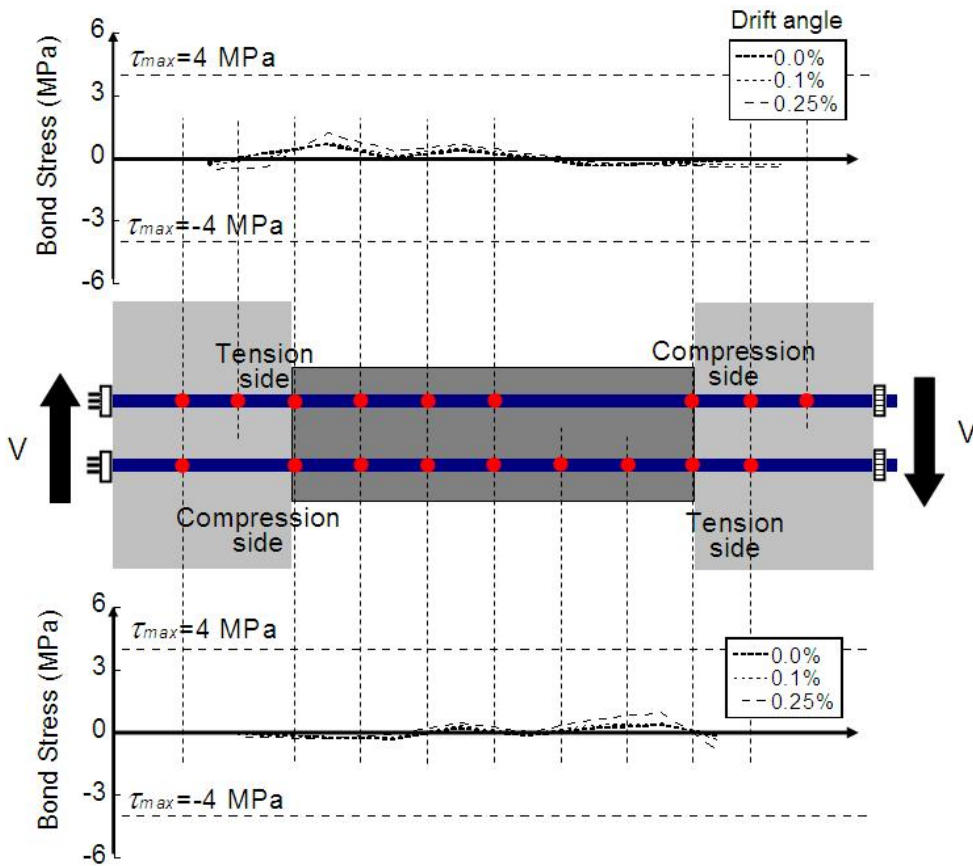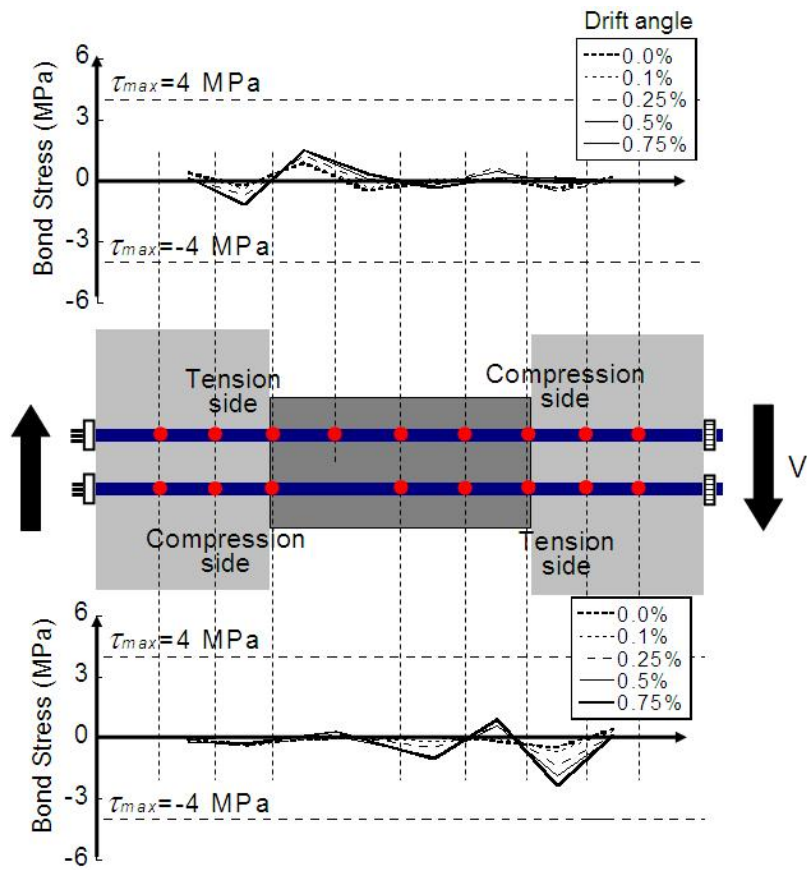
Fig. 3.35 Distribution of bond stress of PT tendon
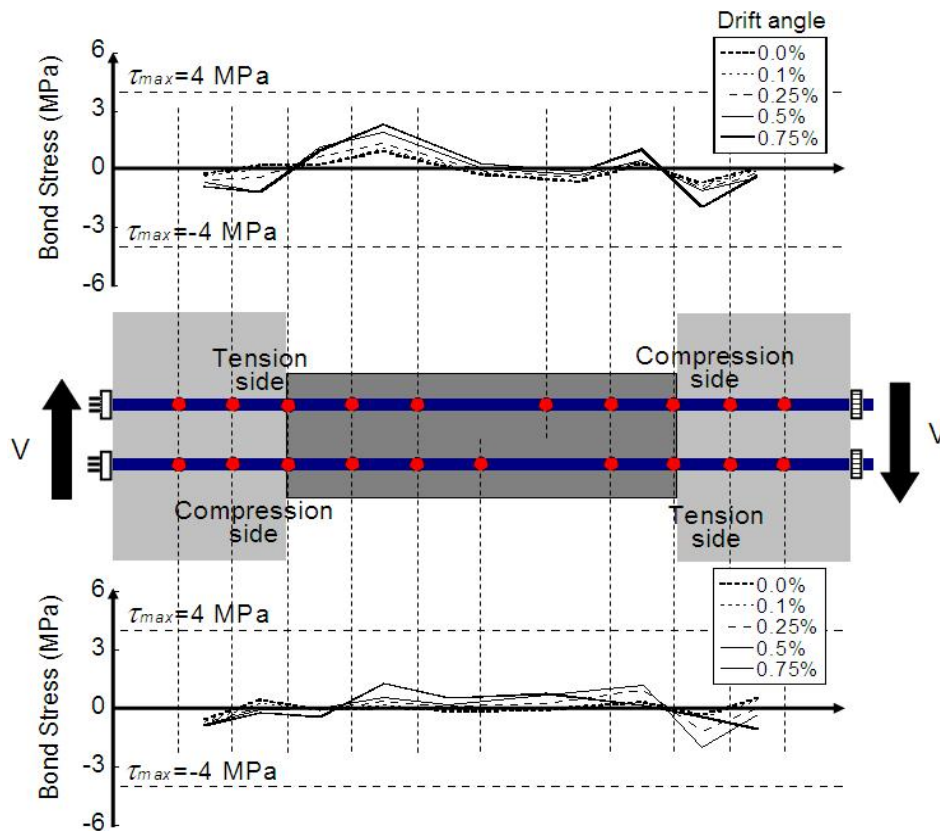
(d) S-15-L10

Fig. 3.35 Distribution of bond stress of PT tendon

(2) Non-prestressed longitudinal bar

Figure 3.36 plots the distribution of bond stress of non-prestressed longitudinal bars. The bond strength of longitudinal bar, τ_{max}, was obtained as shown in Table 3.13 referred to reference [3.7]. As shown in Fig. 3.36, bond stresses in beams failing in diagonal tension (S-10-L10, S-15-L00, and S-15-L10) hardly develop. It points out that a effect of bond stress of longitudinal bar on diagonal tension failure is negligible. On the other hand, bond stress of longitudinal bar in shear tension failed beam (S-10-L21) developed even though it does not reach its bond strength.

Table 3.13 Analytical bond strength [3.7]

Specimen	Analytical bond strength
S-10-L10	5.8
S-10-L21	6.4
S-15-L00	5.2
S-15-L10	5.8
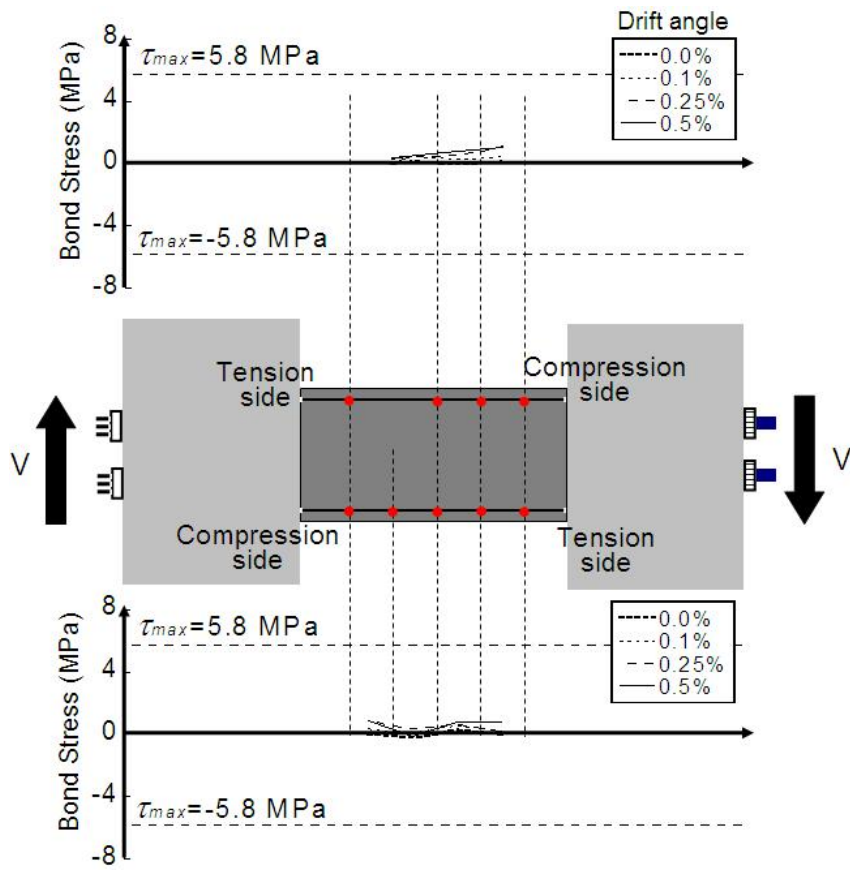
(a) S-10-L10
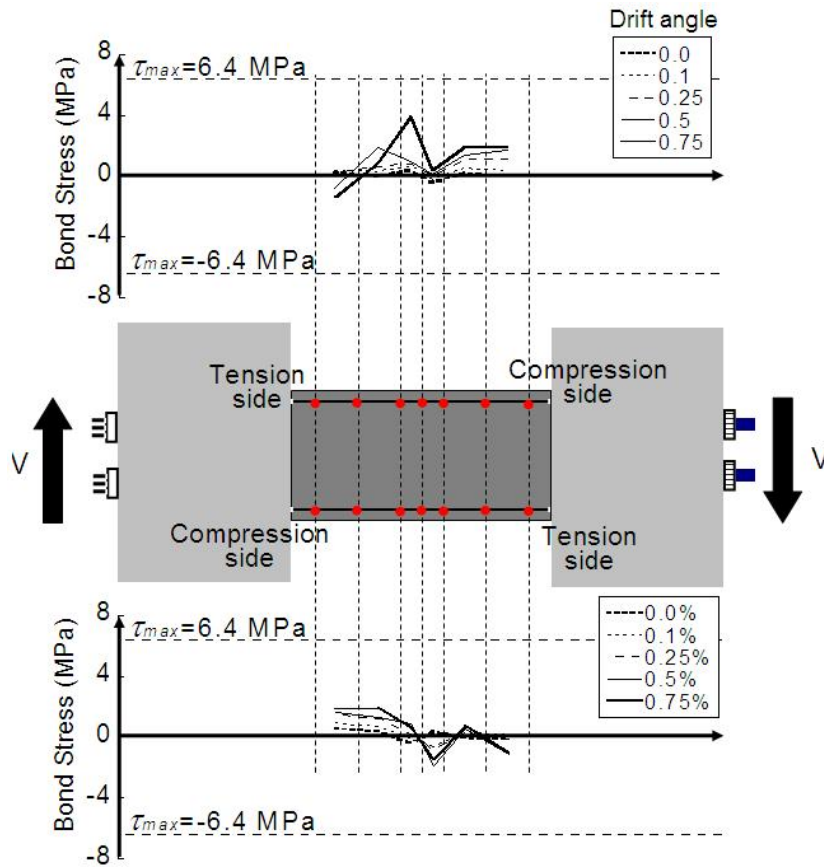
(b) S-10-L21

Fig. 3.36 Distribution of bond stress of non-prestrssed longitudinal bar

１０ ０
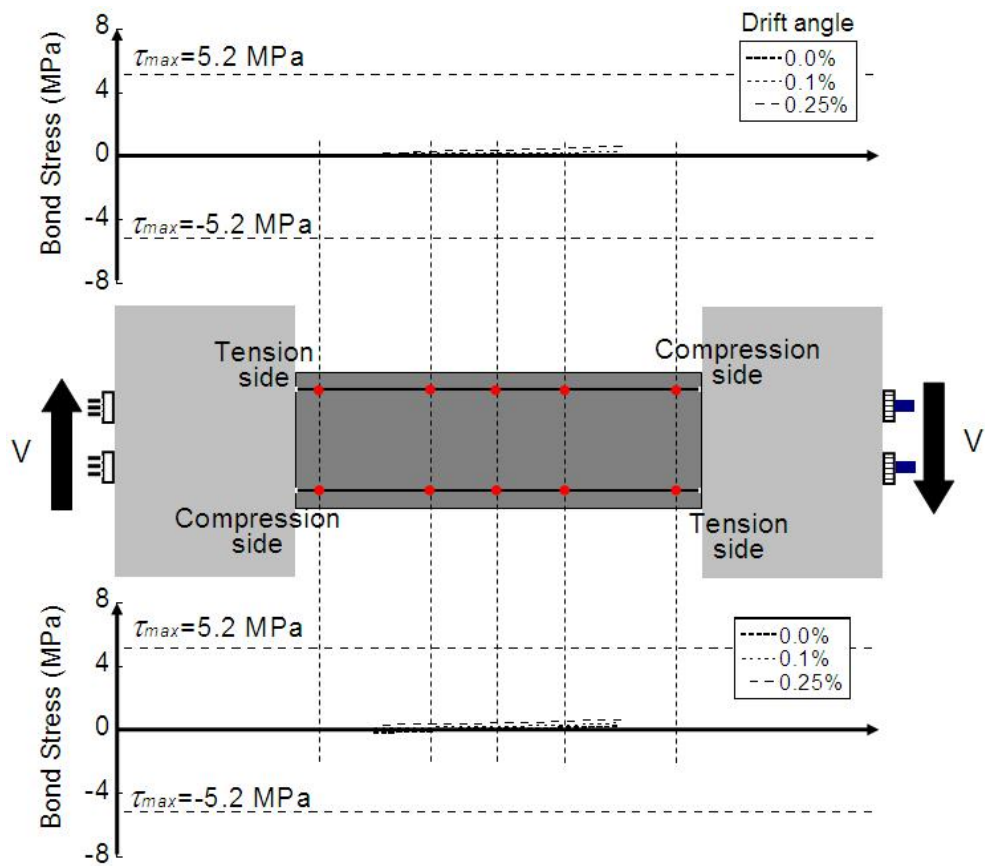
(c) S-15-L00
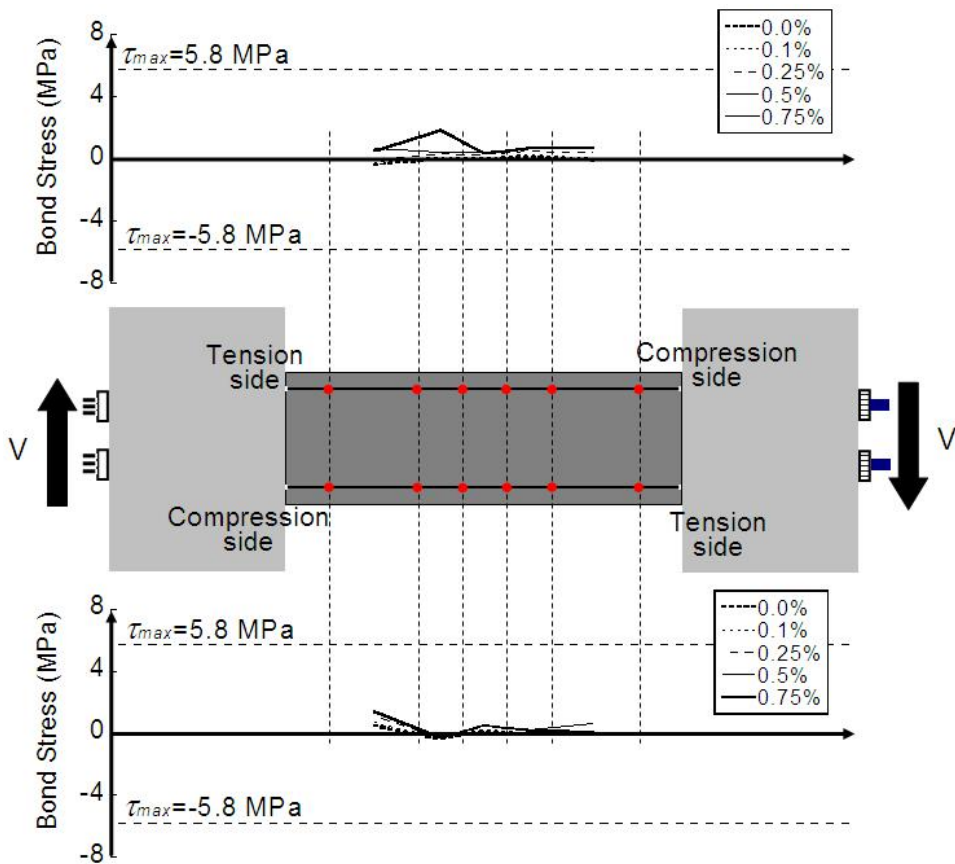
(d) S-15-L10

Fig. 3.36 Distribution of bond stress of non-prestrssed longitudinal bar

3.4 Shear Strength and Shear Failure Mechanism of Prestressed Concrete Members

3.4.1 Experimental Data Used for The Verification

To investigate the applicability of conventional shear analogy to precast / prestressed concrete members, analytical shear cracking and failure strengths by the current shear strength equations are compared to experimental ones.

One hundred three experimental data from previous researches on shear behavior of prestressed / precast concrete members [2.9-2.10, 2.13-2.14, 3.12-3.19] and from this study are used. Table 3.14 shows geometrical and material properties of specimens used in the verification. Experimental shear cracking and failure strength, V_{exp_cr} and V_{exp}, in this study is defined as load carrying the shear capacity of member at primary shear cracking and at peak. Fig. 3.37 plots range of parameters and the distribution of specimens for the verification: (a) compressive strength of concrete; (b) shear span ratio; (c) yield strength of shear reinforcement; (d) shear reinforcement ratio; (e) prestressing and axial force level ($=(P_e+N)/(bDF_c)$); (f) failure mode; (g) prestressing steel and structural type. S, B, and F in Fig. 3.37 (f) indicate shear, bond, and flexural failure, respectively. The definition of shear failure modes, S (ST), S (DT), S (SC), and S (FSC) follow those in section 3.2.4. S(C), R(C), and D(C) in Fig. 3.37 (g) indicate prestressing strand, round, and deformed PT bar in cast-in-situ prestressed concrete member, respectively. The prestressing steel, round, and deformed PT bar in precast prestressed concrete member are indicated as S(P), R(P), and D(P), respectively.
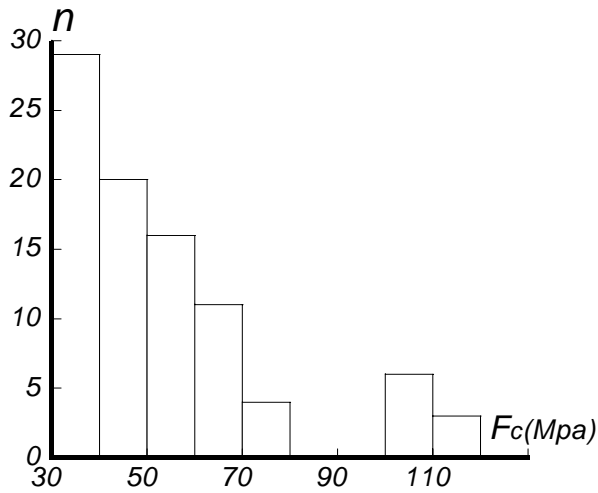
(a) Compressive strength of concrete
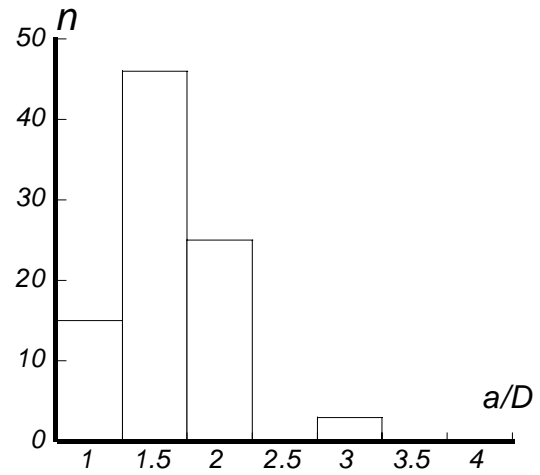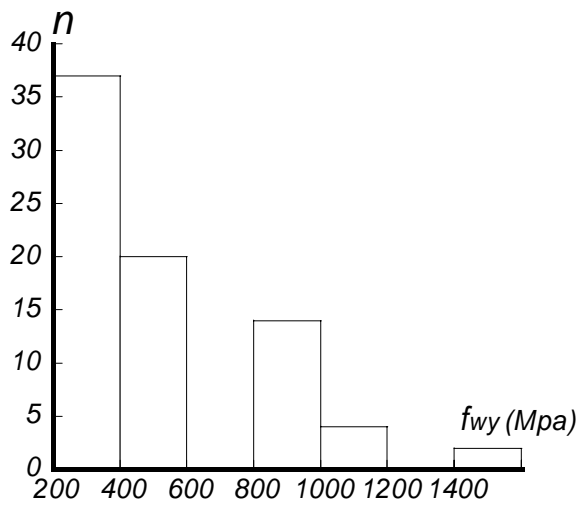
(b) Shear span to overall depth ratio

(c) Yield strength of shear reinforcement
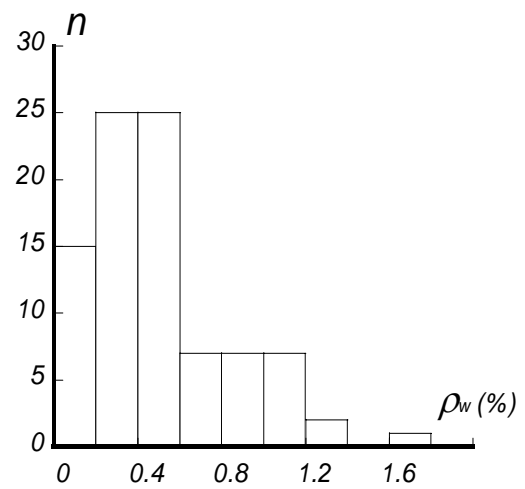
(d) Shear reinforcement ratio
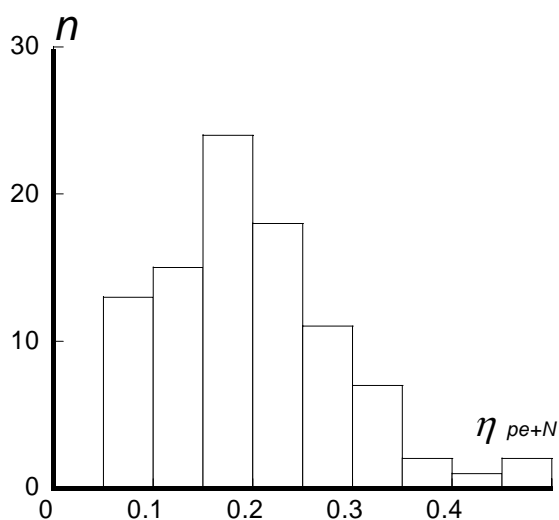
(e) Prestressing and axial force level
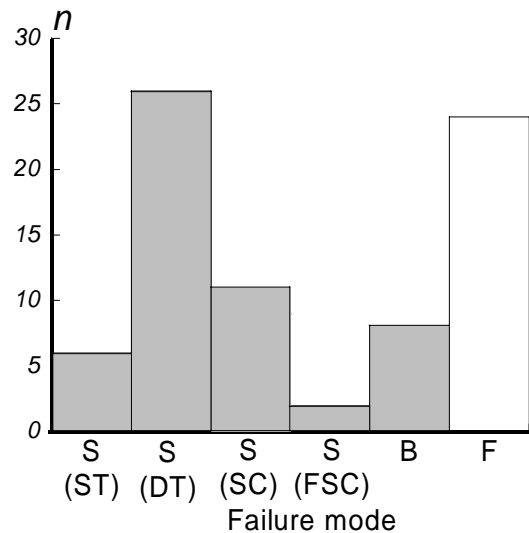
(f) Failure mode

Fig. 3.37 Range of parameters of specimens for the verification
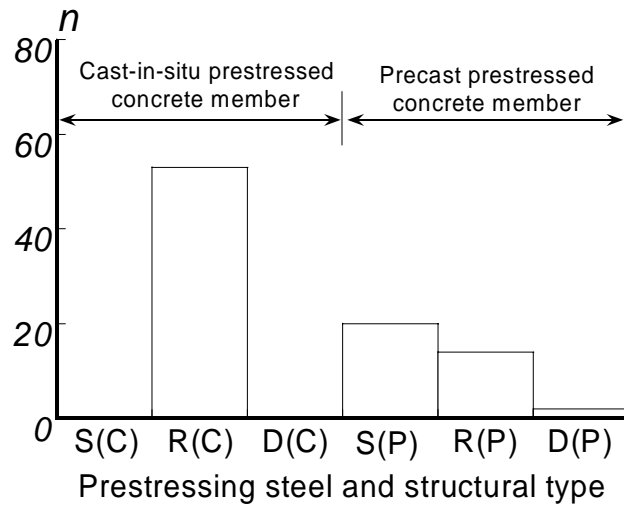
(g) Prestressing steel and structural type

Fig. 3.37 Range of parameters of specimens for the verification

Fig. 3.38 illustrates shear resistance mechanism due to shear reinforcement (truss mechanism) for cast-in-situ and precast prestressed concrete beam, respectively. Shear resistance mechanism of shear reinforcement (Truss mechanism) in cast-in-situ system exists between non-prstressed longitudinal bars in compression and tension because tensile force of non-prestressed longitudinal bar at the ends of member is transferred to anchorage zone as shown in Fig. 3.38. On the other hand, the truss mechanism in precast system with cut-off longitudinal bars significantly distributes between prestressing steel in compression and tension as shown in Fig. 3.38. This is because tensile force of non-prestressed longitudinal bars in precast system is hardly transferred to anchorage zone due to discontinuity of the longitudinal bars at the gap joint. To resolve this problem, Yuasa [2.15] proposed simplified analytical methodology in which distance between   both tensile and compressive reinforcements varies depending on structural type and bond properties of prestressing tendons as follows:

1. In cast-in-situ system, distance between both compressive and tensile reinforcements, j_o, is defined as distance between both non-prestressed longitudinal bars in compression and tension, j_r, regardless of bond properties of prestressing steel.

2. In precast system, j_o varies depending on type of prestressing steel:

    2.1- In the precast system with deformed PT bars or prestressing strands, j_o is defined as distance between both prestressing steel in compression and tension, j_p.

    2.2- In the precast system with round PT tendons, j_o is defined as zero.

(a) Structural type   (b) Truss mechanism
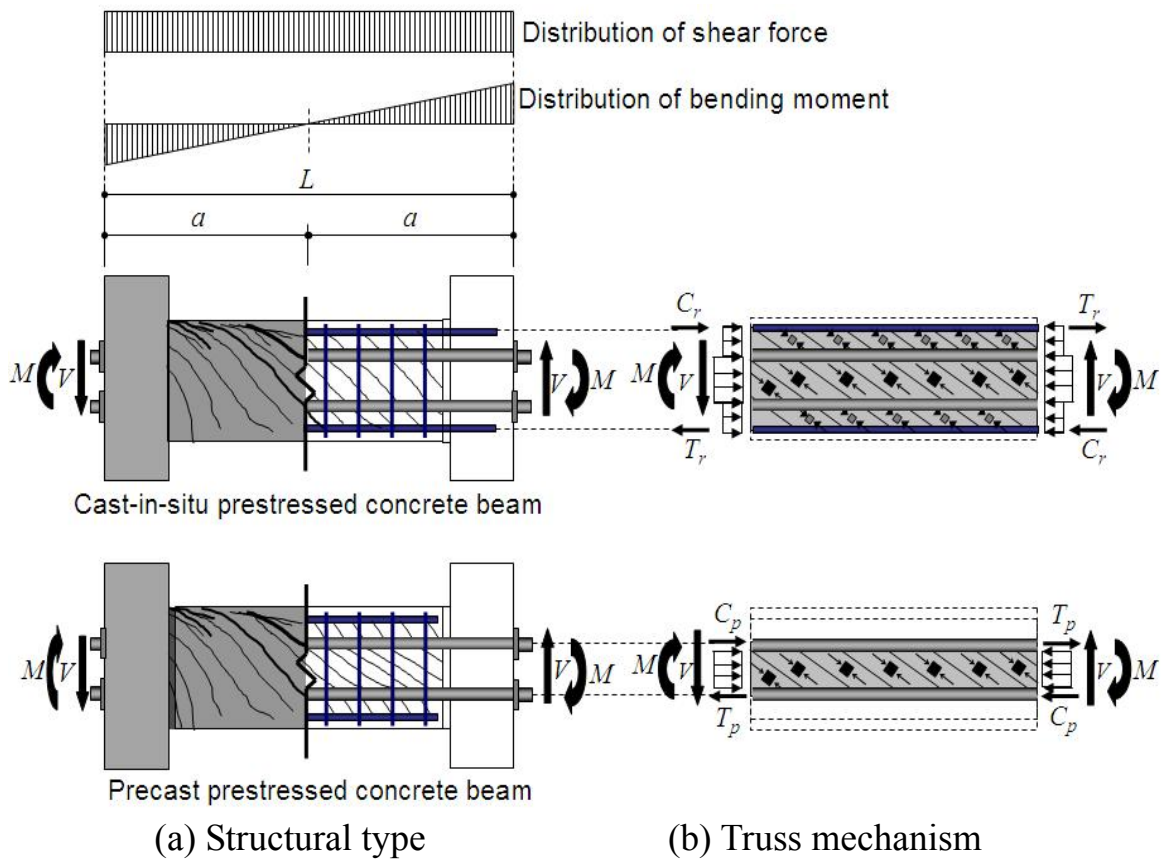
Fig. 3.38 Shear resistance mechanism of cast-in-situ and precast prestressed concrete beam

Table 3.14 Geometrical and material properties of specimens used for the verification

Ref.	No.	Specimen	a/D	Fc (MPa)	Longitudinal bar — Tensile			Longitudinal bar — Compressive			Shear reinforcement			Prestressing steel					ηpe+N	Failure mode	Vexp (kN)
					n	Art (mm)	fry (MPa)	n	Arc (mm)	fry (MPa)	Aw (mm)	ρw (%)	fwy (MPa)	Type	n	Ap (mm)	dp (mm)	fpy (MPa)			
[2.9]	1	B1/3-0.1	1.5	71.6	2		355	2		355	71.3	0.89	355	R(P)	4	415.5	300	1193	0.28	B	810.1
	2	B1/2-0.1		57.8															0.49	B	883.2
	3	B1/2-0.1t		70.4	4	71.3	376	4	71.3	376		1.18	376					1203	0.41	B	878.5
	4	B1/3-0.2			2			2				0.89				804.3		1152	0.27	B	768.5
	5	B1/2-0.2		57.8			355			355			355					1177	0.48	B	811.7
[2.10]	6	R-15-L32	1.5	106.5	3			3			30.0	0.32	988	R(P)	4	530.9	300	1002	0.27	B	1203
	7	R-15-L63			4	71.3	361	4	71.3	361		0.63							0.20	F	1185
	8	R-15-H32			3			3				0.32	1435						0.26	B	1163
	9	R-15-H63			4			4				0.63							0.20	F	1186
	10	D-15-L32			3			3				0.32	988	D(P)		506.7			0.27	B	1253
	11	D-15-L63			4			4				0.63							0.21	F	1230
[2.13]	12	S-PW0	1.5	58.2	2	199	386	2	199	386.0	31.7	0.45	381.0	S(P)	4	227.1	185	1804	0.126	S(DT)	239.0
	13	S-PW04		58.4																B	279.0
	14	S-PW12		56.8							71.3	1.14	381.0						0.130	S(FSC)	316.0
[2.14]	15	S-JP00-PW12		62.8							71.3	1.14	381.0		4	227.1	162	1735	0.117	F	271.0
	16	S-JP075-PW04		59.0							31.7	0.45	347.0						0.125	S(SC)	275.0
	17	S-JP075-PW12		59.7							71.3	1.14	381.0						0.123	F	307.0
[3.13]	18	S-SR1-PW04	1.0	59.4	2	199	328	2	199	328.0	31	0.4	331.0	S(P)	4	227.1	185	1761	0.124	S(SC)	259.0
	19	S-SR1-PW12		59.6							71.3	1.14	366.0						0.123	B	328.0
	20	S-SR2-PW04	2.0	57.8							31.7	0.45	331.0						0.127	FS	215.0
	21	S-SR2-PW12		61.1							71.3	1.14	366.0						0.120	F	240.0
[3.14]	22	NA-PW0	1.5	39.1	0	0	-				0	0	-	R(P)	4	415.5	185	1115		S(DT)	227.0
	23	A-PW0						2	199	360.0	0	0	-	R(C)		227.0		1169	0.188	S(DT)	184.0
	24	A-PW04			2	199	360				31.7	0.45	421.0							S(SC)	244.0
	25	A-PW12									71.3	1.14	355.0							F	270.0

Table 3.14 Geometricaland material properties of specimens used for the verification

Ref.	No.	Specimen	a/D	F_c (MPa)	Tensile n	A_{rt}	f_{ry}	Comp. n	A_{rc}	f_{ry}	A_w	ρ_w	f_{wy}	Type	n	A_p	d_p	f_{py}	η_{pe+N}	Failure mode	V_{exp} (kN)
[3.15]	26	LD2PW04φ13		42.7												132.7		1107	0.087	S(DT)	158.8
	27	LD2PW04φ17										0.42				227.0		1198	0.173	S(DT)	200.9
	28	LD2PW04φ23									12.6		318.5			415.5		1158	0.317	S(DT)	198.5
	29	LD2PW02φ13		42.3												132.7		1107	0.088	S(DT)	149.1
	30	LD2PW02φ17	1.0									0.21		R(C)	2	227.0	210	1198	0.175	S(DT)	183.5
	31	LD2PW02φ23														145.5		1158	0.320	S(DT)	190.5
	32	LD2PW00φ13		46.0									-			132.7		1107	0.081	S(DT)	171.3
	33	LD2PW00φ17									0	0	-			227.0		1198	0.161	S(DT)	162.0
	34	LD2PW00φ23											-			415.5		1158	0.294	S(DT)	165.4
	35	LD3PW04φ13		38.8							12.6	0.42	318.5			132.7		1107	0.096	F	125.1
	36	LD3PW04φ17														227.0		1198	0.191	F	163.4
	37	LD3PW02φ13		38.2	2	71.3	342	2	71.3	342.0	12.6	0.21	318.5			132.7		1107	0.098	FS	129.6
	38	LD3PW02φ17	1.5													227.0		1198	0.194	FS	160.3
	39	LD3PW00φ13									0	0	-			132.7		1107	0.104	F	129.0
	40	LD3PW00φ17		35.8							0	0	-			227.0		1198	0.206	FS	164.8
	41	LD3PW00φ23									0	0	-			415.5		1158	0.377	S(DT)	152.3
	42	LD4PW04φ13		33.8								0.42		R(C)		132.7		1107	0.110	F	91.8
	43	LD4PW04φ17														227.0		1198	0.219	F	116.9
	44	LD4PW02φ13									12.6		318.5			132.7		1107	0.088	FS	94.3
	45	LD4PW02φ17	2.0	42.3								0.21				227.0		1198	0.175	FS	123.7
	46	LD4PW02φ23														415.5		1158	0.320	FS	148.0
	47	LD4PW00φ13									0	0	-			132.7		1107	0.098	FS	93.2
	48	LD4PW00φ17		37.9							0	0	-			227.0		1198	0.195	F	119.4
	49	LD4PW00φ23									0	0	-			415.5		1158	0.357	S(ST)	140.2

Table 3.14 Geometrical and material properties of specimens used for the verification

Ref.	No.	Specimen	a/D	F_c (MPa)	Longitudinal bar						Shear reinforcement			Prestressing steel						Failure mode	V_{exp} (kN)
					Tensile			Compressive													
					n	A_{rt}	f_{ry}	n	A_{rt}	f_{ry}	A_w	ρ_w	f_{wy}	Type	n	A_p	d_p	f_{py}	η_{pe+N}		
[3.16]	50	LD3PW02φ13I	1.5	48.8	2	199	346	2	199	345	12.6	0.21	439.0	R(C)	2	132.7	235	1385	0.089	FS	178.3
	51	LD3PW02φ17I														227.0		1166	0.152	S(DT)	178.7
	52	LD4PW02φ13I	2.0	39.9												132.7		1385	0.108	FS	132.8
	53	LD4PW02φ17I														227.0		1166	0.186	FS	145.9
	54	LD3PW06φ23II	1.5	48.8	3	71.3	353	3	71.3	353	28.3	0.62	432.2			415.5		1017	0.240	FS	243.7
	55	LD4PW06φ23I	2.0	39.9															0.293	F	156.8
	56	LD3PW08φ23II	1.5	48.8								0.83	432						0.240	FS	252.5
	57	LD4PW08φ23II	2.0	39.9															0.293	F	158.1
	58	LD3PW12φ23II	1.5	48.8								1.24							0.240	FS	244.7
[3.17]	59	LD3φ23SD07α30	1.5	39.7	2	127	363	2	127	362	12.6	0.42	434	R(C)	2	415.5	210	1043	0.111	S(SC)	189.3
	60	LD3φ23SD07α45																	0.166	S(SC)	193.9
	61	LD3φ23SD07α60																	0.221	S(ST)	212.6
	62	LD3φ23SD08α60		38.3													240		0.229	S(ST)	200.1
	63	LD3φ26SD07α45														530.9	210	1004	0.219	S(ST)	194.5
	64	LD3φ32SD05α60													1	804.3	150	996	0.221	S(SC)	193.9
	65	LD4φ23SD07α30	2.0	38.3		199	339	2	199	339						415.5		1043	0.114	S(SC)	162.3
	66	LD4φ23SD07α45																	0.171	S(SC)	167.5
[3.18]	67	No.1	2.0	45.8	3	199	445	3	199	445	28.3	0.20	261	R(C)	2		275	1082	0.094	S(SC)	199.1
	68	No.2		48.0															0.179	S(ST)	183.4
	69	No.3		51.1															0.252	S(SC)	271.6
	70	No.4		50.7												804.3			0.169	S(SC)	240.3
	71	No.6		44.8							28.3	0.20	261		1		175	1152	0.191	S(SC)	275.6
	72	No.7	3.0	53.0															0.162	S(SC)	179.5
	73	No.8		71.0															0.181	S(SC)	234.4

Table 3.14 Geometrical and material properties of specimens used for the verification

Ref.	No.	Specimen	a/D	F_c (MPa)	Longitudinal bar						Shear reinforcement			Prestressing steel						Failure mode	V_{exp} (kN)
					Tensile			Compressive													
					n	A_{rt}	f_{ry}	n	A_{rt}	f_{ry}	A_w	ρ_w	f_{wy}	Type	n	A_p	d_p	f_{py}	η_{pe+N}		
[3.18]	74	No.9	3.0	60.1	3	199	445	3	199	445	28.3	0.20	261	R(C)	1	804.3	175	1152	0.285	S(SC)	225.5
[3.19]	75	No.1	1.5	115	2	71.3	364	2	71.3	364	127	1.69	839	R(P)	4	415.5	235	1055	0.09	F	690.0
	76	No.4									71.3	0.95	951							F	698.0
	77	No.5									31.7	0.42	843							S(DT)	698.0
[3.20]	78	9.2J04+1/4	2.0	53.0	4	71.3	295	4	71.3	295	12.6	0.40	480	R(P)	4	66.5	185	1237	0.07	FS	207
	79	11J04+1/3		57.1														1231	0.10	FS	251
	80	11J04+1/8		53.0												95.0		1231	0.10	FS	171
	81	11J04+1/4		57.1															0.10	FS	223
	82	13J04+1/8		61.0												132.7		1213	0.13	FS	209
	83	13J04+1/4																	0.13	FS	251
	84	17J04+1/8														227.0		1050	0.19	FS	217
	85	17J04-1/4																	0.19	FS	262
	86	11J08+1/4		56.8							28.3	0.75	606			95.0		1231	0.10	FS	225
	87	11J12+1/4										1.13							0.10	FS	226
	88	11M04+1/4		54.1							12.6								0.10	FS	227
	89	11J04-3qs/4		57.1															0.10	F	86
	90	11J04+0		53.0							12.6	0.40	480						0.10	F	110
	91	11M04-3qs/4		57.1															0.10	F	84
	92	11J02+1/8		56.8															0.10	F	170
Test1	93	S-10-L42	1.0	57.3	4	71.3	361	4	71.	361	31.7	0.42	984	S(P)	2	592.3	300	1805	0.175	S(FSC)	682.5
	94	S-10-L63										0.63							0.161	FS	741.6
	95	S-15-L21	1.5	62.3								0.21							0.150	S(DT)	509.3
	96	S-15-L42										0.42							0.146	F	509.8
	97	S-15-L63										0.63							0.158	F	530.7

Table 3.14 Geometrical and material properties of specimens used for the verification

Ref.	No.	Specimen	a/D	F_c (MPa)	Longitudinal bar						Shear reinforcement			Prestressing steel						Failure mode	V_{exp} (kN)
					Tensile			Compressive													
					n	A_{rt}	f_{ry}	n	A_{rt}	f_{ry}	A_w	ρ_w	f_{wy}	Type	n	A_p	d_p	f_{py}	η_{pe+N}		
Test1	98	S-20-L21	2.0	55.9	4	71.3	361	4	71.3	361	31.7	0.21	984	S(P)	2	592.3	300	1805	0.212	FS	386.8
	99	S-20-L42										0.42							0.208	F	386.2
Test2	100	S-10-L10	1.0	65.2	4	71.3	381	4	71.3	381	28.3	0.11	1006	S(P)	2	1184.5	500	1763	0.23	S(DT)	1006
	101	S-10-L21										0.21							0.22	S(ST)	1054
	102	S-15-L00	1.5									0.00							0.22	S(DT)	803
	103	S-15-L10										0.11							0.22	S(DT)	884

Note: a/D is Shear span ratio; F_c is compressive strength of concrete in MPa; n is the number of reinforcement; A_{rt}, A_w, and A_p are sectional area of longitudinal bar, shear reinforcement, and prestressing steel in mm; f_{ry}, f_{wy}, and f_{py} are yield strength of longitudinal bar, shear reinforcement, and prestressing steel in MPa; ρ_w is shear reinforcement ratio in %; d_p is effective depth for prestressing steel in mm, and η_{pe+N} is effective prestressing and axial force ratio$(=(P_e+N)/bDF_c)$, respectively.

Type of prestressing steel: R(C) and S(C) are round PT bar and prestressing strand in cast-in-situ prestressed concrete member; R(P), D(P), and S(P) are round PT bar, deformed PT bar, and prestressing strand in precast prestressed concrete member.

3.4.2 Shear Cracking Strength

For the evaluation of shear cracking strength of prestressed concrete members, V_{cr}, a shear cracking strength equation in AIJ guide line [2.8] and a strut mechanism in AIJ PC standard [2.16] are used.

AIJ Shear cracking strength equation [2.8]

The shear cracking strength equation based on principle tensile stress corresponding to tensile strength of concrete (Eq. (3.45)) is used.

$$V_{cr-a} = \frac{1}{1.5} bD \sqrt{F_t \left(F_t + \frac{P_e + N}{bD} \right)}$$
Eq. (3.45)

where b is width of member section, D is overall depth, F_t is tensile strength of concrete, P_e is effective prestressing force, N is axial force, respectively.

AIJ PC Strut Mechanism [2.16]

The shear contribution by concrete (strut mechanism) in AIJ standard for prestressed concrete member [2.16] (Eq. 3.46) is used.

$$V_{cr-b} = 0.5 bD (\nu F_c) \tan \theta$$
Eq. (3.46)

$$\nu = \alpha L_r \left(1 + \frac{P_e}{bDF_c} \right)$$
Eq. (3.47)

$$\tan \theta = \sqrt{(L/D)^2 + 1} - L/D$$
Eq. (3.48)

$$L_r = \frac{a}{2D} \quad \text{and} \quad \alpha = \sqrt{60/F_c}$$
Eq. (3.49)

$$L_r \le 1 \quad \text{and} \quad \alpha \le 1$$
Eq. (3.50)

Figure 3.39 plot comparison between experimental and analytical shear cracking strength by two methods above: (a) for a difference of structural type; and (b) for a difference of failure mode. Vertical and horizontal axis in Fig. 3.39 represent a ratio of observed shear cracking strength to flexural strength, V_{cr-e}/V_{fu}, and a ratio of predicted shear cracking strengths to flexural strength, V_{cr-a}/V_{fu} and V_{cr-b}/V_{fu}, resepetively.

In evaluation by AIJ guide line [2.8], mean value of V_{cr-e}/V_{cr-a}, were 0.2 and 1.3 for specimens failed in SC and DT, respectively. Coefficient of variation (C.V) distributes 0.16 for specimens failed in SC and DT, respectively.

Analytical shear cracking strengths by AIJ standard [2.16] also employed similar

results with those by AIJ guide line [2.8]. For specimens failed in SC and DT, mean value of V_{cr-e}/V_{cr-b} by AIJ standard [2.16] were 0.2 and 0.5, respectively.

It can be seen that two methods provided similar analytical results. However, further investigation for applicability of two methods above to specimens failed in different failure mode needs.

V_{exp_cr}/V_{cr}	R(C)○	S(P)▲
Mean	0.8	1.0
C.V.	0.31	0.17

V_{exp_cr}/V_{cr}	R(C)○	S(P)▲
Mean	0.7	0.8
C.V.	0.24	0.14
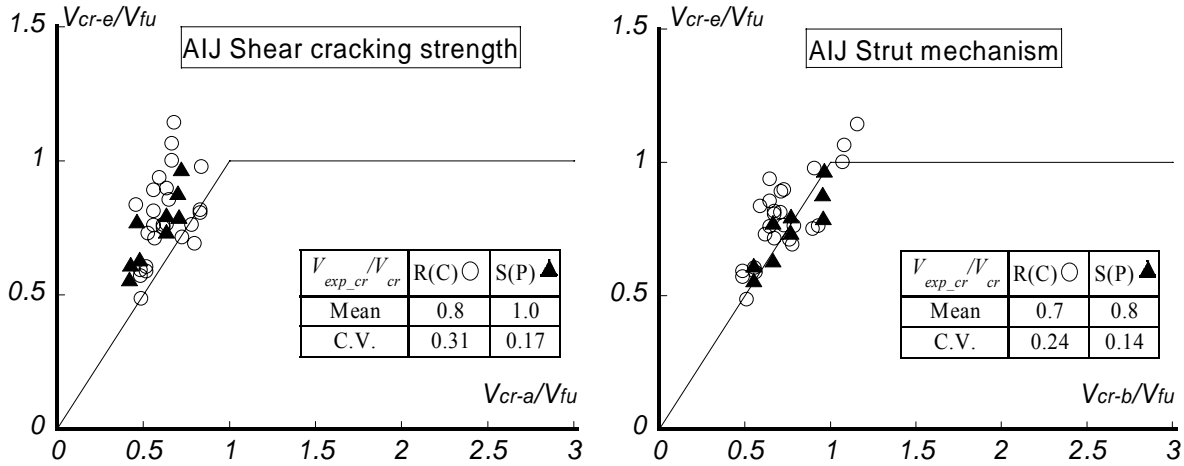
(a) Structural type (R(C) and S(P))

V_{exp}/V_A	S(ST)●	S(SC)▲	S(DT)■	FS○	F△
Mean	1.3	0.2	1.3	1.2	1.1
C.V.	0.16	0.16	0.16	0.24	0.17

V_{exp}/V_A	S(ST)●	S(SC)▲	S(DT)■	FS○	F△
Mean	1.2	0.2	0.5	1.0	1.1
C.V.	0.18	1.01	0.23	0.18	0.13
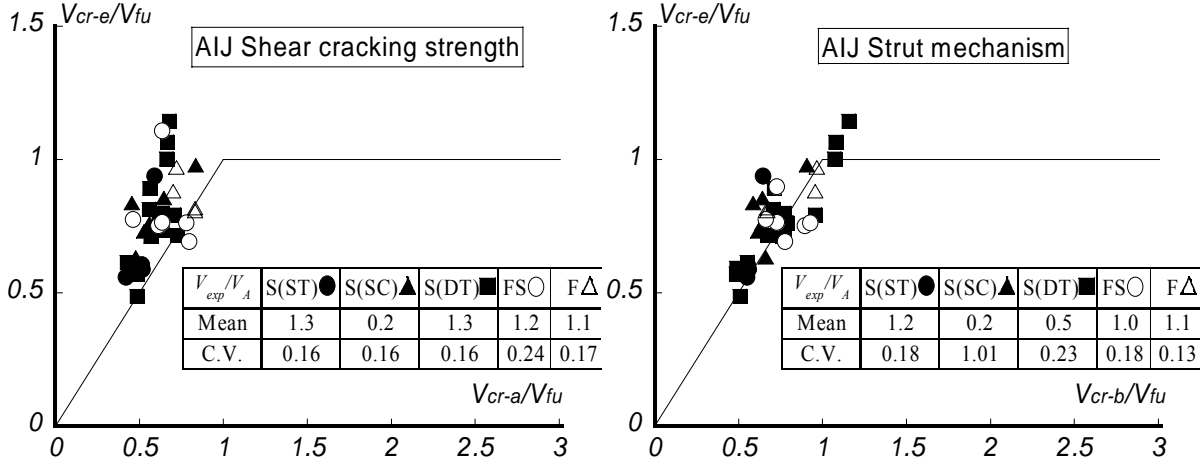
(b) Failure mode

Fig. 3.39 Comparison between observed and analytical shear cracking strength

3.4.3 Shear Failure Strength

For the analytical shear strength of prestressed / precast concrete members, three design equations (ACI shear design equation [2.7], AIJ guide line [2.8] and AIJ standard [2.16]). For the verification of shear failure strength, experimental data of specimens failed in flexure and shear after flexural yielding (F and FS) are excluded.

112

Method A

This is a set of shear design equations of ACI 318-08 [2.7]. The equations were specified in section 2.4.1. Effective depth, d, is defined as distance from extreme compression fiber to tensile longitudinal bar, d_r, in Method A.

Method B

This is a set of shear design equations of ACI 318-08 [2.7] applied the following analytical modification.

1. Effective depth, d, is defined as d_r for cast-in-situ prestressed concrete members and distance from extreme compression fiber to tensile prestressing steel, d_p, for precast prestressed concrete members, respectively.

Method C

The shear design equations from AIJ guide line for reinforced concrete members [2.8] using following modifications are used in Method C. The shear design equations are specified in section 2.4.2.

1. Yuasa's methodology: Effective distance between reinforcing bar in compression and tension, j_e, is defined as a distance between non-prestressed longitudinal bars, j_r, for cast-in-situ prestressed concrete members, and between prestressing steel in compression and tension, j_p for post-tensioned precast concrete members, respectively.

Method D

The shear design equations in Ref. 2.16 applied the following modifications are used in Method D.

1. Yuasa's methodology: Distance between reinforcing bar in compression and tension, j_o, is defined as a distance between non-prestressed longitudinal bars in compression and tension, j_r, for cast-in-situ prestressed concrete members, and between prestressing steel in compression and tension, j_p for precast prestressed concrete members, respectively.

2. Upper limit for yield strength of shear reinforcement ($f_{wy} \leq 295$ MPa) is neglected.

The detail equations were specified in section 2.4.3.

Figure 3.40 plots relationship between experimental and analytical shear

strength: (a) for a different structural type; (b) for a different failure mode. Horizontal and vertical axis in Fig. 3.40 represent a ratio of analytical shear strength to shear force at flexural strength, V_A/V_{fu}, V_B/V_{fu}, V_C/V_{fu}, or V_D/V_{fu}, and a ratio of experimental peak load to shear force at flexural strength, V_{exp}/V_{fu}, respectively. Analytical shear strength, V_A, V_B, V_C, and V_D are shear strength by *Method A*, *B*, *C*, and *D* respectively. Experimental peak load, V_{exp}, in specimen failed in flexure and shear represent flexural and shear strength, respectively. Shear force at flexural strength, V_{fu} in Fig. 3.40 is obtained by M_u/a where M_u is flexural strength by AIJ stress block (Eq. 3.3) and a is shear span, respectively.

V_{exp}/V_A	R(C) ○	S(P) ▲	R(P) ●	D(P) ■
Mean	1.6	1.1	1.2	1.7
C.V.	0.21	0.42	0.43	-

V_{exp}/V_B	R(C) ○	S(P) ▲	R(P) ●	D(P) ■
Mean	1.6	1.2	2.8	1.9
C.V.	0.21	0.37	0.26	-

V_{exp}/V_C	R(C) ○	S(P) ▲	R(P) ●	D(P) ■
Mean	1.6	2.2	4.5	3.0
C.V.	0.32	0.28	0.39	-

V_{exp}/V_D	R(C) ○	S(P) ▲	R(P) ●	D(P) ■
Mean	1.0	0.9	1.1	1.2
C.V.	0.10	0.08	0.15	-
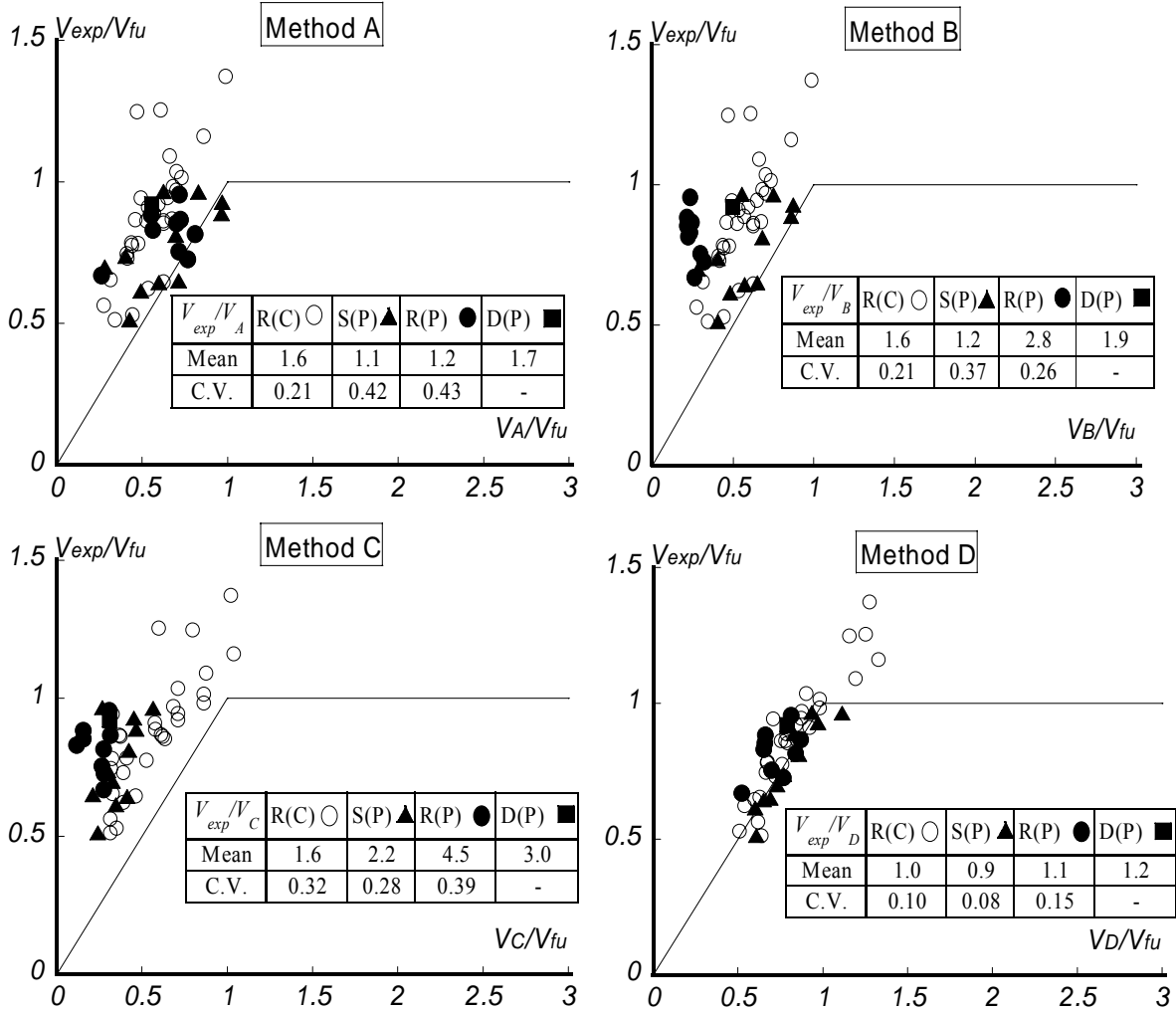
(a) Structural type

Fig. 3.40 Comparison between experimental and analytical shear strength

114

V_{exp}/V_A	S(ST)●	S(SC)▲	S(DT)■	S(FSC)△	B ○
Mean	1.4	1.2	1.6	0.9	1.2
C.V.	0.20	0.30	0.31	0.03	0.22

V_{exp}/V_B	S(ST)●	S(SC)▲	S(DT)■	S(FSC)△	B○
Mean	1.8	1.5	1.7	1.1	2.5
C.V.	0.14	0.23	0.39	0.02	0.36

V_{exp}/V_C	S(ST)●	S(SC)▲	S(DT)■	S(FSC)△	B ○
Mean	2.3	2.4	1.7	2.0	3.2
C.V.	0.26	0.27	0.77	0.05	0.39

V_{exp}/V_D	S(ST)●	S(SC)▲	S(DT)■	S(FSC)△	B ○
Mean	1.1	1.0	1.0	1.0	1.1
C.V.	0.16	0.09	0.12	0.08	0.14
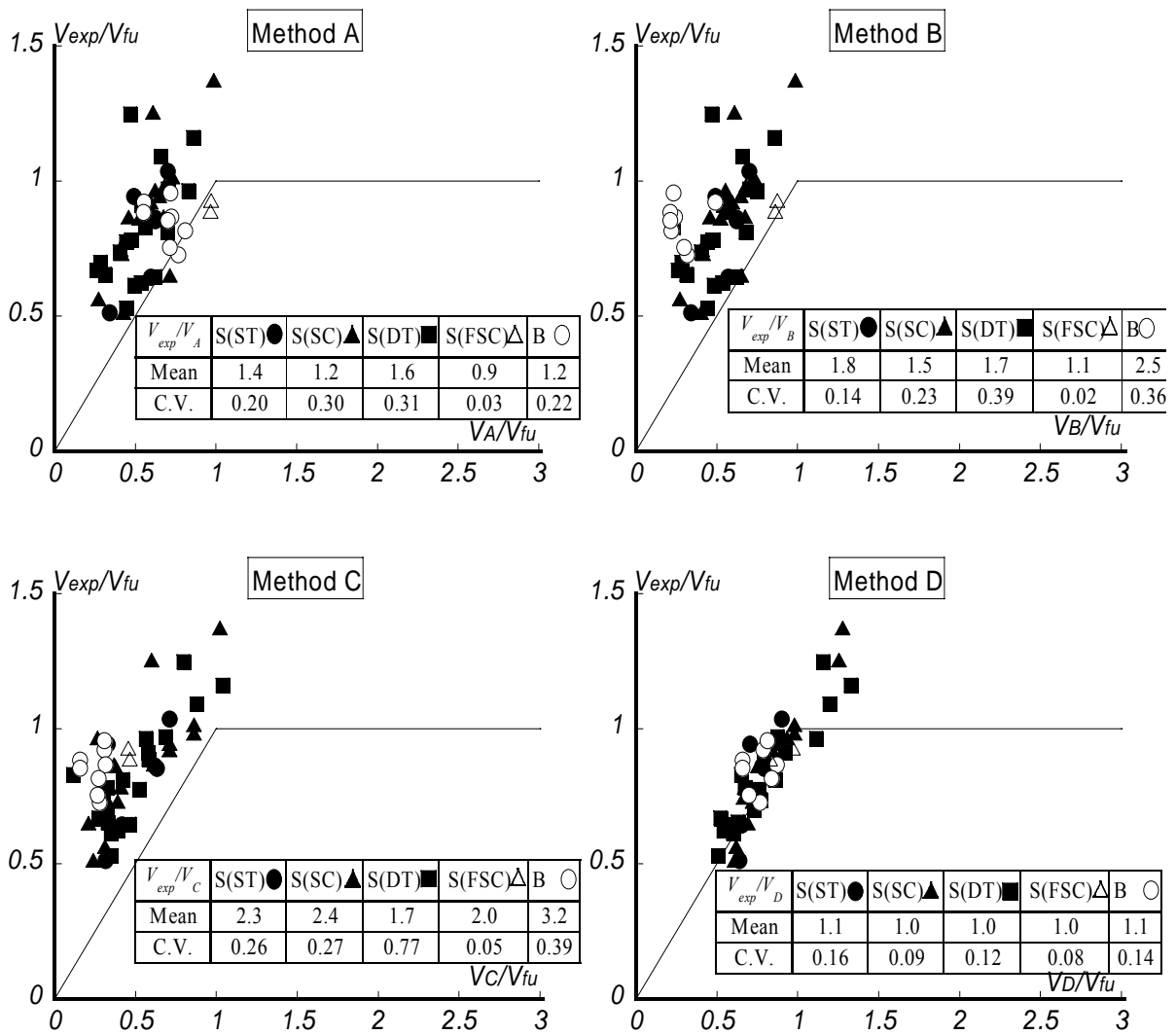
(b) Failure mode

Fig. 3.40 Comparison between experimental and analytical shear strength

As shown in Fig. 3.40 (a), *Method A* provided V_{exp}/V_A of 1.6 for cast-in-situ prestressed concrete members with round PT bar (R(C)). It also produced V_{exp}/V_A of 1.1, 1.2, and 1.7 for precast prestressed concrete member with prestressing strand (S(P)), round PT bar (R(P)), and deformed PT bar (D(P)), respectively. As shown in Fig. 3.40 (b), *Method A* provided V_{exp}/V_A of 1.4, 1.2, 1.6, 0.9, and 1.2 for shear strength of beam failed in shear tension (ST), shear compression (SC), diagonal tension (DT), flexural shear compression (FSC), and bond (B) failure, respectively. Analytical shear strength by *Method A* could not evaluate experimental shear strength within ±20% accuracy. Coefficient of variations of V_{exp}/V_A distributed from 0.21 to 0.43 and from 0.03 to 0.31 for structural type and failure mode, respectively.

Method B gave V_{exp}/V_B of 2.8 for structural type R(P). For other structural types,

Method B provided analytical shear strength in a similar accuracy with *Method A*. In failure mode, *Method B* could not evaluate experimental shear strength of beam failed in shear compression (SC) within ±20% accuracy.

Method C provided V_{exp}/V_C of 2.2, 4.5, and 3.0 for S(P), R(P), and D(P), respectively. No analytical shear strength evaluated experimental ones within ±20% accuracy. Also, large coefficient of variations (C.V = 0.28 to 0.39 and 0.05 to 0.77 for structural type and failure mode) were resulted by *Method C*. It can be seen that most underestimated analytical shear strengths were resulted by *Method C*. It is because a beneficial effect of prestress on shear resistance is not taken into consideration in *Method C*.

Analytical shear strength by *Method D* evaluated experimental shear strength in a best accuracy of four methods. Mean value of V_{exp}/V_D distributed from 0.9 to 1.2 and from 1.0 to 1.1 for structural type and failure mode. Further V_{exp}/V_D of the smallest C.V.s were provided by *Method D*.

3.4.4 Effect of Experimental Parameters on Shear Strength

Figure 3.41 plots relationship between a ratio of experimental to analytical shear strength, V_{exp}/V_A, and experimental parameters: (a) compressive concrete strength, F_c; (b) shear span to overall depth ratio, a/D; (c) yield strength of shear reinforcement, f_{wy}; (d) shear reinforcement ratio, ρ_w; and (e) prestressing level, η_{pe}. Vertical and horizontal axis in Fig. 3.41 represent a ratio of experimental to analytical shear strength and each experimental parameters, respectively. In a same manner, the relationships between a ratio of experimental to analytical shear strength by *Method B* to *D* and experimental parameters are plotted in Fig. 3.42 to 3.44, respectively.

As shown in Fig. 3.41 to 3.44, Analytical shear strengths by *Method D* evaluated experimental ones in best accuracy of four methods regardless of experimental paramters. It points out that beneficial effect of prestress on shear resistance and bond properties of longitudinal and prestressing tendon must be taken into account to evaluate shear strength of prestressed / precast concrete members.
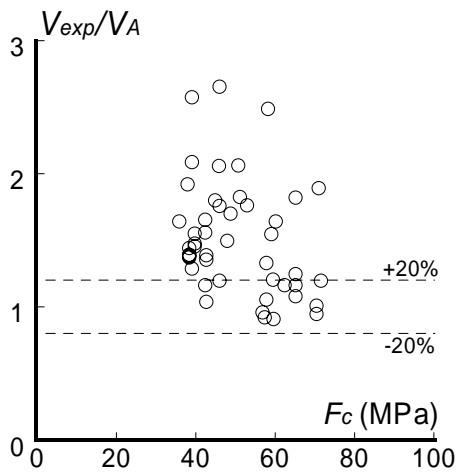
(a) Compressive strength of concrete
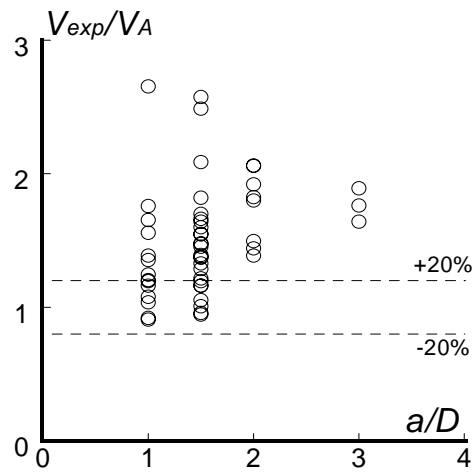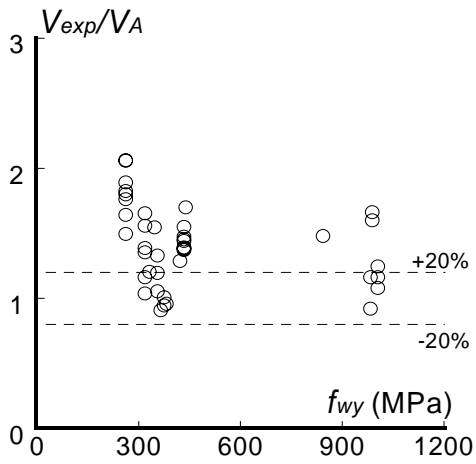
(b) Shear span to overall depth ratio

(c) Yield strength of shear reinforcement
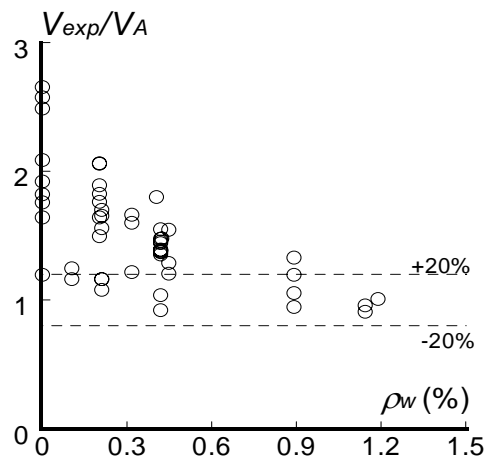
(d) shear reinforcement ratio
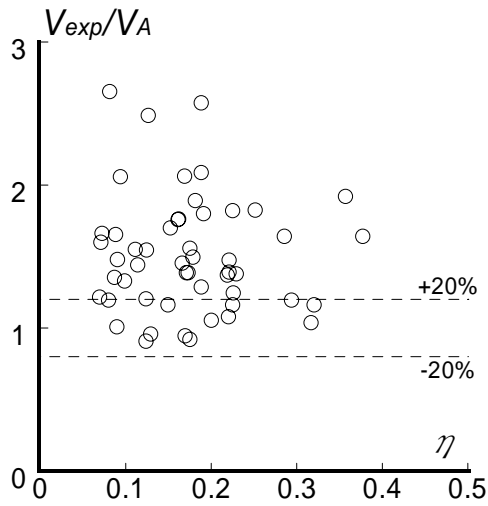
(e) Prestressing level

Fig. 3.41 Relationship between V_{exp}/V_A and experimental paramters
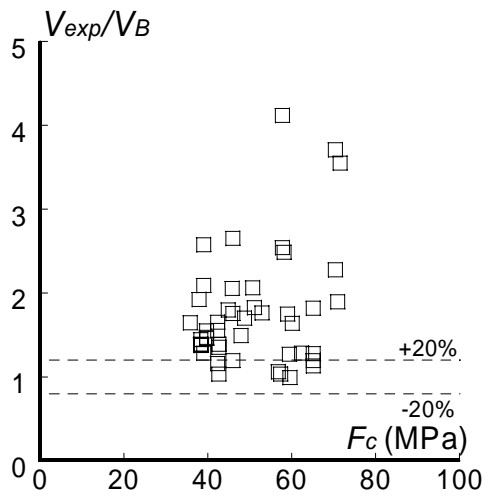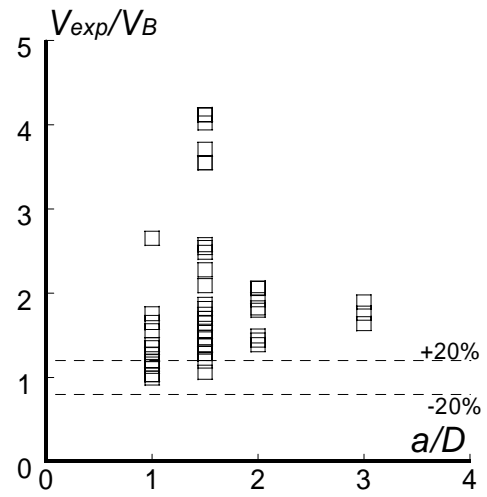
(a) Compressive strength of concrete (b) Shear span to overall depth ratio
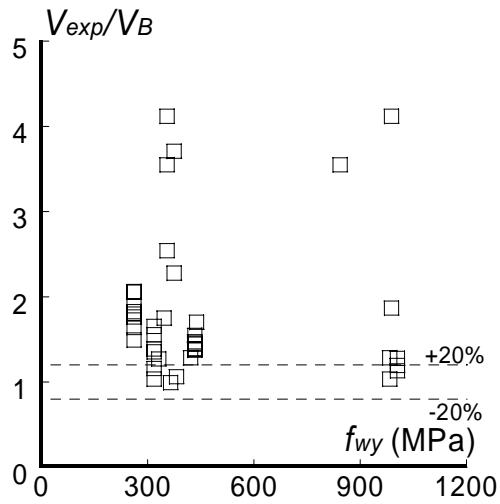
(c) Yield strength of shear reinforcement (d) Shear reinforcement ratio
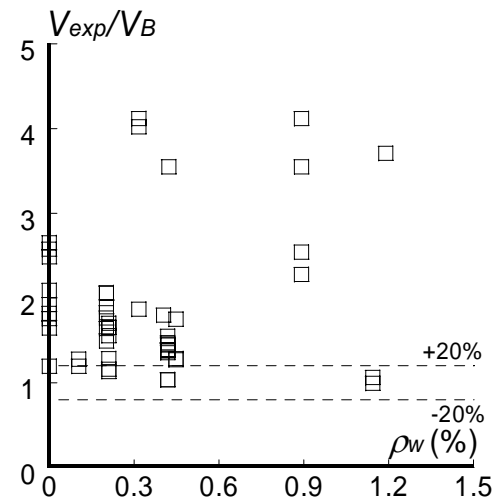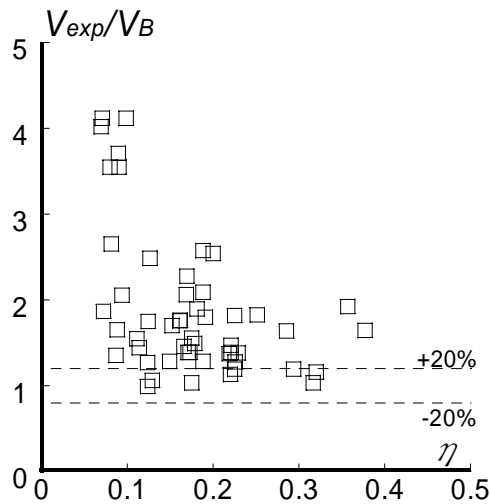
(e) Prestressing level

Fig. 3.42 Relationship between V_{exp}/V_B and experimental paramters
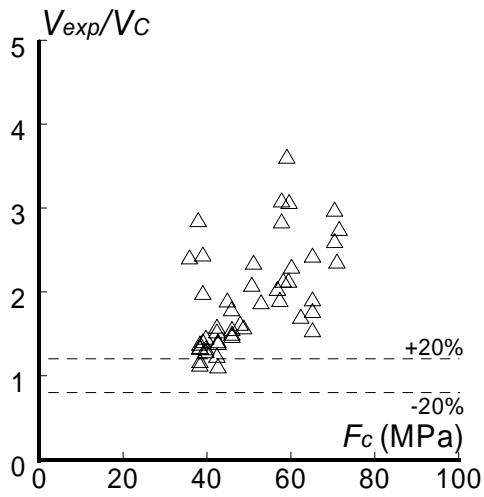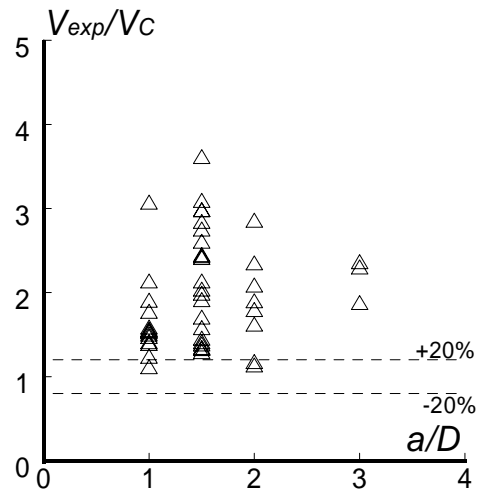
(a) Compressive strength of concrete

(b) Shear span to overall depth ratio
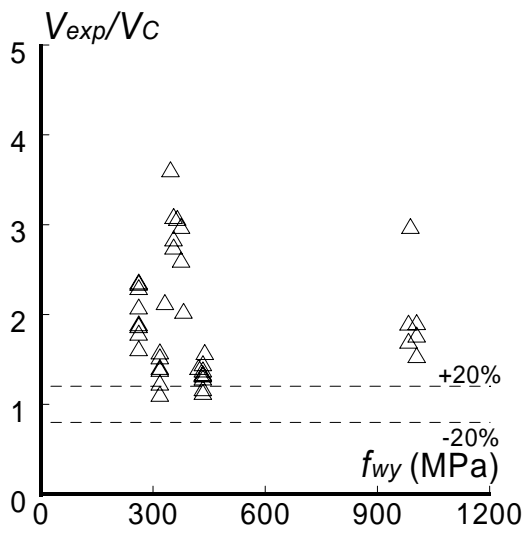
(c) Yield strength of shear reinforcement
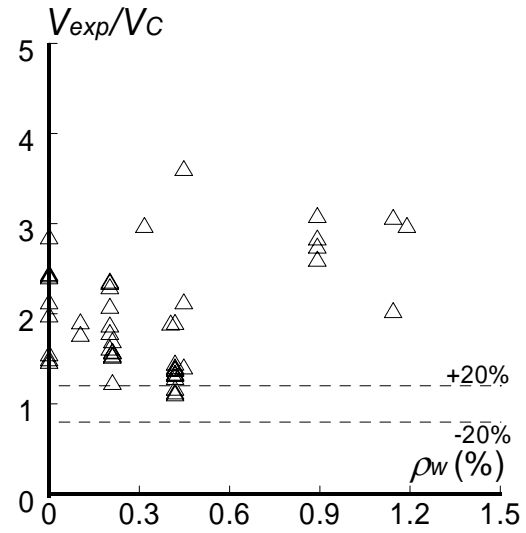
(d) Shear reinforcement ratio
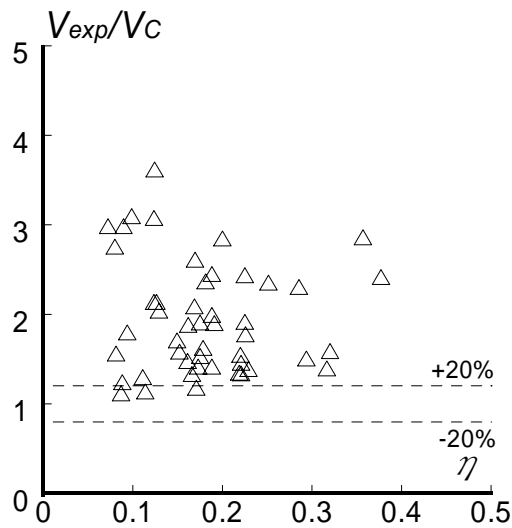
(e) Prestressing level

Fig. 3.43 Relationship between V_{exp}/V_C and experimental paramters

(a) Compressive strength of concrete (b) Shear span to overall depth ratio

(c) Yield strength of shear reinforcement (d) Shear reinforcement ratio

(e) Prestressing level
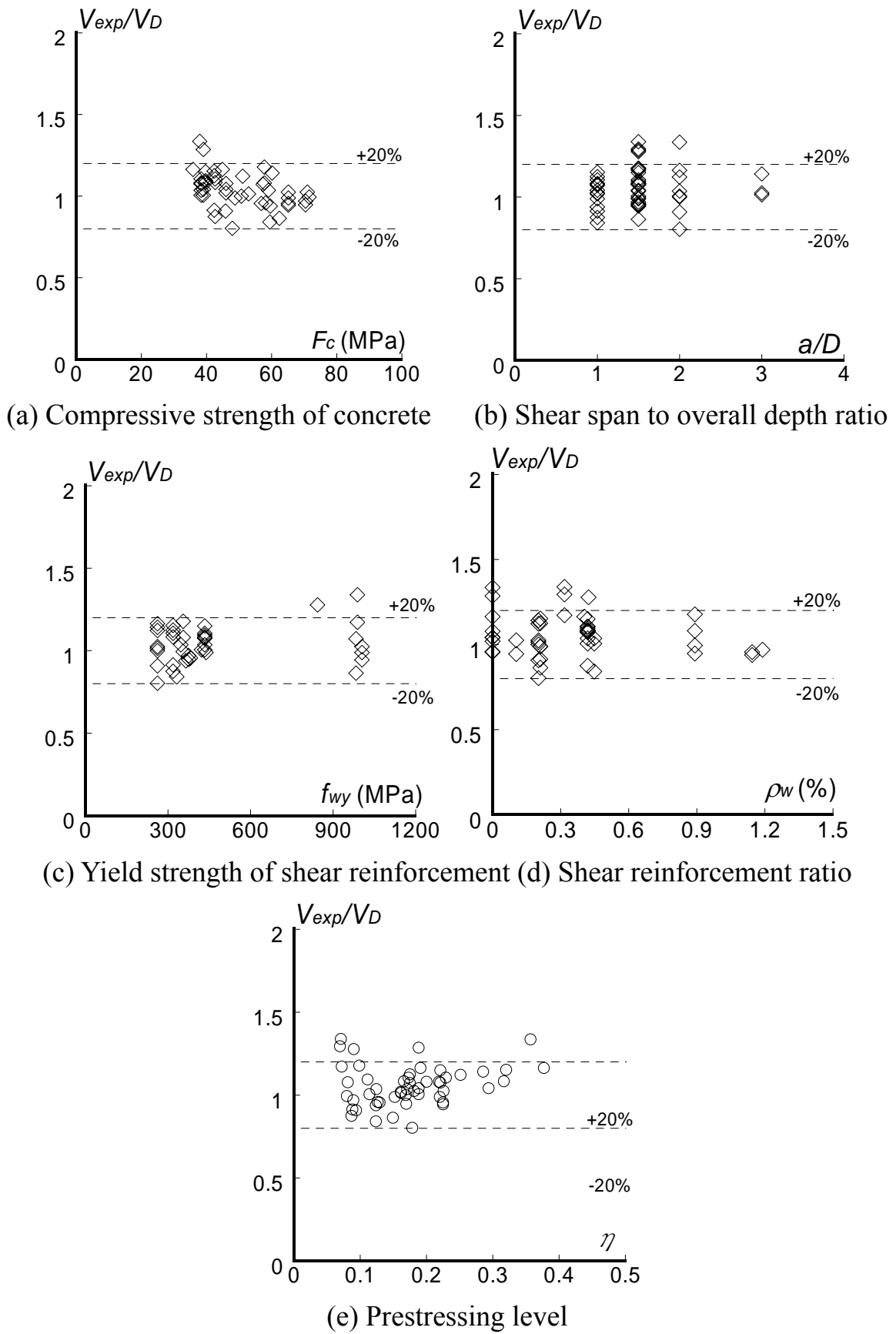
Fig. 3.44 Relationship between V_{exp}/V_D and experimental paramters

3.4.5 Effect of Experimental Parameters on Failure Mode

Figure 3.45 plots relationship between the shear failure mode and experimental parameters. Three shear failure modes, ST, SC, and DT, are accepted in this section. Vertical and horizontal axis in Fig. 3.45 indicate a ratio the number of specimens failed in shear to the number of total specimens and experimental parameters: (a) compressive strength of concrete; (b) shear span to overall depth ratio; (c) yield strength of shear reinforcement; (d) shear reinforcement ratio; and (e) prestressing level, respectively. Symbols, ■, ▲, and ● in Fig. 3.45 represent experimental data of specimens failed in diagonal tension (DT), shear compression (SC), and shear tension (ST), respectively. The numbers in parenthesis in horizontal axis indicate the number of specimens corresponding to each experimental parameter.

(a) Compressive strength of concrete

(b) Shear span to overall depth ratio

(c) Yield strength of shear reinforcement

(d) Shear reinforcement ratio
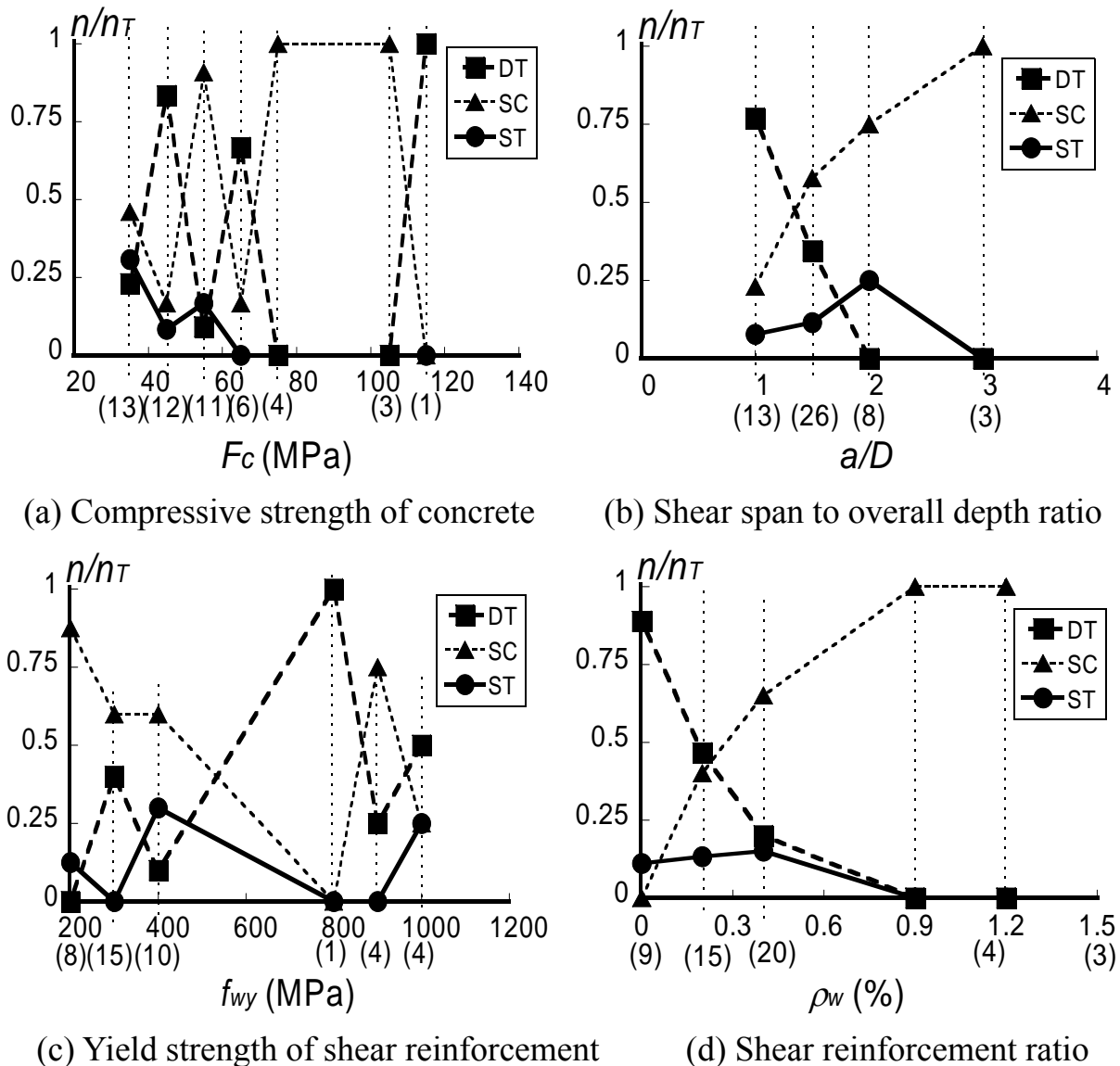
Fig. 3.45 Relationship between shear failure mode and experimental parameters
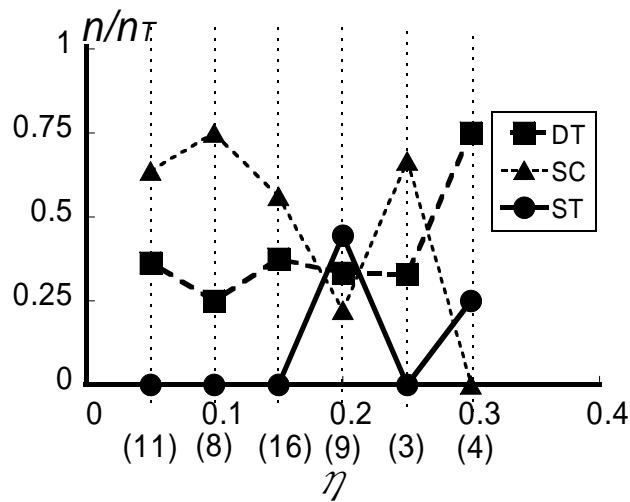
(e) Prestressing level

Fig. 3.45 Relationship between shear failure mode and experimental parameters

As shown in Fig. 3.45, shear compression failure (SC) occurs in prestressed concrete member with high a/D or high ρ_w while diagonal tension failure (DT) does in the member with low a/D or low ρ_w. It points out that shear reinforcement in prestressed concrete member with long span or with large amount of shear reinforcement might not yield at shear failure (SC). Further, it is noted that shear reinforcement in short span member hardly contribute for shear resistance of member.

3.5 Conclusions

In section 3, two series of static loading test on flexural and shear behavior of post-tensioned precast concrete beams had been conducted. Main conclusions by the tests are summarized as follows.

1. Five failure modes (ST, SC, DT, FSC, and F) were observed: shear reinforcement in prestressed concrete beams failed in ST (shear tension) yielded at ultimate state while the shear reinforcement in the beams failed in SC or FSC does not yield. In DT failure, initiation of primary shear crack leads to decay of load carrying the shear capacity of beams,

2. In flexural deformation, tensile stresses of prestressing steel at beam-stub joint were the largest: deformation of post-tensioned precast concrete beam concentrates the beam-stub joints.

3. Tensile stresses of shear reinforcement at mid-span in which moment equals to zero were largest while those at both ends of beam were

approximately zero.

4. In DT failure, shear reinforcement hardly contributed for shear resistance of beam.

5. In FSC failure, the prominent crushing of the concrete at the flexural compression zone was observed.

6. In evaluation of shear failure strength using current shear design equations, *Method D* in which shear equations in Ref. 2.16 were modified evaluated the experimental shear failure strength in the best accuracy.

7. By parametric study using experimental data from previous researches and from this study, it can be seen that shear span to overall depth ratio, *a/D*, and shear reinforcement ratio, ρ_w, significantly affect to failure mode.

The following future works must be resolved to rationally investigate shear and flexural failure mechanism of prestressed / precast concrete members.

1. In shear compression failure (SC), the effect of bonds tress of non-prestressed longitudinal bars or prestressing steels and compressive stress in cover and cracked concrete on shear resistance mechanism of prestressed / precast concrete members needs to be quantified.

2. In diagonal tension failure (DT), relationship between initiation of primary shear crack and shear resistance needs to be investigated.

3. In flexural shear compression failure (FSC), the shear capacity of the concrete at the flexural compression zone needs to be scrutinized.

4. Deformation capacity of post-tensioned precast concrete member at flexural failure must be predicted.

5. An effect of bond stress of prestressing steel on flexural behavior of prestressed / precast concrete members must be scrutinized.

The future works above will be scrutinized in next sections.

[References]

3.1 Okdada M., Hamahara M., Suetsugu H., Motooka J., "Elasto-plastic Hysteretic Behavior of Prestressed Concrete Beams," *Journal of Structural and Construction Engineering*, AIJ, No. 410, April, 1990, pp. 63-69 (in Japanese).

3.2 Sugano S., "Elasto-plastic Hysteretic Behavior of Reinforced Concrete Members," *Concrete Journal*, JCI, Vol. 11, No. 2, Feb., 1973, pp. 1-9.

3.3 Architectural Institute of Japan, "Standard for Structural Design and Construction of Prestressed Concrete Structures," 1998, pp. 184-196 (in Japanese).

3.4 Research Committee on Bond Property in Prestressed Concrete Members and Structures Organized by Japan Prestressed Concrete Engineering Association (2005), "The State of the Art Report on Bond Property in Prestressed Concrete Members and Structures, 2005, pp. 3.7-3.10 (in Japanese).

3.5 Korenaga T., Watanabe H., "Model of the Bond Characteristics between Prestressing Strand and Grout Mortar," *Summaries of Technical Papers of Annual Meeting*, AIJ, 1999, pp. 1083-1084 (In Japanese).

3.6 Kiuchi Y., Katou H., Takamatsu K., "Experimental Study on Bond Property between PC Tendon and Concrete (Part 2. Discussion on Bond-Slip Relationship," *Summaries of Technical Papers of Annual Meeting*, AIJ, Sep., 2000, pp. 1013-1014 (In Japanese).

3.7 Architectural Institute of Japan (AIJ), "Design Guide lines for Earthquake Resistant Reinforced Concrete Buildings Based on Inelastic Displacement Concept," 1999, pp. 175-192 (In Japanese).

3.8 Yoshida K., Kitayama K., Nishikawa T., "Shear Strength of Reinforced Concrete Columns Subjected to Tensile Axial Force," *Proceeding of Japan Concrete Institute,* JCI, Vol. 18, No. 2, 1996, pp. 875-880 (In Japanese).

3.9 Bazant ZP, Xiang Y. Size effect in compression fracture: splitting crack band propagation. *Journal of Engineering Mechanics*, ASCE, Vol.123, No. 2, 1997, pp. 162-172.

3.10 Bazant ZP, Kazemi MT. Size effect on diagonal shear failure of beams without stirrups. *ACI Structural Journal*, Vol. 88, No. 3, 1991, pp. 268-276.

3.11 Yang KH, Chung HS, Lee ET, Eun HC. Shear characteristics of high-strength concrete deep beams without shear reinforcements. *Engineering structures*, Vol. 25, 2003, pp. 1343-1352.

3.12 Ohtaga K., Yuasa N., Hamahara M., "Experimental study on shear behavior of precast prestressed concrete beams," *Summaries of Technical Papers of Annual Meeting*, AIJ, Oct., 2002, 991-992. (In Japanese)

3.13 Ogawa T., Saito A., Iida S., Fukui T., Suetsugu H., Sakiyama K., Hamahara M., "Experimental study on shear behavior of precast prestressed concrete beams," *Summaries of Technical Papers of Annual Meeting*, AIJ, Sep., 1999,

1077-1078. (In Japanese)

3.14 Fukui T., Nagasawa T., Hamahara M., Suetugu H., "Experimental Study on Shear Behavior of Prestressed Concrete Beams," *Summaries of Technical Papers of Annual Meeting*, AIJ, Sep., 1994, 1023-1028. (In Japanese)

3.15 Fukui T., Ookuma A., Hamahara M., Suetugu H., "Experimental Study on Shear Strength and Ductility of Prestressed Concrete Beams," *Summaries of Technical Papers of Annual Meeting*, AIJ, Sep., 1996, 877-880. (In Japanese)

3.16 Ookuma A., Fukui T., Hamahara M., Suetugu H., "Effect of Prestress on Shear Behavior of Prestressed Concrete Beams," *Summaries of Technical Papers of Annual Meeting*, AIJ, Sep., 1997, 847-852. (In Japanese)

3.17 Wakamatsu S, Takizawa K, Takagi H, Shiraishi I. Experimental study on shear properties of prestressed concrete beams, *Summaries of Technical Papers of Annual Meeting*, AIJ, Sep., 1998, 1039-1040. (In Japanese)

3.18 Fukui T., Ookuma A., Hamahara M., Suetugu H., "Ultimate Shear Strength of Prestressed Concrete Beam," *Journal of Structural and Construction Engineering*, AIJ, No. 505, Mar., 1998, pp. 107-114. (In Japanese)

3.19 Yoon W., Hamahara M., Motooka J., "Experimental Study on Restoring Force Characteristics of Precast Prestressed Concrete Columns," *Journal of Structural and Construction Engineering*, AIJ, No. 480, Feb., 1996, pp. 151-160. (In Japanese)

4. Analytical Model 1 for Shear Failure Mechanism of Post-tensioned Precast Concrete Members (SC and ST Model)

4.1 Introduction

Extensive researches have been conducted on shear behavior of reinforced concrete (RC) to investigate their shear resisting mechanisms [2.3, 4.1-4.6]. The original study on the shear resisting mechanism was conducted by Ritter [4.1] who proposed a truss model for computing the shear strength. Extensive experimental researches were then conducted to modify Ritter's model in terms of the inclination of shear crack [4.2]. Then, Mitchell [4.3] proposed the compression field theory (CFT) to account for load level and deformation. Vecchio [2.3] carried out further research to develop modified compression field theory (MCFT), in which tensile stresses in concrete was considered. Ghiassi [4.1] proposed an analytical method for post cracking response of reinforced concrete members using the stresses at the crack surfaces.

Before MCFT model, it was difficult to apply the analytical models developed for RC members to prestressed / precast concrete members since effects of prestressing and bond characteristics of tendons on shear resistance model were not properly evaluated. Collins [2.2] applied MCFT model to prestressed concrete members. As upper limit conditions in the calculation procedure, Collins designated the maximum compressive strength of shear cracked concrete and yield strength of shear reinforcement.

Let's consider a post-tensioned precast concrete member subjected to anti-symmetric bending with shear force, V, axial force N, and bending moment, M as shown in Fig. 1. At either end of the member, the prestressing tendons carry compressive and tensile forces, C_p and T_p, and the ordinary reinforcement

carries compressive and tensile forces, C_r and T_r. It is noted that the ordinary reinforcement are cut off slightly inside the ends in precast members. The former experiments on this type of members showed that the shear reinforcement did not yield when the shear capacity was reached [3.14-3.15, 4.8].
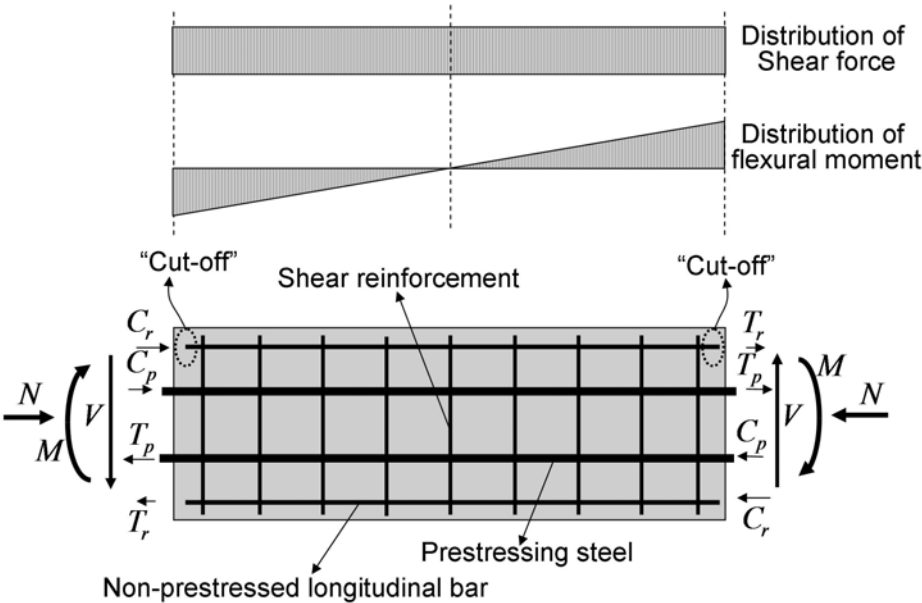
Fig. 4.1 Post-tensioned precast concrete member subjected to pure shear

To account for the fact of non-yielding of shear reinforcement at the shear capacity, Yuasa [2.15] proposed a simplified analytical method based on a truss analogy to take into account shear contribution of shear reinforcement correctly.

In his truss analogy, a distance between both tensile and compressive reinforcements varies depending on types of prestressing tendons. To evaluate concrete contribution to shear capacity, Yuasa used the shear design equation in the design standard of Architectural Institute of Japan [2.16]. He assumed that a distance between tensile and compressive reinforcements is zero if round prestressing bars are used in post-tensioned precast members. In this case, the shear contribution from shear reinforcement on shear strength becomes zero. However, it has been reported by several experiments that tensile stress in shear reinforcement increase and shear reinforcement contribute for shear capacity of post-tensioned precast concrete member [2.9-2.10]. Further, it is not clear the effects of bond characteristics of prestressing tendons on the stress and strain conditions of concrete and reinforcements.

In this chapter, the shear resisting model is proposed for ST, SC, and B failure of post-tensioned precast concrete members with cut-off non-prestressed longitudinal bars by taking into account the bond characteristics of prestressing tendons. The proposed truss model well simulated shear strength, load-deformation response, tensile stress of shear reinforcement, bond stress on prestressing steel, stress in cracked concrete compressive struts in Post-tensioned precast concrete members up to the peak. The accuracy of the proposed model was examined by comparing the simulation with experimental data in terms of shear strength, shear strain, and tensile stress in shear reinforcement.

4.2 Model Outline

4.2.1 Shear Resistance Model of Post-tensioned Prestressed Concrete Member

Figure 4.2 illustrates a new truss model for a post-tensioned precast concrete member. The member has two layers of mild reinforcing bars and two layers of prestressing tendons. It is subjected to anti-symmetric bending moment with constant shear force and axial force. The proposed shear resisting mechanism assumes three zones. Zone 1, represented by ABF or EIJ, is compressive triangles in cover concrete at the top and bottom of the member. Zone 2, BCGF or DEIH, exists between the mild reinforcing bars and tendons and has diagonal cracks with angle θ_2. Zone 3, CDHG, exists between two tendons with diagonal cracks with angle θ_3. The analytical shear force, V_a, is the summation of shear stress at each zone.
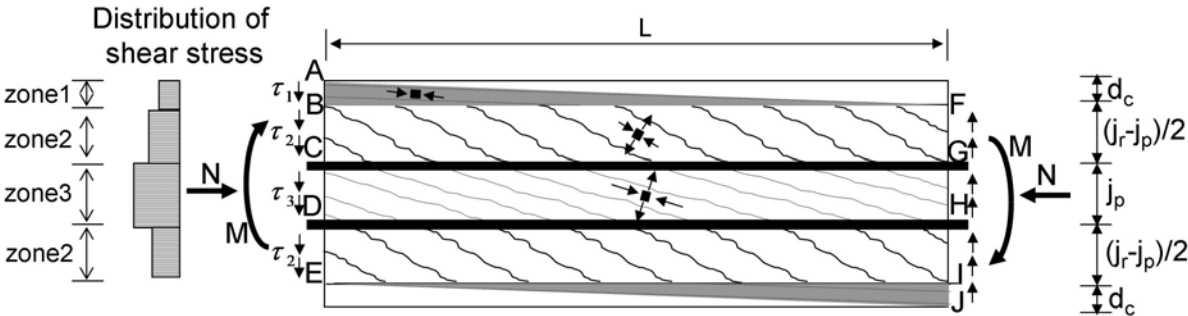
Fig. 4.2 Proposed model for shear resistance mechanism of post-tensioned precast concrete member

In post-tensioned precast concrete members, compressive longitudinal mild bars normally yield before the maximum shear capacity is reached because mild steel, which has the yield strength between 300 MPa – 450 MPa, is used [2.9-2.10]. Since the bond stress of longitudinal reinforcing bars rapidly decreases after yielding [4.6], it is neglected to construct the shear resisting mechanism in this study. Fig. 4.3 illustrates distribution of bond stress of non-prestressed longitudinal bar in: (a) cast-in-situ prestressed concrete member; and (b) precast prestressed concrete member. Ichinose [2.5] showed the existence of additional contribution of lateral force from concrete cover in addition to the bond force of longitudinal bars although the quantification has not been made. In post-tensioned precast concrete member, tensile force of non-prestressed longitudinal bar is hardly transferred to anchorage zone. Then, equivalent bond stress of longitudinal bar distributes along the member length as shown in Fig. 4.3 (b). In this study, it is assumed that cover concrete strut distribute along the whole of a member length because it can be seen that tensile force of longitudinal bar in tension side equals to zero in precast prestressed concrete member. Moreover, the contribution from the concrete cover is quantified to construct a new truss model. Therefore, in post-tensioned precast concrete member, the compressive struts due to cover concrete can be distribute as ABF or EIJ in Fig. 4.2, because longitudinal bars are usually cut off at the end of member.

(a) Cast-in-situ prestressed concrete member
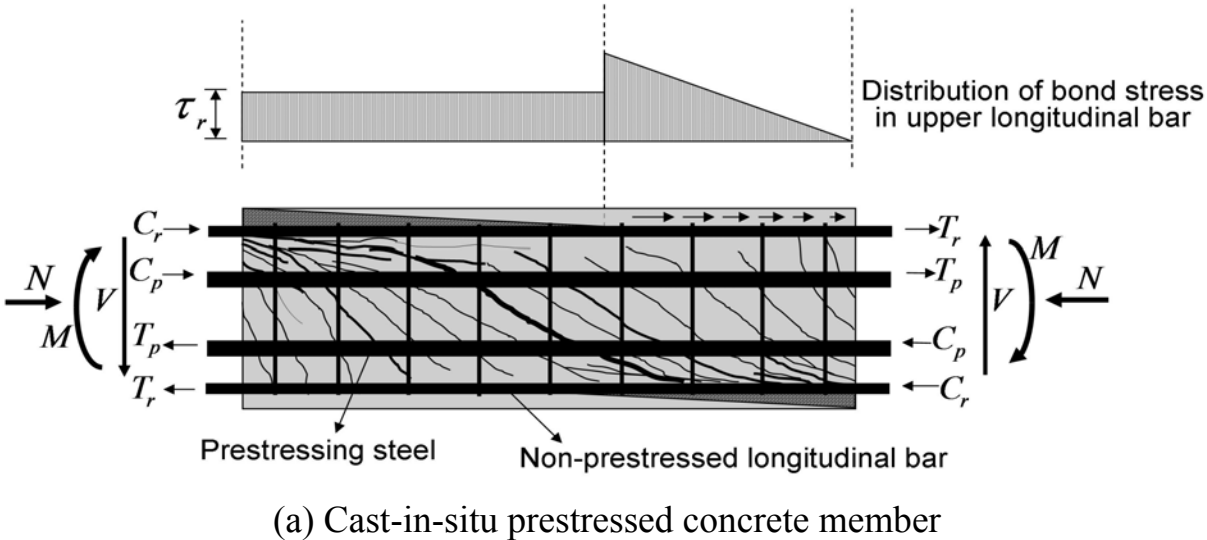
Fig. 4.3 Distribution of bond stress of upper non-prestressed longitudinal bar
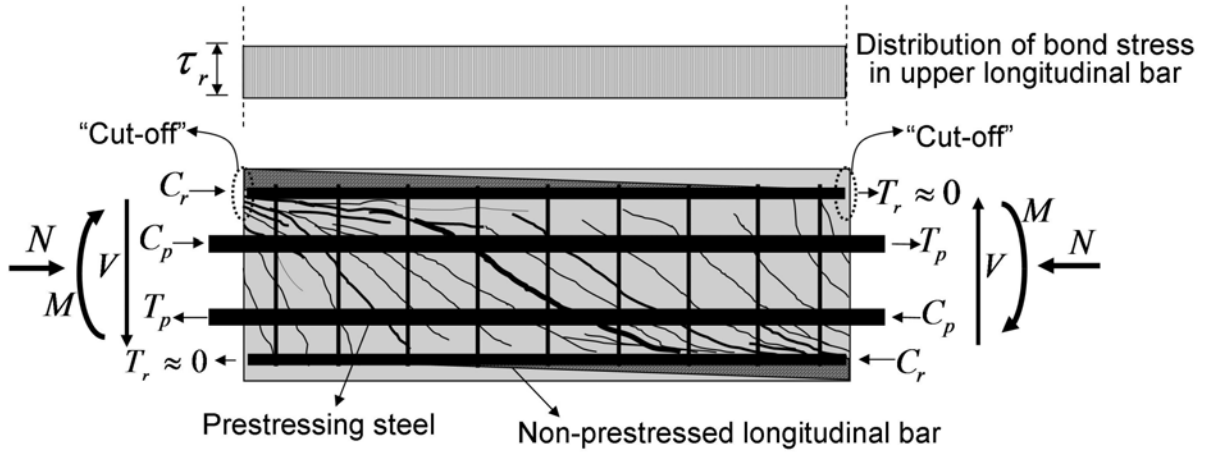
(b) Precast prestressed concrete member

Fig. 4.3 Distribution of bond stress of upper non-prestressed longitudinal bar

The analytical shear force, V_a, by proposed truss model (Fig. 4.2) is calculated by Eq. (4.1).

$$V_a = b(\tau_1 d_c + \tau_2 (j_r - j_p) + \tau_3 j_p) \qquad \text{Eq. (4.1)}$$

where b is the beam width, d_c is the cover concrete depth, j_r is the distance between two non-prestressed longitudinal bars, j_p is the distance between two prestressing tendons, τ_1, τ_2, and τ_3 are shear stresses in Zones 1, 2, and 3, respectively.

For analytical simplification, the following assumptions are made.

Assumption 1: Stresses and strains are uniform in each zone. Hence the mean values are used in formula.

Assumption 2: The principle strain directions coincide with the principle stress directions. Shear cracks are parallel to the compressive principal strain and stress.

Assumption 3: In practice, the width of shear crack is variable in even same zone. However, it is assumed that shear crack width in a zone same because strains are uniform in each zone (Assumption 1). Further, it is assumed that shear crack widths in Zones 2 and 3 in Fig. 4.2 are same because it is difficult to evaluate distribution of shear crack width in two zones.

4.2.2 Equilibrium Requirements of Stresses

In order to consider the equilibrium conditions, stress states in each zone is defined. Fig. 4.4 illustrates stress states and resultant forces in: (a) Zone 1 and 2; (b) Zone 2 to 3; (c) Zone 1 and 3 in Fig. 4.4 at the zero moment section in web spacing, s. Fig. 4.5 illustrates Mohr's stress circle for each zone. Zone 1 is compressed uniaxially with stress, f_{11}, and angle, θ_1, where $\tan\theta 1 = \dfrac{d_c}{L}$. Shear stress in the Zone 1 is given as $\tau_1 = f_{11}\dfrac{Ld_c}{L^2 + d_c^2}$. Zone 2 is under biaxial conditions with the principal stresses, f_{21} and f_{22}. Stress f_{21} is the compressive principal stress with angle θ_2, and it is parallel to the cracking as defined by Assumption 2. Stress f_{22} is the tensile principal stress. Shear stress in Zone 2, τ_2, may be expressed as $\tau_2 = (f_{21} + f_{22})\sin\theta_2\cos\theta_2$ from the Mohr's circle in Fig. 4.5 (b). In a same manner, shear stress in Zone 3, τ_3, may be expressed as $\tau_3 = (f_{31} + f_{32})\sin\theta_3\cos\theta_3$ using the compressive principal stress f_{31}, and tensile principal stress, f_{32} (Fig. 4.5 (c)).

Let's consider equilibrium conditions of free body which consists of Zone 1 and 2 in Fig. 4.4 (a). Assuming that it has one set of shear reinforcement with spacing s and the beam width is b, the equilibrium conditions in longitudinal (horizontal) and transverse (vertical) direction are expressed as follows.

$$\frac{bsLd_c}{L^2 + d_c^2}f_{11} = bs\tau_2 \qquad\qquad \text{Eq. (4.2)}$$

$$bs(f_{21}\sin^2\theta_2 - f_{22}\cos^2\theta_2) = A_w f_{ws2} + \frac{bsd_c^2}{L^2 + d_c^2}f_{11} \qquad\qquad \text{Eq. (4.3)}$$

Solving simultaneous equation, Eq. (4.2) and (4.3), for f_{21} after eliminating f_{22} produces Eq. (4.4).

$$f_{21} = \frac{A_w f_{ws2}}{bs} + \frac{d_c + L\cot\theta_2}{L^2 + d_c^2}d_c f_{11} \qquad\qquad \text{Eq. (4.4)}$$

where s is spacing of shear reinforcement and L is member length.

In a same manner, equilibrium requirements in longitudinal and transverse direction in Zone 2 ~ 3 (Fig. 4.4 (b)) and 1~3 (Fig. 4.4 (c)) are as Eq. (4.5) to (4.8). Unknowns f_{31}, f_{32}, θ_3, τ_p, and f_{ws3} in Eq. (4.5) to (4.8) indicate principle compressive and tensile stress, inclination of shear crack in Zone 3, bond stress

131

on prestressing steel, and tensile stress in shear reinforcement, respectively. From Eq. (4.7), bond stress on the prestressing steel can be expressed as Eq. (4.9).

$$bs(f_{31} + f_{32})\sin\theta_3\cos\theta_3 = \tau_p\psi_p s + \frac{bsLd_c}{L^2 + d_c^2}f_{11} \quad \text{for Zone 1~3} \quad \text{Eq. (4.5)}$$

$$bs(f_{31}\sin^2\theta_3 - f_{32}\cos^2\theta_3) = A_w f_{ws3} + \frac{bsd_c^2}{L^2 + d_c^2}f_{11} \quad \text{for Zone 1~3} \quad \text{Eq. (4.6)}$$

$$(f_{21} + f_{22})\sin\theta_2\cos\theta_2 + \frac{\tau_p\psi_p}{b} = \sin\theta_3\cos\theta_3(f_{31} + f_{32}) \quad \text{for Zone 2~3} \quad \text{Eq. (4.7)}$$

$$f_{31}\sin^2\theta_3 - f_{32}\cos^2\theta_3 = f_{21}\sin^2\theta_2 - f_{22}\cos^2\theta_2 + \frac{A_w(f_{ws3} - f_{ws2})}{bs} \quad \text{for Zone 2~3} \quad \text{Eq. (4.8)}$$

$$\tau_p = \frac{b}{\psi_p}[\sin\theta_3\cos\theta_3(f_{31} + f_{32}) - (f_{21} + f_{22})\sin\theta_2\cos\theta_2] \quad \text{Eq. (4.9)}$$

where ψ_p is sum of perimeters of prestressing steels in one layer.
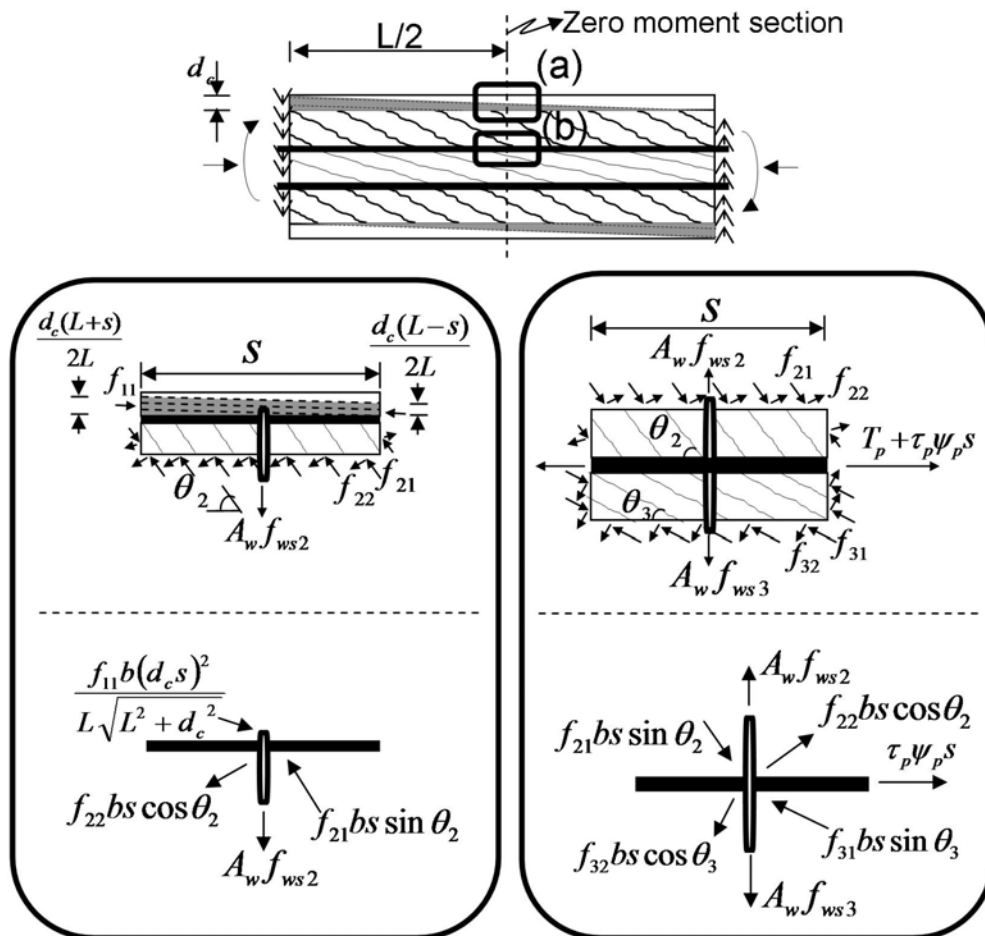
(a) Stress state and resultant forces in Zone 1 ~ 2

(b) Stress state and resultant forces in Zone 2 ~ 3

Fig. 4.4 Stress state and resultant force in each zone
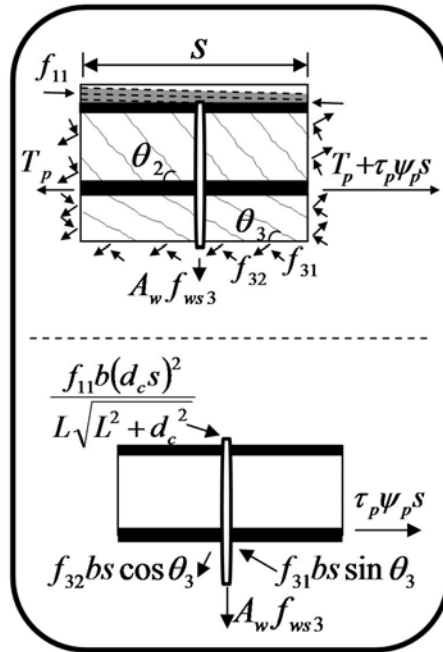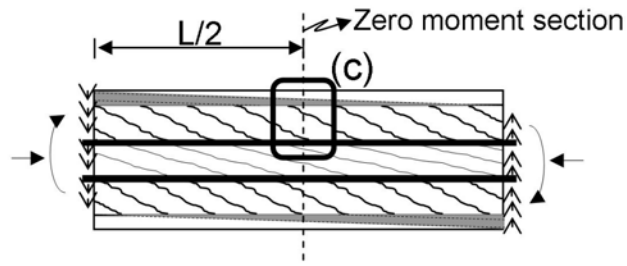
(c) Stress state and resultant
forces in Zone 1 ~ 3

Fig. 4.4 Stress state and resultant force in each zone

(a) Zone 1   (b) Zone 2   (c) Zone 3
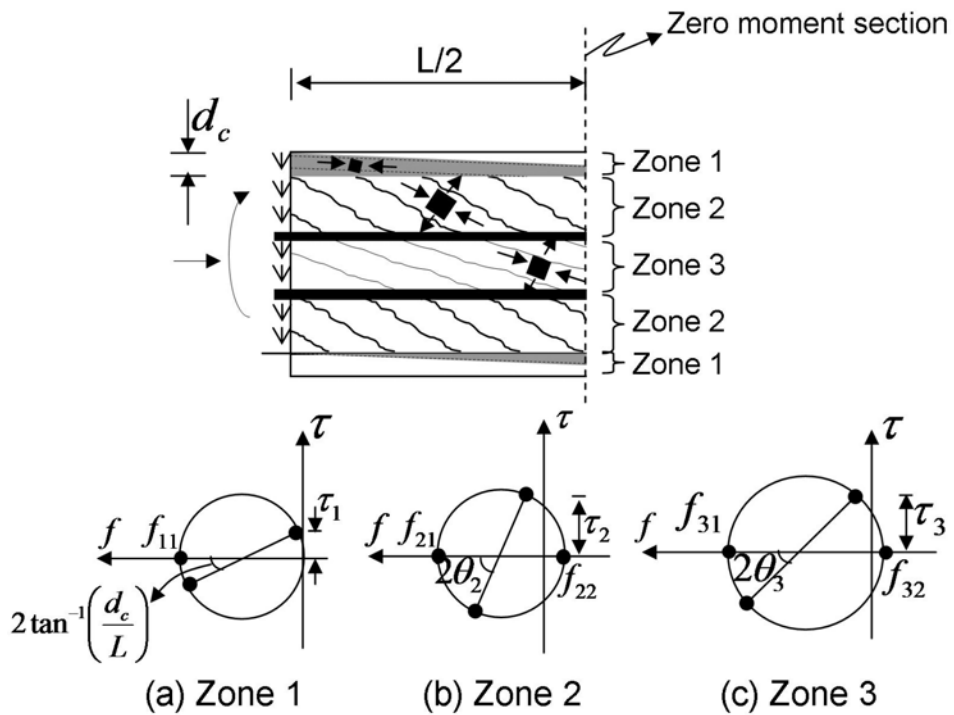
Fig. 4.5 Mohr`s stress circle of each zone

Longitudinal components in concrete and reinforcements must be counteracted by an equal applied axial forces, N. Fig. 4.6 shows the axial stresses at zero moment section in longitudinal direction. As shown in Fig. 4.6, unbalanced longitudinal component of the diagonal cracked concrete stresses and axial force must be equilibrated by tensile stresses in the non-prestressed longitudinal bar and prestressing steel. This longitudinal equilibrium requirement can be expressed as Eq. (4.10). Unknown f_{1x}, f_{2x}, and f_{3x} are longitudinal stress in Zone 1, 2, and 3 which are expressed as Eq. (4.11) to (4.13) by free body (Fig. 4.4) or Mohr's stress circle (Fig. 4.5), respectively.

$$A_r f_{rs} + A_p f_{ps} = f_{2x} b (j_r - j_p) + f_{3x} b j_p + f_{1x} b d_c - N \qquad \text{Eq. (4.10)}$$

$$f_{1x} = f_{11} \frac{L^2}{L^2 + d_c^{\ 2}} \qquad \text{for Zone 1} \quad \text{Eq. (4.11)}$$

$$f_{2x} = f_{21} \cos^2 \theta_2 - f_{22} \sin^2 \theta_2 \qquad \text{for Zone 2} \quad \text{Eq. (4.12)}$$

$$f_{3x} = f_{31} \cos^2 \theta_3 - f_{32} \sin^2 \theta_3 \qquad \text{for Zone 3} \quad \text{Eq. (4.13)}$$

where A_r and A_p are sectional area of non-prestressed longitudinal bar and prestressing steel, f_{rs} and f_{ps} are tensile stress in longitudinal bar and prestressing steel, respectively.
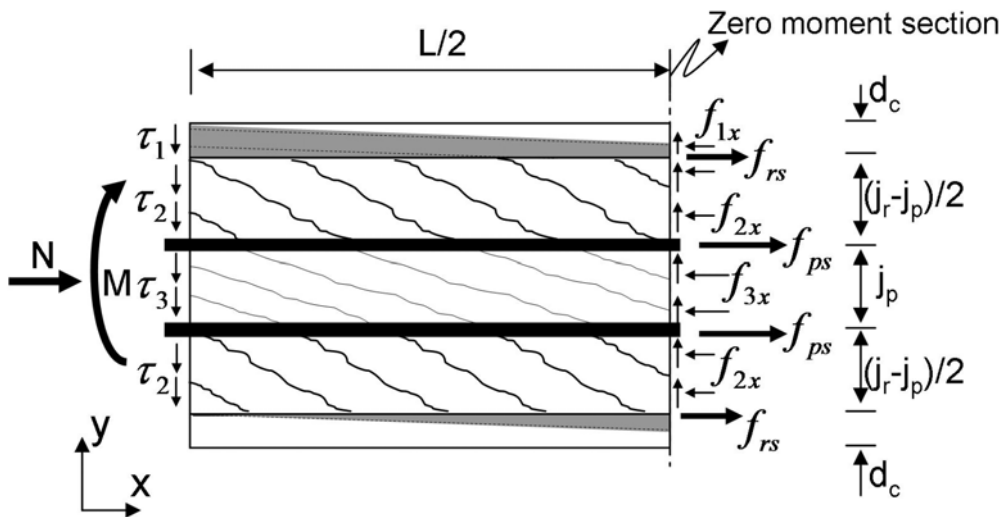
Fig. 4.6 Axial stresses at zero moment section in longitudinal direction

4.2.3 Compatibility Conditions of Strains

Let's consider the compatibility conditions of strains in concrete and reinforcements in Zone 2 and 3. Compatibility condition for concrete in Zone 1 is not mentioned in this section because it is not used to analytical calculation.

Figure 4.7 shows the strain state and Mohr's strain circle of diagonally cracked concrete in Zone 2 and 3. As shown in the Fig. 4.7, diagonally cracked concrete of Zone 2 and 3 are in biaxial state. The longitudinal and transverse average strain in Zone 2 and 3, ε_{2x}, ε_{2y} and ε_{3x}, ε_{3y}, are given by Eq. (4.14) to (4.17) based on Mohr's strain circle in the Fig. 4.7, respectively.

$$\varepsilon_{2x} = \frac{\varepsilon_{22}\tan^2\theta_2 + \varepsilon_{21}}{1+\tan^2\theta_2} \qquad \text{for Zone 2} \qquad \text{Eq. (4.14)}$$

$$\varepsilon_{2y} = \frac{\varepsilon_{22} + \varepsilon_{21}\tan^2\theta_2}{1+\tan^2\theta_2} \qquad \text{for Zone 2} \qquad \text{Eq. (4.15)}$$

$$\varepsilon_{3x} = \frac{\varepsilon_{32}\tan^2\theta_3 + \varepsilon_{31}}{1+\tan^2\theta_3} \qquad \text{for Zone 3} \qquad \text{Eq. (4.16)}$$

$$\varepsilon_{3y} = \frac{\varepsilon_{32} + \varepsilon_{31}\tan^2\theta_3}{1+\tan^2\theta_3} \qquad \text{for Zone 3} \qquad \text{Eq. (4.17)}$$

where ε_{21} and ε_{22} are average compression and tensile strain in Zone 2, ε_{31} and ε_{32} are average compression and tensile strain in Zone 3, θ_2 and θ_3 are inclination of shear crack in Zone 2 and 3.
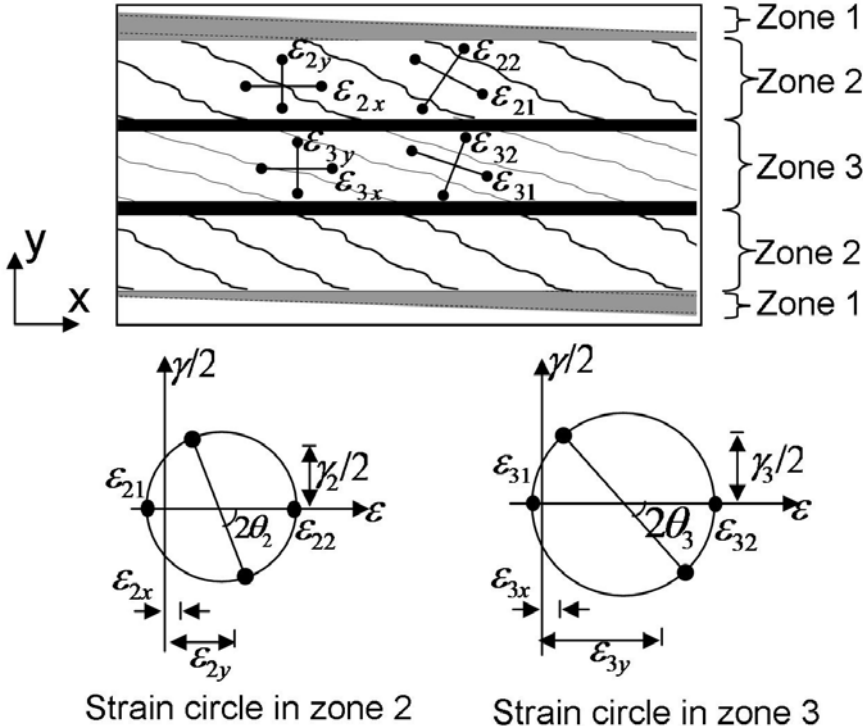
Fig. 4.7 Strain state and Mohr's strain circle of diagonally cracked concrete in Zone 2 and 3

The shear crack width in Zone 2 and 3 can be taken as the product of the

principle tensile strain, and the average spacing of the shear cracks, $\varepsilon_{22}s_{m\theta2}$ and $\varepsilon_{32}s_{m\theta3}$, in Zone 2 and 3, respectively. The shear crack width is obtained as Eq. (4.18) and (4.19). For the average spacing of the shear cracks, $s_{m\theta2}$ and $s_{m\theta3}$, the crack spacing expression of CEB-FIP code [4.9] is used in this study. Refer to CEB-FIP code [4.9] for detail equation of $s_{m\theta}$.

$$w_2 = \varepsilon_{22}s_{m\theta2} \qquad\qquad \text{for Zone 2} \qquad \text{Eq. (4.18)}$$

$$w_3 = \varepsilon_{32}s_{m\theta3} \qquad\qquad \text{for Zone 3} \qquad \text{Eq. (4.19)}$$

where w_2 and w_3 are shear crack width in Zone 2 and 3.

4.2.4 Constitutive Laws

Material constitutive laws for concrete and reinforcements applied in the proposed truss model are introduced in this section. For relationship between stress and strain in concrete of each zone, Vecchio's model [2.3] for shear cracked concrete is introduced. For the principle tensile stress of concrete in Zone2 and 3, f_{22} and f_{32}, corresponding to the principle tensile strain of concrete, ε_{22} and ε_{32}, following model [2.3] is applied in this study.

$$f_{22} = \frac{\alpha_1\alpha_2 f_t}{1+\sqrt{500\varepsilon_{22}}} \quad \text{(MPa)} \qquad \text{for Zone 2} \quad \text{Eq. (4.20)}$$

$$f_{32} = \frac{\alpha_1\alpha_2 f_t}{1+\sqrt{500\varepsilon_{32}}} \quad \text{(MPa)} \qquad \text{for Zone 3} \quad \text{Eq. (4.21)}$$

where f_t is tensile strength of concrete, α_1 and α_2 are factors accounting for the bond characteristics of the reinforcement and the type of loading ($\alpha_1 = 1.0$ for deformed longitudinal bars and 0.7 for plain bars, wires or bonded strands, $\alpha_2 = 1.0$ for short-tern monotonic loading and 0.7 for sustained and/or repeated loads [2.2]).

The resulting principle compressive strain in Zone 2 and 3, ε_{21} and ε_{31}, which corresponding to the principle compressive stresses, f_{21} and f_{31}, are calculated by Eq. (4.22) and (4.23). For maximum compressive stress of diagonally cracked concrete, f_{21max} and f_{31max}, experimental stress-strain relationship by Vecchio [2.3] is used (Eq. (4.24) and (4.25)).

$$\varepsilon_{21} = \varepsilon_c'(1-\sqrt{1-f_{21}/f_{21max}}) \qquad \text{for Zone 2} \quad \text{Eq. (4.22)}$$

$$\varepsilon_{31} = \varepsilon_c'(1-\sqrt{1-f_{31}/f_{31max}}) \qquad \text{for Zone 3} \quad \text{Eq. (4.23)}$$

$$f_{21max} = \frac{f_c'}{0.8+170\varepsilon_{22}} \qquad \text{for Zone 2} \quad \text{Eq. (4.24)}$$

$$f_{31\max} = \frac{f_c'}{0.8 + 170\varepsilon_{32}} \qquad \text{for Zone 3} \quad \text{Eq. (4.25)}$$

where ε'_c is compressive strain corresponding to compressive strength, f'_c.

For the material constitutive laws of reinforcements in each zone, shear reinforcement, longitudinal bar, and prestressing steel is assumed as perfect elasto-plastic material. Hence, the constitutive laws for shear reinforcement, longitudinal bar, and prestressing steel are expressed as Eq. (4.26) to (4.29), respectively. It is assumed that longitudinal strain in longitudinal bar and prestressing steel equals to longitudinal strain of concrete in Zone 2 and 3, respectively.

$$f_{ws2} = E_w\varepsilon_{2y} \text{ for } \varepsilon_{2y} \le \varepsilon_{wy}, \ f_{ws2} = f_{wy} \text{ for } \varepsilon_{2y} > \varepsilon_{wy} \qquad \text{for Zone 2} \quad \text{Eq. (4.26)}$$

$$f_{ws3} = E_w\varepsilon_{3y} \text{ for } \varepsilon_{3y} \le \varepsilon_{wy}, \ f_{ws3} = f_{wy} \text{ for } \varepsilon_{3y} > \varepsilon_{wy} \qquad \text{for Zone 3} \quad \text{Eq. (4.27)}$$

$$f_{rs} = E_r\varepsilon_{2x} \text{ for } \varepsilon_{2x} \le \varepsilon_{ry}, \ f_{rs} = f_{ry} \text{ for } \varepsilon_{2x} > \varepsilon_{ry} \qquad \text{Eq. (4.28)}$$

$$f_{ps} = E_p(\varepsilon_{pe} + \varepsilon_{3x}) \text{ for } \varepsilon_{3x} + \varepsilon_{pe} \le \varepsilon_{py}, \ f_{rs} = f_{ry} \text{ for } \varepsilon_{3x} + \varepsilon_{pe} > \varepsilon_{py} \qquad \text{Eq. (4.29)}$$

where f_{ws2} and f_{ws3} are tensile stress, E_w is elastic modulus of shear reinforcement in Zone 2 and 3, E_r and E_p are elastic modulus of longitudinal bar and prestressing steel, and ε_{pe} is tensile strain in the prestressing steel due to prestress, ε_{wy}, ε_{ry}, and ε_{py} are tensile strain corresponding to yield strength of shear reinforcement, longitudinal bar, and prestressing steel, respectively.

To evaluate the maximum bond stress on prestressing steel, following experimental equation for bond strength of round PT bar and prestressing strands [3.6] is used in this study. Eq. (4.30) and (4.31) is empirical relation for bond stress–slip of prestressing steel proposed by Kiuchi [3.6]. Table 4.1 shows the summarized contents of the empirical parameters for maximum bond stress in Kiuchi`s model [3.6].

$$\tau_{p\max} = 0.31\sqrt{f_g'} \text{ for round PT bar} \quad \text{(MPa)} \qquad \text{Eq. (4.30)}$$

$$\tau_{p\max} = 0.53\sqrt{f_g'} \text{ for prestressing strands} \quad \text{(MPa)} \qquad \text{Eq. (4.31)}$$

where τ_{pmax} is bond strength of prestressing steel and f'_g is compressive strength of grout. For bond strength of deformed prestressing steel, bond strength equation in AIJ guideline [3.7] for deformed reinforcing bar is applied.

Table 4.1 Empirical parameters of PT tendon [3.6]

Parameters		Prestressing strands	Round PT bar
Bond stress (MPa)	τ_{pmax}	$0.53(f_g{'})^{1/2}$	$0.31(f_g{'})^{1/2}$
	τ_f	$0.5\tau_{pmax}$	$0.2\tau_{pmax}$
Slip (mm)	$S_{\tau pmax}$	0.004ϕ	0.045
	$S_{\tau f}$	$3.0S_{\tau pmax}$	$3.0S_{\tau pmax}$

Bond stress-slip relations in Kiuchi model [3.6]

1) Prestressing strands

$\tau = \tau_{pmax}(2X - X^2)$, $X = S / S_{\tau pmax}$, for $0 \leq S < S_{\tau pmax}$

$\tau = \tau_{pmax}(1.25 - 0.25X)$, for $S_{\tau pmax} \leq S < S_{\tau f}$

$\tau = 0.5\tau_{pmax}$, for $S_{\tau f} \leq S$

2) Round PT bar

$\tau = \tau_{pmax}(2X - X^2)$, $X = S / S_{\tau pmax}$, for $0 \leq S < S_{\tau pmax}$

$\tau = \tau_{pmax}(1.4 - 0.4X)$, for $S_{\tau pmax} \leq S < S_{\tau f}$

$\tau = 0.2\tau_{pmax}$, for $S_{\tau f} \leq S$

Note: τ_{pmax} and τ_f are bond strength and frictional stress of prestressing steel, $S_{\tau pmax}$ and $S_{\tau f}$ are slip of prestressing steel corresponding to τ_{pmax} and τ_f, respectively.

4.2.5 Analytical Procedures

Figure 4.8 illustrates calculation procedure by truss model proposed in this study. For the calculation using proposed method, equilibrium conditions for stress, compatibility conditions for strain, and constitutive laws for material properties are used in Zone 1, 2, and 3, respectively.

First, shear stress of concrete in Zone 2, τ_2, is estimated. Second, principal compressive stress in Zone 1, f_{l1}, is obtained by equilibrium condition for stress in Zone1 (Eq. (4.2)). Principal compressive stress in Zone 1, f_{l1}, which is larger than concrete compressive strength, $f_c{'}$, is revised. Third, for Zone 3, principal tensile strain of cracked concrete, angle of shear crack, and tensile stress of shear reinforcement, ε_{32}, θ_3, and f_{ws3}, is estimated. Based on the equilibrium and compatibility conditions for stress and strain in Zone 3, principal stresses and strains of cracked concrete in Zone 3, f_{32}, f_{31}, ε_{31}, ε_{3x}, and ε_{3y} are obtained and revised until they satisfy that f_{31} and f_{ws3} are smaller than their ultimate strengths,

f'_{31max} and f_{wy}, respectively. Forth, for Zone 2, principle tensile strain of cracked concrete, angle of shear crack, and tensile stress of shear reinforcement in Zone 2, ε_{22}, θ_2, and f_{ws2}, is estimated and revised in a same manner with Zone 3. Fifth, axial force is obtained by Eq. (4.10) to (4.13). The axial force must equal to desired value (usually, zero for beam). Last, bond stress and strength in prestressing steel, τ_p and τ_{pmax}, is obtained by Eq. (4.9) and (4.30) to (4.31), respectively.

START

Geometric and material properties

(D) revise τ_2 → estimate τ_2 ← reduce τ_2

f_{11} by Eq. (4.2), $\tau_1 = f_{11}Ld_c/(L^2+d_c^2)$

$f_{11} < f'_c$ — No / Yes

estimate $\varepsilon_{32}, \theta_3, f_{ws3}$ ← reduce ε_{32} revise f_{ws3}

(E) reduce ε_{32}
(F) increase ε_{32} → $S_{m\theta3}$ by CEB-FIP code

f_{32}, f_{31}, and f_{31max} by Eq. (4.21), (4.6), and (4.25)

$f_{31} < f'_{31max}$ — No / Yes

$\varepsilon_{31}, \varepsilon_{3x}$, and ε_{3y} by Eq. (4.23), (4.16), and (4.17)

$f_{ws3} < f_{wy}$ and $E_w\varepsilon_{3y} = f_{ws3}$ — No / Yes

$\tau_3 = (f_{31}+f_{32})\sin\theta_3\cos\theta_3$

(B) revise θ_2 → estimate $\varepsilon_{22}, \theta_2$ ← revise ε_{22}

$S_{m\theta2}$ by CEB-FIP code

(C) revise f_{ws2} → estimate f_{ws2}

w_2, w_3 by Eq. (4.18) and (4.19)

$w_2 = w_3$ — No / Yes

(A)

(A)

f_{22}, f_{21} by Eq. (4.20) and (4.3)

f_{21} by Eq. (4.3) = f_{21} by Eq. (4.4) — No (B)

f_{21max} by Eq. (4.24) ↓Yes

$\varepsilon_{21}, \varepsilon_{2x}$, and ε_{2y} by Eq. (4.22), (4.14), and (4.15)

$E_w\varepsilon_{2y} = f_{ws2}$ — No (C) / Yes

$\tau_2 = (f_{21}+f_{22})\sin\theta_2\cos\theta_2$

τ_2 above = estimated τ_2 — No (D) / Yes

Check N by Eq. (4.10) to (4.13)
If N is not equal to the desired value, make a new estimate of θ_3

τ_p by Eq. (4.9)

τ_{pmax} by Eq. (4.30) or (4.31)

(E) Yes ← $\tau_p > \tau_{pmax}$ / No

$f_{11} = f'_c$ — No → $f_{31} = f'_{31max}$ — No → $\tau_p = \tau_{pmax}$ — No → $f_{ws3} = f_{wy}$ — No (F)

↓Yes: SC | ↓Yes: SC | ↓Yes: B | ↓Yes: ST

END

Fig. 4.9 Calculation procedure of proposed analytical model

An analytical example by proposed model is employed for a post-tensioned precast concrete beam (S-10-L42 in section 3.2). Refer to Table 3.3 and 3.4 for geometrical and material conditions of S-10-L42 for the calculation.

1. Estimate shear stress of cracked concrete in Zone 2, τ_2. Estimate τ_2 as 1.60 MPa.

2. By Eq. (4.2), f_{11} is obtained as 38.9 MPa.

$$f_{11} = \frac{\tau_2}{Ld_c}\left(L^2 + d_c^2\right) = \frac{1.60}{800 \cdot 33}\left(800^2 + 33^2\right) = 38.9 \quad \text{Eq. (4.32)}$$

3. Check that $f_{11} \leq F_c$ where F_c is compressive strength of concrete. If $f_{11} > F_c$, return to step 1 and choose a smaller τ_2.

4. Estimate valuables in Zone 3, ε_{32}, θ_3, and f_{w3}. Estimate them 0.008%, 30 degree, and 4 MPa, respectively.

5. $s_{m\theta3}$ by CEB-FIP code is resulted as 464.3 mm.

$$s_{m\theta3} = \frac{1}{\dfrac{\sin\theta_3}{s_{mx3}} + \dfrac{\cos\theta_3}{s_{my3}}} = \frac{1}{\dfrac{\sin 30°}{972.0} + \dfrac{\cos 30°}{528.2}} = 464.3 \quad \text{Eq. (4.33)}$$

6. Eq. (4.21), (4.6), and (4.25) produces f_{32} of 1.0, f_{31} of 3.3, and f_{31max} of 70.4, respectively.

$$f_{32} = \frac{\alpha_1\alpha_2 f_t}{1+\sqrt{500\varepsilon_{32}}} = \frac{0.7\cdot 0.7\cdot 2.5}{1+\sqrt{500\cdot 0.00008}} = 1.0 \quad \text{Eq. (4.34)}$$

$$f_{31} = \left(\left(A_w f_{ws3} + \frac{bsd_c^2}{L^2+d_c^2}f_{11}\right)\frac{1}{bs} + f_{32}\cos^2\theta_3\right)\frac{1}{\sin^2\theta_3}$$
$$= \left(\left(63.3\cdot 4 + \frac{300\cdot 50\cdot 33^2}{800^2+33^2}38.9\right)\frac{1}{300\cdot 50} + 1.0\cdot\left(\frac{\sqrt{3}}{2}\right)^2\right)\frac{1}{0.5^2} = 3.3 \quad \text{Eq. (4.35)}$$

$$f_{31max} = \frac{f_c'}{0.8+170\varepsilon_{32}} = \frac{57.3}{0.8+170\cdot 0.00008} = 70.4 \quad \text{Eq. (4.36)}$$

7. Check $f_{31} \leq f_{31max}$. If $f_{31} > f_{31max}$, return to step 4 and estimate a smaller ε_{32}. $f_{31} = 3.3 < 70.4 = f_{31max}$, Therefore, go to Step 8.

8. Eq. (4.23), (4.16), and (4.17) give ε_{31} of -0.005%, ε_{3x} of -0.002%, and ε_{3y} of 0.005%, respectively.

$$\varepsilon_{31} = \varepsilon_c'(1-\sqrt{1-f_{31}/f_{31max}}) = -0.0021(1-\sqrt{1-3.3/70.4}) = -0.00005 \quad \text{Eq. (4.37)}$$

$$\varepsilon_{3x} = \frac{\varepsilon_{32}\tan^2\theta_3 + \varepsilon_{31}}{1+\tan^2\theta_3} = \frac{0.00008 \cdot \left(\dfrac{\sqrt{3}}{3}\right)^2 - 0.00005}{1+\left(\dfrac{\sqrt{3}}{3}\right)^2} = -0.00002 \quad \text{Eq. (4.38)}$$

$$\varepsilon_{3y} = \frac{\varepsilon_{32} + \varepsilon_{31}\tan^2\theta_3}{1+\tan^2\theta_3} = \frac{0.00008 - 0.00005 \cdot \left(\dfrac{\sqrt{3}}{3}\right)^2}{1+\left(\dfrac{\sqrt{3}}{3}\right)^2} = 0.00005 \quad \text{Eq. (4.39)}$$

9. Calculate f_{ws3} by Eq. (4.27). It is resulted as 9.7 MPa.

$$f_{ws3} = E_w \cdot \varepsilon_{3y} = 194000 \cdot 0.00005 = 9.7 \qquad \text{Eq. (4.40)}$$

10. Check $f_{ws3} \le f_{wy}$. If $f_{ws3} > f_{wy}$, return to Step 4 and revise a smaller f_{ws3}.

11. Calculate shear stress in cracked concrete of Zone 3, τ_3 by following equation. It results τ_3 of 1.9 MPa.

$$\tau_3 = (f_{31} + f_{32})\sin\theta_3\cos\theta_3 = (3.3+1.0)\frac{1}{2}\cdot\frac{\sqrt{3}}{2} = 1.9 \qquad \text{Eq. (4.41)}$$

12. Estimate ε_{22} and θ_2. Estimate them as 0.01% and 45 degree, respectively.

13. $s_{m\theta 2}$ by CEB-FIP code is resulted as 381.9 mm.

14. Estimate f_{ws2}. Estimate it as 14 MPa.

15. Shear crack width of cracked concrete in Zone 2 and 3, w_2 and w_3, are obtained by Eq. (4.18) and (4.19). They produce 0.038 and 0.037 mm, respectively.

$$w_2 = \varepsilon_{22}s_{m\theta 2} = 0.0001 \cdot 381.9 = 0.038 \qquad \text{Eq. (4.42)}$$

$$w_3 = \varepsilon_{32}s_{m\theta 3} = 0.00008 \cdot 464.3 = 0.037 \qquad \text{Eq. (4.43)}$$

16. Check $w_2 = w_3$. If $w_2 \neq w_3$, return to Step 12 and estimate a smaller ε_{22}. Modified ε_{22} of 0.009% produces w_3 of 0.038. Because of $w_2=w_3$, go to Step 17.

17. Calculate f_{22} and f_{21} by Eq. (4.20) and (4.3), respectively.

$$f_{22} = \frac{\alpha_1\alpha_2 f_t}{1+\sqrt{500\varepsilon_{22}}} = \frac{0.7\cdot0.7\cdot2.5}{1+\sqrt{500\cdot0.00009}} = 1.01 \qquad \text{Eq. (4.44)}$$

$$f_{21} = \left(\left(A_w f_{ws2} + \frac{bsd_c^2}{L^2+d_c^2}f_{11}\right)\frac{1}{bs} + f_{22}\cos^2\theta_2\right)\frac{1}{\sin^2\theta_2}$$
$$= \left(\left(63.3\cdot14 + \frac{300\cdot50\cdot33^2}{800^2+33^2}38.9\right)\frac{1}{300\cdot50} + 1.01\cdot\left(\frac{\sqrt{2}}{2}\right)^2\right)\left(\frac{2}{\sqrt{2}}\right)^2 = 1.3$$

Eq. (4.45)

18. Calculate f_{21} by Eq. (4.4). It results f_{21} = 1.8 MPa

$$f_{21} = \frac{A_w f_{ws2}}{bs} + \frac{d_c + L\cot\theta_2}{L^2 + d_c^2} d_c f_{11} = \frac{63.3 \cdot 14}{300 \cdot 50} + \frac{33 + 800 \cdot 1.04}{800^2 + 33^2} 33 \cdot 389 = 1.8 \quad \text{Eq. (4.46)}$$

19. Check f_{21} in Step 17 = f_{21} in Step 18. If f_{21} in Step 17 $\neq f_{21}$ in Step 18, return to Step 12, and revise θ_2. Modified θ_2 of 35 degree produces f_{21} of 2.4. Go to Step 20.

20. Calculate f21max by Eq. (4.24). It results f_{21max} = 70.2 MPa.

$$f_{21\max} = \frac{f_c'}{0.8 + 170\varepsilon_{22}} = \frac{57.3}{0.8 + 170 \cdot 0.000097} = 70.2 \quad \text{Eq. (4.47)}$$

21. Calculate ε_{21}, ε_{2x}, and ε_{2y} by Eq. (4.22), (4.14), and (4.15), respectively. They give 0.004%, 0.006%, and 0.008%, respectively.

$$\varepsilon_{21} = \varepsilon_c'(1 - \sqrt{1 - f_{21}/f_{21\max}}) = 0.0021(1 - \sqrt{1 - 2.4/70.2}) = 0.00004 \quad \text{Eq. (4.48)}$$

$$\varepsilon_{2x} = \frac{\varepsilon_{22}\tan^2\theta_2 + \varepsilon_{21}}{1 + \tan^2\theta_2} = \frac{0.000097 \cdot 0.7^2 + 0.00004}{1 + 0.7^2} = 0.00006 \quad \text{Eq. (4.49)}$$

$$\varepsilon_{2y} = \frac{\varepsilon_{22} + \varepsilon_{21}\tan^2\theta_2}{1 + \tan^2\theta_2} = \frac{0.000097 + 0.00004 \cdot 0.7^2}{1 + 0.7^2} = 0.00008 \quad \text{Eq. (4.50)}$$

22. Calculate f_{ws2} by $E_w\varepsilon_{2y}$. Check f_{ws2} estimated in Step 14 = $E_w\varepsilon_{2y}$. If necessary, return to Step 14, revise f_{ws2}. Modified f_{ws2} (=15 MPa) in Step 14 produces 15 MPa (=$E_w\varepsilon_{2y}$) in Step 22. Go to Step 23.

23. Calculate shear stress in cracked concrete of Zone 2, τ_2 by following equation. It results τ_2 of 1.6 MPa.

$$\tau_2 = (f_{21} + f_{22})\sin\theta_2\cos\theta_2 = (2.4 + 1.01) \cdot 0.57 \cdot 0.82 = 1.6 \quad \text{Eq. (4.51)}$$

24. Check τ_2 in Step 23 = τ_2 estimated in Step 1. If necessary, return to Step 1, revise τ_2. Because of τ_2 in Step 23 = 1.6 = τ_2 estimated in Step 1, go to Step 25.

25. Check axial force, N, by Eq. (4.10). Eq. (4.10) produces N of 152.3 kN. Return to Step 4, revise θ_3. Modified θ_3 of 28 degree produces axial force, N, of 0.0 kN corresponding to beam. go to Step 26.

26. Calculate bond stress and bond strength of prestressing steel, τ_p and τ_{pmax} by Eq. (4.9) and (4.31), respectively. Check $\tau_p \leq \tau_{pmax}$. If necessary, return to Step 4 and apply a smaller ε_{32}.

27. Shear force of 184.2 kN is obtained by the following equations.

$$V_a = b(\tau_1 d_c + \tau_2(j_r - j_p) + \tau_3 j_p) = 300 \cdot (1.62 \cdot 33 + 1.60 \cdot 134 + 1.73 \cdot 200) = 184.2$$

To obtain the response of the beam at shear force, these calculations above are repeated for an increasing τ_2 until the each shear resistance component reach

their ultimate state ($f_{11}=F_c$, $f_{31}=f_{31max}$, $\tau_p = \tau_{pmax}$, or $f_{ws3} = f_{wy}$).

For the judgement of failure mode, obtained analytical results, f_{11}, f_{31}, τ_p, and f_{ws3}, are compared to their ultimate strength, f'_c, f'_{31max}, τ_{pmax}, and f_{wy}, respectively. If shear reinforcement yields at maximum shear capacity ($f_{ws3} = f_{wy}$), the failure mode is judged as shear tension failure (ST). The failure mode due to crushing of diagonally cracked concrete ($f_{31} = f_{31max}$) or cover concrete ($f_{11}=f'_c$) is judged as shear compression failure (SC). Crushing of concrete after yielding of shear reinforcement is defined as ST in this study. The failure mode due to bond failure of prestressing steel ($\tau_p = \tau_{pmax}$) is judged as bond failure (B).

4.3 Verification of Analytical Results

4.3.1 Experimental Data Used for Verification

To clarify the accuracy of analytical results by truss model proposed in this study, twelve experimental data on half scale of post-tensioned precast concrete members failed in shear compression (SC), shear tension (ST), bond (B) (four beams [2.14, 3.12], eight columns [2.9, 2.10], and two beams from Test 2 in Chapter 3) are used. Those were also used for the verification in section 3.4. Experimental data of post-tensioned precast concrete members failed in diagonal tension (DT) are excluded in this section, because analytical model proposed in this chapter can not cover DT failure. A new analytical model which can cover DT failure of prestressed / precast concrete member will be scrutinized in Chapter 5. Table 4.2 shows geometrical and material properties of specimens used in the verification. Fig. 4.9 plots range of parameters and the distribution of specimens for the verification: (a) compressive strength of concrete; (b) shear span ratio; (c) yield strength of shear reinforcement; (d) shear reinforcement ratio; (e) prestressing and axial force level ($=(P_e+N)/(bDF_c)$); (f) failure mode. The definition of notation on failure mode, SC, B and ST in Fig. 4.9 (f) follow the definition of failure mode in section 3.2.4. Analytical shear strength, failure mode, shear load-deformation response, and tensile stress in shear reinforcement will be compared to experimental results.

Table 4.2 Experimental parameters of specimens used for the verification

Ref.	Specimen	b	D	a/D	F_c	ρ_w	f_{wy}	Type of PT tendon	η_{pe+N}	Failure mode
[2.9]	B-1/3-0.1	400	400	1.5	71.6	0.89	355	R	0.28	B
	B-1/2-0.1	400	400	1.5	57.8	0.89	355	R	0.49	B
	B-1/2-0.1t	400	400	1.5	70.4	1.19	376	R	0.41	B
	B-1/3-0.2	400	400	1.5	70.4	0.89	376	R	0.27	B
	B-1/2-0.2	400	400	1.5	57.8	0.89	355	R	0.48	B
[2.10]	R-15-L32	400	400	1.5	107	0.32	988	R	0.27	B
	R-15-H32	400	400	1.5	107	0.32	1435	R	0.26	B
	D-15-L32	400	400	1.0	107	0.32	988	D	0.27	B
[2.14]	SJP075PW04	250	250	1.5	59.0	0.45	347	S	0.15	SC
[3.12]	SSR1PW04	250	250	1.0	59.4	0.45	331	S	0.15	SC
	SSR1PW12	250	250	1.0	59.6	1.14	366	S	0.15	SC
Test 2	S-10-L21	300	600	1.0	65.2	0.21	1006	S	0.22	ST

Note: b and D are member sectional width and depth in mm, a/D is shear span to overall depth ratio, F_c is compressive strength of concrete in MPa, ρ_w is shear reinforcement ratio in %, f_{wy} is tensile yield strength of shear reinforcement in MPa, η_{p+N} is prestressing and axial force ratio (= $(N+P_e)/bDF_c$) where N and P_e are axial and prestressing force, repectively. R and S in Type of prestressing steel indicate round PT bar and prestressing strands, respectively.
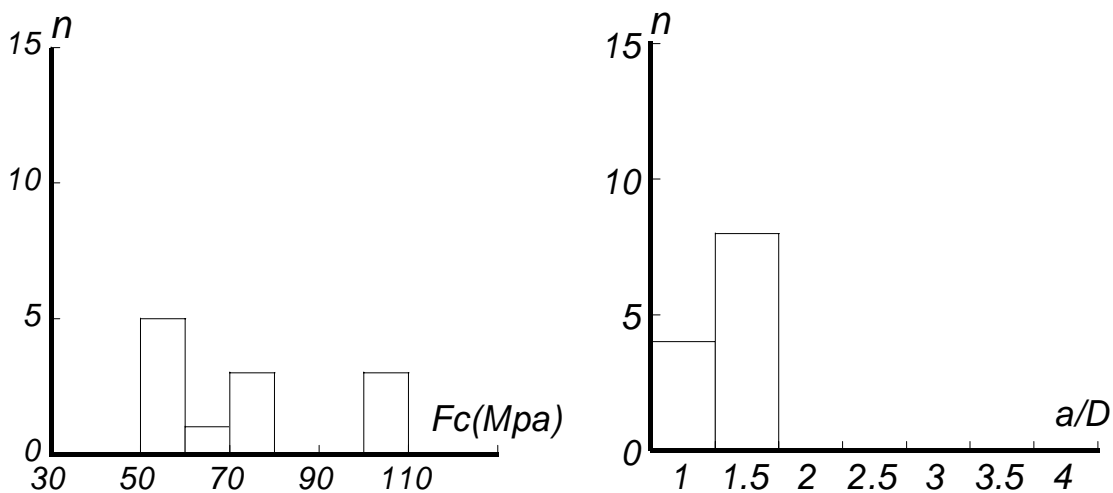
(a) Compressive strength of concrete (b) Shear span to overall depth ratio
Fig. 4.9 Range of parameters and the distribution of specimens for the verification
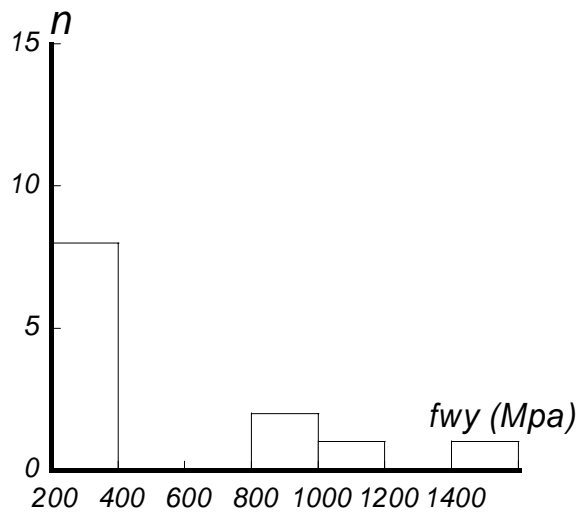
(c) Yield strength of shear reinforcement   (d) Shear reinforcement ratio
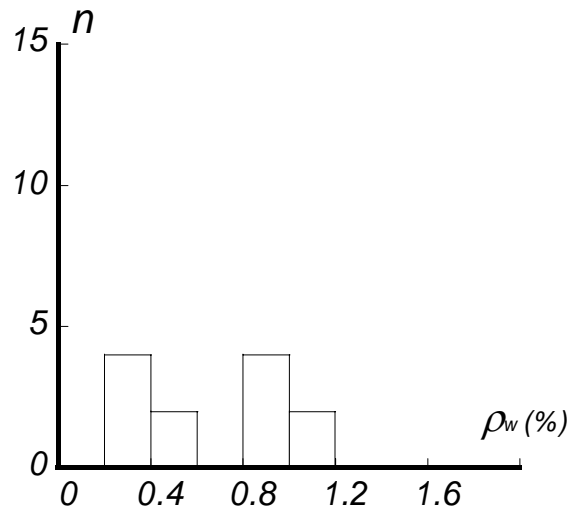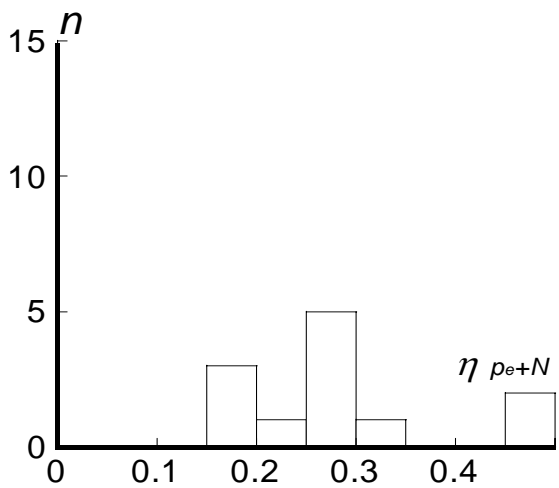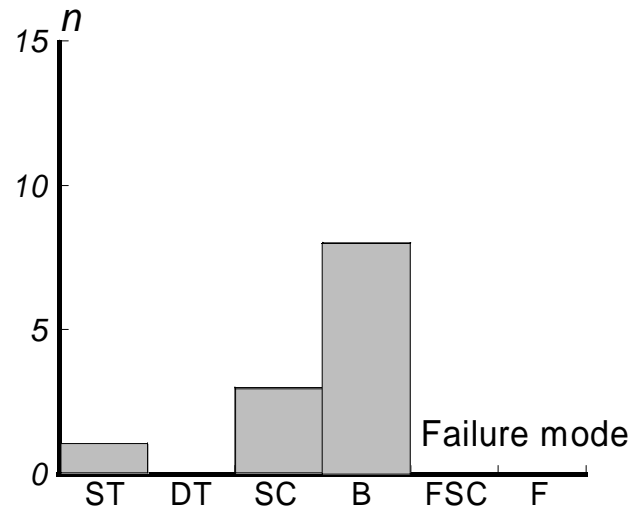
(e) Prestressing and axial force level   (f) Failure mode

Fig. 4.9 Range of parameters and the distribution of specimens for the verification

4.3.2 Shear Failure Strength and Failure Mode

Based on the proposed method, shear failure strength at ultimate state of each shear resistance component ($f_{11}=F_c$, $f_{31}=f_{31max}$, $\tau_p = \tau_{pmax}$, or $f_{ws3} = f_{wy}$) can be obtained. Fig. 4.101 shows the comparison between analytical and experimental shear strength. Vertical and horizontal axis in Fig. 4.10 represents experimental and analytical shear strengths, V_{eu} and V_{au}, respectively. For experimental shear strength, experimental peak load of post-tensioned precast concrete members failed in shear (SC and ST) and bond (B) are used. For analytical shear strength, analytical shear strength by the conventional MCFT for prestressed concrete member [2.2], and a new truss model proposed in this study are shown in Fig. 4.10 (a) and (b), respectively. Circles, squares, and triangles in Fig. 4.10 (b)

represent observed failure mode data of B, SC, and ST, respectively. Solid and open dots in Fig. 4.10 (b) represent data in which predicted failure modes agree and disagree with observed ones, respectively.
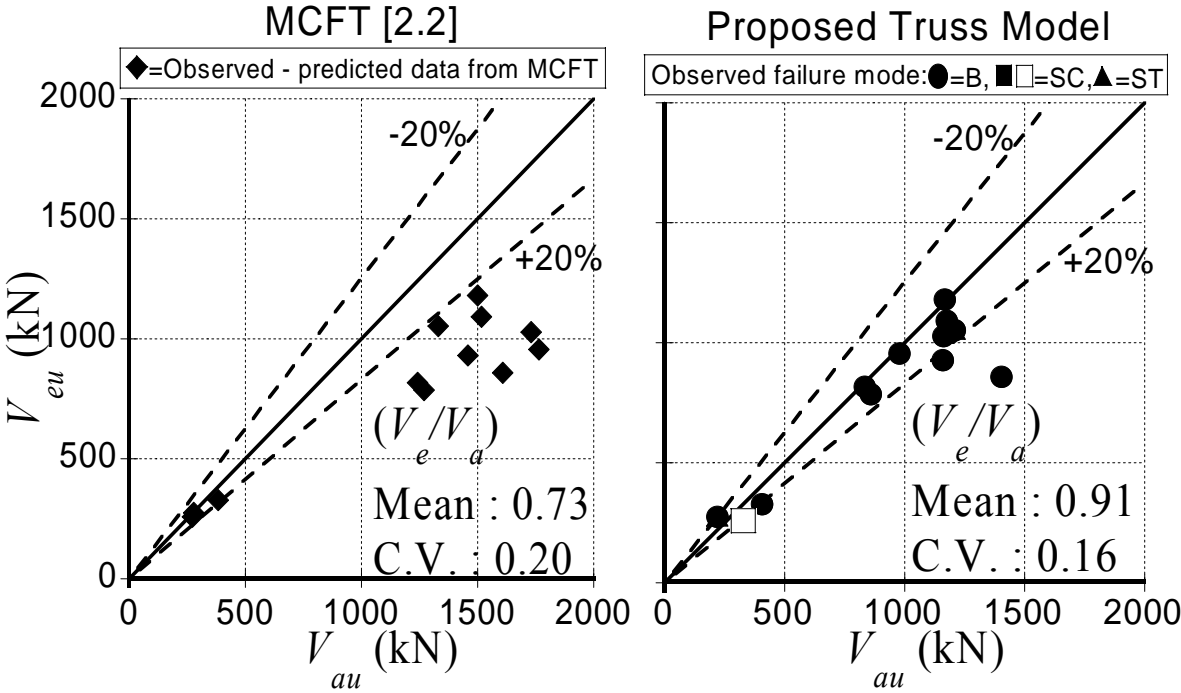
Fig. 4.10 Comparison between experimental and analytical shear strength by: (a) conventional MCFT; (b) proposed truss model.

As shown in Fig. 4.10, analytical shear strengths by the truss model proposed in this study evaluate experimental shear strength in a good accuracy. The conventional MCFT [2.2] produced overestimated analytical shear strength. It is because it designates only the yield strength of shear reinforcement, f_{wy}, and compressive strength of diagonal shear cracked concrete, f_{2max}, as upper limit conditions in the calculation procedure. Further, it noted that thirteen out of fourteen analytical data for failure mode show agreement with observed ones. It points out that the truss model proposed in this study appropriately evaluates the shear strength and failure mode of post-tensioned precast concrete member. For deep understanding on analytical and experimental results, predicted and observed results on Fig. 4.10 are listed Table 4.3. To enhance the accuracy for the evaluation of failure mode, it is necessary to observe quantitatively the failure mode such as crushing of cracked concrete because stress in concrete can not measured in the test. Establishment of quantitative observation method for the failure mode in the test is future work.

Table 4.3 Predicted and observed data in Fig. 4.10

Ref.	Specimen	Observed shear strength V_{eu} (kN)	Predicted shear strength V_{au} (kN)		Observed failure mode	Predicted failure mode
			MCFT	Proposed method		
[2.9]	B-1/3-0.1	817	1242	835	BF	BF
	B-1/2-0.1	929	1459	1160	BF	BF
	B-1/2-0.1t	957	1764	977	BF	BF
	B-1/3-0.2	787	1271	858	BF	BF
	B-1/2-0.2	860	1610	1402	BF	BF
[2.10]	R-15-L32	1181	1501	1168	BF	BF
	R-15-H32	1029	1730	1162	BF	BF
	D-15-L32	1092	1518	1175	BF	BF
[2.14]	SJP075PW04	275	278	221	STF	STF
[3.12]	SSR1PW04	259	272	328	SCF	BF
	SSR1PW12	328	383	405	BF	BF
Test 2	S-10-L21	1054	1330	1208	STF	STF

4.3.3 Load-Deformation Response

An advantage of the proposed analytical method is to be able to predict the load-shear deformation response until shear failure of a post-tensioned precast concrete member. Post-tensioned precast concrete columns (R-15-L32 and R-15-H32 [2.10]) and a beam (S-10-L21 in Test 2) were selected from data base in order to show the load-shear deformation response. In proposed analytical model, shear strains in zone 2 and 3 are different. Therefore, average shear strain, γ_{ave}, can be obtained as Eq. (4.52) using energetic equilibrium condition between external and internal force ($E_{ext} = E_{int}$). Observed shear strain are average shear strain measured by linear displacement transducers which are diagonally attached in the segment of mid-length of member.

$$0.5(V_a + V_{cr})L\gamma_{ave} = bL\{0.5(\tau_1 + \tau_{cr1})\gamma_1 D_1 + (\tau_2 + \tau_{cr2})\gamma_2 D_2 + 0.5(\tau_3 + \tau_{cr3})\gamma_3 D_3\} \quad \text{Eq. (4.52)}$$

where V_{cr} is shear force at initiation of shear crack, τ_{cr1}, τ_{cr2}, and τ_{cr3} are shear stress of concrete in zone 1, 2, and 3 at initiation of shear crack, γ_1 is shear strain in zone 1 which is obtained as τ_1/G_1 ($=2(1+0.2)\tau_1/E_c$), respectively.

Figure 4.11 compares the predicted and observed responses until shear failure of the post-tensioned precast concrete beams and columns. In the figure, solid and

dotted curves indicate the observed and predicted responses. In the figure, black and open squares indicate observed and predicted initiation of shear crack, respectively. The predicted responses were obtained by straight line connecting analytical results as increasing of shear strain. In the response of beams as shown in the Fig. 4.11 (a), the overall response of shear strain predicted by truss model proposed in this study show a good agreement while shear force is little overestimated. However, rapid increase of shear strain in observed results can not be simulated in predicted ones. It is because that stable development of strains in diagonally cracked zone is assumed and fractural behavior of shear crack is not considered in proposed model. In the response of columns in Fig. 4.11 (b), the responses of predicted shear strain show a good agreement while ultimate shear strain of R-15-H32 is underestimated. This is because R-15-H32 failed in shear due to rapid increase of shear strain immediately after initiation of primary shear crack. However, it can be seen that overall behavior of load-deformation of post-tensioned precast concrete member subjected to pure shear can be simulated by proposed method.
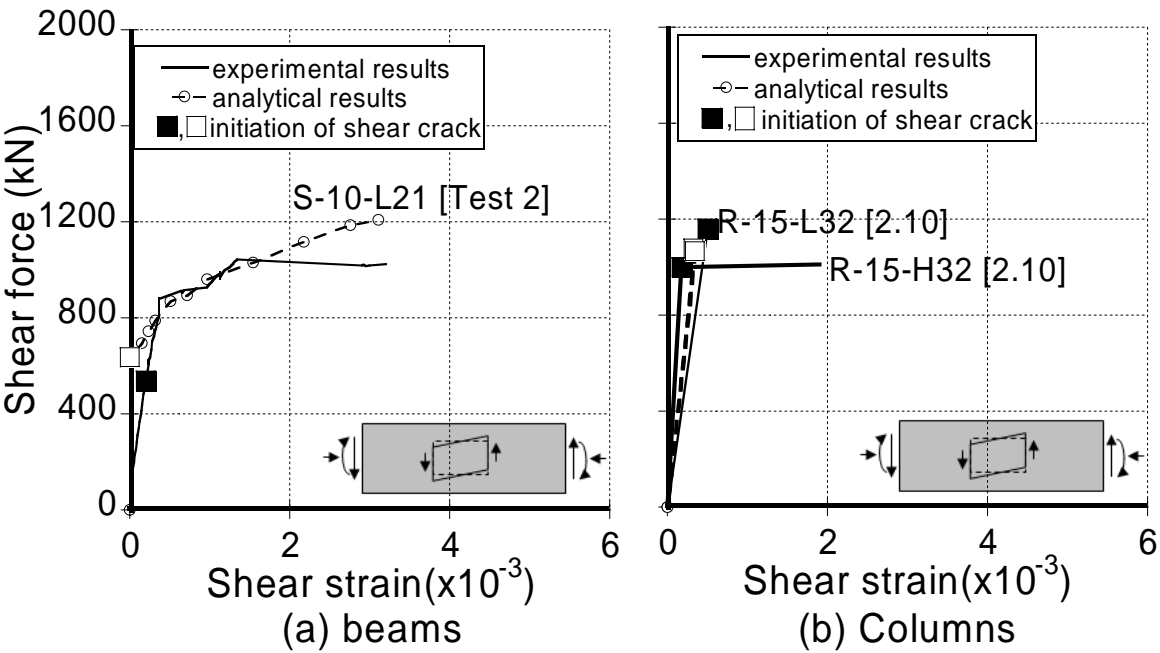

Fig. 4.11 Comparison between experimental and analytical load-deformation response

4.3.5 Tensile Stress in Shear Reinforcement

Figure 4.12 compares the predicted and observed tensile stress in shear reinforcement. In the figure, solid and dotted curves indicate the observed and predicted responses. The observed tensile stresses in the Fig. 4.12 are a product

148

of elastic modulus of shear reinforcement and measured maximum strain in shear reinforcement in mid-length of member, $E_w\varepsilon_y$. The predicted tensile stress are a product of E_w and transverse strain in Zone 3, ε_{3y} $(=E_w\varepsilon_{3y})$. In a same manner with the Fig. 4.11 (a), shear force is little overestimated. It is because observed shear capacity of S-10-L21 decayed due to rapid increase of strain in diagonally cracked zone after yielding of shear reinforcement (ST) while rapid increase of strain in shear reinforcement are not simulated in proposed model. Furthermore, as shown in Fig. 4.11 (b), ultimate tensile stress of shear reinforcement in R-15-H32 is underestimated in the same manner with the Fig. 4.11 (b). It is because of rapid and simultaneous increase of strain in shear reinforcement and bond failure on prestressing steel (B) due to fractural opening of shear crack. However, analytical tensile stresses of shear reinforcement in others show good agreement with those of observed results.
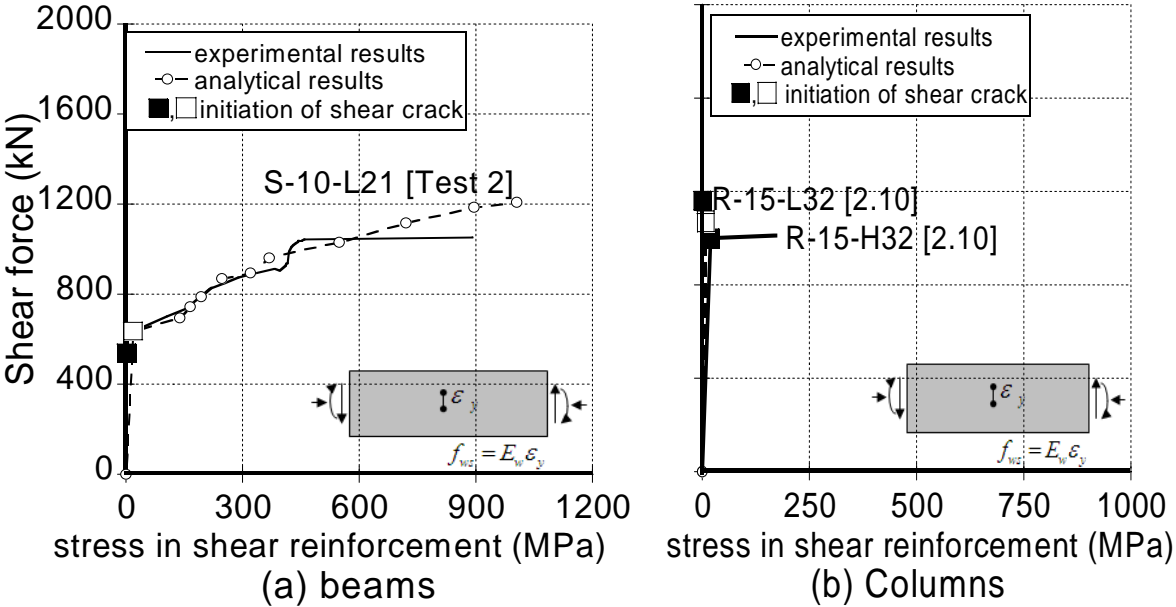
Fig. 4.12 Comparison between experimental and analytical load-tensile stress of shear reinforcement response

From the verifications above, it can be emphasized that the overall load-deformation response, tensile stress in shear reinforcement, bond stress in prestressing steel, as well as ultimate shear strength of post-tensioned precast concrete member are well predicted by proposed truss model. It can be seen that the proposed model can be applied to the post-tensioned precast concrete members with materials in excess of the range of parameters used for the verification because the proposed model is based on the equilibrium condition of stresses and compatibility conditions of strains in concrete and reinforcements.

4.4 Conclusions

A new analytical shear resistance model for post-tensioned precast concrete members had been proposed. In the model, the bond characteristics of prestressing steel and compressive stress in cover concrete were taken in account. To verify the accuracy of analytical results by proposed truss model, experimental data on post-tensioned precast concrete members which failed in shear from previous research [2.9, 2.10, 2.14, 3.12] and from Test 2 in Chapter 3 were used.

The most important conclusions are summarized as follows:

1. Analytical shear strengths of post-tensioned precast concrete member by truss model proposed in this study evaluated experimental shear strength in a better accuracy than those by conventional MCFT [2.2].

2. In thirteen out of fourteen post-tensioned precast concrete members used for verification, analytical failure mode of post-tensioned precast concrete member by proposed model provided results agreed with observed one.

3. Analytical load-deformation response of post-tensioned precast concrete beams and columns showed a good agreement with experimental response while shear strength of post-tensioned precast concrete beam (S-10-L21 in Test 2) was little overestimated.

4. Shear strain and tensile stress in shear reinforcement of post-tensioned precast concrete column with round PT bar (R-15-H32 [2.10]) was underestimated. However, overall behavior of load-displacement of post-tensioned precast concrete member subjected to pure shear was well simulated by proposed method.

Analytical model for DT failure of prestressed concrete member which were excluded in this chapter will be clarified in next chapter.

[References]

4.1 Ritter W. (1899), "Die Bauweise Hennebique (Construction Techniques of Hennebique)," *Schweizererische Bauzeitung*, Zürich, Feb.

4.2 Hognestad, E. (1952), "What Do We Know about Diagonal Tension and Web Reinforcement in Concrete," *University of Illinois Enigineering Experiment Station*, *Circular Series*, No. 64, pp. 47.

4.3 Mitchell D., and Collins M. P. (1974), "Diagonal Compression Field Theory-A Rational Model for Structural Concrete in Pure Torsion," *ACI Journal Proceedings*, V. 71, No. 8, Aug., pp. 396-408.

4.4 Ghiassi B., and Soltani M. (2010), "Local Stress Field Approach for Shear Failure Assessment of Reinforced Concrete Members," *Journal of Advanced Concrete Technology*, V. 8, No. 2, June, pp. 223-238.

4.5 Watanabe F., and Lee J. (1998), "Theoretical Prediction of Shear Strength and Failure Mode of Reinforced Concrete Beams," *ACI Structural Journal*, V. 95, No. 6, Nov.-Dec., pp. 749-757.

4.6 Bentz E. C., Vecchio F. J., Collins M. P., "Simplified Modified Compression Field Theory for Calculating Shear Strength of Reinforced Concrete Elements," ACI Structural Journal, Vol. 103, No. 4, July-Aug., 2006, pp. 614-624.

4.7 Hanai N., Umemura H., Ichinose T., "The Factors Which Influence Strength Deterioration of RC Columns Failing in Shear After Flexural Yielding," *Journal of Structural and Construction Engineering*, No. 593, July, 2005, pp. 129-136. (In Japanese)

4.8 Fukui T., Ookuma A., Hamahara M,, "Shear Strength and Ductility of Prestressed Concrete Beam," *Proceeding of Japan Concrete Institute*, Vol. 21, No. 3, 1999, pp. 931-936.

4.9 CEB-FIP (1978), "Model Code for Concrete Structures, CEB-FIP International Recommendations," 3rd, Comité Euro-International du Béton, Paris, pp. 348.

4.10 Architectural Institute of Japan (AIJ) (1999), "Design Guidelines for Earthquake Resistant Reinforced Concrete Buildings Based on Inelastic Displacement Concept," 175-190. (In Japanese)

5. Analytical Model 2 for Reinforced / Prestressed Concrete Members (DT Model)

5.1 Introduction

In shear failure mode of prestressed / precast concrete member, many members had been failed in diagonal tension (DT) as shown in Fig. 3.37 (f). Moreover, the diagonal tension failure is the most brittle and catastrophic failure mode in shear failure mode. The DT failure is a sudden shear failure induced by a primary diagonal crack which opens excessively, and by deterioration of aggregate interlock resistance [5.1]. It points out that shear reinforcement does not significantly contribute for the shear resistance because the member failed in shear prior to development of tensile stress in shear reinforcement. New analytical model specified in Chapter 4 can not apply to prestressed concrete member failing in DT because it covers shear tension (ST), shear compression (SC), and bond failure (B) of post-tensioned / precast concrete member. Therefore, to prevent prestressed concrete beams from the DT failure and to effectively use shear reinforcement in shear design of prestressed concrete members, the relationship between the aggregate interlock and the opening of shear crack at initiation of shear crack should be investigated.

According to previous studies on the DT failure of reinforced concrete beams [3.9-3.11], the excessive opening of the crack at initiation of shear crack is closely related to the shear span to overall depth ratio, a/D, and beam section width to overall depth ratio, b/D. A decrease in a/D or in b/D leads to a higher energy release rate of crack surface at initiation of shear crack, increasing of crack widths, and deterioration of the load-carrying capacity by aggregate interlocking. From the previous researches on shear behavior of prestressed concrete beams [2.13, 3.12-3.17], it has been experimentally observed that a decrease in the amount of shear reinforcement, ρ_w, also leads to the DT failure.

In Japan, to prevent prestressed members from DT failure, web-shear cracking strength, V_{wc}, based on principal stress corresponding to tensile strength of concrete, f_t, ([2.8], Eq. (3.45)) is conventionally used. It can be judged that the prestressed concrete member does not fail in DT if web-shear cracking strength, V_{wc}, is less than the ultimate shear strength, V_u ([2.16], Eq. (3.46-3.50)). However, its theoretical basis does not reflect the mechanical relationship between opening of shear crack and the aggregate interlock resistance. Further, the verification for the method above using V_{wc} has not been fully conducted.

Therefore, it is necessary to investigate the DT failure of prestressed concrete beam and propose the quantitative relationship between experimental parameters affecting DT failure (the shear span to overall depth ratio, a/D, beam section width to overall depth ratio, b/D and the amount of shear reinforcement, ρ_w) and crack width at initiation of primary shear crack, w.

Based on the experimental results in previous research and in section 3.3, the conventional method using V_{wc} is verified. Hence, an analytical method to evaluate the crack width at the initiation of shear crack and to predict the DT failure is proposed. The analytical results obtained by proposed method such as failure mode, crack width etc. are clarified by comparing observed ones in the researches in the past [2.13, 3.12-3.17].

5.2   Model Outline

5.2.1 Initiation and Development Mechanism of Shear Crack

To propose an analytical method reflecting the mechanism of DT failure, it is necessary to evaluate crack width at initiation of primary shear crack. A relationship between release of fracture energy of concrete on shear crack surface and deformation of reinforcement on shear crack interface is analytically investigated.

Figure 5.1 illustrates the initiation mechanism of tensile crack in a member subjected to pure tension and definition of fracture energy. In fracture mechanics, initiation of crack is recognized as development of micro-crack because it is assumed that initial defects exist in concrete. Increasing in outer force, T, leads

to increasing in elastic energy accumulated in uncracked and produces the energy dissipated to develop of micro-crack. Therefore, fracture energy is defined as difference between work done by outer force, *W, a*nd elastic energy accumulated in member, *U,* per unit area (N.m/m$_2$). If the fractural energy accumulated at tips of micro-crack, *G*, reaches its critical value (critical fracture energy, *G$_f$*), development of micro-crack is initiated (cracking occurs). The critical fracture energy is depended on material properties and is regardless of loading patterns.
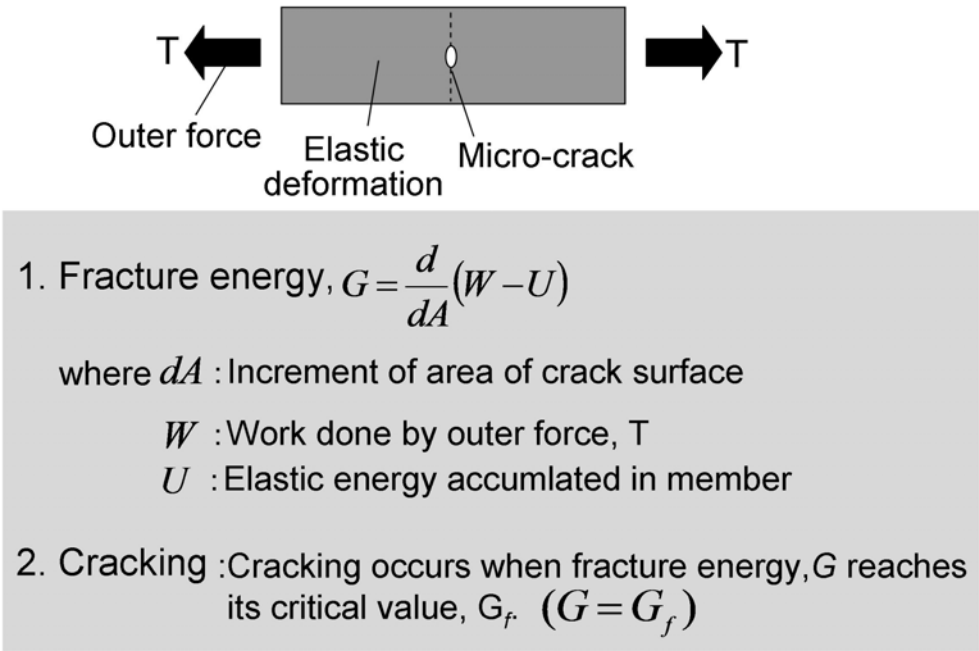

Fig. 5.1 Initiation mechanism of tensile crack in a member subjected to pure tension and definition of fracture energy.

Figure 5.2 illustrates process of from initiation to development of tensile crack in a member subjected to pure tension. As shown in Fig. 5.2 (a), tensile strain in concrete and reinforcement are same before cracking. It is because concrete and reinforcement is strongly bonded and tensile strain in concrete is transferred to both ends of member by the bonded reinforcement. Once primary tensile crack occurs, concrete is released from its encasement (debonding and slip), and crack starts to open by release of fracture energy on crack surface (Fig. 5.2 (b)). The opening of crack continues until total release fracture energy, $G_f A_{cr}$, equals to total energy dissipated by debonding and slip of reinforcement, ΣG. According to elastic fracture mechanics, $G_f A_{cr}$ equals to $(1/2)\Sigma G$. Therefore, it can be seen that initial width of crack, *w*, is closely related to relationship between $G_f A_{cr}$ and $(1/2)\Sigma G$.

(a) Immediately before cracking

(b) Initiation of crack (cracking)
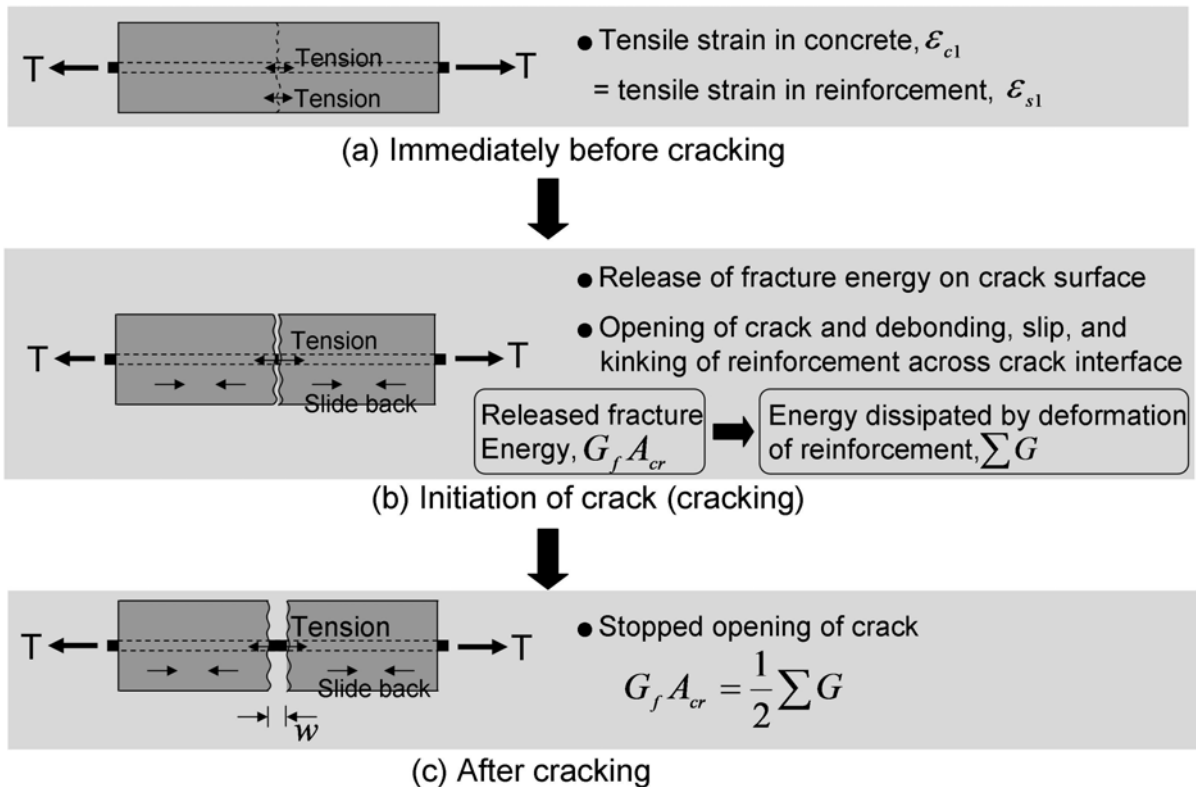
(c) After cracking

Fig. 5.2 Process of from initiation to development of tensile crack

Figure 5.3 illustrates the initiation and development mechanism of a diagonal shear crack in a beam subjected to double curvature and constant shear force. A decrease in the amount of each reinforcement resisting against opening of a shear crack leads to an excessive increase in crack width and deterioration in the load capacity carrying by aggregate interlocking [3.11]. In a same manner with reinforcement across tensile crack, once shear crack has opened or slid, the each reinforcement across the shear crack are released from their concrete encasement (debonding) [5.2]. In initiation and development of shear crack, dowel action of reinforcement also must be considered as well as debonding and slip. Fig. 5.4 illustrates three mechanism of dowel action of reinforcement across shear crack for different crack width. In large crack width, kinking action is prominent as dowel action. Therefore, kinking of reinforcement is applied to analytical model in this study because excessive opening of shear crack is prominent in diagonal tension failure.

In a same manner with initiation and development mechanism of tensile crack, it can be seen that the fracture energy of concrete released on shear crack surface is dissipated by deformation (debonding, sliding, and dowel action) of

155

reinforcement on shear crack interface. Therefore, crack width at initiation of primary shear crack can be evaluated by equilibrium condition between released fracture energy of concrete on crack surface and dissipated deformation energy of reinforcement on crack interface.
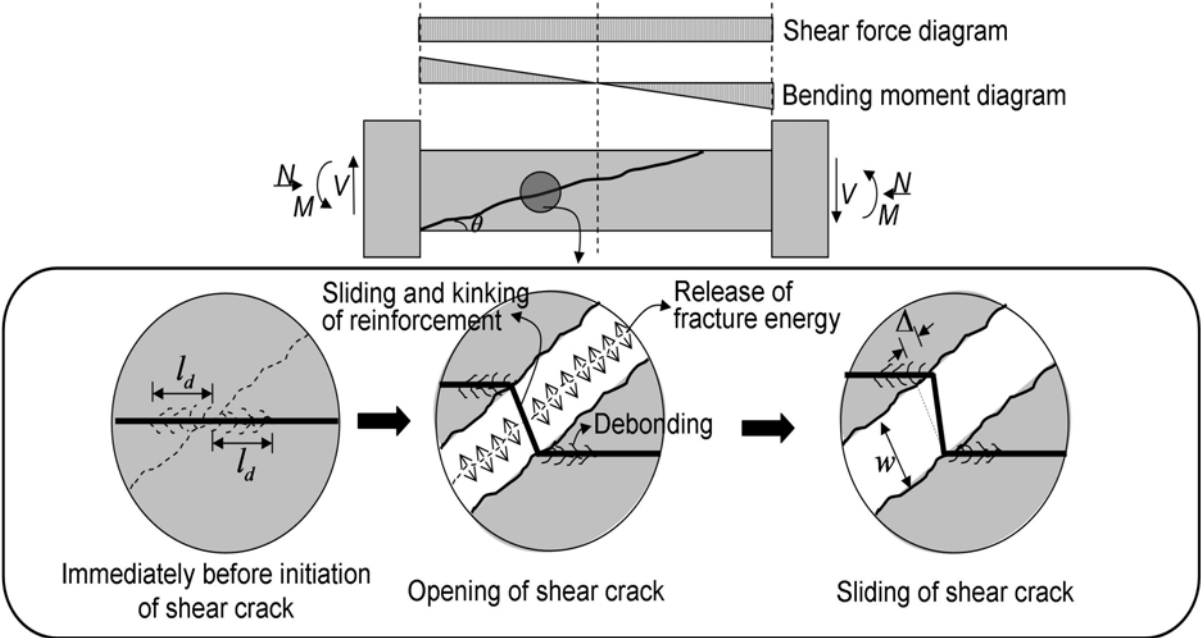

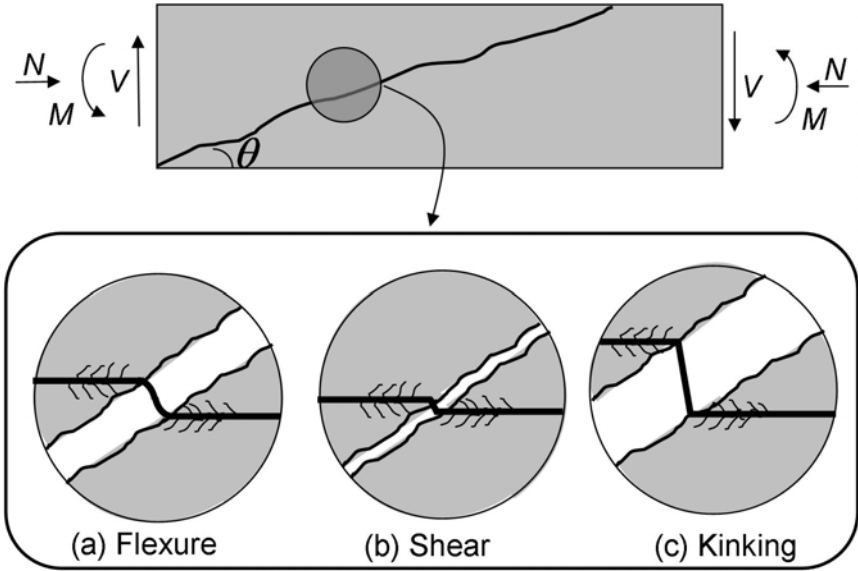Fig. 5.3 Initiation and development mechanism of diagonal shear crack

Fig. 5.4 Dowel action of reinforcement across shear interface

The following assumptions are made to evaluate crack width at initiation of primary shear crack.

Assumption 1: The fracture energy of concrete on the surface of a primary shear crack, $G_f A_{cr}$, is dissipated by the debonding, sliding, and

156

kinking of prestressing steel, longitudinal, and shear reinforcement, respectively.

Assumption 2: Relation of total energy dissipated by each reinforcement and released fracture energy of concrete is linear elastic.

Assumption 3: Dowel action of reinforcing bar across the shear crack is developed as kinking as shown in Fig. 5.4 (c) because dowel strengths of reinforcing bar is obtained as kinking for larger crack width.

Assumption 4: Debonded lengths of reinforcements due to opening of crack are calculated by Dan's model [5.3].

Assumption 5: In bond stress-slip relationships of reinforcement (Fig. 5.5), immediately after bond strength is neglected. Fig. 5.5 illustrates bond stress-slip relationship of reinforcement used in this study. Frictional stress, τ_f, is constant. For bond strength, τ_{max}, slip at bond strength, S_{max}, and frictional stress, τ_f, conventional analytical models [3.6, 5.4, 5.5] are used.
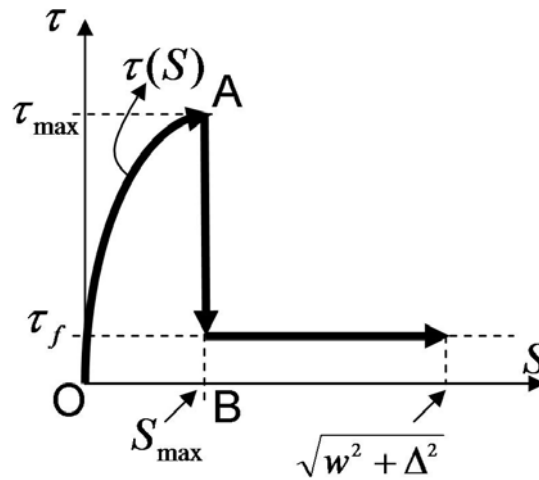
Fig. 5.5 Bond stress-slip relationship applied in this study

5.2.2 Energy Equilibrium Requirements on Shear Interface

Total energy dissipated by deformation of each reinforcement, ΣG, consists of the energy dissipated by debonding, sliding, and dowel action (kinking) of each reinforcement on shear crack, G_d, G_s, and G_k as Eq. (5.1), respectively. The debonding energy, G_d, consists of debonding energy of longitudinal bar, prestressing steel bar, and shear reinforcement as indicated in Eq. (5.2), respectively. In the same manner, the sliding and kinking energy, G_s and G_k can be expressed as Eq. (5.3) and (5.4). The debonding, sliding, and kinking energy

on the shear crack, G_d, G_s, and G_k will be clarified in the section 5.2.4 to 5.2.6.

$$\sum G = G_d + G_s + G_k \qquad \text{Eq. (5.1)}$$

$$G_d = G_{dr} + G_{dp} + G_{dw} \qquad \text{Eq. (5.2)}$$

$$G_s = G_{sr} + G_{sp} + G_{sw} \qquad \text{Eq. (5.3)}$$

$$G_k = G_{kr} + G_{kp} + G_{kw} \qquad \text{Eq. (5.4)}$$

where G_{dr}, G_{dp}, and G_{dw} are debonding energy of longitudinal bar, prestressing steel bar, and shear reinforcement, G_{sr}, G_{sp}, and G_{sw} are sliding energy of longitudinal bar, prestressing steel, and shear reinforcement, G_{kr}, G_{kp}, and G_{kw} are kinking energy of longitudinal bar, prestressing steel, and shear reinforcement, respectively.

5.2.3 Fundamental Relation of Linear Elastic Fracture Mechanics

Since it is assumed that a relation of released fracture energy of concrete, γ_f, and total energy dissipated by deformation of each reinforcement, ΣG, is linear elastic (Assumption 2), a relation between γ_f and ΣG can be expressed as Eq. (5.5). The fracture energy, γ_f, is obtained by CEB-FIP model code 1990 [5.6] as shown in Eq. (5.6).

$$\sum G = 2\gamma_f \qquad \text{Eq. (5.5)}$$

$$G_f = \frac{\gamma_f}{A_{cr}} = \left(0.0469 a_g^2 - 0.5 a_g + 26\right)\left(\frac{f_c}{10}\right)^{0.7} \qquad \text{Eq. (5.6)}$$

where G_f (N.m/m^2) is a fracture energy of concrete per unit area by splitting, a_g (mm) is aggregate size in concrete, f_c (N/mm^2) is compressive strength of concrete, and A_{cr} (mm^2) is a crack surface area.

5.2.4 Debonding Energy on Shear Crack Interface

To evaluate total dissipation energy, ΣG, debonding, sliding, and kinking energy on shear crack interface, G_d, G_s, and G_k, are clarified. Let's first consider the debonding energy of reinforcement. Noting that the debonded surface of reinforcement is $2l_d\psi$ where l_d is debonded length and ψ is perimeter of each reinforcement. Fig. 5.6 illustrates calculation method for debonding energy of reinforcement. As shown in Fig. 5.6, debonding energy of reinforcement can be defined as multiple of total area of debonded surface, $2l_d\psi n$, and area between the simplified bond stress-slip curve and the slip axis from the origin to the slip at the peak stress, OAB in Fig. 5.6 (b). Then, Eq. (5.7) to (5.9) can be made.

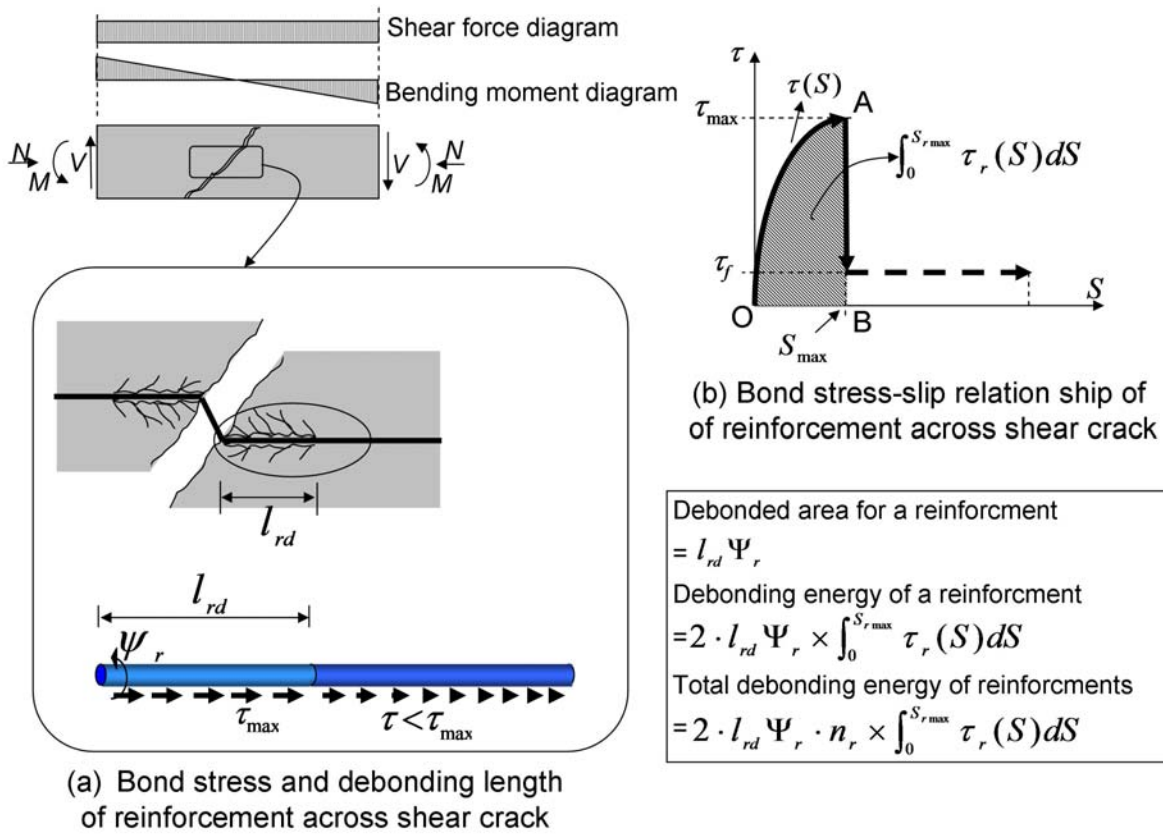Debonded length, l_d, is obtained as Eq. (5.10) to (5.12) [5.3].

(b) Bond stress-slip relation ship of of reinforcement across shear crack

Debonded area for a reinforcment
$= l_{rd} \Psi_r$
Debonding energy of a reinforcment
$= 2 \cdot l_{rd} \Psi_r \times \int_0^{S_{rmax}} \tau_r(S) dS$
Total debonding energy of reinforcments
$= 2 \cdot l_{rd} \Psi_r \cdot n_r \times \int_0^{S_{rmax}} \tau_r(S) dS$

(a) Bond stress and debonding length of reinforcement across shear crack

Fig. 5.6 Calculation method of debonding energy of reinforcement

$$G_{dr} = 2l_d \psi_r n_r \int_0^{S_{rmax}} \tau_r(S) dS \qquad \text{for longitudinal bar} \qquad \text{Eq. (5.7)}$$

$$G_{dp} = 2l_d \psi_p n_p \int_0^{S_{pmax}} \tau_p(S) dS \qquad \text{for prestressing steel} \qquad \text{Eq. (5.8)}$$

$$G_{dw} = 2l_d \psi_w n_w \int_0^{S_{wmax}} \tau_w(S) dS \qquad \text{for shear reinforcement} \qquad \text{Eq. (5.9)}$$

$$l_{dr} = \frac{2.1(f_{ru} - f_{ry})}{\left(f_g\right)^{1.5}} d_r \qquad \text{for longitudinal bar} \qquad \text{Eq. (5.10)}$$

$$l_{dp} = \frac{2.1(f_{pu} - f_{py})}{\left(f_g\right)^{1.5}} d_p \qquad \text{for prestressing steel} \qquad \text{Eq. (5.11)}$$

$$l_{dw} = \frac{2.1(f_{wu} - f_{wy})}{\left(f_g\right)^{1.5}} d_w \qquad \text{for shear reinforcement} \qquad \text{Eq. (5.12)}$$

where S_{rmax}, S_{pmax}, and S_{wmax} are the slip corresponding to the bond strength of longitudinal bar, prestressing steel, and shear reinforcement, l_{rd}, l_{pd}, and l_{wd} are debonded lengths of longitudinal bar, prestressing steel, and shear reinforcement, ψ_r, ψ_p, and ψ_w are perimeter length of longitudinal bar, prestressing steel, and shear reinforcement, n_r, n_p, and n_w are the number of longitudinal bar,

prestressing steel, and shear reinforcement on interface of shear crack, τ_r, τ_p, and τ_w are bond stress of longitudinal, prestressing steel, and shear reinforcement, d_r, d_p, and d_w are diameters of longitudinal bar, prestressing steel, and shear reinforcement, respectively.

For a relationship between bond stress and slip of each reinforcement until maximum bond stress, $\tau_r(S)$, $\tau_p(S)$, and $\tau_w(S)$ in Eq. (5.7) to (5.9), the following analytical models are used.

For longitudinal bar (deformed bar) [5.4, 5.5]

$$\tau_r(S) = \tau_{r\max}(S/S_{r\max})^{\alpha} \qquad \text{Eq. (5.13)}$$

$$\tau_{r\max} = 0.03c^{0.38}f_c \qquad \text{Eq. (5.14)}$$

$$S_{r\max} = 0.003c \le 0.17 \qquad \text{Eq. (5.15)}$$

$$\alpha = 0.13c^{0.18} \qquad \text{Eq. (5.16)}$$

For prestressing steel (prestressing strands and round PT bar) [3.6]

$$\tau_p(S) = \tau_{p\max}\left[\frac{2S}{S_{p\max}} - \left(\frac{S}{S_{p\max}}\right)^2\right] \qquad \text{Eq. (5.17)}$$

$$\tau_{p\max} = 0.53\sqrt{f_g}, \quad S_{p\max} = 4.0\times10^{-3}\phi_p \quad \text{for prestressing strands} \qquad \text{Eq. (5.18)}$$

$$\tau_{p\max} = 0.31\sqrt{f_g}, \quad S_{p\max} = 0.045 \quad \text{for round PT bar} \qquad \text{Eq. (5.19)}$$

For shear reinforcement (plain bar) [5.4, 5.5]

$$\tau_w(S) = \tau_{w\max}(S/S_{w\max})^{\alpha} \qquad \text{Eq. (5.20)}$$

$$\tau_{w\max} = 0.015c^{0.38}f_c \qquad \text{Eq. (5.21)}$$

$$S_{w\max} = 0.6 \qquad \text{Eq. (5.22)}$$

$$\alpha = 0.4 \qquad \text{Eq. (5.23)}$$

where τ_{rmax}, τ_{pmax}, and τ_{wmax} are the bond strength of longitudinal bar, prestressing steel, and shear reinforcement, c is a thickness of cover concrete, and ϕ_p is a nominal diameter of prestressing strands.

5.2.5 Sliding Energy on Shear Crack Interface

Figure 5.7 illustrates distributions of deformation, stress, and strain at a cracked section and debonded zone. A cracking leads to sliding back of concrete as from *ab* to *ac* and elongation of steel as from *de* to *df* in Fig. 5.7 (a), respectively. Then, strains in concrete and steel are also varied as from ε_{c1} to ε_{co} and as from ε_{s1} to ε_{so} in Fig. 5.7 (b), respectively. Variables σ_{co}, σ_{c1}, σ_{so}, σ_{s1}, ε_{co}, ε_{c1}, ε_{so}, and ε_{s1} in the Fig. 5.7 (a) and (b) represent cohesive stress of concrete after cracking,

tensile stress of concrete at cracked section, tensile stress of longitudinal bar at cracked section and tip of debonded zone, and strains corresponding to σ_{co}, σ_{c1}, σ_{so}, and σ_{s1}, respectively. The slip of longitudinal bar is double sum of steel elongation, u_{so}, and concrete slide back, u_{co}, after debonding [5.7] as shown in Fig. 5.7 (a). Since u_{so} and u_{co} can be evaluated from *abc* and *def* in Fig. 5.7 (a), Eq. (5.24) can be made. Tension is assumed as positive in this study. Displacement of reinforcement and concrete, u_s and u_c, can be defined as Eq. (5.25). Total displacement due to elongation of reinforcement and slide back of concrete, u_s-u_c, can be expressed as Eq. (5.26).

(a) Deformation and stress distributions in a steel bar and concrete
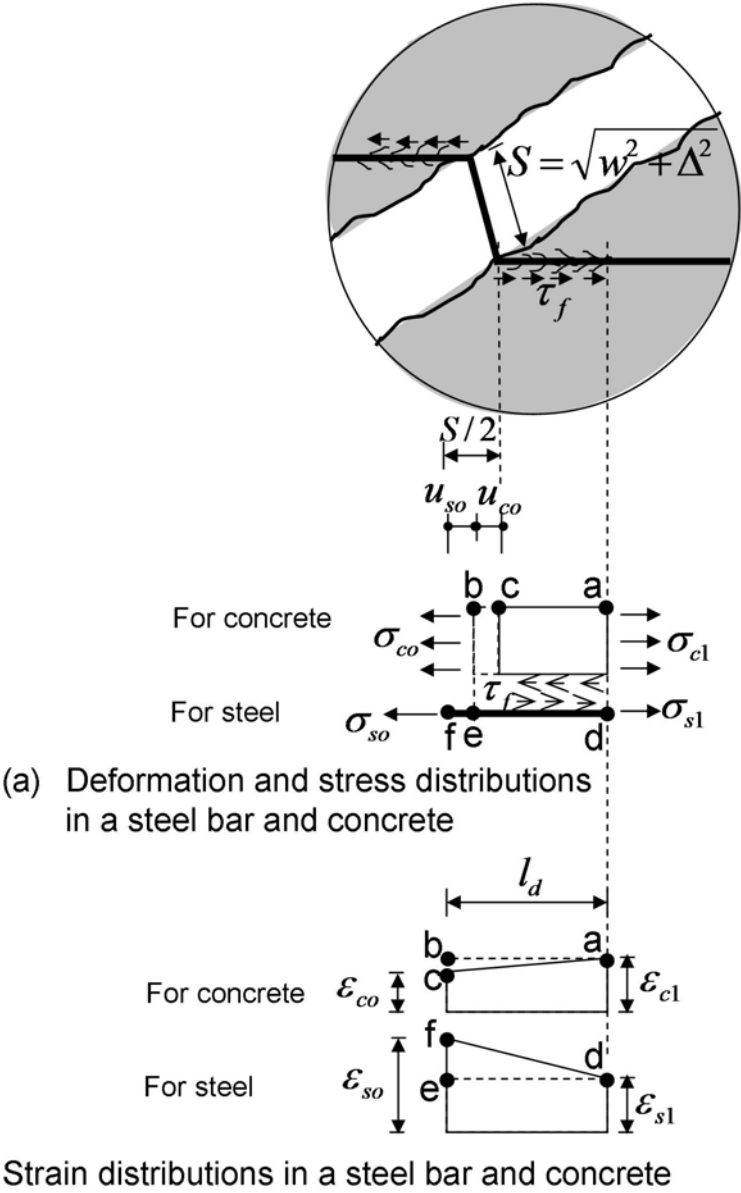
(b) Strain distributions in a steel bar and concrete

Fig. 5.7 Distributions of deformation, stress, and strain at a cracked section and debonded zone

$$S = 2(u_{co} + u_{so}) = l_d(\varepsilon_{so} - \varepsilon_{co}) = \sqrt{w^2 + \Delta^2} \qquad \text{Eq. (5.24)}$$

$$u_s = \int\left(\frac{\varepsilon_{so} - \varepsilon_{c1}}{l_d}S + \varepsilon_{c1}\right)dS, \quad u_c = -\int\left(\frac{\varepsilon_{c1} - \varepsilon_{co}}{l_d}S - \varepsilon_{c1}\right)dS \qquad \text{Eq. (5.25)}$$

$$u_s - u_c = \frac{\varepsilon_{so} - \varepsilon_{co}}{2l_d}S^2 \qquad \text{Eq. (5.26)}$$

Figure 5.8 illustrates calculation method for sliding energy of reinforcement after debonding. Then, the energy dissipated due to sliding of non-prestressed longitudinal bar, G_{sr}, can be expressed as Eq. (5.27) because frictional stress of non-prestressed longitudinal bar, τ_{rf}, is constant (Assumption 6). In the same manner, sliding energy of prestressing steel and shear reinforcement, G_{sp} and G_{sw}, can be expressed as Eq. (5.28) and (5.29), respectively.
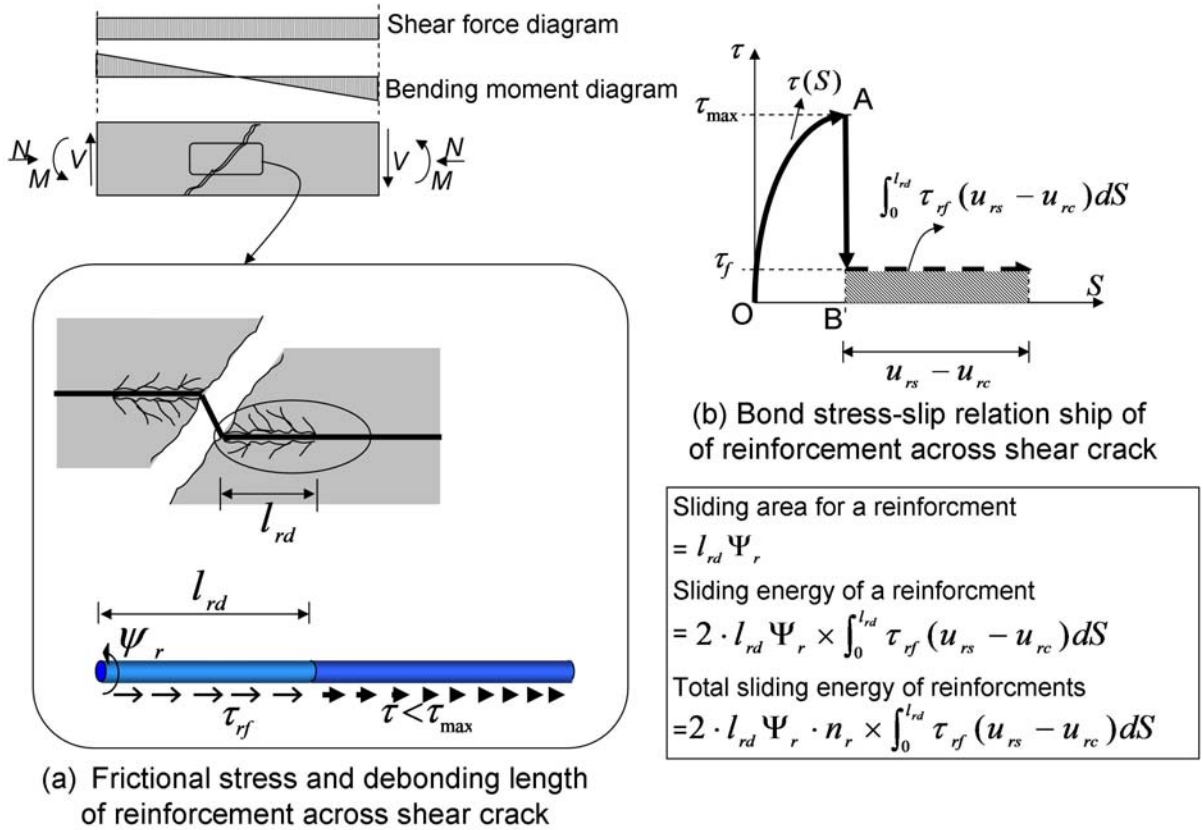

(a) Frictional stress and debonding length
of reinforcement across shear crack

(b) Bond stress-slip relation ship of
of reinforcement across shear crack

Sliding area for a reinforcment
$= l_{rd}\Psi_r$
Sliding energy of a reinforcment
$= 2 \cdot l_{rd}\Psi_r \times \int_0^{l_{rd}} \tau_{rf}(u_{rs} - u_{rc})dS$
Total sliding energy of reinforcments
$= 2 \cdot l_{rd}\Psi_r \cdot n_r \times \int_0^{l_{rd}} \tau_{rf}(u_{rs} - u_{rc})dS$

Fig. 5.8 Calculation method of sliding energy of reinforcement

$$G_{rs} = 2\psi_{rr}n_r\int_0^{l_d}\tau_{rf}(u_{rs} - u_{rc})dS = 2\psi_r n_r\tau_{rf}\frac{\varepsilon_{rso} - \varepsilon_{rco}}{6}l_d^2 = \frac{1}{3}\psi_r n_r l_d\tau_{rf}\sqrt{w^2 + \Delta^2} \quad \text{Eq. (5.27)}$$

$$G_{sp} = \frac{1}{3}\psi_p n_p l_d\tau_{pf}\sqrt{w^2 + \Delta^2}, \quad \sqrt{w^2 + \Delta^2} = l_d(\varepsilon_{pe} + \varepsilon_{pso} - \varepsilon_{pco}) \qquad \text{Eq. (5.28)}$$

$$G_{sw} = \frac{1}{3}\psi_w n_w l_d \tau_{wf} \sqrt{w^2 + \Delta^2}, \quad \sqrt{w^2 + \Delta^2} = l_d(\varepsilon_{wso} - \varepsilon_{wco}) \qquad \text{Eq. (5.29)}$$

where τ_{pf}, τ_{pf}, and τ_{wf} are frictional stresses of non-prestressed longitudinal bar, prestressing steel bar, and shear reinforcement, and ε_{pe} is tensile strain in prestressing steel due to prestress (equals to zero for RC member), respectively.

The frictional stress of non-prestressed longitudinal bar, prestrssing steel bar, and shear reinforcement, τ_{rf}, τ_{pf}, and τ_{wf} in Eq. (5.27) to (5.29) are obtained by Eq. (5.30) to (5.33) [3.6, 5.4, 5.5].

$$\tau_{rf} = 0.15\tau_{r\max} \qquad \text{for longitudinal bar} \qquad \text{Eq. (5.30)}$$

$$\tau_{pf} = 0.5\tau_{p\max} \qquad \text{for prestressing strands} \qquad \text{Eq. (5.31)}$$

$$\tau_{pf} = 0.2\tau_{p\max} \qquad \text{for round PT bar} \qquad \text{Eq. (5.32)}$$

$$\tau_{wf} = 0.15\tau_{w\max} \qquad \text{for shear reinforcement} \qquad \text{Eq. (5.33)}$$

5.2.6 Kinking Energy on Shear Crack Interface

Figure 5.9 illustrates kinking of reinforcement on the shear crack interface of the member. As shown in Fig. 5.9, vertical displacement of the kinked reinforcement equals to $w\cos\theta + \Delta\sin\theta$. Therefore, kinking energy of longitudinal bar is expressed as Eq. (5.34) to (5.37). In Eq. (5.34), A_r and σ_{rso} are the sectional area and tensile stress of longitudinal bar due to elongation after cracking. Tensile stress, σ_{rso}, is defined by the lesser of yield strength of longitudinal bar, f_{ry}, or multiple of Young's modulus and tensile strain in longitudinal bar, $E_r\varepsilon_{rso}$. By Eq. (5.27), ε_{rso} is expressed as Eq. (5.36). Cohesive strain in concrete after cracking, ε_{rco}, is obtained by Shah`s model [5.8] (Eq. (5.37)).

$$G_{kr} = A_r \sigma_{rso} \cos\theta(w\cos\theta + \Delta\sin\theta) \qquad \text{Eq. (5.34)}$$

$$\sigma_{tso} = \min(f_{ry}, E_r\varepsilon_{rso}) \qquad \text{Eq. (5.35)}$$

$$\varepsilon_{rso} = \frac{3G_{sr}}{\psi_r n_r \tau_{rf} l_d^2} + \varepsilon_{rco} \qquad \text{Eq. (5.36)}$$

$$\varepsilon_{rco} = \frac{f_t \exp(-0.06103w^{1.01})}{E_c} \qquad \text{Eq. (5.37)}$$

where f_t and E_c are tensile strength and Young`s modulus of concrete, and w is shear crack width.
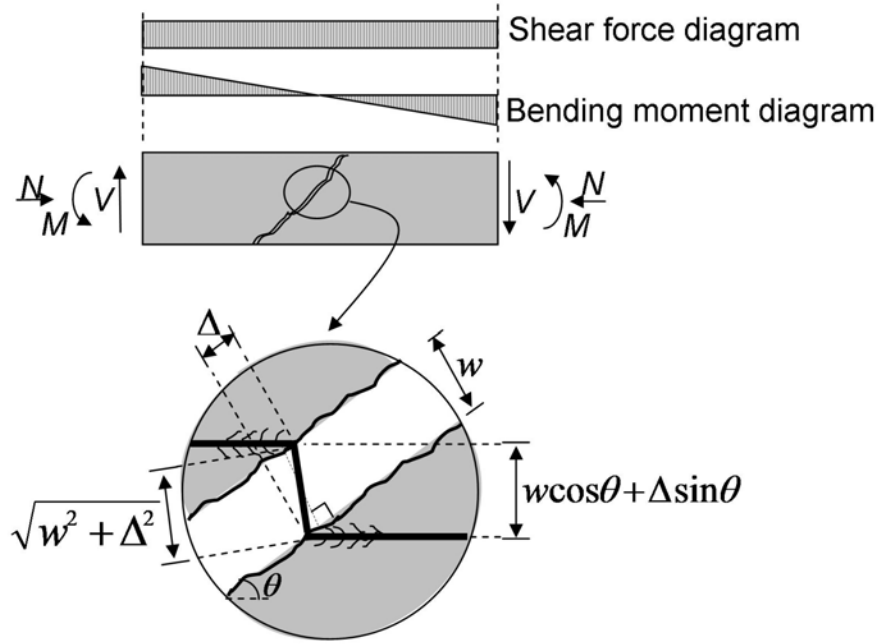
Fig. 5.9 Kinking of reinforcement across shear crack

In a same manner, kinking energy of prestressing steel bar and shear reinforcement can be expressed as Eq. (5.38) and (5.39), respectively.

$$G_{kp} = A_p \sigma_{pso} \cos\theta (w\cos\theta + \Delta\sin\theta) \qquad \text{Eq. (5.38)}$$

$$G_{kw} = A_w \sigma_{wso} \cos\theta (w\cos\theta + \Delta\sin\theta) \qquad \text{Eq. (5.39)}$$

where A_p and σ_{pso} are the sectional area and tensile stress of prestressing steel due to elongation (=min(f_{py}, $E_p\varepsilon_{pso}$)), f_{py} and E_p is yield strength and elastic modulus of prestressing steel, ε_{pso} is tensile strain due to elongation of prestressing steel, A_w and σ_{wso} are the sectional area and tensile stress of shear reinforcement due to elongation (=min(f_{wy}, $E_w\varepsilon_{wso}$)), f_{wy} and E_w is yield strength and elastic modulus of shear reinforcement, ε_{wso} is tensile strain of shear reinforcement due to elongation, respectively.

5.2.7 Axial (longitudinal) Equilibrium Condition

To evaluate opening and sliding of shear crack, w and Δ, equilibrium condition for axial force in member is used as well as energy equilibrium condition (Eq. (5.1) to (5.4), section 5.2.2) in this study. Fig. 5.10 illustrates axial (longitudinal) force components in shear cracked concrete and reinforcements. As shown in Fig. 5.10, the axial (longitudinal) force equilibrium condition is expressed as $N = -F_{rx} - F_{px} - F_{wx} - F_{cix} + V_{cix}$. Then, the equation can be derived as Eq. (5.40). The normal and shear stresses on the surface of shear crack, f_{ci} and v_{ci}, in Eq. (5.40) are estimated by a Li and Maekawa model (Eq. (5.41) and (5.42), [5.9]).

$$N = -\frac{(w\sin\theta - \Delta\cos\theta)}{2l_d}\left[E_p A_p + E_r A_r + E_w b\rho_w j_r \cot\theta\right] - f_{pe}A_p - bj_r\left(f_{ci} - v_{ci}\cot\theta\right) \quad \text{Eq. (5.40)}$$

$$f_{ci}(w,\Delta) = -3.83 f_c^{1/3}\left(0.5\pi - \tan^{-1}\left(\frac{w}{\Delta}\right) - \frac{w\Delta}{w^2 + \Delta^2}\right) \quad \text{Eq. (5.41)}$$

$$v_{ci}(w,\Delta) = 3.83 f_c^{1/3}\frac{\Delta^2}{w^2 + \Delta^2} \quad \text{Eq. (5.42)}$$

where θ is inclination of primary shear crack, s is spacing of shear reinforcement, j_r is a distance between longitudinal bars in tension and compression, and f_{pe} is tensile stress in prestressing steel due to prestress (equals to zero for RC member).

$$N = -F_{rx} - F_{px} - F_{wx} - F_{cix} + V_{cix}$$

$$F_{rx} = \frac{E_r A_r}{2l_d}(w\sin\theta - \Delta\cos\theta)$$

$$F_{px} = \frac{E_p A_p}{2l_d}(w\sin\theta - \Delta\cos\theta) + f_{pe}A_p$$

$$F_{wx} = \frac{E_w A_w}{2l_d}(w\sin\theta - \Delta\cos\theta)$$

$$F_{cix} = f_{ci}bj_r, \quad V_{cix} = v_{ci}bj_r\cot\theta$$
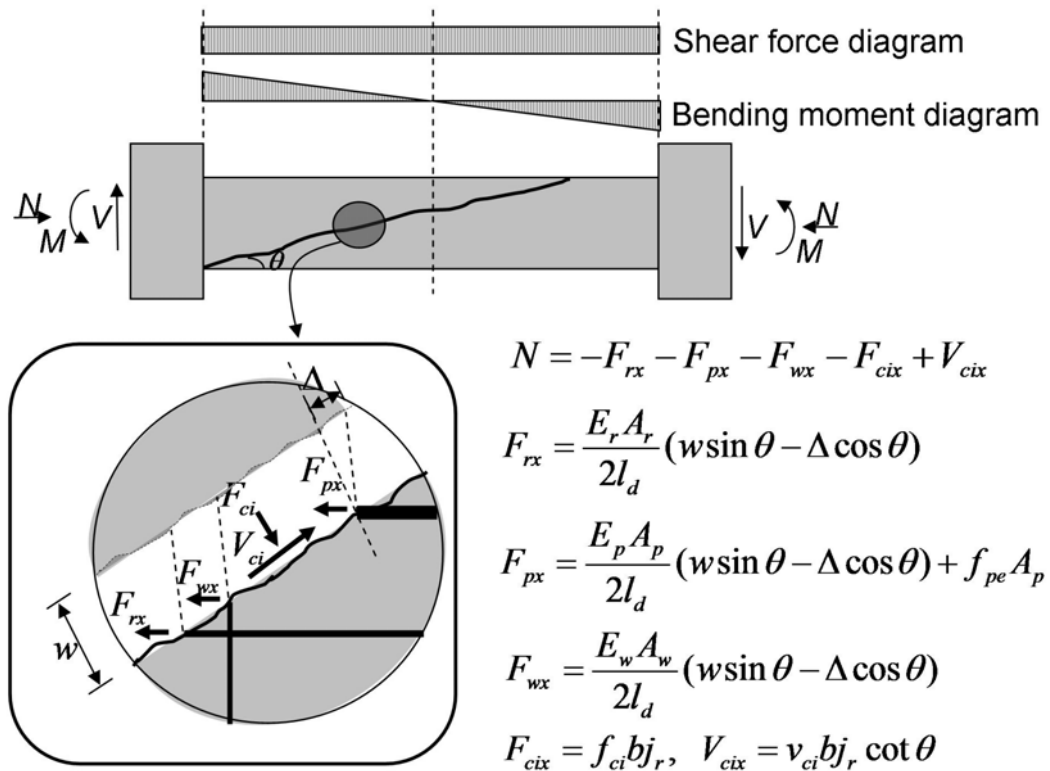
Fig. 5.10 Axial (longitudinal) force components on shear crack interface

5.2.8 Analytical Procedures

The first web-shear cracking load in the beam failing in diagonal tension (DT) represents the ultimate shear strength. To evaluate the web-shear cracking strength, the conventional Modified Compression Field Theory (MCFT) for reinforced/prestressed concrete beams with web reinforcement [2.2] and the simplified MCFT for reinforced concrete beams without web reinforcement [4.6] are used in this study. The first web-shear cracking strength is attained as a shear force when the principle tensile strain reaches f_t/E_c, where f_t and E_c are

tensile strength and Young's modulus of concrete. For more detail about the analytical procedures of the MCFTs, refer to Ref. [2.2] and [4.6].

Figure 5.11 illustrates the calculation procedure for prediction of DT failure. Main calculation procedures are as follows: First, shear cracking strength, V_{wc}, and inclination of primary shear crack, θ, are obtained by the conventional MCFTs [2.2, 4.6]. Then, estimate width and sliding of shear crack, w and Δ. Third, normal and shear stress on the surface of shear crack, fci and vci, are obtained by Li and Maekawa model (Eq. (5.41) to (5.42), [5.9]) using estimated w and Δ. Fourth, check the axial force equilibrium condition by Eq. (5.40). If necessary, revise the Δ. Fifth, bond strength and slip at bond strength of each reinforcement are obtained by Eq. (5.13) to (5.23). Sixth, debonding, sliding, and kinking energy of each reinforcement can be obtained by Eq. (5.7) to (5.12), (5.27) to (5.29), and (5.34) to (5.37), respectively. Total energy dissipated by deformation of reinforcements, ΣG, and fracture energy of concrete, G_f, are obtained by Eq. (5.1) to (5.6) in seventh step. Eighth, equilibrium condition of energy is checked to estimate w. Displacements across and along the primary shear crack, w and Δ, statically increase until the total dissipated energy G equals to $2\gamma_f$ ($=2G_f A_{cr}$). In the final step, if the estimated shear crack width, w, is larger than the critical width, w_{cr}, given by Hordijk`s model (Eq. (5.43)), it is judged that the beam is expected to fail in DT.

$$w_{cr} = 5.14(G_f / f_t) \qquad \text{Eq. (5.43)}$$

where G_f is a fracture energy of concrete per unit area by splitting in N.m/m^2 and f_t is tensile strength of concrete in N/mm$_2$.

An analytical example by proposed model is employed for a post-tensioned precast concrete beam (S-10-L10 in section 3.3). Refer to Table 3.10 and 3.11 for geometrical and material conditions of S-10-L10 for the calculation.

1. Calculate shear cracking strength, V_{wc}, and inclination of primary shear crak, θ, by two MCFTs. They produced 111.9 kN and 20.4 degree, respectively.
2. Estimate displacement across and along the primary shear crak: width, w, and sliding, Δ. Initial value of 5.0 and 3.0 mm for w and Δ are applied.
3. Normal and shear stress on shear crack, f_{ci} and v_{ci}, are given as -1.5 and 4.1 MPa by Eq. (5.42) and (5.42), respectively.

$$f_{ci}(w,\Delta) = -3.83 f_c^{1/3}\left(0.5\pi - \tan^{-1}\left(\frac{w}{\Delta}\right) - \frac{w\Delta}{w^2 + \Delta^2}\right)$$
$$= -3.83(65.2)^{1/3}\left(0.5\pi - \tan^{-1}\left(\frac{5}{3}\right) - \frac{5 \cdot 3}{5^2 + 3^2}\right) = -1.5 \qquad \text{Eq. (5.44)}$$

$$v_{ci}(w,\Delta) = 3.83 f_c^{1/3}\frac{\Delta^2}{w^2 + \Delta^2} = 3.83(65.2)^{1/3}\frac{3^2}{5^2 + 3^2} = 4.1 \qquad \text{Eq. (5.45)}$$

4. Calculate axial force, N, by Eq. (5.40).

5. Check axial force, N. Modified Δ (=1.99 mm) produces axial force of zero.

6. Calculate bond strength and slip at bond strength of each reinforcement by Eq. (5.13) to (5.23).

For longitudinal bar (deformed bar) [5.4, 5.5]

$$\tau_r(S) = \tau_{r\max}(S/S_{r\max})^\alpha = 7.386(S/0.099)^{0.244} \qquad \text{Eq. (5.46)}$$

$$\tau_{r\max} = 0.03c^{0.38}f_c = 0.03 \cdot 33^{0.38} \times 65.2 = 7.386 \qquad \text{Eq. (5.47)}$$

$$S_{r\max} = 0.003c = 0.003 \cdot 33 = 0.099 \qquad \text{Eq. (5.48)}$$

$$\alpha = 0.13c^{0.18} = 0.13 \cdot 33^{0.18} = 0.244 \qquad \text{Eq. (5.49)}$$

For prestressing steel (prestressing strands and round PT bar) [3.6]

$$\tau_p(S) = \tau_{p\max}\left[\frac{2S}{S_{p\max}} - \left(\frac{S}{S_{p\max}}\right)^2\right] = 3.89\left[\frac{2S}{0.22} - \left(\frac{S}{0.22}\right)^2\right] \qquad \text{Eq. (5.50)}$$

$$\tau_{p\max} = 0.53\sqrt{f_g} = 0.53\sqrt{53.9} = 3.89 \qquad \text{Eq. (5.51)}$$

$$S_{p\max} = 4.0 \times 10^{-3}\phi_p = 4.0 \times 10^{-3} \times 55 = 0.22 \qquad \text{Eq. (5.52)}$$

For shear reinforcement (plain bar) [5.4, 5.5]

$$\tau_w(S) = \tau_{w\max}(S/S_{w\max})^\alpha = 3.70(S/0.6)^{0.4} \qquad \text{Eq. (5.53)}$$

$$\tau_{w\max} = 0.015c^{0.38}f_c = 0.015 \cdot 33^{0.38} \cdot 65.2 = 3.70 \qquad \text{Eq. (5.54)}$$

$$S_{w\max} = 0.6 \qquad \text{Eq. (5.55)}$$

$$\alpha = 0.4 \qquad \text{Eq. (5.56)}$$

7. Debonding, sliding, and kinking energy can be obtained by Eq. (5.7) to (5.12), (5.27) to (5.29), (5.34) to (5.37), respectively. Following results are given: G_{dr} = 1.8, G_{dp} = 10.2, G_{dw} = 8.15, G_{sr} = 3.04, G_{sp} = 8.34, G_{sw} = 21.7, G_{kr} = 3.0, G_{kp} = 1.0, and G_{kw} = 0.6 N·m, respectively.

8. Total energy dissipated by debonding, sliding, and kinking energy of each reinforcement, ΣG, is given as 57.83 N·m by Eq. (5.1) to (5.4).

$$\sum G = G_d + G_s + G_k = 20.15 + 33.08 + 4.6 = 57.83 \qquad \text{Eq. (5.57)}$$

$$G_d = G_{dr} + G_{dp} + G_{dw} = 1.8 + 10.2 + 8.15 = 20.15 \qquad \text{Eq. (5.58)}$$

$$G_s = G_{sr} + G_{sp} + G_{sw} = 3.04 + 8.34 + 21.7 = 33.08 \qquad \text{Eq. (5.59)}$$

$$G_k = G_{kr} + G_{kp} + G_{kw} = 3.0 + 1.0 + 0.6 = 4.6 \qquad \text{Eq. (5.60)}$$

9. Fractural energy of concrete on primary shear crack surface, G_f, are obtained as 107.9 N·m/m^2 by Eq. (5.6). Then, $2\gamma_f$ of 82.87 N·m is obtained.

$$G_f = \frac{\gamma_f}{A_{cr}} = \left(0.0469 a_g^2 - 0.5 a_g + 26\right)\left(\frac{f_c}{10}\right)^{0.7} = 107.9 \qquad \text{Eq. (5.61)}$$

10. Check equilibrium condition of energy based on the linear fractural mechanics ($\Sigma G, = 2G_f A_{cr}$, Eq. (5.5)). If necessary, return to step 2 and revise w.

$$\sum G = 57.83 \neq 82.87 = 2\gamma_f \qquad \text{Eq. (5.62)}$$

Therefore, estimated w and Δ must be revised. Reviesed w of 7.82 and Δ of 3.07 mm give zero axial force and ΣG of 41.5 N·m. Go to next step.

11. Calculate the critical shear crack width, w_{cr}, by Eq. (5.43). It results 2.054 mm.

$$w_{cr} = 5.14(G_f / f_t) = 5.14(107.9 \times 10^{-2} / 2.7) = 2.054 \qquad \text{Eq. (5.63)}$$

12. Judge failure mode. S-10-L10 is expected to fail in diagonal tension (DT) because estimated w of 7.82 mm is larger than w_{cr} of 2.054 mm.

To verify the accuracy of analytical results by analytical method proposed in this study, comparison between the analytical and experimental results [2.13, 3.12-3.17]. It will discuss in next section.
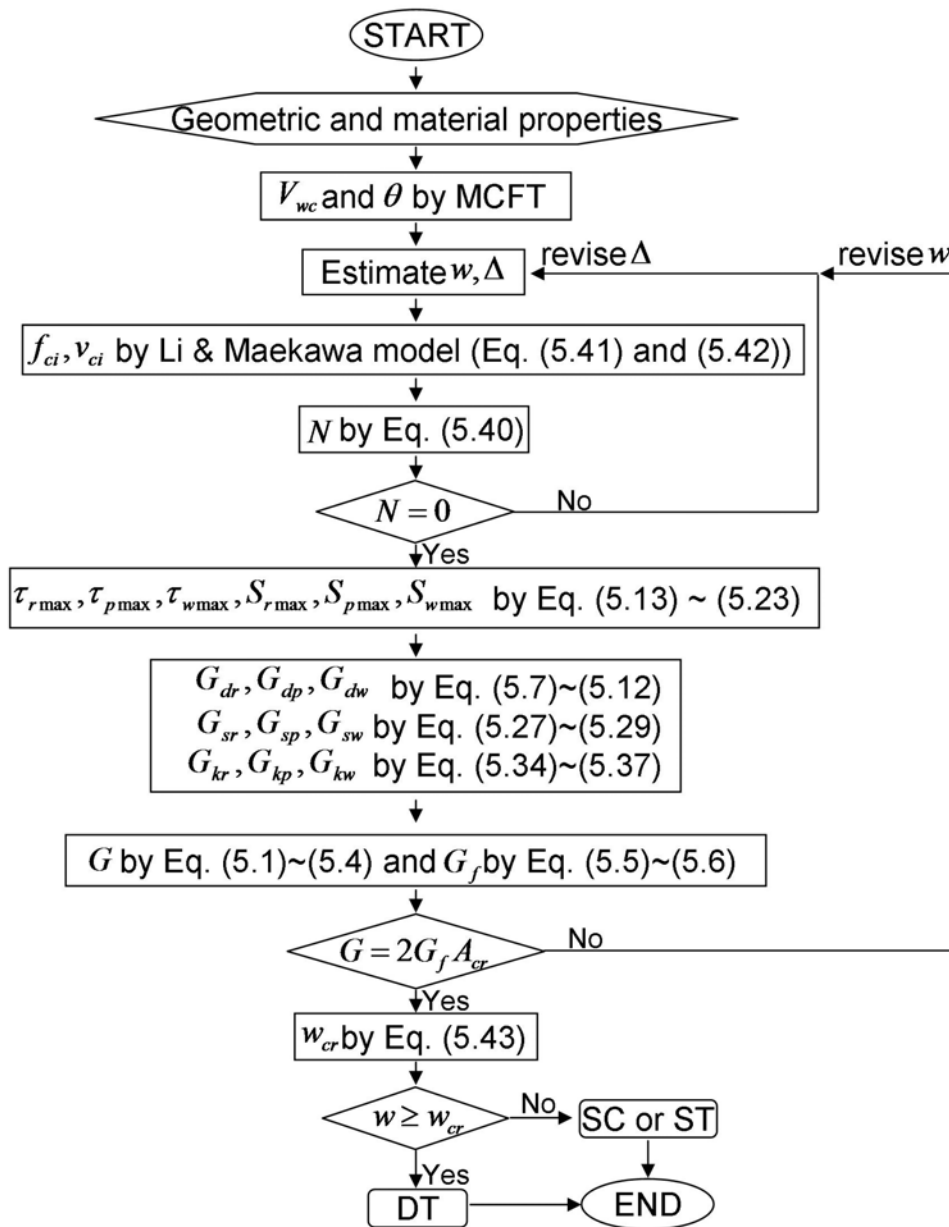
Fig. 5.11 Calculation procedures for prediction of DT failure

5.3 Verification of Analytical Results

5.3.1 Experimental Data Used for Verification

The proposed analytical method is verified by comparing with the test results. A total four prestressed concrete (PC) beams from this study and 36 PC beams from the research in the past [2.13, 3.12-3.17] are taken for the verification. Eighteen reinforced concrete (RC) beams [5.10, 5.11] and 7 RC columns [5.12] are also taken for the verification of shear cracking strength and failure mode, because the model proposed in this study can be applied to RC as well as PC members. Fig. 5.12 shows the range of the main parameters and failure mode of

these test specimens. Horizontal axis in Fig. 5.12 represents the experimental parameters and failure mode. The number of tested specimens for each fraction of the experimental paramaters and failure mode is indicated in vertical axis in Fig. 5.12. DT, SC, ST, and FSC in Fig. 5.12 (d) indicate diagonal tension, shear compression, and shear tension failure, flexural shear compression failure, respectively. Table 5.1 shows the geometrical and experimental parameters of specimens for the verification.

(a) Shear span ratio

(b) Ratio of sectional width to depth

(c) Shear reinforcement ratio
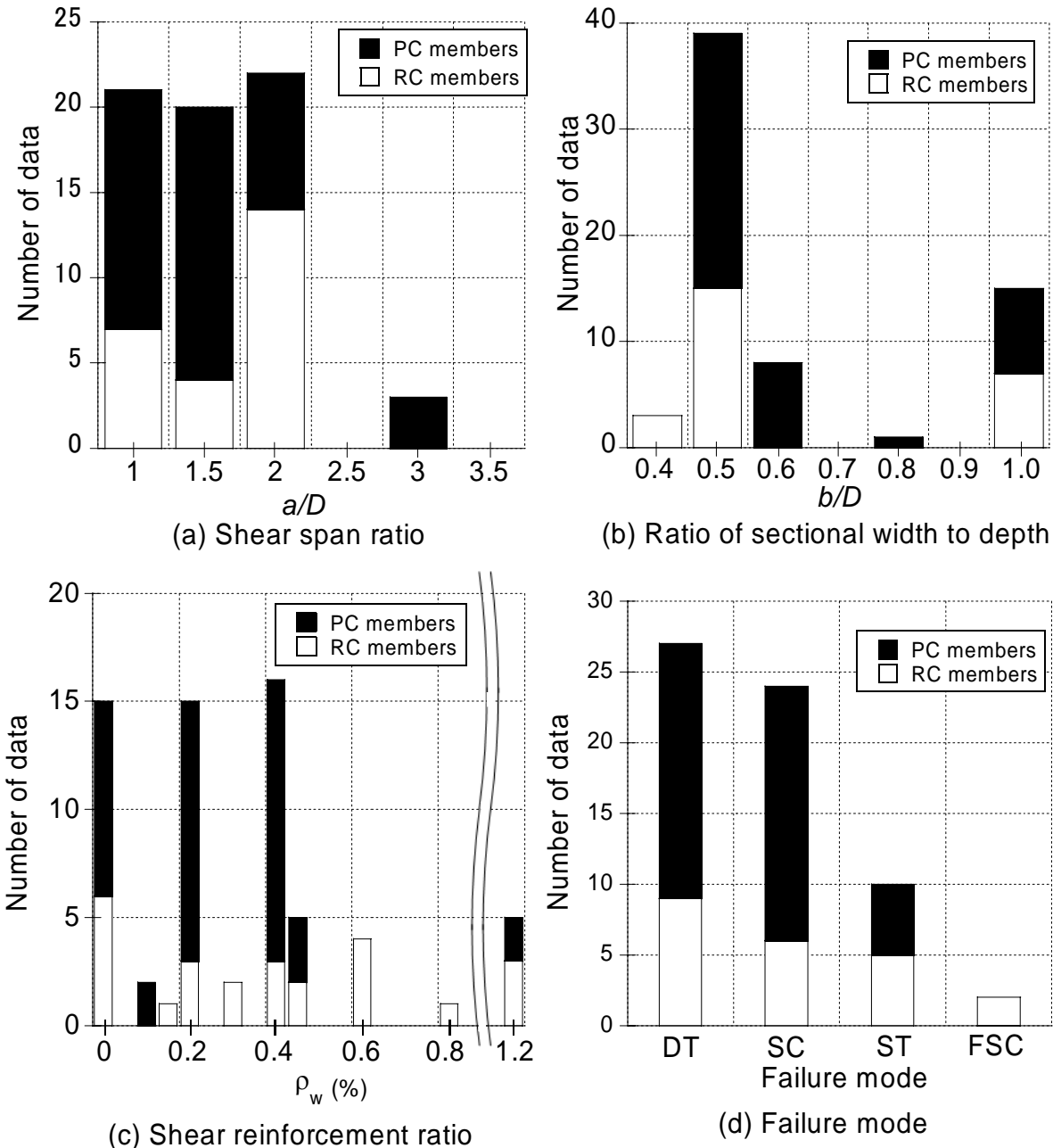
(d) Failure mode

Fig. 5.12 Range of the main parameters and failure mode of specimens for the verification

Table 5.1 Geometrical and experimental parameters of specimens

Type	Ref.	Name	b (mm)	D (mm)	b/D	a/D	F_c (kN)	f_{ry} (MPa)	f_{py} (MPa)	f_{wy} (MPa)	ρ_w (%)
PC beam	[2.13]	S-PW0	250	250	1.0	1.5	58.2	376	1804	-	0.00
		S-PW12					56.8			381	1.14
	[3.12]	S-SR1-PW04	250	250	1.0	1.0	59.4	328	1761	331	0.45
		S-SR1-PW12					59.6			366	1.14
	[3.13]	A-PW0	250	250	1.0	1.5	39.1	360	1169	-	0.00
		A-PW04							1169	421	0.45
		NA-PW0							1115	-	0.00
	[3.14]	LD2PW04φ13	150	300	0.5	1.0	42.7	342	1107	319	0.40
		LD2PW04φ17							1198		
		LD2PW04φ23							1158		
		LD2PW02φ13					42.3		1107		0.20
		LD2PW02φ17							1198		
		LD2PW02φ23							1158		
		LD2PW00φ13					46.0		1107	-	0.00
		LD2PW00φ17							1198	-	
		LD2PW00φ23							1158	-	
		LD3PW00φ23				1.5	35.8			-	
	[3.15]	LD3PW02φ17I	150	300	0.5	1.5	48.8	346	1166	325	0.20
	[3.16]	LD3φ23SD07α30	150	300	0.5	1.5	39.7	363	1043	434	0.40
		LD3φ23SD07α45									
		LD3φ23SD07α60									
		LD3φ23SD08α60									
		LD3φ26SD07α45					38.3		1004		
		LD3φ32SD05α60							996		
		LD4φ23SD07α30							1043		
		LD4φ23SD07α45									
	[3.17]	No.1	200	350	0.6	2.0	45.8	445	1082	261	0.20
		No.2					48.0				
		No.3					51.1				0.20
		No.4					50.7		1152		
		No.6					44.8		1082		0.40
		No.7					53.0				
		No.8					71.0		1152		0.20
		No.9					60.1				

Table 5.1 Geometrical and experimental parameters of specimens

Specimens for the verification			b (mm)	D (mm)	b/D	a/D	F_c (kN)	f_{ry} (MPa)	f_{py} (MPa)	f_{wy} (MPa)	ρ_w (%)
Type	Ref.	Name									
PC beam	Test 1	S-10-L42	300	400	0.75	1.0	57.3	361	1805	984	0.42
		S-15-L21				1.5	62.3				0.21
	Test 2	S-10-L10		600	0.5	1.0	65.2	380	1763	1006	0.10
		S-10-L21									0.21
		S-15-L00				1.5					0.00
		S-15-L10									0.10
RC beam	[5.10]	B-210-0	180	400	0.45	1.5	20.4	798	-	-	0.00
		B-360-0					37.5		-	-	
		B-570-0					53.8		-	-	
RC beam	[5.11]	B-0	200	400	0.5	2.0	34.0	931	-	-	0.00
		B-30-046					32.8		-	349	0.46
		B-30-121					32.2		-	285	1.21
		B-60-030					32.6		-	492	0.30
		B-60-059					32.9		-	554	0.59
		B-80-019					33.3		-	865	0.19
		B-80-046					33.3		-	901	0.46
		B-80-059					33.7		-	901	0.59
		B-80-121					33.8		-	898	1.21
		B-120-019					34.5		-	1061	0.19
		B-120-030					34.8		-	1061	0.30
		B-120-059					34.7		-	1060	0.59
		B-120-121					34.8		-	1065	1.21
		B-150-019					34.9		-	1235	0.19
		B-1.5-0				1.5	35.4		-	-	0.00
RC column	[5.12]	0-10-10-4	400	400	1.0	1.0	93.4	957	-	-	0.00
		20-10-10-4							-	1372	0.15
		60-7-10-2					76.9		-		0.40
		60-10-10-4					93.4		-		
		60-7-10-4					76.9		-		
		90-10-10-4					93.4		-		0.62
		120-10-10-4							-		0.80

b: sectional width, D: sectional depth, a/D: shear span ratio, F_c: compressive strength of concrete, ρ_w: shear reinforcement ratio, f_{ry}, f_{py}, and f_{wy}: yield strength of non-prestressed longitudinal bar, prestressing steel, and shear reinforcement, respectively.

5.3.2 Shear Cracking Strength and Failure Mode

Figure 5.13 shows the comparison between observed shear cracking strength, V_{cr-e} and predicted shear cracking strengths: (a) V_{cr-a}; (b) V_{cr-b}; and (c) V_{cr-c}. Three shear failure modes, ST, SC, and DT failure, were selected in this section. Vertical axis in Fig. 5.13 indicates observed shear cracking strength, V_{cr-e}. Horizontal axis in Fig. 5.13 represents the predicted shear cracking strengths, V_{cr-a}, V_{cr-b}, and V_{cr-c}, respectively. Predicted shear cracking strengths in Fig. 5.13, V_{cr-a}, V_{cr-b}, and V_{cr-c} represent analytical shear cracking strengths by AIJ RC guide line ([2.8], Eq. (3.45)), PC standard ([2.16], Eq. (3.46)), and the proposed method in this study, respectively. Circles, squares, and triangles in Fig. 5.13 indicate observed data for RC and PC members which experimentally failed in diagonal tension (DT), shear compression (SC), and shear tension (ST), respectively.
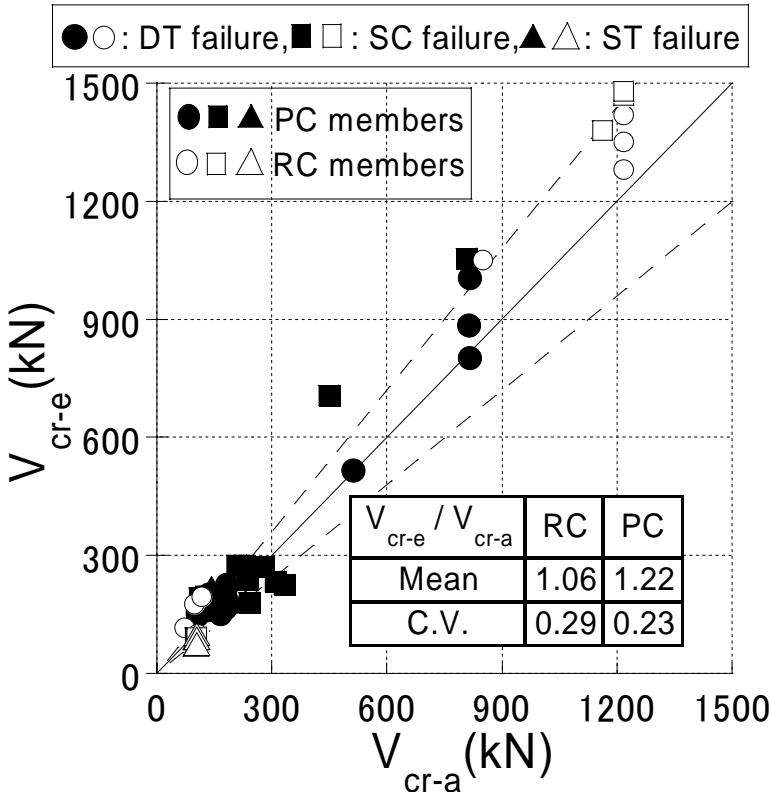
(a) V_{cr-a} by AIJ RC guide line [2.8]

Fig. 5.13 Comparison between observed and predicted shear cracking strength
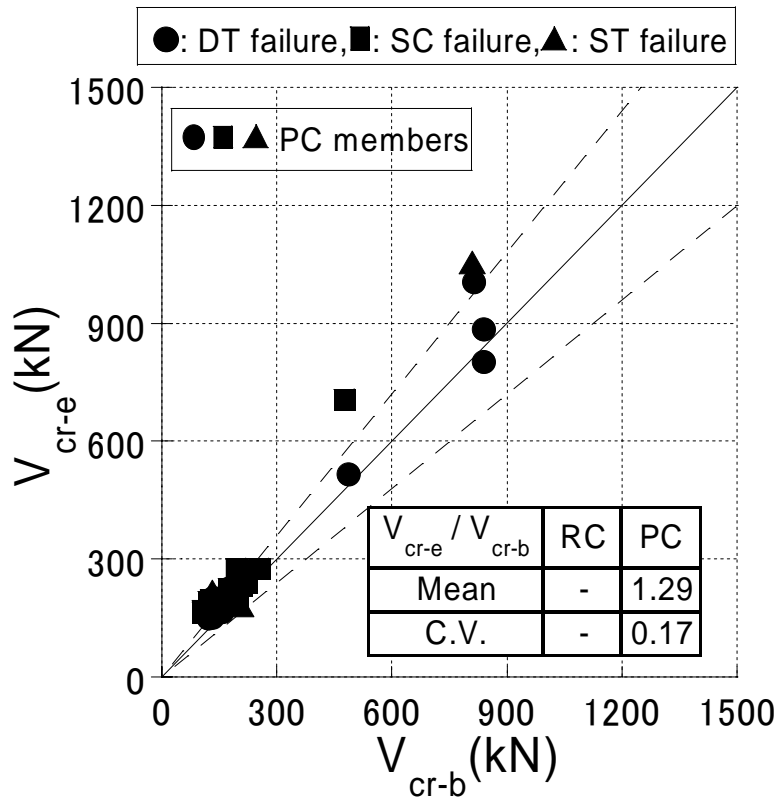
(b) $V_{cr\text{-}b}$ by AIJ PC standard [2.16]
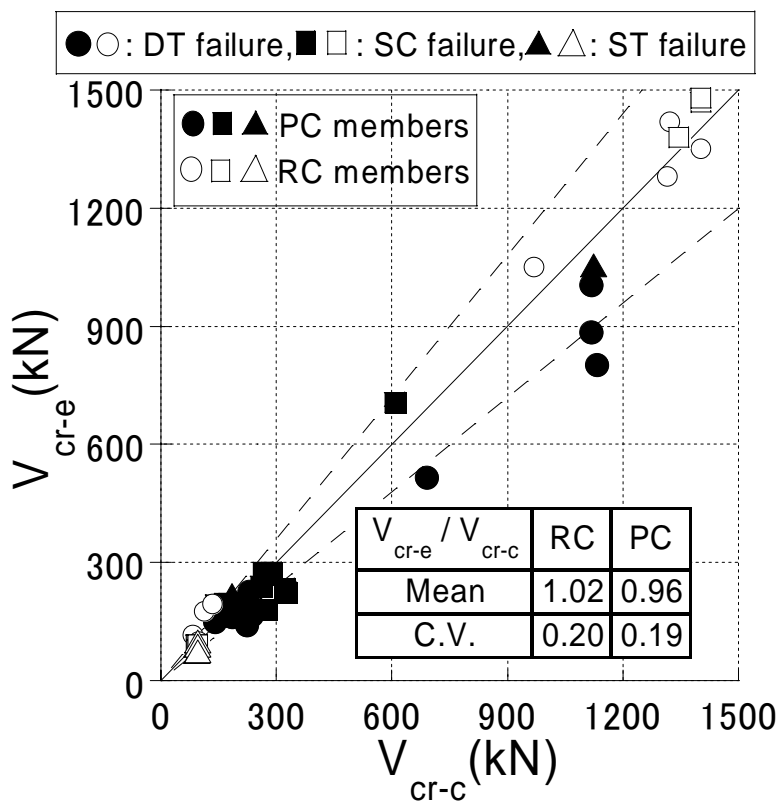
(c) $V_{cr\text{-}c}$ by proposed method

Fig. 5.13 Comparison between observed and predicted shear cracking strength

As shown in Fig. 13 (a), predicted shear cracking strength by AIJ RC guide line ([2.8], Eq. (3.45)) evaluated observed shear cracking strength of RC members in a good accuracy (mean value of V_{cr-e}/V_{cr-a} = 1.06 and coefficient of variation (C.V.) = 0.29). However, V_{cr-a} can not evaluate V_{cr-e} of PC members in a good accuracy (mean value of V_{cr-e}/V_{cr-a} = 1.22 and C.V. = 0.23). It points out that AIJ RC guide line ([2.8], Eq. (3.45)) can not appropriately evaluate shear cracking strength of PC members. The predicted shear cracking strengths show a good agreement with their observed web-shear cracking strength.

Analytical shear cracking strength by AIJ PC standard ([2.16], Eq. (3.46)) V_{cr-b}, can not evaluated observed shear cracking strength of PC member with ± 20% accuracy (mean value of V_{cr-e}/V_{cr-a} = 1.29 and C.V. = 0.17). It is because concrete strength factor, v, in Eq. (3.46) is based on the empirical results of prestressed concrete for evaluation of shear failure strength. It points out that methodology using strut mechanism in Eq. (3.46) to evaluate shear cracking strength of PC member is not appropriate.

As shown in Fig. 5.13 (c), analytical shear cracking strength in proposed method (MCFTs [2.2, 4.6]) evaluated observed shear cracking strength in the best accuracy (mean value of V_{cr-e}/V_{cr-a} = 1.02 and C.V. = 0.20 for RC members, mean value of V_{cr-e}/V_{cr-a} = 0.96 and C.V. = 0.19 for PC members).

Figure 5.14 plots comparison between observed and predicted failure mode by proposed method. Solid and open data in Fig. 5.14 indicate predicted failure modes agree and disagree with the observed ones. Vertical and horizontal axis in Fig. 5.14 represent observed and predicted shear cracking strength. As shown in Fig. 5.14, most predicted failure modes agree with the observed ones except for nine out of 65 specimens. It points out that propose method is appropriately predict diagonal tension failure of RC and PC members.
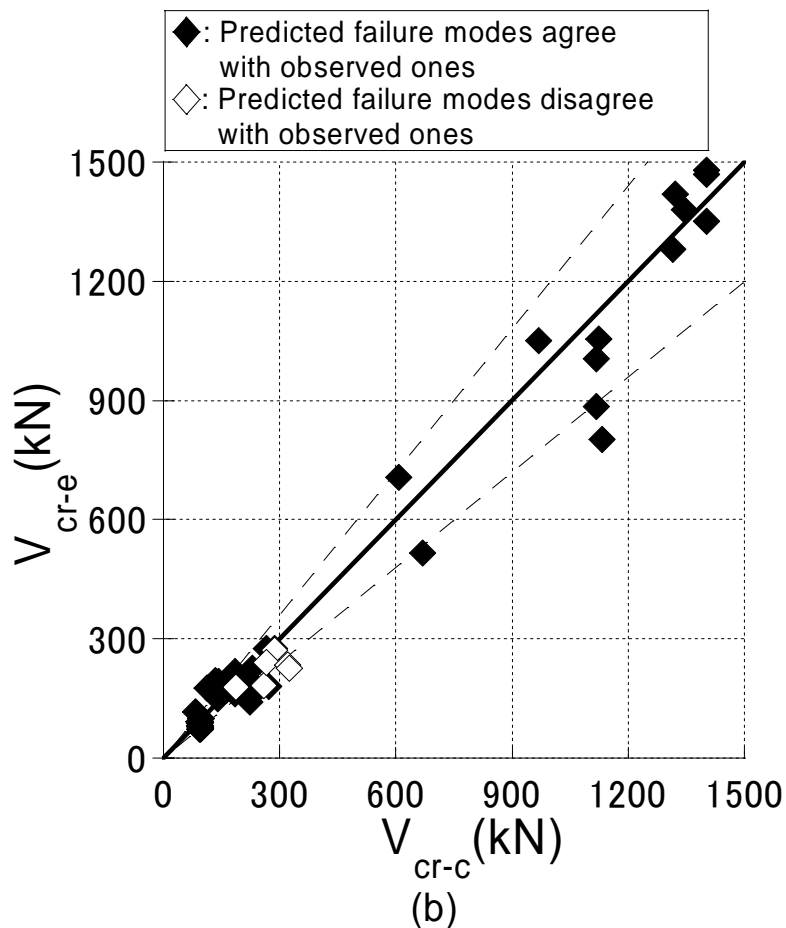
Fig. 5.14 Comparison between observed and predicted failure mode

5.3.3 Primary Shear Crack Width

To verify the analytical method proposed in this study, evaluation of the width of primary shear crack is important. Fig. 5.15 shows comparison of predicted and observed width of primary shear crack. Horizontal and vertical axis in Fig. 5.15 represent predicted and observed width of primary shear crack, respectively. It is difficult to observe the crack width of primary shear crack in beams which failed in DT because the beam simultaneously fails at initiation of primary shear crack. However, it is possible to measure the width of primary shear crack in the beams which failed in other modes than DT (SC and ST etc.) because the crack width gradually increases even after shear cracking. In this study, observed crack widths of primary shear crack in PC beams which failed in ST, SC, FS, and F are used. Notation, ST, SC, FS, and F indicate shear tension, shear compression, shear failure after flexural yielding, and flexural failure. Refer to section 3.2.4 for the definition of the failure modes. As shown in Fig. 5.15, analytical widths of primary shear crack predicted by proposed method evaluate observed crack width at primary shear cracking in a good accuracy. However, further investigation needs because the number of data is quite a few for comparison.

176
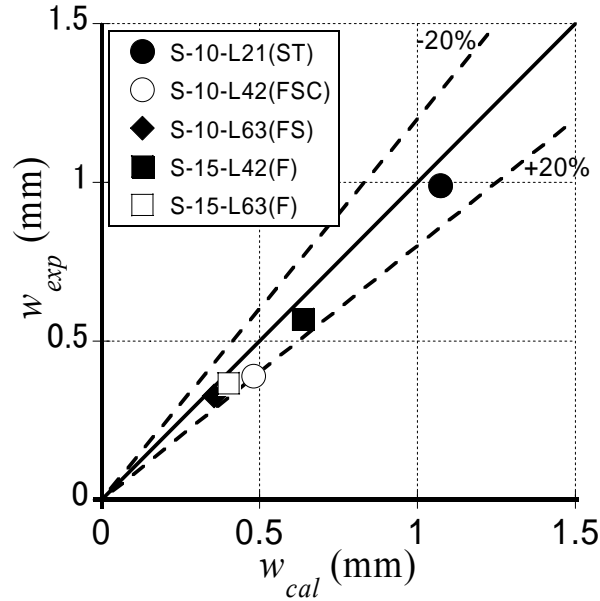
Fig. 5.15 Comparison between predicted and observed width of primary shear crack

5.3.4 Parametric Study

Figure 5.16 plots relationship between a ratio of experimental to analytical shear cracking strength by AIJ RC guide line ([2.8], Eq. (3.45)), V_{cr-e}/V_{cr-a}, and exp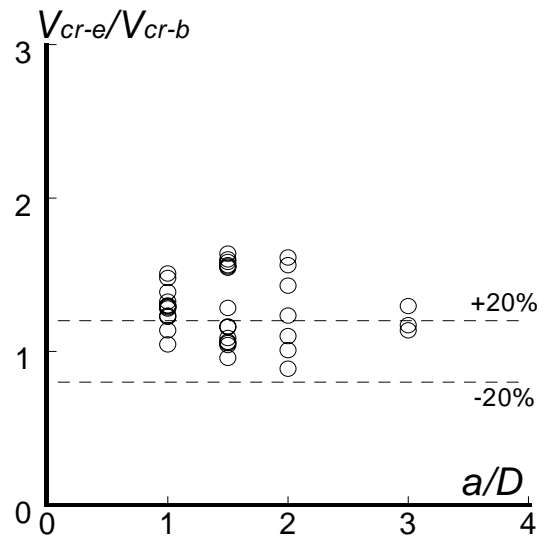erimental parameters: (a) compressive concrete strength, F_c; (b) shear span to overall depth ratio, a/D; (c) yield strength of shear reinforcement, f_{wy}; (d) shear reinforcement ratio, ρ_w; and (e) prestressing level, η_{pe}. Vertical and horizontal axis in Fig. 5.16 represent a ratio of experimental to analytical shear cracking strength and each experimental parameters, respectively. In a same manner, the relationships between a ratio of experimental to analytical cracking shear strength by AIJ PC standard ([2.16], Eq. (3.46)) and proposed method, V_{cr-e}/V_{cr-b}, and V_{cr-e}/V_{cr-c}, and experimental parameters are plotted in Fig. 5.17 to 5.18, respectively.

As shown in Fig. 5.16 to 5.18, analytical shear cracking strengths in proposed method (MCFTs [2.2, 4.6]) evaluated experimental ones in best accuracy of three methods regardless of experimental paramters. Further, it can be seen that the proposed model can be applied to the post-tensioned precast concrete members with materials in excess of the range of parameters used for the verification because the proposed model is based on the equilibrium condition of stresses and compatibility conditions of strains in concrete and reinforcements.
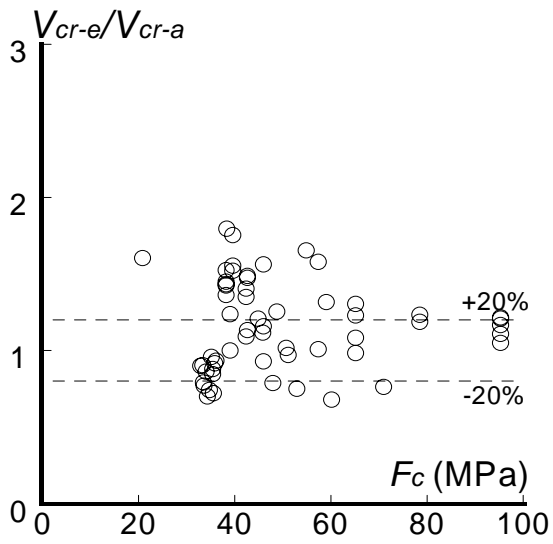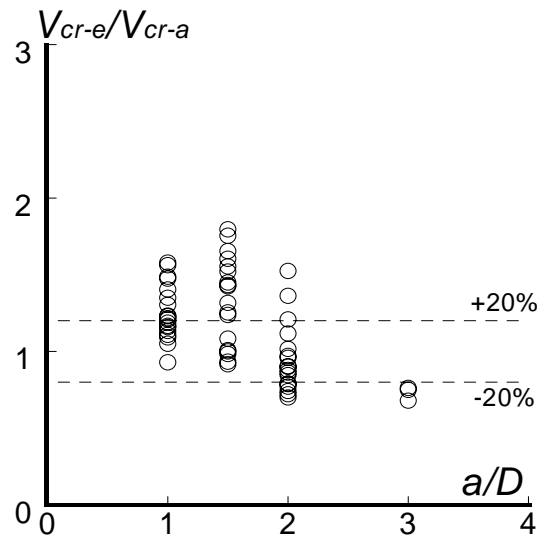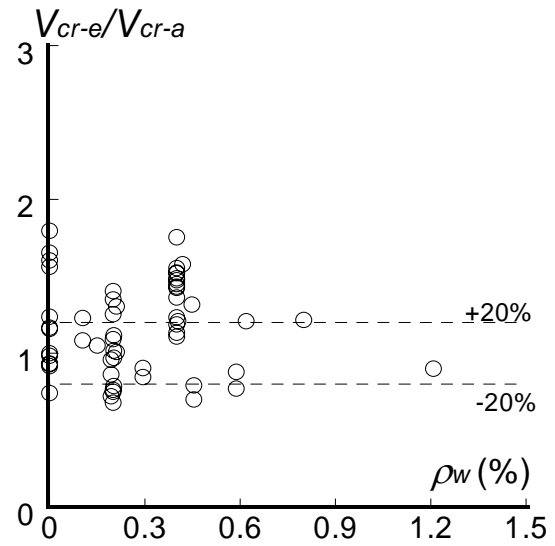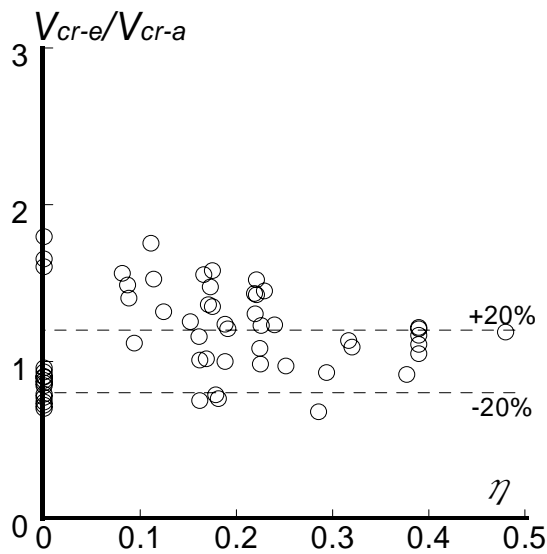
Fig. 5.16 Relationship between a ratio of experimental to analytical shear cracking strength by AIJ RC guide line [2.8] and parameters
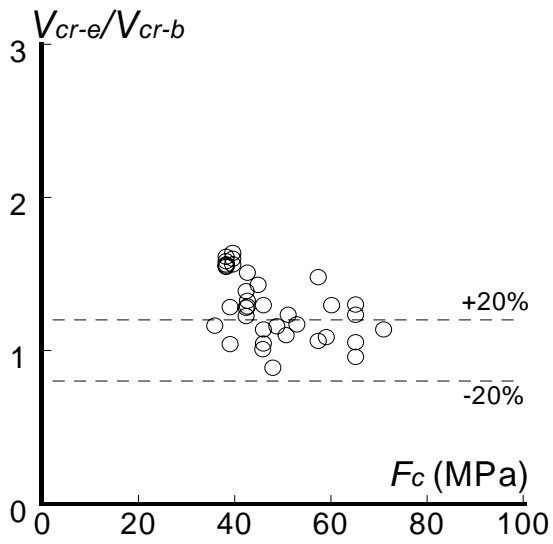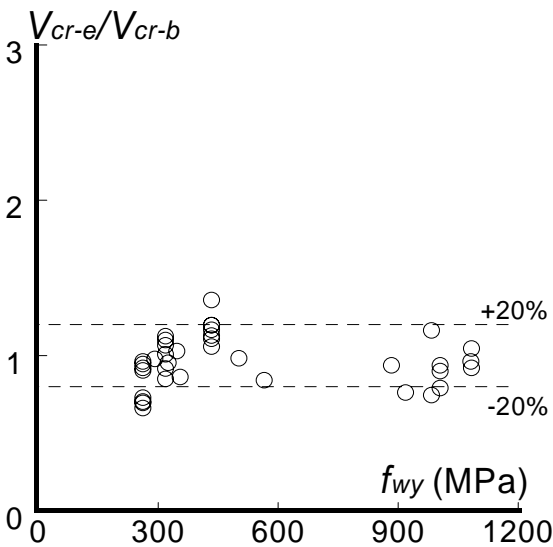
178

(a) Compressive strength of concrete   (b) Shear span to overall depth ratio

(c) Yield strength of shear reinforcement   (d) Shear reinforcement ratio
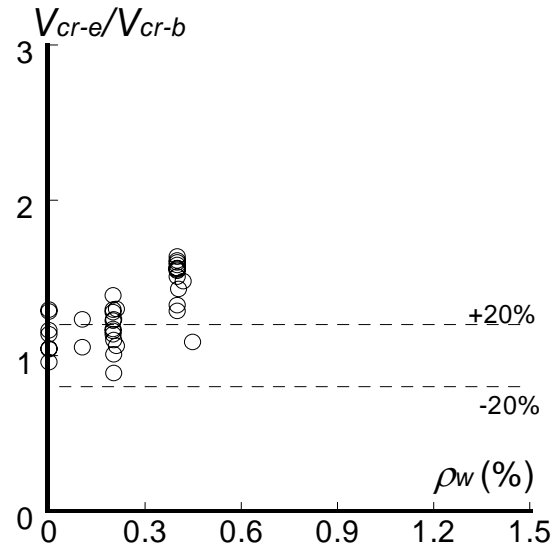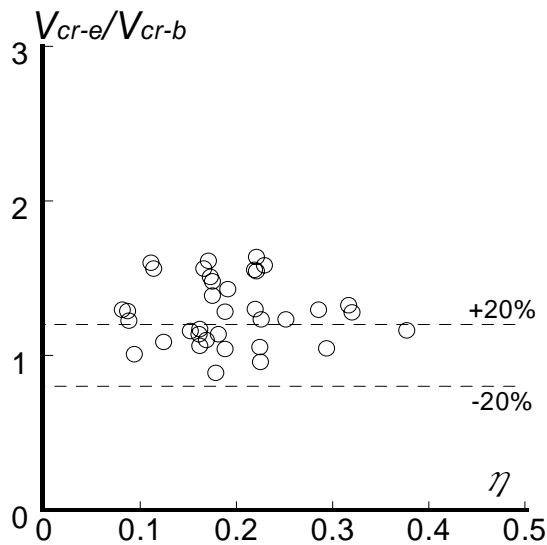
(e) Prestressing level

Fig. 5.17 Relationship between a ratio of experimental to analytical shear cracking strength by AIJ PC standard [2.16] and parameters
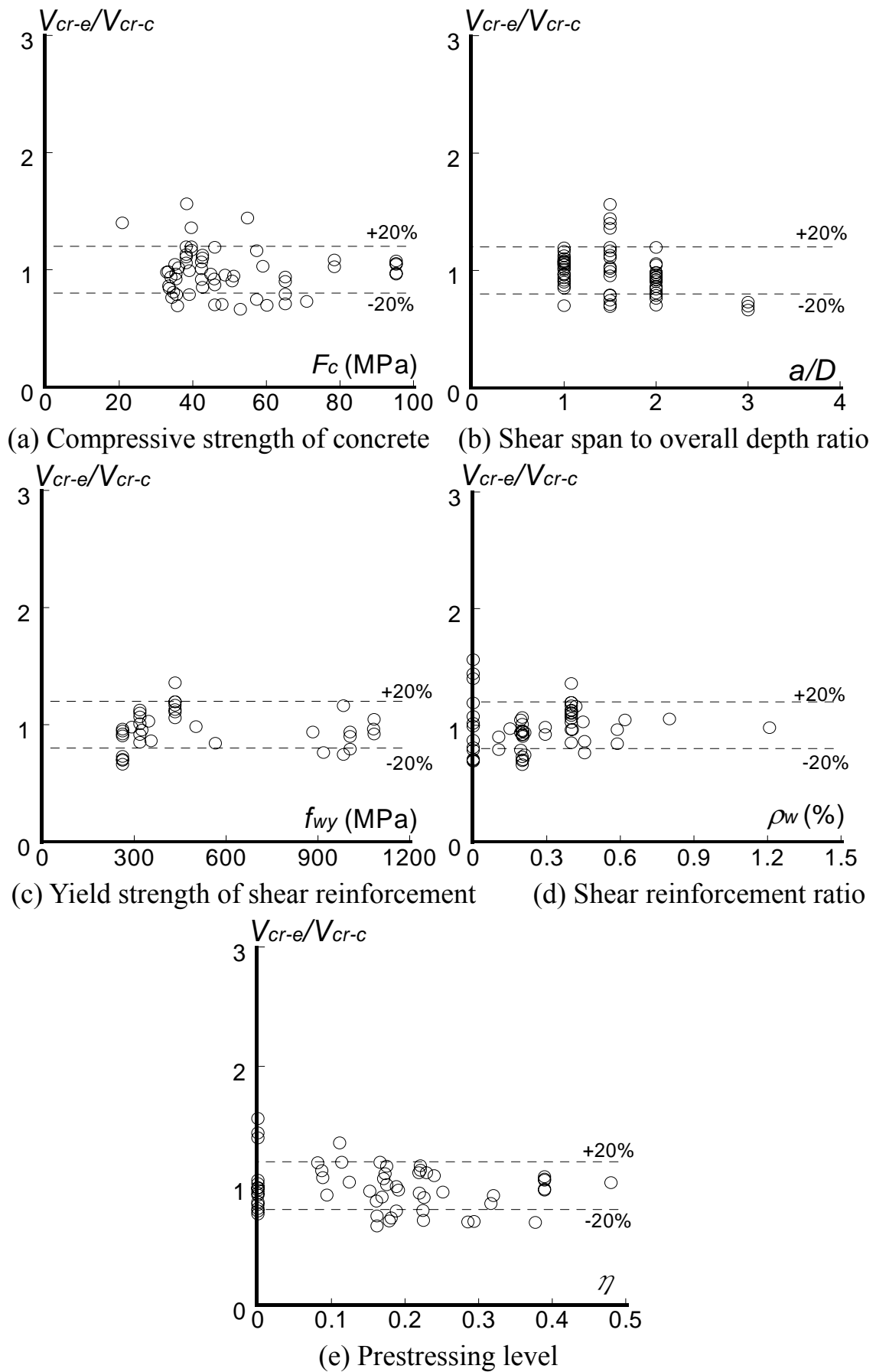
179

(a) Compressive strength of concrete

(b) Shear span to overall depth ratio

(c) Yield strength of shear reinforcement

(d) Shear reinforcement ratio

(e) Prestressing level

Fig. 5.18 Relationship between a ratio of experimental to analytical shear cracking strength by proposed method and parameters

5.3.5 Minimum Ratio of Shear Reinforcement

By the proposed method, failure modes of PC/RC members were predicted in a good accuracy. It points out that the lower limit of shear reinforcement ratio, ρ_m, of member failing in DT and other mode simultaneously can be obtained by proposed method. The lower limit of the shear reinforcement ratio, ρ_m, is important to prevent PC/RC members from DT failure and to effectively use the shear reinforcement in shear design, if a/D and b/D are known.

Figure 5.19 shows required ρ_m to prevent DT failure for difference of a/D and b/D. Material properties of PC beams for this verification in Fig. 5.19 are same with ones of specimens tested in section 3.3. Vertical and horizontal axis in Fig. 5.19 represent shear reinforcement ratio, ρ_w, and member section width/depth ratio, b/D, for difference of shear span/overall depth ratio, a/D; (a) 1.0; (b) 1.5, respectively. Solid curve indicates ρ_m predicted by proposed method. Open circles and square indicate two test specimens which failed in DT (S-10-L10, S-15-L10) and one which failed in ST (S-10-L21) in section 3.2 and 3.3.
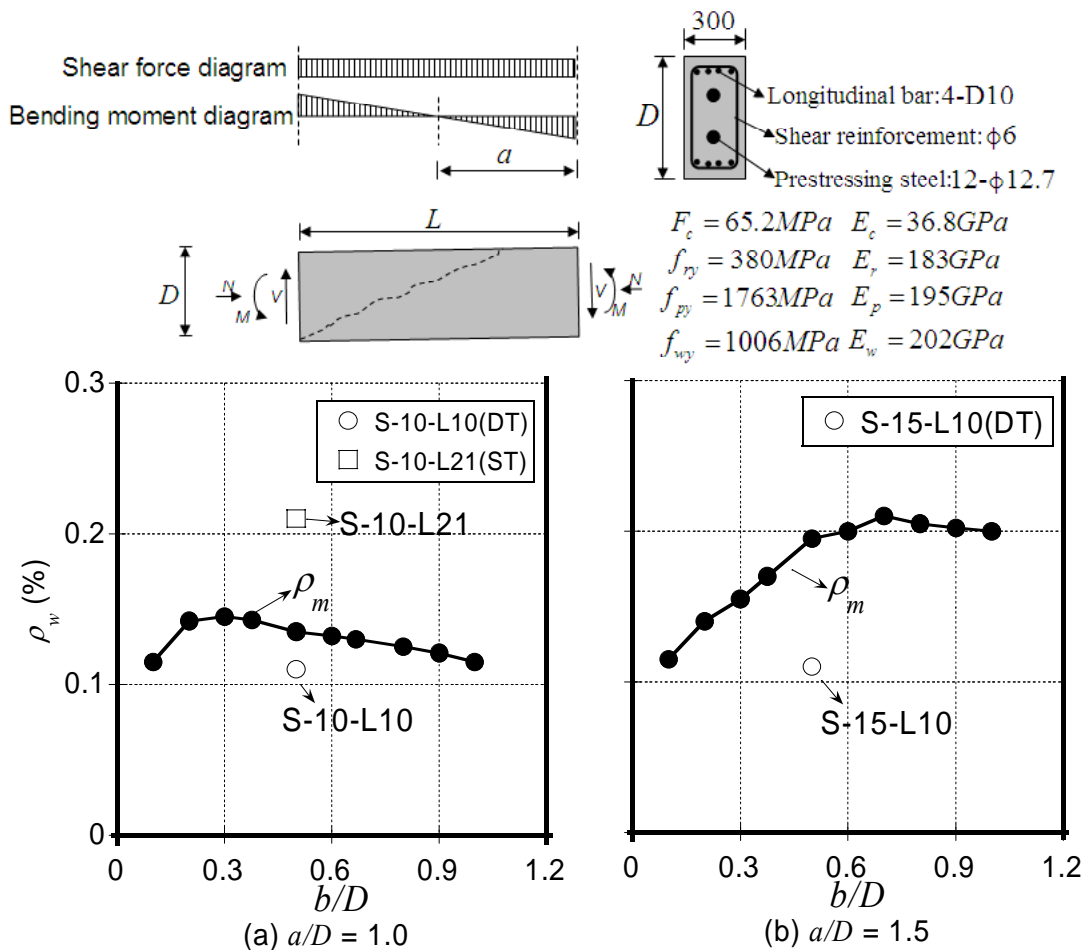
Fig. 5.19 Required minimum ratio of shear reinforcement to prevent DT failure

As shown in Fig. 5.19, a specimen failed in DT if its experimental parameters (b/D-ρ_w) are placed under the solid curve. It points out that analytical method proposed in this study can evaluate ρ_m required to prevent the member from DT failure and be useful to propose ρ_m in shear design of PC and RC members.

For deep understanding on analytical results by proposed method, the analytical results in Fig. 5.13 to 5.19 are shown in Table 5.2.

5.4   Conclusions

An analytical method to predict diagonal tension (DT) failure of RC and PC member was proposed. Based on the fundamental relation in fracture mechanics, debonding, sliding, and kinking energy of each reinforcement (non-prestressed longitudinal bar, prestressing steel, and shear reinforcement) on shear crack interface were obtained. Using the debonding, sliding, and kinking energy, analytical method to predict DT failure was proposed. For the verification of proposed analytical method, predicted web-shear cracking strength, failure modes, and the width of primary shear crack were compared to the observed ones. Analytical results from proposed method showed a good agreement with observed ones such as shear strength, crack width of primary shear crack, and failure mode. Further, minimum shear reinforcement ratio, ρ_m, to prevent the members from DT failure was analytically investigated. It pointed out that proposed method is effective and useful to propose the minimum ratio of shear reinforcement, ρ_m, in shear design of PC and RC members, if a/D and b/D are known.

Table 5.2 Summary of analytical results by proposed method

Specimen Names	Failure mode		Web-shear cracking strength			Crack width		
	Observed	Predicted	V_{wco} (kN)	V_{wcp} (kN)	V_{wcp}/V_{wco}	w (mm)	w_{cr} (mm)	w/w_{cr}
S-10-L10	DT	DT	1006	1119	1.11	2.72	2.08	1.3
S-10-L21	ST	N-DT	913	1125	1.23	1.07	2.08	0.5
S-15-L00	DT	DT	803	1134	1.41	20.0	2.08	9.6
S-15-L10	DT	DT	884	1117	1.26	4.04	2.08	1.9
A-PW0	DT	DT	184	234	1.27	4.49	1.88	2.4
A-PW04	SC	N-DT	-	235	-	0.63	1.88	0.3
NA-PW0	DT	DT	227	230	1.01	2.82	1.88	1.5
S-PW0	DT	DT	-	263	-	5.38	2.04	2.6
S-PW12	SC	N-DT	-	265	-	0.49	2.03	0.2
LD2PW04φ13	DT	DT	159	141	0.89	5.60	1.91	2.9
LD2PW04φ17	DT	N-DT	201	182	0.91	1.39	1.91	0.7
LD2PW04φ23	DT	N-DT	198	232	1.17	0.41	1.91	0.2
LD2PW02φ13	DT	DT	150	140	0.93	8.96	1.91	4.7
LD2PW02φ17	DT	DT	183	182	0.99	3.55	1.91	1.9
LD2PW02φ23	DT	N-DT	190	207	1.09	0.91	1.91	0.5
LD2PW00φ13	DT	DT	171	144	0.84	16.8	1.94	8.7
LD2PW00φ17	DT	DT	162	185	1.14	15.1	1.94	7.8
LD2PW00φ23	DT	DT	165	236	1.43	11.1	1.94	5.7
LD3PW00φ23	DT	DT	152	220	1.45	12.9	1.85	7.0
LD3PW02φ17I	DT	N-DT	178	187	1.05	1.81	1.96	0.9
S-SR1-PW04	SC	N-DT	-	266	-	0.96	2.04	0.5
S-SR1-PW12	SC	N-DT	-	269	-	0.49	2.04	0.2
LD3φ23SD07α30	SC	N-DT	193	142	0.74	0.67	1.88	0.4
LD3φ23SD07α45	SC	N-DT	198	166	0.84	0.70	1.88	0.4
LD3φ23SD07α60	ST	N-DT	217	186	0.86	0.72	1.88	0.4
LD3φ23SD08α60	ST	N-DT	204	184	0.90	0.60	1.87	0.3
LD3φ26SD07α45	ST	N-DT	199	179	0.90	0.45	1.87	0.2
LD3φ32SD05α60	SC	N-DT	198	176	0.89	0.31	1.87	0.2
LD4φ23SD07α30	SC	N-DT	166	139	0.84	0.46	1.87	0.2
LD4φ23SD07α45	SC	N-DT	171	161	0.94	0.49	1.87	0.3
No.1	SC	N-DT	199	216	1.09	1.79	1.94	0.9
No.2	ST	DT	183	260	1.42	2.49	1.96	1.3
No.3	SC	DT	272	287	1.06	3.32	1.98	1.7

Table 5.2 Summary of analytical results by proposed method

Specimen Names	Failure mode		Web-shear cracking strength			Crack width		
	Observed	Predicted	V_{wco} (kN)	V_{wcp} (kN)	V_{wcp}/V_{wco}	w (mm)	w_{cr} (mm)	w/w_{cr}
No.4	SC	DT	240	266	1.11	3.30	1.98	1.7
No.6	SC	N-DT	276	287	1.04	0.34	1.93	0.2
No.7	SC	N-DT	180	272	1.51	3.25	2.00	1.6
No.8	SC	DT	234	320	1.37	7.58	2.12	3.6
No.9	SC	DT	226	324	1.43	5.93	2.05	2.9
S-10-L42	SC	N-DT	706	608	0.86	0.48	2.03	0.2
S-15-L21	DT	DT	516	690	1.34	2.01	1.55	1.3
B-210-0	DT	DT	116	83	0.72	3.79	1.98	1.9
B-360-0	DT	DT	176	112	0.64	3.63	2.24	1.6
B-570-0	DT	DT	194	135	0.70	5.50	2.41	2.3
B-0	DT	DT	77	95	1.23	3.97	2.20	1.8
B-30-046	SC	N-DT	81	93	1.15	0.46	2.18	0.2
B-30-121	SC	N-DT	91	93	1.02	0.21	2.17	0.1
B-60-030	SC	N-DT	92	93	1.01	1.04	2.18	0.5
B-60-059	SC	N-DT	79	94	1.19	0.44	2.18	0.2
B-80-019	ST	N-DT	88	94	1.07	1.23	2.19	0.6
B-80-046	ST	N-DT	72	95	1.32	0.44	2.19	0.2
B-80-059	DC	N-DT	87	95	1.09	0.35	2.19	0.2
B-80-121	DC	N-DT	82	95	1.16	0.20	2.19	0.1
B-120-019	ST	N-DT	100	96	0.96	0.51	2.20	0.2
B-120-030	ST	N-DT	89	96	1.08	0.37	2.21	0.2
B-120-059	SC	N-DT	92	96	1.04	0.19	2.20	0.1
B-120-121	DC	N-DT	74	96	1.30	0.11	2.21	0.0
B-150-019	ST	N-DT	76	96	1.26	0.22	2.21	0.1
B-1.5-0	DT	DT	99	97	0.98	4.26	2.21	1.9
0-10-10-4	DT	DT	1420	1322	0.93	8.67	2.69	3.2
20-10-10-4	DT	DT	1280	1316	1.03	5.67	2.69	2.1
60-7-10-2	DT	DT	1050	969	0.92	2.65	2.59	1.0
60-10-10-4	DT	DT	1350	1402	1.04	3.16	2.69	1.2
60-7-10-4	SC	N-DT	1380	1345	0.97	1.49	2.59	0.6
90-10-10-4	SC	N-DT	1470	1402	0.95	1.49	2.69	0.6
120-10-10-4	SC	N-DT	1480	1402	0.95	0.60	2.69	0.2

[References]

5.1 Sato Y, Tadokoro T, Ueda T., "Diagonal Tension Failure Mechanism of Reinforced Concrete Beams," *Journal of Advanced Concrete Technology*, Vol. 2, No. 3, 2004, pp. 327-341.

5.2 Gastebled O. J., May I. M., "Fracture Mechanics Model Applied to Shear Failure of Reinforced Concrete Beams without Stirrups," *ACI Structural Journal*, Vol. 98, No. 2, 2001, pp. 184-190.

5.3 Dan J. R., Dawn E. L., John F. S., "Bond-Slip Response of Reinforcing Bars Grouted in Ducts," *ACI Structural Journal*, Vol. 99, No. 5, 2002, pp. 568-576.

5.4 Matsumoto T, Higai T, Saito S., "Experimental Study on the Bond Characteristics of Deformed Bar with Small Concrete Cover," *Proceedings of the Japan Concrete Institute*, Vol. 26, No. 2, 2004, pp. 823-828. (In Japanese)

5.5 Comite Euro-International du Beton., CEB-FIP Model Code 1990., Thomas Telford, CEB-FIP, 1990, pp. 82-85.

5.6 Comite Euro-International du Beton., CEB-FIP Model Code 1990., Thomas Telford, CEB-FIP, 1990, pp. 34-37.

5.7 Ouyang C, Shah S. P., "Fracture energy approach for predicting cracking of reinforced concrete tensile members," *ACI Structural Journal*, Vol. 91, No. 1, 1994, pp. 69-78.

5.8 Gopalaratanam V. S., Shah S. P., "Softening response of plain concrete in direct tension," *ACI Proceedings*, Vol. 82, No. 3, 1987, pp. 345-356.

5.9 Li B, Maekawa K, Okamura H., "Modeling of shear transfer in concrete using contact density function," *International Workshop on Concrete Shear in Earthquake (Houston, USA)*, 1991; pp. 226-235.

5.10 Kokusho S., Kobayashi K. et al., "Ultimate Shear Strength of RC Beams with High Tension Shear Reinforcement and High Strength Concrete," *Summaries of Technical Papers of Annual Meeting*, AIJ, Mar., 1987, pp. 83-91. (In Japanese)

5.11 Takagi H., Okude H., Nitta T., "Shear Strength of Beam Depending the Strength of Web Reinforcements," *Proceedings of the Japan Concrete Institute*, Vol. 11, No. 2, 1989, pp. 75-80. (In Japanese)

5.12 Kitada Y., Kawachi T. et al., "Flexural and Shear Strength of Reinforced

Concrete Columns Using Ultra High Strength Materials," *Summaries of Technical Papers of Annual Meeting*, AIJ, Oct., 1988, pp. 697-702. (In Japanese)

6. Analytical Model 3 for Post-tensioned Precast Concrete Members (FSC Model)

6.1 Introduction

Shear failure mechanisms of post-tensioned precast concrete members failed in ST, SC, B, and DT were investigated and shear analogies were developed in Chapter 4 and 5. From the Test 1 in Chapter 3 and experimental research on shear behavior of post-tensioned precast concrete members in the past [2.13], significant deterioration of shear capacity due to crushing of the concrete in flexural compression zone had been observed as shown in Fig. 6.1. Fig. 6.1 illustrates the crack patterns of post-tensioned precast concrete beams failed in shear due to crushing of the concrete in the flexural compression zone. It points out that the deterioration of shear capacity of the concrete at flexural compression zone significantly also affect the shear failure mechanism of post-tensioned precast concrete members. The failure mode in this case is defined as flexural shear compression failure (FSC) in this study.
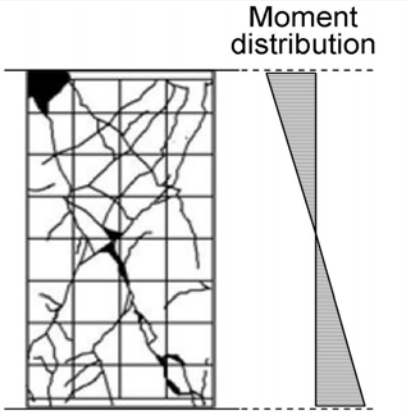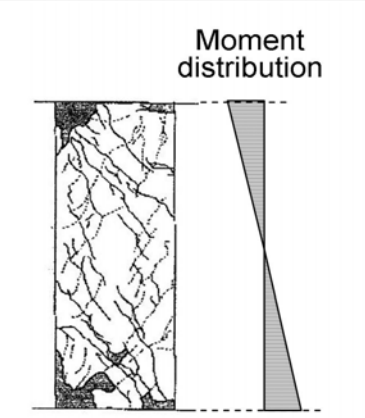
Crack pattern		
Name of specimen	S-10-L42	S-PW12
Reference	*Test 1*	[2.13]
Observed failure mode	FSC	FSC

Fig. 6.1 Crack patterns of post-tensioned precast concrete member failed in FSC

Choi [2.1] proposed the analytical method to evaluate inelastic deformation capacity of reinforced concrete beams using shear capacity of concrete at flexural compression zone in critical section. However, Choi`s model only can be applied to reinforced concrete beams failing in flexure. There is not yet analogy to investigate the FSC failure and to evaluate shear strength of post-tensioned precast concrete member failing in FSC.

To evaluate shear strength of post-tensioned precast concrete members failing in FSC, an analytical model based on the stress state of concrete in the flexural compression zone is proposed in this chapter. Further, failure mode of post-tensioned precast concrete member will be also predicted by the proposed model. For the estimation of deformation capacity of post-tensioned precast concrete member failing in flexure, drift angle at flexural failure using rocking model in which rocking deformation at the joint interface of post-tensioned precast concrete member is considered will be also evaluated by the proposed method. By comparison between analytical and experimental results (shear strength, failure mode, and drift angle at flexural failure), accuracy of analytical results will be clarified.

6.2 FSC Failure Strength

Figure 6.2 illustrates load-displacement relation and shear capacity. F, ST, SC, DT, and FSC failure in Fig. 6.2 indicates flexural, shear tension, shear compression, diagonal tension, and flexural shear compression failure, respectively. As shown in Fig. 6.2, the member in which shear capacity is smaller than shear demand at flexural yielding might fail in shear (DT, ST, SC, or FSC). Fig. 6.3 shows the shear failure types of post-tensioned precast concrete member. Refer to section 3.2.4 for the definition of the failure modes. Excessive opening of shear crack due to yielding of shear reinforcement leads to deterioration of interlock resistance of shear crack and to shear failure (ST). Significant increasing in compressive principle stress in shear cracked concrete leads to compression failure of shear cracked concrete strut (SC). In the member with low shear reinforcement ratio, ρ_w, low member section to depth ratio, b/D, or low shear span to depth ratio, a/D, excessive opening of primary shear crack at initiation of shear crack leads to deterioration of interlock resistance on shear

crack surface and significant decay of load carrying the shear capacity of the member (DT). Shear resistance capacity of the concrete in the flexural compression zone also significantly affect the shear capacity of post-tensioned precast concrete member, because the concrete in flexural compression zone is subjected to shear as well as the axial stress. Shear failure of the concrete in the flexural compression zone leads to deterioration of transferred diagonal compression stress in shear cracked concrete strut and decay of shear capacity (FSC).
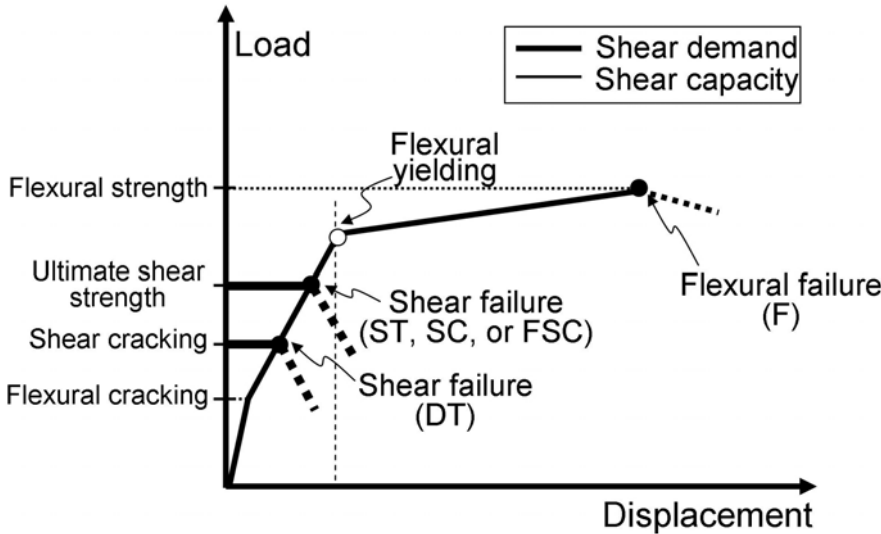
Fig. 6.2 Load-displacement relation and shear capacity
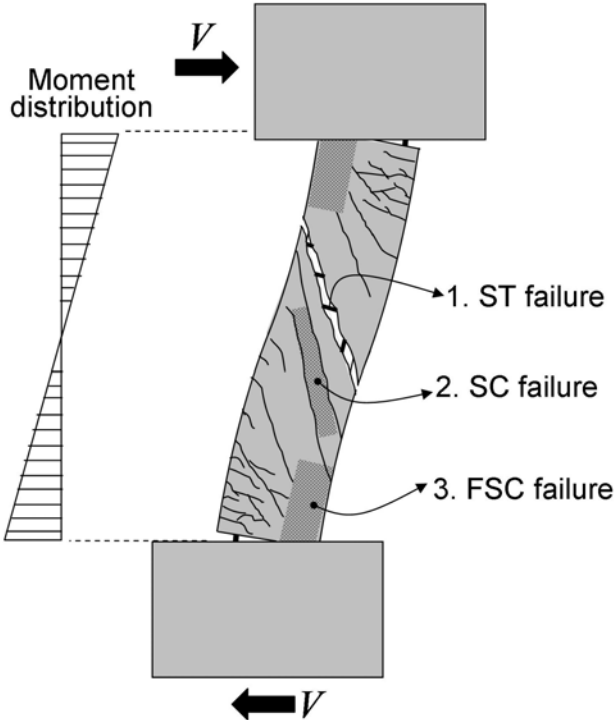
Fig. 6.3 Shear failure type of post-tensioned precast concrete member

Extensive researches on shear behavior of reinforced / prestressed concrete member have applied ST, SC, and DT failure modes to develop or modify the shear analogies. [2.3, 2.9-2.15, 2.17-2.23, 3.12-3.19, 4.1, 4.4-4.8] Also, ST, SC, r DT failure strength can be evaluated by the analytical models proposed in Chapter 4 and 5. However, there is no shear analogy considering the shear capacity of the concrete in the flexural compression zone. In this section, stress state of the concrete at flexural compression zone is investigated. Then, an analytical model to be able to predict the shear strength and failure modes of post-tensioned precast concrete member failing FSC as well as ST or SC will be proposed.

6.2.1 Analytical Assumption

To evaluate the shear strength of a member due to FSC failure, the conventional section analysis with following analytical assumptions is used.

1. The shear force is resisted primarily by the concrete in the compression zone of the critical section after initiation of flexural crack or gap opening, because once a flexural crack (or gap opening) initiates, the tensile crack immediately propagates to the neutral axis at the cross section, and provoke the decreasing of effective depth resisting the shear force [2.1].
2. Plane section before bending remains plane after bending.
3. Prestressing steels do not perfectly bond with concrete. Strain compatibility factor, F, representing a ratio of actual strain on prestressing steel to strain on prestressing steel which is perfectly bonded with concrete is used in this study.
4. The tensile strength of concrete are neglected.
5. Ultimate strain of concrete, ε_{cu}, is assumed as 0.003.
6. For plane and confined stress-strain curve of concrete, Komuro`s model [6.1] is used. Cover concrete is assumed as the plane concrete. The concrete section except for cover is assumed as confined section.

6.2.2 Shear Capacity of Concrete at Flexural Compression Zone

Let`s consider the critical section of-post-tensioned precast concrete to evaluate the shear strength of FSC failure mode. Fig. 6.4 illustrates distribution of stress and strain at critical section in joint interface. For shear stress of the concrete in the flexural compression, Rankine`s failure criteria (Eq. (6.1)), using normal stress, σ_c, and compressive strength of concrete, F_c. As shown in Fig. 6.4, the

part of the compression zone experiencing compressive softening no longer provides the shear stress capacity controlled by compression [2.1]. Shear capacity of the concrete in flexural compression zone, V_{cc}, can be obtained as Eq. (6.2) and (6.3).

$$\tau_c(z) = \sqrt{F_c(F_c - \sigma_c(z))} \qquad \text{Eq. (6.1)}$$

$$V_{cc} = b\int_0^{x_n} \tau_c(z)dz, \text{ for } \varepsilon_c \leq \varepsilon_{cc} \qquad \text{Eq. (6.2)}$$

$$V_{cc} = b\int_0^c \tau_c(z)dz, \text{ for } \varepsilon_c > \varepsilon_{cc} \qquad \text{Eq. (6.3)}$$

where b is cross sectional width of member, ε_{cc} is normal strain corresponding to compressive strength of confined concrete, c is effective depth of shear stress distribution in compression ($=(\varepsilon_c \cdot x_n)/\varepsilon_{cc}$), and x_n is neutral axis depth, respectively.
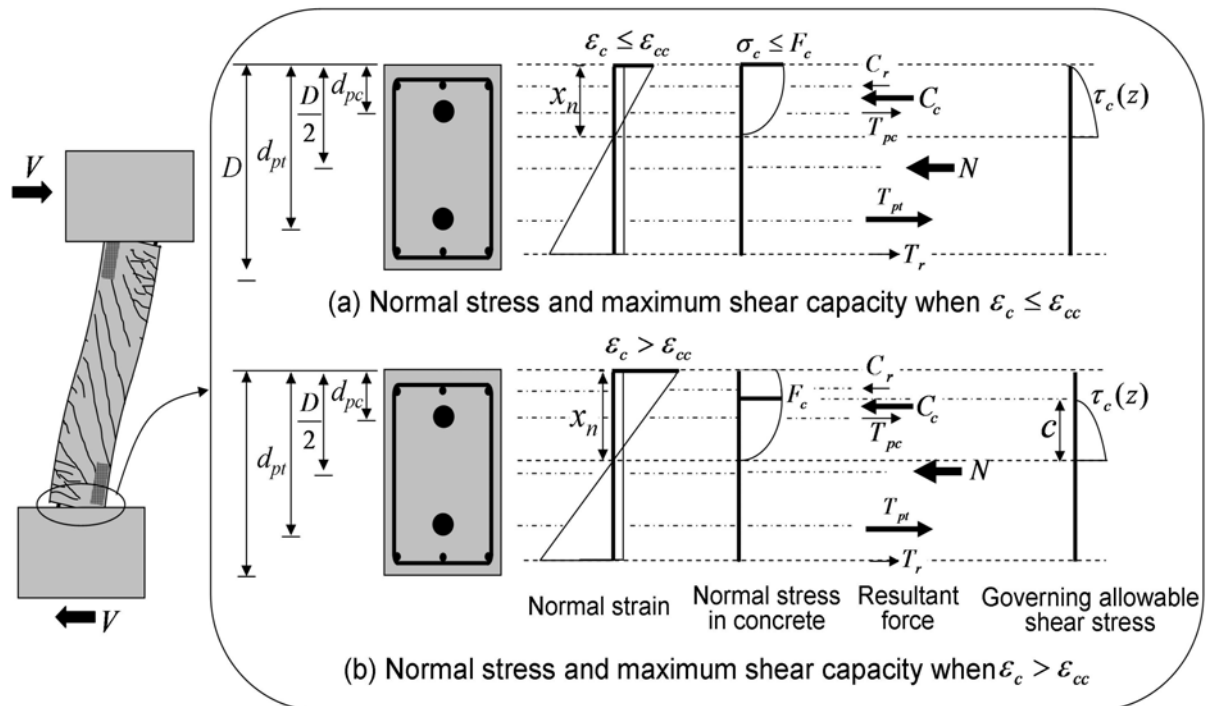
Fig. 6.4 Distribution of stress and strain at critical section in joint interface

6.2.3 Shear Demand of Post-tensioned Precast Concrete Member

In this section, analytical method using the conventional section analysis for the shear demand of post-tensioned precast concrete member will be introduced. For estimated variables, ε_c and x_n in Eq. (6.1) to (6.3), equilibrium condition for resultant forces at critical section (Eq. (6.4)) and compatibility condition for bond stress on prestressing steel (Eq. (6.5)) are used. Sum of resultant forces in

the critical section of member, ΣP, must be equilibrated with axial force, N, as shown in Eq. (6.4). Compressive axial force is defined as positive in this study. Fig. 6.5 illustrates distribution of bond stress and tensile force of prestressing steel at the top and bottom of post-tensioned precast concrete member subjected to double-curvature. When double-curvature flexural deformation is imposed on a member where prestressing steels are symmetrically located at the section, the stress and strain distributions at the top and bottom critical sections are the same. Therefore, the maximum tensile force difference of a prestressing steel between at the top and bottom critical sections, ΔT_{max}, equals to the bond force of a prestressing steel at bond strength, $\tau_{pmax}\psi_p L$. Then, tensile force difference of a prestressing steel between at the top and bottom critical sections, $T_{pt}\text{-}T_{pc}$, can be derived as Eq. (6.5) using compatibility factor, F, defined as a ratio of actual strain on prestressing steel to strain on prestressing steel which is perfectly bonded with concrete as shown in Eq. (6.6) and (6.7) [6.2]. Eq. (6.6) and (6.7) represent strains at prestressing steel in tension and compression, respectively. Then, coefficient F is obtained as Eq. (6.8). Tensile strain increment of prestressing steel at the critical section, $\Delta\varepsilon_p$, is obtained as Eq. (6.9). Then, flexural moment at the critical section of a member is derived as Eq. (6.10). Shear demand at the critical section of member, V_f, is obtained as Eq. (6.11).

$$\Sigma P = C_c + C_r - T_{pc} - T_{pt} - T_r = N \quad , \quad C_c = b\int_0^{x_n} \sigma_c(z)dz \qquad \text{Eq. (6.4)}$$

$$\Delta T_{\max} = \tau_{p\max}\psi_p L \geq T_{pt} - T_{pc} = F\varepsilon_c \frac{d_{pt} - d_{pc}}{x_n} \frac{E_p\Sigma A_P}{2} \qquad \text{Eq. (6.5)}$$

$$\varepsilon_{pt} = \varepsilon_{pe} + F\left(\varepsilon_{cpn} + \varepsilon_c \frac{d_{pt} - x_n}{x_n}\right) \qquad \text{Eq. (6.6)}$$

$$\varepsilon_{pc} = \varepsilon_{pe} + F\left(\varepsilon_{cpn} + \varepsilon_c \frac{d_{pc} - x_n}{x_n}\right) \qquad \text{Eq. (6.7)}$$

$$F = \frac{2x_n\tau_{p\max}\psi_p L}{\varepsilon_c(d_{pt} - d_{pc})E_p\Sigma A_p} \qquad \text{Eq. (6.8)}$$

$$\Delta\varepsilon_p = F\left(\varepsilon_{cpn} + \varepsilon_c \frac{d_{pt} - x_n}{x_n}\right) \qquad \text{Eq. (6.9)}$$

$$M_f = C_c\left(x_n - \frac{\int_0^{x_n} z\sigma_c(z)dz}{\int_0^{x_n} \sigma_c(z)dz}\right) + C_r d_{rc} - T_{pc}d_{pc} - T_{pt}d_{pt} - T_r d_{rt} + N\cdot\frac{D}{2} \quad \text{Eq. (6.10)}$$

$$V_f = \frac{M_f}{a} \qquad \text{Eq. (6.11)}$$

where C_c, C_r, T_r, T_{pc}, and T_{pt} are resultant force of concrete, longitudinal bar in compression and tension side, and prestressing steel in compression and tension side, N is axial force, ε_{pt} and ε_{pc} are tensile strain of prestressing steel in tension and compression, ε_{pe} is tensile strain in prestressing steel due to initial prestress, ε_{cpn} is compressive strain in concrete due to initial prestress, d_{pt} and d_{pc} are distance from extreme compression fiber to centroid of prestressing steel in tension and compression, E_p, A_p, τ_{pmax} are elastic modulus, sectional area, and bond strength of prestressing steel, respectively.
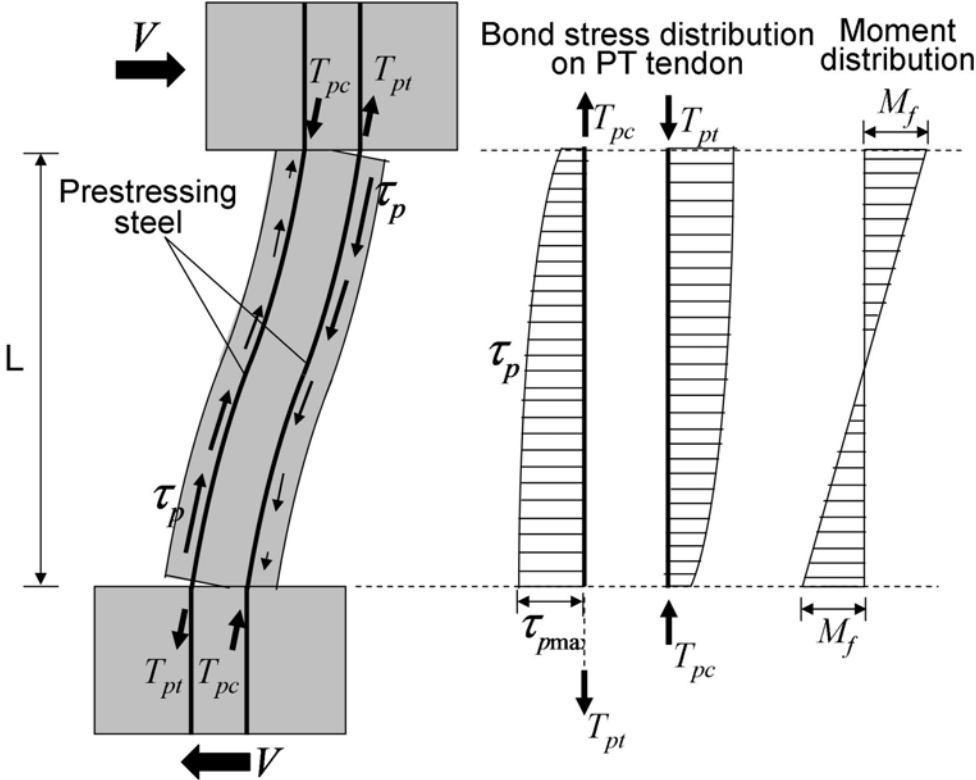
Fig. 6.5 Distribution of bond stress and tensile force of prestressing steel

6.2.4 Prediction of Failure Mode

For the prediction of failure mode, five failure modes, flexural failure (F), shear tension failure (ST), shear compression failure (SC), diagonal tension failure (DT), and flexural shear compression failure (FSC), are accepted. The failure mode of the member is determined by the lesser of flexural strength and shear strength. ST and SC failure strengths are obtained by the analytical model 1 in Chapter 4. DT failure strength is obtained by the analytical model 2 in Chapter 5. Flexural strength of member, V_{fu}, can be obtained by the maximum shear demand at the critical section of member as shown in Fig. 6.2. FSC failure occurs when shear capacity of the concrete at the flexural compression zone, V_{cc},

equals to shear demand, V_f, as shown in Eq. (6.12).

$$V_{cc} = V_f$$ Eq. (6.12)

If the compressive strain of concrete at the extreme compression fiber at the maximum shear demand, ε_{cmax}, is smaller than the compressive strain of concrete at the extreme compression fiber satisfying Eq. (6.12), the member is expected to fail in flexure prior to shear (F). If not, the member is judged to fail in shear (ST, SC, DT, or FSC). Shear failure modes (ST, SC, DT, and FSC) are determined by the lesser of ST, SC, DT, and FSC failure strength. FSC failure occurs when shear capacity of the concrete at the flexural compression zone, V_{cc}, satisfying Eq. (6.12) is smaller than ST or SC failure strength.

6.3 Deformation Capacity of Post-tensioned Precast Concrete Member at Flexural Failure

6.3.1 Analytical Assumptions

For evaluation of deformation capacity of post-tensioned precast concrete members at flexure failure, following analytical assumptions are applied in this study.

1. Shear deformation of post-tensioned precast concrete member is neglected, because shear deformation is much smaller than the flexural deformation in post-tensioned precast concrete member failing in flexure [6.3]. Therefore, total deformation of post-tensioned precast concrete member, R, is evaluated by the flexural deformation only, R_f, as shown in Eq. (6.13).

2. Bond stress on prestressing steel linearly distributes in the longitudinal direction.

3. The length of plastic hinge region in post-tensioned precast concrete member, L_p, equals to overall depth of member cross section ($L_p = 1.0D$).

4. The curvature of member after initiation of plastic hinge, ϕ_p, distributes as shown in Fig. 6.6. The curvature is constant in plastic hinge region.
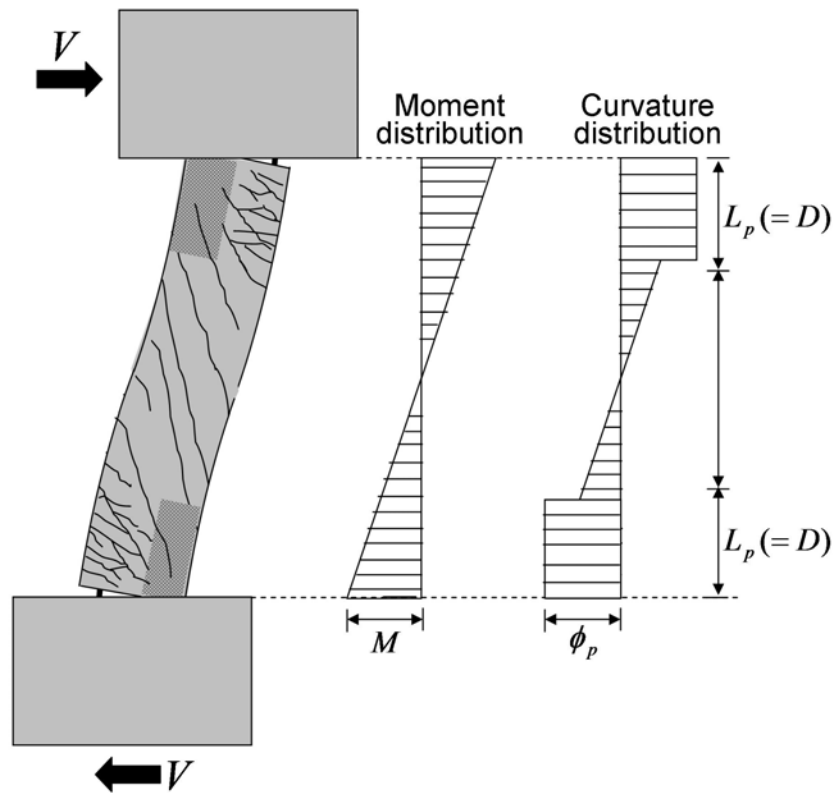
Fig. 6.6 Distribution of curvature after initiation of plastic hinge

6.3.2 Flexural Deformation of Post-tensioned Precast Concrete Member

Flexural deformation consists of pulling-out deformation of prestressing steel at joint interface, $R_{f.pu}$, and flexural deformation in outside joint interface, $R_{f.p}$ (Eq. (6.14)). As the pulling-out deformation model of post-tensioned precast concrete members subjected to double-curvature, the conventional rocking deformation model is applied in this study. Fig. 6.7 illustrates an example of rocking model for a column and stub. The rocking model in Fig. 6.7 is from the conventional pulling-out idea of reinforced concrete member. In the general rocking model, the curvature, ϕ, of post-tensioned precast concrete members concentrates at beam-column or column-foundation joint interface because deformation due to pull-out of prestressing steel is prominent. Variables, δ_p, $\Delta\varepsilon_p$, $\Delta\varepsilon_{pa}$, l_s, and x_n in Fig. 6.7 are pulling-out of prestressing steel, tensile strain increment of prestressing steel at joint interface and anchorage zone, development length of prestressing steel, and neutral axis depth, respectively. Pulling-out of prestressing steel, δ_p, consists of sum of the pulling-out due to slip of prestressing steel from the column and stub, δ_{p1} and δ_{p2}, as shown in Eq. (6.15). If neutral axis, x_n, is larger than distance from extreme compression fiber to centroid of prestressing steel in tension, d_{pt}, pulling-out deformation, $R_{f.pu}$ equals

195

to zero (Eq. (6.16)). Neutral axis, x_n, and tensile strain increment of prestressing steel at joint interface, $\Delta\varepsilon_p$, in Eq. (6.15) and (6.16) are obtained by the section analysis mentioned in section 6.2.3 (Eq. (6.9)). Flexural deformation in outside joint interface, $R_{f.p}$, can be obtained as Eq. (6.17) because curvature of member distributes as shown in Fig. 6.6 [6.4].

$$R \approx R_f \qquad\qquad \text{Eq. (6.13)}$$

$$R_f = R_{f.pu} + R_{f.p} \qquad\qquad \text{Eq. (6.14)}$$

$$R_{f.pu} = \frac{\delta_p}{d_{pt} - x_n} = \frac{\delta_{p1} + \delta_{p2}}{d_{pt} - x_n}, \quad \text{for } (x_n < d_{pt}) \qquad \text{Eq. (6.15)}$$

$$R_{f.pu} = 0, \qquad\qquad \text{for } (x_n \ge d_{pt}) \qquad \text{Eq. (6.16)}$$

$$R_{f.p} = \frac{1}{L}\left[\phi_p \left\{ L_p^2 + L_p(L - 2L_p) \right\} + \frac{2V_p(L/2 - L_p)^3}{3E_c I_e} \right] \qquad \text{Eq. (6.17)}$$

where ϕ_p is curvature of member at plastic hinge ($=\varepsilon_c/x_n$), L_p is length of plastic hinge in longitudinal direction of member, V_p is shear force at initiation of plastic hinge, E_c is Young`s modulus of concrete, and I_e is equivalent moment of inertia for effective area in section, respectively.
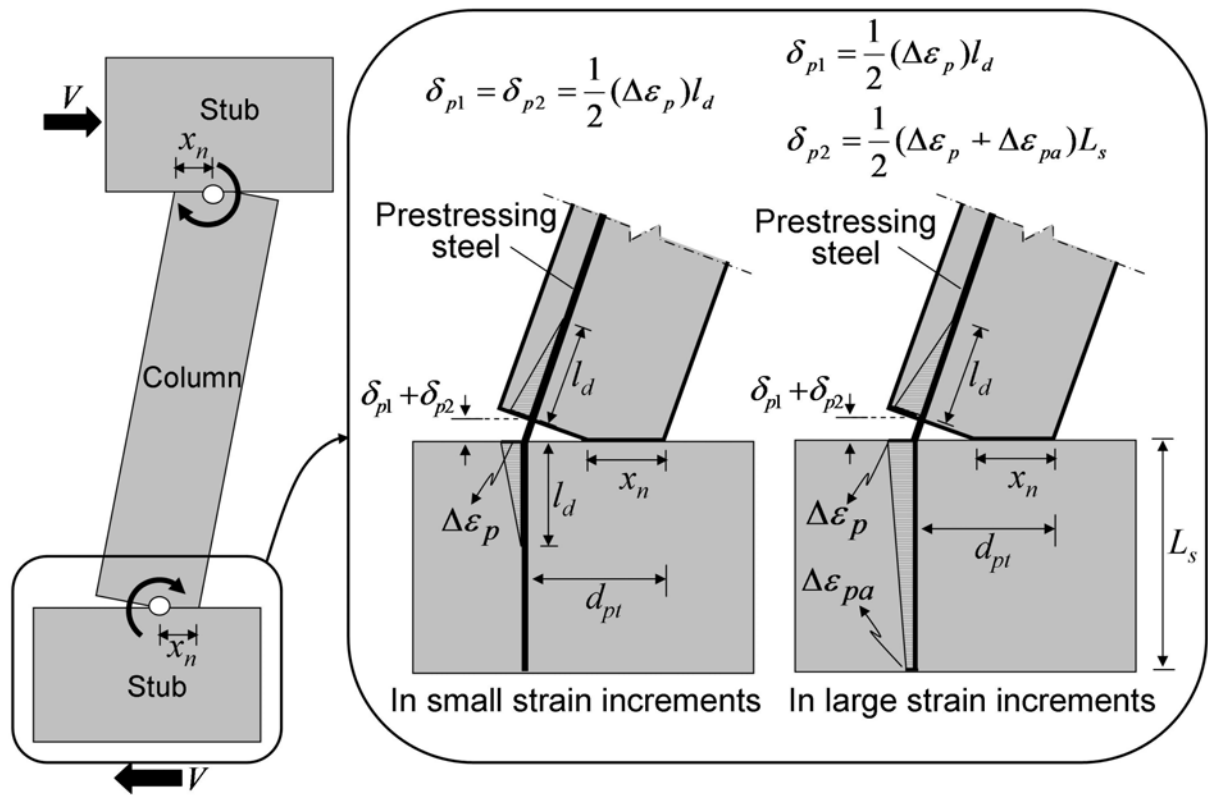
(a) Rocking model

(b) Distribution of bond stress on prestressing steel

Fig. 6.7 Rocking deformation model of post-tensioned precast concrete column

Variables, δ_{p1}, δ_{p2}, $\Delta\varepsilon_{pa}$, and l_d, in Fig. 6.7 and Eq. (6.15) can be obtained by Eq. (6.18) to (6.22). Tensile force of prestressing steel corresponding to bond strength in development length, $\tau_{pmax}\psi_p l_d$, must be equilibrated with $\Delta\varepsilon_p E_{pt} A_{pt}$ where τ_{pmax}, ψ_p, E_{pt}, and A_{pt} are bond strength, perimeter length, elastic modulus, and sectional area of prestressing steel in tension zone, respectively. Therefore, development length of prestressing steel, l_d, can be derived as Eq. (6.18). By substituting stub height, L_s, into l_d in Eq. (6.18), upper limit of tensile strain increment of prestressing steel at joint interface, $\Delta\varepsilon_{pmax}$, is obtained as Eq. (6.19). Because it is assumed that bond stress in prestressing steel linearly distributes, pulling-out of prestressing steel, δ_p, is derived as Eq. (6.21) in a small tensile strain increments ($\Delta\varepsilon_p \leq \Delta\varepsilon_{pmax}$). In large tensile strain increments ($\Delta\varepsilon_p > \Delta\varepsilon_{pmax}$), tensile strain increment at anchorage zone, $\Delta\varepsilon_{pa}$, can be obtained as Eq. (6.20). Then, δ_{p1} and δ_{p2} are derived as Eq. (6.22).

$$l_d = \frac{\Delta\varepsilon_p E_{pt} A_{pt}}{\tau_{p\max}\psi_p} \qquad \text{Eq. (6.18)}$$

$$\Delta\varepsilon_{p\max} = \frac{\tau_{p\max}\psi_p L_s}{E_{pt} A_{pt}} \qquad \text{Eq. (6.19)}$$

$$\Delta\varepsilon_{pa} = \Delta\varepsilon_p - \frac{\tau_{p\max}\psi_p L_s}{E_{pt} A_{pt}} \qquad \text{Eq. (6.20)}$$

$$\delta_{p1} = \delta_{p2} = \frac{1}{2}\Delta\varepsilon_p l_d = \frac{\Delta\varepsilon_p{}^2 E_{pt} A_{pt}}{2\tau_{p\max}\psi_p}, \text{ for } \Delta\varepsilon_p \leq \Delta\varepsilon_{p\max} \quad \text{Eq. (6.21)}$$

$$\delta_{p1} = \frac{1}{2}(\Delta\varepsilon_p + \Delta\varepsilon_{pa})L_s = \left(\Delta\varepsilon_p - \frac{\tau_{p\max}\psi_p L_s}{2E_{pt} A_{pt}}\right)L_s, \delta_{p2} = \frac{\Delta\varepsilon_p{}^2 E_{pt} A_{pt}}{2\tau_{p\max}\psi_p}, \text{ for } \Delta\varepsilon_p > \Delta\varepsilon_{p\max}$$

$$\text{Eq. (6.22)}$$

For bond strength of prestressing steel, τ_{pmax}, following analytical models and assumptions in the report of research committee on bond property in prestressed concrete members and structures organized by Japan Prestressed Concrete Engineering Association [3.4] are used.

$$\tau_{p\max} = 0.53\alpha\sqrt{F_g} \text{ MPa} \quad \text{for prestressing strands} \quad \text{Eq. (6.23)}$$

$$\tau_{p\max} = 1.5 \text{ MPa} \quad \text{for round PT bar} \quad \text{Eq. (6.24)}$$

$$\tau_{p\max} = 6.0 \text{ MPa} \quad \text{for deformed PT bar} \quad \text{Eq. (6.25)}$$

where α equals to 1.0 and 1.17 for seven and nineteen wire strands, F_g is compressive strength of grouting mortar injected in a duct, respectively.

6.4 Calculation Procedure of Proposed Method for The Prediction of Shear Strength, Failure Mode, and Deformation Capacity of Post-tensioned Precast Concrete Members

Figure 6.8 illustrates calculation procedure of shear strength and deformation capacity by proposed method. First, predict the primary shear cracking strength, V_{cr}, and failure modes by the analytical model 2 in Chapter 5. Second, judge the failure mode. If the member is expected to fail in DT, the analytical procedure is teminated. If not, go to next step. Then, section analysis is conducted to obtain the shear strength for FSC failure, V_{cc}, and shear demand at the critical section of member, V_f. In third step, estimate the compressive strain at the extreme compression fiber, ε_c, compatibility factor for bond properties of prestressing steel, F, and the neutral axis depth, x_n. Fourth, check the resultant force based on the estimated ε_c, F, and x_n by Eq. (6.4). If necessary, return to Step 3 and revise x_n. In fifth step, check the coefficient F by Eq. (6.5). If necessary, return to Step 3 and reduce the value of F. In sixth step, calculate the V_{cc} and V_f by Eq. (6.2) to (6.3) and (6.11), respectively. Seventh, check $V_{cc}=V_f$ (Eq. (6.12)). If necessary, return to Step 3 and revise ε_c until satisfying Eq. (6.12). In eighth step, the flexural strength, V_{fu}, is obtained by repeating Step 3 to 7 until the maximum value of V_f is produced. In ninth step, the failure mode is judged by comparison between the lesser of shear strengths, $\min(V_u, V_{cc})$, and the flexural strength, V_{fu}. If V_{fu} is smaller than the lesser of shear strengths, V_u and V_{cc}, it is judged that the member fails in flexure (F). Then, go to Step 12 and calculate the deformation capacity of the member at flexural failure. If not, it is expected that the member fails in shear. Then, go to Step 10 and predict shear strength by analytical model 1 in Chapter 4, V_u. In eleventh step, judge the shear failure mode by the lesser of V_u and V_{cc}. If V_u is smaller than V_{cc}, the member is expected to fail in ST or SC. Then, the failure modes (ST or SC) are predicted by the analytical model 1 in Chapter 4. If V_u is not smaller than V_{cc}, the predicted failure mode is FSC.

From twelfth step, the deformation capacity of member at flexural failure is evaluated using ε_c, x_n, and F obtained at Step 8. In twelfth step, calculate tensile strain increment of prestressing steel, $\Delta\varepsilon_p$, by Eq. (6.9). In thirteen step, check

$\Delta\varepsilon_p \le \Delta\varepsilon_{pmax}$. If $\Delta\varepsilon_p$ is not larger than $\Delta\varepsilon_{pmax}$, go to Step 13 and calculate δ_{p1} and δ_{p2} by Eq. (6.21). If $\Delta\varepsilon_p$ is larger than $\Delta\varepsilon_{pmax}$, go to Step 14 and calculate δ_{p1} and δ_{p2} by Eq. (6.22). Last, calculate the total flexural deformation of the member, R_f, by Eq. (6.13) to (6.17).
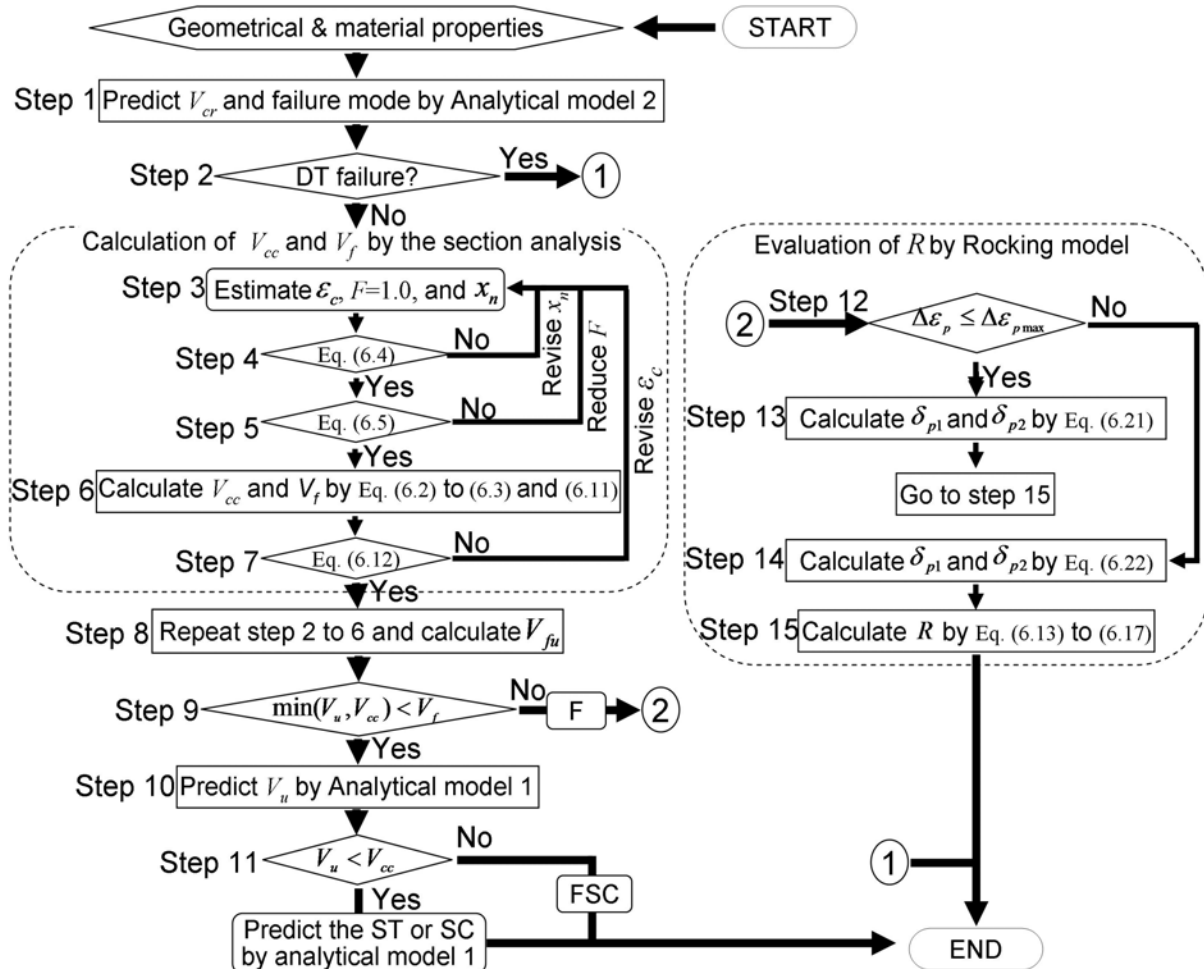
Fig. 6.8 Calculation procedure of proposed method.

6.5 Verification of Analytical Results

6.5.1 Experimental Data Used for Verification

To clarify the accuracy of analytical failure strength and deformation capacity by the proposed method, experimental data on twenty two and seventeen half-scale of post-tensioned precast concrete beam [2.13-2.15, 3.14, 3.20, Test 1 and 2] and columns [2.10, 3.20] are used. The geometrical conditions and experimental results (drift angle at flexural failure, R_u, peak load, V_e, and failure mode) of test specimens used for evaluation in this study are summarized in Table 6.1. Material properties of the specimens are summarized in Table 6.2.

Table 6.1 Geometrical conditions and experimental results of test specimens

	Ref.	Specimen	b	D	L	j_p	d_{pt}	P_e	N	R_u	V_e	Failure mode[†]
Beam	[2.13]	S-PW0	250	250	750	120	185	460	0	-	239	DT
		S-PW12								-	316	FSC
	[2.14]	SJP00-PW12	250	250	750	0	125	460	0	3.8	271	F
		SJP075PW04				75	163			-	275	SC
		SJP075PW12								4.0	307	F
	[2.15]	SSR1PW04	250	250	500	120	185	460	0	-	259	SC
		SSR2PW04			1000				0	-	215	FS
		SSR2PW12							0	-	240	F
	[3.13]	A-PW0	250	250	750	12	18	367	0	-	184	DT
		A-PW04								-	244	DT
	[3.19]	11J04+0	250	250	1000	120	185	354	0	>4.0	110	F
	Test 1	S-10-L42	300	400	800	200	300	1204	0	-	683	FSC
		S-10-L63						1104		-	742	FS
		S-15-L21			1200			1121		-	509	DT
		S-15-L42						1093		2.0	510	F
		S-15-L63						1178		1.9	531	F
		S-20-L21			1600			1419		-	387	FS
		S-20-L42						1396		1.8	386	F
	Test 2	S-10-L10	300	600	1200	400	500	2699	0	-	1006	DT
		S-10-L21						2580		-	1054	ST
		S-15-L00						2580		-	803	DT
		S-15-L10						2580		-	884	DT
Column	[2.10]	R-15-L63	400	400	1200	200	300	1166	3838	1.6	1185	F
		R-15-H63						1192	3805	1.6	1186	F
		D-15-L63						1058	3940	1.8	1230	F
	[3.19]	9.2J04+1/4	250	250	1000	120	185	247	780	-	207	FS
		11J04+1/3						354	1040	-	251	FS
		11J04+1/8						354	390	-	171	FS
		11J04+1/4						354	780	-	223	FS
		13J04+1/8						496	390	-	209	FS
		13J04+1/4						496	780	-	251	FS
		17J04+1/8						733	390	-	217	FS
		17J04-1/4						733	780	-	262	FS
		11J08+1/4						354	780	-	225	FS
		11J12+1/4						354	780	-	226	FS
		11M04+1/4						354	780	1.6	232	F
		11J04-3qs/4						354	-160	>4.0	86	F
		11M04-3qs/4						354	-160	>4.0	84	F
		11J02+1/8						354	390	2.7	170	F

Note : b and D are width and total depth of member section in mm, L is member

length in mm, a/D is shear span ratio, j_p is distance between both prestressing steels in tension and compresson in mm, d_{pt} is distance from extreme compression fiber to centroid of prestressing steel in tension in mm, P_e is effective prestresing force in kN, N is axial load in kN (compressive load is positive), R_u is experimental drift angle of members at design ultimate state in %, V_e is experimental peak load of members in kN, repectively.

Failure mode[†]: ST, SC, and FSC are shear tension, shear compression, and flexural shear compression failure prior to flexural yielding, and F and FS are flexural and shear failure after flexural yielding, respectively.

Table 6.2 Material properties of test specimens for verification

	Ref.	Specimen	Concrete		Shear reinforcement			Longitudinal reinforcement			Prestressing steel		
			F_c	E_c	ρ_w	f_{wy}	E_w	A_r	f_{ry}	E_r	A_p	f_{py}	E_p
Beam	[2.13]	S-PW0	58.2	37	0.45	347	195	199	386	198	227	1804	188
		S-PW12	56.8	34	1.14	381	206						
	[2.14]	SJP00-PW12	62.8	37	1.14	381	206					1804	189
		SJP075PW04	59.0	40	0.45	347	195	199	386	198	227	1735	185
		SJP075PW12	59.7	38	1.14	381	206						
	[2.15]	SSR1PW04	59.4	35	0.45	331	184	199	328	189	227	1761	187
		SSR2PW04	57.8	56	0.45	331							
		SSR2PW12	61.1	34	1.14	366	188						
	[3.13]	A-PW0	39.1	33	0.00	-	-	398	360	184	227	1115	202
		A-PW04			0.45	421	197						
	[3.19]	11J04+0	53.0	32	0.40	480	200	71.3	295	200	95.0	1231	205
	Test 1	S-10-L42	57.3	29	0.42								
		S-10-L63			0.63								
		S-15-L21	62.3	30	0.21								
		S-15-L42			0.42	984	194	71.3	361	178	592	1805	186
		S-15-L63			0.63								
		S-20-L21	55.9	28	0.21								
		S-20-L42			0.42								
	Test 2	S-10-L10	65.2	37	0.10								
		S-10-L21			0.21	1006	202	71.3	381	183	1184	1763	195
		S-15-L00			0.00								
		S-15-L10			0.10								
Column	[2.10]	R-15-L63	106.5	45	0.63	988	197	71.3	361	178	531	1002	193
		R-15-H63			0.63	1435	210						
		D-15-L63			0.63	988	197				507		196
	[3.19]	9.2J04+1/4	53.0	32	0.40	480	200	71.3	295	200	67	1237	
		11J04+1/3	57.1	30							95	1231	205
		11J04+1/8	53.0	32									
		11J04+1/4	57.1	30									
		13J04+1/8	61.0	32							133	1213	204
		13J04+1/4		32									
		17J04+1/8		32							227	1050	
		17J04-1/4		32									
		11J08+1/4	56.8	30	0.75	606	211				95	1231	205
		11J12+1/4		30	1.13	606	211						
		11M04+1/4	53.0	32	0.40	480	200						
		11J04-3qs/4	57.1	30									
		11M04-3qs/4	57.1	30									
		11J02+1/8	56.8	30									

Note : F_c and E_c are compressive strength and Young`s modulus of concrete in MPa and GPa, ρ_w is a ratio of shear reinforcement in %, A_r and A_p are sectional area of a longitudinal bar and prestressing steel in mm^2, f_{wy}, f_{ry}, and f_{py} = yield strength of shear, longitudinal, and prestressing reinforcement in MPa, and E_w, E_r, and E_p = elastic modulus of shear, longitudinal, and prestressing reinforcement in GPa, respectively.

6.5.2 Failure Strength and Failure Mode

Figure 6.9 plots relationship between observed and predicted failure strength and failure mode. The observed failure strength in Fig. 6.9 represents peak load observed in the tests. The predicted failure strengths for the members failed in shear (ST, SC, DT, or FSC) were defined as the analytical shear strength obtained by the lesser of shear strengths (V_{cr}, V_{cc}, and V_u) in the proposed method. For the members failed in flexure (F), the predicted failure strengths indicate the ultimate flexural strength, V_{fu}. Vertical and horizontal axis in Fig. 6.9 represent observed and predicted failure strength, respectively. Circles, squares, triangles, and rhombus in Fig. 6.9 indicate observed data for post-tensioned precast concrete members experimentally failed in each failure modes (ST, SC, FSC, FS, and F), respectively. Solid and open dots in Fig. 6.9 indicate that the predicted failure modes agree and disagree with the experimental observations, respectively. As shown in Fig. 6.9, mean value and C.V. (Coefficient of variations) for observed / predicted failure strength equals to 0.97 and 0.16, respectively. It is clear that analytical failure strengths obtained by the proposed method evaluate experimental failure strength in a good accuracy regardless of failure mode. Further, it can be seen that most predicted failure modes agree with the observed ones except for five specimens. It points out that the proposed method is the effective analytical tool which can be widely applied to evaluate the failure strength and to predict the failure mode of post-tensioned precast concrete members.
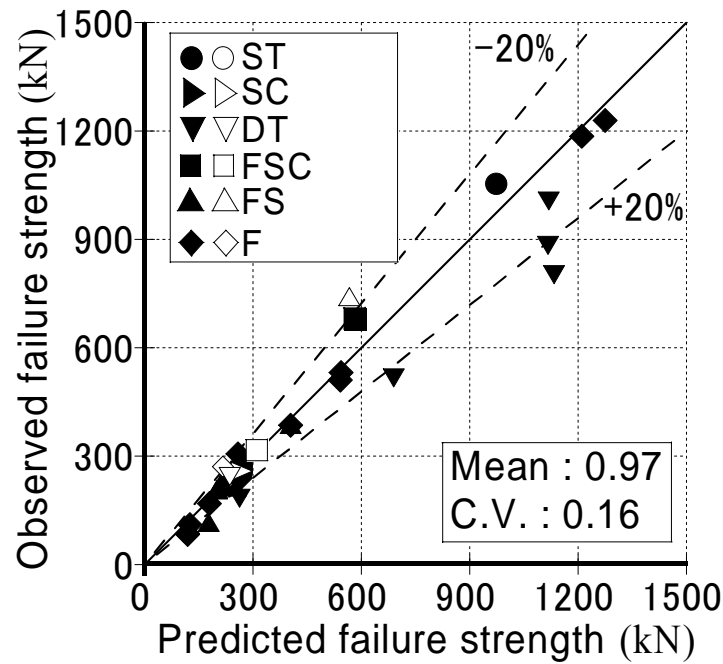
Fig. 6.9 Comparison between observed and predicted failure strength and mode

6.5.3 Deformation Capacity

Figure 6.10 plots the relationship between observed and predicted drift angle at flexural failure of post-tensioned precast concrete members failed in flexure (F). The observed drift angle is defined as the ratio of relative displacement to length of member at peak load. The predicted drift angle is defined as the flexural drift angle, R_f, obtained by Eq. (6.13) to (6.25). Vertical and horizontal axis in Fig. 6.10 indicate observed and predicted drift angle at flexural failure. As shown in Fig. 6.10, the mean value and C.V. for observed / predicted drift angle equals to 1.14 and 0.16, respectively. It can be seen that predicted drift angle at flexural failure, R_f, evaluats observed drift angle at flexural failure in a good accuracy. It is clear that the analytical method proposed in this study is useful tool to evaluate the deformation capacity of post-tensioned precast concrete members failing in flexure.

Further, it can be seen that the proposed model can be applied to the post-tensioned precast concrete members with materials in excess of the range of parameters used for the verification because the proposed model is based on the equilibrium condition of stresses and compatibility conditions of strains in concrete and reinforcements.
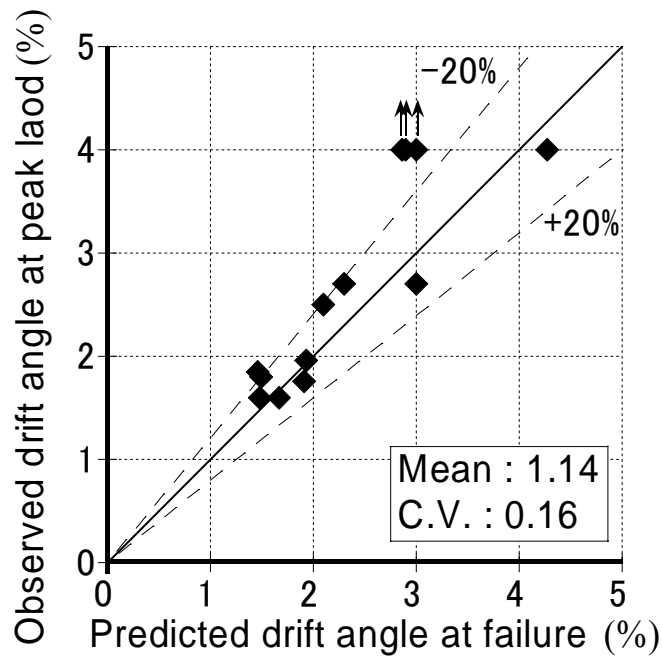
Fig. 6.10 Comparison between observed and predicted drift angle at flexural failure

6.6 Conclusions

To predict failure strength and failure mode of post-tensioned precast concrete member, a new analytical method considering the stress state of the concrete at the flexural compression zone and using the conventional section analysis was proposed. To predict shear strength for ST, SC, or DT failure, analytical models proposed in the Chapter 4 and 5 are used. For the shear strength of FSC failure, the shear capacity of the concrete at the flexural compression zone is assumed to be provided by the intact concrete in the compression zone. Further, drift angle at the flexural failure of post-tensioned precast concrete members was also evaluated by the proposed method using the rocking deformation model. Deformations due to pulling-out of prestressing steel at joint interface and due to flexural deformation in outside joint interface were considered as the total deformation of post-tensioned precast concrete member. For the verification, analytical results such as failure strength, failure mode, and drift angle at flexural failure predicted by the proposed method were compared to observed ones. The principle findings of this study are summarized as follows:

  1. Based on the stress state of the concrete at the flexural compression zone, shear strength due to deterioration of shear capacity of the concrete, V_{cc}, can be obtained.

2. By the comparison between shear strengths and flexural strength, the failure modes were predicted.

3. Rocking deformation model in which only pulling-out deformation of the prestressing steel at joint interface is considered is the effective deformation model to simulate the deformation properties of post-tensioned precast concrete members.

4. The predicted results (shear strength, flexural strength, failure mode, and drift angle at flexural failure) produced by the proposed method evaluated the observed ones in a good accuracy.

[References]

6.1 Komuro T., Imai K., Muramatsu A., Korenaga T., Kawabata I., and Watanabe F., "Compressive Properties of RC Columns Using High Strength Concrete with Compression Strength of 100-180 N/mm^2." *Summaries of Technical Papers of Annual Meeting,* AIJ, Sep., 2003, pp. 161-162. (in Japanese)

6.2 M. Nishiyama, M. Tani, J. Lee, "Ultimate Flexural Strength Evaluation for Prestressed Concrete Columns," *Proceedings of The 10th Japan-Taiwan-Korea Joint Seminar on Earthquake Engineering for Building Structures*, 10-11 Oct. 2008, pp. 277-285.

6.3 Lee J., "Shear Resistance Mechanism of Post-tensioned Precast Concrete Beam," M.S. Thesis, 2010, Kyoto University. (in Japanese)

6.4 Nagasaki M., Watanabe T., and Maeda M., "Evaluation of Yielding Deformation of Reinforced Concrete Members," *Proceedings of the Japan Concrete Institute*, Vol. 18, No. 2, 1996, pp. 797-802. (in Japanese)

7. Effect of Bond Strength and Mild Steel Ratio on Seismic Performance of Prestressed Concrete Beams

7.1 Intoduction

Post-tensioned precast concrete structures are generally constructed with grouted tendon. The grouting is of importance for preventing tendons from corroding and providing bond between tendon and concrete. Unbonded tendon is coated with a corrosion inhibitor such as grease. Prestressed concrete (PC) structures with unbonded tendon systems have been constructed to save work and time for grouting.

The significant development of a new technology using a self-centering function of unbonded PT tendon systems has been established as part of PRESSS project. Unbonded tendon systems once developed to save grouting work help construct a high-performance building for earthquake resistance.

Because of no bond between PT tendon and concrete, the structural behavior of members with unbonded tendon is different from the one of members with bonded tendon [7.1]. Because plane section assumption cannot be applied to unbonded tendon, the flexural strength of prestressed concrete members using unbonded tendon is considered to be 10 - 20% smaller than when bonded tendon is used. However, there are not enough analytical or experimental investigations for the structural behavior of prestressed concrete members with unbonded tendons.

In this study, the structural behaviors of beams with bonded and unbonded PT tendon are compared based on analytical results. FEM analyses using a structural analysis software package, FINAL/99-Rev.2, are carried out. Based on

the analyses results, the effect of bond strength of PT bars and longitudinal mild-steel reinforcing bar ratio on the flexural strength, hysteretic energy dissipation capacity, and residual deformation is investigated.

7.2 Analytical Modeling in Finite Element Method
7.2.1 Outline of Finite Element Analysis Modeling
Finite element analyses are carried out on a prestressed concrete beam with unbonded PT tendons reported in Ref. [7.1] under seismic loading. The analytical results are compared with the experimental results to ensure the applicability of the analyses.

Table 7.1 summarizes the geometrical and material properties of the specimen in Ref. [7.1]. The beam cross sectional dimensions are 160×210 mm. The beam length and shear span depth ratio are 3000 mm and 7.14, respectively. Flexure is considered to be dominant. Reinforcing details are shown in Fig.7.1. The beam was post-tensioned by prestressing steel bars (2-ϕ13), and shear reinforced with mild-strength round bars (ϕ6@150 mm), which were supported by supplementary longitudinal reinforcing bars of mild-strength steel (4-D10). The bond strength of PT tendon is assumed as small as 0.0001 MPa.
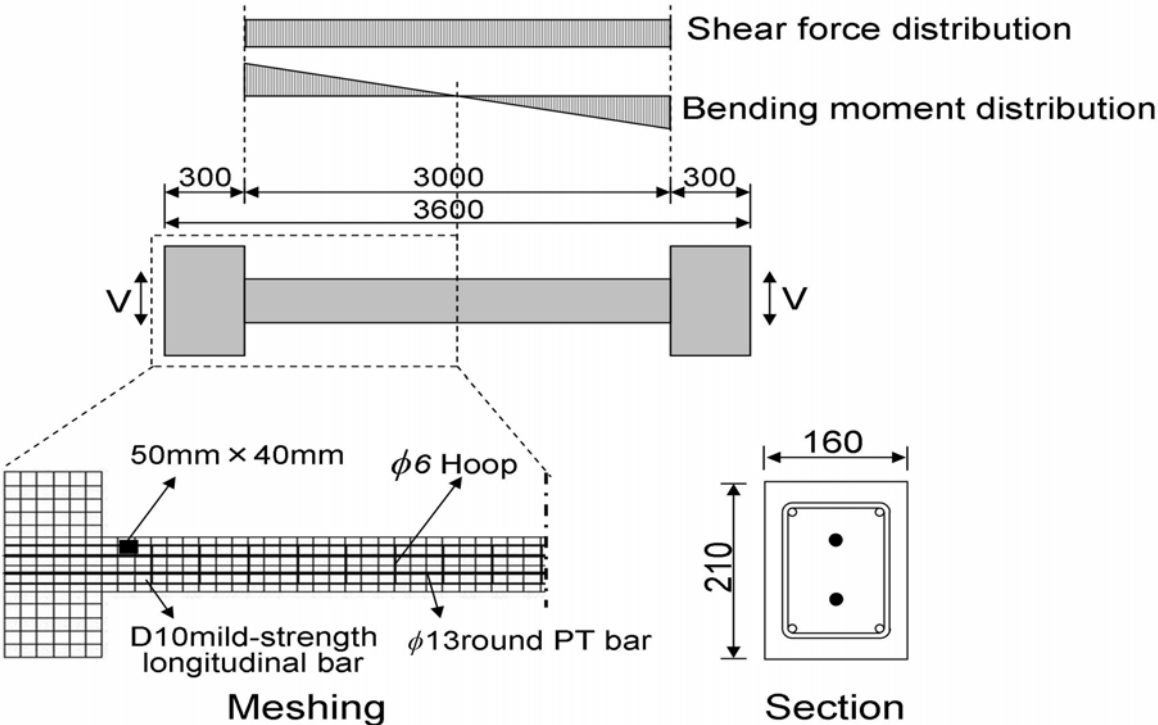
Fig. 7.1 Reinforcing and meshing details

Table 7.1   Geometrical and material properties of the beam in Ref. [7.1]

Section		$b{\times}D$	160×210 mm
Beam length		L	3000 mm
Shear span depth ratio		a/D	7.14
Mild strength longitudinal bar D10	Yield strength	f_{ry}	394 MPa
Shear reinforcement $\phi6$	Yield strength	f_{wy}	394 MPa
	Shear reinforcement ratio	p_w	0.24 %
Post-tensioning bar $\phi13$	Yield strength	f_{py}	1270 MPa
Concrete	Compressive strength	F_c	47.3 MPa
	Young`s modulus	E_c	24.0 GPa
	Tensile strength	F_t	3.8 MPa
Prestressing force ratio		P_e/bDF_c	0.106
Initial prestress / yield strength of PT tendon		f_{pe}/f_{py}	0.50
Ratio of moment capacity due to prestressing steel to the total moment capacity		λ	0.87
Bond strength of PT tendon		τ_{pmax}	0.0001 MPa

Domain discretization: Meshing

Elements formed in the FEM analyses are illustrated in Fig.7.1. An element in the specimen is 50 mm long in the longitudinal direction. The domain discretization in the transverse direction ranges from 30 to 40 mm depending on the location of non-prestressed longitudinal and prestressed reinforcements.

Material constitutive law: concrete

Plane stress elements for concrete with four nodes are used. Modified Ahmad model for stress-strain (*s-s*) curve (Eq. (7.1), [7.2]) is used. Table 7.2 shows the material models for the concrete.

$$\sigma = \frac{\left[A \cdot X + (D-1) \cdot X^2\right]F_c}{1 + (A-2)X + D \cdot X^2} \qquad \text{Eq. (7.1)}$$

where σ: concrete stress, F_c: uniaxial compressive strength of concrete

(for ascending curves)

$$X = \varepsilon / \varepsilon_{max}, \ D = 200 / F_c - (E_c / E_{max} -1)^2, \ E_c = F_c / \varepsilon_{cc} \quad \text{Eq. (7.2)}$$

(for descending curves)

$$X = \left(1 + \frac{\varepsilon - \varepsilon_{max}}{\varepsilon_{max}}\right)^n, \quad n = 0.9 + 3.4(F_c/1000)^2, \quad D = 1 - 1800(F_{max}/F_c - 1)^2/F_c \quad \text{Eq. (7.3)}$$

where, ε: concrete strain, ε_{max}: concrete strain corresponding to the maximum compressive stress in multi-axial stress, F_{max}, E_c and E_{max}: Young's modulus of concrete in uniaxial and multi axial stress, respectively.

Table 7.2   Concrete model for FEM

Stress-strain relationship	Modified Ahmad model [7.2] (Eq. 7.1)
Compression failure criteria	Kupfer-Gerstle`s failure criteria without decay of strength after cracking
Compressive softening effect	Modified Ahmad model [7.2] (Eq. 7.1) No strain softening at compressive strength after cracking Strain at compressive strength (=1.37F_c (kgf/cm^2)+1690 (10^{-6})) [7.3]
Shear transfer characteristic	Naganuma model [7.4]
Tension stiffening effect	Izumo model (c=0.2) [7.5]

Material constitutive law: mild-strength steel

The truss elements with rectangular section are used for longitudinal mild-strength bar. The truss element is formed by connecting pre-defined nodes of concrete as shown in Fig.7.2. Fig.7.3 illustrates the stress-strain curve for longitudinal steel. The relationship is defined as elasto-perfectly-plastic.

Material constitutive law: shear reinforcement

The truss elements with rectangular section like a longitudinal bar element are used for shear reinforcement. The stress-strain curve is also defined as elasto-perfectly-plastic.
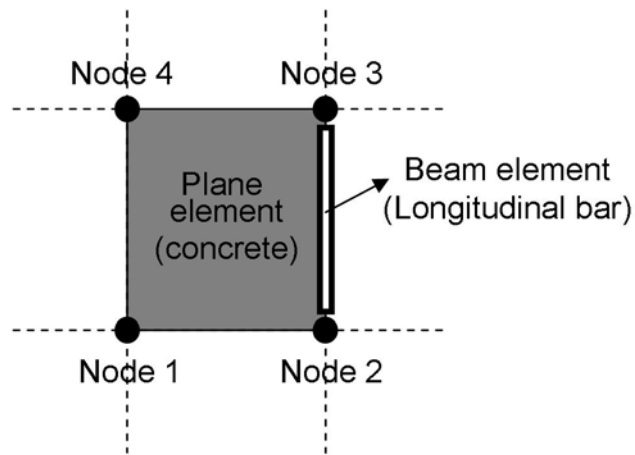
Fig. 7.2 Concrete and longitudinal bar model
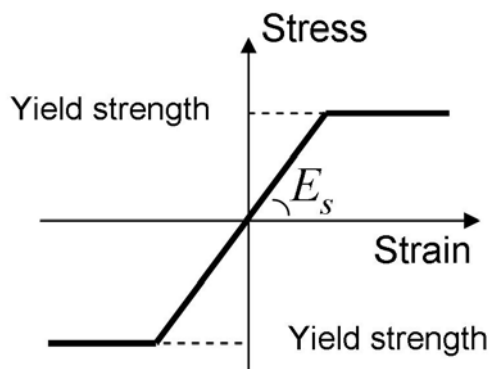
Fig. 7.3 Stress-strain curve for longitudinal mild-strength bar

Material constitutive law: PT bar and bond element

For a tendon element, a truss element with the same sectional area with the tendon is used. The stress-strain curve is defined as an elasto-perfectly-plastic relationship. A bond element between the tendon and concrete is idealized as shown in Fig. 7.4. The property of the bond element is defined in the longitudinal and transverse directions. A bond stress-slip relationship shown in Fig. 7.5 is applied to the longitudinal bond property. Nodes of the tendon element (nodes 5 and 8) are rigidly connected with nodes of concrete element (nodes 6 and 7) in the transverse direction. The anchorage is assumed at both ends of the member, so that the tendon does not have a relative move against concrete at the ends.

Figure 7.5 illustrates a bond stress-slip relationship between unbonded tendon and concrete idealized as a bi-linear model. The slip at the bond strength is assumed as 0.02 mm. The bond strength of unbonded tendon, τ_{pmax}, is assumed as low as 0.0001 MPa because the tendon profile is straight and only friction is available. The difference of unbonded tendon tensile force between the

anchorages, ΔT_p corresponds to frictional resistance. Using bond strength, τ_{pmax} = 0.0001 MPa, the friction force of 2.45 N (=0.0001$\psi_p L$) is calculated, where ψ_p is the perimeter length of tendon and L is the member length. The friction force of 2.45 N corresponds to the friction coefficient of 0.68×10^{-4}/m. The friction coefficient of PT bar in this study is much smaller than the friction coefficient (λ=0.003) of a bonded bar specified in Ref. 7.6 when the prestress is introduced.
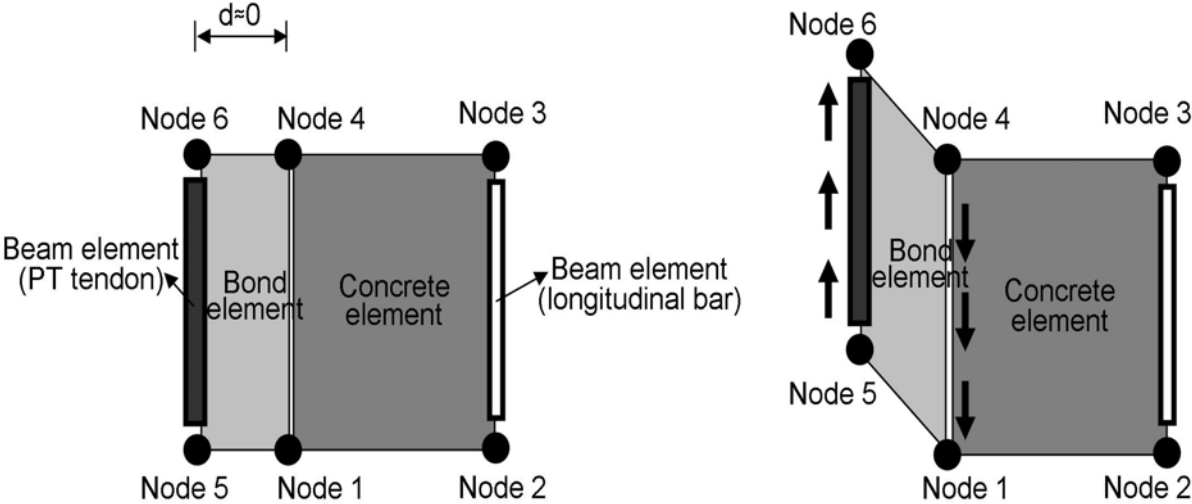
Fig. 7.4 Bond element between concrete and PT tendon
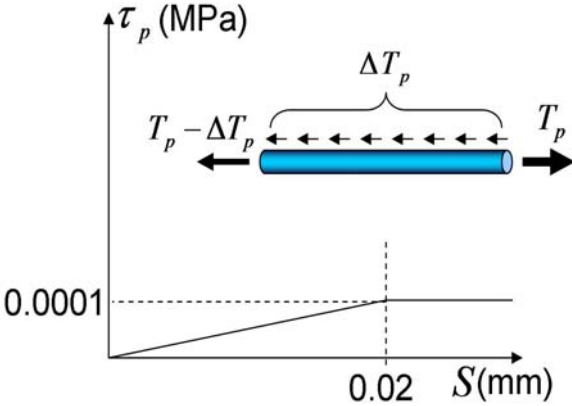
Fig. 7.5 Bond stress-slip relationship

Cracking model
In this study, smeared cracking model is applied because the investigation of the global structural behavior of prestressed concrete beam is a main objective in this FEM analysis.

7.2.2 Verification of Analytical Results

Table 7.3 indicates the summary of the comparison between the analytical and

experimental results. Fig. 7.6 shows load - beam rotation angle relationships obtained analytically and experimentally. As shown in Fig. 7.6 and Table 3, the results by the FEM analyses simulate the experimental results in a good accuracy. Fig. 7.7 plotts tensile stress variations from the initial prestress in one of the two tendons. It can be seen that the FEM analyses appropriately simulates the increment of tensile stress in the unbonded tendon. Fig. 7.8 indicates the comparison between predicted and observed crack patterns of the specimen [7.1]. As shown in Fig. 7.8, crack spacing predicted by FEM analysis is not corresponded to the crack spacing observed in the test [7.1]. It is because the analytical model applied in the FEM analysis is smeared cracking model. Discrete cracking model taking local behavior of cracking into consideration is effective to simulate the local behavior of crack, etc. crack spacing or crack width. It points out that FEM models applied in this study can not simulate the local behavior of cracking of prestressed concrete beam. Establishment of analytical model with discrete cracking model for evaluation of crack spacing and width is future work.
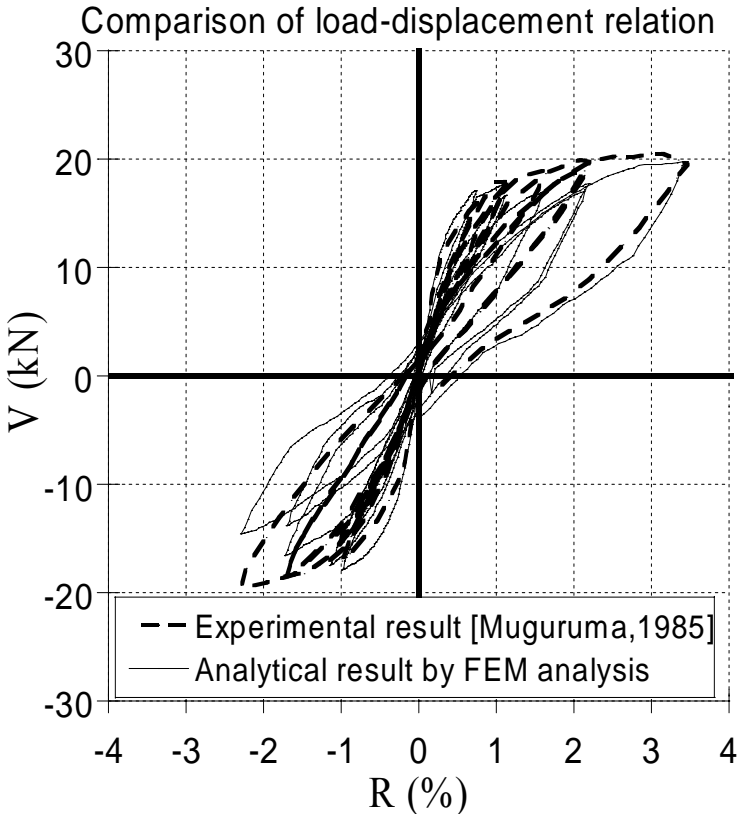
Fig. 7.6 Comparison between analytical and experimental load-displacement relations
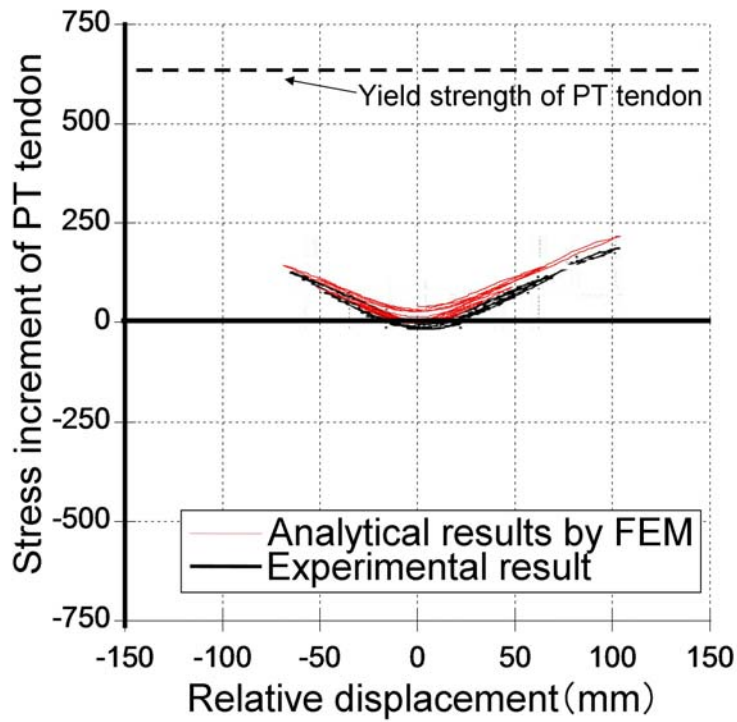
Fig. 7.7 Comparison between analytical and experimental increment of tensile stress in PT tendon

(a) Observed crack pattern [7.1]

(b) Predicted crack pattern by FEM analysis
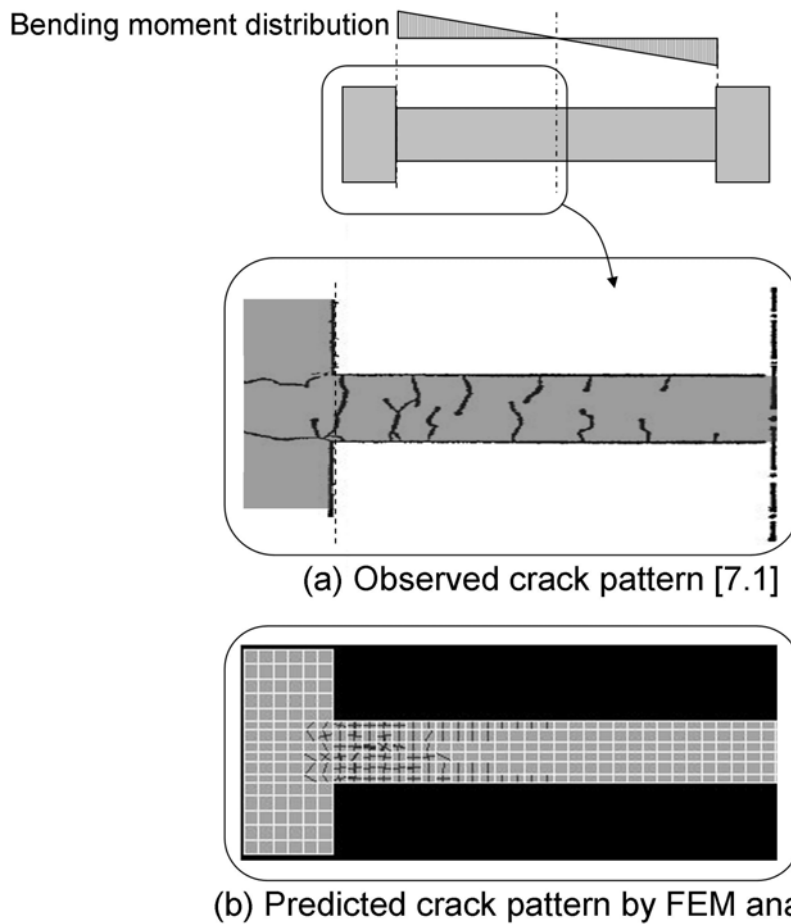
Fig. 7.8 Comparison between analytical and experimental crack patterns

Table 7.3 Summary of the analytical and experimental results

	Experimental results		Analytical results	
	R (%)	V (kN)	R (%)	V (kN)
Flexural cracking	0.18	7.33	0.20	8.90
Yielding of non-prestressed longitudinal bar	1.06	17.5	0.79	16.9
Yielding of PT-tendon	-	-	-	-
Maximum load capacity	3.15	20.5	3.47	19.8

7.3 Effect of Bond Stress and Mild Steel Ratio on Structural Behavior of Prestressed Concrete Beams

7.3.1 Outline of Finite Element Analysis Modeling

To investigate the effect of bond stress of PT tendon and amount of non-prestressed longitudinal mild-strength bars on structural behaviors of a prestressed concrete beam, FEM analyses are carried out. A design example described in Ref. [7.6] is referred. Table 7.4 shows the geometrical and material properties of the prestressed concrete beam. Elements formed in the FEM analyses are illustrated in Fig. 7.9. As shown in Table 7.4 and Fig. 7.9, The beam cross sectional dimensions are 400x1000 mm. The beam length and shear span depth ratio are 7500 mm and 3.75, respectively. The beam was post-tensioned by prestressing bar (4-ϕ21) and shear reinforced with high strength shear reinforcement (D10@200), which were supported by supplementary longitudinal reinforcing bars of mild strength steels (6-D22 or 6-D32). The initial prestressing force corresponding to 70% of the yield strength of the tendon was introduced. Table 7.5 shows the analytical parameters allocated to the beams. They were three levels of bond strength and two levels of longitudinal reinforcement ratio.

Table 7.4　Geometrical and material properties of beam

Section	$b \times D$	400×1000 mm^2
Beam length	L (mm)	7500
Shear span depth ratio	a/D	3.75
Prestressing force ratio	P_e/bDF_c	0.077
Initial prestress / yield strength in PT tendon	f_{pe}/f_{py}	0.70
Ratio of PT tendon contribution to moment capacity	λ	0.8 for 6-D22 0.6 for 6-D32
Concrete	Compressive strength	F_c (N/mm^2)	45
	Tensile strength	F_t (N/mm^2)	2.0
Shear reinforcement	Yielding strength	f_{wy} (N/mm^2)	600
	Shear reinforcement ratio	ρ_w (%)	0.18
PT tendon	Yielding strength	f_{py} (N/mm^2)	1690
	Reinforcement ratio	ρ_p (%)	0.53
Non-prestressed longitudinal bar	Yielding strength	f_{ry} (N/mm^2)	300
	Reinforcement ratio	ρ_r (%)	0.7 for 6-D22 1.4 for 6-D32
Bond strength of PT tendon	τ_{pmax} (N/mm^2)	1.64 for round PT bar 14.3 for deformed PT bar
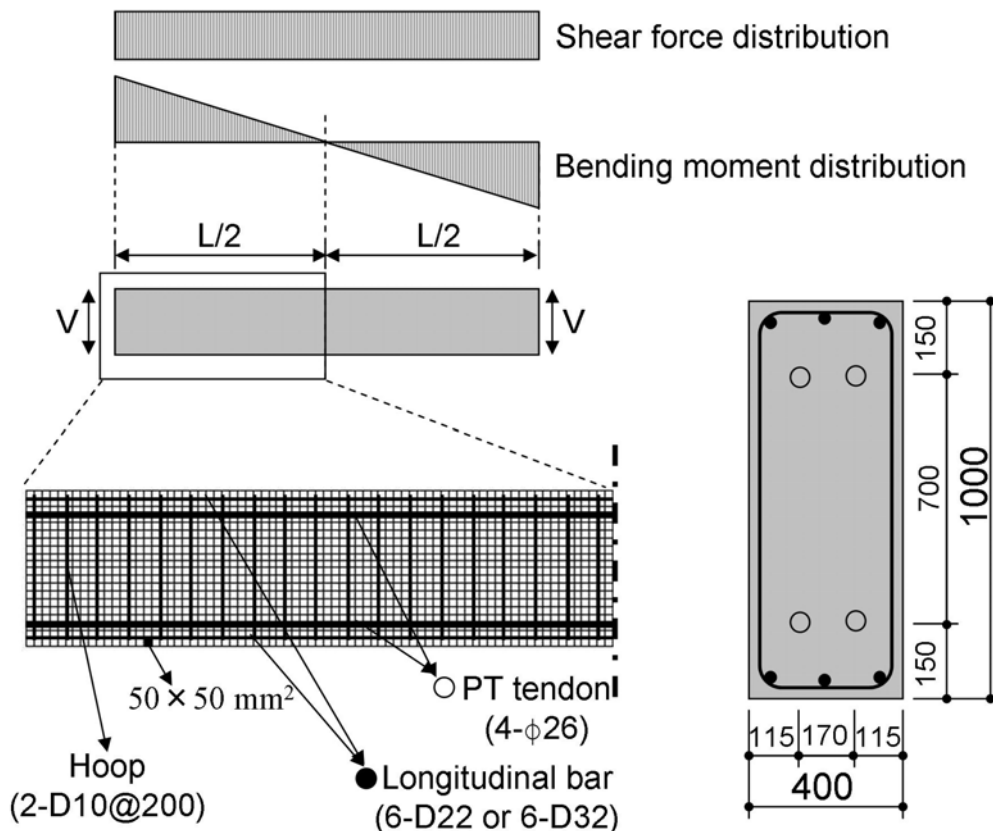
Fig. 7.9 Reinforcing detail

Table 7.5   Analytical parameters allocated to the beams

Type of PT tendon (Bond strength) / Reinforcement ratio of longitudinal bar, ρ_r (%)	Unbonded PT tendon (≈ 0 N/mm^2)	Bonded PT tendon	
		Round tendon (=1.64 N/mm^2)	Deformed tendon (=14.3 N/mm^2)
0.7 (6-D22)	No.1	No.2	No.3
1.4 (6-D32)	No.4	No.5	No.6

Note: $\rho_r = A_r/bd$, where A_r is sectional area of non-prestressed longitudinal bar in mm^2, b and d are the beam width and the effective depth in mm, respectively.

Domain discretization: Meshing

As shown in Fig. 7.9, the longitudinal size of an element is 50 mm. The domain discretization in the transverse direction is dependent on the location of non-prestressed and prestressed reinforcement.

Material constitutive law: concrete, longitudinal bar, shear reinforcement

The same material constitutive laws as the previous section are used.

217

Material constitutive law: PT tendon and bond element

For the unbonded tendon element, the same material constitutive law as the previous section is used. The bond-slip relationships between bonded tendon and concrete are illustrated in Fig. 7.10. Iihosi's model [7.7] (Eq. (7.4) to (7.12)) for the bond stress-slip relationship of bonded tendon (round and deformed bar) is employed.
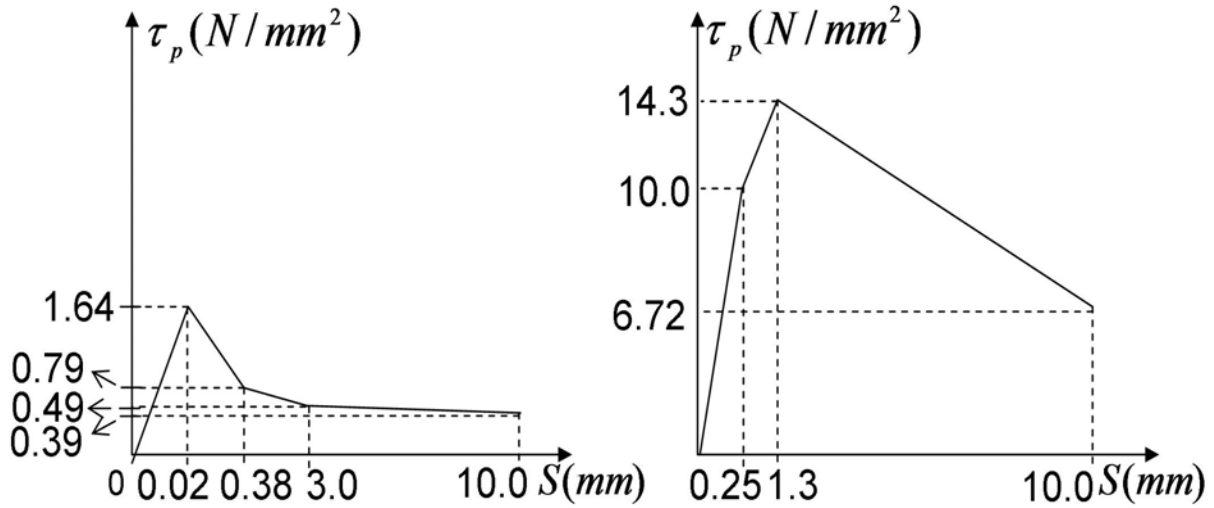
Fig. 7.10 Bond stress-slip relationships

$$\text{(Round PT bar)};\qquad 0 < S \le 0.02mm, \ \tau/\tau_{p\max} = 50 \times S \qquad \text{Eq. (7.4)}$$

$$0.02 < S \le 0.38mm, \quad \tau/\tau_{p\max} = -1.44 \times S + 1.03 \qquad \text{Eq. (7.5)}$$

$$0.38 < S \le 3mm, \quad \tau/\tau_{p\max} = -0.07 \times S + 0.51 \qquad \text{Eq. (7.6)}$$

$$3 < S \le 10mm, \quad \tau/\tau_{p\max} = -0.01 \times S + 0.34 \qquad \text{Eq. (7.7)}$$

$$\tau_{p\max} = 0.18F_g^{0.58} \ \ (=1.64 \ \text{N/mm}^2) \qquad \text{Eq. (7.8)}$$

$$\text{(Deformed PT bar)};\qquad 0 < S \le 0.25mm, \quad \tau/\tau_{p\max} = 2.81 \times S \qquad \text{Eq. (7.9)}$$

$$0.25 < S \le 1.3mm, \quad \tau/\tau_{p\max} = 0.28 \times S + 0.63 \qquad \text{Eq. (7.10)}$$

$$1.3 < S \le 10mm, \ \tau/\tau_{p\max} = -0.06 \times S + 1.07 \qquad \text{Eq. (7.11)}$$

$$\tau_{p\max} = 0.52F_g^{0.87} \ \ (=14.30 \ \text{N/mm}^2) \qquad \text{Eq. (7.12)}$$

7.3.2 Loading and Computations

The loading steps below are applied.

・Step 0: Tensile force corresponding to the initial prestressing force is introduced to PT tendons

・Step 1: The loading cycles indicated in Fig. 7. 11 are imposed.

Figure 7.11 illustrates the loading histories applied to the FEM analyses. The shear forces and displacements at yielding of mild-strength bar, V_y and δ_y, in the loading histories are obtained by a monotonic loading analysis for the beam No.3 (ρ_r=0.7%) and No.6 (1.4%). The results provide V_y of 344 kN for No.3 and 430 kN for No.6. The displacements, δ_y, are 0.41 mm for No.3 and 0.42 mm for No.6.
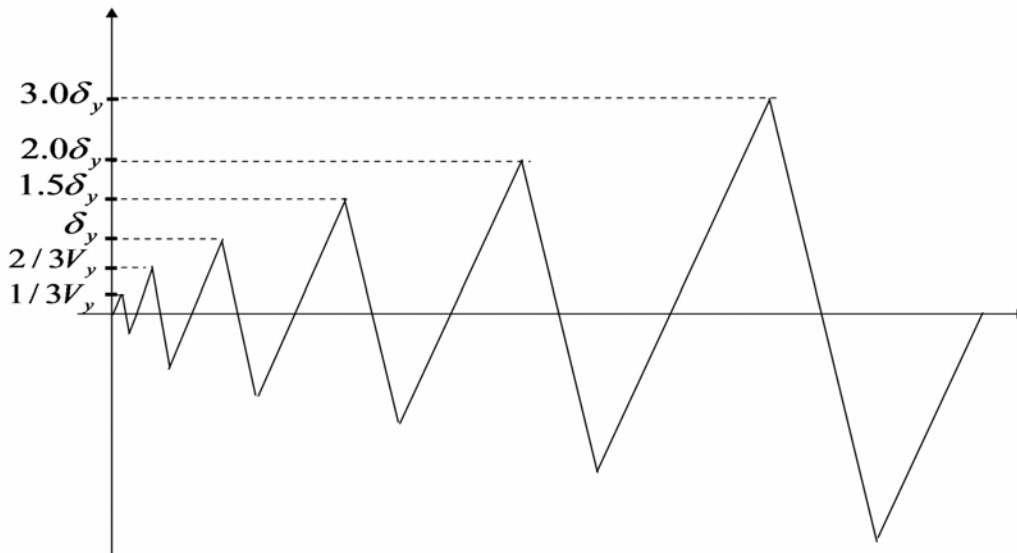
Fig. 7.11 Loading histories

7.4 Discussion on Analytical Results

7.4.1 Load-Displacement Relation

Figures 7.12 to 7.14 show the load, V - drift angle, R, relationships. Table 7.6 summarizes the load-displacement relationships of specimens. The drift angle, R, is obtained by δ/L, where δ and L are relative vertical displacements between the ends of the beam and beam length, respectively. As shown in Figs. 7.12 to 7.14, no deterioration of load carrying capacity is observed in all beams.

In the beams with ρ_r = 0.7%, a first flexural crack occurred at R = 0.06%. The maximum load capacities of the beams with bonded tendons were approximately 30 kN larger than those with unbonded tendons. The longitudinal mild-strength steel in all beams yielded at R = 0.25%. The unbonded bar did not yield while the round and deformed bars yielded at R = 0.48 and 0.39%, respectively. Cover concrete in the beams with unbonded, round, and deformed bars reached the strain of 0.23 % corresponding to compressive strength at R = 0.48, 0.47, and

0.43%, respectively.

In the beams with ρ_r = 1.4%, a first flexural crack occurred at R = 0.06%. The longitudinal mild-strength bar in all beams yielded at R = 0.29%. The beams with unbonded, round, and deformed bars reached their maximum load capacity at R = 1.25, 0.63, and 0.63%, respectively. The unbonded bar did not yield while the round and deformed bars yielded at R = 0.64 and 0.61%, respectively. The softening of cover concrete started at R = 0.63, 0.63, and 0.51% for the beams with the unbonded, round, and deformed bars, respectively.

Table 7.6 Summary of load-displacement relations

Specimens		Flexural cracking		Yielding of longitudinal bar		Yielding of PT tendon		Peak of load	
		$R(\%)$	V(kN)	$R(\%)$	V(kN)	$R(\%)$	V(kN)	$R(\%)$	V(kN)
p_r = 0.7%	Unbonded	0.06	133.0	0.25	300.0	-	-	0.82	326.5
	Round bar	0.06	131.1	0.25	312.1	0.48	316.0	0.41	351.0
	Deformed bar	0.06	133.1	0.25	311.0	0.39	347.8	0.61	356.1
p_r = 1.4%	Unbonded	0.06	140.4	0.29	384.6	-	-	1.25	412.2
	Round bar	0.06	140.4	0.28	394.3	0.64	426.5	0.63	450.2
	Deformed bar	0.06	140.4	0.28	390.5	0.61	441.1	0.63	441.7

□:Flexural cracking ○:Yielding of longitudinal bar △:Yielding of PT tendon ■:Crusing of concrete
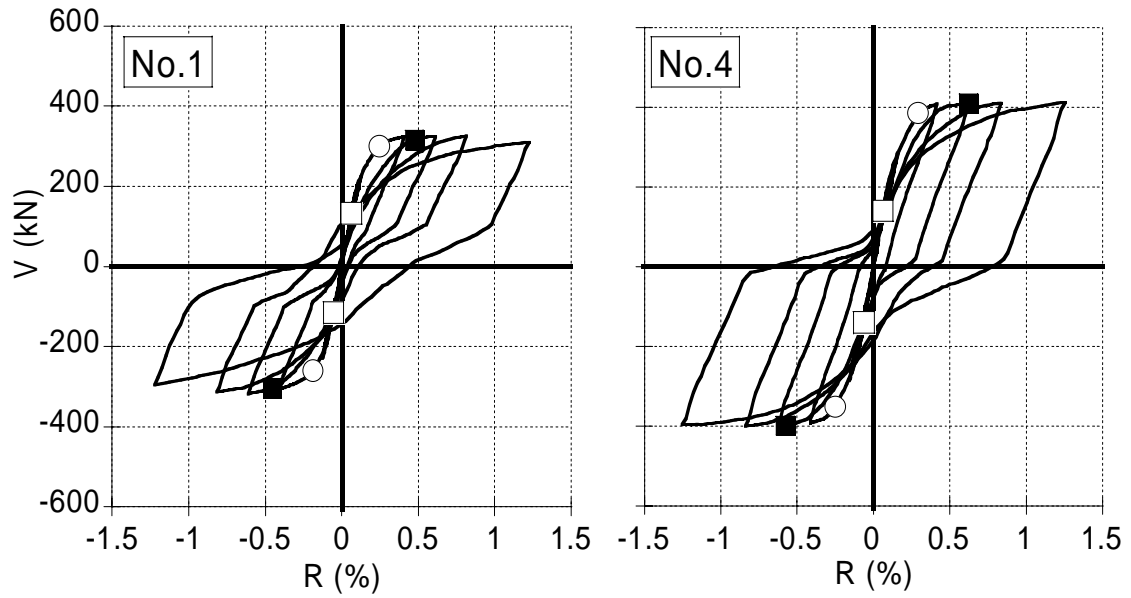
(a) $\rho_r = 0.7\%$ (b) $\rho_r = 1.4\%$

Fig. 7.12 Load-drift angle relation for the beams with unbonded tendon
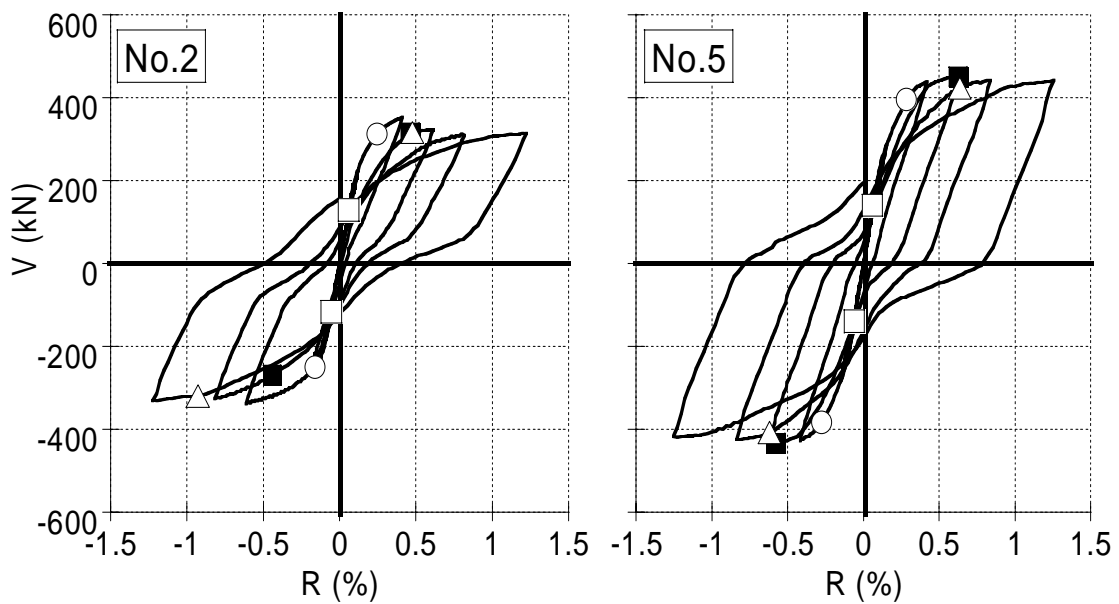
(a) $\rho_r = 0.7\%$ (b) $\rho_r = 1.4\%$

Fig. 7.13 Load-drift angle relation for the beams with bonded round bar

(a) $\rho_r = 0.7\%$　　　　　　　　(b) $\rho_r = 1.4\%$
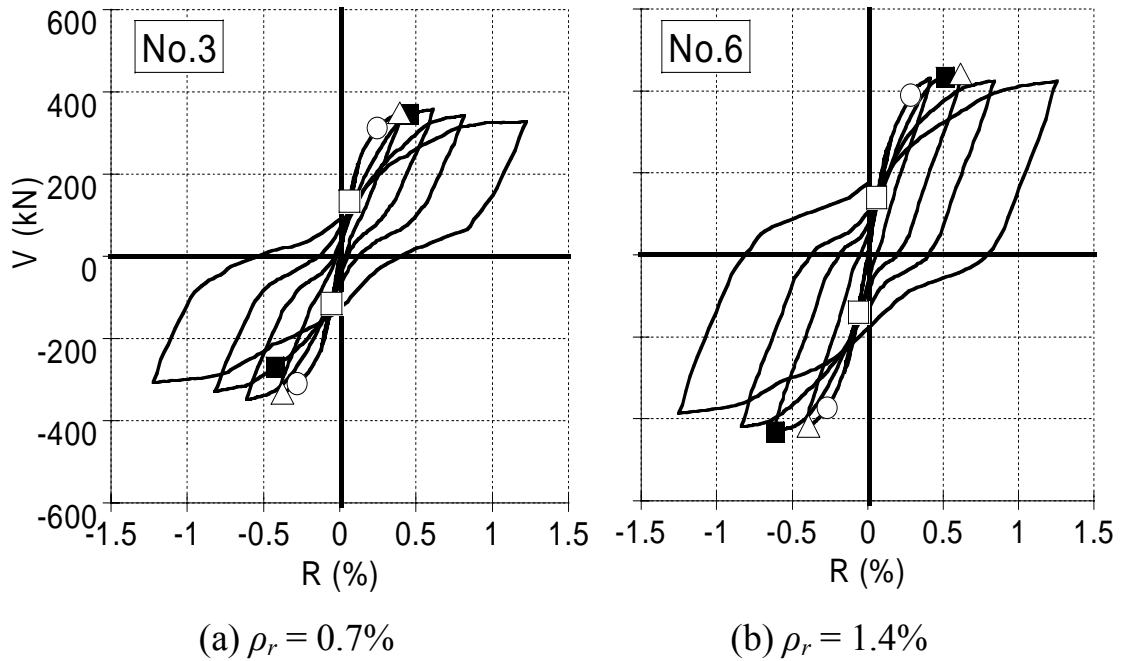
Fig. 7.14 Load-drift angle relation for the beams <u>with bonded deformed bar</u>

7.4.2 Tensile Stress Variation of PT Tendon

Figures 7.15 to 7.17 illustrate tensile stress variations of tendons for No.1 to 6. As shown in Fig. 7.15, the maximum tensile stress increment of the unbonded tendon was 250 MPa, which indicated it remained elastic. For the bonded tendon, the tensile stress increment reached 500 MPa, which indicated it reached its yield strength.

(a) $\rho_r = 0.7\%$　　　　　　　　(b) $\rho_r = 1.4\%$
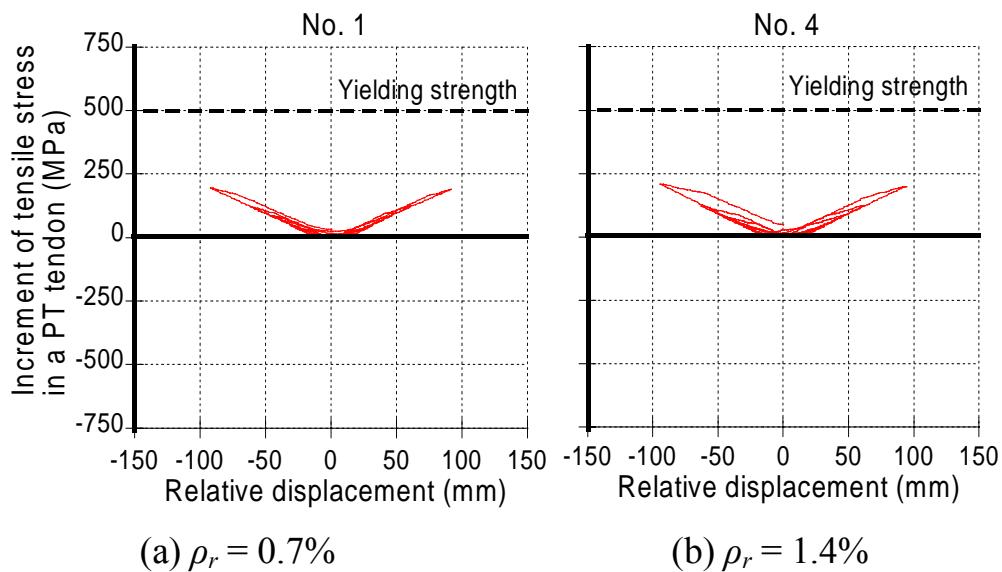
Fig. 7.15 Stress variation in tendon for beams <u>with unbonded tendon</u>

(a) $\rho_r = 0.7\%$ (b) $\rho_r = 1.4\%$
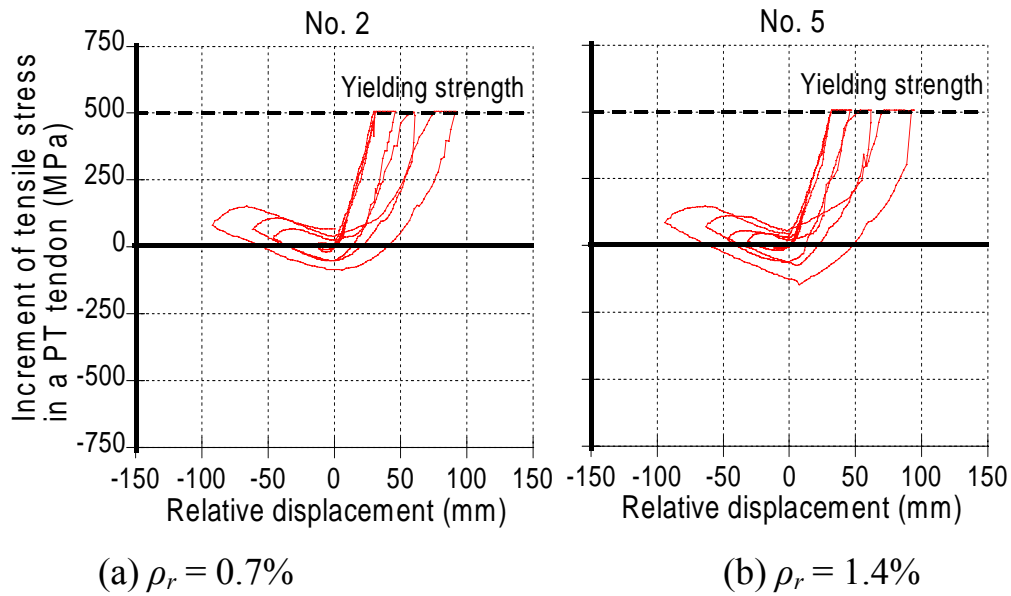
Fig. 7.16 Stress variation in tendon for beams <u>with bonded round bar</u>

(a) $\rho_r = 0.7\%$ (b) $\rho_r = 1.4\%$
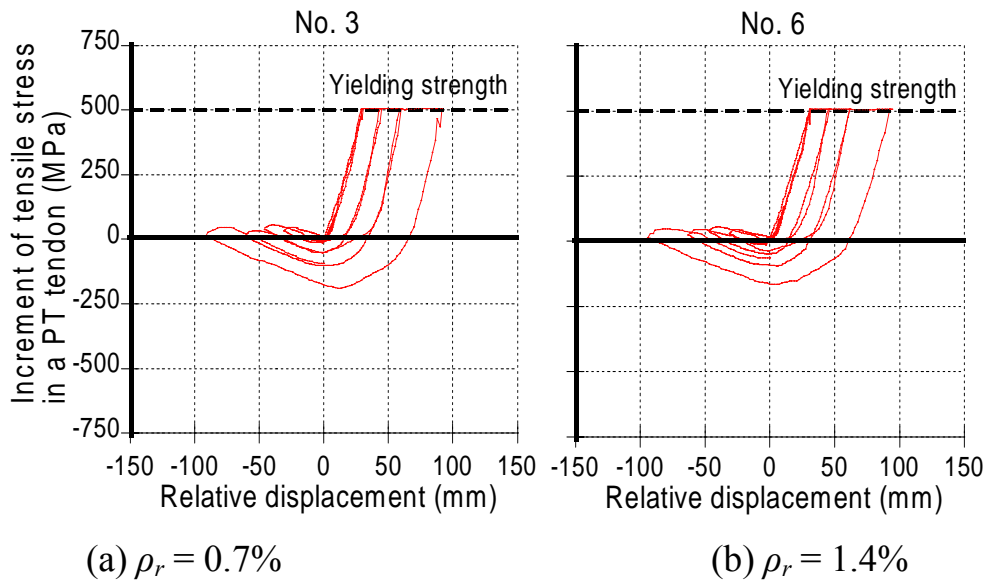
Fig. 7.17 Stress variation in tendon for beams <u>with bonded deformed bar</u>

7.4.3 Crack Patterns

Figure 7.18 shows the crack patterns of the analytical specimens. As shown in Fig. 7.18, flexural cracks distribute in wide region for specimens with high ρ_r (No. 4, 5, 6). Significant effect of bond stress on crack patterns does not observed. As mentioned in section 7.2.2, further analytical discrete cracking model to be able to simulate the local behavior of cracking needs.
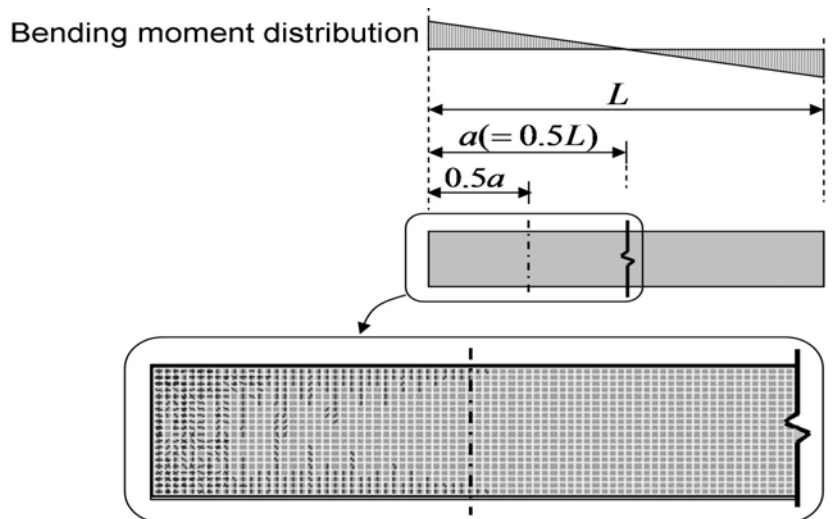
(a) No.1 (with unbonded PT tendon, ρ_r=0.7%)
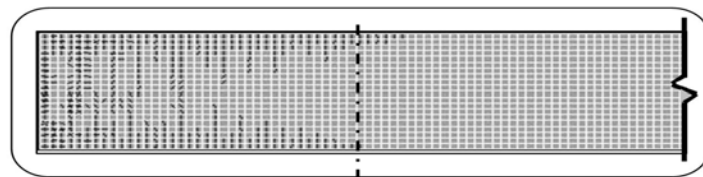
(b) No.2 (with round PT tendon, ρ_r=0.7%)
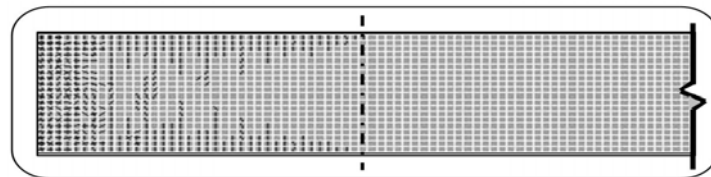
(c) No.3 (with deformed PT tendon, ρ_r=0.7%)
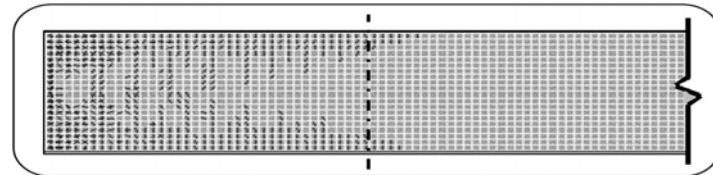
(d) No.4 (with unbonded PT tendon, ρ_r=1.4%)
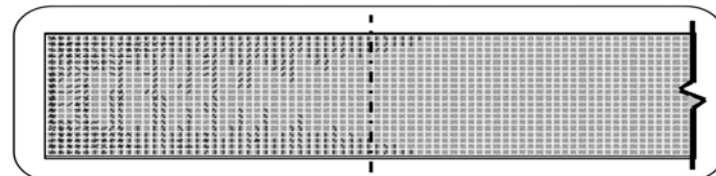
(e) No.2 (with round PT tendon, ρ_r=1.4%)
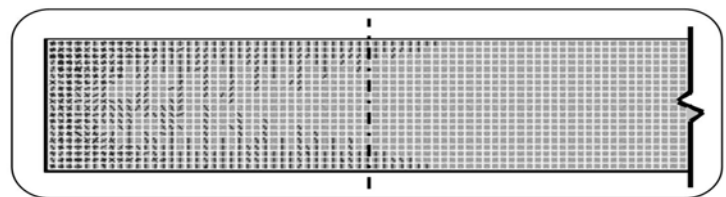
(c) No.3 (with deformed PT tendon, ρ_r=1.4%)

Fig. 7.18 Crack patterns

7.4.4 Energy Dissipation Capacity

Figure 7.19 shows equivalent viscous damping factor, h_{eq}, plotted against beam rotation angle. Fig. 7.20 plots the comparison of energy dissipation capacity among materials such as concrete, mild-strength longitudinal bar, and PT tendon which are located at the critical section of the member. At R=1.2%, the beams with ρ_r = 1.4% developed the energy dissipation capacity of h_{eq} = 0.47 while those with ρ_r = 0.7% developed the energy dissipation capacity of h_{eq} = 0.4. It can be pointed out that increase in ρ_r leads to increase in h_{eq}. This is because most hysteretic energy was dissipated by yielding of the non-prestressed mild-strength longitudinal bars as shown in Fig. 7.20.

As shown in Fig. 7.20, it can be seen that there is no significant difference of energy dissipation capacity in beam between with bonded deformed PT bar and with others. It is because the energy dissipation capacity due to mild-strength longitudinal bar decreases as energy dissipation capacity due to PT tendon increases. owever, it is clear that the bond stress of tendon did not significantly affect hysteretic energy dissipation capacity.
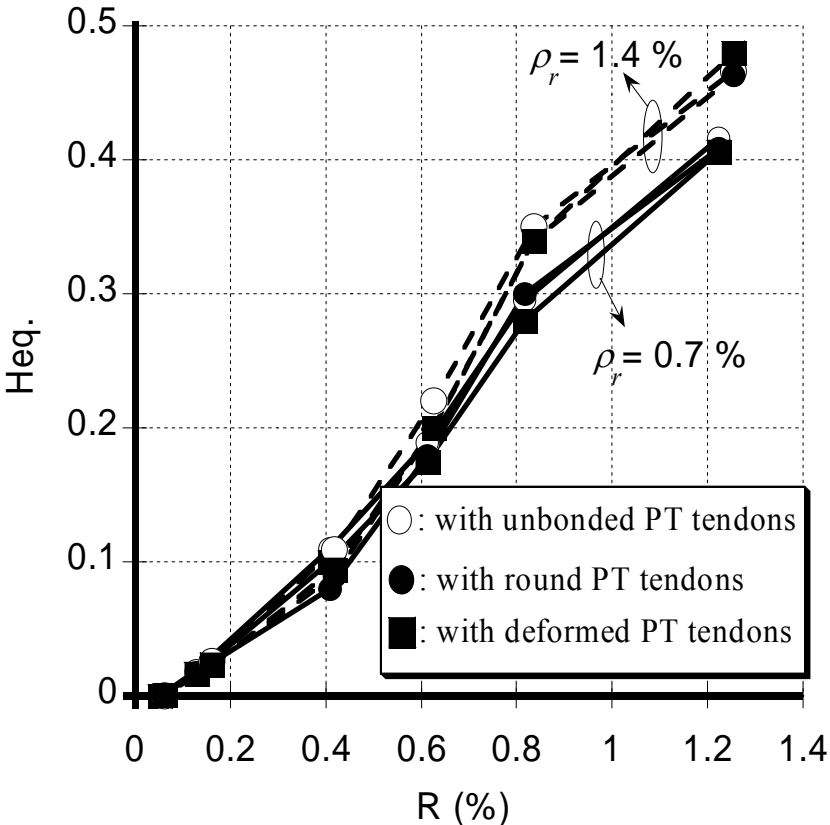
Fig. 7.19 Equivalent viscous damping, h_{eq}
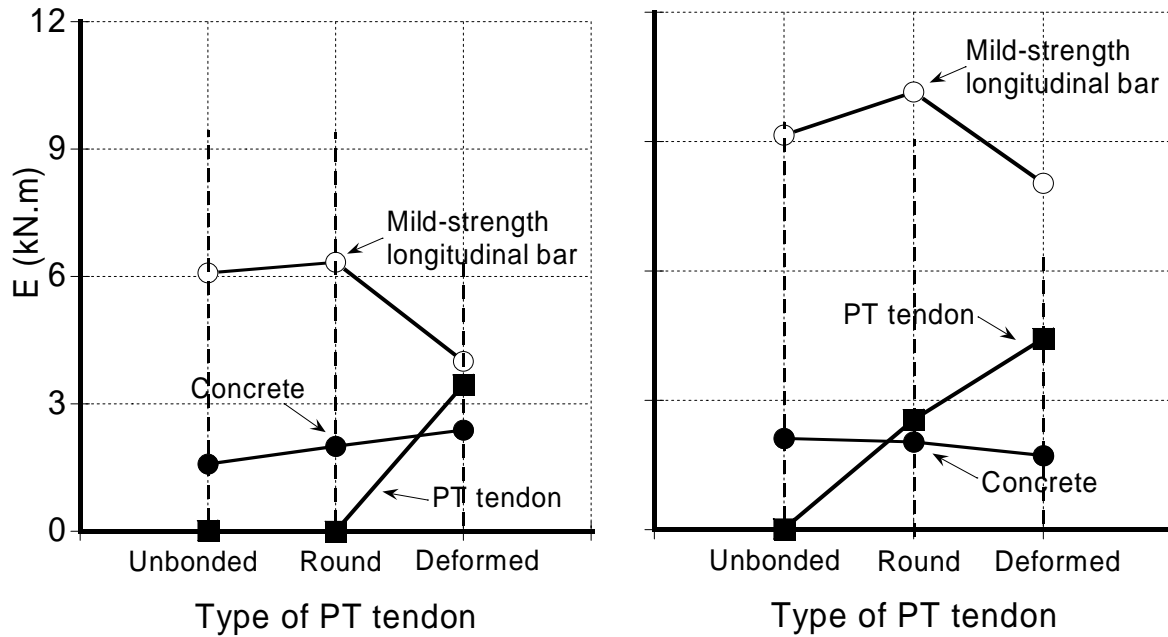
Fig. 7.20 Comparison of energy dissipation capacity among materials

7.4.5 Residual Deformation

Residual drift angles are plotted in Fig.7.21. A residual drift angle is the drift angle at zero load after unloading in the positive direction. As shown in Fig.7.12, no significant difference in residual drift angle among the beams is observed until R=0.4%. When the peak drift angle exceeds 0.6%, the amount of non-prestressed mild-strength longitudinal bar affects the residual drift angle. At R=1.2%, the residual drift angles of 0.8% in the beams with ρ_r = 1.4% develop while those of 0.4% in the beams with ρ_r = 0.7% does. It can be seen that the higher ρ_r is provided, the larger residual drift angle is observed. Compression force by prestress needed to push back the longitudinal mild-strength bar yielded in the previous loading cycle to the opposite sign of strain should be provided. It is noted that the larger amount of mild-strength steel ratio, ρ_r, was provided, the larger residual deformation was observed. It is pointed out that the tendon type does not significantly affect residual deformation and reduction in prestress in tendon while the mild-strength steel ratio, ρ_r, does.

Based on the analytical results above, the bond stress of the tendons affects the maximum load capacity of the beams while the amount of non-prestressed mild-strength longitudinal bars has an influence on hysteretic energy dissipation capacity and residual deformation.

226
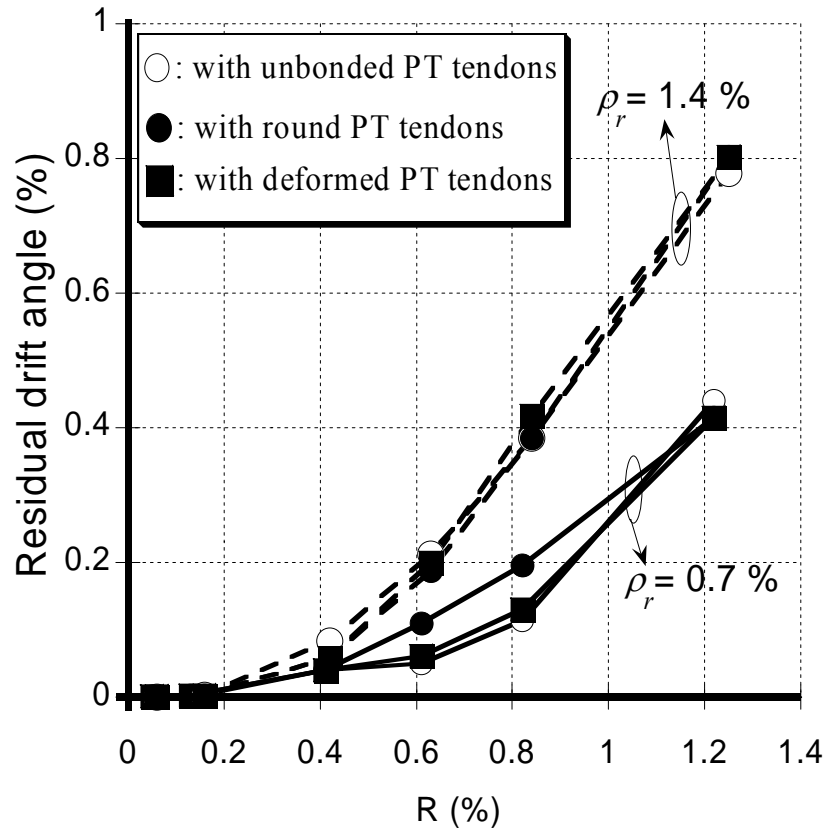
Fig. 7.21 Residual drift angle

7.5 Conclusions

The main purpose of this study was to investigate the effect of bond stress in PT tendon and the amount of non-prestressed longitudinal mild-strength bars on structural behaviors of prestressed concrete beams. Based on the FEM analyses, the structural behaviors of the beams with unbonded and bonded tendons were discussed. The conclusions obtained are summarized as follows.

1. The maximum load capacities of the beams with bonded tendons (round or deformed bars) were approximately 10% larger than those of the beams with unbonded tendons.

2. The larger amount of non-prestressed mild-strength longitudinal bars was provided, the larger hysteretic energy dissipation capacity (equivalent viscous damping factor, h_{eq}) was obtained: at $R=1.2\%$, the beams with ρ_r = 1.4% developed the energy dissipation capacity of h_{eq} = 0.47 while those with ρ_r = 0.7% developed the energy dissipation capacity of h_{eq} = 0.4.

3. The larger amount of non-prestressed mild-strength longitudinal bars was provided, the larger residual deformation was observed: at $R=1.2\%$, the

residual drift angles of 0.8% in the beams with $\rho_r = 1.4\%$ developed while those of 0.4 % in the beams with $\rho_r = 0.7\%$ did.

[References]

7.1 Muguruma H., Watanabe F., and Nishiyama M., "Structural Behaviours of Statically Indeterminate Unbonded Prestressed Concrete Beam," *Journal of Prestressed Concrete, JPCEA*, Vol. 27, No. 2, Mar., 1985, pp. 66-73 (in Japanese).

7.2 Naganuma K., "Stress-strain Relationship for Concrete under Triaxial Compression," *Journal of Structural and Construction Engineering*, AIJ, No. 474, Aug., 1995, pp.163-170 (in Japanese).

7.3 Amemiya A., Noguchi H., "Development of Finite Element Analytical Program for High Strength Reinforced Concrete Members (Development of Concrete Model, Part 1)", *Summaries of Technical Papers of Annual Meeting, AIJ*, Sep., 1990, pp. 639-640 (in Japanese).

7.4 Naganuma, K., "Nonlinear Analytical Model for Reinforced Concrete Panels under In-plane Stresses(Study on Nonlinear Analytical Method for Reinforced Concrete Wall Structures, Part 1)", *Journal of Structural and Construction Engineering*, AIJ, No. 421, Mar., 1991, pp.39-48. (in Japanese)

7.5 Izumo J., "Analytical model for Reinforced Concrete Plate Element Subjected to In-plane Stresses", *Concrete Research and Technology, JCI*, No. 87, Sep., 1987, pp. 107-120 (in Japanese)

7.6 Architectural Institute of Japan, "Satandard of Structural Design and Construction of Prestressed Concrete Structures," 1998, pp. 97-101 (in Japanese).

7.7 Iihoshi F,, Mizoguchi S., Nakatsuka T., "The Experimental Study Regarding The Bond Characteristic between The PC Steel Bars, The Grout and The Sheath," *Proceedings of The 17th Symposium on Developments in Prestressed Concrete, JPCEA*, Nov., 2008, pp. 397-402 (Japanese).

8. Major Conclusions and Future Work

8.1 Major Conclusions

Concluding remarks regarding the results from the study undertaken have generally been given at the end of each chapter. They are summarized again as follows:

8.1.1 Chapter 2

Ichinose's truss analogy takes into account the shear contribution of compressive cover concrete and required bond stress of reinforcing bar. It points out that Ichinose's truss analogy can be applied to reinforced concrete members which are subjected to axial force or with insufficient bond stress of reinforcing bars. However, the truss model does not make quantitative relationships between valuables.

MCFT proposed by Vecchio and based on the stress and strain status of concrete and reinforcement simulated shear force-deformation relation very well. As an upper limit condition for calculation procedures Vecchio used yield strength of shear reinforcement, f_{wy}, and softened compressive strength of concrete strut, f_{c2max}, respectively. However, MCFT does not take into account shear contribution of compressive cover concrete. Moreover, shear resistance mechanism for reinforced / prestressed concrete members with multiple layered reinforcing bars can not be investigated by MCFT. It is necessary to develop a new shear resistance model for reinforced / prestressed concrete with shear contribution of compressive cover concrete or with multiple layered reinforcing bars.

Current shear design equations in ACI provision [2.7] and AIJ guideline [2.8, 16] were introduced. Shear design equations in the ACI provision consist of shear contribution of concrete and shear reinforcement. The shear contribution

of concrete in the ACI provision was empirical equations based on the experimental parameters affecting shear behavior of reinforced concrete member. Therefore, the design equations can not be applied to the member in which geometric or material properties are exceed to applicable coverage. An equation for the shear reinforcement contribution in ACI provision underestimates the experimental results because it is based on the conventional 45 degree angle truss model. Shear design equations in AIJ guide lines were based on the strut and truss analogies as shear contribution of concrete and shear reinforcement, respectively. In order to apply the equations in AIJ guide line to prestressed concrete member with cut-off longitudinal bar at ends of the member, further investigations on the effect of bond stress of PT tendons and cover concrete on the shear behavior need.

In order to investigate inelastic deformation capacity of reinforced concrete beams failing in flexure and shear after flexural yielding, analytical methods proposed by Choi [2.1] and Nakatsuka [2.4] were introduced. Choi used Rankine's failure criteria to investigate stress-strain relationship of concrete in flexural compression zone. Based on the shear capacity of concrete in flexural compression zone, Choi developed the analytical method to investigate the deterioration of shear capacity of slender reinforced concrete beams. However, the model can not be applied to reinforced concrete beam failing in shear or short beam. Also, to apply the model to prestressed concrete members, further investigations need.

To investigate the deterioration of shear capacity of reinforced concrete failing in shear after flexural yielding, Nakatsuka proposed analytical model based on the Mohr-Columb's failure criteria. To simulate deterioration of shear capacity after flexural yielding, Nakatsuka used the shear resistance capacity of concrete in flexural compression and shear reinforcement. Nakatsuka's model is effective tool to investigate the deterioration of shear capacity of reinforced concrete beams failind shear after flexural yielding.

8.1.2 Chapter 3

In section 3, two series of static loading test on flexural and shear behavior of post-tensioned precast concrete beams had been conducted. Main conclusions by the tests are summarized as follows.
    1. Five failure modes (ST, SC, DT, FSC, and F) were observed: shear

reinforcement in prestressed concrete beams failed in ST (shear tension) yielded at ultimate state while the shear reinforcement in the beams failed in SC or FSC does not yield. In DT failure, initiation of primary shear crack leads to decay of load carrying the shear capacity of beams,

2. In flexural deformation, tensile stresses of prestressing steel at beam-stub joint were the largest: deformation of post-tensioned precast concrete beam concentrates the beam-stub joints.

3. Tensile stresses of shear reinforcement at mid-span in which moment equals to zero were largest while those at both ends of beam were approximately zero.

4. In DT failure, shear reinforcement hardly contributed for shear resistance of beam.

5. In FSC failure, the prominent crushing of the concrete at the flexural compression zone was observed.

6. In evaluation of shear failure strength using current shear design equations, *Method D* in which shear equations in Ref. 2.15 were modified evaluated the experimental shear failure strength in the best accuracy.

7. By parametric study using experimental data from previous researches and from this study, it can be seen that shear span to overall depth ratio, *a/D*, and shear reinforcement ratio, ρ_w, significantly affect to failure mode.

8.1.3 Chapter 4

A new analytical shear resistance model for post-tensioned precast concrete members had been proposed. In the model, the bond characteristics of prestressing steel and compressive stress in cover concrete were taken in account. To verify the accuracy of analytical results by proposed truss model, experimental data on post-tensioned precast concrete members which failed in shear from previous research [2.9, 2.10, 2.14, 3.12] and from Test 2 in Chapter 3 were used.

The most important conclusions are summarized as follows:

1. Analytical shear strengths of post-tensioned precast concrete member by truss model proposed in this study evaluated experimental shear strength in a better accuracy than those by conventional MCFT [2.2].

2. In thirteen out of fourteen post-tensioned precast concrete members used

for verification, analytical failure mode of post-tensioned precast concrete member by proposed model provided results agreed with observed one.

3. Analytical load-deformation response of post-tensioned precast concrete beams and columns showed a good agreement with experimental response while shear strength of post-tensioned precast concrete beam (S-10-L21 in Test 2) was little overestimated.

4. Shear strain and tensile stress in shear reinforcement of post-tensioned precast concrete column with round PT bar (R-15-H32 [2.10]) was underestimated. However, overall behavior of load-displacement of post-tensioned precast concrete member subjected to pure shear was well simulated by proposed method.

Analytical model for DT failure of prestressed concrete member which were excluded in this chapter will be clarified in next chapter.

8.1.4 Chapter 5

An analytical method to predict diagonal tension (DT) failure of RC and PC member was proposed. Based on the fundamental relation in fracture mechanics, debonding, sliding, and kinking energy of each reinforcement (non-prestressed longitudinal bar, prestressing steel, and shear reinforcement) on shear crack interface were obtained. Using the debonding, sliding, and kinking energy, analytical method to predict DT failure was proposed. For the verification of proposed analytical method, predicted web-shear cracking strength, failure modes, and the width of primary shear crack were compared to the observed ones. Analytical results from proposed method showed a good agreement with observed ones such as shear strength, crack width of primary shear crack, and failure mode. Further, minimum shear reinforcement ratio, ρ_m, to prevent the members from DT failure was analytically investigated. It pointed out that proposed method is effective and useful to propose the minimum ratio of shear reinforcement, ρ_m, in shear design of PC and RC members, if a/D and b/D are known.

8.1.5 Chapter 6

The main purpose of this study was to propose the prediction method for failure strength and deformation capacity of post-tensioned precast concrete members. To predict failure strength and failure mode of post-tensioned precast concrete member, a new analytical method considering the stress state of the concrete at

flexural compression zone and using the conventional section analysis was proposed. To predict shear strength for ST, SC, or DT failure, analytical models proposed in the Chapter 4 and 5 are used. For the shear strength for FSC failure, the shear capacity of the concrete at flexural compression zone is assumed to be provided by the intact concrete in the compression zone. Further, drift angle at flexural failure of post-tensioned precast concrete members also is evaluated by the proposed method using the rocking deformation model. Deformations due to pulling-out of prestressing steel at joint interface and due to flexural deformation in outside joint interface are considered as the total deformation of post-tensioned precast concrete member. For the verification, analytical results such as failure strength, failure mode, and drift angle at flexural failure predicted by the proposed method were compared to observed ones. The principle findings of this study are summarized as follows:

1. Based on the stress state of the concrete at the flexural compression zone, shear strength due to deterioration of shear capacity of the concrete, V_{cc}, can be obtained.

2. By the comparison between shear strengths, V_{cc} and V_u, and the flexural strength, V_{fu}, the failure modes were predicted.

3. Rocking deformation model in which only pulling-out deformation of prestressing steel at joint interface is considered is the effective deformation model to simulate deformation properties of post-tensioned precast concrete members.

4. The predicted results (shear strength, flexural strength, failure mode, and drift angle at flexural failure) produced by the proposed method evaluated the observed ones in a good accuracy.

8.1.6 Chapter 7

The main purpose of this study was to investigate the effect of bond stress in PT tendon and the amount of non-prestressed longitudinal mild-strength bars on structural behaviors of prestressed concrete beams. Based on the FEM analyses, the structural behaviors of the beams with unbonded and bonded tendons were discussed. The conclusions obtained are summarized as follows.

4. The maximum load capacities of the beams with bonded tendons (round or deformed bars) were approximately 10% larger than those of the beams with unbonded tendons.

5. The larger amount of non-prestressed mild-strength longitudinal bars was provided, the larger hysteretic energy dissipation capacity (equivalent viscous damping factor, h_{eq}) was obtained: at R=1.2%, the beams with ρ_r = 1.4% developed the energy dissipation capacity of h_{eq} = 0.47 while those with ρ_r = 0.7% developed the energy dissipation capacity of h_{eq} = 0.4.

6. The larger amount of non-prestressed mild-strength longitudinal bars was provided, the larger residual deformation was observed: at R=1.2%, the residual drift angles of 0.8% in the beams with ρ_r = 1.4% developed while those of 0.4 % in the beams with ρ_r = 0.7% did.

8.2 Future work

Several additional problems encountered during the research work for the thesis could not be directly applied to practical structural design field. To establish the rational structural design procedure and development of prestressed / precast concrete structures, the following research topics are suggested.

1. New analytical model proposed in this study (Chapter 4 to 6) can not be applied to practical structural design procedure because of sophisticate calculation procedures. Therefore, more simplified and rational structural design procedure reflecting the failure mechanism of prestressed / precast concrete members needs to be developed.

2. In Chapter 6, drift angle post-tensioned precast concrete members at flexural failure was predicted by the proposed analytical model. However, predicted drift angel by the analytical method did not evaluate some observed drift angle in a good accuracy. Therefore, further investigation on estimation of total deformation of post-tensioned precast concrete members is expected.

3. As shown in Chapter 7, amount of mild-strength longitudinal bar significantly affect the structural behavior of prestressed concrete beams. However, effect of other analytical parameters such as compressive strength of concrete, yield strength of shear reinforcement, amount of prestressing steel in a section on structural behavior is not clear yet. Moreover, structural behavior of post-tensioned precast concrete member was not investigated by FEM analysis. Further investigation on structural

behavior of members with various structural type and parameters needs.

本論文は，筆者の過去 5 年間の研究成果をまとめたものであります。この間，多くの先生方，同僚の皆様より暖かい御指導及び御鞭撻を頂きました。

京都大学工学研究科教授西山峰広先生には，私が研究生活に入りました 2008 年より，研究者のあるべき姿を教えていただく伴に，本研究全般に亘る御指導を賜りました。ここに多大な感謝の意を表します。

京都大学防災研究所教授田中仁史先生には，将来研究者として歩いていくべき研究者像や研究に関する様々なアドバイスを頂きました。なお，本論文の審査も頂き，ここに感謝の意を表します。

東京工業大学応用セラミックス研究所教授河野進先生及び京都大学工学研究科助教坂下雅信先生には，実験研究における試験体設計・製作や実験装置運営に関する御教えを頂きました。ここに深く感謝いたします。

本論文を審査していただきました京都大学教授吹田啓一郎先生からは，有意義な御意見，厳しいご指摘をいただきました。

蔚山大学教授朴淳規先生，公州大学副教授金吉熙，成均館大学教授李槙允先生からは，留学生活及び学業に関する様々な助言などを頂きました。御礼を申し上げます。

大阪工業大学教授仲塚佶先生，大阪大学教授倉本洋先生，ソウル大学教授朴鴻根先生・洪性傑先生，建築研究所研究員谷昌典さんからは，PC 構造に関する膨大な知識及び助言を頂きました。御礼を申し上げます。

京都大学工学研究科技官岩本敏憲さん及び野村昌弘さんには実験に必要な技術と知識を一から教えて頂き、実験作業のすべてにおいて御協力及び御指導頂きました。秘書の津田有輝子さんには、研究室の研究活動を円滑に進められるよういつも環境を整えてくださいました。皆様に御礼申し上げます。

最後に，私事で恐縮でありますが，私が，勉学・研究に専念できる環境を与えてくれました両親，そして妻・敏姫に心より感謝いたします。

2013 年 3 月

이재만

Appendices

A.1 Stress-Strain Relationship of Materials in Test 1
A.1.1 Concrete

Figure A. 1 plots the stress-strain relationship of concrete used in Test 1.
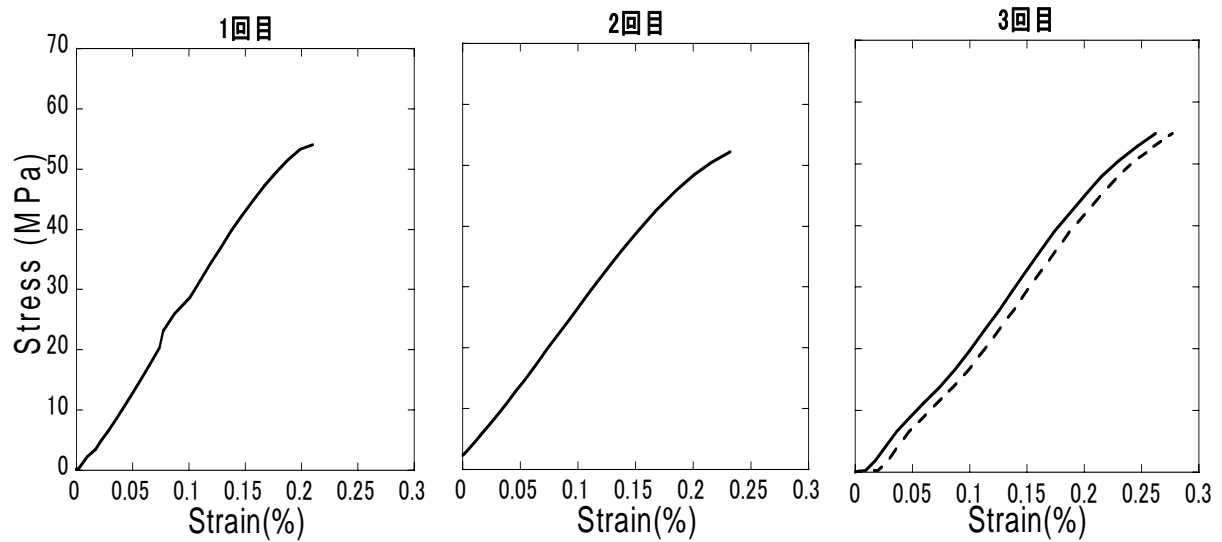
(a)　S-10-L42、S-10-L63(Before loading)
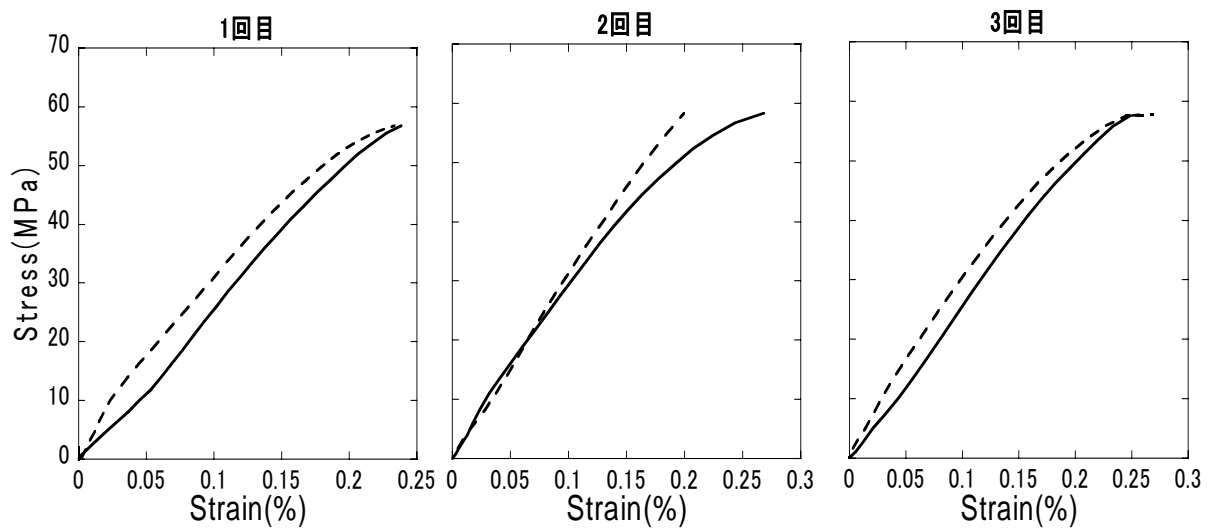
(b)　S-10-L42、S-10-L63(After loading)

Fig. A.1　Strain-strain relationship of concrete in Test 1
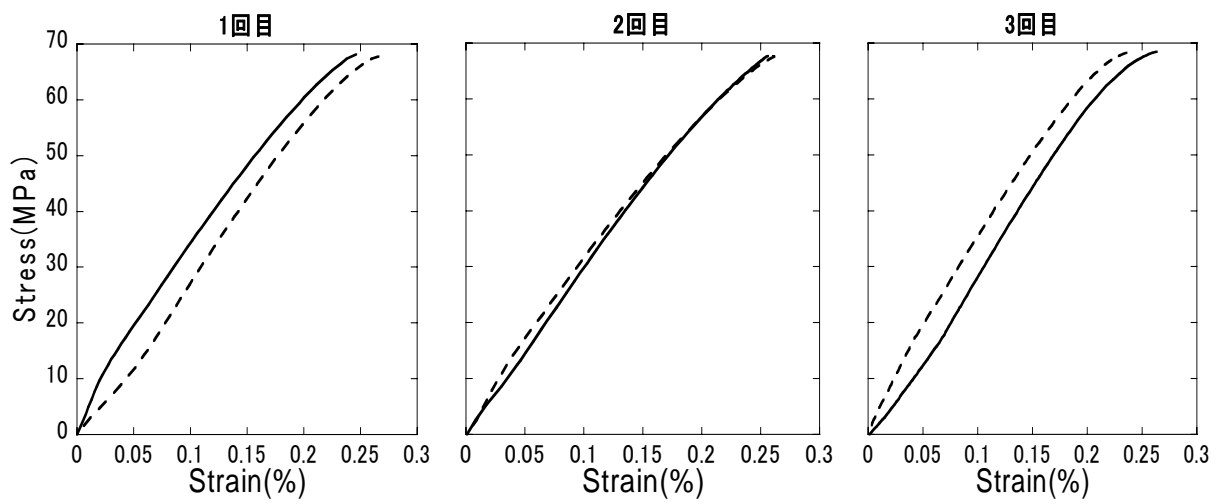
(c)　S-15-L21、S-15-L42、S-15-L63(Before loading)
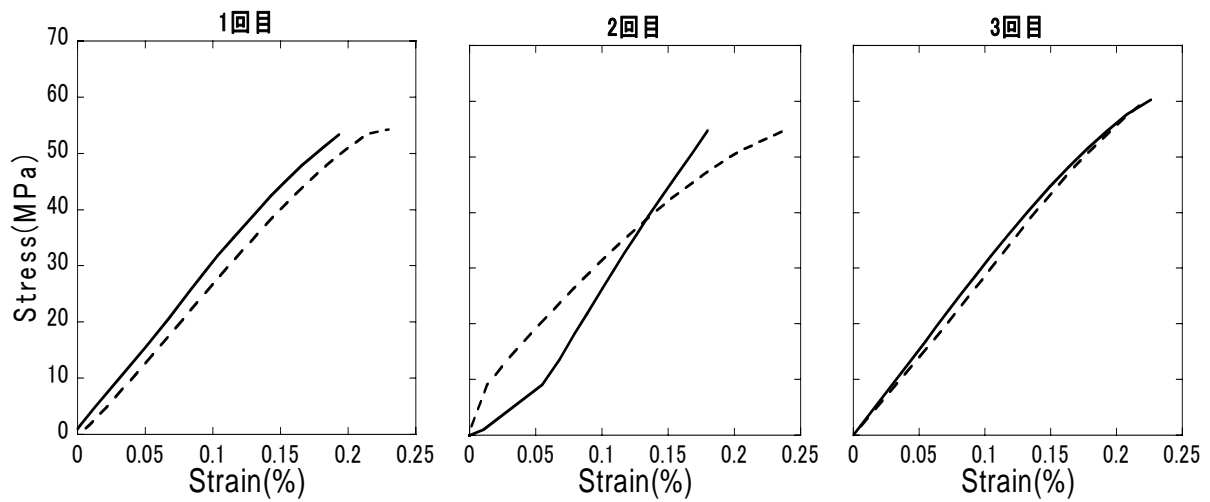
(d)　S-15-L21、S-15-L42、S-15-L63(After loading)
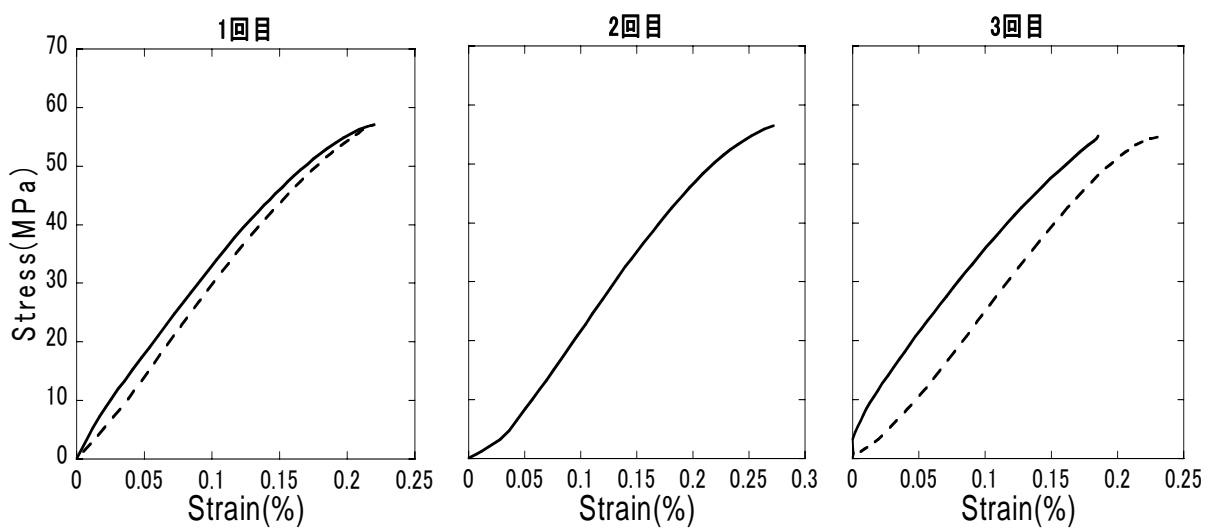
(e)　S-20-L21、S-20-L42(Before loading)

Fig. A.1　Strain-strain relationship of concrete in Test 1
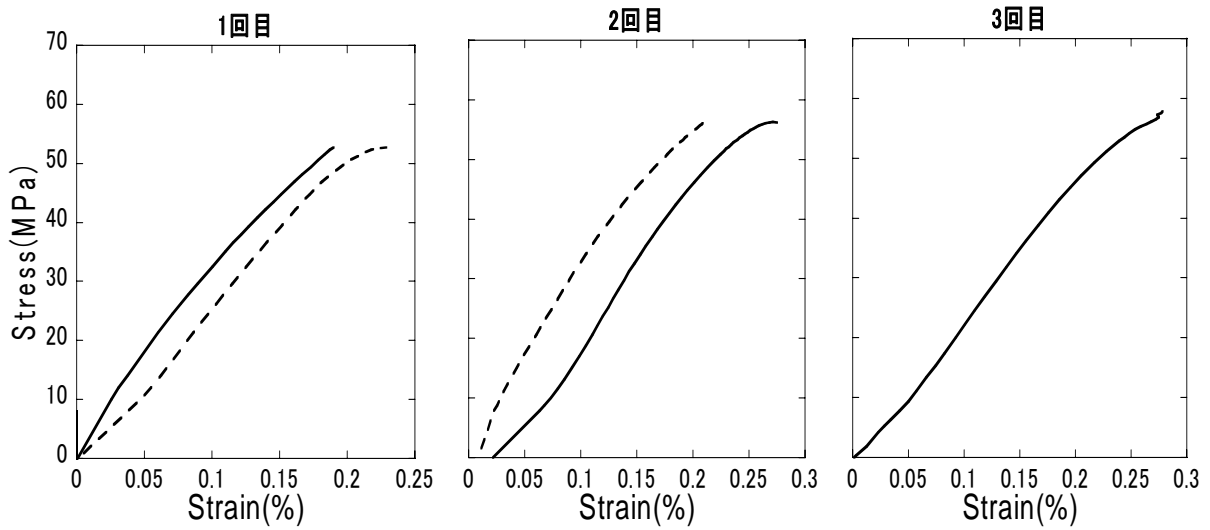
(f) S-20-L21、S-20-L42(After loading)

Fig. A.1 Strain-strain relationship of concrete in Test 1

A.1.2 Joint Mortar

Figure A. 2 plots the stress-strain relationship of joint mortar used in Test 1.
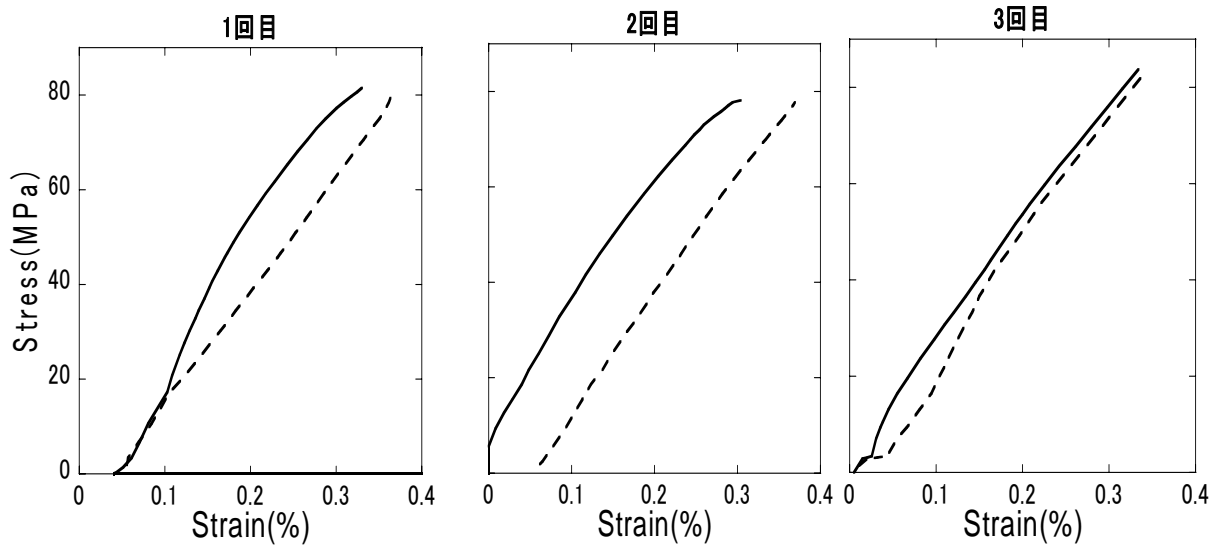
(a) S-10-L42、S-10-L63

Fig. A.2 Strain-strain relationship of joint mortar in Test 1
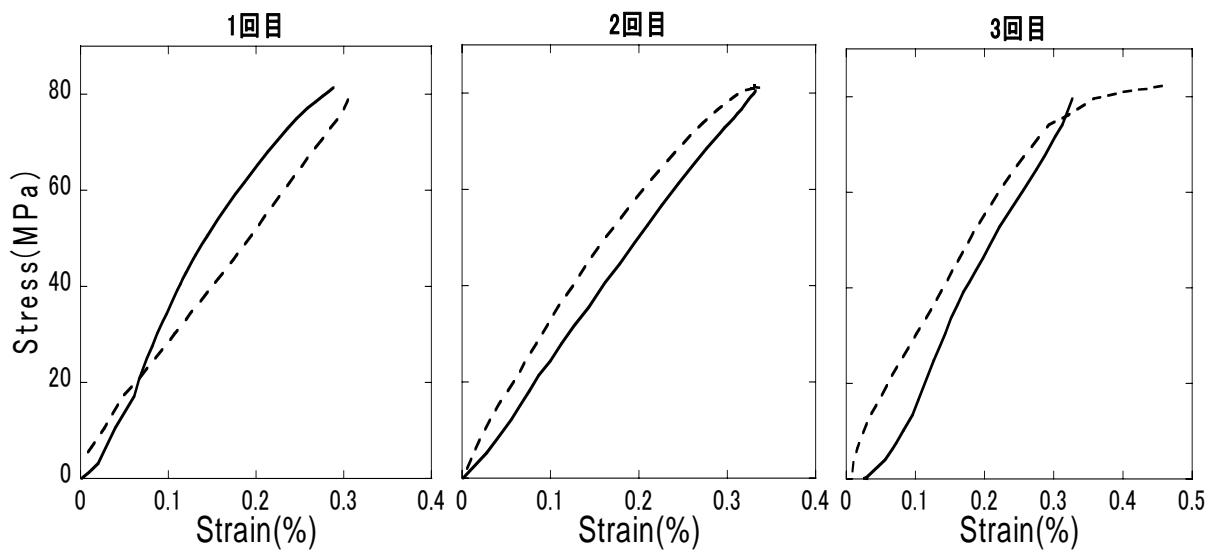
(b)　S-15-L21、S-15-L42、S-15-L63
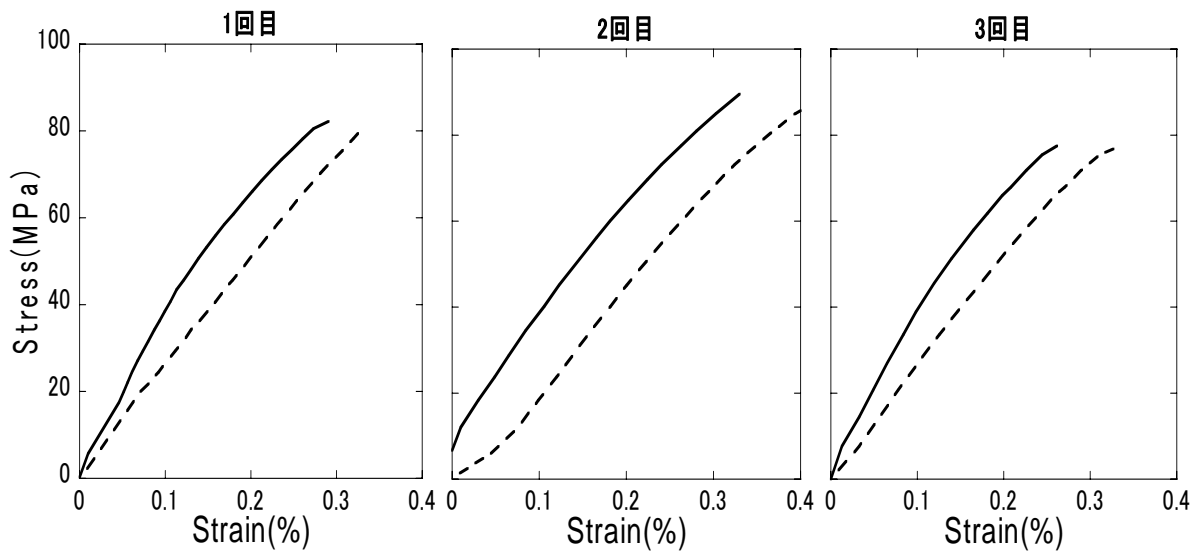
(c)　S-20-L21、S-20-L42

Fig. A.2　Strain-strain relationship of joint mortar in Test 1

A.1.3 Grouting Mortar

Figure A. 3 plots the stress-strain relationship of grouting mortar used in Test 1.
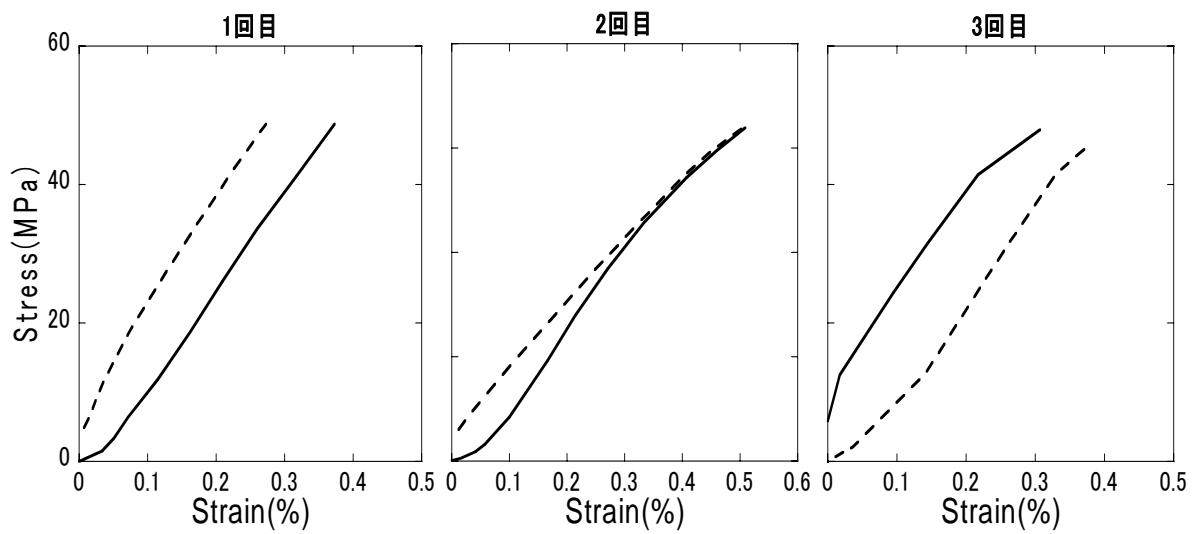
(a)　S-10-L42、S-10-L63
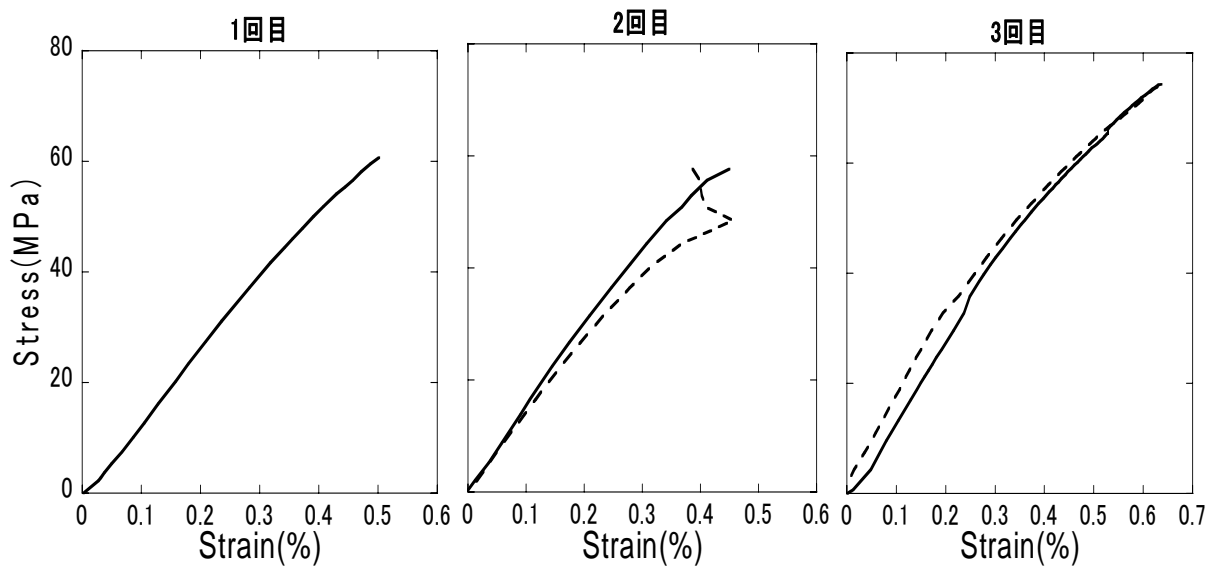
(b)　S-15-L21、S-15-L42、S-15-L63

Fig. A.3　Strain-strain relationship of grouting mortar in Test 1
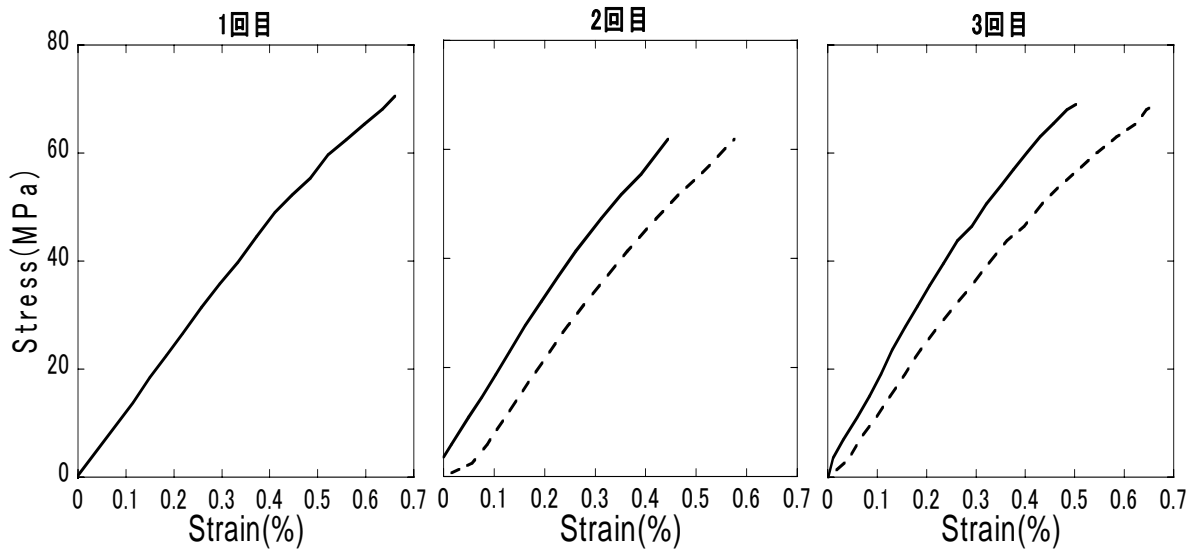
(c) S-20-L21、S-20-L42

Fig. A.3   Strain-strain relationship of grouting mortar in Test 1

A.1.4 Prestressing Strand

Seven-wired strands were used in the Test 1. Fig. A. 4 plots the stress-strain relationship of prestressing strands. The experimental result on seven seven-wired strands is plotted in Fig. A. 4.
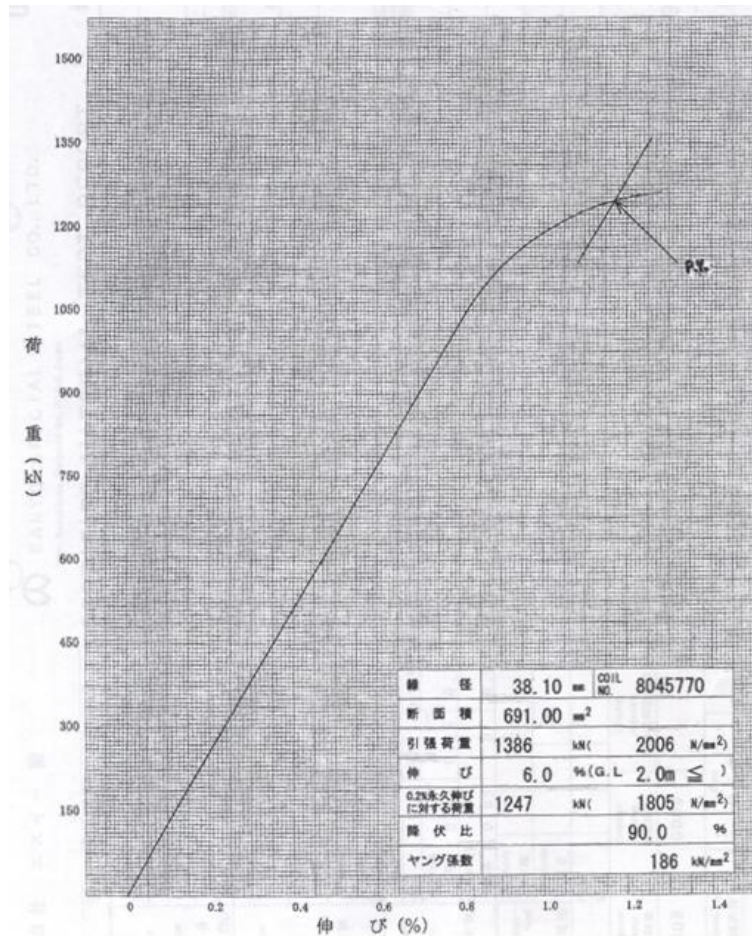
Fig. A.4   Strain-strain relationship of prestressing strands in Test 1

A.1.5 Non-Prestressed Longitudinal Bar

Figure A. 5 plots the stress-strain relationship of longitudinal bars used in Test 1.
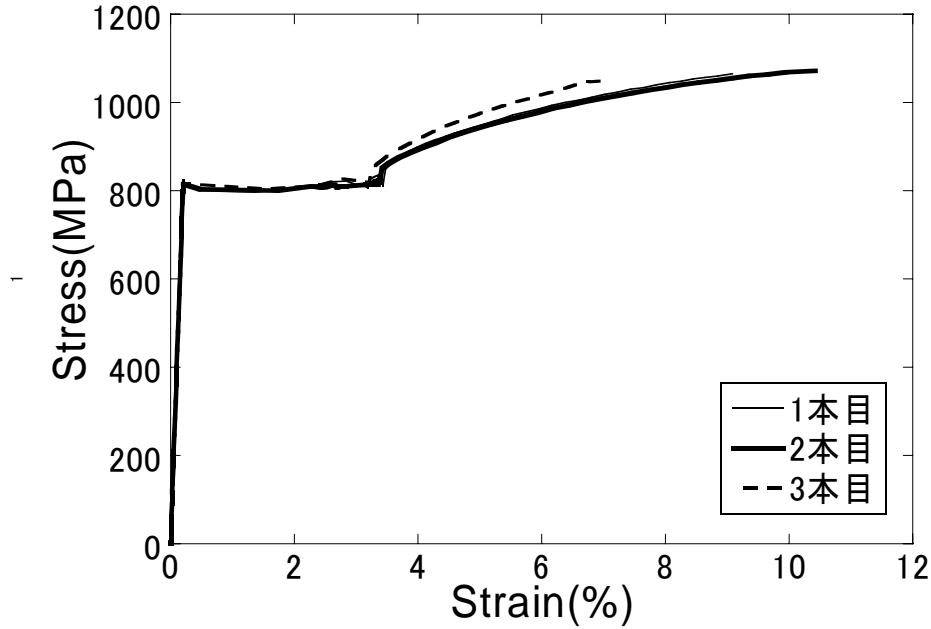
Fig. A.5   Strain-strain relationship of non-prestressed longitudinal bars in Test 1

A.1.6 Shear Reinforcement

Figure A. 6 plots the stress-strain relationship of shear reinforcements used in Test 1.
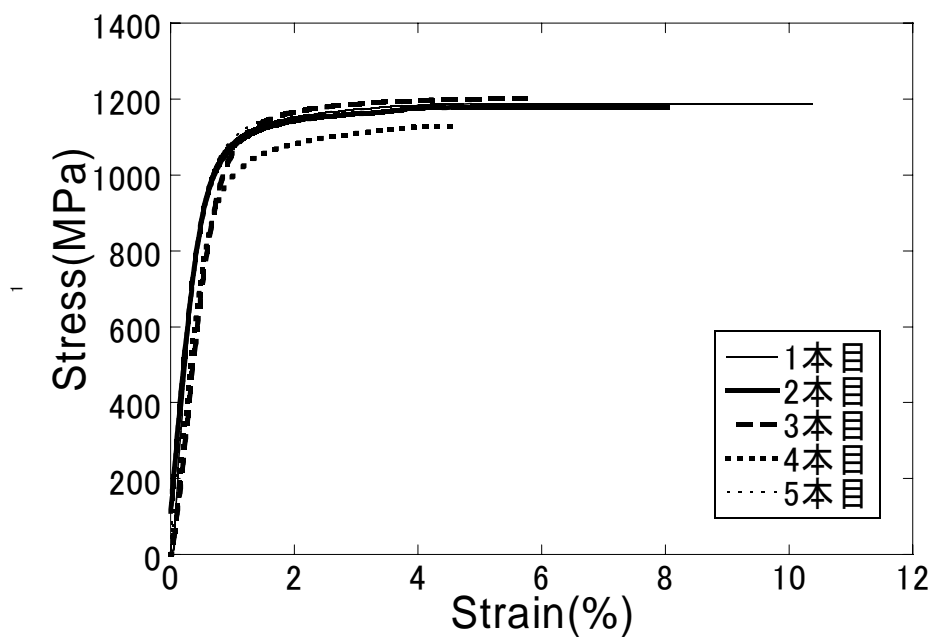
Fig. A.6   Strain-strain relationship of shear reinforcements in Test 1

A.2 Stress-Strain Relationship of Materials in Test 2
A.2.1 Concrete

Figure A. 7 plots the stress-strain relationship of concrete used in Test 2.
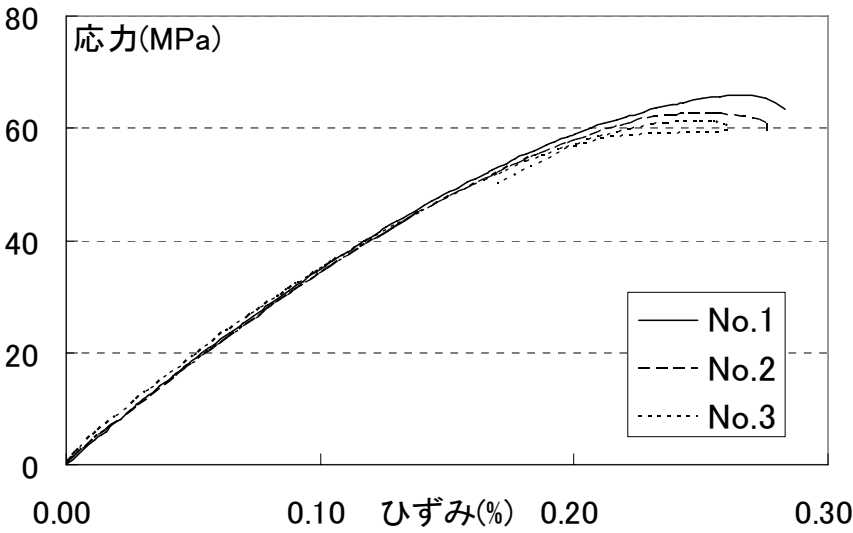
(a) Before loading
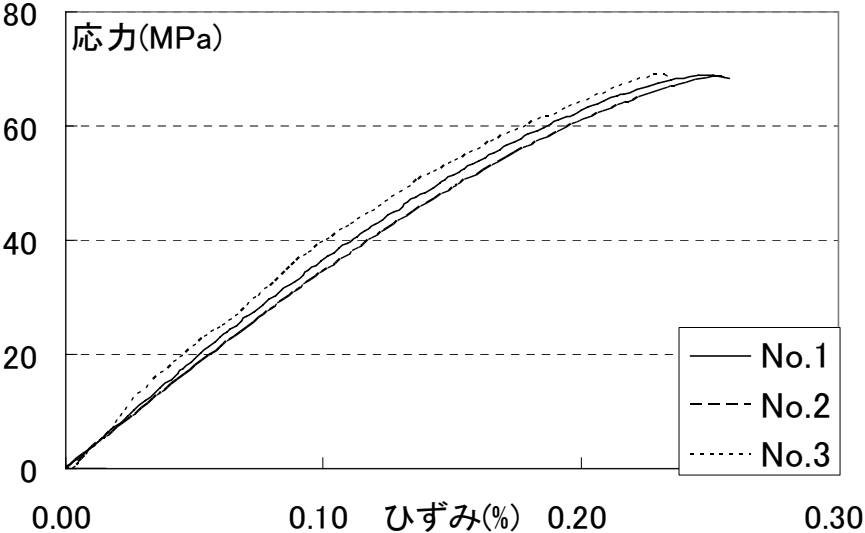
(b) After loading

Fig. A.6　Strain-strain relationship of concrete in Test 2

A.2.2 Joint Mortar

Figure A. 8 plots the stress-strain relationship of joint mortar used in Test 2.
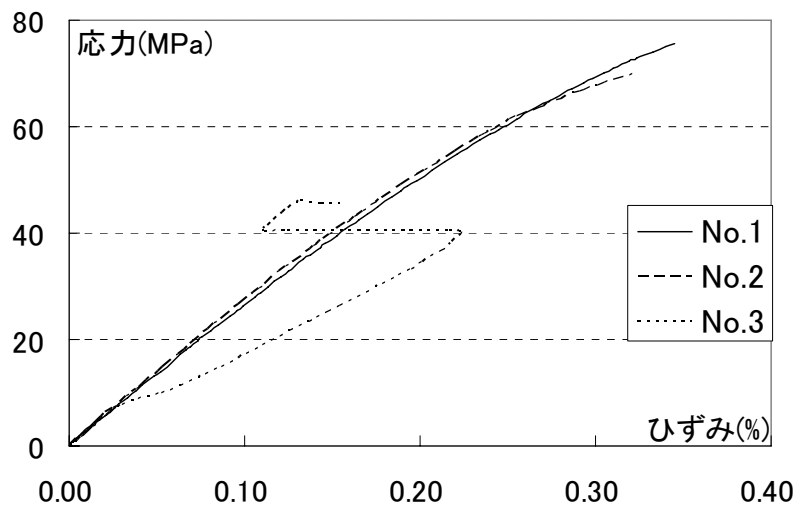
Fig. A.8　Strain-strain relationship of joint mortar in Test 2

A.2.3 Grouting Mortar

Figure A. 9 plots the stress-strain relationship of grouting mortar used in Test 2.
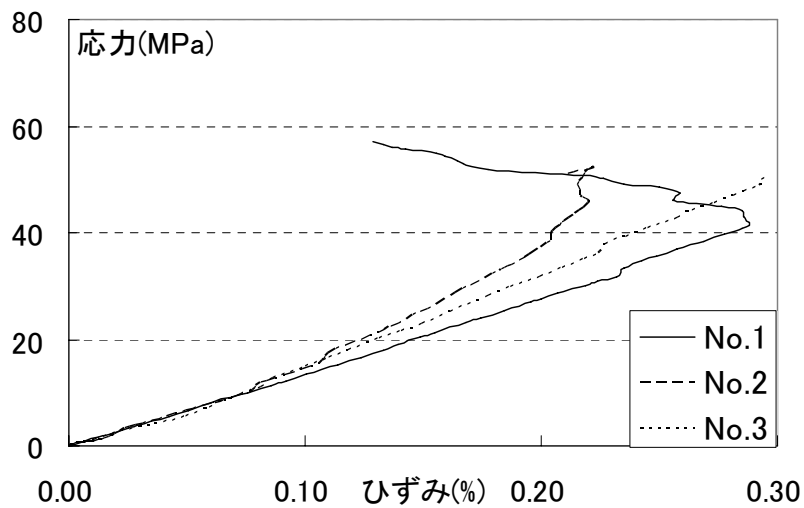
Fig. A.9　Strain-strain relationship of grouting mortar in Test 2

A.2.4 Prestressing Strand

Table A. 1 summarizes the material properties of prestressing strand used in Test 2.

Table A.1　Summary of material properties of prestressing strands in Test 2

Yielding force (kN)	Tensile force (kN)	Elongations (%)	Elastic modulus (Gpa)
2088	2316	7.0	194.7

A.2.5 Non-Prestressed Longitudinal Bar

Figure A. 10 plots the stress-strain relationship of non-prestressed longitudinal bars used in Test 2.
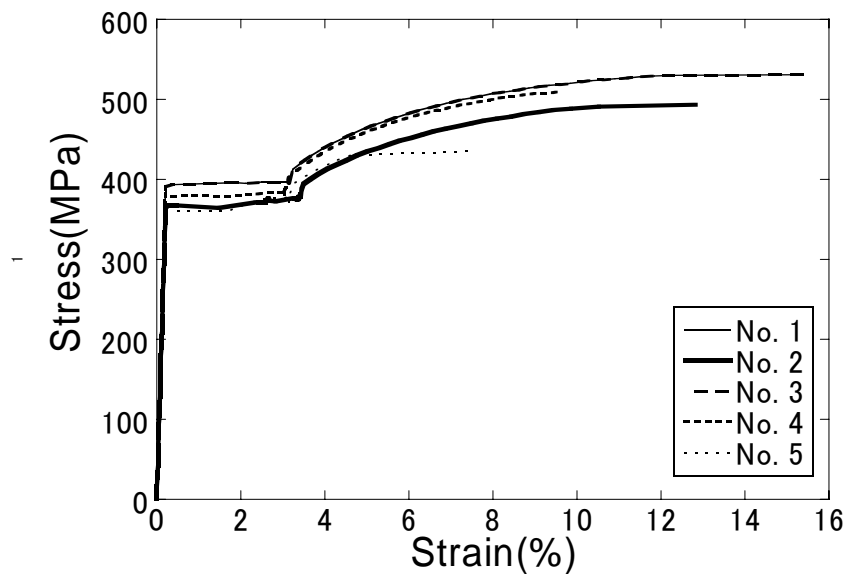
Fig. A.10　Strain-strain relationship of non-prestressed longitudinal bars in Test 2

A.2.6 Shear Reinforcement

Figure A. 11 plots the stress-strain relationship of shear reinforcement used in Test 2.
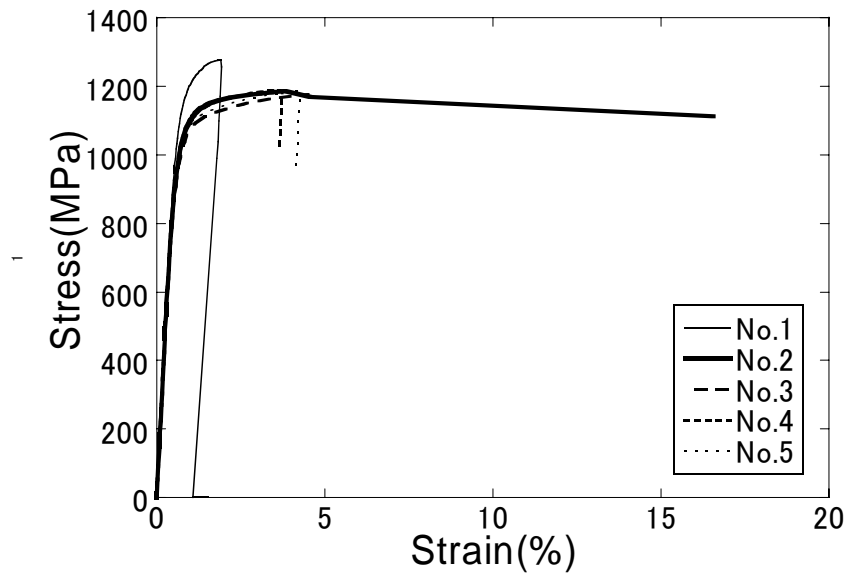
Fig. A.11　Strain-strain relationship of shear reinforcement in Test 2

A.3 Strain Distributions of Materials in Test 1
A.3.1 Prestressing Strands

Figure A. 12 plots the strain distributions of prestressing strands used in Test 1.
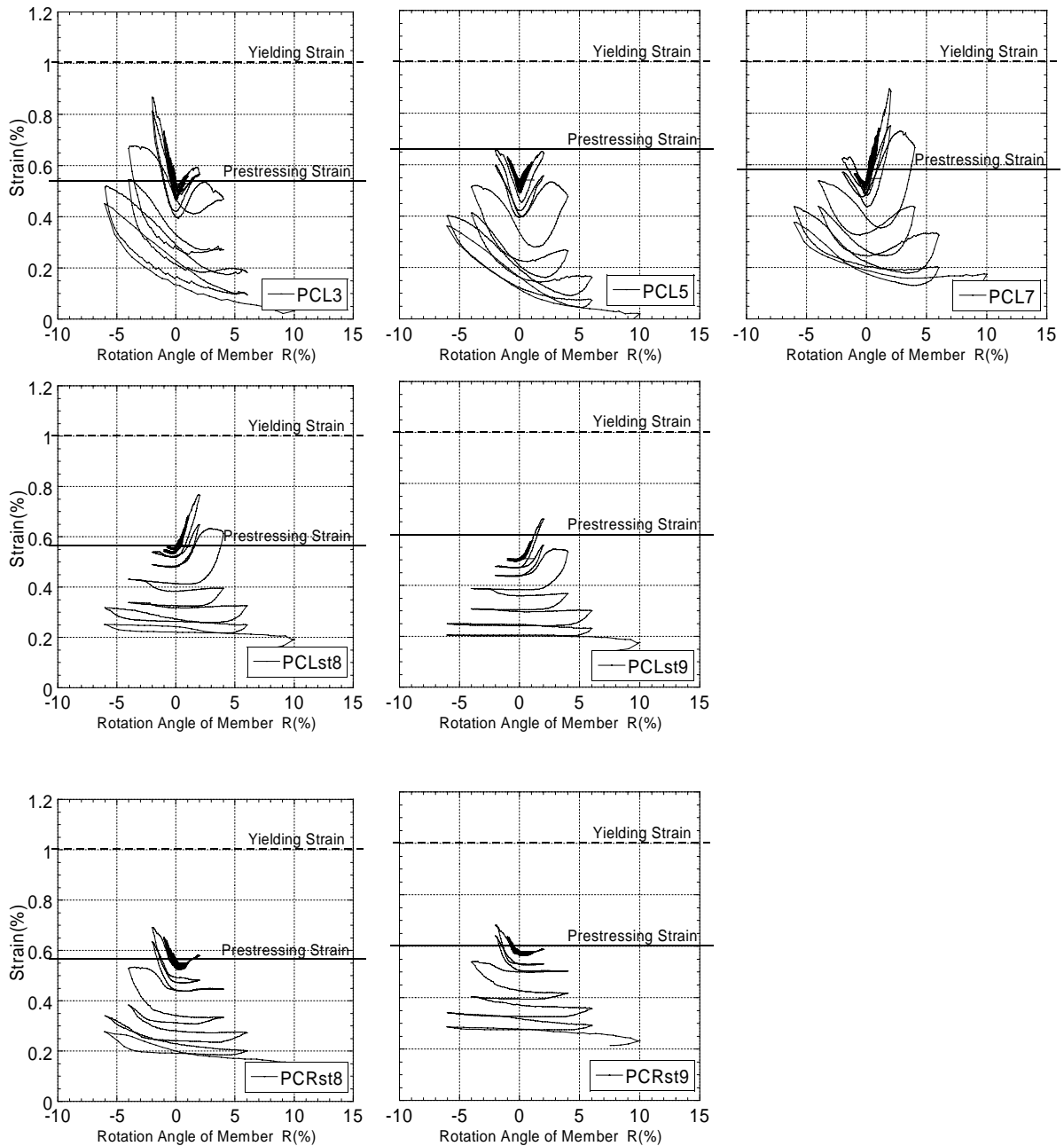
(a)   S-10-L42

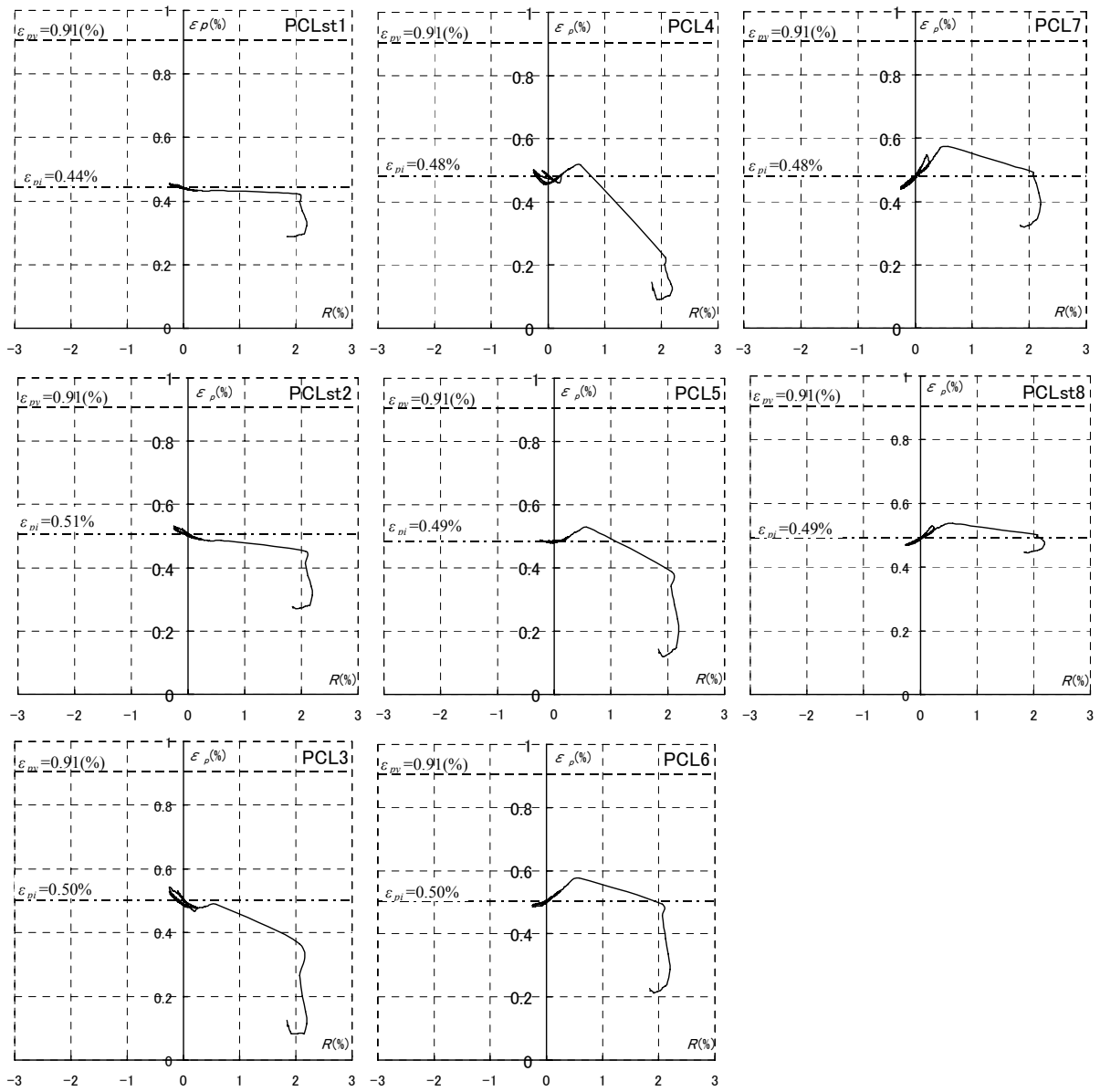Fig. A.12   Strain distribution of prestressing strands in Test 1
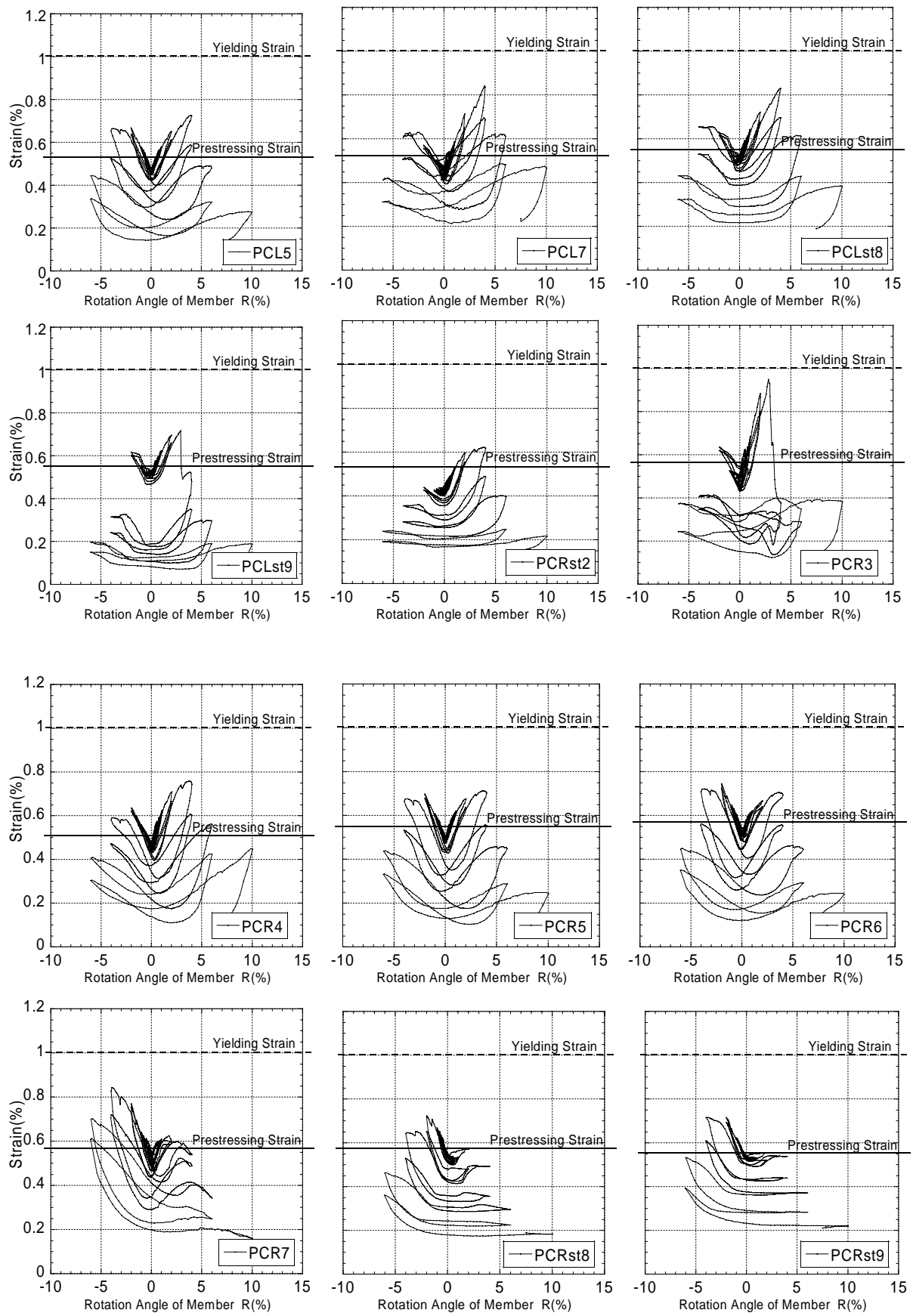
(b)   S-10-L63

Fig. A.12   Strain distribution of prestressing strands in Test 1

249
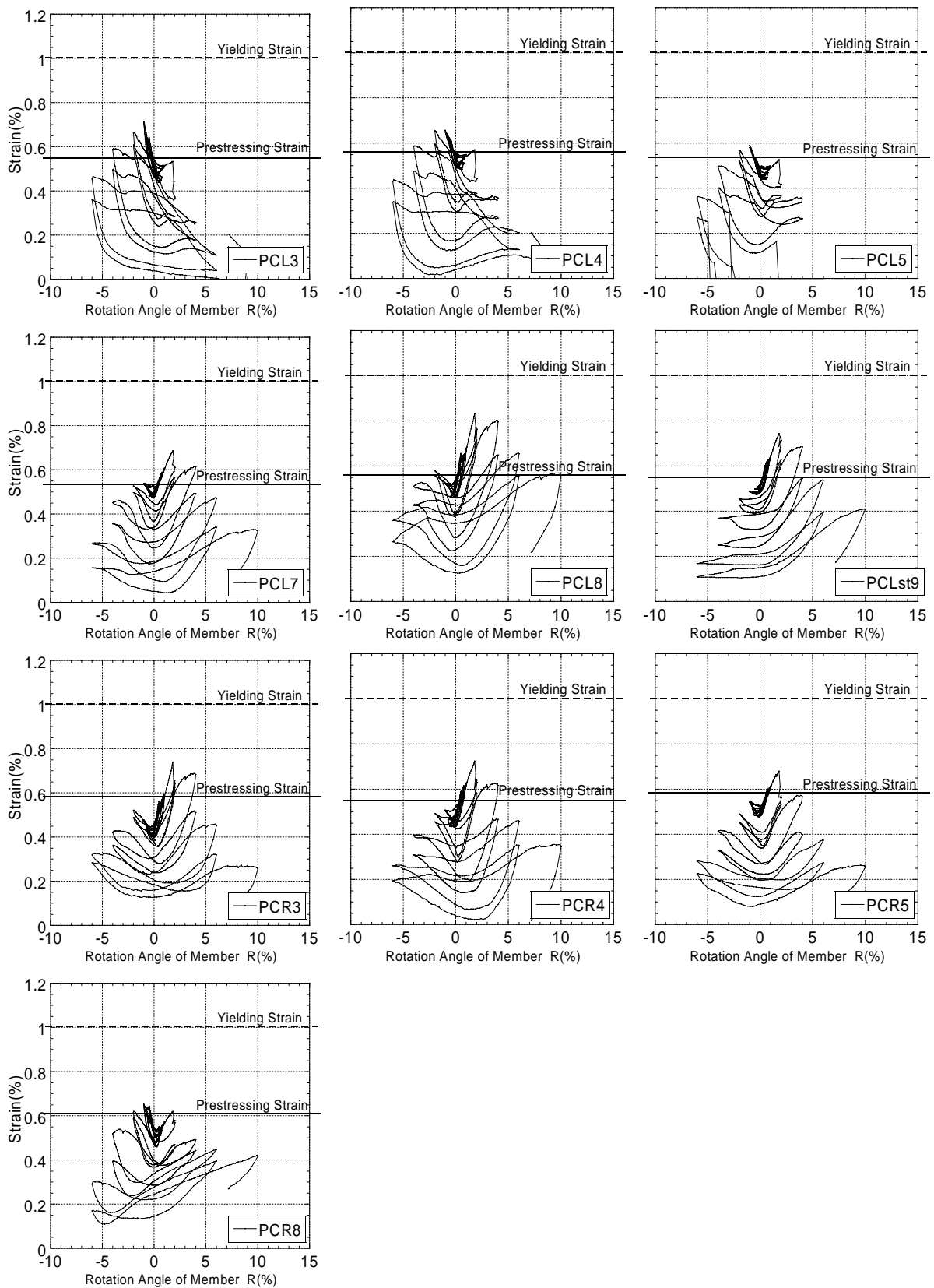
(c) S-15-L21
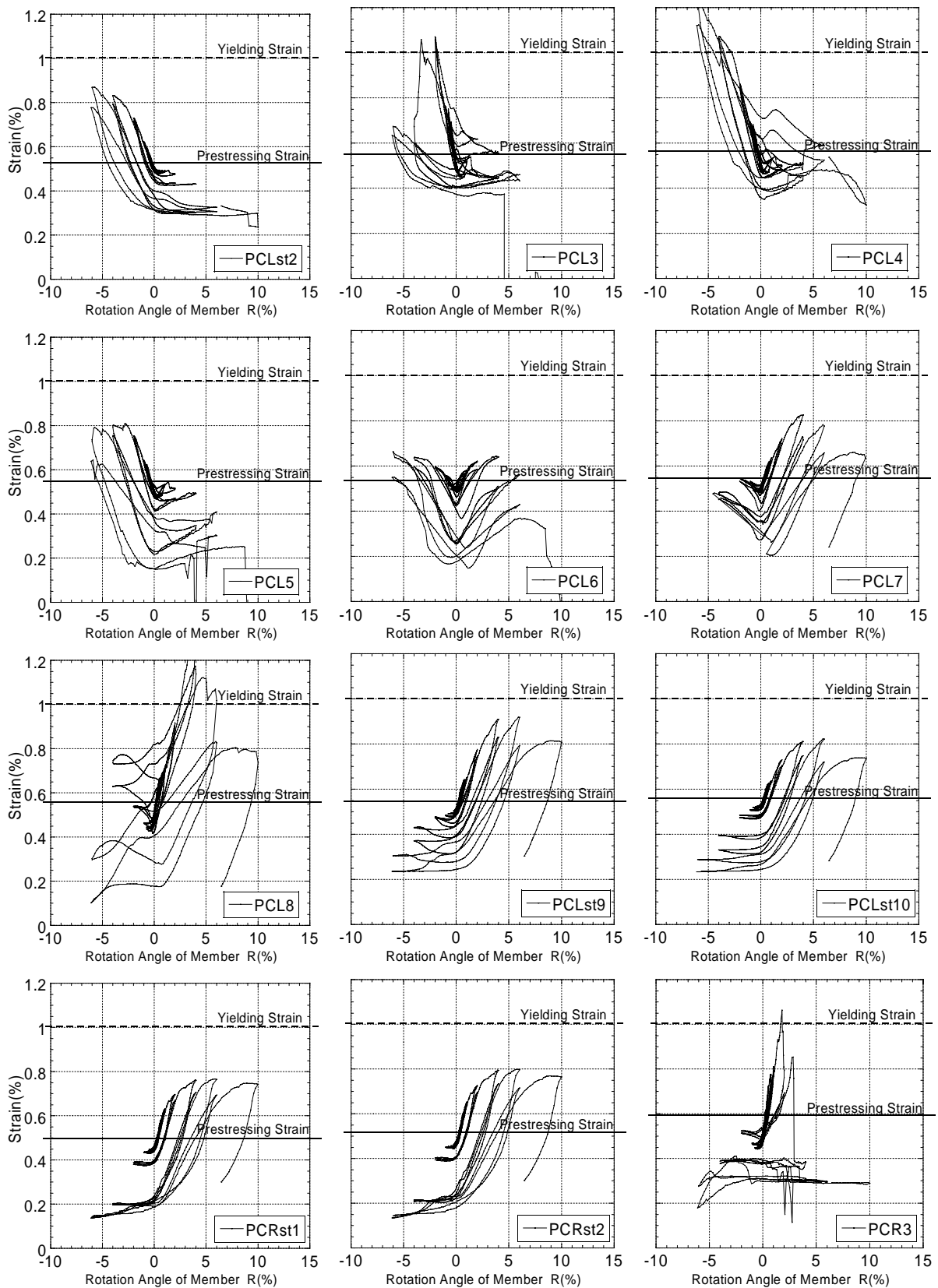
Fig. A.12 Strain distribution of prestressing strands in Test 1

(d) S-15-L42

Fig. A.12 Strain distribution of prestressing strands in Test 1

251

(d)　S-15-L42

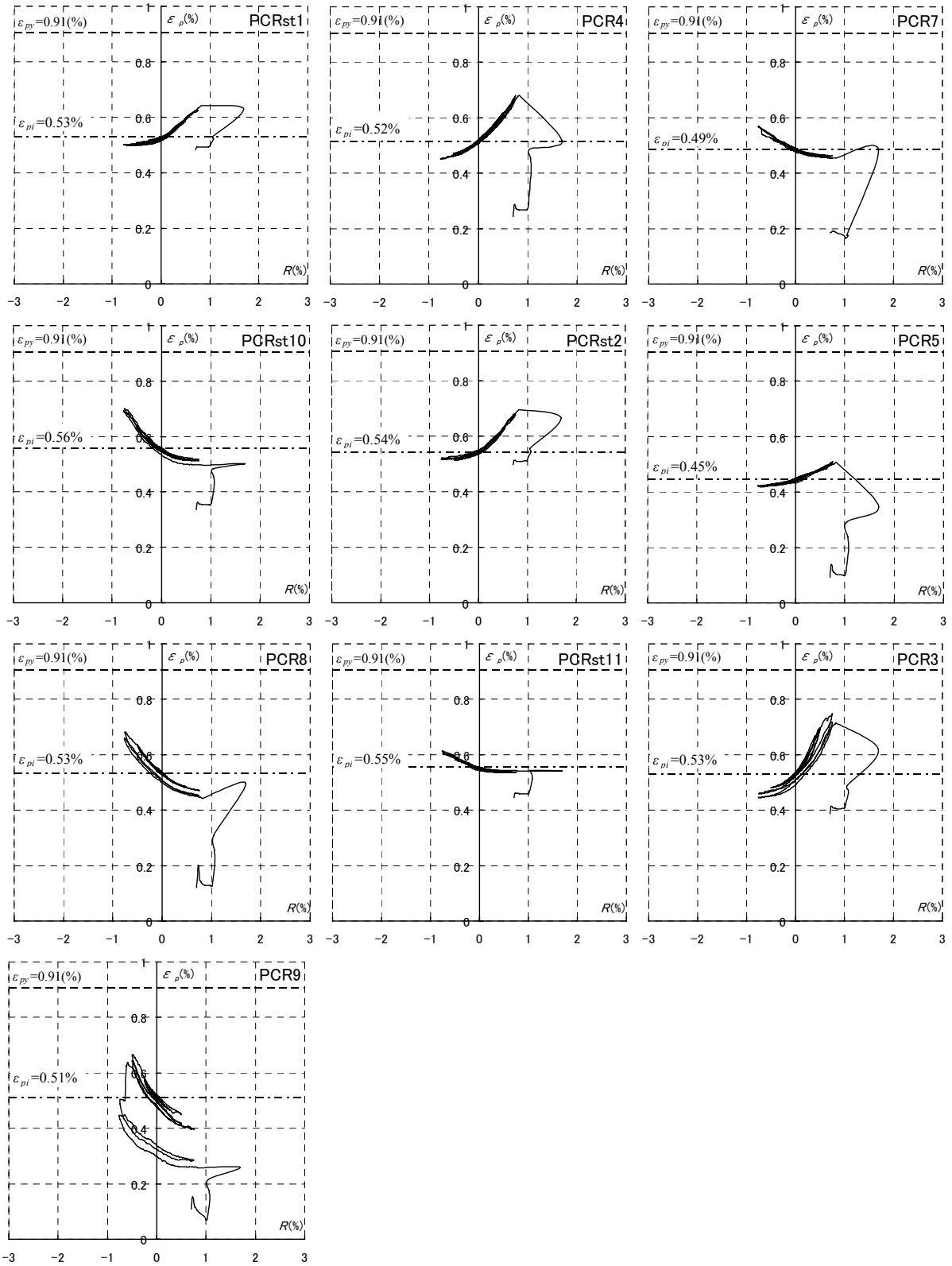Fig. A.12　Strain distribution of prestressing strands in Test 1

252
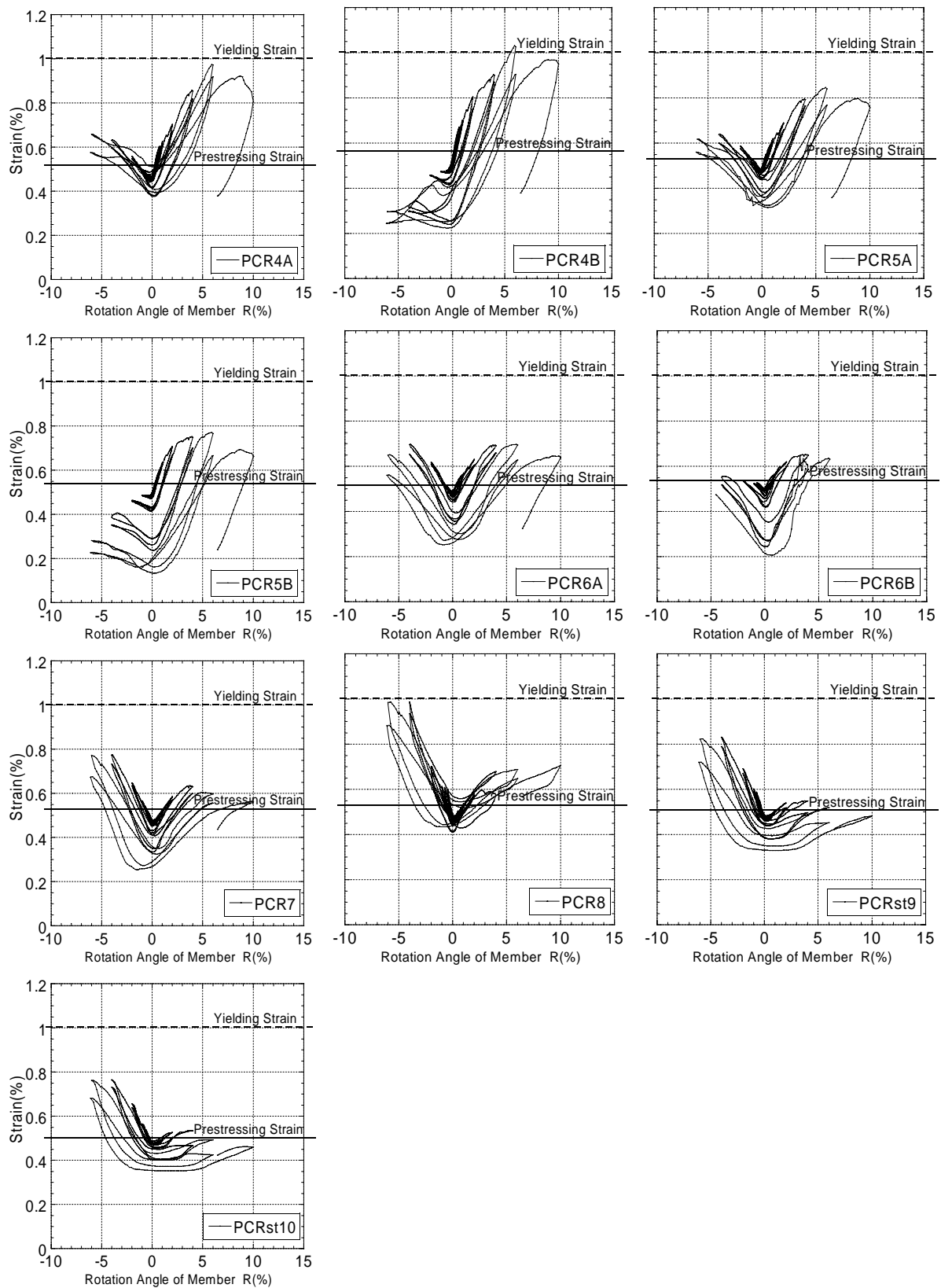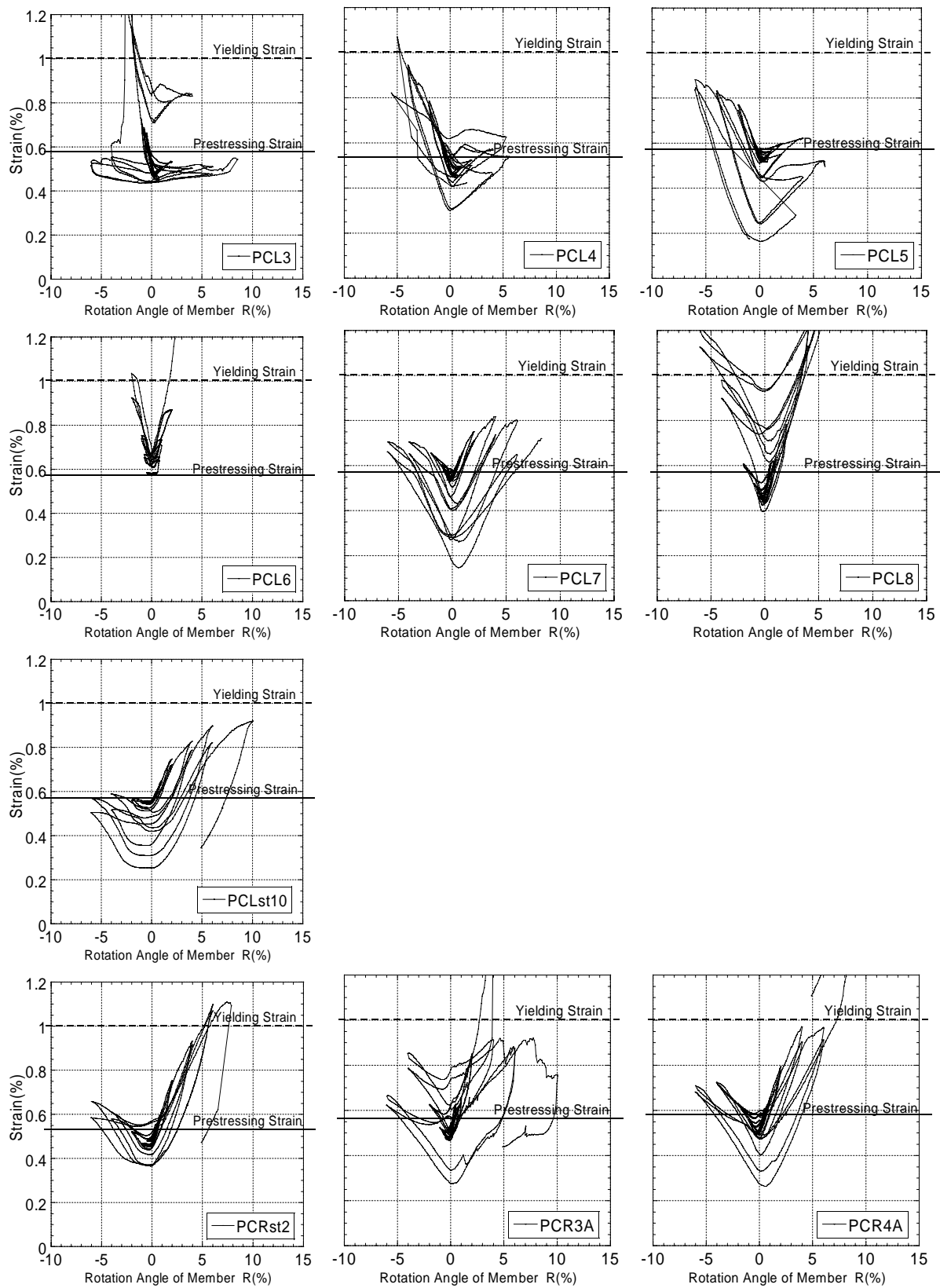
(e) S-15-L63

Fig. A.12 Strain distribution of prestressing strands in Test 1

253

(e)   S-15-L63

(f)   S-20-L21

Fig. A.12   Strain distribution of prestressing strands in Test 1

254
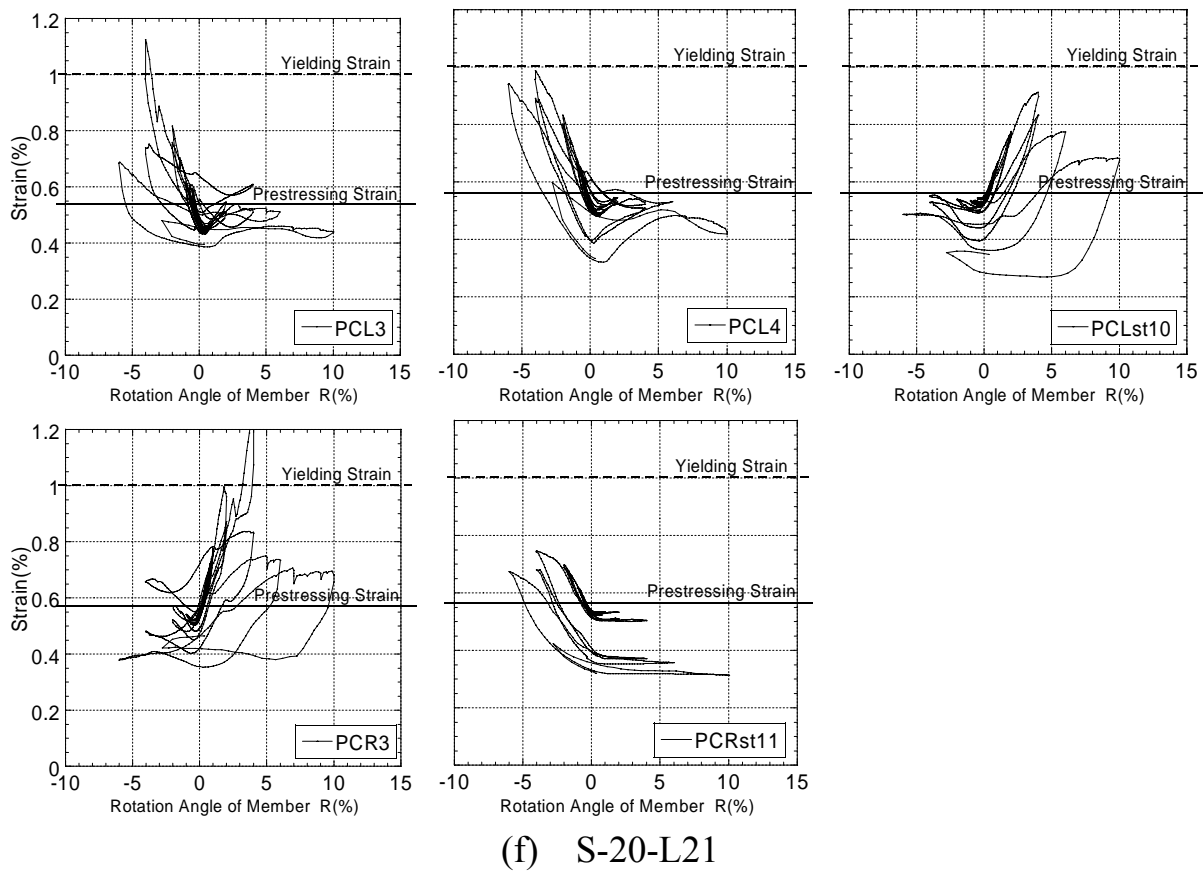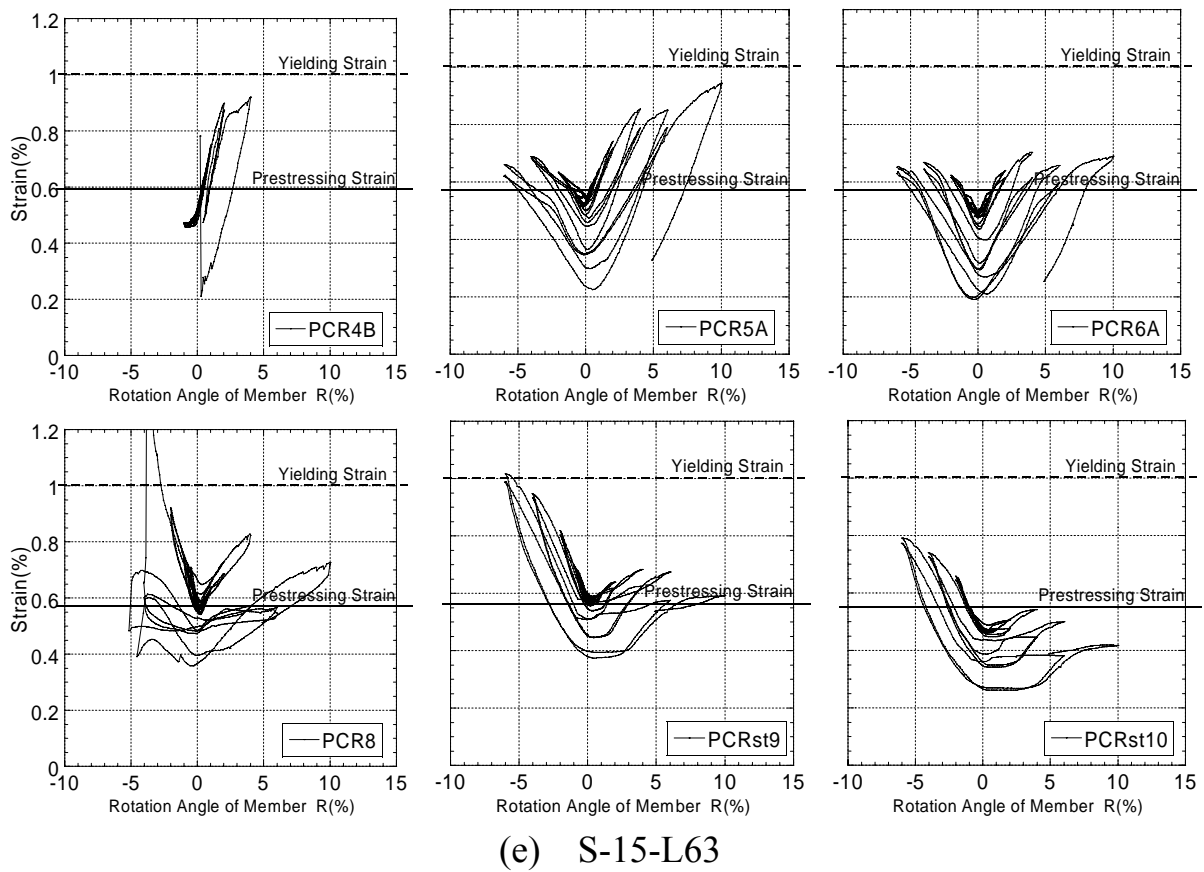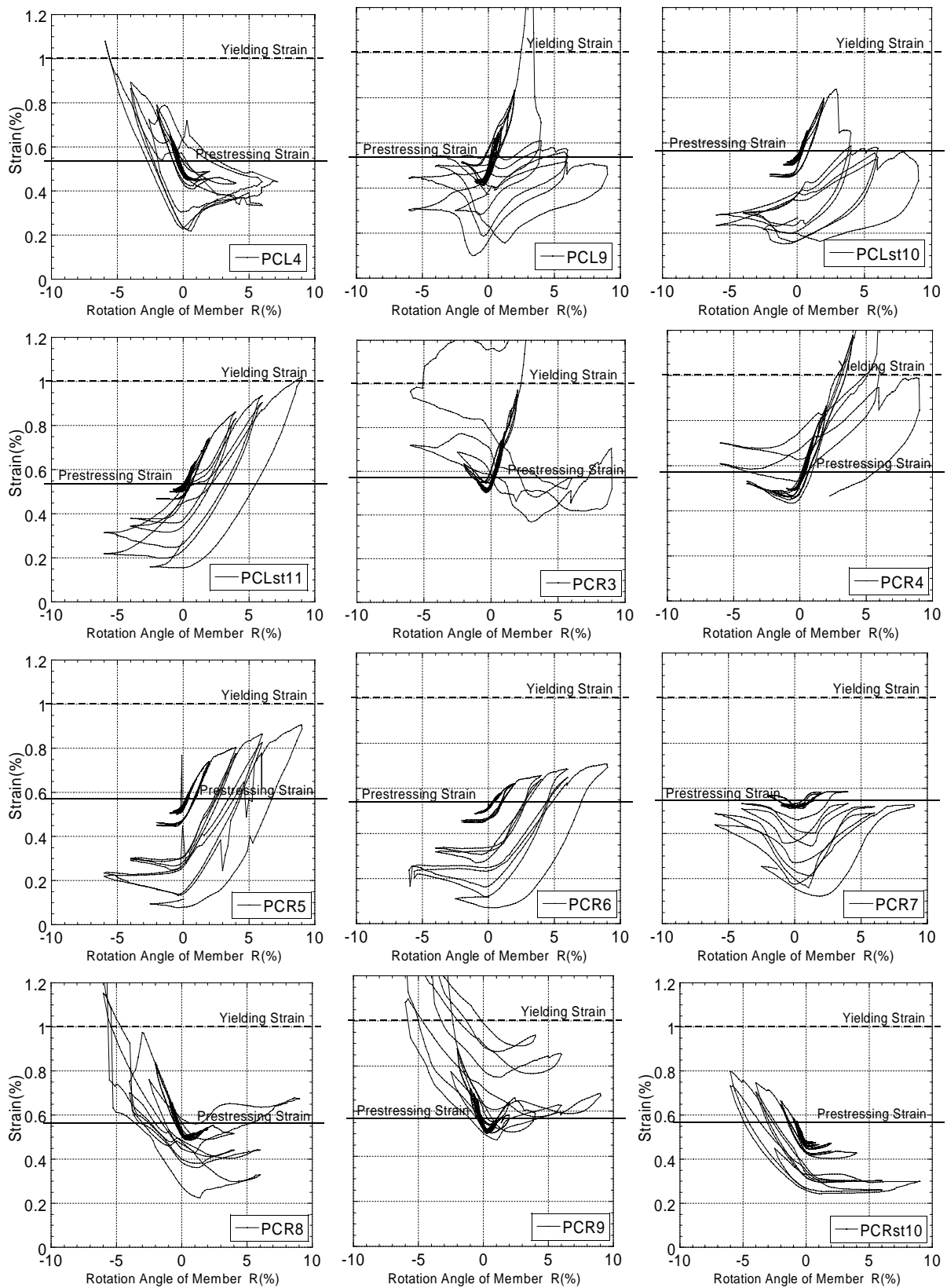
(g) S-20-L42
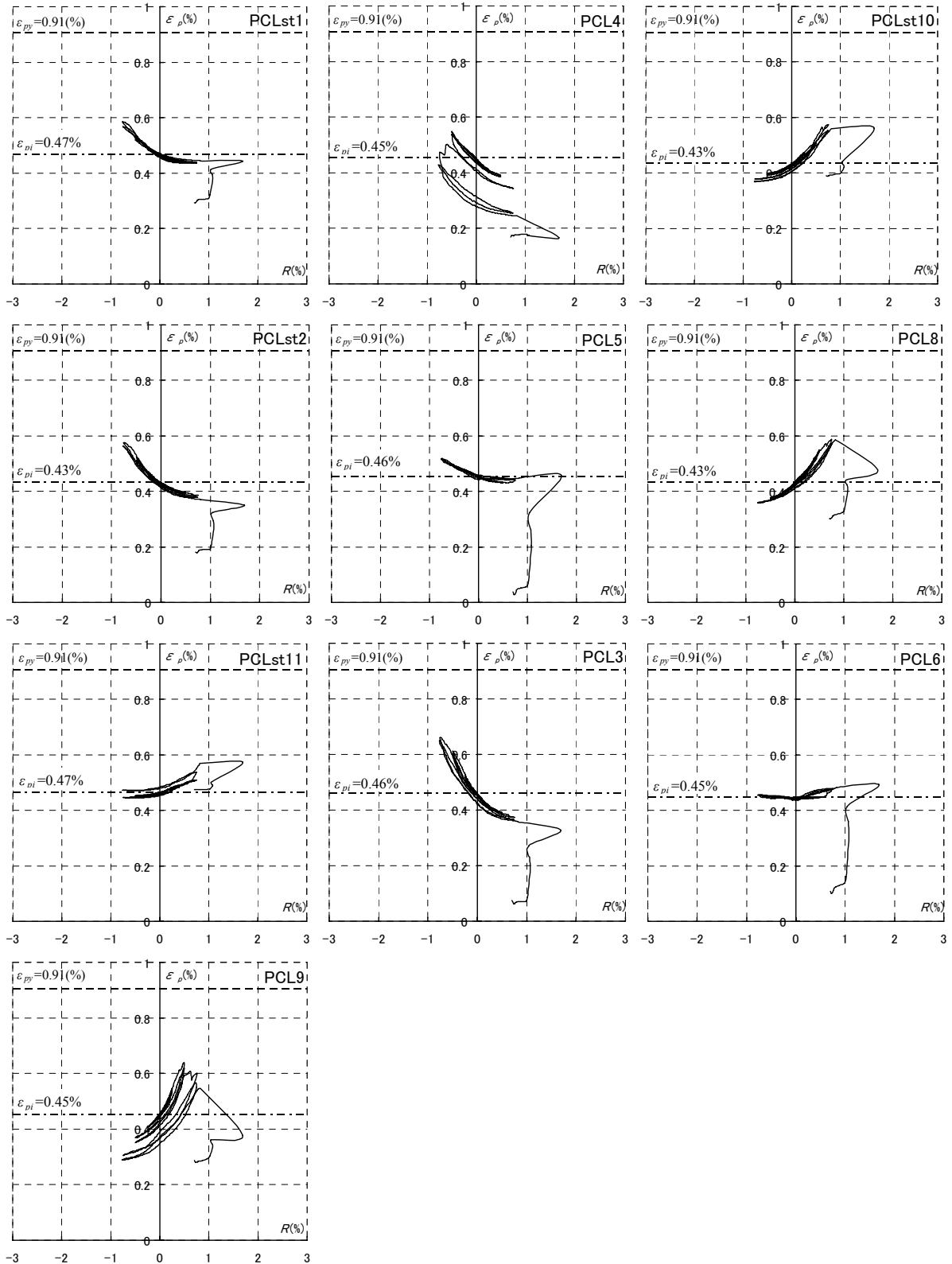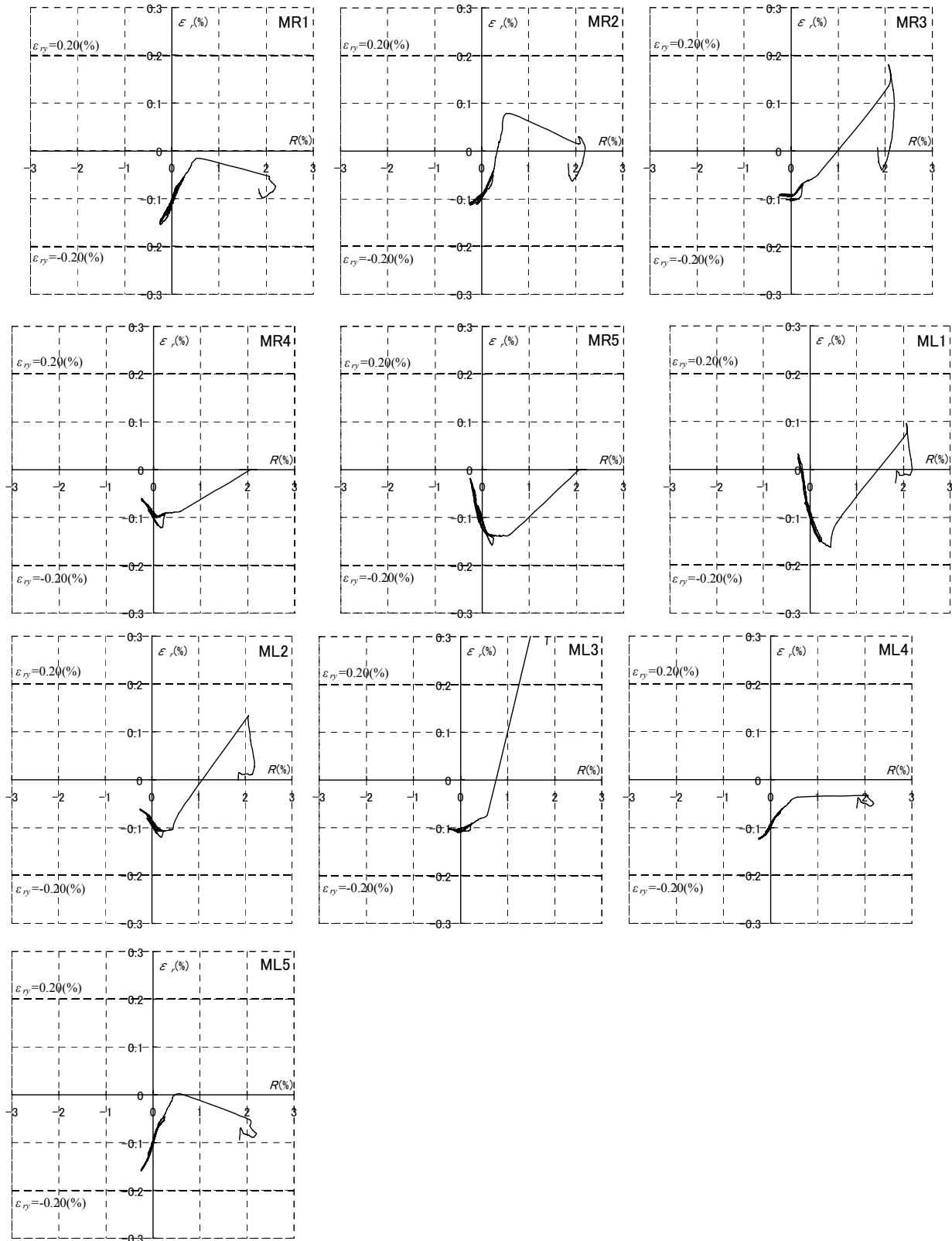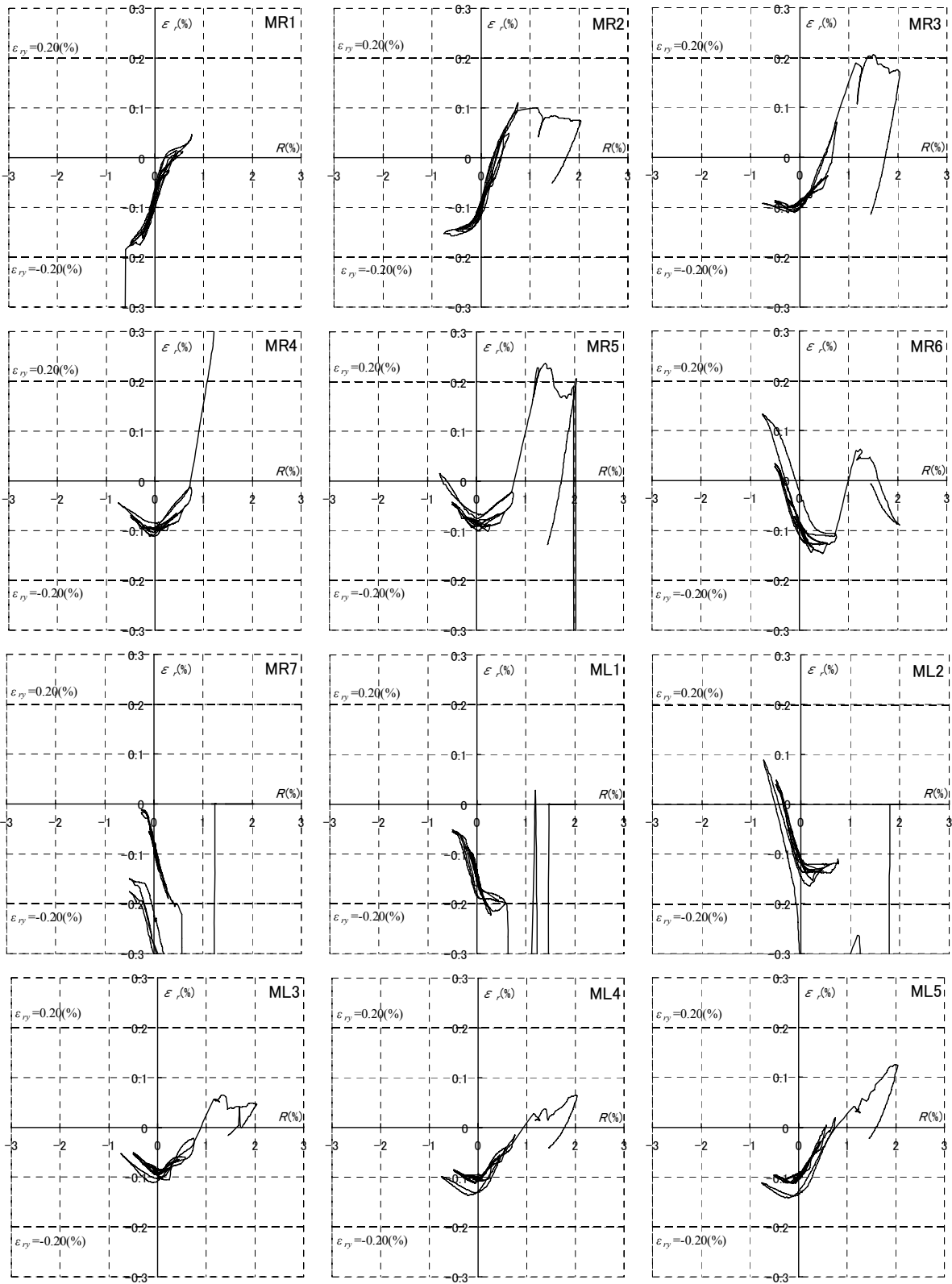
Fig. A.12 Strain distribution of prestressing strands in Test 1

255

A.3.2 Non-Prestressed Longitudinal Bar

Figure A. 13 plots the strain distributions of non-prestressed longitudinal bars used in Test 1.

(a)　S-10-L42
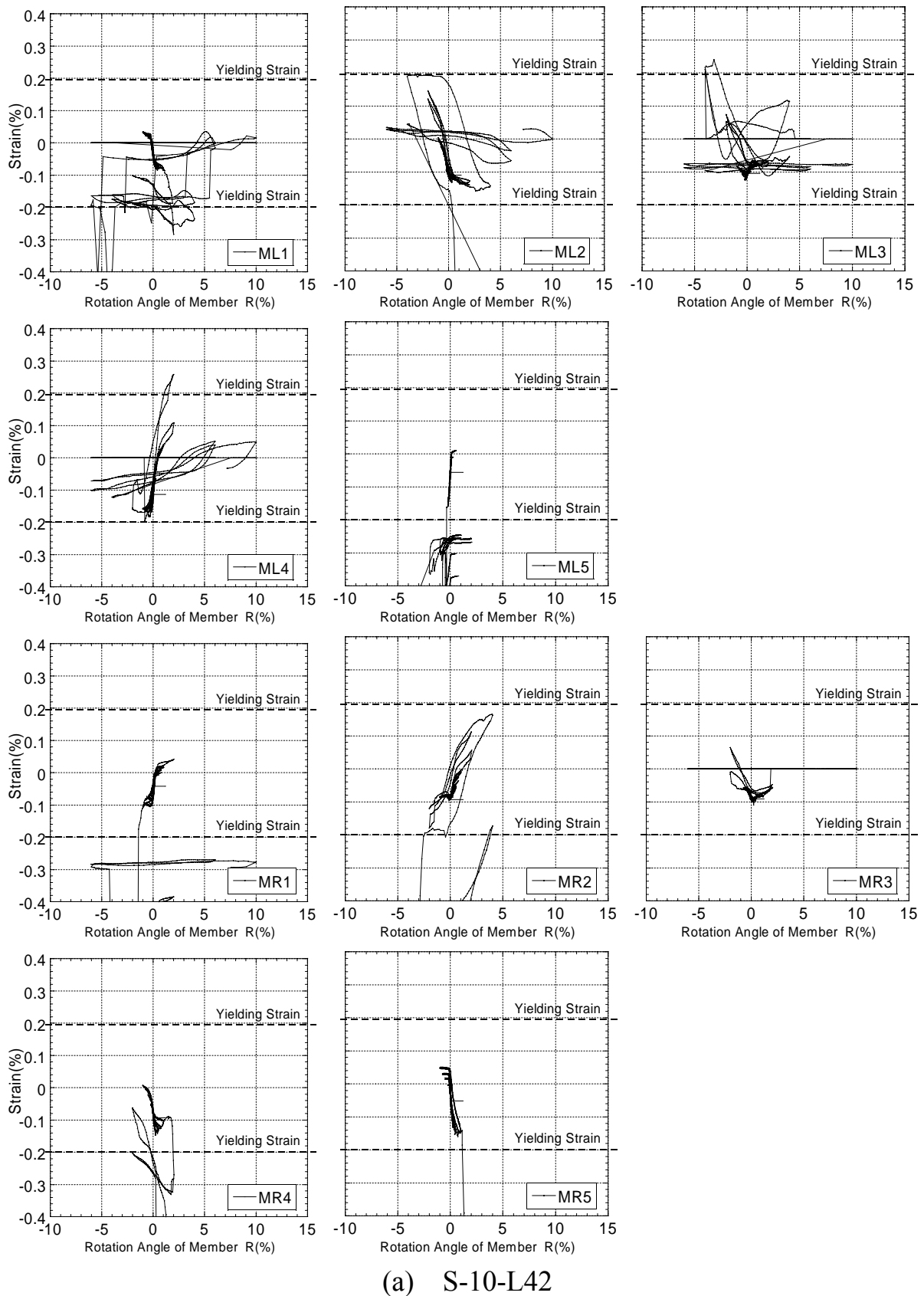
Fig. A.13　Strain distribution of non-prestressed longitudinal bars in Test 1
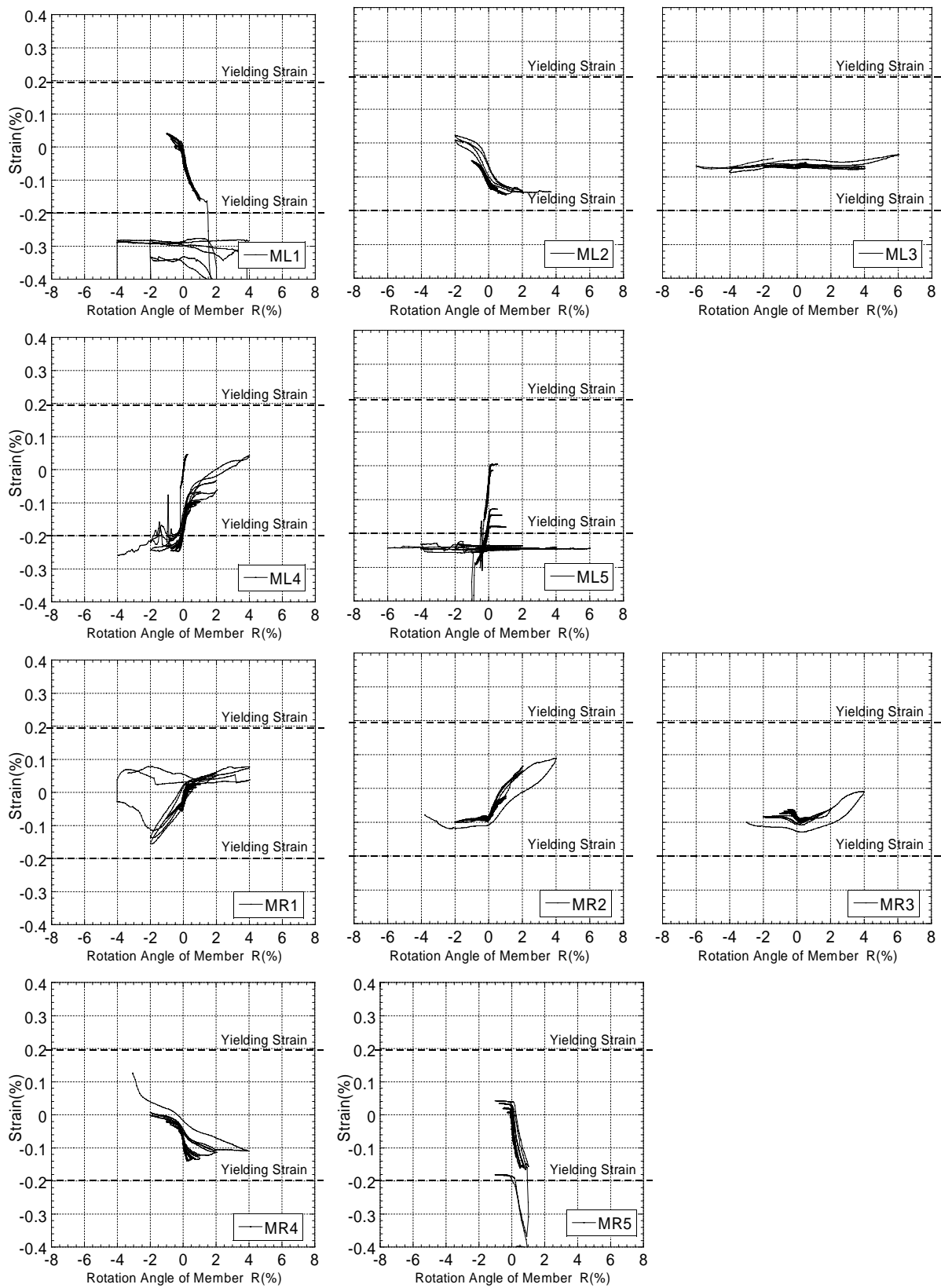
(b) S-10-L63

Fig. A.13 Strain distribution of non-prestressed longitudinal bars in Test 1
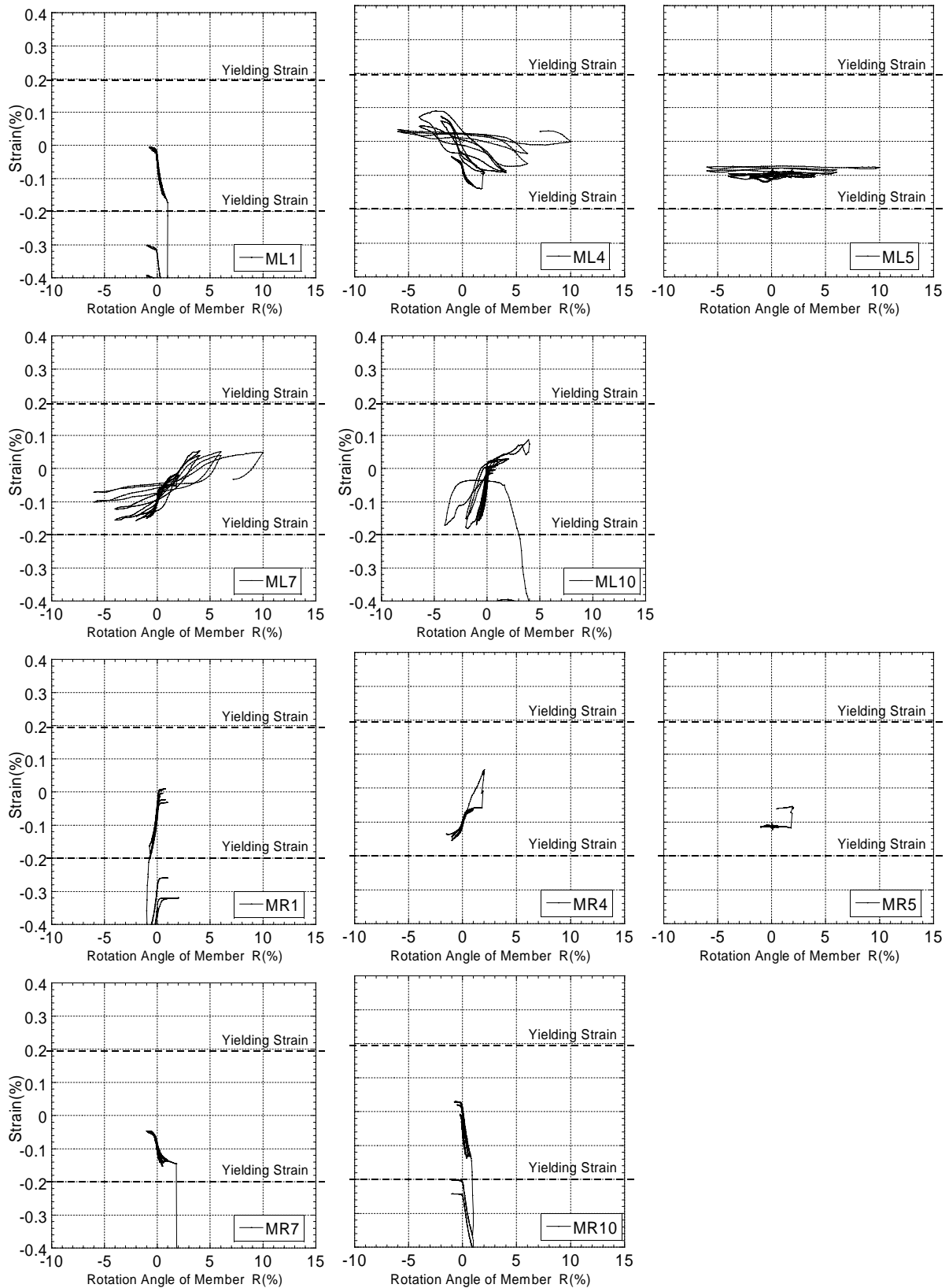
(c)   S-15-L21

Fig. A.13   Strain distribution of non-prestressed longitudinal bars in Test 1
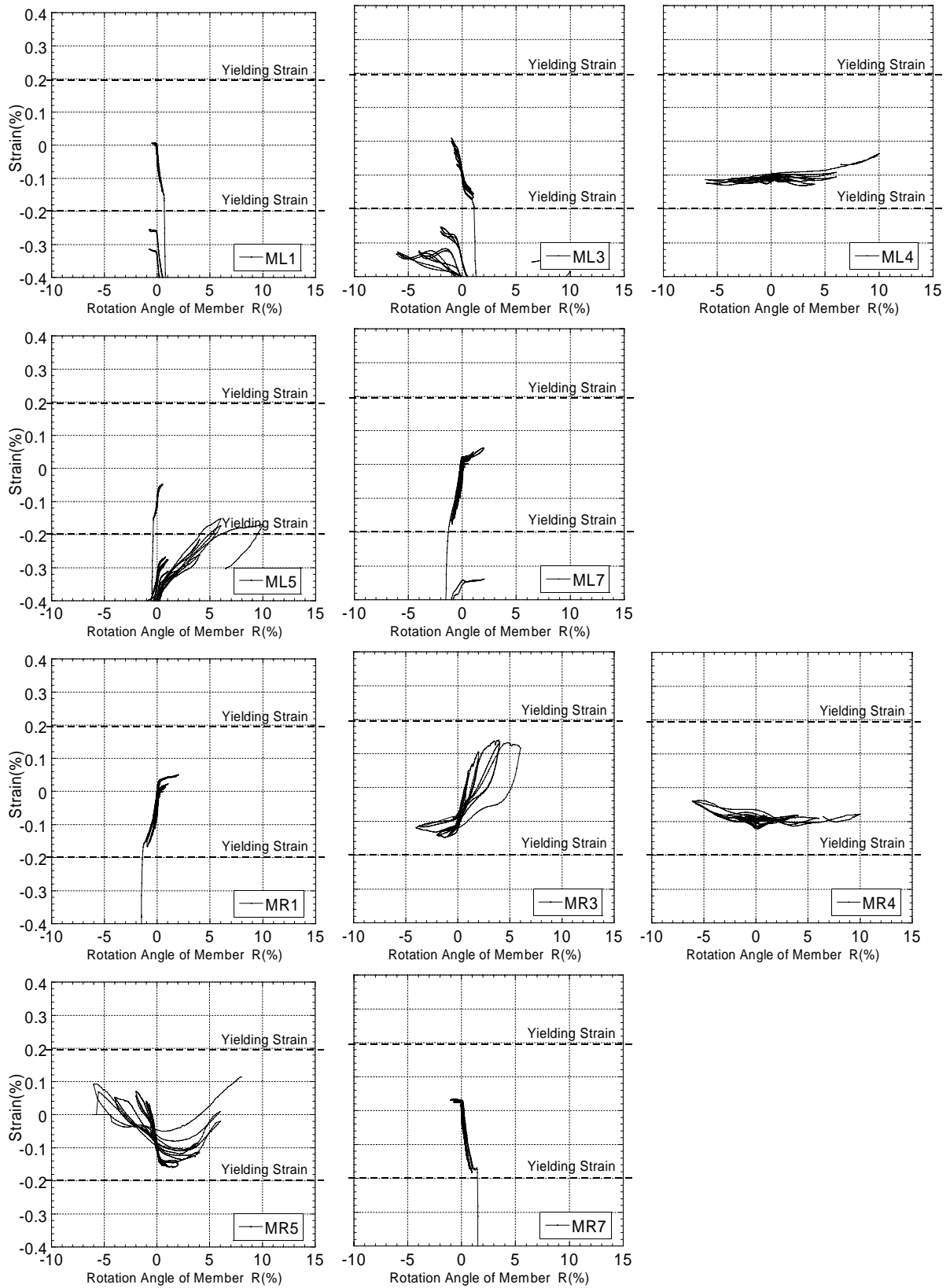
(d) S-15-L42

Fig. A.13   Strain distribution of non-prestressed longitudinal bars in Test 1
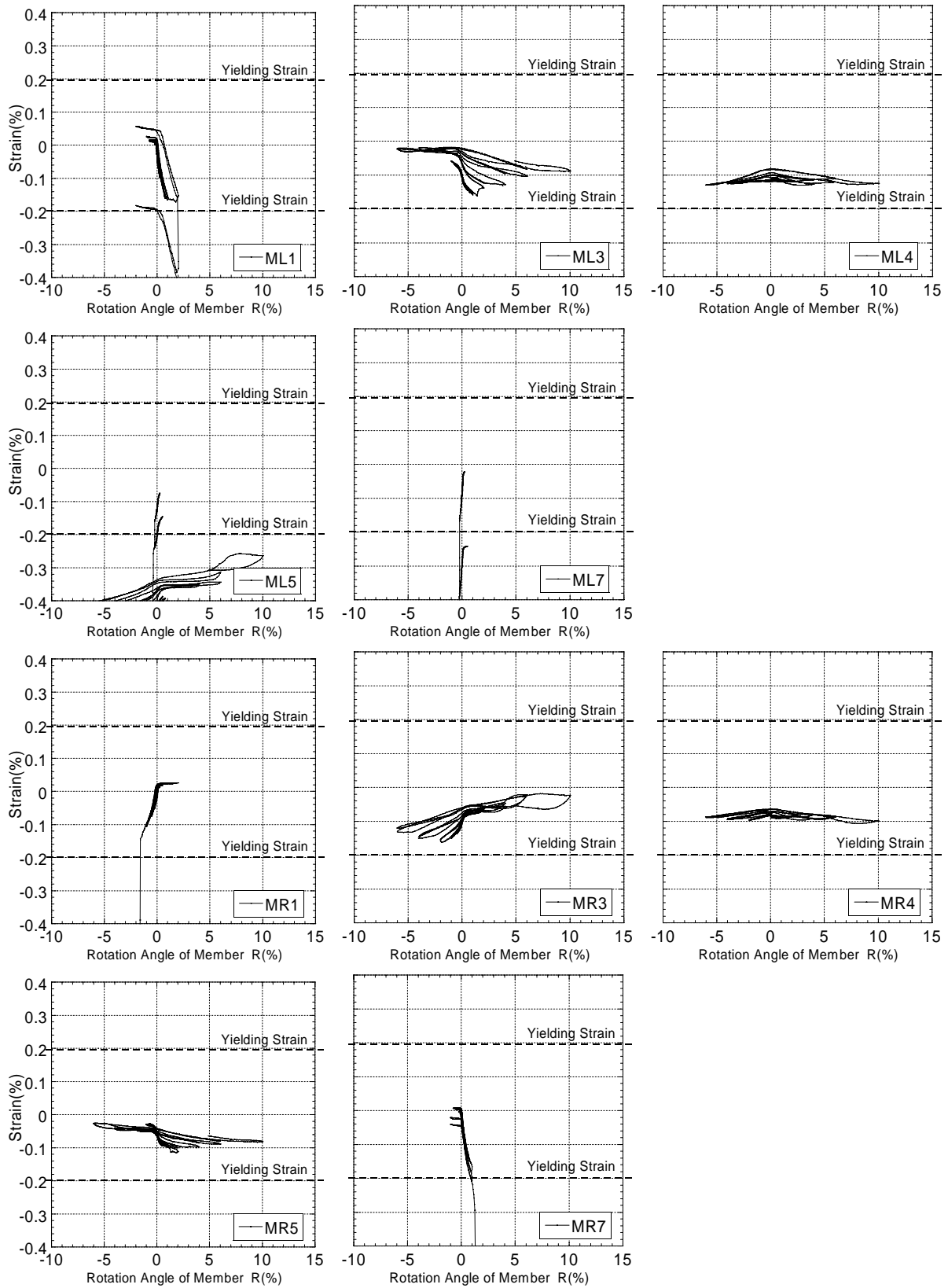
(e) S-15-L63

Fig. A.13 Strain distribution of non-prestressed longitudinal bars in Test 1

260
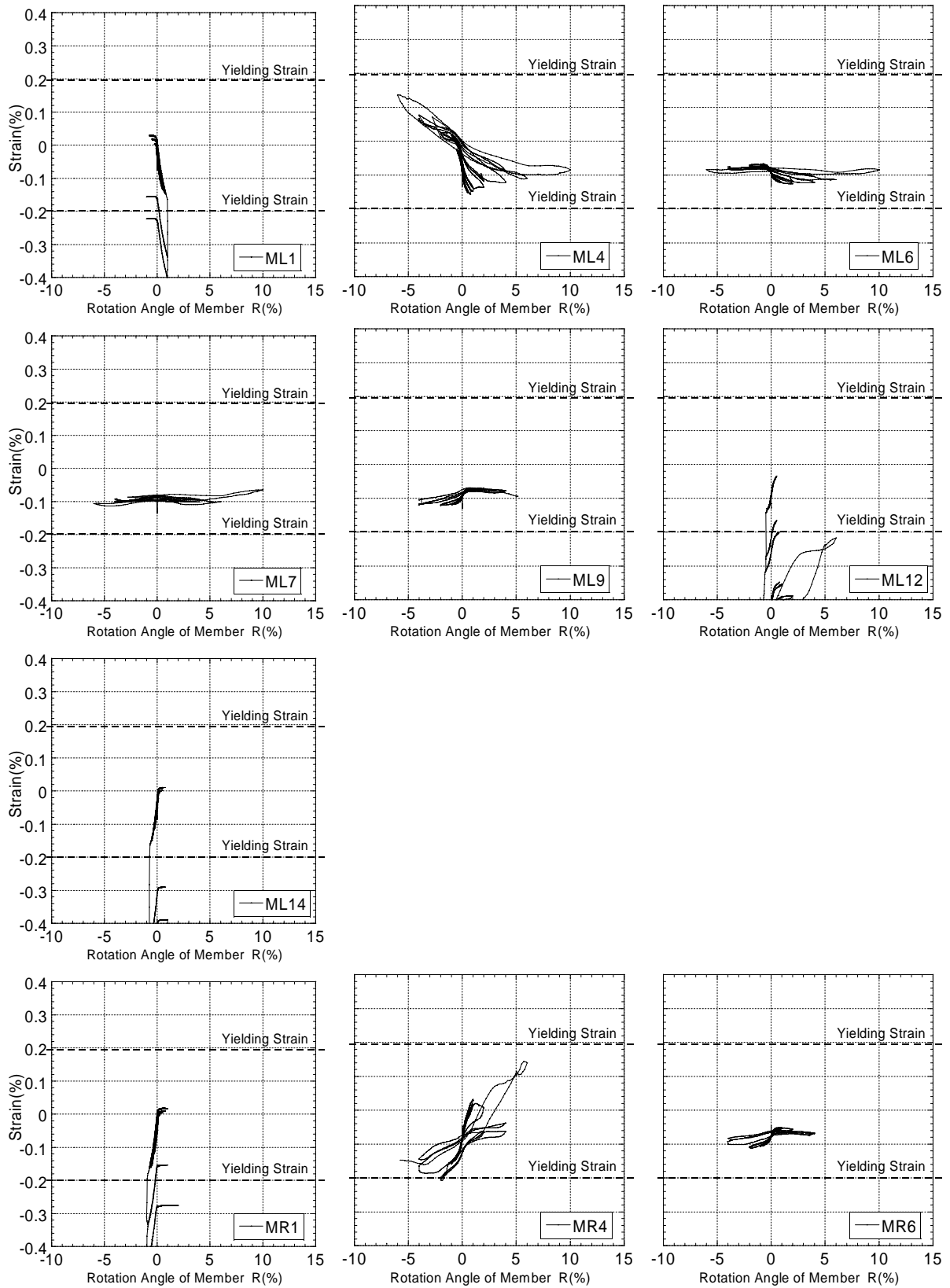
(f) S-20-L21

Fig. A.13 Strain distribution of non-prestressed longitudinal bars in Test 1
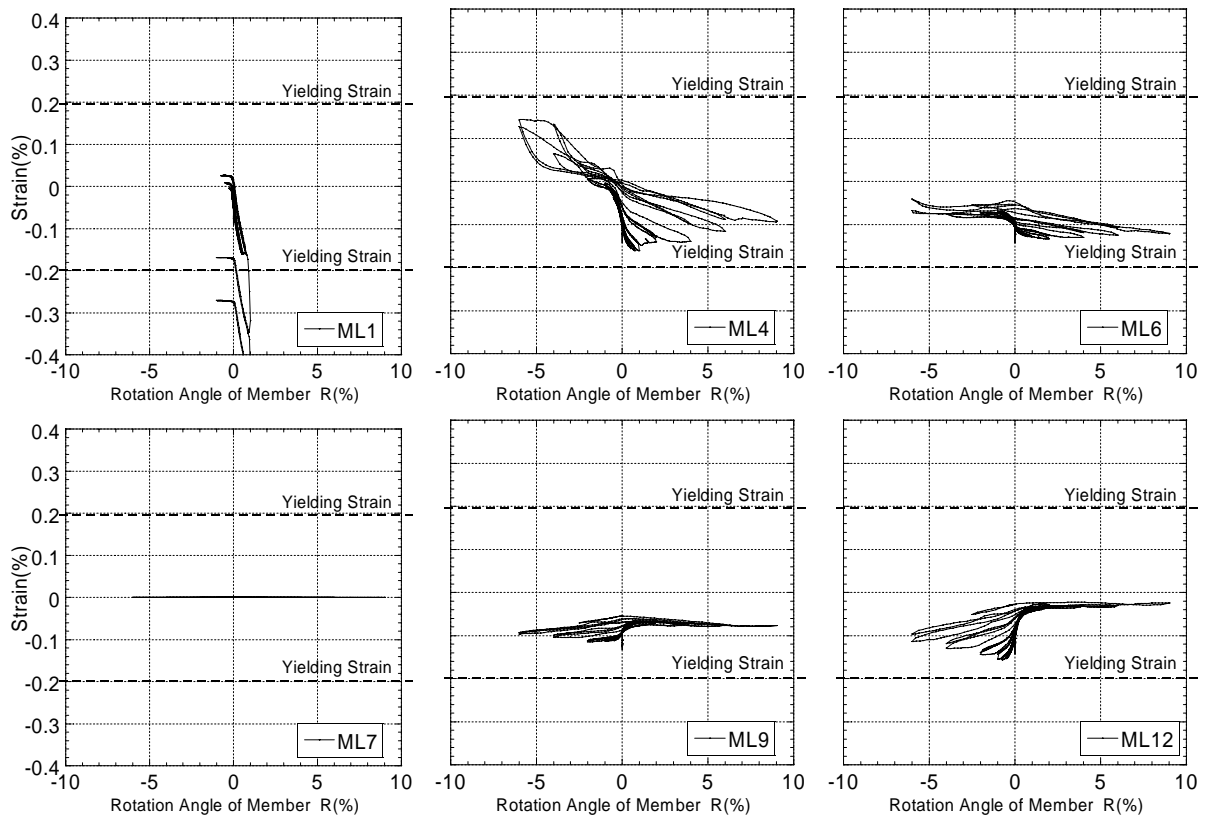
261

(f) S-20-L21

(g) S-20-L42

Fig. A.13 Strain distribution of non-prestressed longitudinal bars in Test 1
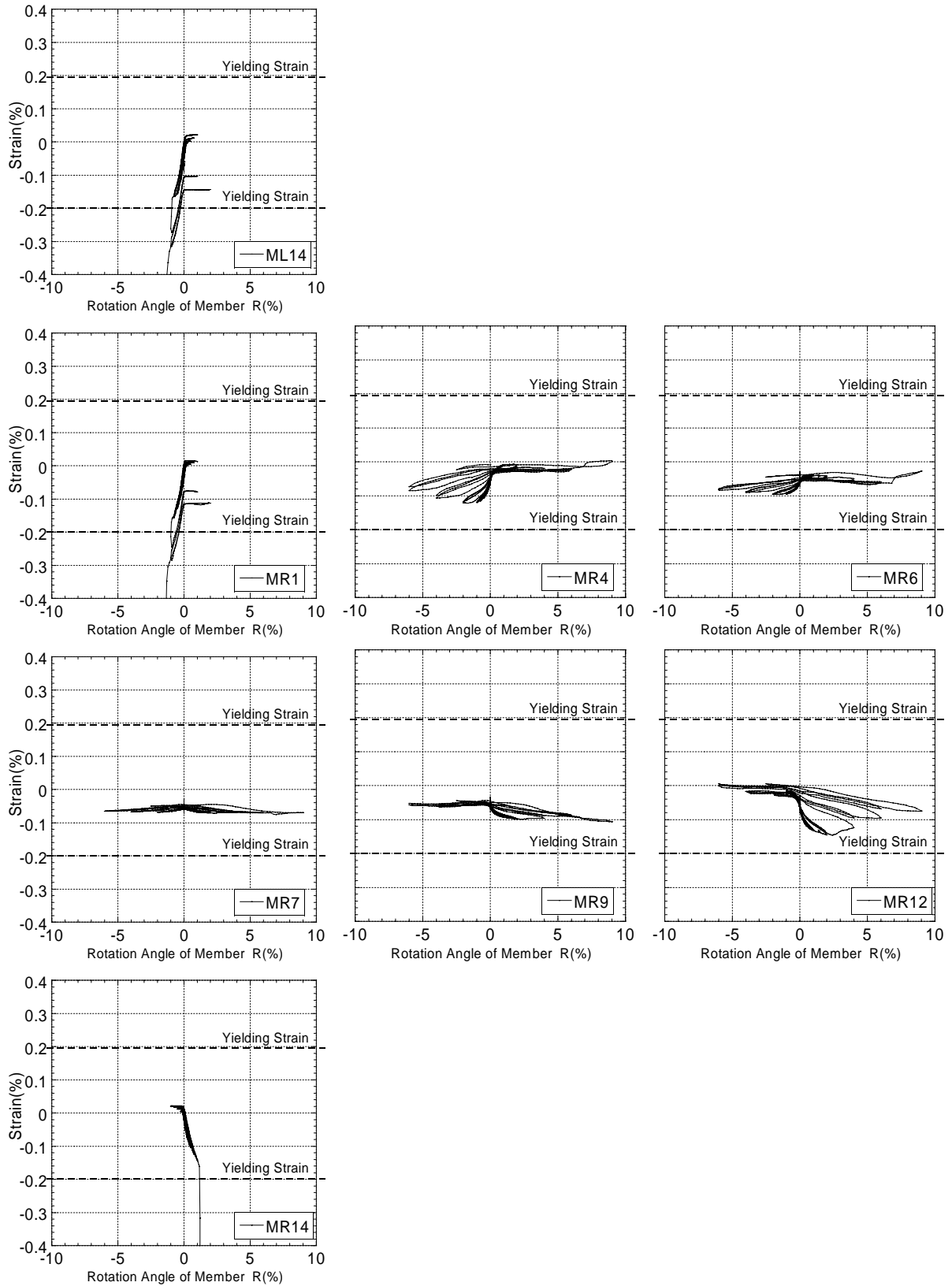
262

(g) S-20-L42

Fig. A.13   Strain distribution of non-prestressed longitudinal bars in Test 1

263

A.3.3 Shear Reinforcement

Figure A. 14 plots the strain distributions of shear reinforcements used in Test 1.
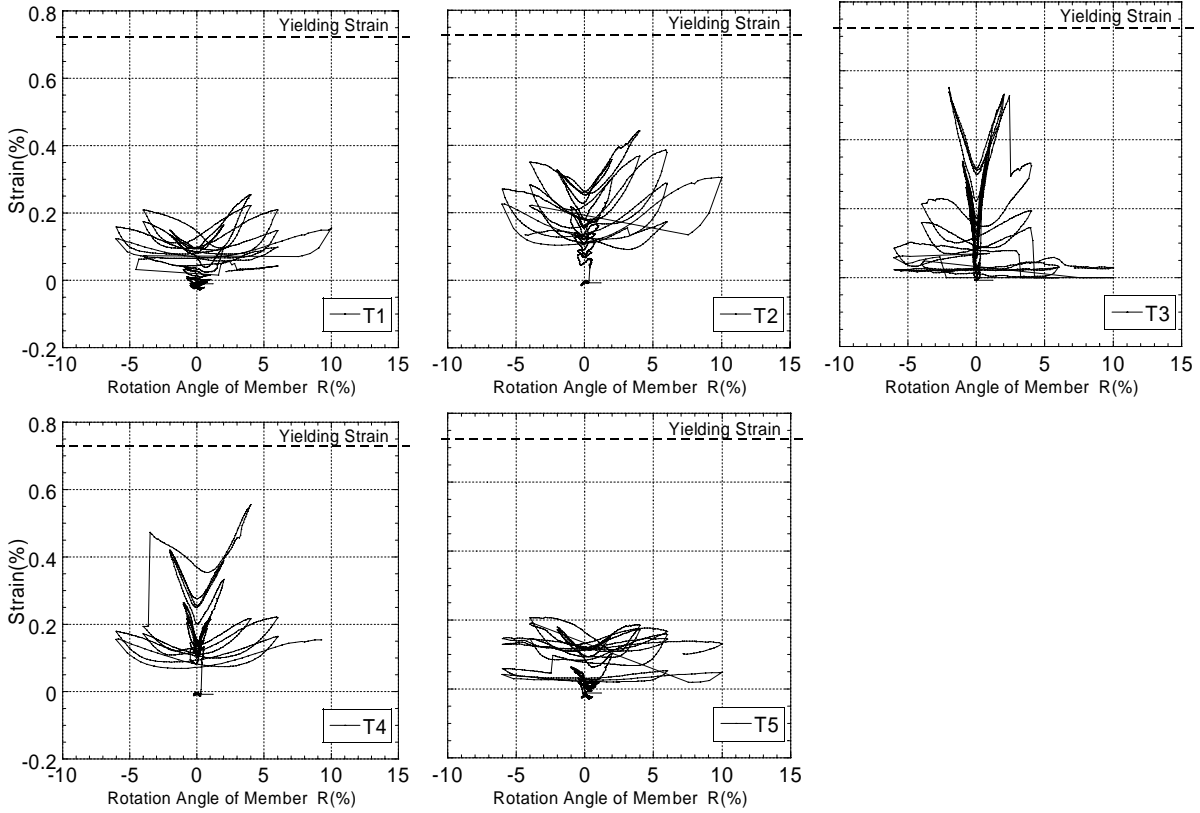
(a)   S-10-L42

Fig. A.14   Strain distribution of shear reinforcements in Test 1
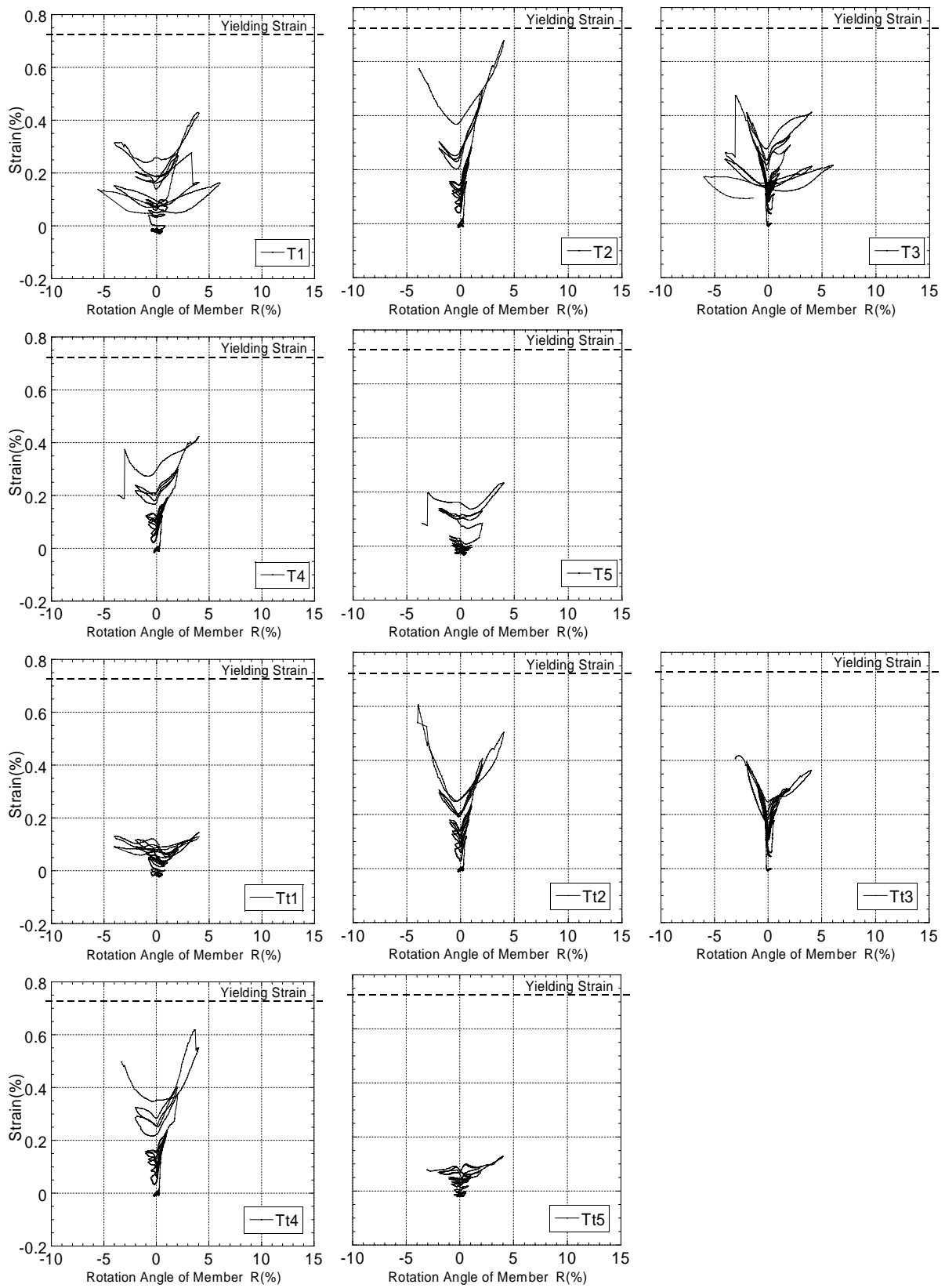
(b)　S-10-L63

Fig. A.14　Strain distribution of shear reinforcements in Test 1

265
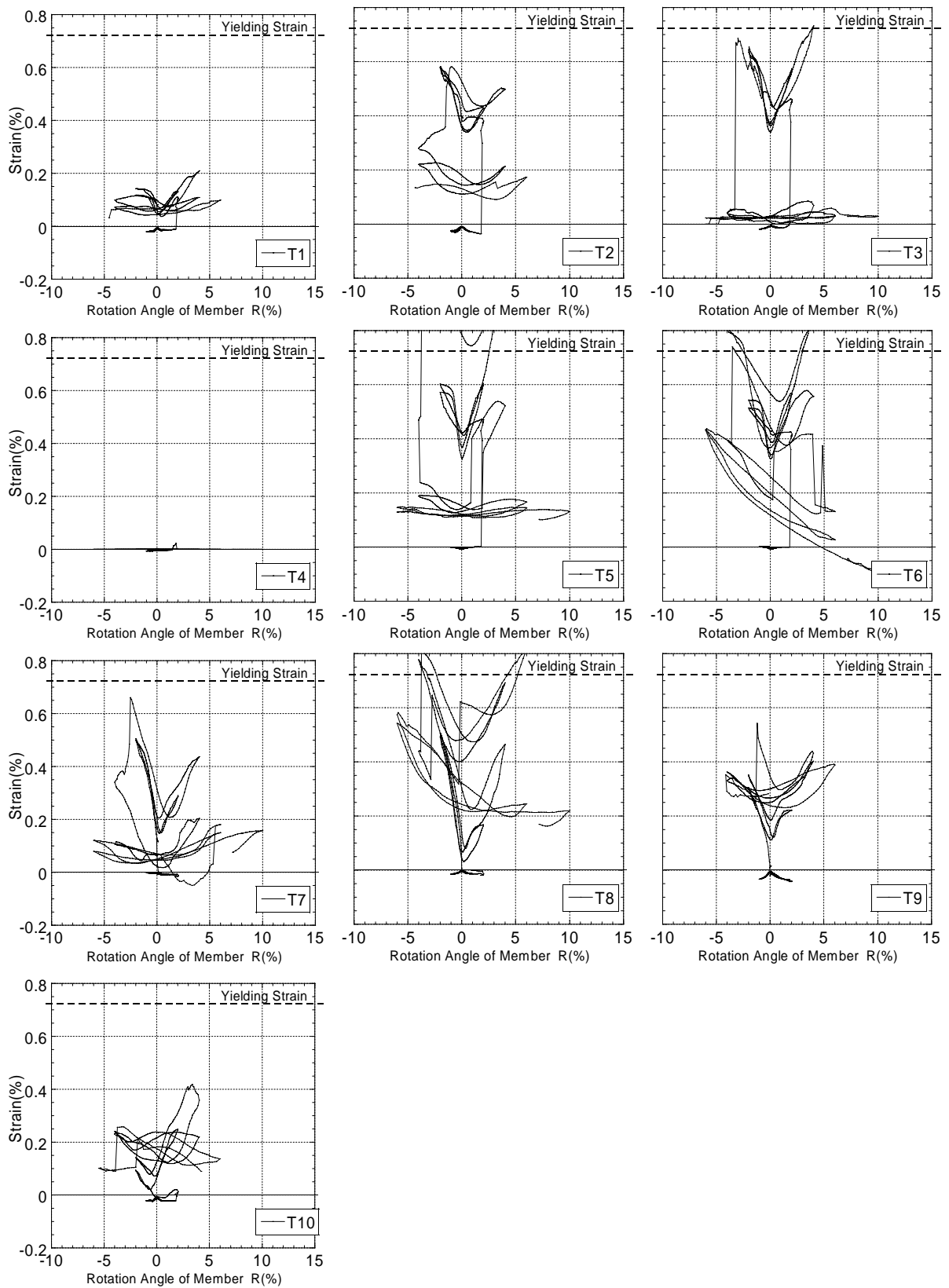
(c) S-15-L21

Fig. A.14 Strain distribution of shear reinforcements in Test 1
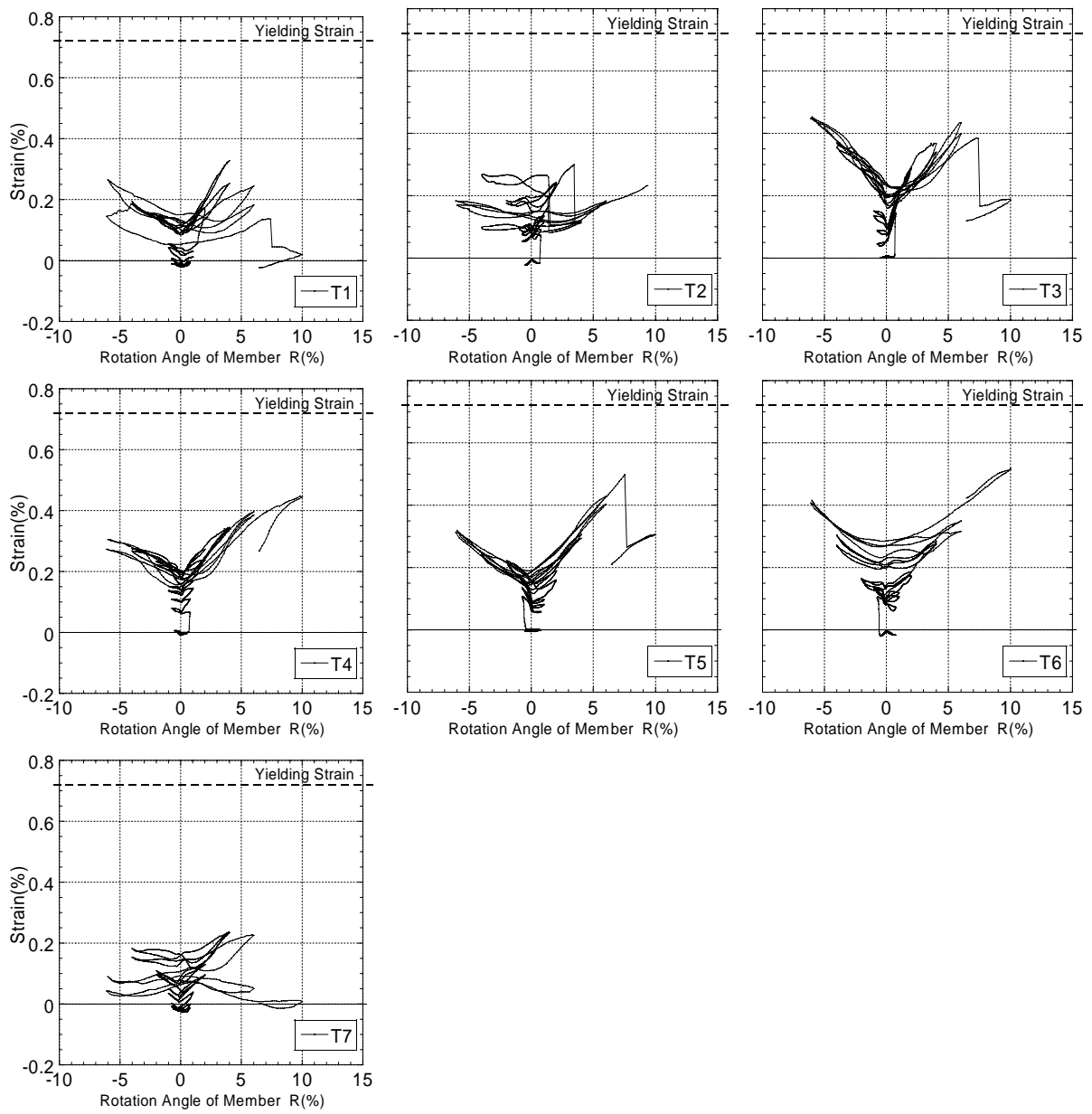
(d)   S-15-L42
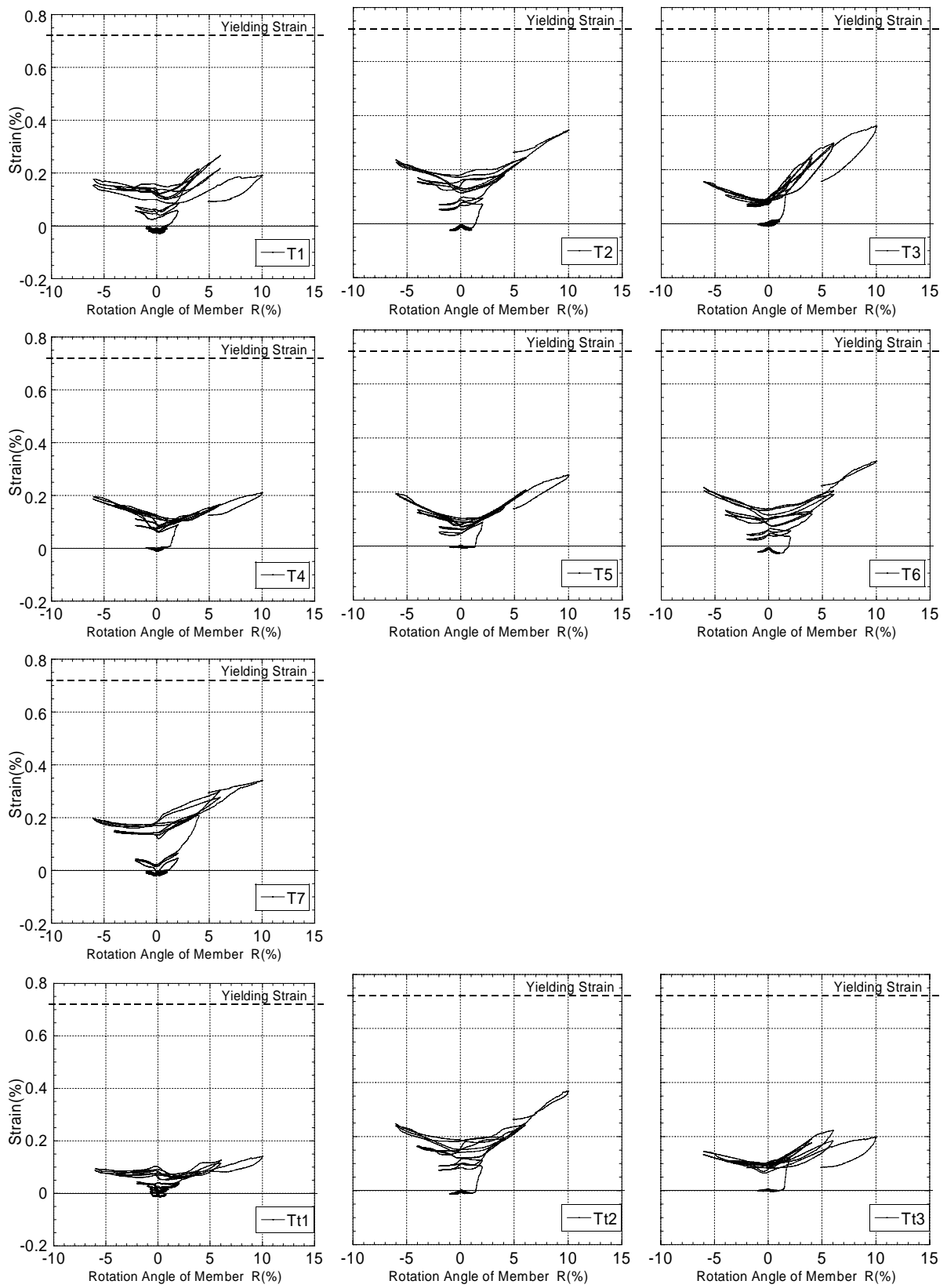
Fig. A.14   Strain distribution of shear reinforcements in Test 1

(e)   S-15-L63

Fig. A.14   Strain distribution of shear reinforcements in Test 1

268

(e)　S-15-L63

Fig. A.14　Strain distribution of shear reinforcements in Test 1

269
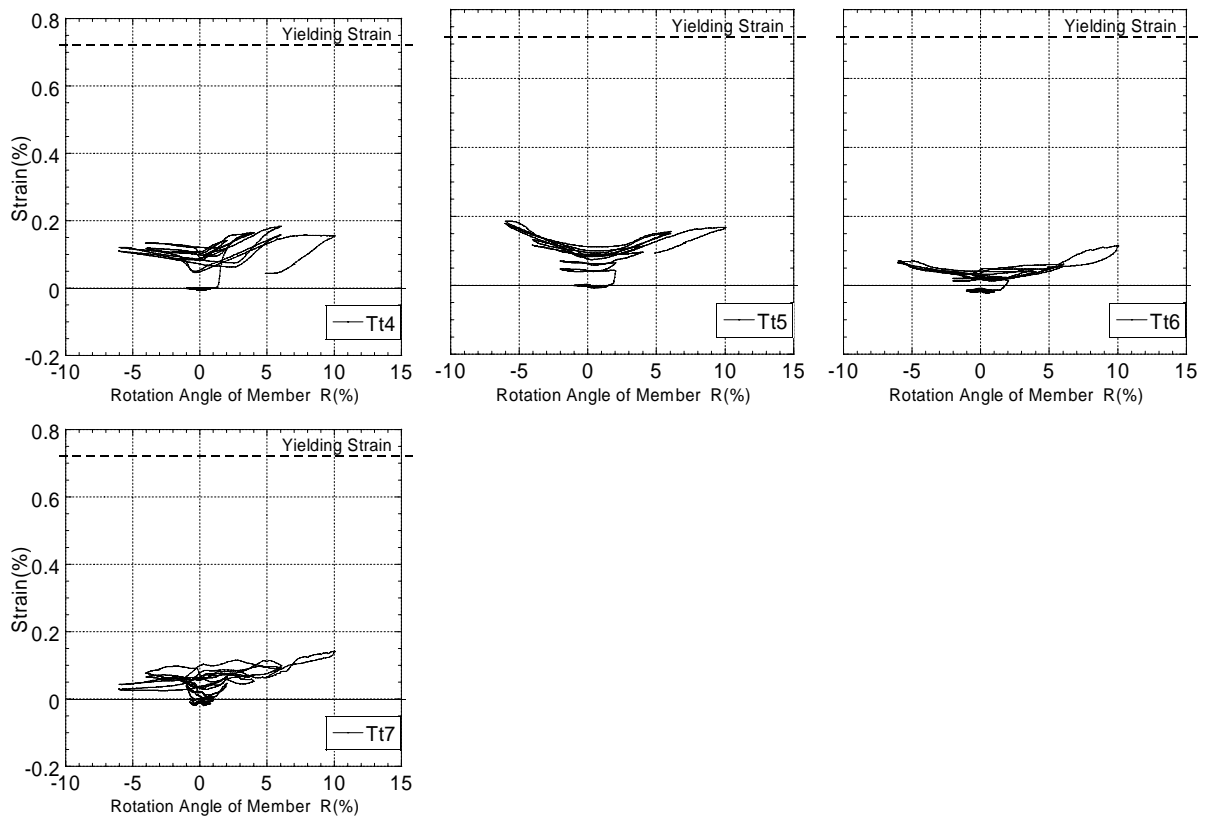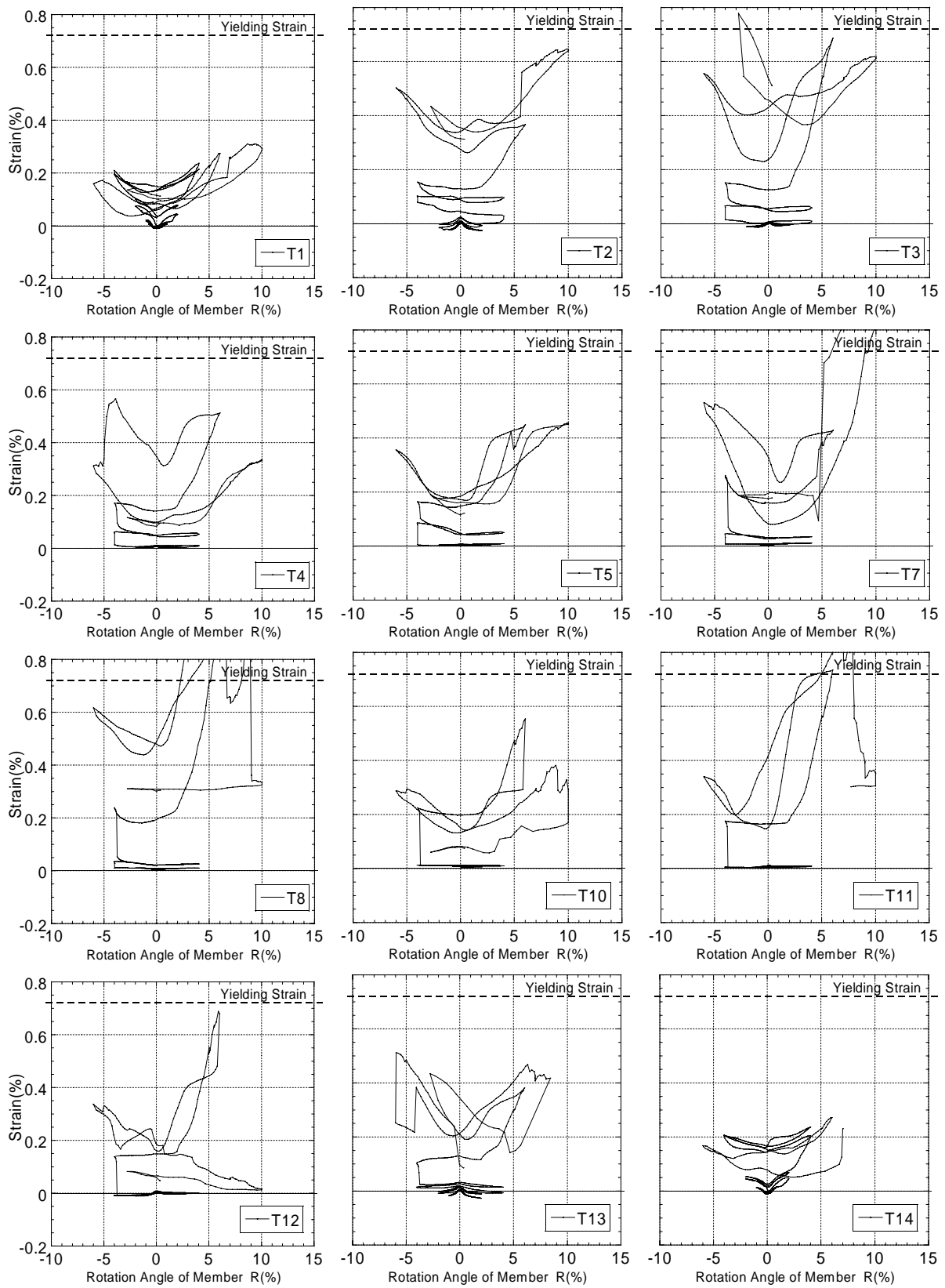
(f) S-20-L21

Fig. A.14   Strain distribution of shear reinforcements in Test 1
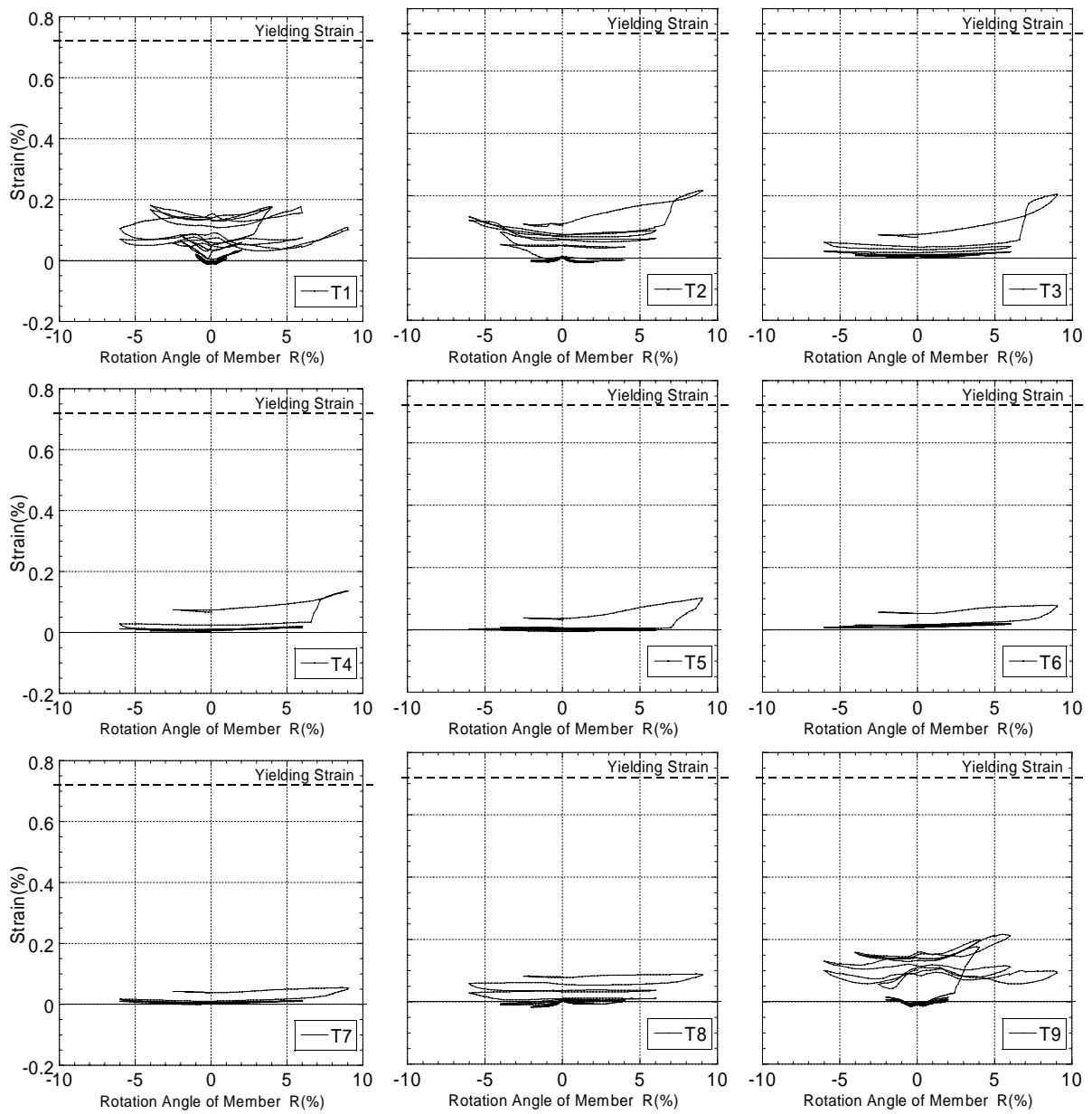
(f)   S-20-L42

Fig. A.14   Strain distribution of shear reinforcements in Test 1

271

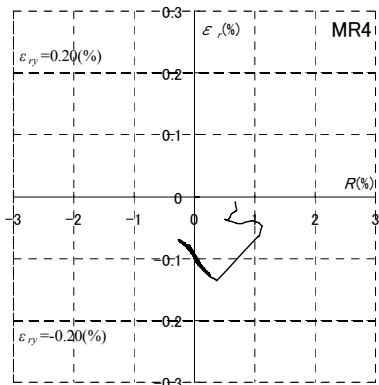# A.4 Strain Distributions of Materials in Test 2
A.4.1 Prestressing Strands

Figure A. 15 plots the strain distributions of prestressing strands used in Test 2.
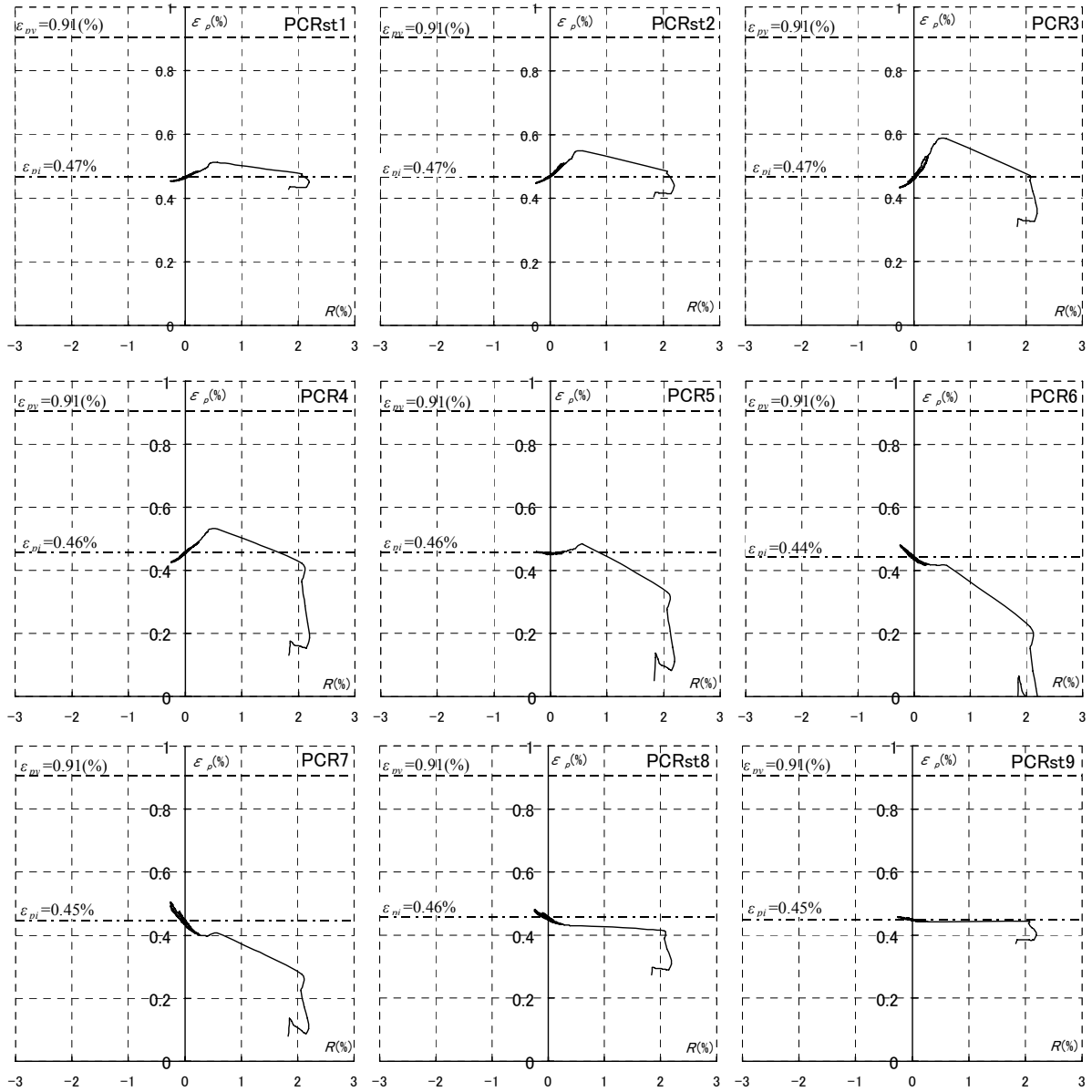
Fig. A.15   Strain distribution of prestressing strands (S-10-L10, PCR) in Test 2

Fig. A.15　Strain distribution of prestressing strands (S-10-L10, PCL) in Test 2

273
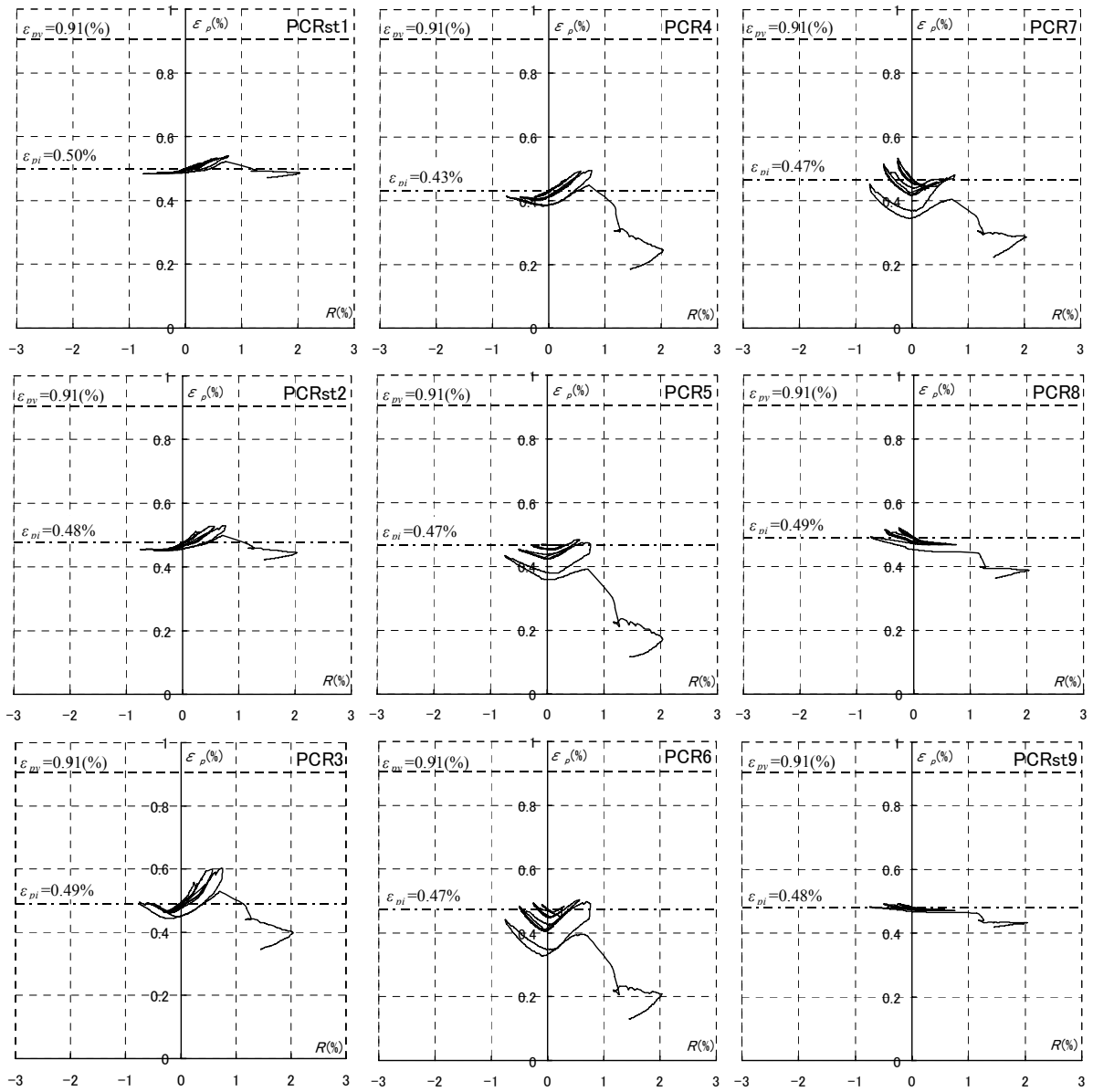
Fig. A.15   Strain distribution of prestressing strands (S-10-L21, PCR) in Test 2

274
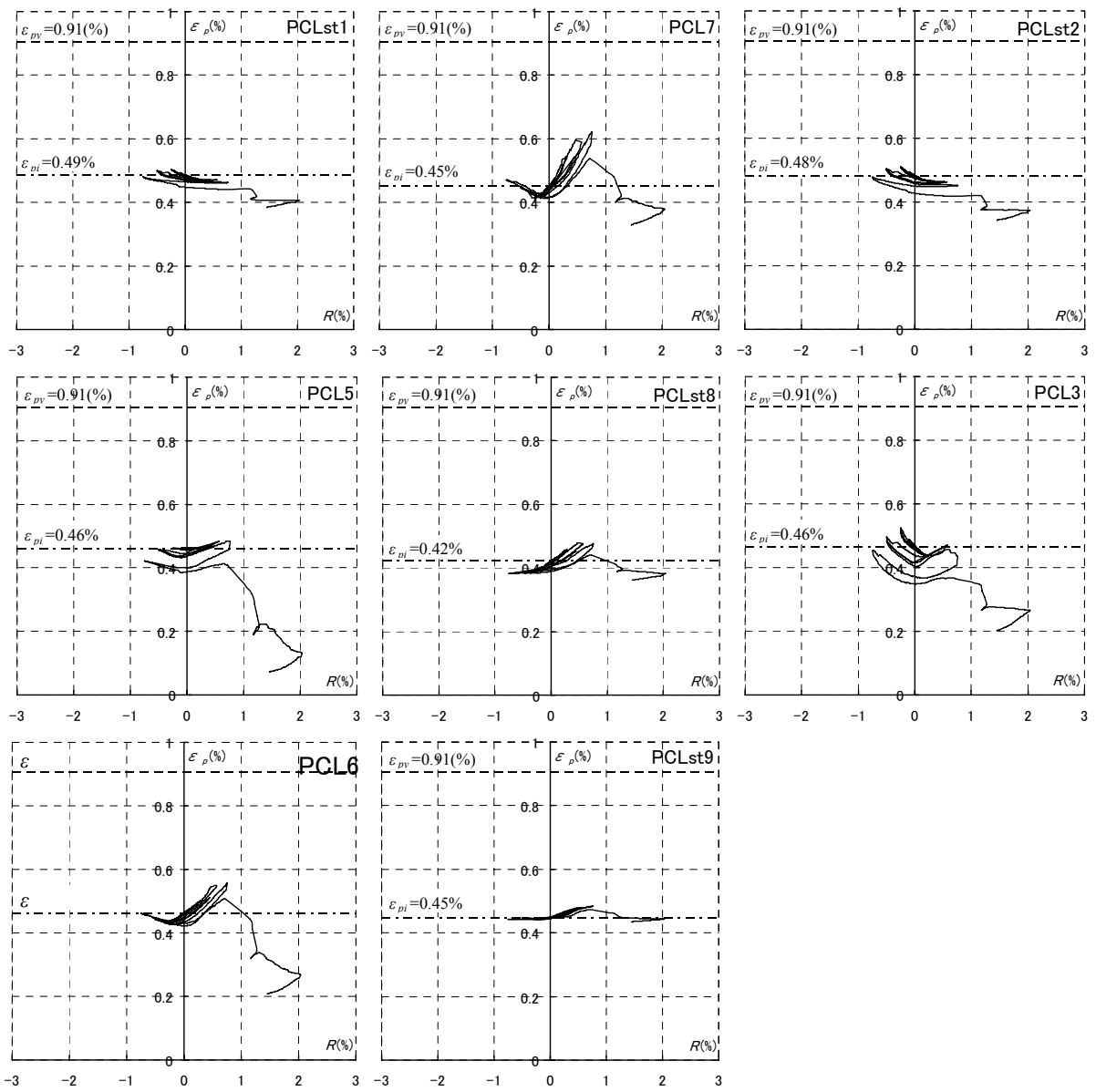
Fig. A.15   Strain distribution of prestressing strands (S-10-L21, PCL) in Test 2
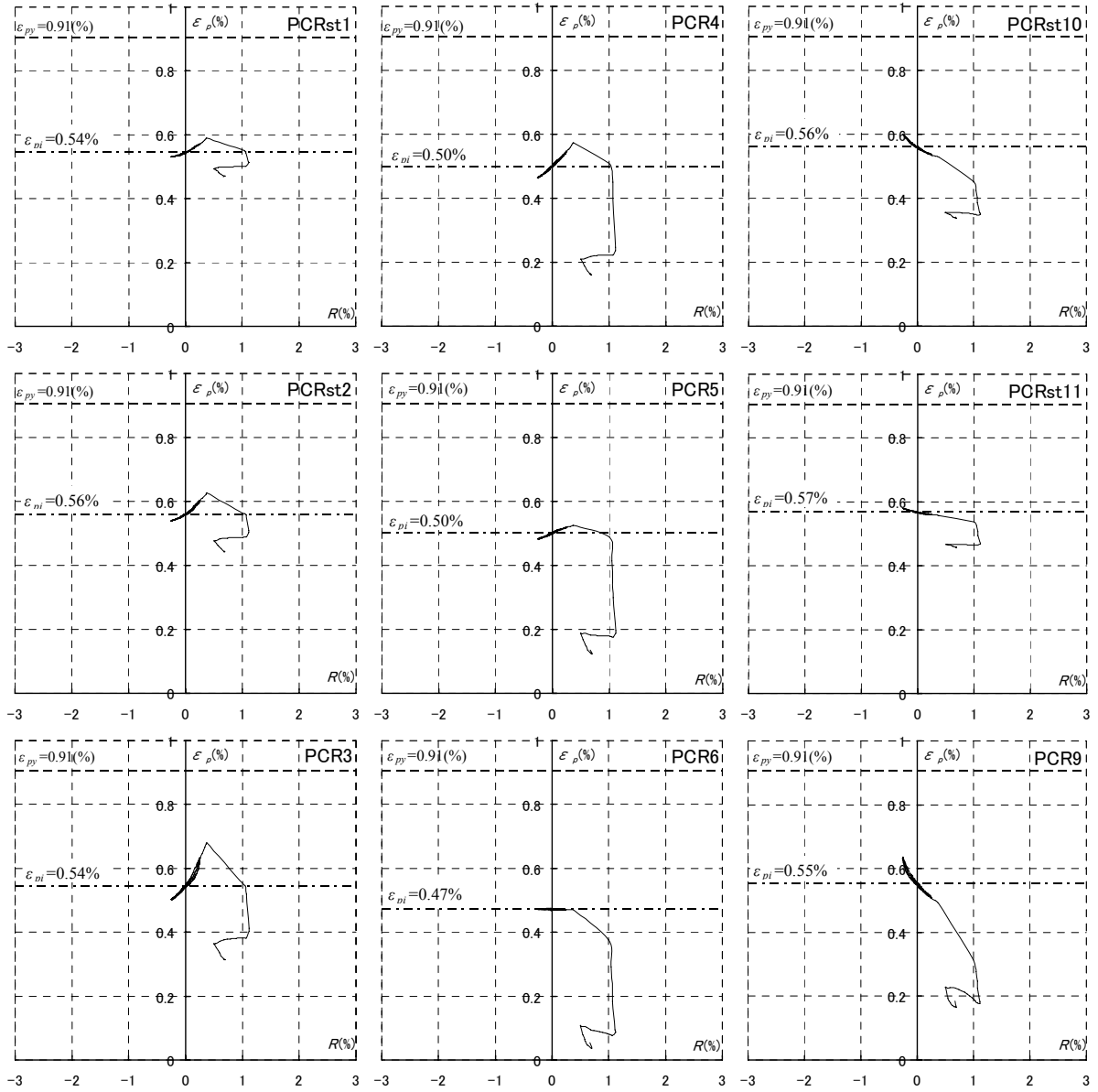
Fig. A.15   Strain distribution of prestressing strands (S-15-L00, PCR) in Test 2

276
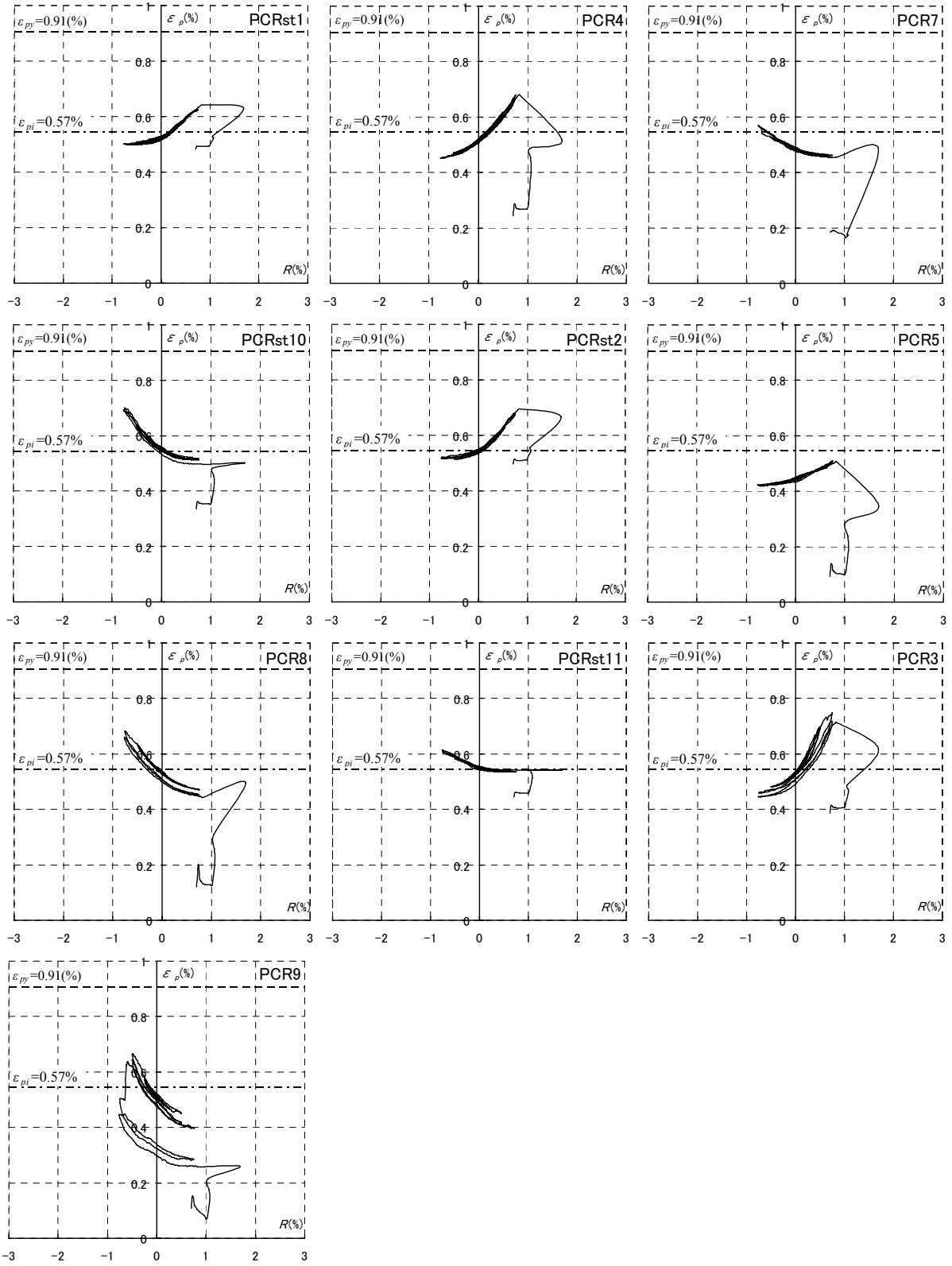
Fig. A.15   Strain distribution of prestressing strands (S-15-L00, PCL) in Test 2

Fig. A.15   Strain distribution of prestressing strands (S-15-L10, PCR) in Test 2

Fig. A.15　Strain distribution of prestressing strands (S-15-L10, PCL) in Test 2

A.4.2 Non-Prestressed Longitudinal Bar

Figure A. 16 plots the strain distributions of non-prestressed longitudinal bars used in Test 2.

(a) S-10-L10

(b) S-10-L21

281

(c) S-15-L00
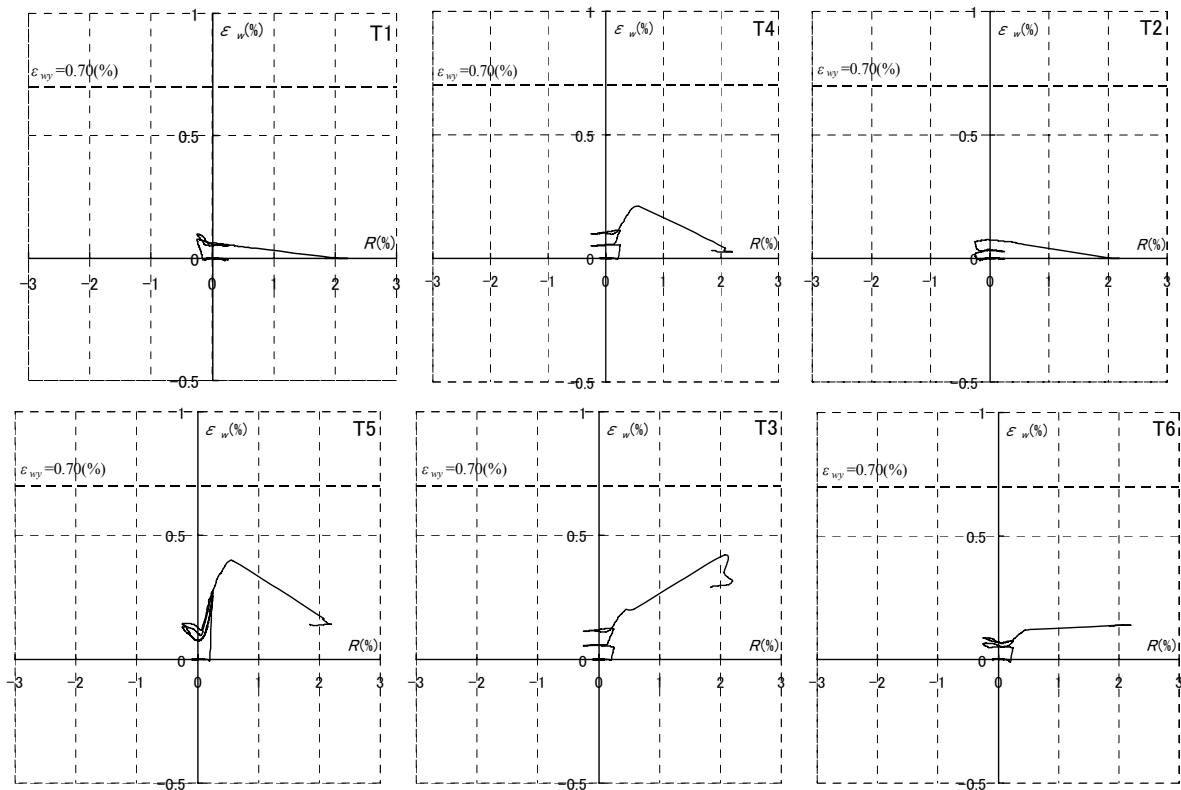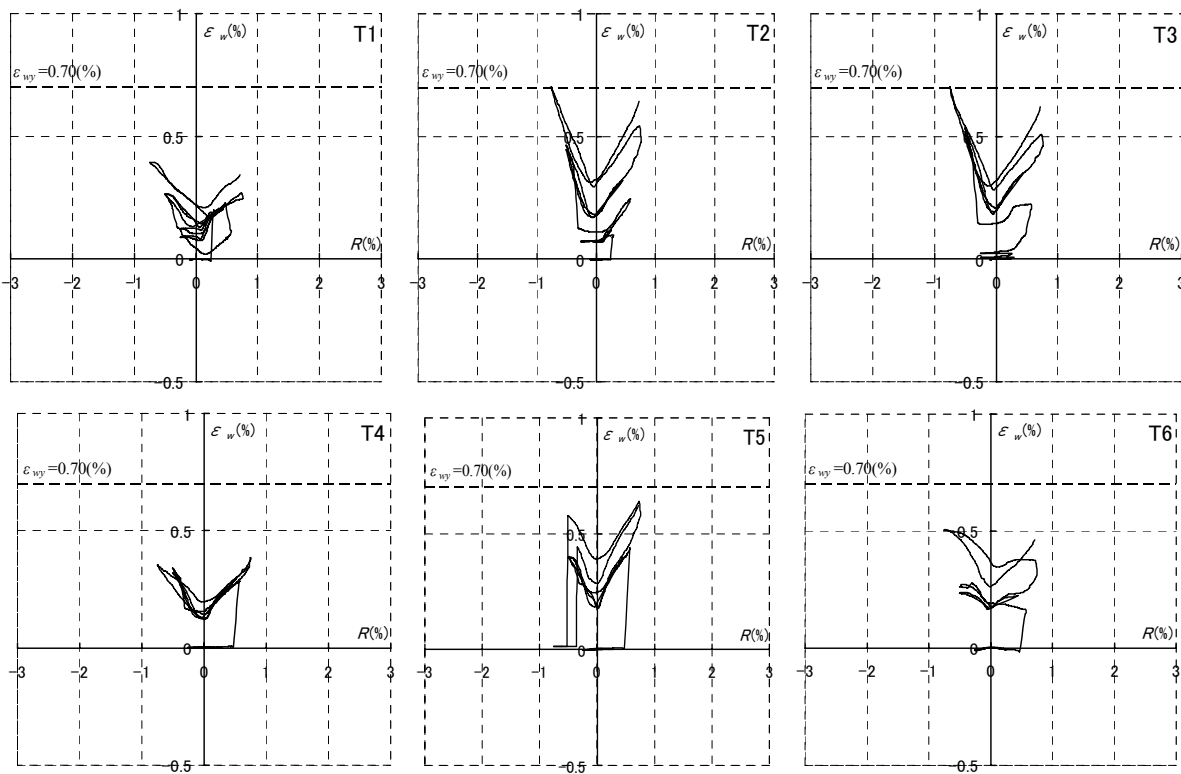
282

(d) S-15-L10

283
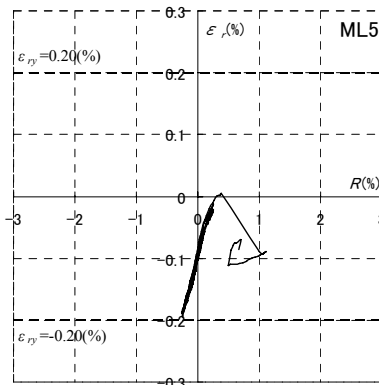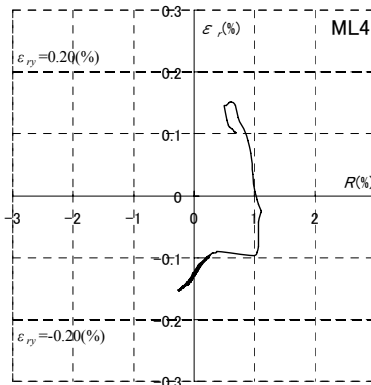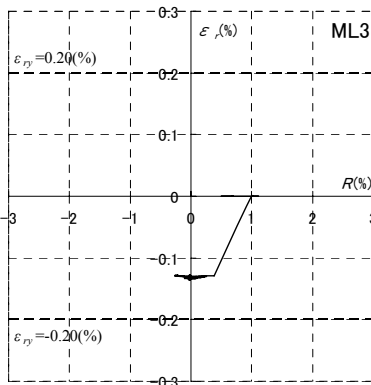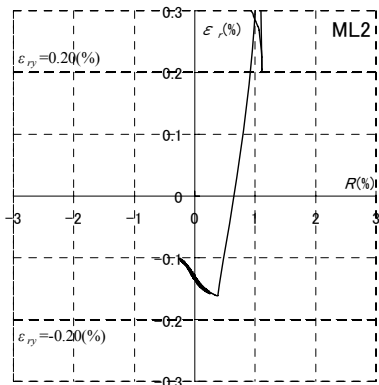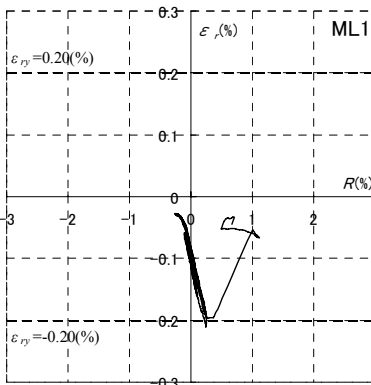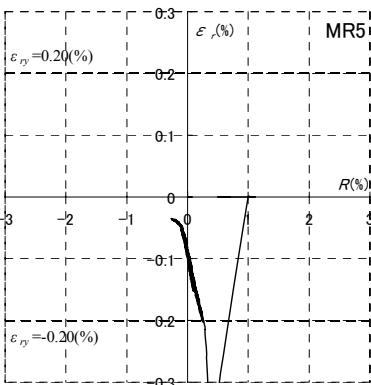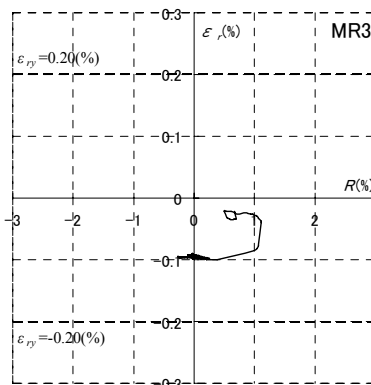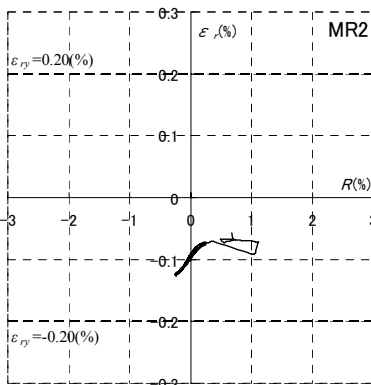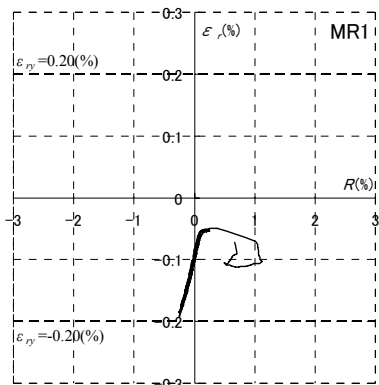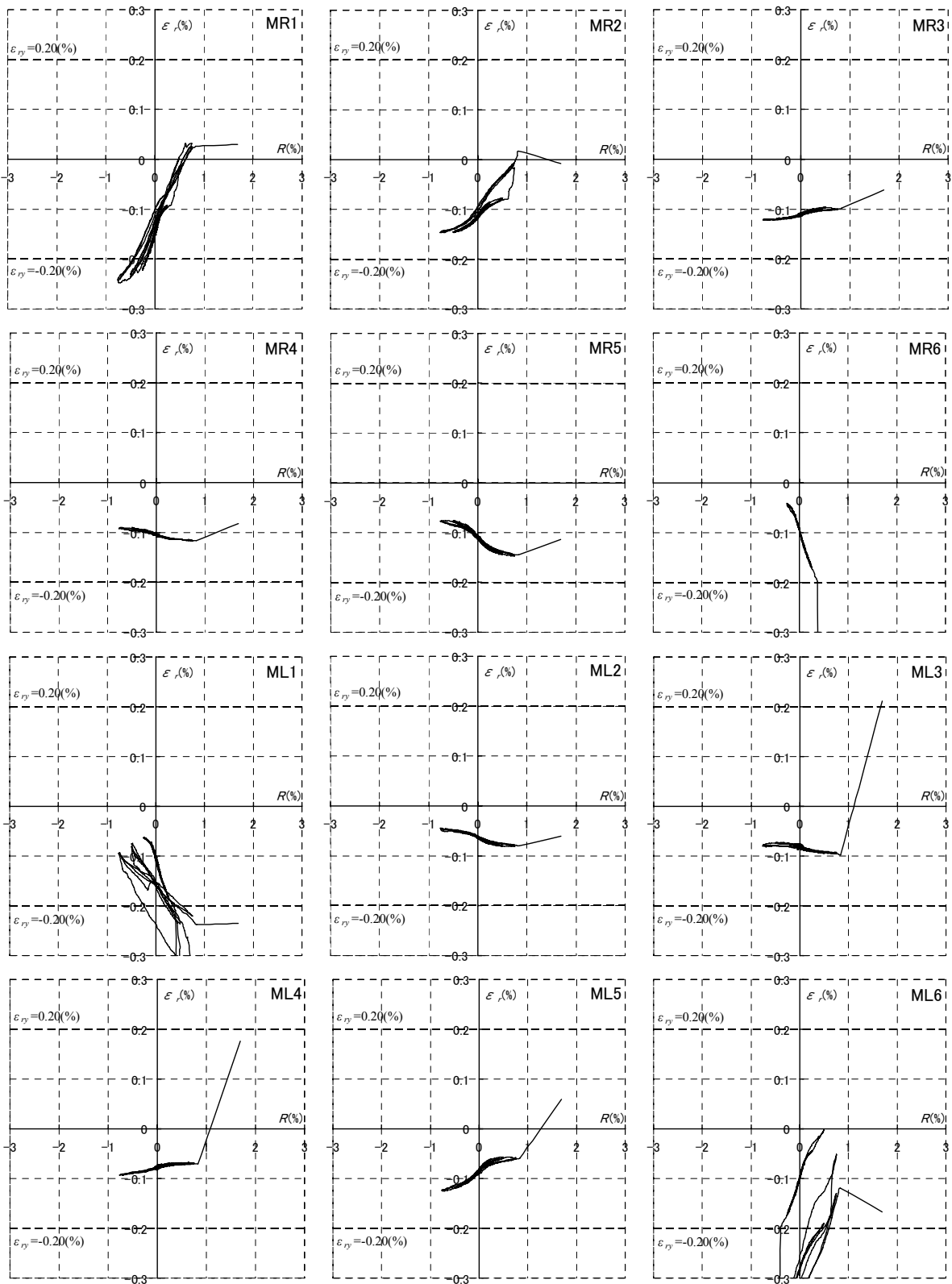
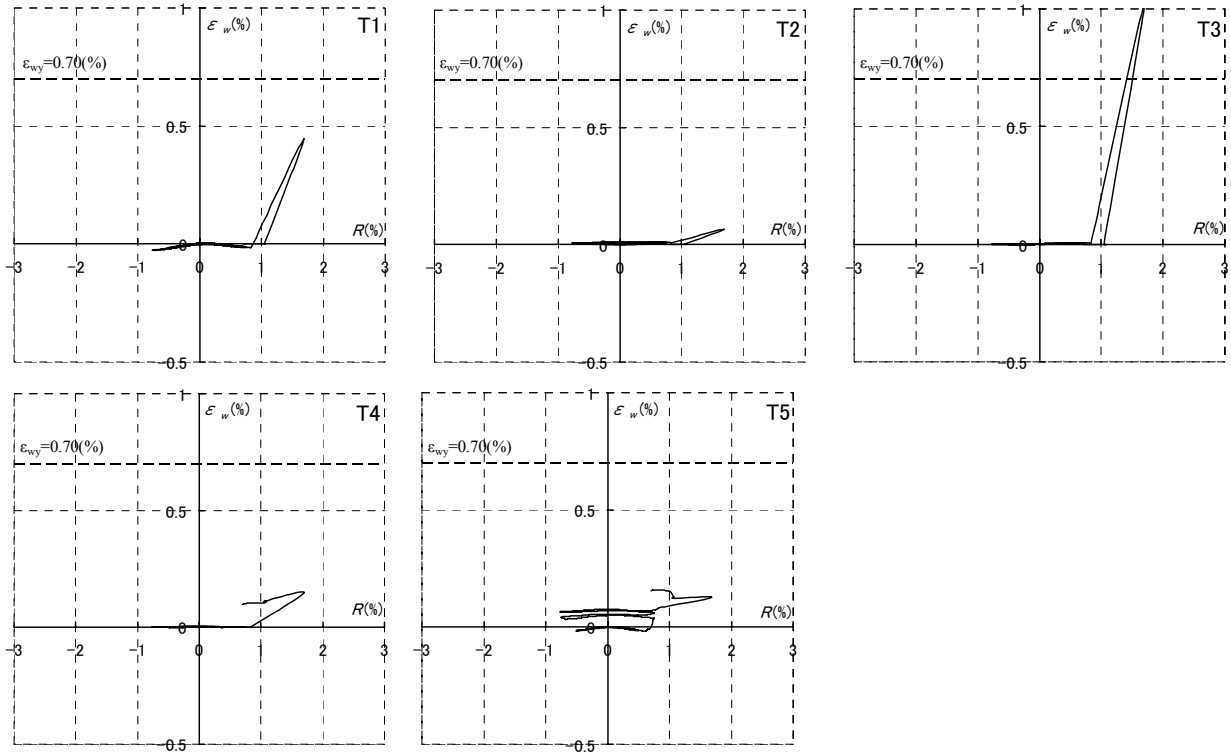# A.4.3 Non-Prestressed Longitudinal Bar

Figure A. 17 plots the strain distributions of shear reinforcements used in Test 2.

(a) S-10-L10

(b) S-10-L21

(c S-15-L10

Fig. A.17   Strain distribution of shear reinforcements in Test 2